Hydro-mechanical behavior of lime-treated/untreated soils under the effects of salinity and wetting-drying cycles

Zi Ying

École des Ponts ParisTech

THÈSE DE DOCTORAT

de l'École des Ponts ParisTech

Hydro-mechanical behavior of lime-treated/untreated soils under the effects of salinity and wetting-drying cycles

École doctorale N°531 - SIE (Sciences, Ingénierie et Environnement)

Spécialité: Géotechnique

Laboratoire Navier/CERMES

Date: 20 September 2021

by

Zi YING

Composition du jury:

Prof. Farimah MASROURI Université de Lorraine	President
Prof. Mahdia HATTAB Université de Lorraine	Reporter
Prof. Said TAIBI Université le Havre Normandie	Reporter
Dr. Valéry FERBER Charier	Examiner
Dr. Gontran HERRIER Lhoist Research and Development	Examiner
Prof. Yu-Jun CUI Ecole des Ponts ParisTech	Supervisor
Dr. Nadia BENAHMED INRAE	Co-supervisor
Dr. Myriam DUC Université Gustave Eiffel	Co-supervisor

Acknowledgements

The work presented in this thesis would not have been possible without the help of many people. I would like to take this opportunity to express my sincere gratitude to all people who directly or indirectly helped me in the course of my Ph.D study.

First, I would like to express my deep and sincere gratitude to my supervisor, Prof. **Yu-Jun CUI**, for his endless guidance, constructive advice, trust and encouragement during my Ph.D study. I have learned from him how to carry out research, write a paper, think in a logic way and present outcomes, as well as how to guide students and what kind of teacher to be in my future life. He also taught me how to deal with life: live modestly, do greatly. These will benefit me all of my life.

I would also extend my sincere appreciation to my co-supervisors, Dr. **Nadia BENAHMED** and Dr. **Myriam DUC.** Thanks for their attendance in every meeting with their valuable suggestions and guidance. Thank them for providing me the opportunity to work in their laboratory and to communicate with other groups who have the same scientific interests. Their guidance and advice have significantly contributed to the accomplishment of this dissertation.

Besides, I wish to acknowledge the reporters and examiners of my thesis: Prof. **Said TAIBI**, Prof. **Mahdia HATTAB**, Prof. **Farimah MASROURI**, Dr. **Valéry FERBER** and Dr. **Gontran HERRIER** for their constructive suggestions and comments which greatly helped improve this dissertation.

The experimental work cannot be completed without the precious assistance from the technical team of CERMES. I specially thank **Emmanuel De Laure** for his fantastic ideas and uncountable helps in my experiments. I also thank **Marine Lemaire**, **Xavier Boulay**, **Baptiste Chabot** and **Loïc Lesueur**, who helped a lot for my experimental work.

I am also grateful to my Chinese friends, who helped me to adapt to living in France. We accompanied and encouraged each other, and made progress together. I also thank my colleagues at CERMES for their assistance and company. That is really a memorable experience with all of you.

I am particularly grateful to Prof. **Zhen-Shun HONG,** who was the supervisor for my master degree and introduced me to Prof. Yu-Jun CUI. Many thanks for his constant encouragement, help, advices and concerns. I would also thank Prof. **Ling-Ling ZENG**, Prof. **Xia BIAN** and Prof. **Jian-Wen DING**, who helped me a lot when I applied for the financial support from China Scholarship Council.

The financial supports from China Scholarship Council (CSC), Ecole des Ponts ParisTech (ENPC) and Institut national de recherche pour l'agriculture, l'alimentation et l'environnement (INRAE) are greatly acknowledged.

Last but not least, I would like to express my love and gratitude to my parents, my grandparents my sister and my aunts for their care and encouragement. I wish to specially thank my boyfriend who always understand and support me, as well as accommodate my willfulness and temper.

Abstract

Lime treatment can enhance the workability and hydro-mechanical properties of soil through different physical-chemical reactions, such as cations exchange and pozzolanic reaction. The effectiveness of lime treatment is expected to be water chemistry and climate dependent. To understand the effects of water chemistry and climate on lime-treated soils, the project DIGUE 2020 was set up involving a dike constructed at les Salin-de-Giraud using local saline soils. In this PhD study, a laboratory work was conducted on the soils taken from Salin-de-Giraud with and without lime treatment, with emphasis put on the effects of salinity and wetting-drying cycles.

In order to well characterize the salinity effect, new methods were proposed to determine the dissolved salinity and the induced osmotic suction for unsaturated soils with consideration of dissolved and precipitated salts. The mechanisms of salinity effect on the liquid limit and compaction behaviour of untreated soil, and of the drying effect on the microstructure of compacted saline soil were clarified. The optimum lime content of soil mixed with deionized water, synthetic seawater, mixed salts solution were determined by pH method. Results showed that the optimum lime content increased with the increase of salt concentration, which can be attributed to the consumption of OH^- ions by Mg^{2+} and Ca^{2+} ions in the salt solution, producing the precipitations of $Mg(OH)_2$ and $CaCO_3$ in the alkaline environment.

The effects of salinity and aggregate size on the mineralogy, microstructure and water retention property of lime-treated saline soil were investigated. Results showed that there was no cementitious compounds detecting on X-ray diffraction pattern even after a curing time as long as 150 days, due to its low quantity and poorly crystallized or amorphous phase. As a result, the microstructure of lime-treated soil varied slight during curing. The matric suction of lime-treated specimens increased significantly during curing, while the total suction increased slightly. Both total and matric suctions of lime-treated specimens increased as salinity increased. The lime-treated specimens with larger aggregates exhibited a larger modal size and thus had a smaller air entry value.

The mechanical behaviour and durability of lime-treated soils were investigated by performing mercury intrusion porosimetry, bender element and oedometer tests on untreated/lime-treated specimens and the specimens subjected to wetting-drying cycles. The lime-treated specimens, as compared to untreated specimens, exhibited higher resistance to wetting-drying cycles, with the pore size distributions keeping almost reversible. The wetting-drying cycles led to reversible changes of small stain shear modulus (G_{max}) and an increase of soil compressibility. The

synthetic seawater, compared to deionized water, resulted in higher G_{max} and higher compressibility for lime-treated soil. After wetting-drying cycles, the lime-treated specimens with lager aggregates (D_{max} = 5 mm) exhibited higher yield stress and lower compressibility than the lime-treated specimens with smaller aggregates (D_{max} = 0.4 mm).

Keywords: Lime-treated/untreated soil; hydro-mechanical behaviour; mineralogy; microstructure; salinity; wetting-drying cycles

Résumé

Le traitement à la chaux peut améliorer la maniabilité et les propriétés hydromécaniques des sols grâce à différentes réactions physico-chimiques telles que l'échange cationique et la réaction pouzzolanique. L'efficacité du traitement à la chaux pourrait dépendre de la chimie de l'eau et du climat. Afin de comprendre les effets de la salinité et du climat sur les sols traités à la chaux, le projet DIGUE 2020 a été mis en place avec une digue construite aux Salin-de-Giraud en employant des sols salins locaux. Dans l'étude de cette thèse, un travail expérimental au laboratoire a été réalisé pour caractériser le comportement hydromécanique des sols prélevés des Salin-de-Giraud avec et sans traitement à la chaux, en mettant l'accent sur les effets de la salinité et des cycles d'humidification-séchage.

Afin de bien caractériser l'effet de la salinité, de nouvelles méthodes ont été proposées pour déterminer la salinité dissoute et la succion osmotique induite pour les sols non saturés, en tenant compte des sels dissous et précipités. Les mécanismes liés à l'effet de la salinité sur la limite de liquidité et le comportement de compactage des sols non traités, et à l'effet de la dessiccation sur la microstructure des sols salins compactés ont été clarifiés. La teneur en chaux optimale des sols avec l'eau déminéralisée, l'eau de mer synthétique et une solution d'un mélange de sels a été déterminée par la méthode du pH. Les résultats ont montré que la teneur en chaux optimale augmentait avec l'augmentation de la concentration en sel, ce qui peut être attribué à la consommation d'ions OH^- par les ions Mg^{2+} et Ca^{2+} dans la solution saline, provoquant les précipitations de $Mg(OH)_2$ et de $CaCO_3$.

Les effets de la salinité et de la taille des agrégats sur la minéralogie, la microstructure et la propriété de rétention d'eau des sols salins avec et sans traitement à la chaux ont été étudiés. Les résultats ont montré qu'il n'y avait pas de produits cimentaires détectés sur le diagramme de diffraction des rayons X même après un temps de cure aussi long que 150 jours, en raison de sa faible quantité et de sa phase mal cristallisée ou amorphe. En conséquence, la microstructure du sol traité à la chaux variait légèrement pendant la cure. La succion matricielle des éprouvettes traitées à la chaux a augmenté de manière significative pendant la cure, tandis que la succion totale a légèrement augmenté. Les succions totales et matricielles des éprouvettes traitées à la chaux augmentaient à mesure que la salinité augmentait. Les éprouvettes traitées à la chaux avec des agrégats plus gros présentaient une taille modale plus grande et avaient donc une valeur d'entrée d'air plus petite.

Le comportement mécanique et la durabilité des sols traités à la chaux ont été étudiés en effectuant des essais de porosimétrie par intrusion de mercure, d'élément piézo-électrique et à l'oedomètre sur des échantillons non traités/traités à la chaux et des échantillons soumis à des cycles d'humidification-séchage. Les éprouvettes traitées à la chaux, par rapport aux éprouvettes non traitées, présentaient une résistance plus élevée aux cycles d'humidification-

séchage, les distributions de la taille des pores restant presque réversibles. Les cycles d'humidification-séchage ont conduit à des changements réversibles du module de cisaillement de petites déformations (G_{max}) et à une augmentation de la compressibilité du sol. L'eau de mer synthétique, par rapport à l'eau déminéralisée, a entraîné un G_{max} plus élevé mais une compressibilité plus grande pour le sol traité à la chaux. Après les cycles d'humidification-séchage, les éprouvettes traitées à la chaux avec des agrégats plus gros (D_{max} = 5 mm) avaient une limite élastique plus élevée et une compressibilité plus faible que les échantillons traités à la chaux avec des agrégats plus petits (D_{max} = 0.4 mm).

Mots clés: Sols avec et sans traitement à la chaux; comportement hydromécanique; minéralogie; microstructure; salinité; cycles humidification-séchage

Publications

Journal papers

1. **Ying Zi**, Cui Yu Jun, Benahmed Nadia, Duc Myriam. (2021). Drying effect on the microstructure of compacted salted silt. **Géotechnique**. Doi.org/10.1680/jgeot.20.P.319.
2. **Ying Zi**, Cui Yu Jun, Duc Myriam, Benahmed Nadia, Bessaies-Bey Hela, Chen Bo. (2021). Salinity effect on the liquid limit of soils. **Acta Geotechnica**. 16(4), 1101-1111. Doi: 10.1007/s11440-020-01092-7.
3. **Ying Zi**, Cui Yu Jun, Benahmed Nadia, Duc Myriam. (2021). Changes of microstructure and water retention property of a lime treated saline soil during curing. **Acta Geotechnica**, Doi: org/10.1007/s11440-021-01218-5.
4. **Ying Zi**, Cui Yu Jun, Benahmed Nadia, Duc Myriam. (2021). Salinity effect on the compaction behaviour, matric suction, stiffness and microstructure of a silty soil. **Journal of Rock Mechanics and Geotechnical Engineering**. 13(4), 855-863. Doi: org/10. 1016/j. jrmge.2021.01.002.
5. **Ying Zi**, Duc Myraim, Cui Yu Jun, Benahmed Nadia. (2021). Salinity assessment for salted soil considering both dissolved and precipitated salts. **Geotechnical Testing Journal**. 44(1):130-147. Doi: org/10.1520/GTJ20190301.
6. **Ying Zi**, Cui Yu Jun, Benahmed Nadia, Duc Myriam. (2021). Investigating the salinity effect on water retention property and microstructure changes along water retention curves for lime-treated soil. **Construction and Building Materials**. 303: 124564. Doi.org/10.1016/j.conbuildmat.2021.124564.
7. **Ying Zi**, Cui Yu Jun, Benahmed Nadia, Duc Myriam. (2021). Changes of small strain shear modulus and microstructure for a lime-treated silt subjected to wetting-drying cycles. **Engineering Geology**. 293: 106334. Doi.org/10.1016/j.enggeo.2021.106334..
8. **Ying Zi**, Cui Yu Jun, Duc Myriam, Benahmed Nadia. (2021). Effect of salt solution on the optimum lime contents of bentonite and silt. **Acta Geotechnica**, under review.
9. **Ying Zi**, Benahmed Nadia, Cui Yu Jun, Duc Myriam. (2021). Determination of osmotic suction from electrical conductivity for unsaturated low-plasticity soils. **Journal of Rock Mechanics and Geotechnical Engineering,** under review.
10. **Ying Zi**, Benahmed Nadia, Cui Yu Jun, Duc Myriam. (2021). Wetting-drying cycle effect on the compressibility of lime-treated soil accounting for wetting fluid nature and aggregate size. **Journal of Rock Mechanics and Geotechnical Engineering**, under review.

Conference paper

1. **Ying Zi**, Cui Yu Jun, Benahmed Nadia, Duc Myriam. (2020). Changes in mineralogy and microstructure of a lime-treated silty soil during curing time, **4th European Conference on Unsaturated soils**. Lisbon. (2020). Doi.org/10.1051/e3sconf/202019503044

Contents

General Introduction

Context

Nowadays, in order to move towards more sustainable engineering practice and reduce economic, environmental and ecological impacts of earth structures such as embankments, roads, highways, landfills, dikes, etc., there is an increasing requirement to re-use the soils located at the site of constructions. However, in most cases, the local soils cannot meet the required mechanical performance. In that case, geotechnical improvement enhancing the resistance of soils becomes indispensable prior to their use. Stabilization with lime treatment is often employed to improve the soil mechanical performance through different physical-chemical reactions such as cation exchange and pozzolanic reaction (Locat et al., 1990; Bell, 1996; Tang et al., 2011a; Mavroulidou et al., 2013; Vitale et al., 2017; Wang et al., 2017a, 2017b; Cuisinier et al., 2020).

The effectiveness of lime treatment is expected to be water chemistry and climate dependent. In order to understand the effects of water salinity and climate on the hydro-mechanical behaviour of lime-treated soils, the project DIGUE 2020 was set up involving a dike constructed using local saline soils at les Salin-de-Giraud in southern France. As shown in Figure 1, the research platform with a width of 4 m (zone I) is constructed on the base of reinforced soil and along the old dike Symadrem (zone II). On the dike Symadrem, there is a track with 4 m width. The dike is close to the Fangassier and Galabert ponds. To identify the effects of lime content, dry density and water chemistry, the research area with a length of about 1 km consists of five research plots (Faisant et al., 2019):

(i) 2% lime-treated soils compacted to 95% of OPN (normal optimum proctor);
(ii) 2% lime-treated soils compacted to 98% of OPN;
(iii) 2% lime-treated soils compacted to 98% of OPN by mixing with seawater;
(iv) 1% lime-treated soils compacted to 98% of OPN;
(v) Untreated soils compacted to 98% of OPN.

The project DIGUE 2020 contains the following five Modules (Faisant et al., 2019; De Baecque, 2019):

(A) The construction of a research platform in the Southern France, on the coast Mediterranean, allowing a permanent in-situ monitoring;

(B) The investigation of the changes in properties of untreated and lime-treated soils (laboratory test and in-situ monitoring);

(C) The durability of dike subjected to marine environment (laboratory test and in-situ monitoring);

(D) Assessment of the risk of marine submersion;

(E) Coordination and communication.

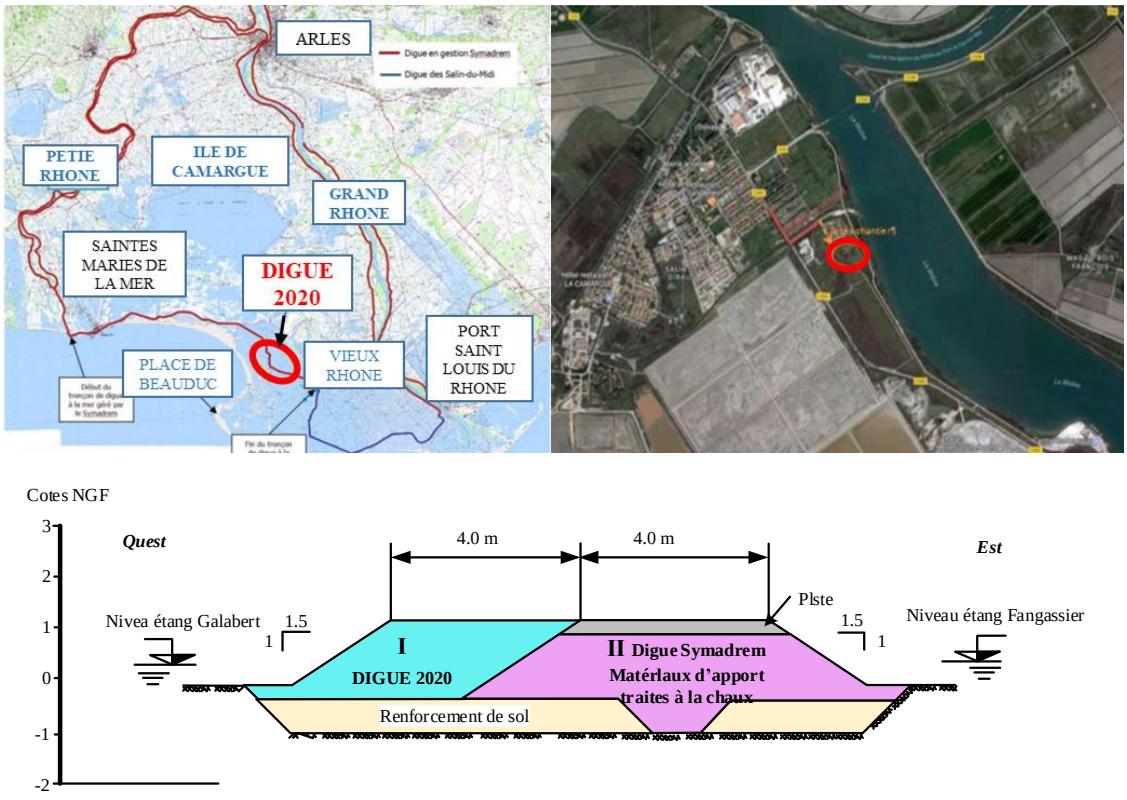

Figure 1. The location and sketch of dike construction at les Salin-de-Giraud (After SYMADREM).

As the DIGUE 2020 is constructed using saline soils and near the sea, the salinity effect on the hydro-mechanical behaviour of soils has to be investigated. As the soils in the shallow depth of construction are unavoidably subjected to climate effect, their water contents can change constantly. This can in turn change the quantities of dissolved and precipitated salts inside the soils and thus the soil osmotic suction. The dissolved salt and osmotic suction are expected to play an important role in soil hydro-mechanical behaviour, while the precipitated salt can be regarded as solid. Therefore, in order to well characterize the salinity effect in the context of dike construction, it is of paramount importance to determine the quantity of dissolved salt and the induced osmotic suction. Once the phenomenon of salt dissolution is clarified in the

construction site environment, the salinity effect on the geotechnical property of untreated soils can be clarified, prior to investigating the case of lime-treated soils.

Many studies have focused on the lime treatment effect on the mineralogy, microstructure, water retention property, hydraulic conductivity, and mechanical behaviour of soils (Locat et al., 1990; Bell, 1996; Guney et al., 2007; Tedesco and Russo, 2008; Le Runigo et al., 2009; Al-Mukhtar et al., 2010a, 2010b; Cuisinier et al., 2011a; Tang et al., 2011a; Lemaire et al., 2013; Mavroulidou et al., 2013; Russo and Modoni, 2013; Di Sante et al., 2014; Tran et al., 2014; Vitale et al., 2017; Wang et al., 2015, 2016, 2017a, 2017b, 2020a). Tang et al. (2011a), Dong (2013) and Wang et al. (2015, 2017a, 2017b) reported that the soil aggregate size influenced the production of cementitious compounds, water retention property and mechanical behaviour of lime-treated soils. Several studies had studied the strength, permeability, compressibility of lime-treated marine soils with special emphasis on the sulfate effect (Rajasekaran and Rao, 2000, 2001, 2002). While dealing with constructions in contact with water, such as dikes, dams, water levees, reservoirs, etc., the leaching and water circulation effects on the evolution of mineralogy, microstructure and permeability of lime-treated soils were investigated (McCallister and Petry., 1990, 1992; Le Runigo et al., 2009, 2011; Deneele et al. 2016). As the lime-treated soils in field are in general exposed to wetting-drying cycles due to water evaporation and rainfall, it appears important to evaluate the effect of wetting-drying cycles on the hydro-mechanical performance of soils in order to further assess the durability and sustainability of the involved constructions. In this regard, the wetting-drying cycle effect on the swelling and shrinkage of lime-treated expansive soils (Guney et al., 2007; Cuisinier and Deneele, 2008; Stoltz et al., 2012), and on the microstructure and hydro-mechanical behavior of lime-treated soils (Aldaood et al., 2014a; Stoltz et al., 2014; Rosone et al., 2016, 2018; Nabil et al., 2018, 2019; Cuisinier et al., 2020) were explored. However, the seawater (with mixed salts) effect on the effectiveness of lime treatment and the wetting-drying cycle impact on the durability of lime-treated saline soils have not been investigated yet. In particular, the roles of the maximum soil aggregate size and the wetting fluids nature in lime-treated saline soils during curing and during wetting-drying need to be clarified.

Objective and organization of the thesis

The present PhD thesis contributes to Modulus B and C of DIGUE 2020 project through laboratory testing. It aims at clarifying the effects of curing time, salinity, maximum soil

aggregate size and wetting-drying cycles on the hydro-mechanical behaviour of untreated and lime-treated soils. The main objectives are as follows:

(i) To propose a new method to determine the salt concentration and osmotic suction for unsaturated soils.
(ii) To investigate the salinity effect on the geotechnical properties and the microstructure of untreated soils subjected to drying.
(iii) To clarify the seawater effect on the optimum lime content.
(iv) To study the effects of salinity and maximum soil aggregate size on the mineralogy, microstructure and water retention property of lime-treated saline soils during curing.
(v) To investigate the wetting fluids nature and aggregate size effects on the mechanical behaviour (small strain shear modulus and compressibility) and microstructure of lime-treated soils subjected to wetting-drying cycles.

The results of this PhD study are presented in eleven published/submitted papers (ten journal papers and one conference paper). The dissertation is organized with six chapters, a chapter of literature review followed by five chapters organized with published/submitted papers in their original forms.

The first chapter is devoted to a literature review. In this chapter, the techniques of soil stabilization, especially for lime treatment (mechanism and determination of optimum lime content) are presented. Then, the geotechnical properties of untreated saline soils and lime-treated soils are described. Afterwards, the factors influencing the mineralogy and microstructure of lime-treated soils during curing are introduced. Finally, the lime treatment effect on the hydro-mechanical behaviour of lime-treated soils is detailed, with emphasis put on the effects of salinity and wetting-drying cycles.

The second chapter focuses on the salinity assessment and osmotic suction determination for unsaturated soils, which corresponds to two published/submitted papers. The first paper, published in “Geotechnical Testing Journal”, proposed three approaches to determine the dissolved water salinity and dissolved soil salinity of salt-amended unsaturated soils with decreasing water content by combining the electrical conductivity-water salinity relationship of mixed salts solution (synthetic seawater) and the relationship between water salinity and soil salinity. The second paper, submitted to “Journal of Rock Mechanics and Geotechnical

Engineering", dealt with the osmotic suction determination for unsaturated soils. A new equation to calculate soil osmotic suction from electrical conductivity was proposed, taking into account the dissolved and the precipitated salts. In order to verify the relevance of the proposed equation, the calculated osmotic suctions were compared with the indirectly measured osmotic suction which was the difference between the total and matric suctions. The total and matric suctions were measured by the chilled-mirror dew-point hygrometer (WP4C) and by the contact filter paper method, respectively.

The third chapter corresponds to three published papers, focusing on the salinity effect on the soil liquid limit, the compaction behaviour, the drying effect on the microstructure of untreated soils, respectively. In the first paper published in "Acta Geotechnica", the cone penetration method was applied to determine the liquid limit of two soils (silt and bentonite) at different water salinities. Sedimentation and rheological tests were carried out on the two soils prepared with and without salt to ascertain the salt effect on liquid limit. In the second paper published in "Journal of Rock Mechanics and Geotechnical Engineering", the standard Proctor compaction test was first conducted on soil specimens with different salinities. To further understand the salinity effect on soil compaction behaviour, filter paper method, bender element test and mercury intrusion porosimetry (MIP) test were carried out on specimens compacted on dry side, at optimum and on wet side. The third paper, published in "Géotechnique", investigated the drying effect on the microstructure of compacted saline soils by means of mercury intrusion porosimetry (MIP) and environmental scanning electron microscope (ESEM).

The forth chapter is devoted to the determination of optimum lime content for saline soils. The pH method was adopted to determine the optimum lime content of two soils (silt and bentonite) which were mixed with deionized water, 35 g/L synthetic seawater and 70 g/L mixed salts solutions, respectively. Then, the base titration test with measuring pH was performed on the soil suspensions. After pH measurement, the supernatants of soil-lime/NaOH suspensions were removed and acidified for chemical analysis by Inductively Coupled Plasma/Optical Emission Spectroscopy (ICP/OES). The results are presented in a paper submitted to "Acta Geotechnica".

The fifth chapter presents the changes in mineralogy, microstructure and water retention property of lime-treated soils, which corresponds to three published papers. The curing time effect on the mineralogy and microstructure of lime-treated soils during curing was investigated by performing X-ray diffraction (XRD) and MIP tests. The results are presented in a conference

paper. The results of aggregate size effect on the changes of microstructure and water retention property of a lime-treated saline soils during curing are presented in a paper published in “Acta Geotechnica”. The results of investigating the salinity effect on the water retention property (total and matric suctions) during curing and the changes of microstructure along water retention curve (during drying) for lime-treated soils are presented in the third paper published in “Construction and Building Materials”.

The sixth chapter is devoted to the mechanical behaviour and durability of lime-treated soils, which includes two published/submitted papers. In the first paper published in “Engineering Geology”, the changes in small strain shear modulus (G_{max}) and microstructure of compacted lime-treated soils under wetting-drying cycles were studied, with consideration of the effects of wetting fluid (deionized water and synthetic seawater) and maximum soil aggregate size. The second paper submitted to “Journal of Rock Mechanics and Geotechnical Engineering”, investigated the wetting-drying cycle effect on the compressibility of lime-treated soils accounting for the wetting fluid nature and aggregate size.

Finally, a general conclusion is presented, together with some perspectives for the future research.

Chapter 1. Literature Review

1.1. Introduction

Lime treatment is recognised as an effective improvement technique for soils with poor physical and mechanical characteristics (Bell, 1989, 1996; Locat et al., 1990). To days, the hydro-mechanical behaviour of lime-treated soil has been broadly investigated. In this chapter, an overview of the geotechnical properties of saline soils, the mechanism of lime treatment, the changes in mineralogy and microstructure, and the hydro-mechanical behaviour of lime-treated soils is presented. The techniques of soil stabilization and the mechanism of lime treatment are described in Section 1.2. A comprehensive literature review about the geotechnical property of saline soil, the changes in microstructure and mineralogy of lime-treated soil is presented in Section 1.3. The lime treatment effect on the hydro-mechanical behaviour of lime-treated soils is discussed in Section 1.4, with emphasis put on the salinity and wetting-drying cycle effects.

1.2. Lime treatment

1.2.1. Soil stabilization

From a socio-economic point of view, there is an increasing need of using local soils in geotechnical and geo-environmental constructions such as embankments, dikes, slopes and municipal waste barriers. However, in most cases, the local soils with relatively low geotechnical properties cannot meet the required mechanical performance of structures. In this context, soil stabilization becomes indispensable prior to using such soils.

Soil stabilization is a widely applied technique to improve soil hydro-mechanical behaviour by blending or mixing with binders. Lime, cement, fly ash, pozzolanas, bitumen, blast furnace slag, rice husk ash, polymer and the combination of these materials or other additives are the commonly used binders (Bell, 1989, 1996; Locat et al., 1990; Ramesh et al., 1999; Basha et al., 2005; Rao and Shivananda, 2005a; Bisanal and Badiger, 2007; Brooks, 2009; Cokca et al., 2009; Cuisinier et al., 2011a; Harichane et al., 2011; Tang et al., 2011a; Russo and Modoni, 2013; Tran et al., 2014; Zhang et al., 2014; Wang et al., 2015; Al-Swaidani et al., 2016; Deng et al., 2017; Roy, 2017; Liu et al., 2018a, 2018b, 2019a, 2019b; Thomas et al., 2018; Consoli et al., 2019; Andavan and Maneesh Kumar, 2020; Bian et al., 2021). Lime treatment has been the most common technique in soil stabilization due to its economical and effective characteristics

as compared to the other stabilization agents. The types of lime used in soil stabilization are quicklime (calcium oxide CaO), hydrated lime (calcium hydroxide $Ca(OH)_2$) and hydrated lime slurry (Afrin, 2017; Firoozi et al., 2017). Quicklime is the most widely used lime, as it has the following advantages as compared to the hydrated lime and hydrated lime slurry: i) it has a higher free calcium content per unit mass; ii) the generation of heat in lime hydration process decreases soil water content and accelerates the soil strength improvement (Afrin, 2017).

1.2.2. Mechanisms of lime treatment

Lime treatment can improve the geotechnical and hydro-mechanical properties of soils through a series of physical-chemical reactions, such as lime hydration, cation exchange, pozzolanic reaction and carbonation (Bell, 1996; Le Runigo et al., 2009; Al-Mukhtar et al., 2010a, 2010b; Cuisinier et al., 2011a; Mavroulidou et al., 2013; Deneele et al., 2016; Vitale et al., 2017; Zhang et al., 2017a; Wang et al., 2020a):

(1) Hydration of quicklime

When quicklime is mixed with soil and water, the lime hydration takes place rapidly, consuming a large amount of water and releasing heat:

$$CaO + H_2O \rightarrow Ca(OH)_2 \quad \Delta H = -57.86 \text{ kJ/ mol} \tag{1-1}$$

The following ionization of calcium hydroxide ($Ca(OH)_2$) provides a large quantity of calcium ions (Ca^{2+}) and hydroxide ions (OH^-):

$$Ca(OH)_2 \rightarrow Ca^{2+} + 2OH^- \tag{1-2}$$

(2) Cation exchange

The free Ca^{2+} cations can be adsorbed on the clay minerals by replacing the monovalent cations (i.e., Na^+, K^+, etc.) previously held by the soil, leading to the flocculation of soil particles and forming coarser aggregates (Guney et al., 2007; Al-Mukhtar et al., 2010a; Di Sante et al., 2014). These modifications induced by lime addition will further improve the soil workability by reducing the soil plasticity, shrinkage and swelling (Bell, 1996; Khattab and Fleureau, 2007; Al-Mukhtar et al., 2012; Al-Swaidani et al., 2016).

(3) Pozzolanic reaction

The released OH^- ions from $Ca(OH)_2$ give rise to the increase of pH to 12.4 which is equivalent to the pH of a lime-saturated solution. This high pH environment promotes the dissolution of silicon ions (Si^{4+}) and aluminium ions (Al^{3+}) from clay minerals, quartz and feldspar. Then, the dissolved Si^{4+} and Al^{3+} ions react with Ca^{2+}, forming cementitious compounds, such as calcium aluminate hydrate (C-A-H), calcium silicate hydrate (C-S-H) and calcium aluminium silicate hydrate (C-A-S-H):

$$Ca^{2+} + 2OH^- + Al_2O_3 \rightarrow \text{Calcium aluminate hydrate(C-A-H)} \quad (1\text{-}3)$$

$$Ca^{2+} + 2OH^- + SiO_2 \rightarrow \text{Calcium silicate hydrate (C-S-H)} \quad (1\text{-}4)$$

$$Ca^{2+} + 2OH^- + Al_2O_3 + SiO_2 \rightarrow \text{Calcium aluminium silicate hydrate (C-A-S-H)} \quad (1\text{-}5)$$

These reactions are termed as pozzolanic reaction that would last long time, as long as the Ca^{2+}, Al^{3+} and Si^{4+} ions are available and the high pH is maintained in soil pore water (Locat et al., 1990; Rao and Shivananda, 2005a; Vitale et al., 2017). Pozzolanic reaction plays a major role in enhancing soil mechanical performance, as the produced cementitious compounds coat the surface of aggregates and bond the adjacent soil particles together (Bell, 1996). This results in an increase of unconfined compressive strength (Al-Mukhtar et al., 2010a; Muntohar et al., 2013), stiffness (Tang et al., 2011a; Wang et al., 2020a) and shear strength (Sivapullaiah et al., 2000), and a reduction of compressibility (Rao and Shivananda, 2005a; Vitale et al., 2017; Wang et al., 2017a).

(4) Carbonation

Lime carbonation is the reaction of Ca^{2+} ions with carbon dioxide in the atmosphere, attenuating the production of cementitious compounds and hence reducing the enhancement by lime treatment (Ciancio et al., 2014).

1.2.3. Determination on optimum lime content

After mixing soil-lime-water together, the Ca^{2+} ions from hydrated lime ($Ca(OH)_2$) are first absorbed on the inter- and intra- layer surface of clay minerals by replacing the monovalent cations (i.e., Na^+, K^+, etc.). Hilt and Davidson (1960) pointed out that the amount of lime absorbed on the clay particles was denoted as the lime fixation point (L_m) or initial consumption of lime (ICL) which can be determined according to the fraction of clay-size particles ($\leqslant$ 2μm), as follows:

$$L_m = \frac{Clay\ \ fraction\,(\%)}{35} + 1.25 \qquad (1\text{-}6)$$

This lime fixation point is highly related to the cation exchange process, but this equation does not take the different types of clay minerals into account. For instance, the cation exchange capacities are 3-15 meq./100 g for kaolinite, 15-40 meq./100 g for illite, and up to 80-150 meq./100 g for smectite (Mitchell and Soga, 2005). The higher the cation exchange capacity, the more the amount of lime required to provide sufficient Ca^{2+} ions for the cation exchange. This is confirmed by the results obtained by Al-Mukhtar et al. (2014) who reported that, immediately after lime addition, the smectite had the highest lime consumption, while the kaolinite had the lowest lime consumption, the illite being in between, as shown in Figure 1-1.

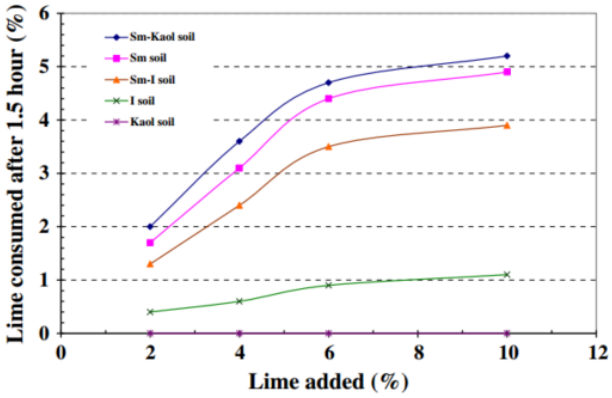

Figure 1-1. Immediate lime consumption by different clayey soils tested (Al-Mukhtar et al., 2014).

Nelson and Miller (1997) indicated that the initial consumption of lime can be determined by soil consistency limits. The initial consumption of lime corresponds to the amount of lime needed for modifying the plasticity of soil, and beyond which no further change in the plasticity occurs. Thus, it is also termed as lime modification optimum of soil (Marks and Haliburton, 1972; Bhuvaneshwari et al., 2013). As shown in Figure 1-2a, the liquid limit and plastic limit of a silt increases with increasing lime content to 2%, then keeps constant with further increasing lime content (Celauro et al., 2012). Kavak and Akyarlı (2007) reported that, for clayey soil, the liquid limit decreased while the plastic limit increased as the lime content increased, giving rise to a significant reduction of plasticity index (Figure 1-2b). Similar phenomenon was obtained by Al-Mukhtar et al. (2010a) on an expansive soil and by Al-Swaidani et al. (2016) on a mixture of clayey soil and pozzolana (Figure 1-2c). This reduction of soil plasticity is due to the cation exchange which reduces the diffused double layer of clay minerals and thus results in the flocculation of soil particles and the formation of coarser aggregates.

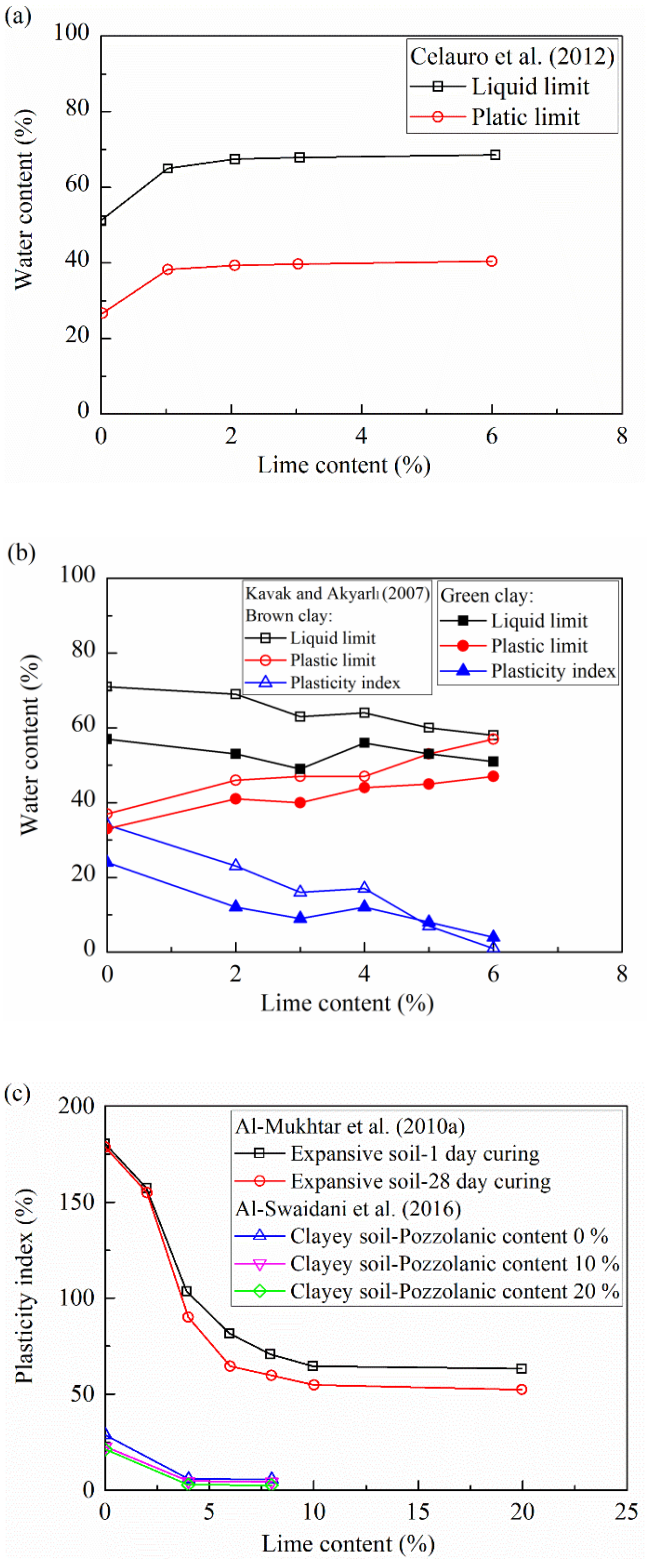

Figure 1-2. Variations of Atterberg limits with lime content.

Eades and Grim (1966) defined the optimum lime content (by weight of dry soil) as the lowest amount of lime which could provide sufficient Ca^{2+} ions for the cation exchange and pozzolanic reaction. This optimum lime content corresponds to the lime stabilization of optimum of soil,

which allows the soil to obtain the maximum mechanical performance. The quickest procedure to estimate the optimum lime content is the pH method (Eades and Grim, 1966): the optimum lime content corresponds to the minimum lime content required to maintain the pH of soil-lime-water mixtures to be 12.4 which is equivalent to the pH of a lime-saturated solution. As shown in Figure 1-3, the pH in the soil-lime-distilled water mixture increased gradually with the addition of lime, until it reached the maximum value (Kavak and Akyarlı, 2007; Al-Mukhtar et al., 2010a; Celauro et al., 2012; Sharma et al., 2012; Saride et al., 2013; Di Sante et al., 2014; Negawo et al., 2019).

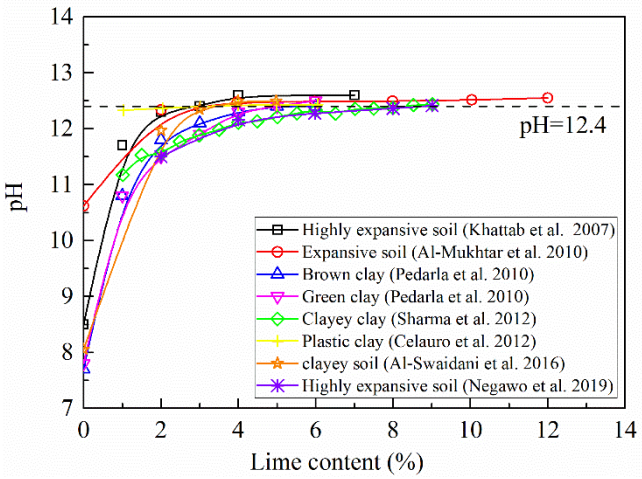

Figure 1-3. pH variations with deionized water-lime mixtures.

This pH method is adopted in ASTM standard (D6276-19, 2019). It is specified that distilled water should be used in the pH measurement for the optimum lime content determination in most cases, while the site water should be used if the pH of the site water is highly acidic (< 6) or highly basic (> 9). Emarah and Seleem (2018) used the Red Sea water with a pH of 8.2~8.7 to prepare the soil suspensions for the identification of optimum lime content. Results showed that the pH of seawater-soil suspensions increased continuously with the increase of lime content to 3%, then it kept almost constant from 3% to 4% lime content before a second increase of pH to 12.4 with further addition of lime (Figure 1-4).

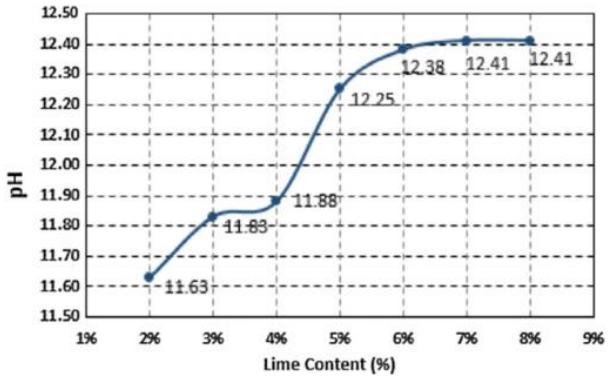

Figure 1-4. pH variations with seawater-lime mixtures (Emarah and Seleem, 2018).

Ciancio et al. (2014) determined the optimum lime content by measuring the unconfined compressive strength (UCS) of lime-treated rammed earth materials and then selected the minimum lime content which produced the maximum strength as the optimum one. Figure 1-5 presents the results of UCS as compared to the results for plastic limit and pH variations. It can be observed that the optimum lime content determined by UCS at maximum strength (4%) is in agreement with the results of pH method and plastic limit.

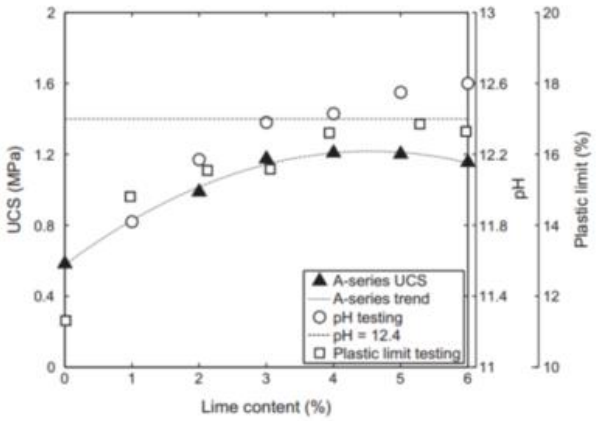

Figure 1-5. Variations of USC, plastic limit and pH with lime content (Ciancio et al., 2014).

1.3. Geotechnical property, mineralogy and microstructure

1.3.1. Saline soil

Saline soils are usually formed from the marine deposits and seawater immersion, which displays undesirable properties such as salt swelling and erosion effects (Li et al., 2016; Liu et al., 2016a). While dealing with constructions of dams, dikes, pavements with saline soils, a number of phenomena might occur, such as differential settlement, cracking and collapse

(McRobert and Foley 1999; Sivapullaiah et al., 2000; Rajasekaran and Rao, 2002; Liu et al., 2019b). Thus, it appears essential to clarify the salinity effect on the lime stabilization to assess the sustainability of geotechnical constructions with lime-treated saline soils.

1.3.1.1. Description of saline soil

As shown in Figure 1-6, a saline soil consists of soil solids, salt, water and gas (Noorany, 1984; ASTM D4542-95, 2001). The corresponding terms are listed in Table 1-1. The salinity (r) which is the ratio of salt mass to salty water mass, is usually used to evaluate the salt concentration. However, this salinity always changes with the variations of water quantity. To avoid this change, Magistad et al. (1945) and Reitemeier (1946) proposed that the salt concentration can be expressed on the oven-dried soil basis, in the unit of equivalent per million (e.p.m.) which was identical to 1 m.e. per kilogram of soil. The salt concentration on the soil basis can be converted to that of solution basis by the following equation:

$$E.p.m._{solution} = \frac{E.p.m._{soil}}{water\ content\ (\%)} \tag{1-7}$$

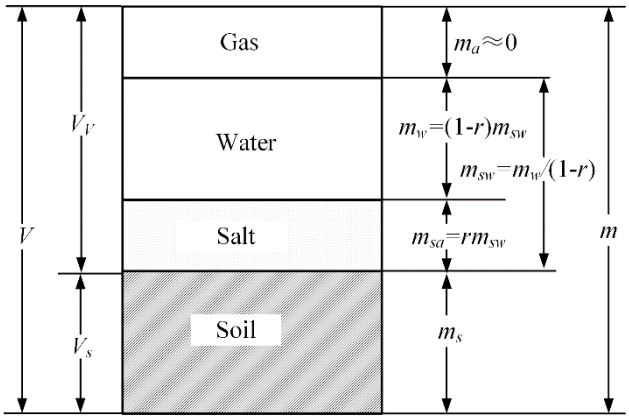

Figure 1-6. Mass composition of a saline soil.

Table 1-1. Terms used to describe a saline soil.

Terms	Significance
m	Total wet soil mass (soil particles, salt and water)
m_s	Mass of dry soil particles
m_{sa}	Mass of salt
m_{sw}	Mass of fluid = $m_w + m_{sa}$
m_w	Mass of pure water = $m_{sw} - m_{sa}$
m_d	Oven-dried mass at 105 °C = $m_s + m_{sa}$
r	Water salinity = m_{sa} / m_{sw}
V	Total volume
V_s	Volume of soil particles
V_V	Volume of voids

For a saline soil, the water content (w) determined from the conventional Equation (1-8) is not correct without considering the presence of salts, while the fluid content (w') of saline soil should be computed from Equation (1-9) which is the ratio of fluid mass (m_{sw}) to the mass of soil solid (m_s) (Siddiqua et al., 2011):

$$w = \frac{m_w}{m_d} \tag{1-8}$$

$$w' = \frac{m_{sw}}{m_s} = \frac{w}{1 - r(1+w)} \tag{1-9}$$

1.3.1.2. Assessment of salt concentration

There are several definitions of salt concentrations: mass concentration (percent composition, %), mass-volume concentration (grams per liter, g/L) or molar concentration (molarity, mol/L). In practice, salt concentration of soil pore water can be determined by measuring the electrical conductivity of soil solution extracts separated from soil slurry which were prepared at 1:1 or 1:5 distilled water:soil dilution, or saturated soil paste (United States Salinity Laboratory Staff, 1954; Rhoades, 1981, 1982; Chi and Wang, 2010; Hardie and Doyle, 2012; Monteleone et al., 2016), or by the chemical composition analysis of soil solution extracts by Inductively Coupled Plasma/Atomic Emission Spectroscopy (ICP/AES) (McLaughlin et al., 1994; Stevens et al., 2003). Besides, the salt mass of a certain amount of dry soil can be estimated from the mineral composition analysis that can determine the quantity of Halite (NaCl) (Aldabaa et al., 2015), as well as from the evaporation of soil solution extracts at 105°C (Magistad et al. 1945; Hardie and Doyle, 2012; Song et al., 2017). Nevertheless, the measured salt quantity by mineral composition analysis only reflects the quantity of NaCl. As for the

measurement of soil solution extracts, the salt cannot be extracted out completely by only one solution extraction, leading to underestimation of salt quantity. Meanwhile, the addition of water to prepare soil slurry resulted in dilution of salt present in soils and distorted the original salt concentration of soil pore water (ASTM D 4542-95, 2001). ASTM D 4542-95 (2001) stated that natural soil pore water can be squeezed out with the aid of external pressure without adding water. However, with this procedure, it was often impossible to obtain enough soil pore water for accurate measurement, especially for soils at low water contents.

1.3.1.3. Soil osmotic suction effect

Soil osmotic suction, which is related to the salinity of soil pore water, is one of the major components influencing the hydro-mechanical behaviour of soil with salinity. Barbour and Fredlund (1989) proposed that the osmotic suction induced osmotic volume change in clayey soil by two ways, namely osmotically induced consolidation and osmotic consolidation. The salt solution results in a reduction of diffused double layer of clay minerals and this, in turn, causes repulsive force diminution and net attractive force increase (Mitchell and Soga, 2005; Israelachvili, 2011). Thus, the separation of clay particles decreases, making the specimens compress to a lower void ratio. This process is denoted as osmotic consolidation (Di Maio, 1996; Loret et al., 2002; Musso et al., 2003; Rao and Thyagaraj, 2007a, 2007b; Thyagaraj and Rao, 2010; Witteveen et al., 2013), as shown in Figure 1-7. Osmotically induced consolation occurs when the soil pore water flows out of the clay due to the osmotic gradient (Di Maio, 1996; Musso et al., 2003; Rao and Thyagaraj, 2007a, 2007b; Thyagaraj and Rao, 2010). The outflowing of water induces negative pore water pressure which corresponds to an increase of effective stress and thus leads to a decrease of volume.

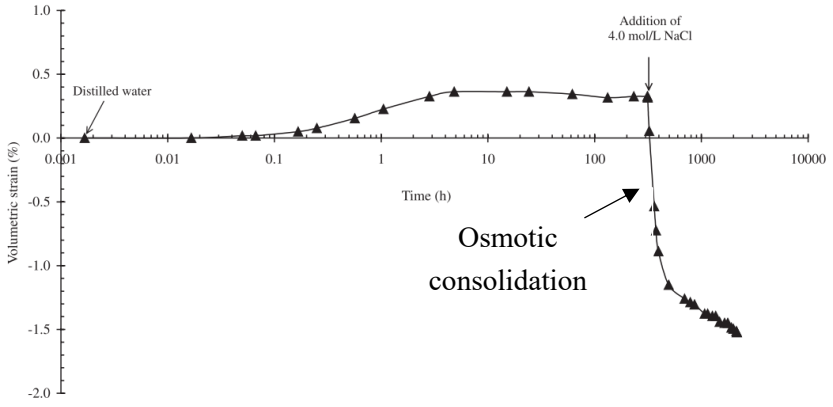

Figure 1-7. Swelling and osmotic consolidation of compacted clay at total vertical stress of 200 kPa (Rao and Thyagaraj, 2007a).

In addition, the modification of diffused double layer of clay minerals induced from osmotic suction is also responsible for the variations of swelling strain. Rao et al. (2006) reported that, for compacted samples with low initial salt content, the swelling magnitude was decreased by the osmotic gradient between soil pore water and reservoir salt solution. Rao and Shivananda (2005b) indicated that the swelling potential of salt-amended expansive soils was independent of initial osmotic suction, while the rate of swelling decreased with increasing osmotic suction (Figure 1-8).

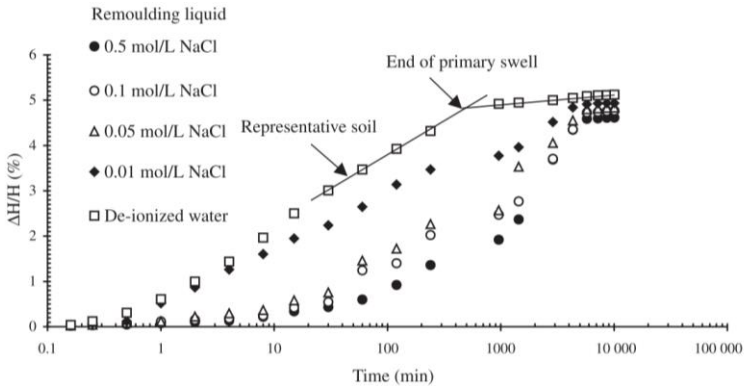

Figure 1-8. Swelling strain of salt-amended expansive soils with inundation of deionized water (Rao and Shivananda, 2005b).

Witteveen et al. (2013) performed chemical loading on a compacted non-swelling illite by replacing soil pore water with sodium chloride (NaCl) solution, and found that the initial stiffness and yield stress decreased as osmotic suction increased. Mokni et al. (2014) reported that the osmotic suction caused a decrease of compressibility and an increase of pre-consolidation stress for compacted Boom Clay. By contrast, Leong and Abuel-Naga (2018) indicated that the osmotic suction had no effect on the shear strength of unsaturated high plasticity silty soil.

1.3.1.4. Determination of soil osmotic suction

The osmotic suction, which results from the presence of dissolved solutes in soil pore water, is often considered as the difference between the total suction and the matric suction (Edil and Motan, 1984; Wan et al., 1995; Sreedeep and Singh, 2006; Abedi-Koupai and Mehdizadeh, 2008; Dao et al., 2008; Liu et al., 2016b). However, Miller and Nelson (1993) and Tang et al. (2002) indicated that the matric suction and osmotic suction were not simply additive. Arifin and Schanz (2009) reported that the difference between the total and the matric suctions corresponded to the osmotic suction and hydration force component for expansive soils. Krahn

and Fredlund (1972) also stated that the difference between the total and the matric suctions was almost equal to the measured osmotic suction for Till, whereas it was higher than the measured one for Regina clay. Therefore, considering the osmotic suction as the difference between total and matric suctions might not be applicable for all kinds of soils.

The osmotic suction of salted soils can be also deduced from the relationship between electrical conductivity and salt/ion concentrations of soil pore water. Several equations for its determination were reported in the literatures, as listed in Table 1-2. Among them, van't Hoff equation was the widely used one (Mitchell and Soga, 2005; Rao and Thyagaraj, 2007a, 2007b; Witteveen et al., 2013). As shown in Figure 1-9, the United States Salinity Laboratory Staff (1954) gave the variations of the osmotic suction with the electrical conductivity for a single salt solution and saturation extract of soil pore water in saline soils. Based on such variations, Mata et al. (2002) derived the relationship between the osmotic suction and the electrical conductivity of soil pore water (Eq. 1-11); Rao and Shivananda (2005b) established the calibration curve as expressed in Eq. (1-12), relating the electrical conductivity of soil pore water to osmotic suction; Leong et al. (2007) estimated the osmotic suction for NaCl solution using Eq. (1-13); Arifin and Schanz (2009) calculated the osmotic suction from the measured electrical conductivity of soil pore water using Eq. (1-14). Witteveen et al. (2013) described the relationship between the measured osmotic suction and the corresponding concentration of NaCl solution by Eq. (1-15), as shown in Fig. 1. The United States Salinity Laboratory Staff (1954) also gave a relationship between the osmotic suction of saturated soil water extract and its electrical conductivity, expressed by Eq. (1-16). Abedi-Koupai and Mehdizadeh (2008) indicated that the soil osmotic suction, at a given water content, can be transformed from the osmotic suction of saturated soil water extract by assuming a linear dilution for salt concentration (Eq. 1-17). Mokni et al. (2014) proposed a relationship between osmotic suction and sodium nitrate ($NaNO_3$) solution, expressed by Eq. (1-18).

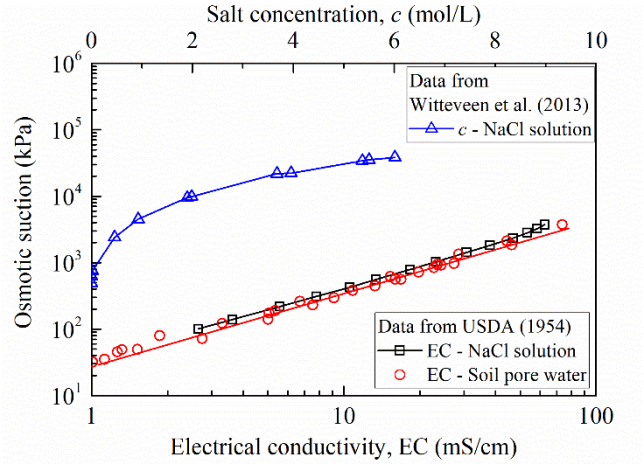

Figure 1-9. Relationship between osmotic suction and electrical conductivity/salt concentration.

Table 1-2. Equations for determination of soil osmotic suction.

Eq.	Equations	References
1-10	$\pi = vcRT$	van't Hoff equation. Mitchell and Soga, (2005)
1-11	$\pi = 0.019\left(\frac{EC}{1\,\mu S/cm}\right)^{1.074}$	Mata et al., (2002)
1-12	$\pi = 31.92EC^{1.08}$	Rao and Shivananda, (2005b)
1-13	$\pi = P_a\left(0.31EC^{1.15}\right)$	Leong et al., (2007)
1-14	$\pi = 38.54EC^{1.0489}$	Arifin and Schanz, (2009)
1-15	$\pi = 0.407c^2 + 3.88c + 0.61$	Witteveen et al., (2013)
1-16	$\pi_e = -360EC_e$	United States Salinity Laboratory Staff, (1954)
1-17	$\pi = \pi_e\left(\frac{w_s}{w}\right)$	Abedi-Koupai and Mehdizadeh, (2008)
1-18	$\pi = -\frac{RT\rho_1}{M_W}\ln\left[1-\left(\frac{cM_S}{\rho_1}\right)\right]^2$	Mokni et al., (2014)

Note: c: salt concentration; v: van't Hoff factor (number of constituent ions); $v{\cdot}c$: ion concentration; EC: electrical conductivity; EC_e: electrical conductivity of saturated soil water extract; M_w: molar mass of water; M_s: molar mass of salt; P_a: atmospheric pressure; R: universal gas constant; T: absolute temperature; w: actual water content of soil; w_s: water content of soil at saturated state; ρ_1: liquid density; π: osmotic suction; π_e: osmotic suction of saturated soil water extract.

To determine the soil osmotic suction by the above quoted equations, it is essential to obtain soil pore water which can be squeezed out with the aid of pore fluid squeezer (ASTM D4542-

95, 2001; Rao and Shivananda, 2005b; Rao et al., 2006; Leong et al., 2007; Thyajaraj and Rao, 2010; Thyagaraj and Salini, 2015). Arifin and Schanz (2009) indicated that the osmotic suction of soil pore water decreased with increasing squeezing pressure due to the restrictive membrane effect, resulting in lower diffusion of ions at higher squeezing pressure. In addition, with the squeezing technique, it was often impossible to obtain enough soil pore water for accurate measurement, especially for unsaturated soils at low water content. Thus, a soil-water slurry was usually prepared to extract enough soil pore water for osmotic suction determination (Krahn and Fredlund 1972; Abedi-Koupai and Mehdizadeh, 2008). In practice, the addition of deionized water to prepare soil slurry induced dilution of salt present in the soil, thus distorting the initial osmotic suction of the soil pore water (Boso et al., 2005).

1.3.2. Salinity and lime effects on the geotechnical property

1.3.2.1. Liquid limit

The soil liquid limit (w_L) is defined as the limiting water content between liquid and plastic states (Sridharan and Prakash, 1998a). It is commonly a strength-based measurement (Sridharan and Prakash, 2000) and a parameter usually used for the classification of soils (ASTM standard D4318-10, 2014). The soil liquid limit is also correlated with other soil properties such as permeability (Mishra et al., 2009), shear strength (Anson and Hawkins, 1998; Sridharan and Prakash, 1999, 2000) and compressibility (Marcial et al., 2002; Yukselen-Aksoy et al., 2008; Hong et al., 2010, 2012). However, the liquid limit is usually affected by several factors, such as salt solution or lime addition.

Previous studies stated that, with increasing salinity, the liquid limit of expansive soils decreased, while the liquid limit of non-expansive soils increased. Sridharan et al. (2002) stated that the diffused double-layer water had a predominant role in liquid limit for expansive soils. The main clay mineral in expansive soils is montmorillonite/smectite. As shown in Figure 1-10, this clay mineral consists of three-layer mineral with 2:1 structural unit constituted by one octahedral aluminium sheet sandwiched between two tetrahedral siliceous sheets with isomorphic substitutions (Mitchell and Soga, 2005). During hydration, the inter-basal spacing of montmorillonite/smectite is known to increase from 9.6 Å (0.96 nm) to infinite due to the successive adsorption of water molecule layers (Figure 1-10).

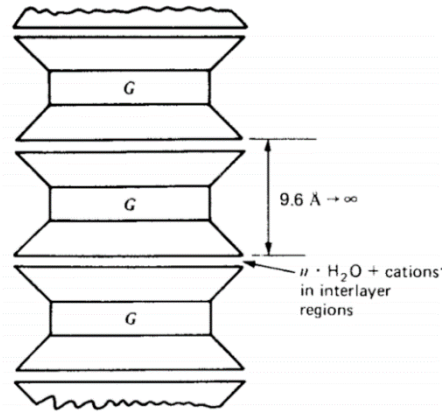

Figure 1-10. Schematic diagram of the structure of smectite mineral (Mitchell and Soga, 2005).

In fact, the thickness of diffuse double layer varies inversely with the square root of the ion concentration and it decreases gradually with increasing salt concentration:

$$d = \sqrt{\frac{\varepsilon kT}{2n_0 e^2 v^2}} \tag{1-19}$$

where ε is the dielectric constant of pore water ($80\times8.85\times10^{-12}$ $C^2/(J\cdot m)$ for deionized water); k is the Boltzmann constant (1.38×10^{-23} J/K); T is the temperature; e is the electronic charge (1.602×10^{-19} C); n_0 is the ion concentration (ion number/m^3) and v is the ionic valence.

According to the DLVO theory (Figure 1-11), at low salt concentration, the particles are repulsive, as the interactions are controlled by the diffused double layer interaction, while at high salt concentration, the interaction is dominated by the van der Waals attractive force (Israelachvili, 2011; Trefalt and Borkovec, 2014). Thus, an increase of salt concentration is accompanied by an increase of net attractive force, which leads soil particles to associate with each other at a lower inter-particle distance. As the double-layer water is expelled out significantly, the liquid limit decreased (Warkentin, 1961; Sridharan and Venkatappa Rao, 1975). In other words, the shrinkage of diffused double layer caused a reduction of liquid limit for expansive soils (Rao et al., 1993; Anson and Hawkins, 1998; Sridharan and Prakash, 2000; Sridharan et al., 2002; Arasan and Yetimoğlu, 2008; Yukselen-Aksoy et al., 2008; Horpibulsuk et al., 2011).

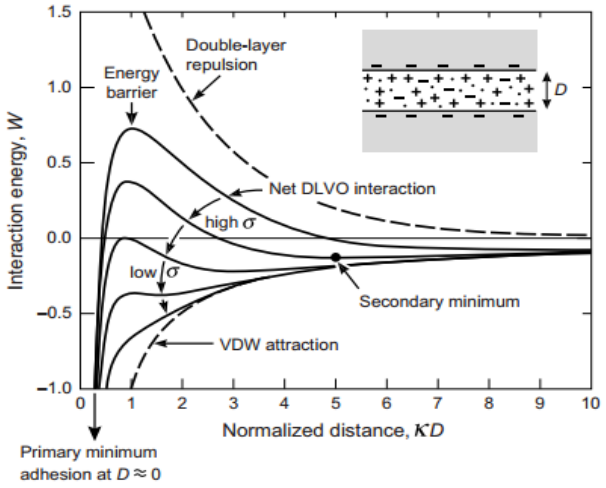

Figure 1-11. Schematic diagram of DLVO theory (Israelachvili, 2011).

However, in the case of non-expansive clays such as kaolinite, illite or chlorite, it is deemed that the increased net attractive force favours the flocculation of soil particles, leading to an increase of liquid limit because more water could be entrapped in a more flocculated structure (Anson and Hawkins, 1998; Sridharan and Prakash, 1999; Sridharan et al., 2002; Horpibulsuk et al., 2011). The increased liquid limit of non-expansive soils with salinity increase is also attributed to the dispersion of clay particles in salt solution (Arasan and Yetimoğlu, 2008) or explained by the formation of new expansive compounds which could increase the liquid limit (Sivapullaiah and Manju, 2005).

The lime addition induced the cation exchanges between soil pore water and the surface of clay minerals, promoting the flocculation of soil particles. This also resulted in an increase of liquid limit of silty soil and a reduction of liquid limit for expansive soil or clayey soils (Bell. 1996; Kavak and Akyarlı, 2007; Al-Mukhtar et al. 2010a; Celauro et al., 2012), as showed previously in Figure 1-2.

1.3.2.2. Compaction behaviour

The soils usually need compaction prior to being used in geotechnical and geo-environmental constructions such as subgrades, dikes, dams and municipal waste barriers. Tatsuoka (2015) and Tatsuoka and Correia (2018) reported that the optimum saturation degree of compacted soil was nearly 82%, independent of soil type and compaction energy level. However, the compaction behaviour in terms of optimum water content and maximum dry density are affected by the salinity. Liu and Zhang (2014) reported that both the maximum dry density and

optimum water content decreased with increasing salinity for saline soils with 3% ~ 8% clay-size fraction. Nevertheless, Ajalloeian et al. (2013) indicated that salinity had negligible effect on the compaction behaviour of fine-grained soils with 28 % clay-size fraction. Abdullah et al. (1997, 1999) stated that the salt solution led to an increase in maximum dry density and a reduction of optimum water content for highly plastic clay whose main minerals were illite and smectite. The same observations were made on clayey soils with 48% clay minerals consisting of montmorillonite, polygorskite and kaolinite (Abood et al., 2007) and on expansive soils (Shariatmadari et al., 2011; Durotoye et al., 2016). They attributed this phenomenon to the decrease of diffused double layer thickness and the more oriented face-to-face clay particle contacts with the increase of salinity.

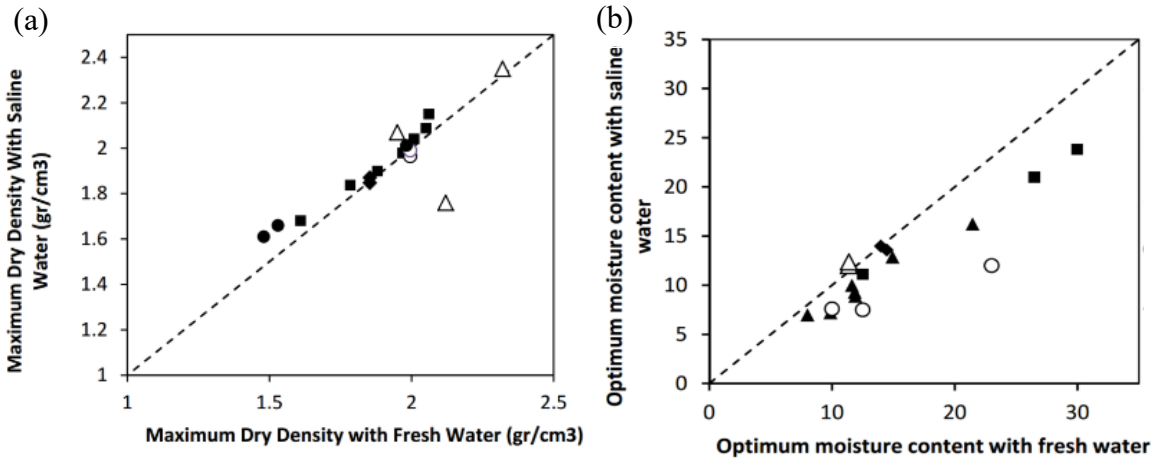

Figure 1-12. Salt solution effect on the compaction behaviour: (a) Maximum dry density; (b) Optimum water content (Ajalloeian et al., 2013).

In general, the addition of lime to soils gives rise to an increase of optimum water content and a decrease of maximum dry density for the same compaction effort (Bell, 1996; Ramesh et al., 1999; Tedesco and Russo, 2008; Le Runigo et al., 2009; Tang et al., 2011a; Di Sante et al., 2014; Al-Swaidani et al., 2016; Wang et al., 2016; Baldovino et al., 2018;). Bell (1996) attributed this reduction in dry density to the immediate formation of cementitious products which reduced the compatibility of lime-treated soil and hence the density.

1.3.3. Mineralogy and microstructure of lime-treated soil

In long term, the pozzolanic reaction consumes the activated silicon ions (Si^{4+}) and aluminium ions (Al^{3+}) ions dissolved from clay minerals, quartz, and feldspar, producing the cementitious compounds and thus leading to the changes of soil mineralogy in lime-treated soil. The cementitious compounds can be in the forms of calcium silicate hydrate (C-S-H), calcium

aluminate hydrate (C-A-H) and calcium aluminium silicate hydrate (C-A-S-H) (Bell, 1996; Guney et al., 2007; Al-Mukhtar et al., 2010a, 2010b; Lemaire et al., 2013; Di Sante et al., 2014; Tran et al., 2014; Keramatikerman et al., 2016; Vitale et al., 2017; Wang et al., 2017b).

1.3.2.1. X-ray diffraction

X-ray diffraction (XRD) is a non-destructive technique for characterizing crystalline materials and providing information on structures, phases, preferred crystal orientations, etc., on the basis of constructive interference of monochromatic X-rays and a crystalline sample. It is widely used to investigate the mineralogical variations and the newly-formed cementitious compounds in lime-treated soils.

Al-Mukhtar et al. (2010a) performed XRD test on lime-treated Impersol with 20% lime, and observed the new reflections of C-A-H phase at d-spacing of 0.76 nm and 0.367 nm in all treated specimens after 7-day curing and the intensity of these reflections increased with curing time. Lemaire et al. (2013) conducted XRD test on treated silt specimens with 1 % lime and 5 % cement and found a very slight new peak of a poorly crystallized compound of C-(A)-S-H in the range from 29° to 29.5° 2θ. Similarly, Keramatikerman et al. (2016) reported that the reflection of C-S-H phase was detected at 2θ between 29° and 30°, and the XRD reflection of C-A-H phase was at 2θ equal to 18° for lime-treated kaolinite at 28-day curing. Vitale et al. (2017) indicated that the peak of C-A-H at 2θ equal to 13° was detected for lime treated kaolinite, while no XRD reflections of C-S-H was detected. By contrast, the crystalline compounds of C-S-H was observed on lime-treated bentonite (Vitale et al., 2017). Wang et al. (2017b) performed XRD tests on lime-treated silt with different maximum aggregate sizes and found that the peak of C-S-H phase at 2θ equal to 34.2° (d ~ 3.04 Å) was identified on the XRD pattern for lime-treated specimens with larger aggregates of 1 mm and 5mm at 1-year curing, whereas no XRD reflection of C-S-H phase was detected for lime-treated specimens with 0.4 mm aggregates after 1 year curing, as shown in Figure 1-13. In addition, Wang et al. (2017b) pointed out that, except for the C-S-H phase, the other minerals in the lime-treated soil were similar to those of untreated soil.

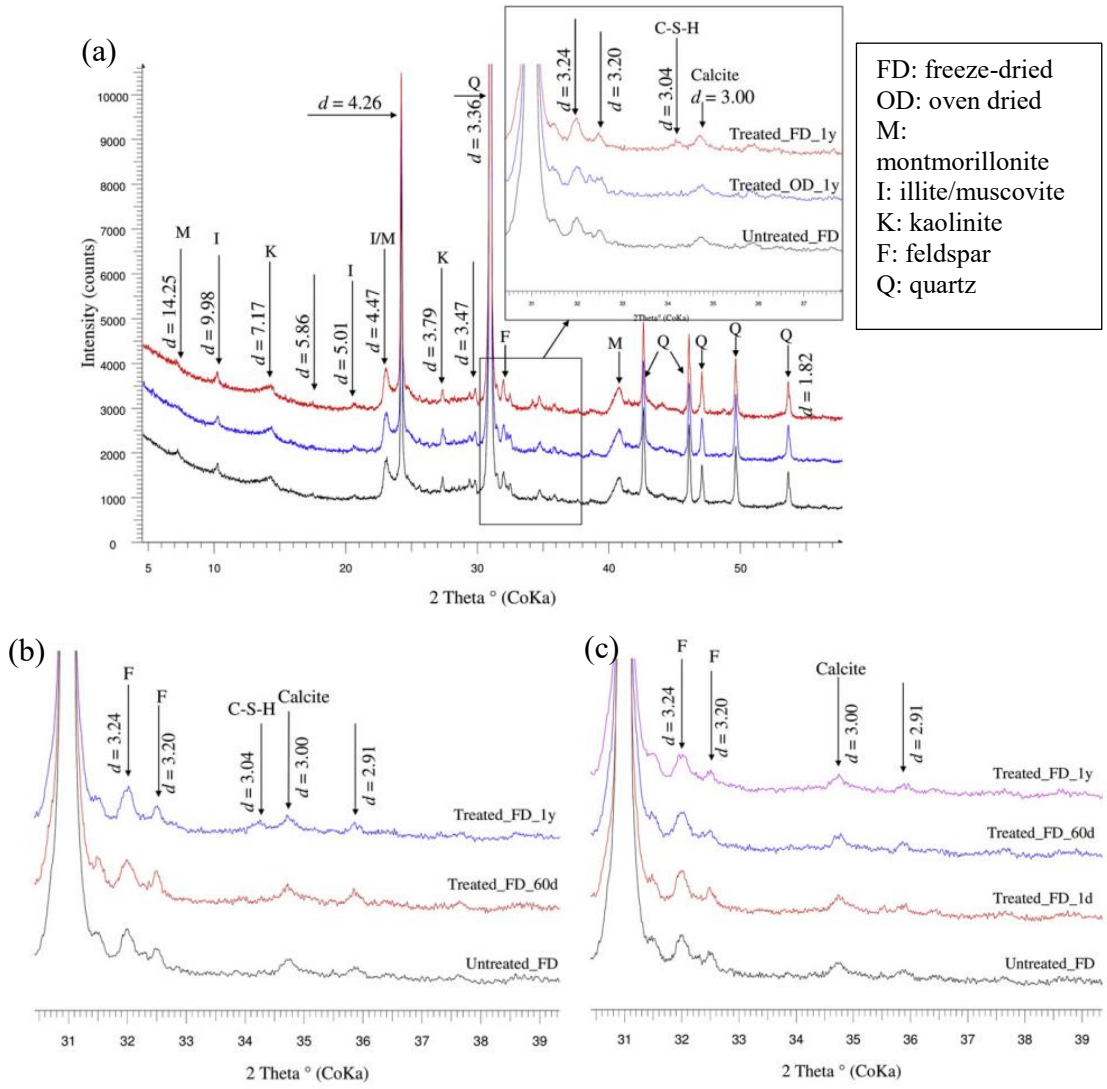

Figure 1-13. X-ray diffraction patterns of untreated and lime-treated specimens: (a) specimens S1 (D_{max} = 1 mm); (b) specimens S5 (D_{max} = 5 mm); (c) Specimens S0.4 (D_{max} = 0.4 mm) (Wang et al., 2017b).

The production of cementitious compounds is affected by the existence of salts in soil. Ramesh et al. (1999) reported that the sodium salts in fly ash-lime mixtures could promote the formation of sodium calcium silicate hydrate as compared to calcium silicate hydrate (C-S-H). Modmoltin and Voottipruex (2009) indicated that sodium chloride (NaCl) and calcium chloride ($CaCl_2$) promoted the dissolution of silicate and aluminate from soil, leading to more production of C-S-H in cemented-treated clay. Xing et al. (2009) stated that the Al^{3+} and Ca^{2+} ions in cemented salt-rich soil improved the formation of cementitious compounds, while the Mg^{2+}, Cl^- and SO_4^{2-} ions impeded such formation. They pointed out that the Mg^{2+} ions in cemented soil could replace the Ca^{2+} ions to produce low strength Mg-S-H instead of the formation of C-S-H; the

Cl^- ions first interacted with Ca^{2+} and Al^{3+} ions to form soft $Ca_2Al(OH)_6Cl(H_2O)_2$ which deposited on the surface of clays, preventing the clay mineral from being combined with $Ca(OH)_2$; SO_4^{2-} ions were combined with $3CaO.Al_3O_3$ to form expansive production.

In addition, the formations of ettringite and thaumasite are usually detected in lime-treated soils including gypsum ($CaSO_4$) or any other sulphate salts (Ramesh et al., 1999; Sivapullaiah et al., 2000, 2006; Rajasekaran and Rao, 2002; Aldaood et al., 2014a, 2014b; Behnood, 2018; Nabil et al., 2019). Mohamed (2000) and Yong and Ouhadi. (2007) indicated that, in the case of lime/cement treated soil, the presence of palygorsite and sepiolite in marls provided a favourable condition for the formation of ettringite. This ettringite is a hydrous mineral that exhibits expansive behaviour, weakening the system of lime-treated soil with time (Wild et al., 1999; Rajasekaran and Rao, 2002; Little et al., 2010; Celik and Nalbantoglu, 2013).

The calcium carbonate is another production in lime-treated soil due to the carbonation reaction between lime and carbon dioxide (CO_2) from atmosphere (Diamond and Kinter, 1965; Wild et al., 1986; Bell, 1996; Al-Mukhtar et al., 2010a, 2010b; Le Runigo et al., 2011).The carbonation plays a negative role in enhancement of soil strength as the consumption of lime by carbonation reduces the available lime to be available for pozzolanic reaction (Wild et al., 1987).

1.3.2.2. Scanning electron microscope

Scanning Electron Microscopy (SEM) is a useful technique that produces images of a sample by scanning the surface with a focused beam of electrons. The electrons interact with atoms in the sample, producing various signals that contain information about the surface topography and composition of the sample. SEM can be also coupled with Energy Dispersive X-ray Spectroscopy (EDS) to qualitatively or semi-quantitatively analyse the chemical compositions at the selected locations of sample.

Locat et al. (1990) conducted SEM observation on lime-treated Buckingham soil with 4% quicklime, and observed the platy C-A-S-H phase and reticular C-S-H phase connecting the adjacent soil particles in treated soil at 100-day curing. Lemaire et al. (2013) performed SEM observation on lime/cement treated silt and observed that the lime/cement binders were distributed in a continuous pattern surrounding the agglomerates and thus the production of hydrated gel stayed localized at the agglomerate periphery. Tran et al. (2014) observed the reticular C-S-H phase in the inter-aggregate pores in lime-treated clay. Al-Mukhtar et al. (2012)

and Sharma et al. (2018) indicated that the flat and large particles of untreated specimens were highly divided into a huge number of small connected particles with the addition of lime, and the products of C-S-H and C-A-H in pozzolanic reaction coated the surface of soil particles. The similar observation was obtained by Al-Swaidani et al. (2016) who reported that, for lime-treated and natural pozzolana-lime-treated clayey soil, the cementation products such as C-S-H and C-S-A-H covered the surface of clayey soil.

Jha and Sivapullaiah (2015) indicated that the microstructure of lime-treated soil was influenced by the curing time and lime content. They pointed out that when the lime content was below 4% or the curing time is shorter, only aggregated soil particles were observed on SEM images, while for the specimens with higher lime content and longer curing time, the production of cementitious compounds coated the surface of aggregates and filled the pores, as shown in Figure 1-14. Vitale et al. (2017) applied this technique on the lime-treated kaolin at different curing times, and found that the soil particles became lager at short curing time (t = 24 h). In the long term (t = 270 days), the products of C-A-H were located at the surface of clay particles and filled the intra-aggregate porosity.

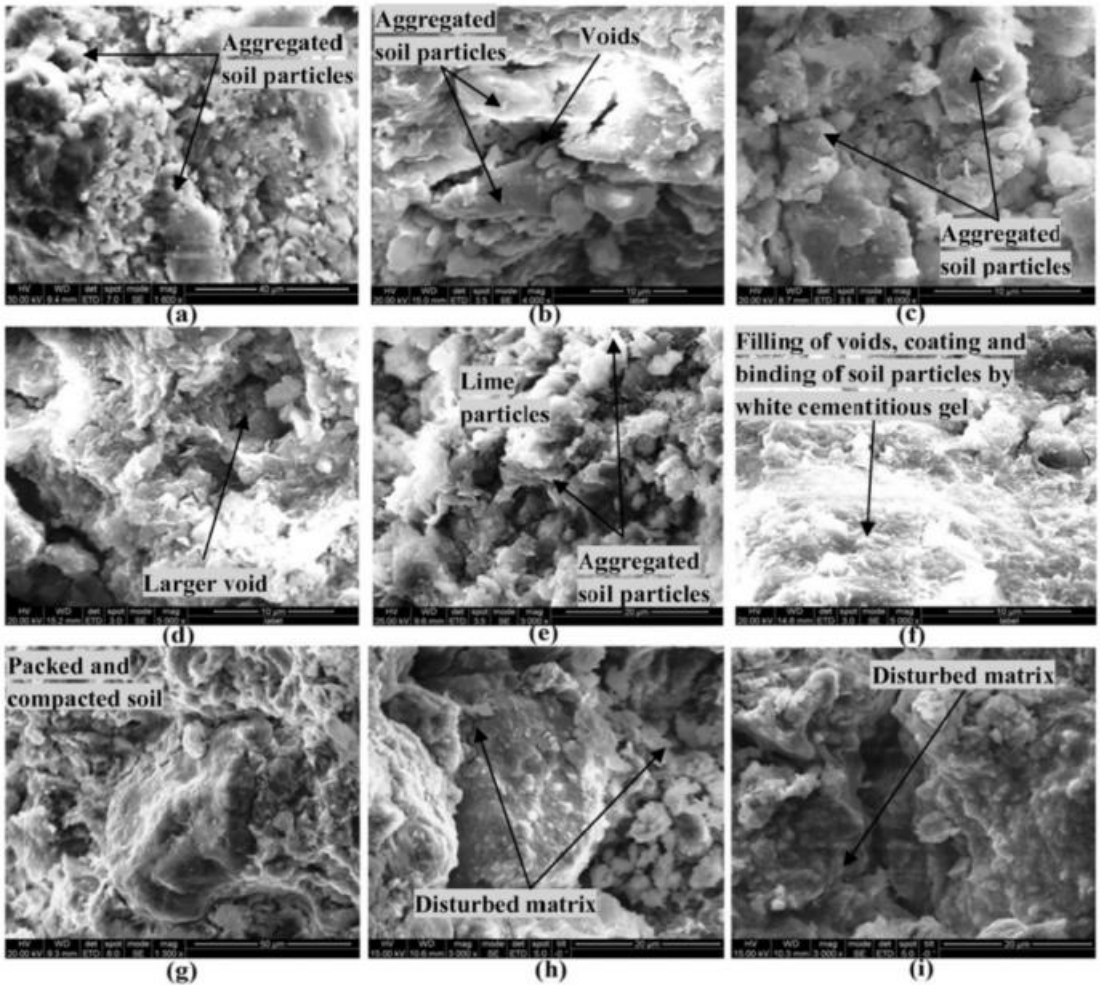

Figure 1-14. SEM micrographs of (a) Soil + 2% lime, 0 day; (b) Soil + 2% lime, 28 day; (c) Soil + 4% lime, 0 day; (d) Soil + 4% lime, 28 day; (e) Soil + 6% lime, 0 day; (f) Soil + 6% lime, 28 day; (g) Soil + 6% lime, 90 day; (h) Soil + 6% lime, 180 day; (i) Soil + 6% lime, 365 day curing period (Jha and Sivapullaiah, 2015).

Di Sante et al. (2014) reported that the curing condition affected the morphology of cementitious compounds produced in lime-treated clay: an amorphous and uniformly distributed cementitious compounds were observed in the unsaturated curing conditions, while a crystalline with more brittle structure was detected in the lime-treated clay cured in saturated condition.

In addition to the cementitious compounds in phases of C-S-H, C-A-H and C-A-S-H, the crystalline of ettringite was usually detected in lime-treated soil with sulphate. Keramatikerman et al. (2016) indicated that amorphous and fibrous cementitious compounds (C-S-H, C-A-H and C-S-A-H) and needle-line ettringite were observed in the ground granulated blast furnace slag (GGBFS) and lime-treated kaolinite. Aldaood et al. (2014a) reported that the

formation of ettringite in lime-treated gypseous soil, not only enhanced the inter-cluster bonding but also filled the pore space. By contrast, Li et al. (2016) stated that, in lime-treated soil, the chlorine salt did not participate in the reaction of lime, but was only adsorbed onto the soil surface or into soil pores.

1.3.2.3. Mercury intrusion porosimetry

Mercury Intrusion Porosimetry (MIP) is a widely used technique to determine the pore size distribution of soils. It is based on the principle that a non-wetting liquid (mercury) does not enter a porous material, unless a pressure is applied (Diamond, 1970; Delage and Lefebvre, 1984; Delage and Pellerin, 1984). The applied pressure ranges from around 3.6 kPa to 230 MPa, and the corresponding intruded diameter varies from 0.006 μm to 350 μm, providing a wide range of pore sizes (Wang et al., 2016; Zeng et al., 2017; Bian et al., 2019). The pressure is related to the entrance pore radius by Laplace's law:

$$p = \frac{2\sigma \cos\theta}{r} \tag{1-20}$$

where r is the entrance pore radius; σ is the surface tension; θ is the contact angle and p is the applied pressure.

To days, most studies have been focused on the effect of lime treatment on the changes in microstructure. It is widely admitted that the quantity of inter-aggregate pores increased with the immediate addition of lime, which is attributed to the cation exchanges and the consequent flocculation of soil particles (Bell, 1989; Locat et al., 1990; Guney et al., 2007; Khattab and Fleureau, 2007; Le Runigo et al., 2009; Cuisinier et al., 2011a; Tran et al., 2014; Wang et al., 2016). Khattab and Fleureau (2007) indicated that such change induced a more homogeneous pore size distribution in the treated specimen as the particles were less oriented due to flocculation than in the untreated specimen. In the long term, the formation of cementitious compounds in pozzolanic reaction coated the surface of aggregates and gradually filled the pore space, clogging some entrances of intra-aggregate pores and resulting in a reduction of inter-aggregate porosity (Locat et al., 1990; Tedesco and Russo, 2008; Guney et al., 2007; Lemaire et al. 2013; Tran et al., 2014; Liu et al., 2019b).

Russo et al. (2007) reported that microstructure changes of lime-treated soil during curing was affected by the initial moulding water content: the more significant fabric variation was observed on lime-treated samples at optimum water content and on the wet side of optimum,

and less change was identified on dry sample, as shown in Figure 1-15. Wang et al. (2016) indicated that the pore size distribution of the lime-treated specimens compacted dry of optimum exhibited bi-modal characteristics with two populations of micro-pores and macro-pores, while that of the specimens compacted on wet side showed typical uni-modal characteristics. During curing, the modal sizes of both macro-pores and micro-pores decreased.

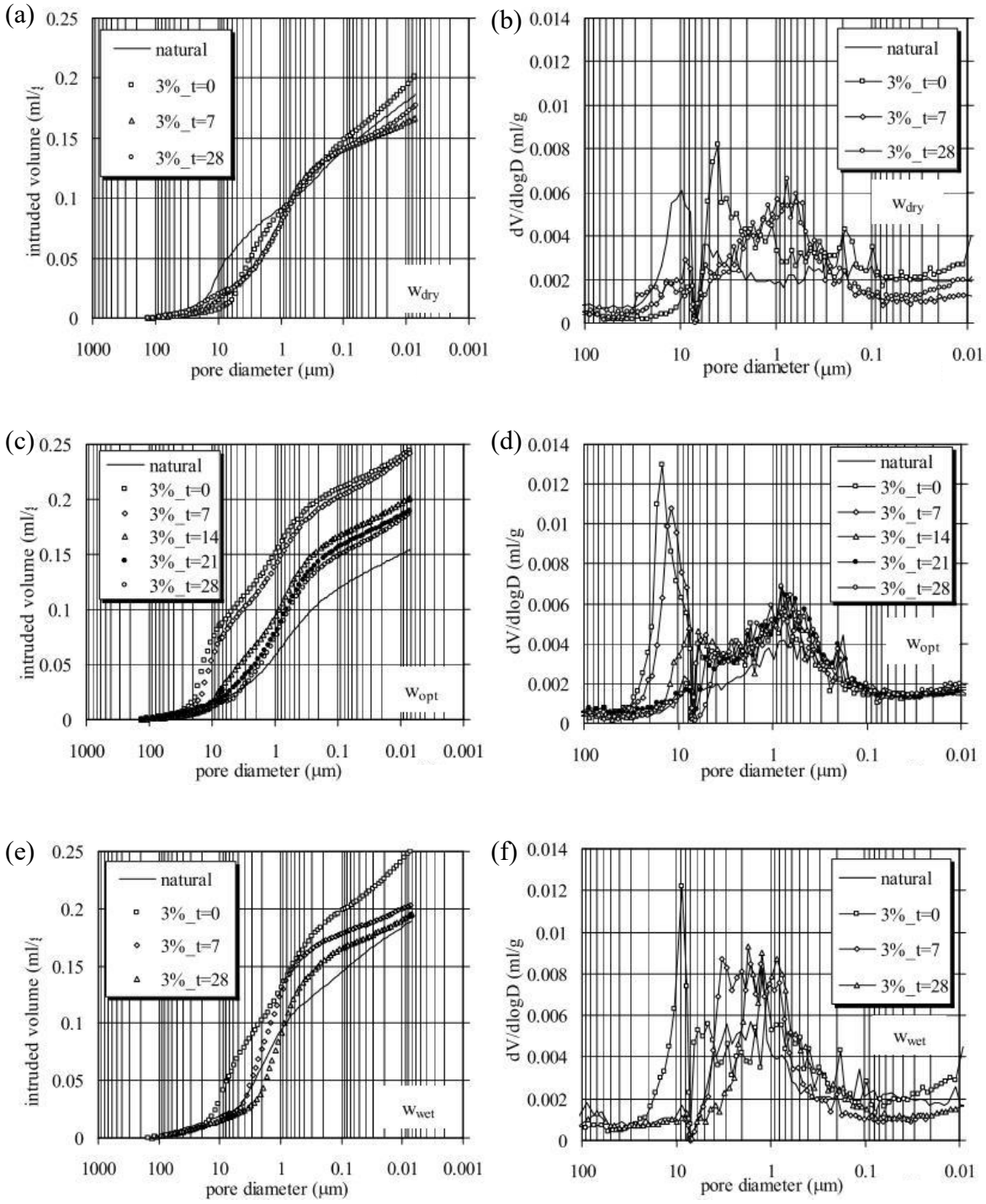

Figure 1-15. Cumulative intrusion curves and pore size distribution of lime-treated samples compacted: (a) and (b) dry of optimum; (b) and (c) at optimum state; (d) and (e) wet of optimum (Russo et al., 2007)

Tedesco and Russo (2008) and Russo and Modoni (2013) reported that a third pore population at diameter ranging from 0.007 to 0.2 μm developed in lime-treated silty soil at longer curing time. This was also identified by Cuisinier et al. (2011a), Le Runigo et al. (2009) and Wang et al. (2017b). They attributed this development of nano-pores to the formation of cementitious compounds which had a pore radius usually less than 0.2 μm. Wang et al. (2017b) reported that the creation of nano-pores was significantly influenced by the maximum soil aggregate size - at given curing time, less quantity of nano-pores were observed in lime-treated specimens with smaller soil aggregates, as shown in Figure 1-16.

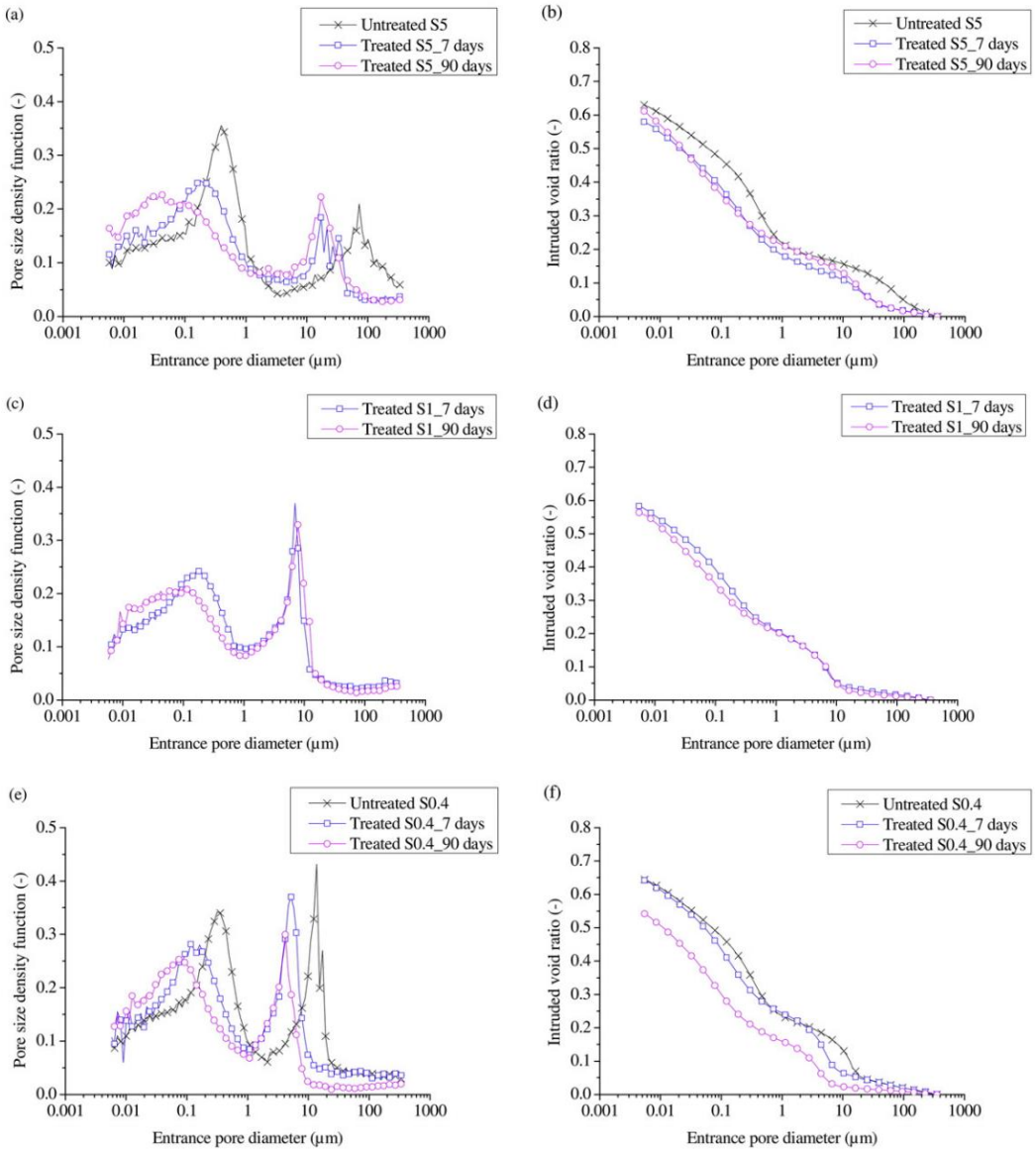

Figure 1-16. Pore size distribution and cumulative intrusion curves of untreated and lime-treated soils with different aggregate sizes (D_{max} = 5 mm for S5, D_{max} = 1 mm for S1, D_{max} = 0.4 mm for S0.4,) (Wang et al., 2017b)

1.4. Hydro-mechanical behaviour of lime-treated soil

1.4.1. Hydraulic behaviour

The hydraulic behaviour is important in evaluating the ability of soil to retain water or the ability to transmit fluid through pore spaces. While dealing with the constructions in contact with water, such as river levees, dams, dikes, reservoir, etc., the effect of lime treatment on the hydraulic behaviour has to be investigated. In this section, the lime treatment effect on the water retention property and the hydraulic conductivity is introduced.

1.4.1.1. Water retention property

The water retention property describing the relationship between suction and either water content or degree of saturation, is an indicator of water retention capacity of soils (Fredlund et al., 1994). It is widely used to predict the permeability (Romero, 1999; Gao et al., 2021), shear strength (Kim and Borden, 2011) and deformation (Tu and Vanapalli, 2016) for unsaturated soils.

A typical soil water retention curve of silty soil is presented in Figure 1-17 (Fredlund et al., 1994). The air-entry value is the matric suction where air starts to enter the largest pores in the soil, and the residual water content is the water content where a large suction change is required to remove more water from the soil. The adsorption curve is different from the desorption curves, due to the hysteresis.

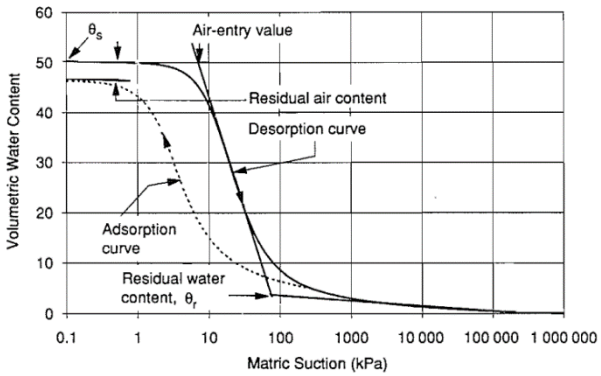

Figure 1-17. Typical soil water retention curve for a silty soil (Fredlund et al., 1994)

The soil water retention curves (SWRCs) can be determined experimentally by the chilled-mirror dew-point hygrometer (Leong et al., 2003) and non-contact filter paper method (ASTM

D5298-16, 2016; Thyagaraj and Salini, 2015) for the total suction measurement, as well as by contact filter paper method (ASTM D5298-16, 2016), insertion tensiometer (Sreedeep and Singh, 2005) and axis-translation technique (Fredlund and Rahardjo, 1993; Leong et al., 2007) for the matric suction measurement. The SWRCs in terms of matric suction can be also derived from the pore size distribution (PSD) curves obtained from mercury intrusion porosimetry (MIP) test (Romero et al., 1999). However, some difference between the SWRCs from direct measurements and from MIP tests is often observed. This difference is mainly attributed to the volume change due to suction changes, because the SWRC determined directly involved the effect of volume change, while the SWRC derived from MIP test did not (Muñoz-Castelblanco et al., 2012; Wang et al., 2015; Sun and Cui, 2020).

Romero et al. (1999, 2011) indicated that the water retention property was dominated by the capillary force in low suction range, whereas the adsorptive force was the important factor in high suction range. The capillarity is highly related to the soil mineralogy and pore size distribution (Lu and Khorshidi, 2015; Ng et al., 2016), while the adsorption was associated with soil mineralogy (Lu and Khorshidi, 2015) and the specific surface area of the clayey fraction (Romero and Vaunat, 2000; Tuller and Or, 2005). Tuller and Or (2005) reported that the soil with higher specific surface area presented higher water adsorption capacity. The specific surface area of lime-treated soil is found to increase over curing time as the cementitious compounds are produced in the long-term reaction (Halperin et al., 1994; Vitale et al., 2017; Sharma et al., 2018). Muller (2014) calculated the specific surface area of cementitious compounds (C-S-H) in cement paste using the results from Nuclear Magnetic Resonance (NMR) test. It is reported that the specific surface areas are 91 m^2/cm^3 for C-S-H gel pores and 175 m^2/cm^3 for interlayer spaces (Muller, 2014), which are higher than that of untreated soil. Indeed, Locat et al. (1996) reported that the produced cementitious compounds gave rise to higher water retention potential, due to the higher overall specific surface area and the very fine pore space in cementitious compounds which acted like a sponge and could store more water.

It is widely reported that the water retention property of lime-treated soil increases with curing time (Figure 1-18), due to the microstructure changes induced by soil-lime reaction (Khattab and Al-Taie, 2006; Petry and Jiang, 2007; Cecconi and Russo, 2008; Tedesco and Russo, 2008; Russo and Modoni, 2013; Wang et al., 2015; Bian et al., 2021). Cecconi and Russo (2008) attributed the increase in water retention capacity to the reduction of interconnection of inter-aggregate pores and the increase of occluded intra-aggregate pores. Tedesco and Russo (2008)

proposed that the cementitious compounds between soil aggregates can be represented by ink-bottle pores, and these pores can improve the water retention capacity by retaining water in the large inner pores. Wang et al. (2016) indicated that the increase of water retention capacity induced by lime addition was related to the decreased sizes of both inter-aggregate pores and intra-aggregated pores. However, Mavroulidou et al. (2013) and Zhang et al. (2017a) reported that the lime treatment applied to London clay resulted in a reduction of water retention capacity, which was attributed to a more open structure enabled by the flocculation and chemical bonding effects.

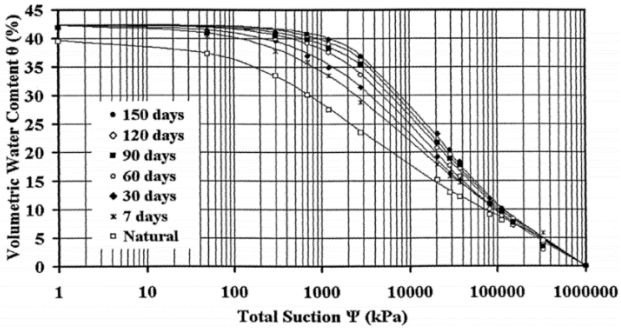

Figure 1-18. Soil water retention curve of lime-treated expansive soil (Khattab and Al-Taie, 2006)

Tedesco (2006) indicated that the water retention property of lime-treated was influenced by the initial remoulding water content - at the same suction, the treated specimens compacted dry of optimum exhibits a lower water content as compared to those compacted wet of optimum. They attributed this phenomenon to the different soil fabrics of soil specimens: the specimens on dry of optimum exhibited macro-pores which reduced the water retention capacity of specimens. Wang et al. (2015) indicated that the lime-treated silt with smaller aggregates had relatively smaller modal size of macro-pores and consequently exhibited a higher air entry value and higher water retention capacity (Figure 1-19).

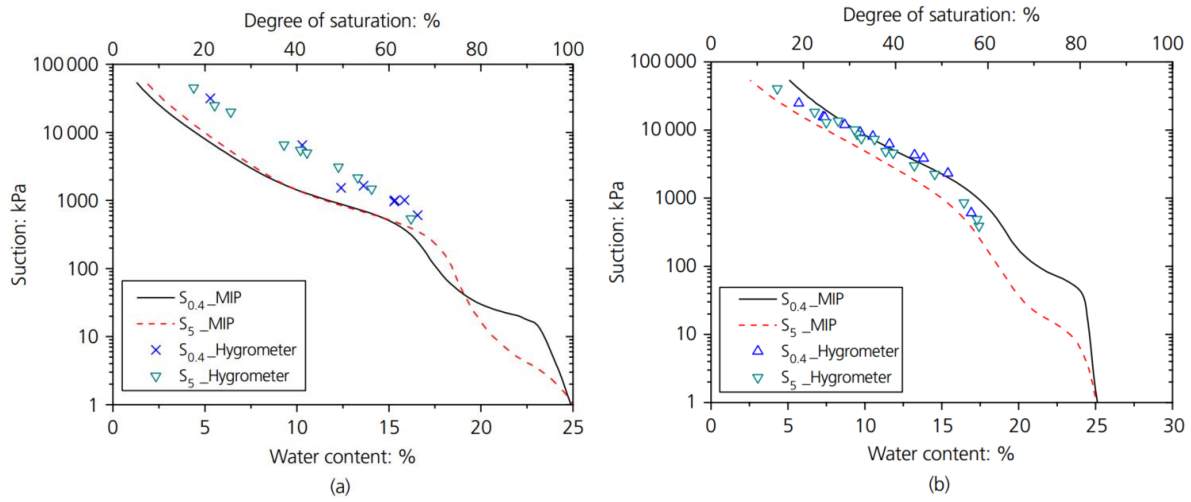

Figure 1-19. Effect of aggregate size on water retention curves: (a) untreated soil; (b) 2% lime-treated soil at curing time of 90 days (Wang et al., 2015)

1.4.1.2. Hydraulic conductivity

To days, lots of studies have focused on the variation of hydraulic conductivity of lime-treated soil, and different results are obtained by different researchers. Several studies indicated that the permeability of lime-treated specimens increased as compared to that of untreated specimens, because the treated soil lost their cohesive properties and behaved as a granular material (McCallister and Petry., 1990, 1992; Rajasekaran and Rao, 2001; Nalbantoglu and Tuncer, 2001; Al-Mukhtar et al., 2012; Sun et al., 2020), whereas others asserted that the lime treatment reduced the permeability (Herrier et al., 2012; Di Sante et al., 2014; Quang and Chai, 2015; Jha and Sivapullaiah, 2016). Makki-Szymkiewicz et al. (2015) reported that the permeability of lime-treated silty soil was the same as that of untreated specimens.

Locat et al. (1996) reported that the hydraulic conductivity of lime-treated soil was affect by the lime content: i) the small addition of lime led to an increase of hydraulic conductivity due to the flocculation of soil particles resulting from cation exchange; ii) at higher lime content, both cation exchange and pozzolanic reaction took place in lime-treated soil and the production of cementitious compounds filled the pore space. Thus, the hydraulic conductivity was reduced by almost one order of magnitude compared to that of the untreated clay. The similar observation was obtained by Osinubi (1998) on lime-treated lateritic soil at standard compaction energy in which the permeability increased to a maximum at 4% lime content and then decreased with further addition of lime, as illustrated in Figure 1-20. They also reported that, for the specimens compacted at higher compaction energy (West African Standard), the

permeability always decreased with increasing lime content, due to the closer packing of soil-lime mixture at higher compaction energy.

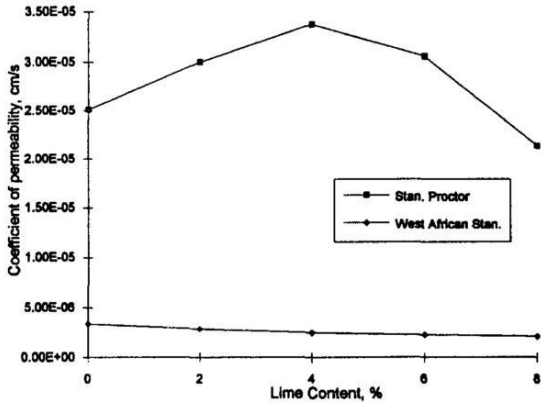

Figure 1-20. Variations of coefficient of permeability of treated samples with lime content (Osinubi, 1998)

The curing time is also an important factor influencing the hydraulic conductivity of lime-treated soil. Tran et al. (2014) reported that the hydraulic conductivity of a lime-treated clay increased progressively during the first 3 days, and stabilized during the next 4 days, which was attributed to the increase of inter-aggregate pore size induced by the lime hydration and modification. Moreover, they also indicated that the hydraulic conductivity might decrease in longer curing time due to the formation of cementitious compounds. Similar results were reported by Locat et al. (1996) on lime-treated clay and by Osinubi (1998) on lime-treated lateritic soil.

De Brito Galvão et al. (2004) pointed out that the variation of hydraulic conductivity of lime-treated soil during curing depended on the soil type. They investigated the permeability of two kinds of treated soils (a brown saprolitic soil and a red lateritic soil) and found that the hydraulic conductivity of brown saprolitic soil increased with increasing lime to 2%, and decreased thereafter with further addition of lime, while that of lateritic soil always decreased as lime content increased.

Le Runigo et al. (2009) investigated the effect of compaction condition on the hydraulic conductivity of lime-treated silt and found that lower permeability can be expected when compacting the specimens on the wet side of optimum or when overcompacting it. Similar observations were obtained by Cuisinier et al. (2011a) who reported that the specimens on wet

side of optimum or the specimens with higher dry density exhibited lower hydraulic conductivity. They explained that the wet specimens or the specimens with higher dry density exhibited less large pores, thus a lower hydraulic conductivity.

Di Sante et al. (2014) studied the effect of curing condition (e.g., saturated or unsaturated conditions) on the hydraulic conductivity of lime-treated clay. They reported that the hydraulic conductivity decreased over time for the specimens at unsaturated condition and it tended to decrease more significantly during curing for the specimens cured for longer time at unsaturated condition, as presented in Figure 1-21. This different behaviour is ascribed to the different microstructure of specimens cured at unsaturated or saturated condition. In the case of specimens after immediate saturation, the production of crystalline cementitious compounds was localized around the aggregates, making the structure locally open, giving rise to higher permeability. However, in the specimens with delayed saturation, the cementitious compounds in gel form partially filled the pores and reduced the connectivity of larger pores, causing a reduction of hydraulic conductivity.

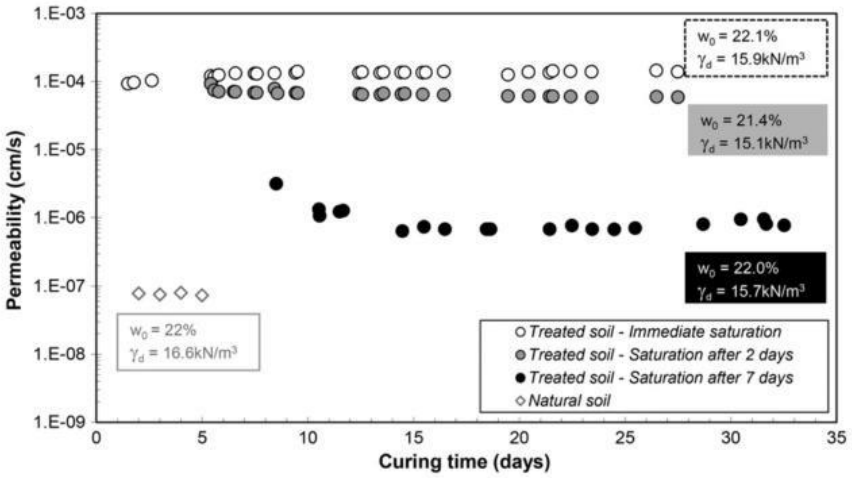

Figure 1-21. Results of permeability tests carried out under 35 kPa confining stress on specimens saturated after different times (Di Sante et al., 2014)

Cuisinier et al. (2020) measured the saturated hydraulic conductivity of lime-treated specimens subjected to wetting-drying cycles with different protocols. The first protocol is AG method by immersing the specimens in demineralized water for 2 days and then oven-drying at 60°C for another 2 days, while the second one is HR method by wetting the specimens through capillary rise and drying the specimens under a relative humidity of 54% and a temperature of 20°C. They found that the imposition of HR cycles resulted in a significant increase of permeability

from 1.0×10^{-9} m/s to 8.3×10^{-6} m/s after 6 cycles, and then the permeability remained stable between 6 and 12 cycles (Figure 1-22). The AG cycles led to a progressive increase of permeability to 6×10^{-7} m/s after 3 cycles, and then the permeability decreased slightly and remained almost constant after 6 cycles (Figure 1-22).

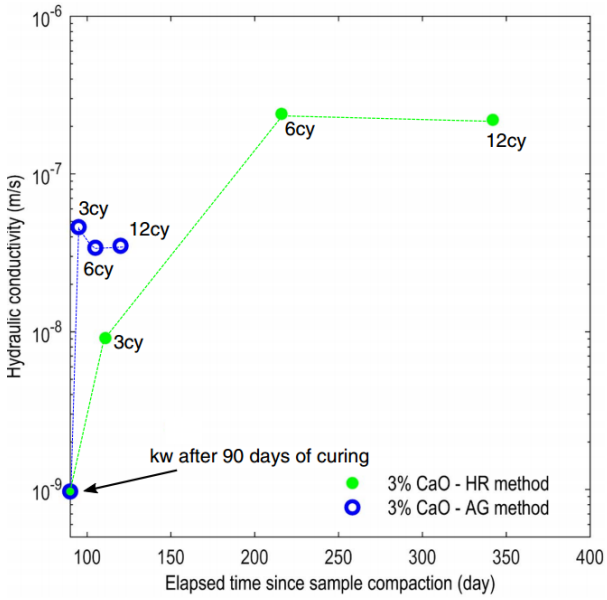

Figure 1-22. Impact of wetting-drying cycles on the saturated hydraulic conductivity of treated silt with 3% of quicklime (Cuisinier et al., 2020).

1.4.2. Mechanical behaviour

The effectiveness of lime treatment is usually evaluated by the mechanical behaviour. In this section, the lime treatment effect on the soil compressibility, unconfined compressive strength, shear strength and small strain shear modulus is presented.

1.4.2.1. Compressibility

It is widely recognised that the compressibility is an important parameter for evaluating the mechanical performance of soils (Olson and Mesri, 1970; Burland, 1990; Hong et al., 2010). Delage and Lefebvre (1984) and Marcial et al. (2002) reported that, when the clayey soil was compressed in oedometer cell, the decrease of volume corresponded to the collapse of macro-pores (or inter-aggregate pores) at low pressure and to the modification of micro-pores (intra-aggregate pores) at higher stress level, which made the soil particles become denser and more oriented. On the contrary, for the granular soils, the volume change during compression was characterised by the re-arrangement of silt/sand particles at low stress level and by the breakage

of grains at higher stress stage (Mesri and Vardhanabhuti, 2009; Mun and McCartney, 2017; Zhao et al., 2020).

To days, lots of studies have involved the lime effect on the soil compressibility. Locat et al. (1996) and Rajasekaran and Rao (2002) reported that the addition of lime induced an increase of pre-consolidation pressure, due to the aggregation and cementation effects. Nalbantoglu and Tuncer (2001) reported that the vertical effective yield stress increased and the compressibility decreased with increasing lime content for expansive clay, as shown in Figure 1-23. The similar results were reported by other researchers: the higher the lime content or the longer the curing time, the lower the compressibility of soils (Sakr et al., 2009; Mavroulidou et al., 2013; Moghal et al., 2014; Jha and Sivapullaiah, 2015; Yunus et al., 2015; Vitale et al., 2016). Rao and Shivananda (2005a) performed one-dimensional oedometer tests on saturated lime-treated clay samples and reported that the compression curve consisted of an initial region (25~100 kPa) where no breakage of cementation bonds, an initial yield stage (100 ~ 3200 kPa) where some bonds started to break, and a second yield stage (> 3200 kPa) with large plastic strain due to bond failure. Wang et al. (2017a) indicated that the compression behavior of lime-treated soil is affected by the soil aggregate size - the specimens with smaller aggregates exhibited lower compressibility and higher oedometer modulus, as lime was distributed more homogeneously inside the soil in the case of smaller aggregates, resulting in more cementitious compounds production.

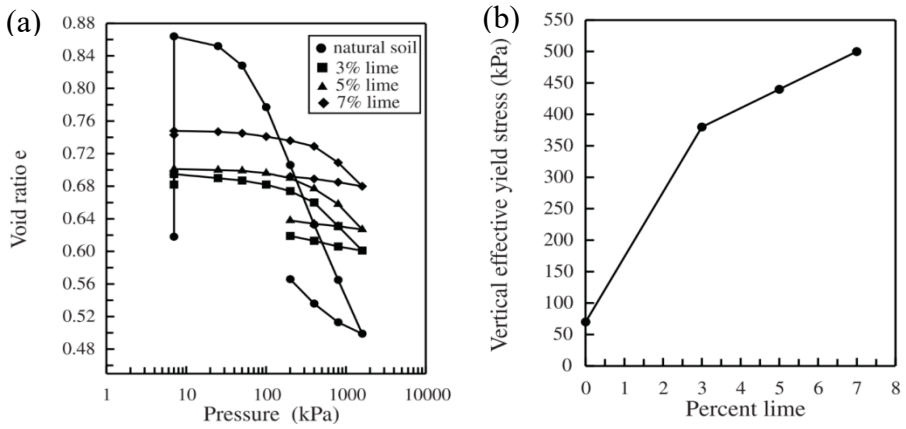

Figure 1-23. Lime treatment effect on the compression behaviour of lime-treated expansive clay: (a) e-logσ_v curve; (b) vertical effective yield stress (Nalbantoglu and Tuncer, 2001)

The compressibility of lime-treated soil is also affected by salts. Rajasekaran et al. (1997) reported that the addition of calcium sulphate and calcium chloride in lime-treated marine clay

led to an increase of shear strength and a reduction of compressibility. They attributed the salt effect to the diffusion of additional calcium ions from salts within lime-treated clay promoting the formation of cementitious compounds. Yunus et al. (2013) performed oedometer test on lime-treated organic clay with different concentrations of chloride salts. They found that the compression index of lime-treated soil reduced to the minimum value at 0.5% of chloride salts, and thereafter increased with increasing salt content, as shown in Figure 1-24. This significant decrease of compressibility at 0.5% salt content is attributed to the closer flocculation of soil particles promoted by salts which could provide more contact surface for pozzolanic reaction, while the further increase of compressibility is ascribed to the deflocculation of soil structure as the excessive salts cause an imbalance in the positive charge surrounding clay surface.

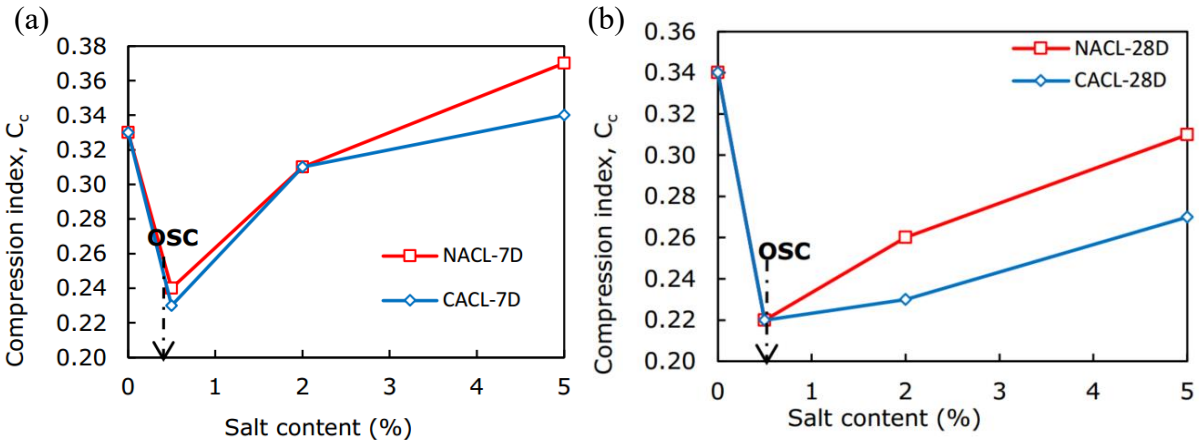

Figure 1-24. Effect of salt contents on the compression index (*Cc*) of lime-treated clay: (a) curing of 7 days; (b) curing of 28 days (Yunus et al., 2013).

Di Sante et al. (2014) investigated the effect of curing condition on the compression behaviour of lime-treated soil by conducting oedometer test on lime-treated clayey soil cured in either saturated or unsaturated conditions. Thy found that a significant reduction in compressibility was observed for all lime-treated specimens as compared to untreated specimens, and the lime-treated specimens cured in saturated condition exhibited higher compressibility than that cured in unsaturated condition. Stoltz et al. (2014) and Rosone et al. (2018) performed odometer tests on the lime-treated specimens which were subjected to wetting-drying cycles and reported that the wetting-drying cycles led to an increase of compressibility and a significant reduction of yield stress (Figure 1-25). This was attributed to the softening of cementitioud bonds and soil structure during wetting-drying cycles, causing a loss of mechanical performance.

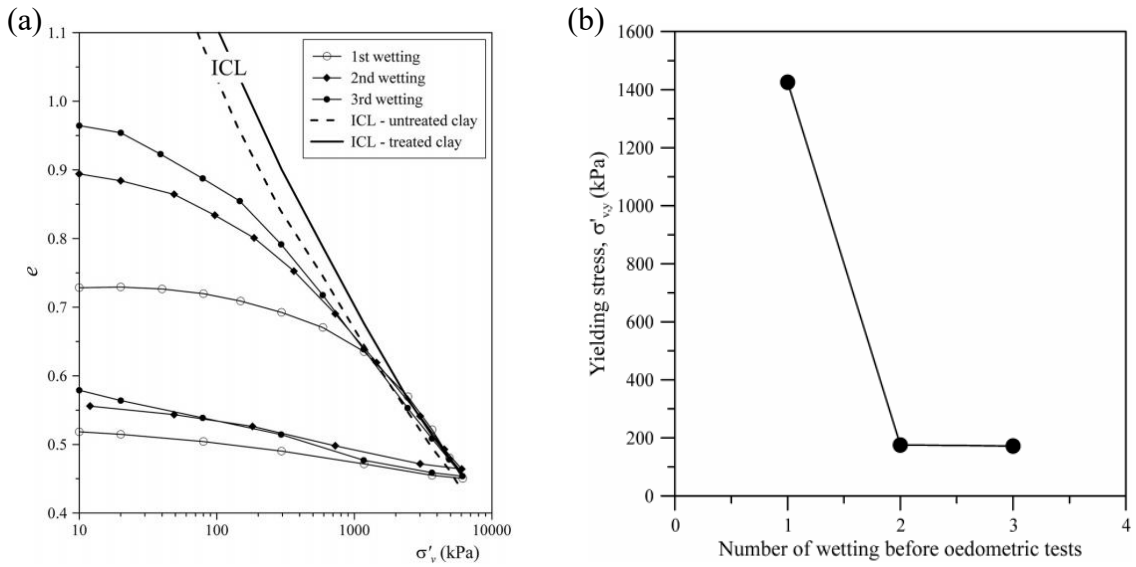

Figure 1-25. Wetting-drying effect on the compression behaviour of lime-treated soil: (a) e-logσ_v curve; (b) yield stress (Rosone et al., 2018)

1.4.2.2. Unconfined compressive strength

Previous studies stated that the lime treatment effectively improved the unconfined compressive strength, UCS (Locat et al., 1990; Bell, 1996; Al-mukhtar et al., 2010a; Ciancio et al., 2014; Baldovino et al., 2018). Locat et al. (1990) reported that the lime-treated specimens obtained 10-fold increase in strength over 200-day curing, reflecting the cumulative effects of cementation process. Al-Mukhtar et al. (2010a, 2010b, 2012) indicated that the UCS is significantly enhanced by the addition of lime and curing, due to the production of cementitious compounds. Consoli et al. (2014) reported that the UCS increased non-linearly with the increase of lime content, but increased linearly with the reduction of porosity of compacted lime-treated specimens. Ciancio et al. (2014) indicated that the UCS of lime-treated rammed earth increased to the maximum value as lime content increased, and then kept almost constant with further addition of lime. Jha and Sivapullaiah (2016) illustrated that the cementation of soil particles and the filling with cementitious compounds of the voids induced by lime treatment significant increased the UCS. Baldovino et al. (2018) mentioned that the UCS presented an exponential relation with lime content, and a linear relationship with the logarithm of curing time, as shown in Figure 1-26. Puppala et al. (1996) reported that the increase in UCS with respect to lime treatment was higher for the specimens compacted wet of optimum than for the specimens compacted dry of optimum, indicating the better stabilization for specimens with higher water content.

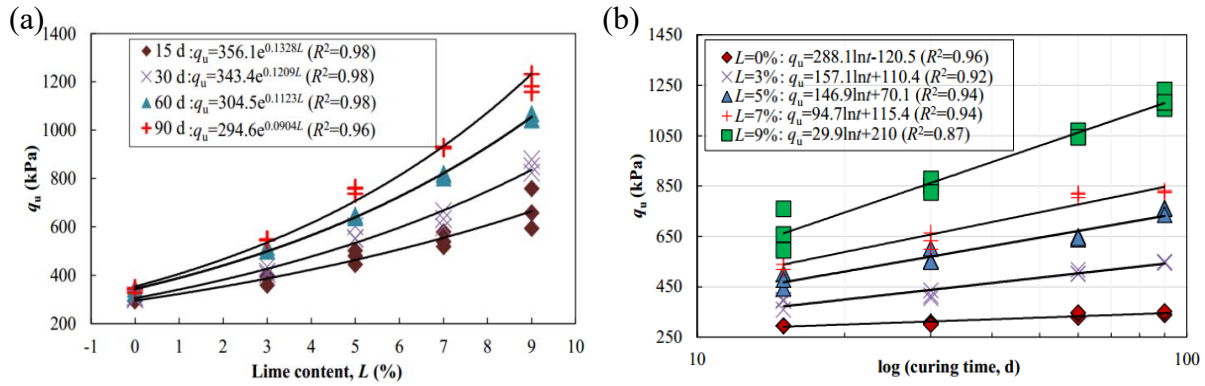

Figure 1-26. The relationships of compressive strength with: (a) lime content; (b) curing time (Baldovino et al., 2018)

Bell (1996) performed unconfined compressive tests on lime-treated montmorillonite, kaolinite and quartz. They reported that the UCS of montmorillonite increased rapidly with increasing lime content to 4% and then decreased significantly with further increase of lime content, while that of kaolinite and quartz increased noticeably with addition of lime until an optimum lime content beyond which the UCS kept almost constant, as illustrated in Figure 1-27. Similarly, Kassim and Chern (2004) indicated that, for different lime-treated soils, the UCS followed different evolutions with curing: the UCS of stabilised Jerangau clay increased very slowly at the first 14 days, followed by a noticeable increase up to 450 kPa by two-fold at 56-day curing; the strength of Tapah Kaolin increased linearly from 60 kPa to 270 kPa with curing, while that of Sg Buluh clay, Kulai clay and Pelepas marine increased slightly during curing due to the less reactive clay minerals.

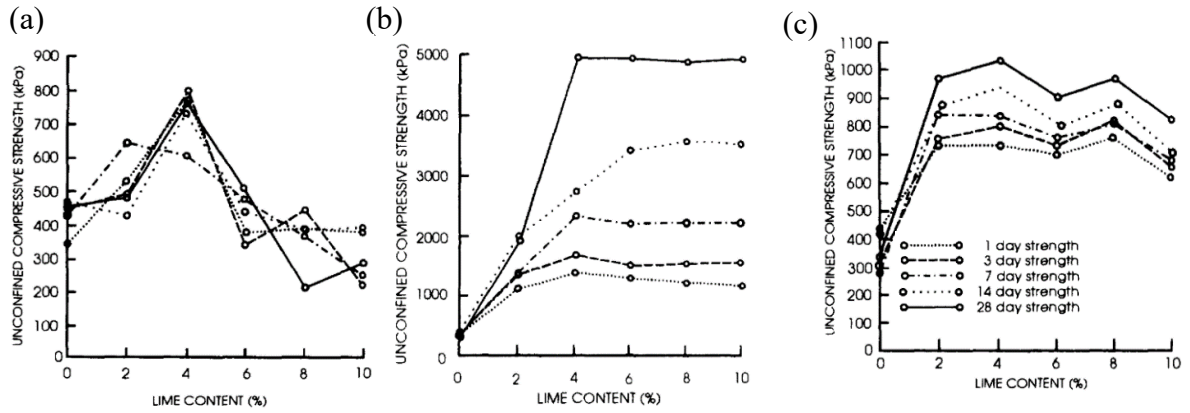

Figure 1-27. Unconfined compressive strength of lime-treated soils: (a) Montmorillonite; (b) Kaolinite; (c) Quartz (Bell, 1996).

The salt content is an important factor influencing the UCS of lime-treated soil. Cuisinier et al. (2011b) investigated the effects of nitrates, phosphates and chloride on the UCS of lime and cement treated soil. They found that the influence of salt effect on soil stabilization and the mechanical behaviour was combined with the curing conditions, the nature of soil (silt or fine sand) and the type of cement. Li et al. (2016) reported that chloride salt had adverse effect on the improvement of UCS, because the salt promoted the flocculation of soil particles and thus reduced the total contact surface of soil and lime which provided less opportunity for pozzolnaic reaction. Liu et al. (2018b) indicated that the UCS decreased with increasing amount of sodium chloride. They attributed this decrease of UCS to the salt expansion which led to some tiny cracks on the one hand, and to the effect of moisture absorption and softening of lime-treated soil at higher salt content on the other hand.

Aldaood et al. (2014a) reported that the UCS of lime-treated gypseous soil increased with curing time and the UCS increased significantly with 5% gypsum but less for higher gypsum percentages (15% and 25%). The 5% gypsum promoted the formation of C-S-H and/or C-A-H and ettringite which gave rise to an increase of strength, while the higher percentage of gypsum decreased the production of C-S-H and/or C-A-H but increased the formation of ettringite which inhibited the increase of strength. As a result, the lime-treated specimens with 15 and 25% gypsum exhibited a lower durability to wetting-drying cycles, as compared to the specimens with 5% gypsum and without gypsum. The decrease of unconfined compressive strength of treated soil with wetting-drying cycles was attributed to the increase in water content during these cycles, cracks propagation during drying and gypsum dissolution during wetting (Aldaood et al., 2014a). Nabil et al. (2019) pointed out that the lime-treated specimens with higher lime content could resist more wetting-drying cycles. As shown in Figure 1-28, the largest reduction of UCS was obtained after the first cycle for the treated specimens in the wetting stage, and the reduction decreased to the minimum value in the 12^{th} cycles for the treated specimens with higher lime contents of 6% and 8%, and in the 6^{th} cycle for the treated specimens with 4% lime content. The untreated specimens and the treated specimens with 2% lime was damaged during the 1^{st} cycle. Cuisinier et al. (2020) investigated the impact of different wetting-drying protocols on the unconfined compressive strength of lime-treated soil. The first protocol is AG method in which the specimens were successively immersed in demineralized water for 2 days and then oven-dried at 60°C for another 2 days, while the second one is HR method by wetting the specimens through capillary rise and drying the specimens under a relative humidity of 54% at a temperature of 20°C. Results showed that the AG cycles

led to a significant decrease of the strength during 12 cycles, and the HR method resulted in a noticeable decrease of strength until 3 cycles, but the subsequent cycles had insignificant effect on the strength, as shown in Figure 1-29.

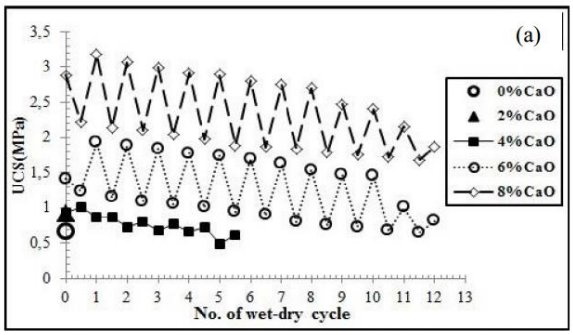

Figure 1-28. The variation of unconfined compressive strength with wetting-drying cycles for lime-treated specimens at curing time of 180 days (Nabil et al., 2019).

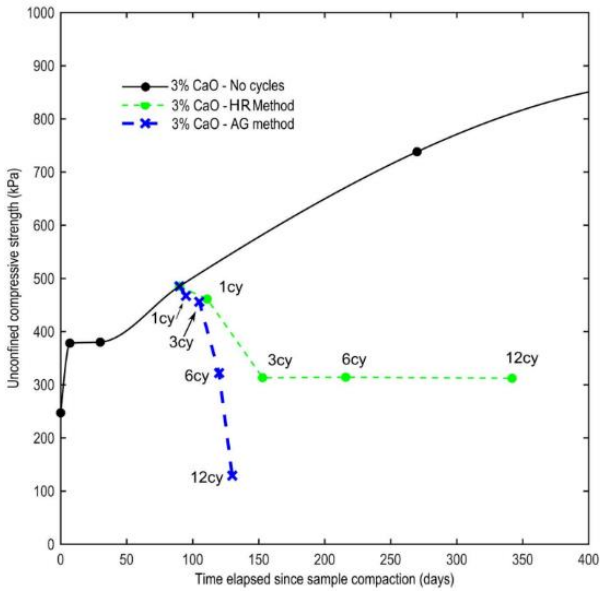

Figure 1-29. Impact of wetting-drying cycles on the UCS of specimens treated with 3% quicklime (Cuisinier et al., 2020).

1.4.2.3. Shear strength

Soil shear strength is a term used to describe the magnitude of the shear stress that a soil can sustain. The shear resistance of soil is a result of friction and interlocking of soil particles, and possibly cementation or bonding at particle contacts. Many studies have focused on the changes in shear strength of lime-treated soils and reported that the lime treatment induced an increase of shear strength (Locat et al., 1990; Liu and Pemberton, 2010; Le Runigo et al., 2011; Ghobadi et al., 2014; Yunus et al., 2015; Anggraini et al., 2016).

Locat et al. (1990) investigated the quicklime stabilization of sensitive clay and found that, even at a water content above the liquid limit, significant strength increase can be obtained if enough time and lime were allowed, due to the physical bridge between soil particles created in the cementation process. Rajasekaran and Rao (2000) performed laboratory vane shear test on undisturbed samples taken from the experimental site at different radial distances to the lime column. They found that the shear strength increased by six to eight times than that of untreated soil at a radial distance of 80 mm, and by four to six times for the lime-treated soil at a radial distance of 200 mm.

Le Runigo et al. (2011) conducted undrained triaxial tests on silt specimens treated with 1% and 3% lime, and reported that the lime treatment gave a significant increase of shear strength while the difference in shear strength between 1% and 3% was quite small. Nevertheless, when the triaxial tests were performed on the lime-treated specimens after leaching, a significant decrease of shear strength was observed for 1% lime addition, while a negligible decrease was obtained for 3% lime treatment, as shown in Figure 1-30. Rosone et al. (2020) suggested that stress-strain behaviour of lime-treated clay was strongly dilatant with a higher peak of strength, which increased with curing time and lime content. However, the increase of shear strength induced by lime-treatment would be lost while subjected to wetting-drying cycles due to the softening of cementitious bonding (Rosone et al., 2018).

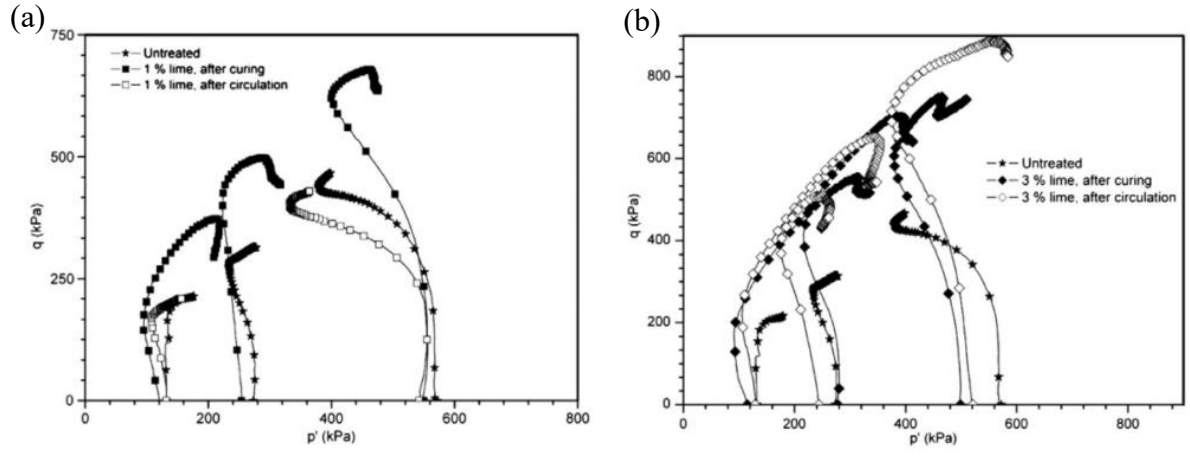

Figure 1-30. Effect of water circulation on the shear strength: (a) 1% lime treatment; (b) 3% lime treatment (Le Runigo et al., 2011).

Rajasekaran and Rao (2000) pointed out that the calcium chloride with quicklime resulted in considerable increase of shear strength, while the sodium sulphate did not. Sivapullaiah et al.

(2000, 2006) indicated that, for a lime-treated montmorillonitic natural black cotton soil and a lime-treated kaolinitic soil, after long curing period of one year, the presence of sulphate led to a reduction of shear strength which was reflected in the reduction of effective cohesion (c'). This was attributed to the prevention of cementitious of particles by sulphate and the formation of ettringite.

1.4.2.4. Small strain shear modulus

Small strain shear modulus, G_{max} ($\varepsilon_s < 0.0001$ %) is an important parameter for describing the elastic properties of soils, and for predicting the dynamic response and ground deformation of engineering structures (Zhou and Chen, 2005; Ng and Yung, 2008; Tang et al., 2011a; Chakraborty et al., 2018). The small stain shear modulus can be obtained by a pair of bender elements (Ng et al., 2009; Tang et al., 2011a; Heitor et al., 2013; Wang et al., 2020a), resonant column (Youn et al., 2008; Yao et al., 2020), torsional shear tests (Youn et al., 2008; Zou et al., 2019), and flat transducers and accelerometers (Wicaksono and Kuwano, 2009; Ferreira et al., 2014).

The bender elements technique is widely used to determine the shear wave velocity, and hence the small strain shear modulus G_{max} of lime-treated soil, due to its simplicity, economy, and non-destructive characteristic. The G_{max} of lime-treated soil is affected by the lime content, compacted dry density, moulding water content, aggregate size and curing time, etc. (Consoli et al., 2011; Tang et al., 2011a; Dong, 2013; Wang et al., 2020a).

Consoli et al. (2011) measured the initial shear modulus G_0 (or the small strain shear modulus G_{max}) of lime-treated soil by bender element technique and reported that G_0 increased linearly with the increase of lime content, whatever the different compacted dry densities, as shown in Figure 1-31. They also pointed out that, at the same lime content, G_0 increased with increasing dry density, while it decreased as the porosity increased.

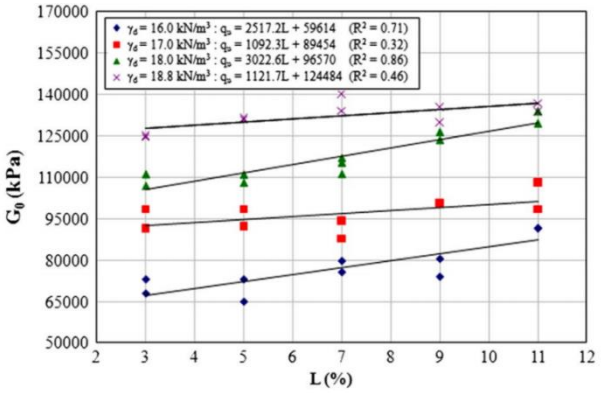

Figure 1-31. Variation of initial shear modulus (G_0) with lime content (L) for clayey sand-lime mixtures (Consoli et al., 2011).

Dong (2013) indicated that the G_{max} variation of lime-treated soil during curing can be divided into two non-linear phase: the first phase due to the cation exchange and the second phase attributable to the pozzolanic reaction. Wang et al. (2020a) reported that the G_{max} and suction changes followed the same two-phase pattern in which the G_{max} and suction increased slowly in the first phase corresponding to the flocculation process, and then increased significantly in the second phase owing to the production of cementitious compounds from pozzolanic reaction, as shown in Figure 1-32.

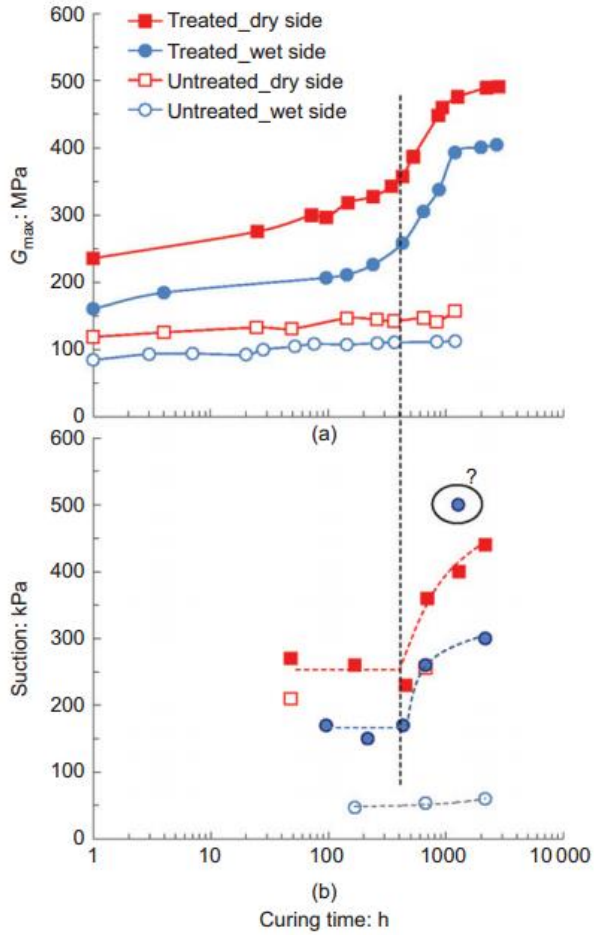

Figure 1-32. Changes in (a) G_{max} and (b) suction for both lime-treated and untreated soil during curing (Wang et al., 2020a).

Tang et al. (2011a), Dong (2013) and Wang et al. (2020a) focused on the effect of moulding water contents on the G_{max} variations of lime-treated soil during curing. Dong (2013) indicated that the lime-treated specimens compacted dry of optimum exhibited higher G_{max} than the specimens compacted wet of optimum, since the soil aggregates are much softer at higher water content. Tang et al. (2011a) reported that, after immediate lime treatment, the G_{max} values of lime-treated clayey soil compacted at dry side (w = 14%) was higher than those of specimens compacted wet of optimum (w = 18%). The G_{max} increased much more significantly with curing for the lime-treated specimens in the case of higher water content, making the stabilized G_{max} of wet specimens increase to the values of dry specimens, as presented in Figure 1-33. They explained that the G_{max} of compacted specimens was mainly governed by the contacts between adjacent soil particles which was dominated by the capillary suction after the compaction. Thus, the higher the suction of the specimen compacted on dry side, the higher the G_{max}. When the stabilization was reached, the G_{max} was governed by the cementation bonds and the effect of suction became less significant. As a result, the stabilized G_{max} of lime-treated specimens at

both dry and wet sides were similar. Nevertheless, Wang et al. (2020a) indicated that the dry specimens had a relatively higher stabilized G_{max} as compared to that of the wet specimens (Figure 1-32). They explained that the combined effect of the relatively lower suction and cementitious compounds resulted in lower G_{max} for lime-treated specimens on wet of optimum.

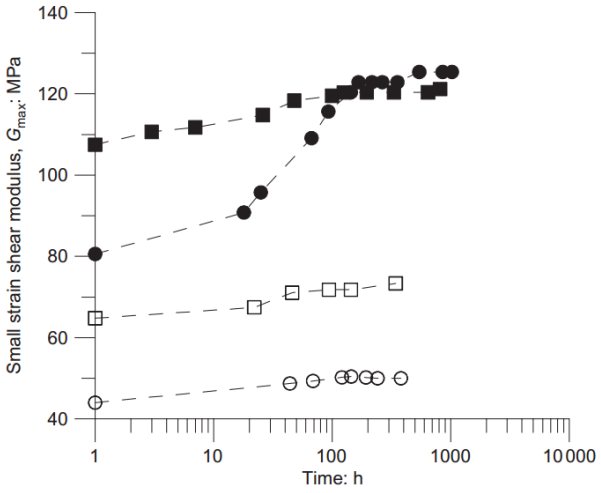

Figure 1-33. Evolutions of small strain shear modulus during curing for specimens with maximum soil aggregates of 0.4 mm (Tang et al., 2011a)

The maximum soil aggregate size is another important factor influencing the G_{max} of lime-treated soil. It is reported that the larger the soil aggregate size, the lower the G_{max} (Tang et al., 2011a; Dong 2013). This is attributed to the more production of cementitious compounds of lime-treated specimens with smaller aggregate size, because of its larger total surface of aggregates and therefore more soil-lime reaction.

Puppala et al. (2006) stated that the presence of sulfate in lime-treated soil would influence the enhancement of G_{max} - the lime-treated clays with low sulfate concentration of 1000 ppm showed considerable increase of G_{max}, while the same lime-treated soil at higher concentration of 10 000 ppm showed less increase of G_{max} due to the sulfate heaving.

Tang et al. (2011a) investigated the changes of G_{max} of untreated and lime-treated specimens during wetting-drying cycles by performing bender element tests. They concluded that the cyclic wetting-drying induced significant decrease of G_{max} of untreated specimens due to the appearance of microcracks, while it had insignificant effect on the G_{max} of lime-treated specimens. In the case of lime-treated specimens, only an intensive drying to very low water content induced microcracks and thus a decrease in G_{max} with subsequent wetting, as shown in

Figure 1-34.

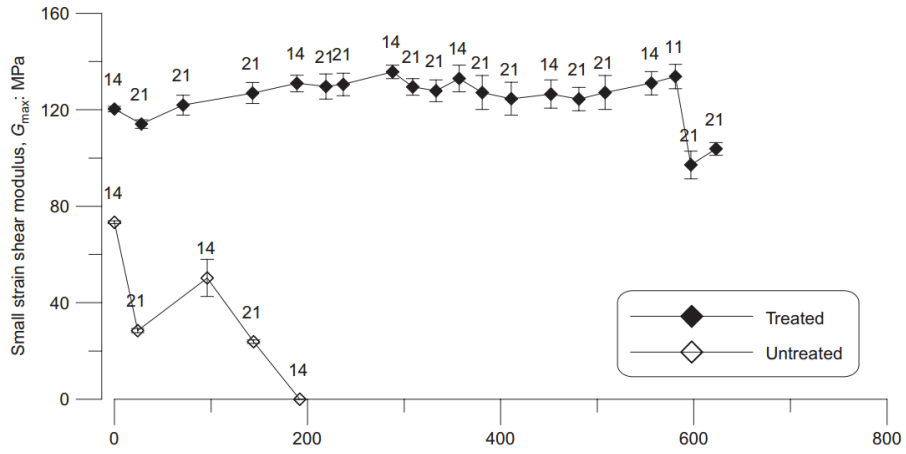

Figure 1-34. Changes in G_{max} upon wetting-drying cycle for specimens with maximum aggregate size of 0.4 mm (the number of 14 and 21 corresponds to the water content) (Tang et al., 2011a)

1.5. Conclusions

This chapter firstly introduces the techniques of soil stabilization, the mechanism of lime treatment, and the methods to determine the optimum lime content. Then, the geotechnical properties of untreated saline soils and lime-treated soils were presented, together with the changes in mineralogy and microstructure of lime-treated soil during curing. Finally, the lime treatment effect on the hydro-mechanical behaviour of lime-treated soils is reviewed, with emphasis put on the effects of salinity and wetting-drying cycles. The following conclusions can be drawn:

(1) Previous studies proposed that the presence of salts should be considered in saline soil and several methods were provided to determine the salt concentration and osmotic suction of saline soils. As the soils in shallow depth of constructions usually interact with the atmosphere, their water contents change constantly. This influences, in turn, the quantities of dissolved and precipitated salts in soils. However, these methods did not pay attention to the difference between dissolved salts and precipitated salts while assessing the salt concentration and osmotic suction for unsaturated soils.

(2) The aforementioned studies stated that, with increasing salinity, the decreased liquid limit for expansive soils was attributed to the shrinkage of diffuse double layer, while the increased liquid limit for non-expansive soils was explained by the growing particle flocculation.

However, these two mechanisms seem to be controversial and it is difficult to understand how an increasing salinity can promote soil flocculation. Similarly, concerning the compaction behaviour, even though a lot of studies had focused on the salinity effect on the compaction behaviour, these results were not consistent and the mechanism was not clarified. Furthermore, the salinity effect on the microstructure evolutions of compacted soils upon drying was not investigated.

(3) The previous studies provided several methods to determine the optimum lime content in which the pH method is the quickest and the most widely used procedure. The deionized water is usually used in the pH measurement, while the presence of salts would influence the pH variations. However, there is no study focusing on the salt solution effect on the optimum lime content and exploring the relevant mechanism.

(4) A number of studies have focused on the changes of mineralogy, microstructure and water retention property of lime-treated saltless soil during curing. However, there is a lack of studies that focus on the salinity effect on the variations of water retention property and microstructure of lime-treated saline soil during curing, as well as the microstructure evolution along the water retention curve (during drying) for lime-treated saline soils. Even though the effect of wetting-drying cycles on the mechanical behavior was widely reported, there is no study focusing on the wetting fluid effect on the mechanical behaviour of lime-treated soils subjected to wetting-drying cycles.

Chapter 2. Assessment of dissolved salinity and osmotic suction

Introduction

The soils in shallow depth are usually subjected to water evaporation, leading to a decerase of water content. For saline soils, the dissolved salt starts to precipitate or crystalize with decreasing water content, due to the saturation of salt in soil pore water. In reality, only dissolved salt and the induced osmotic suction have significant effect on the hydro-mechanical behaviour of saline soils, whereas the precipitated salt can be regarded as soil solid. However, while dealing with unsaturated soils, they do not have enough soil pore water to be extracted for the determination of dissolved salinity and osmotic suction.

This chapter deals, firstly, with the assessment of dissolved salinity for unsaturated soils. The relationship between dissolved water salinity (the mass ratio of dissolved salt to salty water) and dissolved soil salinity (the mass ratio of dissolved salt to dry solid) was established. For mixed salts solution having the same salt composition as synthetic seawater, the relationship between electrical conductivity (EC) and either total water salinity or dissolved water salinity (r) was investigated. Afterwards, three approaches were proposed to calculate the dissolved water salinity and dissolved soil salinity of salt-amended soils. Finally, the calculated results were compared with the measured ones. This work was published in “Geotechnical Testing Journal”.

Then, the determination of soil osmotic suction was explored for unsaturated soils. First, the total and matric suctions of compacted soils were measured by the chilled-mirror dew-point hygrometer (WP4C) and by the contact filter paper method. Then, a new equation to calculate soil osmotic suction from electrical conductivity was proposed, taking into account the dissolved and the precipitated salts. The calculated soil osmotic suctions were compared with the indirectly measured osmotic suction which was the difference between the total suction and the matric suctions. This constitutes a paper submitted to “Journal of Rock Mechanics and Geotechnical Engineering”.

The articles are presented here in their original versions.

Ying, Z., Duc, M., Cui, Y.J., Benahmed, N. 2021. Geotechnical Testing Journal, 44(1): 130-147.

Salinity assessment for salted soil considering both dissolved and precipitated salts

Zi Ying[1], Myriam Duc[2], Yu-Jun Cui[1], Nadia Benahmed[3]

Abstract: In practice, the soils in shallow depth are usually subjected to the effect of wetting-drying cycles, leading to water content variations. As water content decreases, the dissolved salt starts to precipitate or crystalize, due to the saturation of salt in soil pore water. In reality, only dissolved salt has significant effect on thermo-hydro-mechanical behaviour of salted soils, whereas the precipitated salt can be regarded as soil solid. However, the existing description of salted soil compositions and salinity assessment do not take the salt state into account, limiting thus its application to salted soils which undergo significant water content changes. In this study, the description of salted soil compositions was revised considering both dissolved and precipitated salts. Then, the relationship between dissolved water salinity (the mass ratio of dissolved salt to salty water) and dissolved soil salinity (the mass ratio of dissolved salt to dry solid) was established. Considering the complex chemical compositions of soil pore water, the relationship between electrical conductivity (EC) and water salinity (r) of mixed salt solution which had the same salt compositions as synthetic sea water was plotted to further transform the measured electrical conductivity of soil pore water to water salinity. Salt quantity in both natural soils and salt-amended soils was determined by centrifuge and EC-r relationship of the mixed salt solution, allowing water salinity and soil salinity to be determined. Besides, the ion compositions and concentrations of soil pore water and site water were estimated by Inductively Coupled Plasma/Atomic Emission Spectroscopy. The similar ion compositions and concentrations obtained for soil pore water and site water proved that the adopted salinity assessment method was relevant. This was also confirmed by the results obtained on salt-amended soils with the measured salinities agreeing well with the target ones. Based on the obtained results, three approaches were proposed to determine the dissolved water salinity of salt-amended soils with decreasing salty water content. This allowed the dissolved soil salinity to be obtained according to the relationship between dissolved water salinity and dissolved soil salinity.

Keywords: salinity assessment; soil salinity; water salinity; dissolved salt; precipitated salt; electrical conductivity

[1]: Ecole des Ponts ParisTech, Laboratoire Navier/CERMES, 6 – 8 av. Blaise Pascal, Cité Descartes, Champs-sur-Marne, 77455 Marne-la-Vallée cedex 2, France
[2]: Université Paris Est, IFSTTAR/GERS/SRO, 14-20 boulevard Newton - Champs-sur-Marne, 77447 Marne-la-Vallée, France
[3]: Irstea, Unité de Recherche RECOVER / Equipe G2DR, 3275 route Cézanne, CS 40061, 13182 Aix En Provence Cedex 5, France

1. Introduction

From environmental and socio-economic points of view, it is recommended to build infrastructures using local soils. In coastal area, while dealing with constructions of dams, dikes etc., the local soils contain some salts, and it is important to investigate the effect of salinity on the thermo-hydro-mechanical behaviour of soils. Moreover, the soils in shallow depth of constructions usually interact with the atmosphere, leading to constant changes in their water content. Thus, some dissolved salt might precipitate or crystalize as water content decreases, and some precipitated salt present as solid particles can be dissolved again with increasing water content. Normally, only dissolved salt has an effect on soil thermo-hydro-mechanical behaviour, whereas the precipitated salt can be regarded as soil solids. Thus, it appears important to determine the quantity of dissolved salt of salted soils, especially for soils which undergo significant water content changes under the climatic effect, which are in general unsaturated.

There are several definitions of salt concentrations: mass concentration (percent composition, %), mass-volume concentration (grams per liter, g/L) or molar concentration (molarity, mol/L). In practice, salt concentration of soil pore water can be determined by measuring electrical conductivity of soil solution extracts separated from soil slurry which were prepared at 1:1 or 1:5 distilled water:soil dilution, or saturated soil paste (U.S. Salinity Laboratory Staff 1954; Rhoades 1981, 1982; Chi and Wang 2010; Hardie and Doyle 2012; Monteleone et al. 2016), or by the chemical composition analysis of soil solution extracts by Inductively Coupled Plasma/Atomic Emission Spectroscopy (ICP/AES) (McLaughlin et al. 1994; Stevens et al. 2003). Besides, salt mass of a certain amount of dry soils can be estimated from the mineral composition analysis that can determine the quantity of Halite, gypsum, blodite and thenardite (Aldabaa et al. 2015), as well as from the evaporation of soil solution extracts at 105°C (Magistad et al. 1945; Hardie and Doyle 2012; Song et al. 2017). As for the measurement of soil solution extracts, the salt cannot be extracted out completely by only one solution extraction, leading to underestimation of salt quantity. Meanwhile, the addition of water to prepare soil slurry resulted in dilution of salt present in soils and distorted the original salt concentration of soil pore water (ASTM D 4542-95 2001). ASTM D 4542-95 (2001) stated that natural soil pore water can be squeezed out with the aid of external pressure without adding water. However, with this procedure, it was often impossible to obtain enough soil pore water for accurate measurement, especially for soils at low water contents. Thus, it appeared that there was still an uncertainty for salinity assessment of soils, especially for soils with presence of both dissolved and precipitated salts.

The experiments aiming at investigating the salt concentration effect on soil behaviour were usually achieved by saturating soil samples by circulating salt solution through samples for fully replacing the pore water (Nguyen et al. 2013; Ye et al. 2014; Zhang et al. 2016a), or by immersing samples in salt solution at constant vertical stress (Di Maio 1996; Musso et al. 2003; Thyagaraj and Rao 2013; Ye et al. 2017), or by preparing salt-amended samples with desired volume and concentration of salt solution (Rao and Shivananda 2005; Thyagaraj and Rao 2010; Song et al. 2017). In these cases, salt concentration was regarded as constant during the experiments. Moreover, salt concentration was also considered as constant when the soil samples were dried to analyse the shrinkage behaviour (He et al. 2016; Mishra et al. 2019). In reality, salt concentration always increased with decreasing water content during water evaporation, and some salts could precipitate at low water contents. To avoid the change of salt concentration, Magistad et al. (1945) and Reitemeier (1946) proposed that ion concentration can be expressed on the oven-dried soil basis, in unit of equivalent per million (e.p.m.) which was identical to 1 m.e. per kilogram of soil. Similarly, salt content, as the mass ratio of salt to dry soil powder, was adopted to analyze the salt effect on soil shrinkage behavior during the drying process (Sun et al. 2013; Zhang et al. 2016b, 2017). From these studies, it can be found that whatever the salt concentration definitions, on the basis of either the salty water quantity or the salt content with respect to dry soil mass, they were always regarded as constant in the experiments mentioned above, without considering the salt precipitation that would occur at low water contents. Besides, Noorany (1984) and ASTM D4542-95 (2001) described the compositions of salted soils as soil solids, salt, water and gas, without distinguishing dissolved and precipitated salts.

This paper aimed at developing a method allowing assessment of the salinity of salted soils, which took into account the quantities of dissolved and precipitated salts. The description of salted soil compositions was first revised considering the presence of both dissolved and precipitated salts. To represent the water and dissolved salt content of salted soils, Noorany (1984) and ASTM D4542-95 (2001) recommended to use the definition (fluid content) of mass ratio of fluids to soil solids. However, this definition becomes confusing when dealing with unsaturated soils because in that case fluids refer to both water (liquid or vapour) and air. Thus, the term of fluid content was replaced by salty water content in this study. Based on the new description of salted soil compositions, the relationship between dissolved water salinity (r_d) referring to the ratio between dissolved salt mass and salty water mass and dissolved soil salinity (r_d') which was expressed as the mass ratio of dissolved salt to dry solid (dry soil and

precipitated salt) was established. Besides, the electrical conductivity (EC) variations with water salinity (r) of mixed salt solution were investigated. Soil solution extracts were obtained by several washings in centrifuge. After that, the water salinity and soil salinity were determined. The ion compositions and concentrations of natural soil pore water and site water were determined by Inductively Coupled Plasma/Atomic Emission Spectroscopy (ICP/AES). Two groups of salt-amended soil samples were prepared at dry and wet sides of optimum salty water content to verify the validity and accuracy of the adopted salinity assessment method. Further, the dissolved water salinity and dissolved soil salinity variations of salt-amended soils with decreasing salty water content were determined on the basis of EC-r relationship of mixed salt solution and also the relationship between dissolved water salinity and dissolved soil salinity.

2. Relationship between water salinity and soil salinity

To distinguish dissolved and precipitated salts, the well-known mass compositions for salted soils (Noorany 1984; ASTM D4542-95 2001) needed to be modified considering two salt phases, as shown in figure 1. The corresponding terms are listed in Table 1. Dissolved water salinity (r_d) which was the ratio of dissolved salt mass to salty water mass always changed with water quantity variations. Thus, dissolved soil salinity (r_d', in equation (1)), defined as the ratio of dissolved salt mass to dry solid mass, was also adopted. The total water salinity and the total soil salinity were obtained if all salts were regarded as dissolved salt without distinguishing dissolved and precipitated salts.

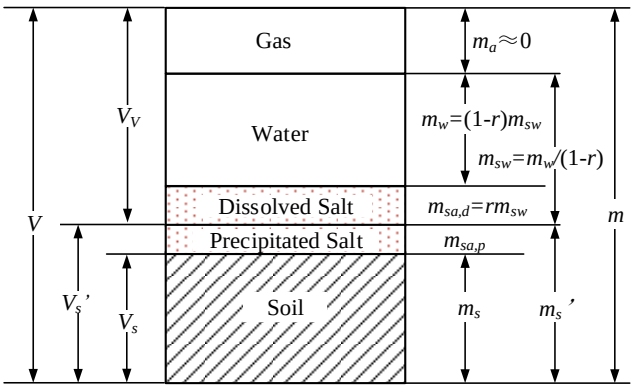

Figure 1. Mass compositions of salted soil.

Table 1. Terms used to describe salted soil.

Terms	Significance
m	Total wet soil mass (soil particles, salt and water)
m_s	Mass of dry soil particles
$m_{sa,d}$	Mass of dissolved salt
$m_{sa,p}$	Mass of precipitated salt
m_s'	Solid mass = $m_s + m_{sa,p}$
m_{sw}	Mass of salty water
m_w	Mass of pure water = $m_{sw} - m_{sa,d}$
m_d	Oven-dried mass (105 °C) = $m_s + m_{sa,d} + m_{sa,p} = m - m_w$
r_d	Dissolved water salinity = $m_{sa,d} / m_{sw}$
V	Total volume
V_s	Volume of soil particles
V_s'	Volume of solid
V_V	Volume of voids

$$r_d^{'} = \frac{m_{sa,d}}{m_s^{'}} = \frac{m_{sa,d}}{m_s + m_{sa,p}} \quad (‰ \text{ or g of dissolved salt/kg of dry solid}) \qquad (1)$$

When the dissolved soil salinity kept constant, there was no precipitated salt. Equation (1) became:

$$r_d^{'} = \frac{m_{sa,d}}{m_s} \quad (‰ \text{ or g of dissolved salt/kg of dry solid}) \qquad (2)$$

In turn, the dissolved water salinity (r_d) referred to the ratio of dissolved salt mass to salty water mass:

$$r_d = \frac{m_{sa,d}}{m_{sw}} = \frac{m_{sa,d}}{m_w + m_{sa,d}} \quad (‰ \text{ or g of dissolved salt/kg of salty water}) \qquad (3)$$

In equation (3), the unit 'kg' can be substituted by 'L' if the salty water density was taken equal to 1 in the case of low salt concentration. More globally, the dissolved water salinity (r_d) can be related to salt concentration (c) in g/L by equation (4):

$$r_d = \frac{1}{\rho_{sw}} c \qquad (4)$$

where ρ_{sw} was the density of salty water.

Consequently, the dissolved salt mass ($m_{sa,d}$) can be derived from equation (3):

$$m_{sa,d} = \frac{r_d m_w}{1 - r_d} \tag{5}$$

The salty water content (w') was expressed by equation (6):

$$w' = \frac{m_{sw}}{m_s'} = \frac{m_w + m_{sa,d}}{m_d - m_{sa,d}} \tag{6}$$

Substituting dissolved salt mass ($m_{sa,d}$) given by equation (5) into equation (6), the salty water content (w') of salted soils became:

$$w' = \frac{m - m_d}{m_d - r_d m} \tag{7}$$

Combining equations (3) and (6), the dissolved salt mass ($m_{sa,d}$) expressed by salty water content (w'), oven-dried mass (m_d) and dissolved water salinity (r_d) was derived:

$$m_{sa,d} = \frac{r_d w' m_d}{1 + r_d w'} \tag{8}$$

Thereby, the dry solid mass (m_s') containing soil and precipitated salt can be obtained:

$$m_s' = m_d - m_{sa,d} = \frac{m_d}{1 + r_d w'} \tag{9}$$

Substituting the dissolved salt mass ($m_{sa,d}$) and the dry solid mass (m_s') from equations (8) and (9) into equation (1), the relationship between dissolved water salinity (r_d) and dissolved soil salinity (r_d') was established in equation (10):

$$r_d' = r_d w' = r_d \frac{m - m_d}{m_d - r_d m} \tag{10}$$

This relationship can be also applied to the total water salinity and the corresponding total soil salinity without distinguishing dissolved and precipitated salts.

3. Materials and methods

3.1 Tested materials

Natural soil was taken at the site of Salin-de-Giraud, France. Its geotechnical properties are presented in Table 2. The grain size distribution determined by the dry sieving method (NF P 94-056 1996) and by the hydrometer method (NF P 94-057 1992) is shown in figure 2. This soil had 81% fine-fraction (< 80 μm) and 17% clay size fraction (< 2 μm). According to French/European standard NF P 11-300 (1992), this soil belonged to category A1, corresponding to a clayey soil of low plasticity (CL) on the basis of Unified Soil Classification System (ASTM D2487-00 2000). The main minerals in soil determined by X-ray diffraction coupled with Rietveld analysis were quartz (39%), calcite (35%), illite (10.8%), feldspar (9.5%), chlorite (3.6%), kaolinite (1.3%) and NaCl crystallized on halite form (0.8%). The presence of crystallized halite in soil was in agreement with the ion compositions of sodium and chloridion in near sea site water (Table 3). The salt concentration of site water was estimated at 10.5 g/L by summarising the ion concentrations determined from chemical analysis by Inductively Coupled Plasma/Atomic Emission Spectroscopy (ICP/AES). The main ion species were Cl^-, Na^+, Ca^{2+}, K^+ and Mg^{2+}, the same as for the synthetic sea water (NF P 18-837 1993) (Table 4). Thus, for practical reasons, the five main salts of synthetic sea water were used in this study.

Table 2. Geotechnical properties of the tested soil.

Property	Value
Specific gravity, G_s	2.71
Liquid limit, w_L (%)	28.9
Plastic limit, w_p (%)	18.8
Plasticity Index, I_p	10.1
Optimum salty water content (%)	17.3
Maximum dry density (Mg/m^3)	1.68

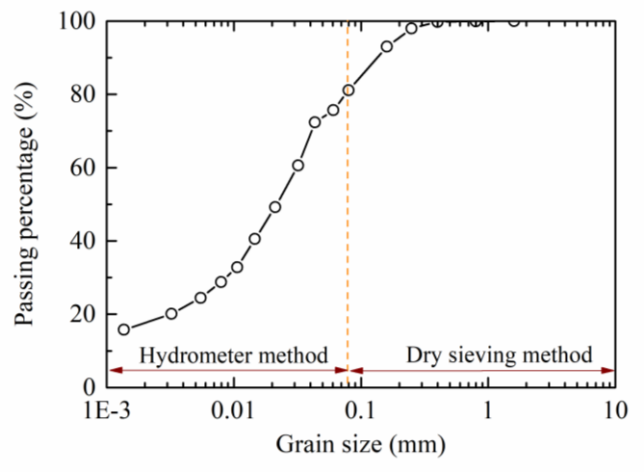

Figure 2. Grain size distribution of natural soil.

Table 3. Chemical compositions of site water.

Solution	Chemical compositions (mg/L) ICP/AES method					Salt concentration, *c* (g/L)
	Cl	Na	Ca	K	Mg	
Site water	6480	3358	173	95	367	10.5

Table 4. Chemical compositions of synthetic sea water (NF P 18-837 1993).

Salts	NaCI	$MgCI_2 \cdot 6H_2O$	$MgSO_4 \cdot 7H_2O$	$CaSO_4 \cdot 2H_2O$	$KHCO_3$
Salt concentration (g/L)	30.0	6.0	5.0	1.5	0.2
Percentage (%)	70.26	14.05	11.71	3.51	0.47

3.2 Methodological approach adopted for salinity assessment

3.2.1 Relationship between electrical conductivity (EC) and water salinity (r)

The relationship between electrical conductivity and NaCl concentration was commonly used to transform the measured electrical conductivity of soil pore water extracts to total dissolved salt concentration (Rao and Shivananda 2005; Rao and Thyagaraj 2007a, 2007b). The evolution of the measured electrical conductivity with different water salinities of NaCl solution is presented in figure 3. Its curve can be expressed by equation (11):

$$EC = -0.0027r^2 + 1.6656r + 0.3822 \quad (11)$$

In addition to sodium chloride, other salts co-existed in soil pore water, as evidenced by the site water analysis (Table 3). As the electrical conductivity of mixed salt solutions was different

from the single NaCl solution at the same concentration (Smith and Gortner 1933), five different salts, corresponding to the chemical compositions of synthetic sea water (Table 4) were used for preparing the mixed salt solutions. This was performed by keeping the same proportion for each salt as for the synthetic sea water. The electrical conductivity of mixed salt solution was measured directly by conductivity meter. As the solubility was different for different salts, for the mixed salt solution, one electrical conductivity value corresponded to two water salinities when there were salt precipitations, namely total water salinity and dissolved water salinity. In this study, the masses of additive salt and additive deionized water were used to calculate the total water salinity directly. Note that the additive salt mass used for the total water salinity calculation was subtracted by the hydrated water mass (i.e. 7 moles of water molecule are hydrated for 1 mole of $MgSO_4 \cdot 7H_2O$ salt, as shown in Table 4). The dissolved water salinity was determined in two different ways. The first was to transform the measured electrical conductivity of mixed salt solution to dissolved water salinity according to the EC-*r* relationship of NaCl solution, expressed in figure 3 and equation (11). The second was to filter the mixed salt solution at different concentrations using a 0.45 μm filter paper to separate dissolved salt solution and precipitated salt (Walton 1989). The collected filtered salt solution and precipitated salt were first oven-dried at 105 ℃ to remove out the free water and some hydrated water, then further oven-dried at 180 ℃ to fully eliminate the remaining hydrated water (Walton 1989). The dissolved water salinity was determined by the masses of oven-dried dissolved salt and additive deionized water. Finally, the relationships between electrical conductivity and total water salinity, as well as dissolved water salinity were established for the mixed salt solution.

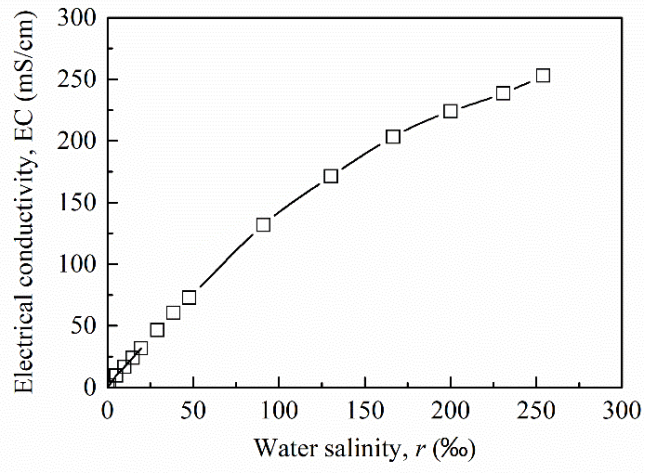

Figure 3. Electrical conductivity variations with water salinity of NaCl solution.

3.2.2 Water salinity (r) and soil salinity (r') measurement

The determination of water salinity (r) and soil salinity (r') required the estimation of total salt mass firstly. The method adopted to estimate the total salt mass in soil consisted in extracting salt from soil by repeated washing steps with pure water through centrifugation, then to measure the electrical conductivity of the collected soil solution extracts. For the soil with a natural salty water content, the measured total salt mass corresponded to the dissolved salt only or the sum of dissolved and precipitated salts.

The test procedure for salinity measurement is shown in figure 4. Two samples of initial wet soil with similar weight were prepared. The first one was oven-dried at 105°C to determine the soil pore water mass (m_w) and the oven-dried mass (m_d), while the second one was immerged in pure water (18Mohm) until it reached a slurry state. The slurry was then shaken for 1 h and centrifuged at 10,000 rpm for 10 min to separate water from soil. After centrifugation, the soil solution extracts were collected and their electrical conductivity was measured. The remaining soil was put again in contact with pure water and the previous operations were repeated, until the electrical conductivity of last collected soil solution extracts was less than 500 μS/cm. This electrical conductivity value corresponded to a water salinity of 0.2‰ (or g of dissolved salt/kg of salty water) that can be considered as negligible. The centrifugation process for soil solution extracts was lengthened until 30 min and the speed was increased to 19,000 rpm if some soil colloids remained in extracts. At the end, the remaining soil and colloid were oven-dried at 105°C to determine the dry soil mass (m_s). The weight and the electrical conductivity of all soil solution extracts were then determined. The electrical conductivity was transformed to water salinity of soil solution extracts. Then, the salt mass (m_{sa}) was calculated according to the water salinity and the mass of collected extracts. The water salinity (r) of soil at natural salty water content state was determined by the masses of salt (m_{sa}) and pure water (m_w). The soil salinity (r') was obtained by the masses of salt (m_{sa}) and oven-dried soil (m_s) after centrifugation. Note that the pure water mass obtained by the oven-drying was used to calculate the water salinity of soil pore water rather than using the mass of collected extracts to avoid the dilution effect with water addition. Besides, the chemical compositions and ion concentrations of soil solution extracts were determined by Inductively Coupled Plasma/Atomic Emission Spectroscopy (ICP/AES). The ion concentrations of soil solution extracts were transformed to ion concentrations of soil pore water according to the dilution ratio which was the mass ratio of pure water to soil solution extracts. The initial salinity of natural soils was determined firstly according to the procedure above.

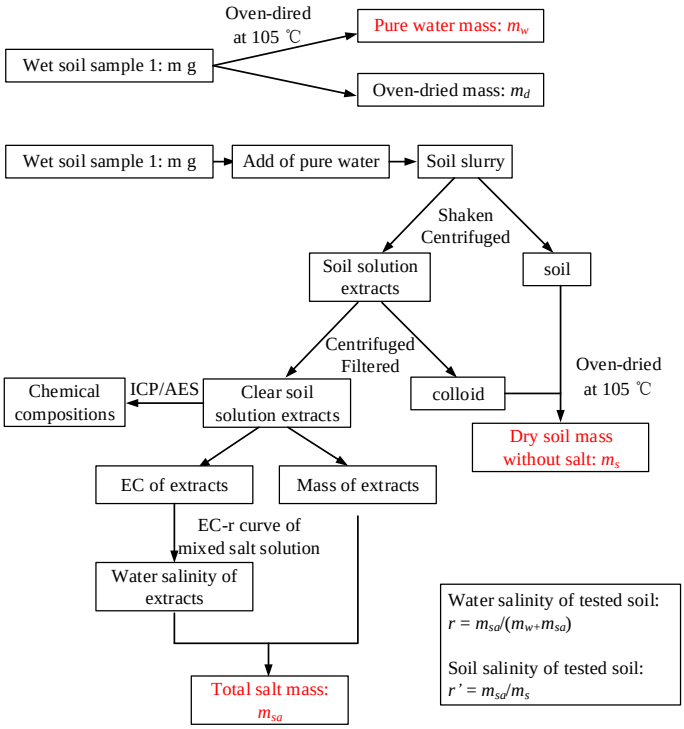

Figure 4. Test procedure of salinity measurement.

3.2.3 Preparation of salt-amended soils

Salt-amended soils with target salinity were prepared to verify the validity and accuracy of the adopted salinity assessment method. The procedure of spraying salt solution on soils was adopted to prepare salt-amended soils to target salinity which was higher than the initial salinity.

If soil did not contain any salt initially, the additive salt mass and water mass were determined easily according to the target soil salinity and water salinity. However, the tested soil in this study had initial salt inside, thus the additive salt mass and water mass to reach the desired salinity and the salty water content required to be calculated. The total additive salt mass was proportioned to each salt mass according to the proportions of the five different salts in synthetic sea water (Table 4).

Air-dried natural soils were used to prepare salt-amended soils in order to add enough quantity of deionized water allowing a complete dissolution of additive salt to reach the desired salty water content and salinity. A small quantity of air-dried soils were oven-dried at 105°C to determine the salty water content. Assuming that all salts were dissolved in soil pore water, the water salinity of air-dried soils was obtained using equation (12) which was derived by combining equations (7) and (10):

$$r = \frac{r' m_d}{m - m_d + r' m} \tag{12}$$

In equation (12), the soil salinity (r') of air-dried soils was the measured soil salinity of natural soils. Knowing the initial water salinity of air-dried soils, the initial salty water content can be determined by equation (7). According to the initial water salinity (r_0), initial soil salinity (r_0'), initial salty water content (w_0') of air-dried soils and target water salinity (r_t), target salty water content (w_t') of salt-amended soils, the additive salt mass and additive water mass could be calculated as follows.

To prepare salt-amended soils from a quantity (m) of air-dried soils, the solid mass (m_d) including dry soils and salt was derived from equation (7).

$$m_d = \frac{m\left(1+w_0' r_0\right)}{1+w_0'} \tag{13}$$

Thus, the water mass (m_w) was given by:

$$m_w = m - m_d \tag{14}$$

Using equation (5), the dissolved salt mass ($m_{sa,d}$) present in air-dried soils was obtained:

$$m_{sa,d} = \frac{r_0 m_w}{1 - r_0} \tag{15}$$

Assuming that salts dissolved fully in soil pore water, the dry soil mass (m_s) was calculated as:

$$m_s = m_d - m_{sa,d} \tag{16}$$

The water salinity (r_1) of air-dried soils at target salty water content was derived using equation (17). In this process, only water quantity increased, whereas the soil mass and salt mass were kept constant. Thus, the soil salinity remained unchanged.

$$r_1 = \frac{r_0'}{w_t'} \tag{17}$$

The water salinity (r_1) can be written as:

$$r_1 = \frac{m_{sa,d}}{m_w + m_{sa,d} + \Delta m_w} \tag{18}$$

Thus, the additive water mass (Δm_w) to reach target salty water content was obtained:

$$\Delta m_w = \frac{m_{sa,d}}{r_1} - m_w - m_{sa,d} \tag{19}$$

From the definition of water salinity, the target water salinity (r_t) was given by equation (20):

$$r_t = \frac{m_{sa,d} + \Delta m_{sa}}{m_w + \Delta m_w + m_{sa,d} + \Delta m_{sa}} \tag{20}$$

Then, the additive salt mass (Δm_{sa}) to reach the target salinity was obtained:

$$\Delta m_{sa} = \frac{r_t \left(m_w + \Delta m_w + m_{sa,d} \right) - m_{sa,d}}{1 - r_t} \tag{21}$$

Note that the real salty water content ($w_r^{'}$) of salt-amended soils needed to be calibrated by equation (22):

$$w_r^{'} = \frac{m_w + \Delta m_w + m_{sa,d} + \Delta m_{sa}}{m_s} \tag{22}$$

The soil salinity at target state can be derived using equation (23):

$$r_t^{'} = \frac{m_{sa,d} + \Delta m_{sa}}{m_s} = r_t w_r^{'} \tag{23}$$

The salt-amended samples were prepared at two salty water contents, dry side (w_t' = 15.2 %) and wet side (w_t' = 19.1 %) of optimum, respectively. The target water salinity of wet sample was fixed at r = 32.38‰ (or g of dissolved salt/kg of salty water) which corresponded to the water salinity of synthetic sea water and to a soil salinity of 6.32‰ (or g of dissolved salt/kg of dry solid). For the sample prepared on dry side, the soil salinity was kept the same as that of wet side (i.e. 6.32‰), whereas the water salinity varied from 32.38‰ to 40.29‰ (or g of dissolved salt/kg of salty water). Note that the soil salinity for both prepared samples and the water salinity for the sample prepared on dry side needed to be calculated step by step following equation (12) to equation (23).

The mixed salt solution prepared by additive salt and additive deionized water was sprayed to air-dried soils layer by layer. The salt-amended soils were divided into two parts. One part was used to verify the salinity after 24 h conservation and the second part was sealed and to be used

to verify the salinity after 20-day conservation following the salinity measurement procedure.

4. Results and discussions

4.1 Relationships between electrical conductivity (EC) and water salinity (r)

Figure 5 shows the changes of electrical conductivity (EC) with total water salinity (*r*) of NaCl solution and mixed salt solution. It can be observed that the EC-*r* curve of mixed salt solution coincided well with that of NaCl solution when the total water salinity was lower than 40‰ (or g of dissolved salt/kg of salty water). However, above this value, the EC-*r* curve of mixed salt solution deviated and was located below the EC-*r* curve of NaCl solution. The deviation of the EC-*r* curve of mixed salt solution can be attributed to the presence of the precipitated salt in the mixed salt solution. The total water salinity of the mixed salt solution was the sum of both dissolved and precipitated salinities; but the electrical conductivity reflected only the dissolved ions mobility (Kwak and Hayes 1975; Wu and Berezansky 1995; Golnabi et al. 2009). Thus, the electrical conductivity of the mixed salt solution was lower than that of NaCl solution due to the partial dissolution of mixed salts, even though the total water salinities of the mixed salt solution and NaCl solution were the same.

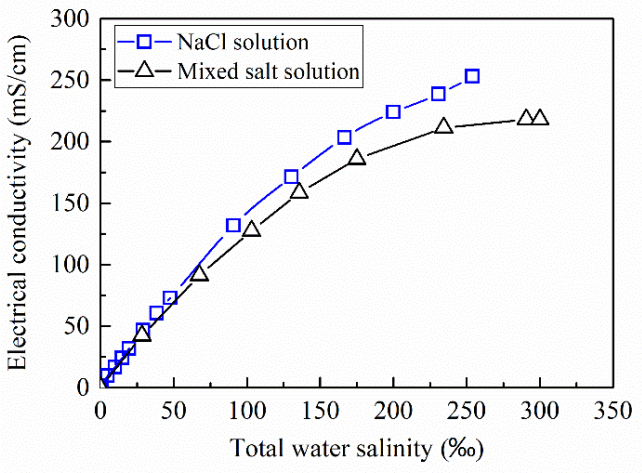

Figure 5. Relationship between electrical conductivity and total water salinity of NaCl solution and mixed salt solution.

The electrical conductivity variations with water salinity (total water salinity and dissolved water salinity) of the mixed salt solution are shown in figure 6. Note that the dissolved water salinity was transformed from the EC-*r* relationship of NaCl solution in figure 6A and it was calculated directly from the masses of oven-dried dissolved salt and salty water in figure 6B. Each curve corresponds to a formula in Table 5. It was observed that the dissolved water salinity

calculated by oven-dried dissolved salt mass and salty water mass was different from that transformed from NaCl solution. In figure 6A, a critical point (r_d = 34‰ or g of dissolved salt/kg of salty water, EC = 52 mS/cm) from where the dissolved water salinity curve deviated from the total water salinity curve was noticed. This was related to the first appearance of precipitated salt in the mixed salt solution. In figure 6B, the critical point on the dissolved water salinity curve was not easy to be distinguished compared to that in figure 6A. It was taken here as point (r_d = 76‰ or g of dissolved salt/kg of salty water, EC = 100 mS/cm), according to the first occurrence of precipitated salt on 0.45 μm filter paper.

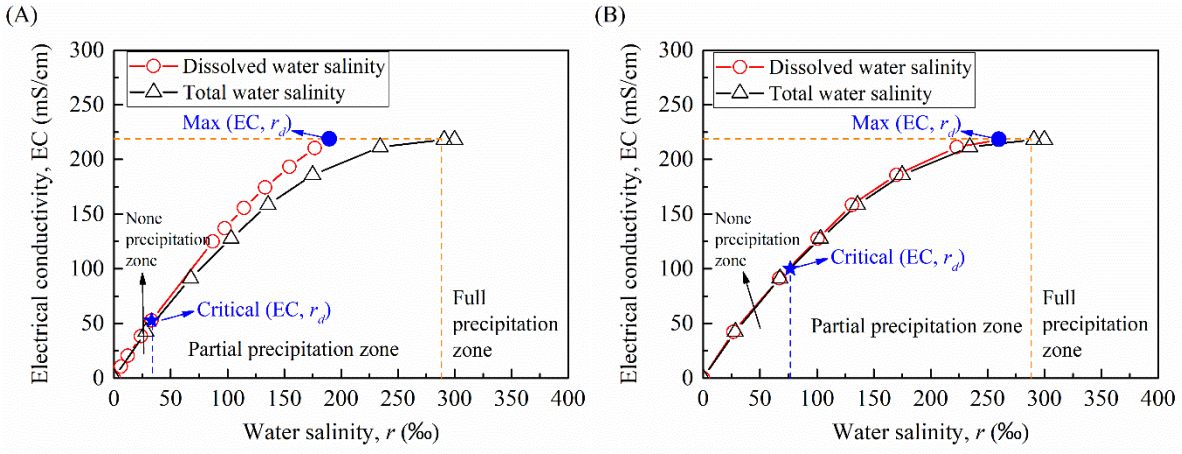

Figure 6. Electrical conductivity variations with water salinity of mixed salt solution: (A) dissolved water salinity is transformed from EC-*r* curve of NaCl solution; (B) dissolved water salinity is the mass ratio of oven-dried dissolved salt to salty water.

Table 5. Relationship between electrical conductivity and water salinity of mixed salt solution.

Curve	Equation	No.
EC versus total water salinity	$EC = -0.0027r^2 + 1.5228r + 0.4093$	(24)
EC versus dissolved water salinity transformed from EC-*r* curve of NaCl solution	$EC = -0.003r^2 + 1.7091r - 0.2284$	(25)
EC versus dissolved water salinity calculated from masses of oven-dried dissolved salt and salty water	$EC = -0.0028r^2 + 1.5573r + 0.6785$	(26)

From the critical point and the end point of EC-*r* curves, a none precipitation zone, partial precipitation zone and full precipitation zone of the mixed salt solution can be defined, as shown in figure 6. wgTherefore, the electrical conductivity reached a maximum value ($r_{d,max}$ = 260‰ or g of dissolved salt/kg of salty water, EC_{max} = 219 mS/cm) and then kept constant. For the none or partial precipitation zone, the relationship between the dissolved soil salinity and the

dissolved water salinity can be expressed by equation (10). For the full precipitation zone, the dissolved water salinity (r_d) should be substituted by the maximum dissolved water salinity ($r_{d,max}$). Finally, the relationships between the dissolved water salinity and the dissolved soil salinity were obtained in all zones, as follows:

$$r_d^{'} = \begin{cases} r_d w^{'} = r_d \dfrac{m - m_d}{m_d - r_d m} & \text{None-partial precipitation zone} \\ r_{d,\max} w^{'} = r_{d,\max} \dfrac{m - m_d}{m_d - r_{d,\max} m} & \text{Full precipitation zone} \end{cases} \tag{27}$$

As shown by figure 7, the dissolved salt mass obtained directly from oven-dried method was higher than the dissolved salt mass transformed from EC-*r* curve of NaCl solution. This explained the observations made on figure 6, suggesting that at the same electrical conductivity, the dissolved water salinity obtained directly from oven-dried salt mass was larger than the dissolved water salinity transformed from EC-*r* curve of NaCl solution. In addition, the transformed total salt mass from EC-*r* curve of NaCl was much lower than the total additive salt mass minus hydrated waters (fig. 7A), whereas the total salt mass which was the sum of the oven-dried dissolved salt mass and the precipitated salt mass was close to the total additive salt mass minus hydrated waters (fig. 7B). This suggested that the determination of salt quantity of the mixed salt solution from EC-*r* curve of NaCl solution led to underestimation. Therefore, even though the underestimation was not significant in figure 7B, to be accurate, the dissolved water salinity for the mixed salt solution should be determined directly from oven-dried dissolved salt mass rather than transforming from EC-*r* curve of NaCl solution. Consequently, the water salinity of soil pore water can be determined precisely by transforming its measured electrical conductivity to water salinity using EC-*r* relationship of mixed salt solution.

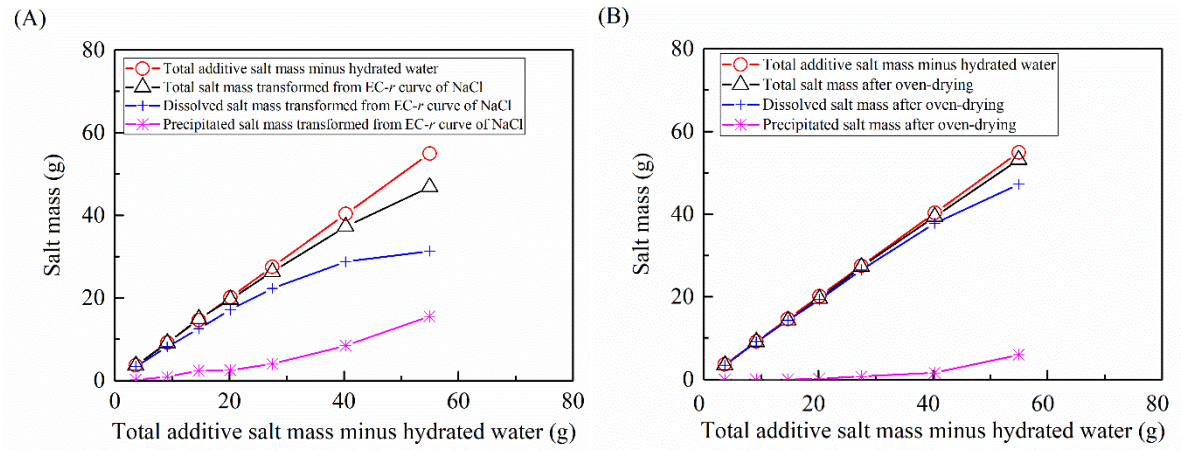

Figure 7. Comparisons of salt mass for different phases: (A) salt mass is transformed from EC-*r* curve of NaCl solution; (B) salt mass is obtained directly by oven-drying.

4.2 Salinity measurement on natural soils and salt-amended soils

As mentioned before, the natural soils were taken from costal area, containing a certain amount of salt inside. The salinity measurement results on two replicated natural soils are presented in Table 6. It can be observed that the obtained salinities of soil 1 and soil 2 were rather close, showing a good repeatability of the results. The difference, which was negligible, between the oven-dried mass (m_d) determined by oven-drying at 105 ℃ and the total mass of dry soil (m_s) and salt (m_{sa}) obtained after centrifugation was only about 0.5 ~ 0.7 g. This can be attributed to the possible loss of soil particles during the centrifugation process. The average water salinity and soil salinity were about 13.3‰ (or g of dissolved salt/kg of salty water) and 2.1‰ (or g of dissolved salt/kg of dry solid), respectively. The ion compositions and concentrations of natural soil pore water and site water are shown in Table 7. The similar ion compositions and fairly equal salt concentrations of natural soil pore water and site water indicated that the adopted salinity assessment method can provide good salinity estimation.

Table 6. Salinity of natural soil.

Natural soil	Wet soil mass, m (g)	Water mass, m_w (g)	Oven-dried mass, m_d (g)	Dry soil mass without salt, m_s (g)	Salt mass, m_{sa} (mg)	Water salinity, r (‰)	Soil salinity, r' (‰)	Average water salinity (‰)	Average soil salinity (‰)
Soil 1	259.1	34.5	224.5	223.5	468.5	13.40	2.10	13.3	2.1
Sois 2	259.9	34.6	225.4	224.3	463.1	13.21	2.06		

Table 7. Chemical compositions of site water and natural soil pore water.

Solutions	Chemical composition (mg/L) – ICP/AES method								c (g/L)	
	Cl	Na	Ca	K	Mg	Fe	Al	Si	c (sum of ICP)	c (derived from EC)
Site water	6480	3358	173	95	367	/	/	/	10.5	12.3
Natural soil pore water	7521	5096	215	225	176	18	7	39	13.3	13.8

To further verify the adopted salinity assessment method, the salinities of salt-amended soils were measured. The salinity verification results are shown in Table 8. Sample 1-1 and sample 1-2 were prepared on dry side (w_t' = 15.2%) and sample 2-1, 2-2 were prepared on wet side (w_t' = 19.1%). The relative error of soil salinity was defined as the difference between the target soil salinity and the measured soil salinity divided by target soil salinity. The relative errors of

soil salinity of sample 1-1 (w_t' = 15.2%) and sample 2-1 (w_t' = 19.1%) tested after 24 h conservation were respectively 4.75% and 6.96%, while the relative errors of samples after 20-day conservation were respectively 4.75% and 0.16%. Comparison of measured salt mass between sample 2-1 and sample 2-2 showed that only 0.1 g difference could make 7% relative error. This acceptable difference can be attributed to the accuracy of total salt mass determination due to partial salt still remaining in soil after several washings or little loss of soil solution extracts. On the whole, the relative errors were acceptable, suggesting that the adopted salinity assessment could lead to reliable salinity measurement. The similar results between the measurements after 24 h and after 20 days showed that the salt content became homogeneous after 24 h conservation.

Note that the measured water salinities of natural soils and salt-amended soils were both much lower than the critical dissolved water salinity (76‰ or g of dissolved salt/kg of salty water). In that case, salt dissolved completely in soil pore water and the measured total salinity corresponded to dissolved salinity.

Table 8. Salinity verification of salt-amended soil.

Sample condition	Sample	Target w_t' (%)	Measured w' (%)	Measured salt mass, m_{sa} (g)	Water salinity, r (‰)		Soil salinity, r' (‰)		Relative error, $\delta = (r_t' - r_m')/r_t'$ (%)
					Measured value, r_m	Target value, r_t	Measured value, r_m'	Target value, r_t'	
Salinity verification after 24 h	Sample 1-1	15.2	16.00	1.3283	37.61	40.29	6.02	6.32	4.75
	Sample 2-1	19.1	19.82	1.2694	29.65	32.38	5.88	6.32	6.96
Salinity verification after 20 days	Sample 1-2	15.2	15.70	1.3298	38.33	40.29	6.02	6.32	4.75
	Sample 2-2	19.1	19.69	1.3657	32.03	32.38	6.31	6.32	0.16

4.3 Determination of dissolved water salinity and dissolved soil salinity during soil drying

As mentioned previously, all salts dissolved in salt-amended soil pore water when the water salinity was lower than the critical dissolved water salinity (76‰ or g of dissolved salt/kg of salty water). However, some salt may precipitate with water loss, for instance during soil drying by water evaporation. To avoid the water salinity measurement of soil at each salty water

content with a known total soil salinity, dissolved water salinity and dissolved soil salinity were determined by combining the EC-*r* relationship of the mixed salt solution (Fig. 6B; equations (24) and (26))and the relationship between water salinity and soil salinity (equation (27)). Firstly, a small amount of soil was oven-dried at 105 ℃ to determine the quantity of water and solid. Afterwards, the total water salinity of soil pore water was obtained by equation (12). Then, the following three approaches were considered to determine the dissolved water salinity for the salt-amended soils with decreasing salty water content:

(i) If the calculated total water salinity was lower than the critical water salinity ($r_{total} < r_{critical}$), as the point of (r, EC) was located in the none precipitation zone, the calculated total water salinity was the dissolved water salinity.

(ii) If the calculated total water salinity was larger than the maximum dissolved water salinity ($r_{total} > r_{d,max}$) and the corresponding EC value was equal to the maximum EC value (EC = EC_{max}), the point of (r, EC) was located in the full precipitation zone; thus, the dissolved water salinity was equal to the maximum dissolved water salinity.

(iii) If the calculated total water salinity was larger than the critical water salinity but lower than the maximum dissolved water salinity ($r_{critical} < r_{total} < r_{d,max}$), it was in the partial precipitation zone: the total water salinity and dissolved water salinity corresponded to the same electrical conductivity. Thus, the electrical conductivity was obtained by substituting the calculated total water salinity into equation (24), subsequently, the corresponding dissolved water salinity was calculated out by equation (26).

The dissolved soil salinity was equivalent to the total soil salinity when the total water salinity was lower than the critical water salinity ($r_{total} < r_{critical}$). Otherwise, the dissolved soil salinity was determined by equation (27) on the basis of known dissolved water salinity (obtained by the three approaches above) and salty water content (calculated by equation (7)). Similarly, if the measured water salinity of natural soils or salt-amended soils was larger than the critical water salinity, the dissolved water salinity and the dissolved soil salinity were also determined following the same procedure.

The variations of water salinity and soil salinity with salty water content are plotted in figure 8. From the definitions of total water salinity and total soil salinity, it can be noticed that the total water salinity increased with decreasing salty water content (Fig. 8A), and the total soil salinity

kept constant at any salty water content (Fig. 8B). As far as the dissolved water salinity and the dissolved soil salinity variations were concerned, they were more complex than the variations of total salinity. The dissolved water salinity increased with decreasing salty water content when the dissolved water salinity was lower than the maximum dissolved water salinity (260‰ or g of dissolved salt /kg of salty water). Then, it kept the maximum value with further decreasing salty water content (Fig. 8A). The dissolved soil salinity kept constant when the dissolved water salinity was lower than the critical dissolved water salinity (76‰ or g of dissolved salt /kg of salty water). Then, it decreased with the decrease of salty water content. This can be explained by the solubility of the mixed salts. All salts dissolved in solution when the dissolved water salinity was lower than the critical dissolved water salinity. Thus, the dissolved soil salinity kept constant and the dissolved water salinity increased with the decrease of water quantity. The sparingly soluble salt with low solubility precipitated gradually when the dissolved water salinity was larger than the critical dissolved water salinity. Thus, the dissolved soil salinity decreased with decreasing salty water content. All salts reached the solubility with further decreasing salty water content and the mixed salt solution kept saturated state; as a result, the dissolved water salinity reached the maximum value and the dissolved soil salinity decreased rapidly. The measured average water salinity and the soil salinity of salt-amended soils prepared on dry and wet sides of optimum are also presented in figure 8. It appeared that the measured water salinity and the soil salinity were consistent with the calculated salinities, justifying the proposed measurement and calculation methods.

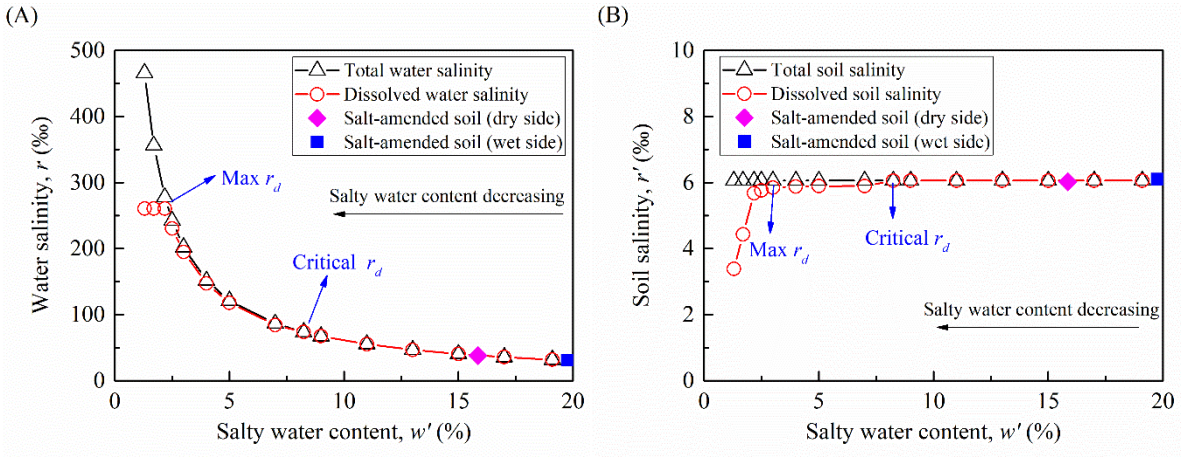

Figure 8. Variations of salinity with the decrease of salty water content: (A) water salinity; (B) soil salinity.

5. Conclusions

This study focused on the determination of dissolved salt quantity for salted soils. To achieve

this goal, the description of salted soil compositions was first revised, taking dissolved and precipitated salts into account. On the basis of this description, the relationship between dissolved water salinity and dissolved soil salinity was established. The electrical conductivity variations with water salinity of mixed salt solution were then investigated. The dissolved water salinity of mixed salt solution was obtained by transforming its electrical conductivity to water salinity using the EC-*r* relationship of NaCl solution on one hand, and by the masses of oven-dried dissolved salt and additive water on the other hand. Results showed that the transformation from NaCl solution underestimated the quantity of dissolved salt even though the main component of the mixed salt solution was sodium chloride. Thus, the dissolved water salinity of mixed salt solution should be determined directly from oven-dried dissolved salt mass rather than transforming from EC-*r* curve of NaCl solution.

In the salinity assessment for salted soils, the relationship between electrical conductivity and water salinity of mixed salt solution was used to transform the measured electrical conductivity to salt quantity of soil pore water. The soil salinity and water salinity were determined on the basis of all salts and soil separated in centrifuge and certain quantity of soil pore water. The similar ion compositions and concentrations for soil pore water and site water indicated that the adopted salinity assessment method could provide accurate measurement. Besides, this was also verified by the salinity measurement of two groups of salt-amended soils: the measured salinities agreed well with the target salinities.

Three approaches were proposed to determine the dissolved water salinity and dissolved soil salinity of salt-amended soils with decreasing salty water content by combining the EC-*r* relationship of mixed salt solution and the relationship between dissolved water salinity and dissolved soil salinity. Results showed that the measured salinities of salt-amended soils coincided well with the calculated values.

Using the proposed method, the dissolved water salinity and the dissolved soil salinity at any salty water content can be determined for a soil with a certain amount of salt, on the basis of the relationship between electrical conductivity and water salinity of mixed salt solution and the relationship between water salinity and soil salinity.

Acknowledgements

The authors wish to acknowledge the support from ENPC and IRSTEA. The support from

China Scholarship Council (CSC) is also gratefully acknowledged.

References

ASTM International. 2000. Standard Practice for Classification of Soils for Engineering Purposes (Unified Soil Classification System). ASTM D2487-00 (2000). West Conshohocken, PA: ASTM International, approved March 10, 2000. https://doi: 10.1520/D2487-00

ASTM International. 2001. Standard Test Method for Pore Water Extraction and Determination of the Soluble Salt Content of Soils by Refractometer. ASTM D4542-95 (2001). West Conshohocken, PA: ASTM International, reapproved, 2001. https://doi: 10.1520/D4542-95

Aldabaa, A. A. A., D. C. Weindorf, S. Chakraborty, A. Sharma, and B. Li. 2015. "Combination of proximal and remote sensing methods for rapid soil salinity quantification". *Geoderma* 239-240 (February): 34-46. https://doi.org/10.1016/j.geoderma.2014.09.011

Chi, C. M. and Z. C. Wang. 2010. "Characterizing salt-affected soils of Songnen Plain using saturated paste and 1: 5 soil-to-water extraction methods." *Arid Land Res Manag* 24, no. 1 (January): 1-11. https://doi.org/10.1080/15324980903439362

Di Maio, C. 1996. "Exposure of bentonite to salt solution: osmotic and mechanical effects." *Géotechnique* 46, no. 4 (December): 695-707. https://doi.org/10.1680/geot.1996.46.4.695

Golnabi, H., M. R. Matloob, M. Bahar, and M. Sharifian. 2009. "Investigation of electrical conductivity of different water liquids and electrolyte solutions." *Iran Phys J* 3, no. 2 (September): 24-28.

Hardie, M. and R. Doyle. 2012. "Measuring soil salinity." *In Plant Salt Tolerance*. Humana Press, Totowa, NJ: 415-425. https://doi.org/10.1007/978-1-61779-986-0_28

He, Y., W. M. Ye, Y. G. Chen, B. Chen, B. Ye, and Y. J. Cui. 2016. "Influence of pore fluid concentration on water retention properties of compacted GMZ01 bentonite." *Appl Clay Sci* 129 (August): 131-141. https://doi.org/10.1016/j.clay.2016.05.020

Kwak, Jan C. T. and R. C. Hayes. 1975. "Electrical conductivity of aqueous solutions of salts of polystyrenesulfonic acid with univalent and divalent counterions." *J Phys Chem* 79, no. 3 (January): 265-269. https://doi.org/10.1021/j100570a014

Magistad, O. C., R. F. Reitemeier, and L. V. Wilcox. 1945. "Determination of soluble salts in soils." *Soil Sci* 59, no. 1 (January): 65-76.

McLaughlin, M, J., L. T. Palmer, K. G. Tiller, T. A. Beech, and M. K. Smart. 1994. "Increased soil salinity causes elevated cadmium concentrations in field-grown potato tubers." *J Environ Qual* 23, no. 5 (September): 1013-1018. doi:10.2134/jeq1994.00472425002300

050023x

Mishra, P. N., A. Scheuermann, T. Bore, and L. Li. 2019. "Salinity effects on soil shrinkage characteristic curves of fine-grained geomaterials." *J Rock Mech Geotech Eng* 11, no. 1 (February): 181-191. https://doi.org/10.1016/j.jrmge.2018.06.008

Monteleone, M., G. Lacolla, G. Caranfa, and G. Cucci. 2016. "Indirect measurement of electrical conductivity and exchangeable cations on soil water extracts: Assessing the

precision of the estimates." *Soil Sci* 181, no. 9/10 (September/October): 465-471. doi: 10.1097/SS.0000000000000181

Musso, G., E. R. Morales, A. Gens, and E. Castellanos. 2003. "The role of structure in the chemically induced deformations of FEBEX bentonite." *Appl Clay Sci* 23, no. 1-4 (August): 229-237. https://doi.org/10.1016/S0169-1317(03)00107-8

NF P 11-300, 1992. Standard for classification of materials for use in the construction of embankments and capping layers of road infrastructures.

NF P 18-837, 1993. Standard for special products for hydraulic concrete construction-Hydraulic binder based needling and/or sealing products-Testing of resistance against seawater and/or water with high sulphate contents.

NF P 94-056, 1996. Standard Test for Soils Investigation and Testing-Granulometric Analysis-Dry Sieving method after Washing.

NF P 94-057, 1992. Standard Test for Soils Investigation and Testing-Granulometric Analysis-Hydrometer method.

Nguyen, X. P., Y. J. Cui, A. M. Tang, Y. F. Deng, X. L. Li, and L. Wouters. 2013. "Effects of pore water chemical composition on the hydro-mechanical behavior of natural stiff clays." *Eng Geol* 166, no. 8 (November): 52-64. https://doi.org/10.1016/j.enggeo.2013.08.009

Noorany, I. 1984. Phase relations in marine soils. *J Geotech Eng* 110, no. 4 (April): 539-543. https://doi.org/10.1061/(ASCE)0733-9410(1984)110:4(539)

Rao, S. M. and P. Shivananda. 2005. "Role of osmotic suction in swelling of salt-amended clays." *Can Geotech J* 42, no. 1 (March): 307-315. https://doi.org/10.1139/t04-086

Rao, S. M. and T. Thyagaraj. 2007a. "Role of direction of salt migration on the swelling behaviour of compacted clays." *Appl Clay Sci* 38, no. 1/2 (December): 113-129. https://doi.org/10.1016/j.clay.2007.02.005

Rao, S. M. and T. Thyagaraj. 2007b. "Swell–compression behaviour of compacted clays under chemical gradients." *Can Geotech J* 44, no. 5 (May): 520-532. https://doi.org/10.1139/t

07-002

Reitemeier, R. F. 1946. "Effect of moisture content on the dissolved and exchangeable ions of soils of arid regions" *Soil Sci* 61, no. 3 (March): 195-214.

Rhoades, J. D. 1981. "Predicting bulk soil electrical conductivity versus saturation paste extract electrical conductivity calibrations from soil properties." *Soil Sci Soc Am J* 45, no. 1 (January): 42-44. https://doi:10.2136/sssaj1981.03615995004500010009x

Rhoades, J. D. 1982. "Soluble salts." *Methods of soil analysis* Part 2.2: 167-178.

Smith, A. K. and R. A. Gortner. 1933. "The Electrical Conductivity of Mixed Salt Solution." *J Phys Chem* 37, no. 1 (January): 79-86. https://doi.org/10.1021/j150343a011

Song, M. M., L. L. Zeng, and Z. S. Hong. 2017. "Pore fluid salinity effects on physicochemical-compressive behaviour of reconstituted marine clays." *Appl Clay Sci* 146, no. 15 (September): 270-277. https://doi.org/10.1016/j.clay.2017.06.015

Stevens, D. P., M. J. McLaughlin, and M. K. Smart. 2003. "Effects of long-term irrigation with reclaimed water on soils of the Northern Adelaide Plains, South Australia." *Soil Res* 41, no. 5 (September): 933-948. https://doi.org/10.1071/SR02049

Sun, D. A., J. Y. Zhang, and G. S. Song. 2013. "Experimental study of soil-water characteristic curve of chlorine saline soil (in Chinese)." *Rock Soil Mech* 34, no. 4: 955-960.

Thyagaraj, T. and S. M. Rao. 2010. "Influence of osmotic suction on the soil-water characteristic curves of compacted expansive clay." *J Geotech Geoenviron Eng* 136, no. 12 (May): 1695-1702. https://doi.org/10.1061/(ASCE)GT.1943-5606.0000389

Thyagaraj, T. and S. M. Rao. 2013. "Osmotic swelling and osmotic consolidation behaviour of compacted expansive clay." *Geotech Geol Eng* 31, no. 2 (April): 435-445. https://doi 10.1007/s10706-012-9596-0

U.S. Salinity Laboratory Staff. 1954. "Diagnosis and improvement of saline and alkali soils." *USDA Agriculture Handbook* no. 60. U.S. Government Printing Office, Washington, D.C.

Walton, N. R. G. 1989. "Electrical conductivity and total dissolved solids-what is their precise relationship?." *Desalination* 72, no. 3 (December): 275-292. https://doi.org/10.1016/0011-9164(89)80012-8

Wu, Y. C. and P. A. Berezansky. 1995. "Low electrolytic conductivity standards." *J. Res Natl Inst Stand Technol* 100, no. 5 (September/October): 521-527. https://doi: 10.6028/jres.100.039

Ye, W. M., F. Zhang, B. Chen, Y. G. Chen, Q. Wang, and Y. J. Cui. 2014. "Effects of salt solutions on the hydro-mechanical behavior of compacted GMZ01 Bentonite." *Environ Earth Sci* 72, no. 7 (October): 2621-2630. https://doi 10.1007/s12665-014-3169-x

Ye, W. M., F. Zhang, Y. G. Chen, B. Chen, and Y. J. Cui. 2017. "Influences of salt solutions and salinization-desalinization processes on the volume change of compacted GMZ01 bentonite." *Eng Geol* 222, no. 18 (May): 140-145. https://doi.org/10.1016/j.enggeo. 2017.04.002

Zhang, F., W. M. Ye, Y. G. Chen, B. Chen, and Y. J. Cui. 2016a. "Influences of salt solution concentration and vertical stress during saturation on the volume change behavior of compacted GMZ01 bentonite." *Eng Geol* 207, no. 3 (June) 48-55. https://doi.org/10.1016/j.enggeo.2016.04.010

Zhang, Y., W. M. Ye, B. Chen, Y. G. Chen, and B. Ye. 2016b. "Desiccation of NaCl-contaminated soil of earthen heritages in the Site of Yar City, northwest China." *Appl Clay Sci* 124-125 (May): 1-10. https://doi.org/10.1016/j.clay.2016.01.047

Zhang, Y., W. M. Ye, Y. G. Chen, and B. Chen. 2017. "Impact of NaCl on drying shrinkage behavior of low-plasticity soil in earthen heritages." *Can Geotech J* 54, no. 12 (November): 1762-1774. https://doi.org/10.1139/cgj-2016-0403

Ying, Z., Benahmed, N., Cui, Y.J., Duc, M. 2021. Submitted to Journal of Rock Mechanics and Geotechnical Engineering, under second round review.

Determination of osmotic suction from electrical conductivity for unsaturated low-plasticity soils

Zi Ying[1], Nadia Benahmed[2], Yu-Jun Cui[1], Myriam Duc[3]

Abstract: Determination of soil osmotic suction from the electrical conductivity (EC) of soil pore water was widely reported in the literature. However, while dealing with unsaturated soils, they do not have enough soil pore water to be extracted for the reliable measurement of EC. In this paper, the chilled-mirror dew-point hygrometer and contact filter paper method were used to determine the total and matric suctions for low-plasticity soils with different salinities (0.05‰, 2.10‰ and 6.76‰). A new piecewise function was proposed to calculate the osmotic suction, with the piecewise point corresponding to the first occurrence of precipitated salt in mixed salts solution (synthetic seawater). The electrical conductivity, ion and salt concentrations used for osmotic suction calculation were transformed from the established relationships of mixed salts solution instead of experimental measurement. The calculated osmotic suction by the proposed equation and the equations in the literature was compared with the indirectly measured one (the difference between the measured total and matric suctions. Results showed that the calculated osmotic suction, especially the one calculated using the proposed function, was in fair agreement with the indirectly measured osmotic suction (especially for specimens with higher salinity of 6.76‰), suggesting that the transformation of EC and concentrations from the established relationship is a good alternative to direct measurement for low-plasticity soil. In particular, the proposed method could be applied for unsaturated low-plasticity soils which do not have enough soil pore water for a proper EC measurement.

Keywords: unsaturated soils; mixed salts solutions; osmotic suction; electrical conductivity

1. Introduction

Osmotic suction, which is correlated to the salinity of soil pore water, is one of the major components influencing the hydro-mechanical behaviour of soil with salinity. Rao and Shivananda (2005) investigated the swelling potential of salt-amended expansive soils by using

[1]: Ecole des Ponts ParisTech, Laboratoire Navier/CERMES, 6 – 8 av. Blaise Pascal, Cité Descartes, Champs-sur-Marne, 77455 Marne-la-Vallée cedex 2, France
[2]: INRAE, Aix Marseille Univ, Unité de Recherche RECOVER, 3275 route Cézanne, CS 40061, 13182 Aix-en-Provence, France
[3]: Université Gustave Eiffel, IFSTTAR/GERS/SRO, 14-20 boulevard Newton, Champs-sur-Marne, 77447 Marne-la-Vallée, France

deionised water and observed that this one was independent of initial osmotic suction. However, they found that the rate of swelling decreased with increasing osmotic suction. By contrast, Rao et al. (2006) reported that, for compacted specimens with low initial salt content, the swelling magnitude was decreased by the osmotic gradient between reservoir salt solution and soil pore water. Witteveen et al. (2013) performed chemical loading on a compacted non-swelling illite by replacing soil pore water with sodium chloride (NaCl) solution, and found that the initial stiffness and yield stress decreased as osmotic suction increased. Mokni et al. (2014) reported that the osmotic suction caused a decrease of compressibility and an increase of pre-consolidation stress for compacted Boom Clay. Therefore, it appears that the determination of soil osmotic suction is indispensable and crucial for better understanding the hydromechanical behaviour of saline soils.

Miller and Nelson (1993) and Tang et al. (2002) indicated that the total suction was not simple addition of matric and osmotic suctions. Krahn and Fredlund (1972) stated that the difference between the total and the matric suctions was the measured osmotic suction for Till (low-plasticity soil), whereas it was higher than the measured one for Regina clay (high-plasticity soil). Arifin and Schanz (2009) reported that the difference between the total and matric suctions corresponded to the osmotic suction and hydration force for expansive soils. In general, it has been admitted that considering the osmotic suction as the difference between total and matric suctions was problematic for high-plasticity soils due to the effect of hydration force, but plausible for low-plasticity soils, as reported by Edil and Motan (1984), Wan et al. (1995), Sreedeep and Singh (2006) and Dao et al. (2008).

The osmotic suction of salted soils can be deduced from the relationship between electrical conductivity, salt and ion concentrations of soil pore water. Several equations for its determination were reported in the literature, as listed in Table 1. van't Hoff equation was the widely used one in determining the osmotic suction of salt solution (Mitchell and Soga 2005; Rao and Thyagaraj 2007a, 2007b; Witteveen et al. 2013). As shown in Fig. 1, the United States Salinity Laboratory Staff (1954) gave the variations of osmotic suction with the electrical conductivity for a single salt solution and saturation extract of soil pore water in saline soils. Based on such variations, Mata et al. (2002) derived the relationship between the osmotic suction and the electrical conductivity of soil pore water (Eq. 2); Rao and Shivananda (2005) established the calibration curve as expressed in Eq. 3, relating the electrical conductivity of soil pore water to osmotic suction; Leong et al. (2007) estimated the osmotic suction for NaCl

solution using Eq. 4; Arifin and Schanz (2009) calculated the osmotic suction from the measured electrical conductivity of soil pore water using Eq. 5. Witteveen et al. (2013) described the relationship between the measured osmotic suction and the corresponding concentration of NaCl solution by Eq. 6, as shown in Fig. 1. The United States Salinity Laboratory Staff (1954) also gave a relationship between the osmotic suction of saturated soil water extract and its electrical conductivity, represented by Eq. 7. Abedi-Koupai and Mehdizadeh (2008) indicated that the soil osmotic suction, at a particular water content, can be transformed from the osmotic suction of saturated soil water extract by assuming a linear dilution for salt concentration (Eq. 8). Mokni et al. (2014) proposed a relationship between osmotic suction and sodium nitrate (NaNO3) solution, expressed by Eq. 9.

Table 1. Equations for determination of soil osmotic suction.

Eq.	Equations	References
1	$\pi = vcRT$	van't Hoff equation.
2	$\pi = 0.019\left(\frac{EC}{1\ \mu S/cm}\right)^{1.074}$	Mata et al., (2002)
3	$\pi = 31.92EC^{1.08}$	Rao and Shivananda, (2005b)
4	$\pi = P_a\left(0.31EC^{1.15}\right)$	Leong et al., (2007)
5	$\pi = 38.54EC^{1.0489}$	Arifin and Schanz, (2009)
6	$\pi = 0.407c^2 + 3.88c + 0.61$	Witteveen et al., (2013)
7	$\pi_e = -360EC_e$	United States Salinity Laboratory Staff, (1954)
8	$\pi = \pi_e\left(\frac{w_s}{w}\right)$	Abedi-Koupai and Mehdizadeh, (2008)
9	$\pi = -\frac{RT\rho_1}{M_W}\ln\left[1-\left(\frac{cM_S}{\rho_1}\right)\right]^2$	Mokni et al., (2014)

Note: c: salt concentration; v: van't Hoff factor (number of constituent ions); $v \cdot c$: ion concentration; EC: electrical conductivity; EC_e: electrical conductivity of saturated soil water extract; M_w: molar mass of water; M_S: molar mass of salt; P_a: atmospheric pressure; R: universal gas constant; T: absolute temperature; w: actual water content of soil; w_s: water content of soil at saturated state; ρ_1: liquid density; π: osmotic suction; π_e: osmotic suction of saturated soil water extract.

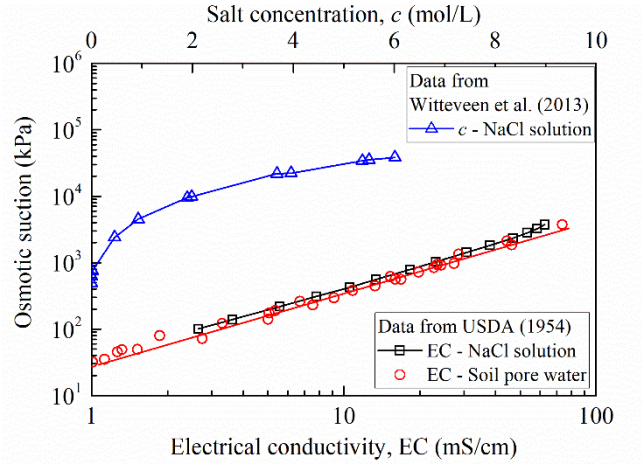

Fig. 1. Relationship between osmotic suction and electrical conductivity/salt concentration.

To determine the soil osmotic suction by the aforementioned equations, it is essential to obtain soil pore water which can be squeezed out with the aid of pore fluid squeezer (ASTM D4542-95 2001; Rao and Shivananda 2005; Rao et al. 2006; Leong et al. 2007; Thyajaraj and Rao 2010; Thyagaraj and Salini 2015). Arifin and Schanz (2009) indicated that the osmotic suction of soil pore water decreased with increasing squeezing pressure due to the restrictive membrane effect, resulting in lower diffusion of ions at higher squeezing pressure. For unsaturated soils, even with the squeezing technique, they still do not have enough pore water to be obtained. Thus, a soil-water slurry was usually prepared to obtain soil pore water (Krahn and Fredlund 1972; Abedi-Koupai and Mehdizadeh 2008). In practice, the deionised water adding to soil slurry would also induce the dilution of salt concentration in soil, thus distorting the initial osmotic suction (Boso et al. 2005).

In this study, to calculate the osmotic suction of compacted specimens, the electrical conductivity (EC), ion/salt concentration of soil pore water were derived from the established relationships of mixed salts solution (EC versus water salinity, EC versus ion/salt concentrations) instead of the direct measurement. This is of paramount importance for unsaturated soils which do not have enough soil pore water for chemical analysis. The water salinity (the mass ratio of salt to salty water) of compacted specimens was derived from the soil water content and soil salinity (the mass ratio of salt to dry soil). Then, the EC was transformed from the water salinity. Once the EC was obtained, the ion and salt concentrations were determined, allowing hence the calculation of osmotic suction by the equations in Table 1. Besides, a new equation to calculate soil osmotic suction from electrical conductivity was proposed, taking into account the dissolved and the precipitated salts. In order to verify the

relevance of the proposed equation, the calculated osmotic suction using the latter was compared with the value calculated from the several equations in Table 1, as well as with the indirectly measured osmotic suction (the difference between the total and the matric suctions). The measurement of the total suction was carried out by the chilled-mirror dew-point hygrometer (WP4C), and that of the matric suction by the contact filter paper method.

2. Materials and methods

2.1 Materials

The tested material is a natural soil collected from les Salin-de-Giraud, in south of France. This soil consists of 30% fine sand (0.075 ~ 2 mm), 53% silt (0.002 ~ 0.075 mm) and 17% clay fraction (< 0.002 mm). Table 2 illustrates the geotechnical properties of tested soil. This soil belongs to low plasticity sandy silt (ASTM D2487-00, 2000). Thus, its osmotic suction can be considered as the difference between total and osmotic suctions, as indicated previously. This soil is saline, with a soil salinity of 2.10‰ (g of salt/kg of dry soil). The salt composition and concentration of soil pore water are listed in Table 3.

Table 2. Geotechnical characteristics of the tested soil.

Property	Value
Specific gravity	2.71
Liquid limit (%)	29
Plastic limit (%)	19
Plasticity Index	10
Specific surface area (m^2/g)	24
Optimum water content (%)	17.10
Maximum dry density (Mg/m^3)	1.68

Table 3. Salt composition and concentration of natural soil pore water.

Solution	Chemical compositions (mg/L)					Salt concentration, c (g/L)
	Cl	Na	Ca	K	Mg	
Soil pore water	7521	5096	215	225	176	13

The mineral composition of tested soil was detected by X-Ray diffraction (XRD) analysis. The D8 Advance diffractometer was used to collect the XRD pattern. Minerals were quantified with EVA and TOPAS software coupled with ICDDPdf2 database. The XRD pattern of the tested soil is presented in Fig. 2. It indicates that this soil is composed of 15.7% clay minerals and 84.3% non-clay minerals. The clay minerals are identified as illite, chlorite and kaolinite. The non-clay minerals are quartz, calcite, feldspars and halite NaCl. This soil is highly crystallized without organic minerals (De Baecque 2019).

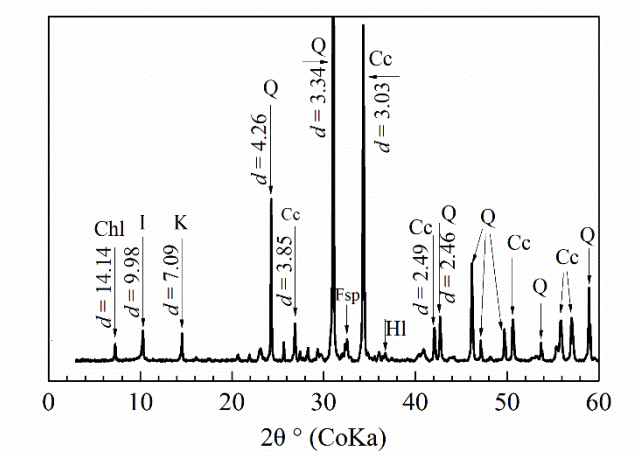

Fig. 2. X-ray diffraction pattern of tested soil (Chl: chlorite; I: illite; K: kaolinite; Q: quartz; Cc: calcite; Fsp: feldspar; Hl: halite).

2.2 Soil salinity adjustment

Five different salts of synthetic seawater (Table 4, French standard AFNOR NF P 18-837, 1993) were used to reconstitute mixed salts solution needed for preparing the salted soils. The target soil salinity was fixed at r' = 6.76‰ (g of salt/kg of dry soil), corresponding to the water salinity of soil pore water of r = 35‰ (g of salt/kg of salty water) for salted soils at water content of 20%. This water salinity was exactly the salinity of synthetic seawater. To avoid destroying soil aggregates, the mixed salts solution was gently sprayed over natural soils layer by layer to reach the required salinity level. The salinity precision of prepared salted soils was verified and the relative error between the target salinity and measured salinity was found less than 4.75%. More details about the calculation of additive salts and preparation for salted soils can be found in Ying et al. (2021a).

Table 4. Salt composition of synthetic seawater.

Salts	NaCl	$MgCl_2 \cdot 6H_2O$	$MgSO_4 \cdot 7H_2O$	$CaSO_4 \cdot 2H_2O$	$KHCO_3$
Salt mass (g) in 1000 g deionized water	30.0	6.0	5.0	1.5	0.2
Percentage (%)	70.26	14.05	11.71	3.51	0.47

To prepare the salted soils with a salinity lower than the initial one, leaching equipment was used and deionised water was flowed through natural soil from bottom to top (Ying et al., 2021b), as shown in Fig. 3. The water head and water flow rate were controlled to be lower than 1 m and 0.3 mL/s respectively to avoid destroying soil aggregates and migration of fine particles. Leached water (or effluent) at the top of the specimen was collected for the electrical conductivity control. Once the electrical conductivity was close to that of deionised water, the leaching process was stopped. The final measured soil salinity of leached soil was down to 0.05‰ (g of salt/kg of dry soil), which was sufficiently low and could be ignored in further analysis.

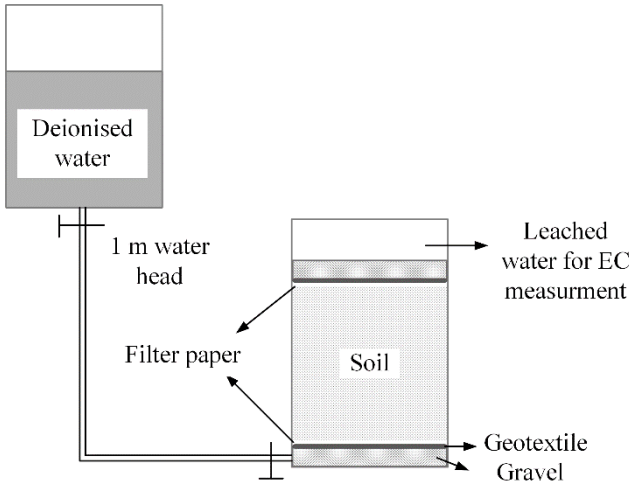

Fig. 3. Equipment for salt leaching test (after Ying et al. 2021b).

2.3 Sample preparation

The natural saline soil, salted soil and leached soil were air-dried, ground and passed through 0.4 mm sieve. The dry soil powders with different soil salinities of 0.05‰, 2.10‰ and 6.76‰ were then humidified by spraying a certain quantity of deionised water to reach the target water content (17%). Then, they were thoroughly mixed and statically compacted to the target dry

density (1.63 Mg/m^3). The compacted specimens had the same respective soil salinities as dry soil powders.

2.4 Matric suction measurement

The matric suction was measured by the contact filter paper method (Sun et al. 2010; ASTM D5298-16 2016) which has high accuracy for matric suction measurement in the range of 10 to 100 000 kPa. The used filter papers was Whatman No. 42, which were oven-dried before usage. The compacted specimens (d = 50 mm, h = 20 mm) were air-dried to reach different target water contents that were 14%, 11%, 8.5%, 6%, 4%, 3% and 1.5%. The water content of air-dried specimens (w) was preliminarily controlled by monitoring the mass of soil specimen during drying (Tang et al. 2011):

$$w = \frac{(1+w_0')m_a}{m_0} - 1 \tag{10}$$

where w_0' is the compacted water content of specimen (17%); m_0 is the mass of as-compacted specimen, and m_a is the mass of air-dried specimen.

After air-drying, two replicated specimens with the same water content were used for one matric suction measurement. A filter paper used for matric suction analysis was sandwiched between two other filter papers whose diameter was slightly larger to prevent the central one from the direct contact with soil. To measure the matric suction, the stacked filter papers were put in the middle of two specimens (Fig. 4). The specimens with filter papers were carefully wrapped and covered to avoid water evaporation. Then, they were stored for two weeks to allow the fluid transfer between specimens and filter papers. Afterwards, the water contents of specimen and filter paper were measured by oven-drying at 105°C. Then, the water content (w') of salted specimen was calculated by Eq. 11 (Ying et al. 2021a):

$$w' = \frac{m_{sw}}{m_s} = \frac{m - m_d}{m_d - rm} \tag{11}$$

where r is the water salinity; m_d is the oven-dried mass (dry soil and salt); m is the mass of wet soil; m_{sw} is the salty water mass, and m_s is the dry soil mass.

To convert the soil salinity ($r' = m_{sa}/m_s$) to water salinity ($r = m_{sa}/m_{sw}$), the following equation was used (Ying et al. 2021a):

$$r = \frac{r'}{w'} \tag{12}$$

The soil matric suction (ψ_m) was determined from the water content of filter paper (w_f) using Eq. (13) (calibration equation for Whatman No.42, ASTM D5298-16 2016):

$$\log \psi_m = \begin{cases} 5.327 - 0.0779 w_f & w_f \le 45.3\% \\ 2.412 - 0.0135 w_f & w_f > 45.3\% \end{cases} \tag{13}$$

The accuracy and reliability of Eq. (13) were also confirmed by Leong et al. (2002).

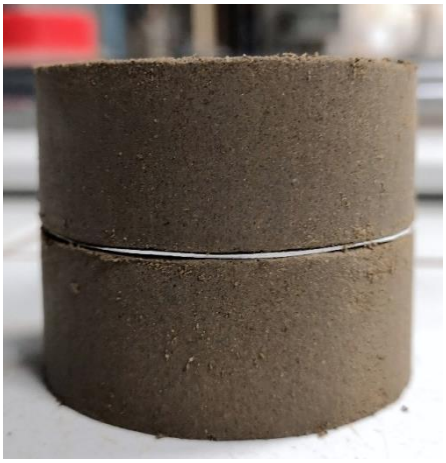

Fig. 4. Matric suction measurement by contact filter paper method.

2.5 Total suction measurement

Chilled-mirror dew-point hygrometer (WP4C) was used to determine the total suction of soil specimens (Fig. 5a). It has higher precision for total suction measurement in comparison to non-contact filter paper method (Bulut et al. 2002; Leong et al. 2003, 2007). This technique is based on the relative humidity measurement (Leong et al. 2003, 2007; Sun et al. 2014, 2020). The total suction was determined through Kelvin's equation:

$$\psi = \frac{RT}{M_w} \ln RT \tag{14}$$

where ψ is the total suction, R is the universal gas constant (8.31 J/mol·K), T is the absolute temperature, M_w is the molar mass of water.

After compaction, each specimen (d = 38 mm, h = 100 mm) was cut into small slices (Fig. 5b).

Then, they were air-dried to different water contents. It appears from Fig. 5b that the drying process did not induce macro-cracks on the surface of specimens. After air-drying, they were enveloped for 24 h for water equilibrium. Then, the total suction of these soil slices were measured by WP4C.

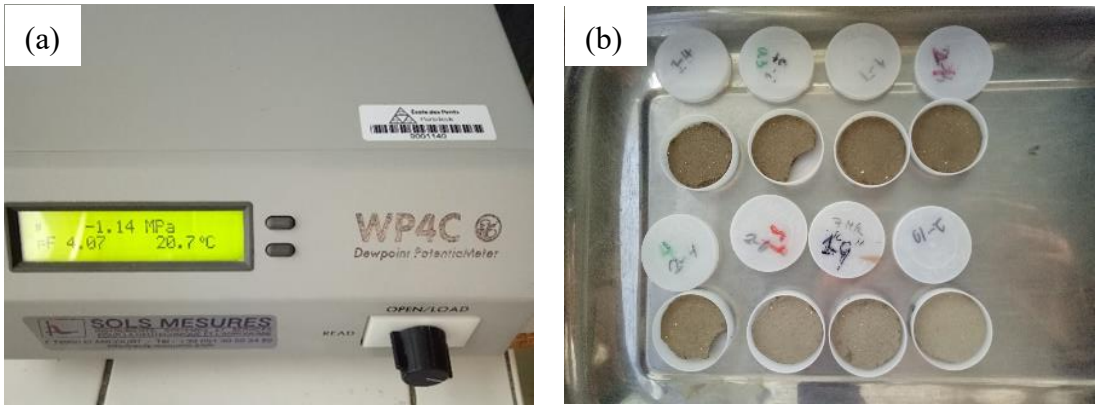

Fig. 5. Setup of total suction measurement: (a) chilled-mirror dew-point hygrometer device (WP4C); (b) specimens.

2.6 Osmotic suction determination

Soil osmotic suction can be measured by several techniques, or computed from the electrical conductivity of soil pore water extract. In this study, first, the osmotic suction of mixed salts solutions prepared by five different salts (Table 4), was measured by WP4C. Afterwards, the electrical conductivities of these mixed salts solutions were systematically measured by a conductivity meter. The conductivity meter was calibrated by the standard solution prior to the measurement. The measured electrical conductivity is the value at 25°C. Then, the relationship between the measured osmotic suction and electrical conductivity is plotted in Fig. 6 and the following equation is established:

$$\pi = \begin{cases} 23.15EC^{1.17} & EC \le 100\ mS/cm \\ 0.28EC^{2.12} & EC > 100\ mS/cm \end{cases} \quad (15)$$

where π is the osmotic suction (kPa) and EC is the electrical conductivity (mS/cm) of mixed salts solution. This equation is a piecewise function, with a piecewise point at EC of 100 mS/cm. Ying et al. (2021a) prepared the same mixed salts solution and filtered them by 0.45-μm filter paper. They found that some salts started to precipitate at EC of 100 mS/cm. It indicates that the piecewise point of the proposed equation (Eq. 15) is the critical point where the precipitated salts occurred. The relationship between the total water salinity and electrical conductivity is

also shown in Fig. 6. Note that the total water salinity consisted of dissolved and precipitated salts when the electrical conductivity was higher than 100 mS/cm..

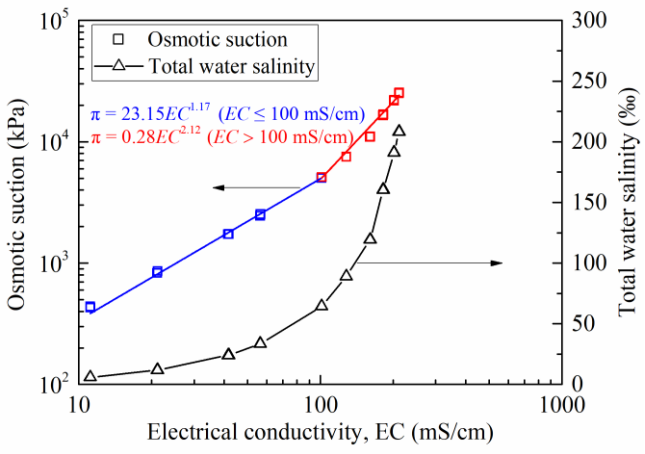

Fig. 6. Relationship between osmotic suction/water salinity and electrical conductivity for mixed salts solutions.

Since the mixed salts solution (Table 4) had the same chemical composition of the soil pore water (Table 3), the osmotic suction of soil specimens could be estimated by Eq. (15) once the electrical conductivity was determined. To this end, the relationship between the electrical conductivity and the dissolved/total water salinities of mixed salts solution established by Ying et al. (2021a) was used, as shown in Fig. 7. The relationship between the electrical conductivity (EC) and the total water salinity (r) is expressed as:

$$EC = -0.0027r^2 + 1.5228r + 0.4039 \tag{16}$$

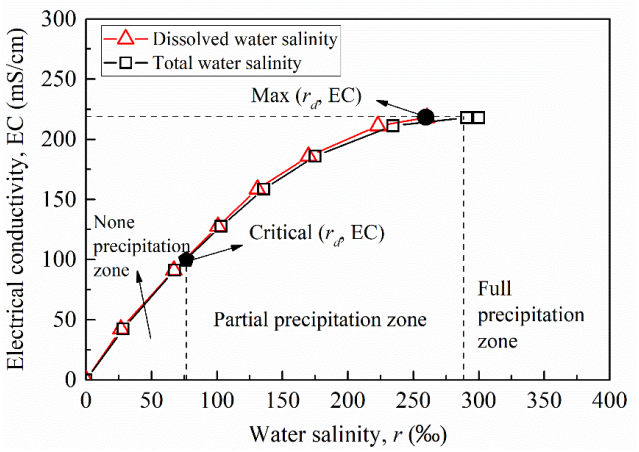

Fig. 7. Electrical conductivity variation with water salinity for mixed salts solution (after Ying et al. 2021a).

The total water salinity was the mass ratio of total salt to additive deionised water. The dissolved water salinity was the mass ratio of dissolved salt to additive deionised water, with dissolved salt mass obtained by oven-drying the filtered clear salt solution (without precipitated salt) at 180°C. None, partial and full precipitation zones of the mixed salts solution were identified according to the critical point (r_d = 76‰ or g dissolved salt/ kg of salty water, EC = 100 mS/cm) and the maximum value of electrical conductivity (219 mS/cm). When adding salts in water, some salts having high solubility were dissolved, while some other salts with low solubility started to precipitate when the water salinity was higher than the value at the critical point. When the salts quantity reached a certain level, the water could not dissolve the salts anymore leading to the maximum values of dissolved water salinity and electrical conductivity. In the none precipitation zone, the total and the dissolved water salinity were the same, whereas in the partial and full precipitation zones, the total water salinity consisted of dissolved and precipitated salts. It is worth pointing out that the total and dissolved water salinities are related to the same electrical conductivity value, because there is no contribution of precipitated salts to the value of electrical conductivity.

As mentioned previously, unsaturated soils usually do not have enough soil pore water for the electrical conductivity measurement. Thus, the following calculation was used to obtain the electrical conductivity of soil pore water as an alternative to direct measurement. Firstly, the total water salinity of soil specimen after total suction measurement was obtained by combining Eqs. (11) and (12). Secondly, the corresponding electrical conductivity of soil pore water was calculated using Eq. (16). Substituting the electrical conductivity into Eq. (15), the osmotic suction of the soil specimen at a given water content was obtained. It should be pointed out that if the calculated total water salinity was higher than the maximum dissolved water salinity, the corresponding electrical conductivity was regarded as the maximum value.

In this study, Eq. (1) to Eq. (6) were also used to calculate the osmotic suction for a comparison with the newly proposed equation (Eq. 15). To this end, the ion concentration (i, mol/L) and salt concentration (c, mol/L) of soil pore water were needed to be determined. Concerning the mixed salts solution, the relationship between the electrical conductivity and the dissolved water salinity in Fig. 7 can be transformed to the relationships between the electrical conductivity and the dissolved ion concentration (i) as well as dissolved salt concentration (c). Firstly, each salt quantity (mol) was obtained by the salt mass divided by molar mass. Ion quantity (mol) was determined according to the molecular formula of salt (Table 4). Afterwards,

the total ion and salt concentrations (mol/L) were determined as the ratio of the quantity of total ion (mol) or salt (mol) to the volume of additive deionised water (L). The dissolved ion concentration and dissolved salt concentration were determined by the total concentration multiplying the percentage of dissolved salt which was the ratio of dissolved salt mass to total salt mass. The electrical conductivity variations with dissolved ion concentration (i) and dissolved salt concentration (c) of mixed salts solution are presented in Fig. 8. The corresponding relationships were expressed in Eq. (17) and Eq. (18), respectively:

$$EC = -2.0426i^2 + 42.241i \tag{17}$$

$$EC = -8.5963c^2 + 86.655c \tag{18}$$

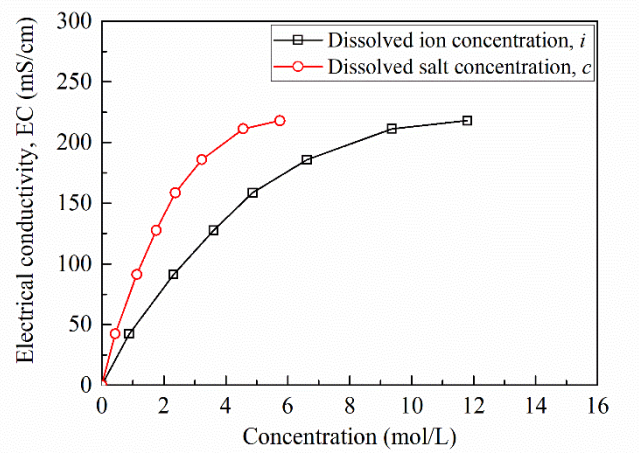

Fig. 8. Electrical conductivity variations with ion concentration/salt concentration.

With the electrical conductivity obtained from Eq. (16), the dissolved ion and salt concentrations can be obtained from Eq. (17) and Eq. (18), respectively. Then, substituting the electrical conductivity, the dissolved ion concentration and the dissolved salt concentration into Eqs. (1) to (6), the osmotic suction was obtained from different equations. Note that the determinations of ion and salt concentrations as well as electrical conductivity at different water contents did not take into account the cation exchange and adsorption, because the low-quantity and low-activity clay minerals (illite, chlorite and kaolinite) in the tested soil, as well as its small specific surface area (24 m^2/g) led to low cation exchange and adsorption.

3. Results and discussions

3.1 Total and matric suctions

The water retention curves with the matric suction obtained from contact filter paper method and the total suction determined by WP4C are presented and discussed in this section. Figure 9 represents the global void ratio of air-dried specimens versus water content. It is worth noting that the void ratio was almost constant during the drying process. This was confirmed by MIP tests conducted by Ying et al. (2021c) on the same soil that the total mercury intruded void ratio was close to the global one without volume shrinkage during drying. They also pointed out that for the tested soil with as low as 17% clay-size particles, upon drying, the clay shrinkage led to the changes of pore size distribution but without the development of shrinkage cracks. Therefore, the effect of shrinkage cracks on the suction variation was not considered in this study.

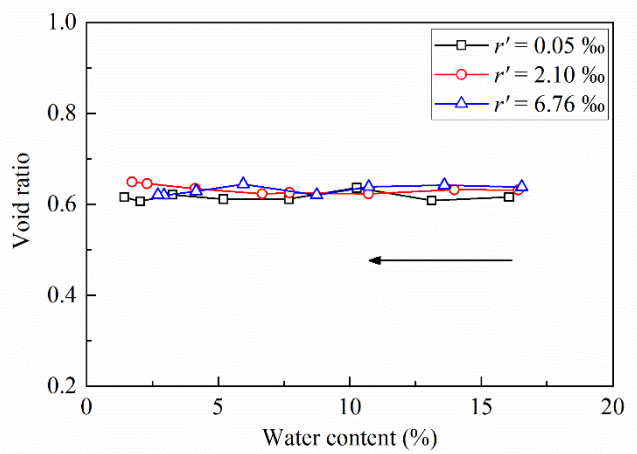

Fig. 9. Void ratio variation during drying.

The suction measurements of soil specimen with soil salinity of 2.10‰ were duplicated to check the test reproducibility. As shown in Figs. 10 and 11, the two water retention curves of soil specimens with 2.10‰ soil salinity were fairly similar, implying a good repeatability of the matric suction and total suction measurements. The average values of the duplicated measurements of specimens with 2.10‰ were used in this study.

It can be seen from Fig. 10 that there was no significant distinction between water retention curves of matric suction for specimens with different soil salinities: at the same water content, the values of matric suction for specimens with negligible soil salinity (0.05‰) and with soil salinities of 2.10‰ and 6.76‰ were close to each other. This result suggested that the matric suction was not affected significantly by salt.

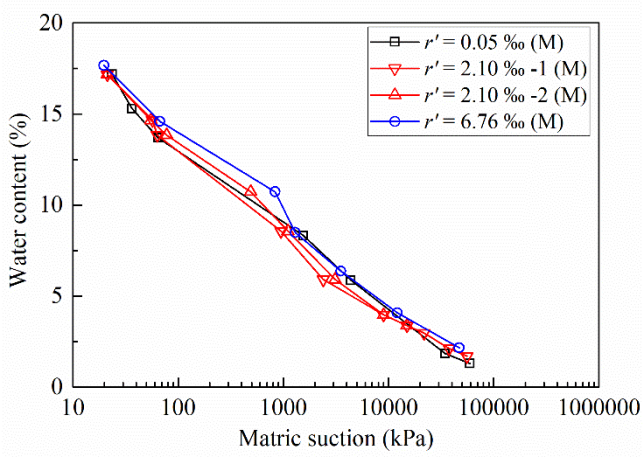

Fig. 10. Water retention curves in terms of matric suction.

From Fig. 11, it appears that the total suction were different when varying the salinity level, indicating clearly that the total suction was significantly affected by soil salinity. Besides, the curves of specimens at higher salinity lied above those of specimens at lower soil salinity. It appears also that the curves converged gradually with decreasing water content.

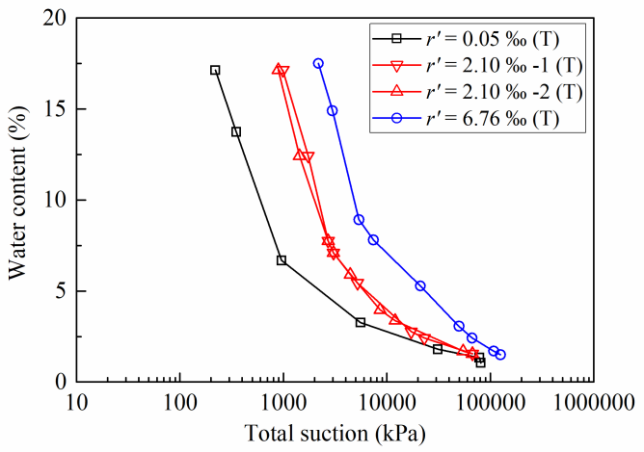

Fig. 11. Water retention curves in terms of total suction.

The variations of the total and matric suctions with water content are depicted in Figs. 12a and 12b for specimens with soil salinities of 2.10‰ and 6.76‰, respectively. It is observed that the total suction was quite higher as compared to matric suction. The difference between the total and matric suctions can be attributed to the contribution of the osmotic suction, which is generated from the dissolved salt in soil pore water. As shown in Fig. 12a, for specimens with 2.10‰ soil salinity, the matric suction curve converged towards the total suction curve with decreasing water content. When the water content was lower than 4.3%, the two curves are similar within the accuracy of the measurement leading to an osmotic suction close to zero. This overlapping phenomenon of total suction and matric suction at lower water content was in

agreement with the results obtained by Arifin and Schanz (2009) and Sreedeep and Singh (2006). It might be attributed to the dominant vapour transfer among specimens and contact filter papers at low water content (Arifin and Schanz 2009). Thus, the suction measured by contact filter paper method consisted of capillary and osmotic components which are close to the total suction. In the case of specimens with 6.76‰ soil salinity, at low water content, the matric suction curve also converged towards the total suction curve but remained relatively lower than the latter (Fig. 12b). It can be inferred that the fluid transfer was still predominant at low water content due to the expanded channels for fluid transfer that were resulted from the shrinkage of diffuse double layer, giving rise to a more precise measurement of matric suction.

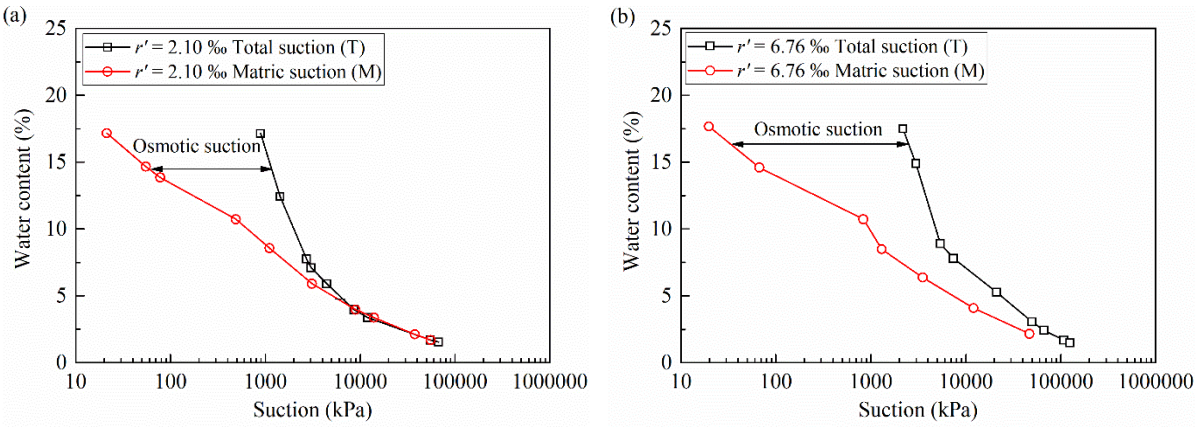

Fig. 12. Water content versus total and matric suctions: (a) *r'* = 2.10‰; (b) *r'* = 6.76‰.

The water retention curves in terms of osmotic suction defined by the difference between the total suction (T) and the matric suction (M) are shown in Fig. 13. It is worth noting that the osmotic suction of soil specimen with soil salinity below 0.05‰, which is a negligible level, was not considered here due to, (i) the low accuracy of total suction measurement below 1000 kPa and, (ii) the non-reliable osmotic suction determination at such low salinity. For specimens with 2.10‰ soil salinity, the osmotic suction increased slightly as the water content decreased to 10%, then stayed in the range between 1200 kPa to 1450 kPa when the water content was in the range of 5% to 10%. Below the water content of 5%, the osmotic suction tended towards zero which corresponded to the section of the curves where the matric and total suctions overlapped as shown in Fig. 12a. In the case of the specimens with soil salinity of 6.76‰, the osmotic suction increased as the water content decreased, and the rate of this increase was higher when the water content was lower than 8%. The osmotic suction was highly correlated to the dissolved water salinity in soil pore water. Ying et al. (2021a) stated that, for this salted soils (the same soil as in this study) with salinity of 6.32‰ close to the one used in this study

(6.76‰), the dissolved water salinity increased slightly from 35‰ to 70‰ when the water content decreased from 17% to 8.5%, then it increased drastically to 260‰ as the water content decreased to 2.5%, and stayed constant at the maximum value with further drying. Consequently, for specimens with 6.76‰ soil salinity, the dissolved water salinity increased slightly when the water content decreased down to 8%, then increased significantly with further decrease of the water content. Therefore, the osmotic suction has a generic trend with two slopes increase with the water content: a low increase followed by a higher one as highlighted in Fig. 13. Concerning the specimens with soil salinity of 2.10‰, the dissolved water salinity increased slightly as the water content decreased to 5%. As a result, the osmotic suction varied slightly during drying.

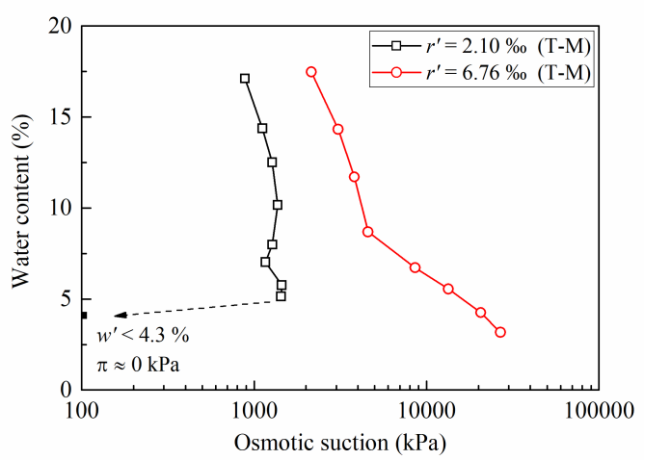

Fig. 13. Water retention curves in terms of osmotic suction.

3.2 Osmotic suction evaluation

The values of osmotic suction determined from indirect measurement (T-M) and calculated from the piecewise function (Eq. 15) proposed in this study for specimens with soil salinities of 2.10‰ and 6.76‰ are shown in Figs. 14 and 15, respectively. For comparison, the values of osmotic suction calculated by Eqs. 1-6 from the literature are also presented. It appears that the osmotic suction calculated from the relationships for single salt solution, such as those of Eqs. (1), (4) and (6), exhibited higher values, whereas the calculated osmotic suction obtained from the relationships of soil pore water was lower (Eqs. 2, 3 and 5). This can be attributed to the different basis of these equations. Indeed, as shown in Fig. 1, at the same electrical conductivity, the NaCl solution gave higher osmotic suction in comparison to the soil pore water (United States Salinity Laboratory Staff 1954).

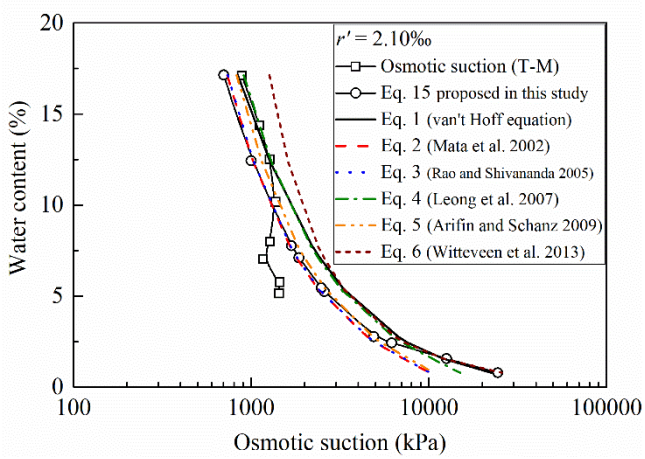

Fig. 14. Comparison of osmotic suction for specimens at 2.10 ‰ soil salinity.

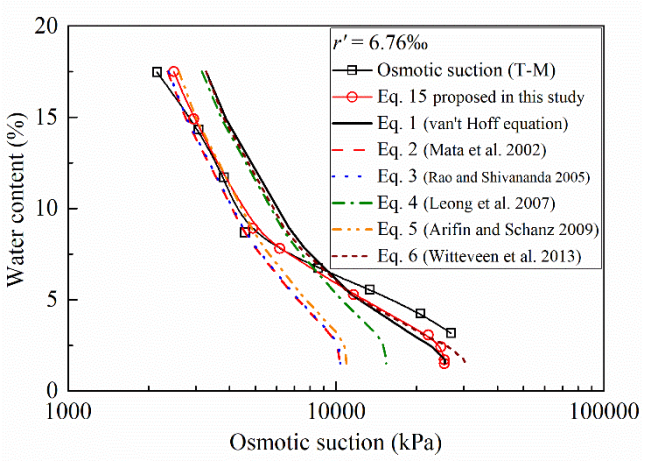

Fig. 15. Comparison of osmotic suction for specimens at 6.76‰ soil salinity.

Figure 14 shows that for specimens with 2.10‰ soil salinity, the osmotic suction calculated using Eq. (15) proposed in this study on the basis of mixed salts solution matched quite well with the one calculated using Eqs. (2), (3) and (5) when the water content was higher than 2.5%, while they were consistent with the osmotic suction calculated using Eqs. (1), (4) and (6) as the water content was lower than 2.5%. The same observation was made on soil specimens with 6.76‰ soil salinity, as shown in Fig. 15. The osmotic suction calculated from Eq. (15) proposed in this study coincided with the value calculated from Eqs. (2), (3) and (5) when the water content was higher than 8%, whereas they became gradually consistent with the value calculated from Eqs. (1), (4) and (6). Interestingly, the osmotic suction for specimens with 2.10‰ soil salinity at water content of 2.5% and for the specimens with 6.76‰ soil salinity at 8% water content was around 5000 kPa. This value corresponded to the piecewise point (EC = 100 mS/cm, π = 5110 kPa) of Eq. (15). In the first section (EC < 100 mS/cm, π < 5110 kPa),

the calculated osmotic suction coincided with the value calculated from the equations based on soil pore water, due to the similar basis used to derive Eq. (15) and these equations with respect to soil pore water. With an increase of water salinity or subsequent electrical conductivity, some mixed salts with low solubility started to precipitate as indicated in Fig. 7 (partial precipitation zone). In this range, the value calculated from Eq. (15) was consistent with the value obtained by the equations on the basis of single salt solution. It was also observed that, for specimens with 6.76‰ soil salinity, the calculated osmotic suction varied slight when the water content was lower than 2.5%, which might be attributed to the constant values of maximum electrical conductivity or dissolved ion and salt concentrations in soil pore water at such low water content. This was consistent with the observation made by Mata et al. (2002), stating that the osmotic suction was constant at water content lower than the micro-structural water content.

The calculated osmotic suction was also compared with the indirectly determined osmotic suction from the difference between the measured total and matric suctions (T-M). In the case of the specimens with 2.10‰ soil salinity, the indirectly measured osmotic suction (T-M) was in the range of the calculated osmotic suction when the water content was higher than 10%, whereas the indirectly measured value was lower than the calculated value when the water content was in the range of 5% to 10%. This is because the measured matric suction by the contact filter paper method at low water content gave a higher value which partially included osmotic component (Arifin and Schanz 2009), thus leading to a lower osmotic suction which was taken as the difference between measured total suction and matric suction. The indirectly measured osmotic suction (T-M) for the soil specimens with soil salinity of 6.76‰ was in good agreement with the calculated osmotic suction, especially for the value calculated by Eq. (15) proposed in this study. It indicated that Eq. (15), a piecewise function for osmotic suction calculation, described both dissolved and precipitated salts, providing thereby precise determination of the osmotic suction for highly salted soils. The coincidence of experimental osmotic suction (T-M) and calculated one also suggested that the determination of electrical conductivity, ion concentration and salt concentration of soil pore water from the relationships shown in Figs. 7 and 8 and expressed by Eqs. (16) to (18), was an appropriate approach. Using this determination method, the osmotic suction of soil specimens (especially at higher salinity of 6.76‰) at any considered water contents can be determined satisfactorily instead of using an elaborate experimental measurement, avoiding the difficulties of extracting soil pore water for unsaturated soils.

However, it should be mentioned that the proposed piecewise function for osmotic suction determination is only appropriate for the low-plasticity soils with limited cation exchange capacity and its soil pore water has similar salt composition to synthetic seawater. Further exploration on the extension of the proposed method to high-plasticity soils will be conducted, with considering the cation exchange and adsorption between soil particles and soil pore water.

4. Conclusions

The matric suction and total suction of compacted specimens were determined by the contact filter paper method and chilled-mirror dew-point hygrometer (WP4C), respectively. Then, the osmotic suction was determined as the difference between the total and matric suctions. Furthermore, a relationship between electrical conductivity and osmotic suction was established for a mixed salts solution, and a new piecewise function was proposed. This mixed salt solution had the same salt composition as soil pore water. Similarly, series of equations in literature were used to calculate the osmotic suction for comparison. Based on the obtained results, the following conclusions are drawn:

(1) The osmotic suction calculated by different equations in the literature presented different values: the osmotic suction calculated by the equations considering the main salt (NaCl) was higher than the value derived from the relationship based on the soil pore water.

(2) The proposed equation taking dissolved and precipitated salts into account was a piecewise function whose piecewise point (EC = 100 mS/cm, π = 5110 kPa) was related to the first appearance of precipitated salt in mixed salts solution. When the osmotic suction was lower than around 5000 kPa (close to piecewise point), the osmotic suction calculated by the piecewise function coincided with the calculated value from the equations on the basis of soil pore water. When the osmotic suction was beyond 5000 kPa, the osmotic suction obtained by the piecewise function converged with the higher value obtained from the equations for single salt solution.

(3) The indirectly determined osmotic suction (T-M) and calculated osmotic suction were in good agreement for soil specimens with 2.10‰ soil salinity when water content was higher than 10%, and for soil specimens with 6.76‰ soil salinity in the whole considered range of water contents. This highlighted that the osmotic suction can be accurately determined from electrical conductivity, ion and salt concentrations for low-plasticity soils. It is worth noting

that this method is more precise for highly salted soils. By this method, the osmotic suction can be determined more easily for saturated low-plasticity soils. Most importantly, this method can be applied to unsaturated low-plasticity soils, which do not have enough pore water for EC measurement.

Author statement

Zi Ying: Validation, Investigation, Writing - original draft. **Nadia Benahmed:** Investigation, Resources, Writing - review & editing. **Yu-Jun Cui:** Conceptualization, Methodology, Writing - review & editing. **Myriam Duc:** Investigation, Resources.

Declaration of competing interest

The authors declare that they have no known competing financial interests or personal relationships that could have appeared to influence the work reported in this paper..

Acknowledgements

The authors would like to thank the China Scholarship Council (CSC). The support provided by Ecole des Ponts ParisTech and INRAE is also greatly acknowledged.

References

Abedi-Koupai, J., and Mehdizadeh, H. 2008. Estimation of osmotic suction from electrical conductivity and water content measurements in unsaturated soils. Geotech. Test. J., 31(2), 142-148.

Arifin, Y. F., and Schanz, T. 2009. Osmotic suction of highly plastic clays. Acta Geotech., 4(3), 177-191.

ASTM D2487-00. 2000. Standard Practice for Classification of Soils for Engineering Purposes (Unified Soil Classification System). ASTM International, West Conshohocken, PA.

ASTM D4542-95. 2001. Standard Test Method for Pore Water Extraction and Determination of the Soluble Salt Content of Soils by Refractometer. ASTM International, West Conshohocken, PA.

ASTM D5298-16. 2016. Standard Test Method for Measurement of Soil Potential (Suction) Using Filter Paper. ASTM International, West Conshohocken, PA.

Boso, M., Romero, E., and Tarantino, A. 2005. The use of different suction measurement techniques to determine water retention curves. Unsaturated Soils: Experimental Studies Springer, Berlin, Heidelberg, 169-181.

Bulut, R., Hineidi. S. M., and Bailey, B. 2002. Suction measurements-filter paper and chilled mirror psychrometer. In Proceedings of the Texas section American Society of Civil Engineers, Fall Meeting, Waco, Texas, October, 2002, 2-5.

Dao, V. N. T., Morris, P. H., and Dux, P. F. 2008. On equations for the total suction and its matric and osmotic components. Cem. Concr. Res., 38(11), 1302-1305.

De Baecque, M., 2019. Caractérisation multi-physique de la durabilité d'un sol traité à la chaux pour une application aux digues maritimes. PhD Dissertation, Université Paris-Est.

Edil, T. B., and Motan, S. E. 1984. Laboratory evaluation of soil suction components. Geotech. Test. J., **7**(4), 173-181.

French standard AFNOR NF P 18-837. 1993. Standard for special products for hydraulic concrete construction-Hydraulic binder based needling and/or sealing products-Testing of resistance against seawater and/or water with high sulphate contents. Association Francaise de Normalisation.

Krahn, J., and Fredlund, D. G. 1972. On total, matric and osmotic suction. Soil Sci., 114(5), 339-348.

Leong, E. C., He, L., and Rahardjo, H. 2002. Factors affecting the filter paper method for total and matric suction measurements. Geotech. Test. J., 25(3), 322-333.

Leong, E. C., Tripathy, S., and Rahardjo, H. 2003. Total suction measurement of unsaturated soils with a device using the chilled-mirror dew-point technique. Géotechnique, 53(2), 173-182.

Leong, E. C., Widiastuti, S., Lee, C. C., and Rahardjo, H. 2007. Accuracy of suction measurement. Géotechnique, 57(6), 547-556.

Mata, C., Romero, E., and Ledesma, A. 2002. Hydro-chemical effects on water retention in bentonite-sand mixtures. In Proceeding of the 3rd International Conference on Unsaturated soil. Recife, Brazil, Swets & Zeitlinger, Lisse, 2002, 283-288.

Miller, D. J., and Nelson, J. D. 1993. Osmotic suction as a valid stress state variable in unsaturated soil mechanics. Unsaturated Soils, 64-76

Mitchell, J. K., and Soga, K. 2005. Fundamentals of soil behaviour. 3rd edn. John Wiley &Sonc, Inc.

Mokni, N., Romero, E., and Olivella, S. 2014. Chemo-hydro-mechanical behaviour of compacted Boom Clay: joint effects of osmotic and matric suctions. Géotechnique, 64(9), 681-693.

Rao, S. M., and Shivananda, P. 2005. Role of osmotic suction in swelling of salt-amended clays. Can. Geotech. J., 42(1), 307-315.

Rao, S. M., and Thyagaraj, T. 2007a. Role of direction of salt migration on the swelling behaviour of compacted clays. Appl. Clay. Sci., 38(1-2), 113-129.

Rao, S. M., and Thyagaraj, T. 2007b. Swell-compression behaviour of compacted clays under chemical gradients. Can. Geotech. J., 44(5), 520-532.

Rao, S. M., Thyagaraj, T., and Thomas, H. R. 2006. Swelling of compacted clay under osmotic gradients. Géotechnique, 56(10), 707-713.

Sreedeep, S., and Singh, D. N. 2006. Methodology for determination of osmotic suction of soils. Geotech. Geol. Eng., 24(5), 1469-1479.

Sun, D. A., Sun, W. J., Yan, W., and Li, J. 2010. Hydro-mechanical behaviours of highly compacted sand-bentonite mixture. J. Rock Mech. Geotech. Eng., 2(1), 79-85.

Sun, W. J., and Cui, Y. J. 2020. Determining the soil-water retention curve using mercury intrusion porosimetry test in consideration of soil volume change. J. Rock Mech. Geotech. Eng., 12(5), 1070-1079.

Sun, W. J, Sun, D. A., Fang, L., and Liu, S. Q. 2014. Soil-water characteristics of Gaomiaozi bentonite by vapour equilibrium technique. J. Rock Mech. Geotech. Eng., 6(1), 48-54.

Tang, A. M., Vu, M. N., and Cui, Y. J. 2011. Effects of the maximum soil aggregates size and cyclic wetting-drying on the stiffness of a lime-treated clayey soil. Géotechnique, 61(5), 421-429.

Tang. G. X., Graham, J., and Blat, J. 2002. Suctions, stresses and strengths in unsaturated sand-bentonite. Eng. Geol., 64(2-3), 147-156.

Thyagaraj, T., and Rao, S. M. 2010. Influence of osmotic suction on the soil-water characteristic curves of compacted expansive clay. J. Geotech. Geoenviron. Eng. 136(12), 1695-1702.

Thyagaraj, T., and Salini, U. 2015. Effect of pore fluid osmotic suction on matric and total suctions of compacted clay. Géotechnique, 65(11), 952-960.

United States Salinity Laboratory Staff, 1954. Diagnosis and improvement of saline and alkali soils. USDA Agriculture Handbook no. 60. U.S. Government Printing Office, Washington, D.C. 1954.

Wan, A. W. L., Gray, M. N., and Graham, J. 1995. On the relations of suction, moisture content and soil structure in compacted clays. 1st International Conference on Unsaturated Soils, Paris, France, 1995, 215-222.

Witteveen, P., Ferrari. A., and Laloui, L. 2013. An experimental and constitutive investigation on the chemo-mechanical behaviour of a clay. Géotechnique, 63(3), 244-255.

Ying, Z., Duc, M., Cui, Y. J., and Benahmed, N. 2021a. Salinity assessment for salted soil considering both dissolved and precipitated salts. Geotech. Test. J., 44(1), 130-137.

Ying, Z., Cui, Y.J., Benahmed, N., Duc, M., 2021b. Salinity effect on the compaction behaviour, matric suction, stiffness and microstructure of a silty soil. J. Rock Mech. Geotech. Eng., 13(4), 855-863.

Ying, Z., Cui, Y.J., Benahmed, N., Duc, M., 2021c. Drying effect on the microstructure of compacted salted soil. Géotechnique. https://doi.org/10.1680/jgeot.20.P.319

Chapter 3. Geotechnical property and drying-induced microstructure of untreated soils

Introduction

The soil geotechnical properties such as liquid limit and compaction behaviour are significantly affected by the salt solution. It was reported that, with increasing salt concentration, the liquid limit of expansive soils decreased due to the shrinkage of diffused double layer, while that of non-expansive soils increased due to the growing particle flocculation (Rao et al., 1993; Sridharan and Prakash, 2000; Di Maio et al., 2004; Mishra et al., 2009; Dutta and Mishra, 2015; Durotoye et al., 2016; Song et al., 2017). These two mechanisms seem to be controversial and it is difficult to understand how an increasing salinity can promote soil flocculation. Thus, the mechanism of salinity effect on the liquid limit of expansive soil and non-expansive soil was first clarified in this chapter by coupling with the sedimentation and rheological tests.

As regards the compaction behaviour, several studies indicated that the maximum dry density increased and the optimum water content decreased with increasing salinity for clays which had high clay fraction and swelling minerals (Abdullah et al., 1997, 1999; Abood et al., 2007; Shariatmadari et al., 2011; Durotoye et al., 2016), whereas others asserted that the salinity had no significant effect on compaction behaviour or led to a reduction of both maximum dry density and optimum water content for soils with low clay fraction (Ajalloeian et al., 2013; Liu and Zhang, 2014). Furthermore, the mechanism of salinity effect on the maximum dry density and optimum water content was not clarified. This constitutes the second work in this chapter. The salinity effect on the compaction behaviour was investigated by performing standard Proctor compaction test, suction measurement, bender element and mercury intrusion porosimetry (MIP) tests. In the third part, the drying-induced microstructure of compacted saline soils was studied by means of mercury intrusion porosimetry (MIP) and environmental scanning electron microscope (ESEM).

The results were presented in three papers. The results on the liquid limit were presented in the first paper published in “Acta Geotechnica”. The results on compaction behaviour were presented in the second paper published in “Journal of Rock Mechanics and Geotechnical Engineering”. The findings about drying-induced microstructure corresponded to the third paper published in “Géotechnique”. The articles are presented here in their original versions.

Ying, Z., Cui, Y.J., Duc, M., Benahmed, N., Bessaies-Bey, H., Chen, B. 2021. Acta Geotechnica, 16(4), 1101-1111.

Salinity effect on the liquid limit of soils

Zi Ying[1], Yu-Jun Cui[1], Myriam Duc[2], Nadia Benahmed[3], Hela Bessaies-Bey[4], Bo Chen[5]

Abstract: Previous studies stated that, with increasing salinity, the decreased liquid limit for expansive soils was attributed to the shrinkage of diffuse double layer, while the increased liquid limit for non-expansive soils was explained by the growing particle flocculation. These two mechanisms seem to be controversial and it is difficult to understand how an increasing salinity can promote soil flocculation. This study aims at clarifying the mechanism controlling liquid limit by conducting cone penetration test, sedimentation and rheological tests on MX80 bentonite and silty soil. Results showed that the liquid limit and yield stress of MX80 increased then decreased with increasing salinity, while they increased slightly for the silty soil. In sedimentation test, faster settling rate and smaller sediment volume were identified for MX80 and silt suspensions in NaCl solution, evidencing the shrinkage of diffuse double layer and the formation of denser aggregated structure. This suggested that the change of liquid limit is the result of two mechanisms in competition, which depend on the compression rate of diffuse double layer: (i) the water storage in nano-fissures which correspond to the nanoscale spaces among interlayers of clay particles resulting from the slight shrinkage of diffuse double layer, and (ii) the water expulsion into larger pores with significant shrinkage of diffuse double layer. For the MX80 at low salinity and for the silt soil, the first mechanism prevailed and the increasing liquid limit was attributed to the requirement of more water to fill the nano-fissures. In contrast, for MX80 at high salinity, the second mechanism prevailed - the diffuse double layer was compressed significantly, changing the double-layer water to free water and giving rise to the decrease of liquid limit.

Keywords: silty soil; expansive soil; liquid limit; sedimentation; yield stress

[1]: Ecole des Ponts ParisTech, Laboratoire Navier/CERMES, 6-8 av. Blaise Pascal, Cité Descartes, Champs-sur-Marne, 77455 Marne-la-Vallée cedex 2, France
[2]: Université Gustave Eiffel, IFSTTAR GERS/SRO, 14-20 boulevard Newton, Champs-sur-Marne, 77447 Marne-la-Vallée, France
[3]: INRAE, Aix Marseille Univ, RECOVER, Equipe G2DR, 3275 route Cézanne, CS 40061, 13182 Aix-en-Provence, France
[4]: Université Gustave Eiffel, IFSTTAR MAST/CPDM, 14-20 boulevard Newton, Champs-sur-Marne, 77447 Marne-la-Vallée, France
[5]: College of Civil Engineering and Architecture, Quzhou University, Zhejiang, 324000, P. R. China

1. Introduction

The soil liquid limit (w_L or LL) is defined as the limiting water content between liquid and plastic states [44]. It is commonly a strength-based measurement [46] and a parameter usually used for the classification of soils [9, 26]. The soil liquid limit was also correlated with other soil properties such as permeability [34], shear strength [7, 45, 46] and compressibility [21, 22, 32, 60]. Sridharan and Prakash [44] adopted the viscometer test to investigate the yield shear strength of soil-water slurries at liquid limit and settling limit water contents and reported that the yield shear strength at setting limit was smaller than that at liquid limit water content. Indeed, all soils have their proper yield shear strengths at their corresponding liquid limits that vary in the range of 0.5 ~ 5.6 kPa [46]. Kenney [27] tried to give a rheological interpretation for the liquid limit test (percussion cup test) which was not a strength test, but was a stress-controlled and strain-dependent measurement. Basically, the rheological test reflects the relationship between the shear stress and the shear rate/shear strain [30]. There is a peak stress which is commonly termed as "yield stress", corresponding to a critical strain at which flow occurs [10]. Hajela and Bhatnagar [20] reported that the liquid limit increased while the yield stress decreased with increasing ratios of plastic index to specific surface area.

Furthermore, according to ASTM standard D 4318-10 [9], distilled water or deionized water should be used in the liquid limit measurement. However, while investigating the salt effect, salt solution with different concentrations was adopted by several authors [13, 14, 18, 19, 34, 43] and previous studies showed that increasing salt concentration could either decrease or slightly increase the liquid limit. Table 1 shows the soil information and resources in the case of decrease of liquid limit with the increase of salt concentration. In this case, mainly expansive soils with significant montmorillonite/smectite fractions are involved. The variations of liquid limit with salt concentration for the soils shown in Table 1 are displayed in Fig. 1a and in Fig. 1b for the salt concentration ranging from 0 to 1.2 mol/L and 0 to 8 mol/L, respectively. In Fig. 1a, the liquid limit decreased more significantly for the soil with higher clay content [16] or with higher montmorillonite/smectite fraction [34]. The same observation can be made from Fig. 1b. The salt effect was more significant for commercial bentonite with almost pure smectite [12] and Ponza bentonite with 70 ~ 80% Na-smectite [14] as compared to the Bisaccia clay and Marino clay [14] which had only 30% Ca-smectite and 10% mixed layer illite-smectite, respectively.

Table 1. Sample information for soils whose liquid limit decreased with increasing salt concentration.

Soil	Minerals or properties	References	Figures
Bentonite A	57% of clay content, 43% silt content; CEC = 27.2 meq/100g; ESP = 38.8%; SSA= 339 m^2/g.	Dutta and Mishra [16]	Fig. 1a
Bentonite B	68% of clay content, 32% silt content; CEC= 44.6 meq/100g; ESP= 54.2 %; SSA= 456 m^2/g.		
Bentonite and basalt soil mixed in a mass ratio of 20:100	Bentonite A (27.7% montmorillonite); Bentonite B (57.1% montmorillonite); Bentonite C (42.8% montmorillonite); Bentonite D (50.1% montmorillonite); Basalt soil (12% clay content).	Mishra et al. [34]	
Commercial bentonite	Pure smectite	Calvello et al. [12]	Fig. 1b
Ponza bentonite	70-80% Na-smectite + 20% kaolinite.	Di Maio et al. [14]	
Bisaccia clay	30% Ca-smectite, 20% illite, 10% kaolinite, 10% chlorite, 15% quartz, 10% calcite, 5% Feldspars.		
Marino clay	30% kaolinite, 10% illite, 10% mixed layer illite-smectite, 10% chlorite, 30-40% quartz.		

Note: CEC: cation exchange capacity; ESP: Exchangeable sodium percentage; SSA: Specific surface area

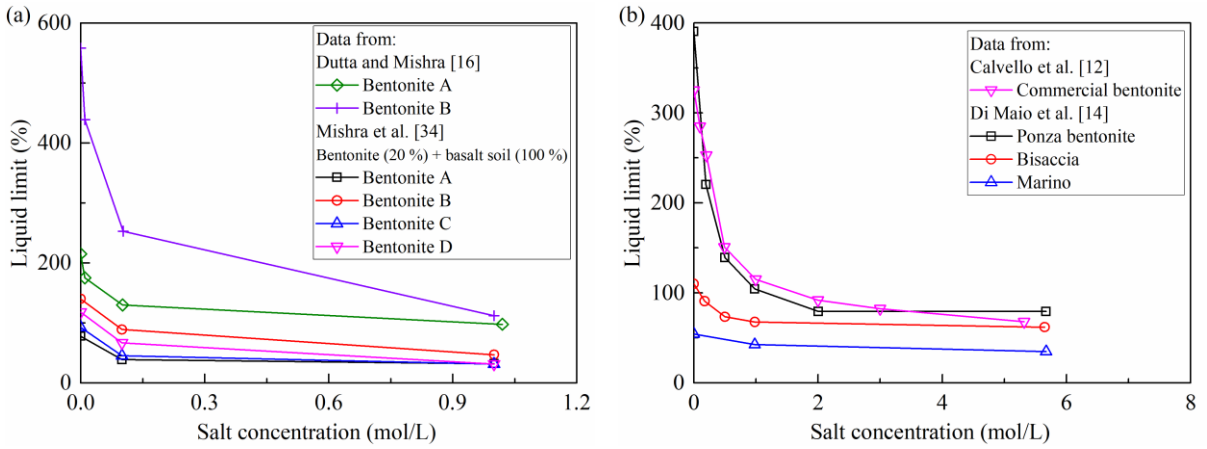

Fig. 1. Salt concentration effect on liquid limit of expansive soil.

Table 2 shows the soil mineralogy and the corresponding resources in the case of slight increase or constant value of liquid limit when the salt concentration increased. In this case, the soils involved were mainly kaolinite [14, 23], chlorite [19] and illite [43]. Figure 2 shows the variations of liquid limit with salt concentration. Seven soils exhibited an increase of liquid limit with salt concentration and three soils showed constant liquid limit values with changes of salt concentration.

Table 2. Sample information for soils whose liquid limit increased or kept constant with increasing salt concentration.

Soil	Minerals	References
Commercial kaolin	75-80% kaolinite, 8-10% illite, < 5% smectite, 10% quartz and feldspars.	Di Maio et al. [14]
Mink creek	41% chlorite, 37% illite, 22% kaolinite.	Geertsema and Torrance [19]
Kaolin	31% silt, 69% clay.	Horpibulsuk et al. [23]
Bangkok clay	39% silt, 61% clay.	
Megurie clay	Smectite, mica, vermiculite, kaolinite, chlorite, quartz, feldspars, cristobalite.	Ohtsubo et al. [38]
Lianyungang clay	68% illite, 11% chlorite, 8% kaolinite, 13% smectite.	Song et al. [43]
Wenzhou clay	76% illite, 11% chlorite, 13% kaolinite.	
Kawazoe	11.5% smectite, 9.9% kaolinite, 10.7% vermiculite, 18.9% illite, 49% non-clay minerals.	Sridharan et al. [48]
Kubota	15.1% smectite, 9.2% kaolinite, 11.5% vermiculite, 22.3% illite, 41.9% non-clay minerals.	
Isahaya	12.8% smectite, 12.8% kaolinite, 14.7% vermiculite, 25.6% illite, 34.1% non-clay minerals.	

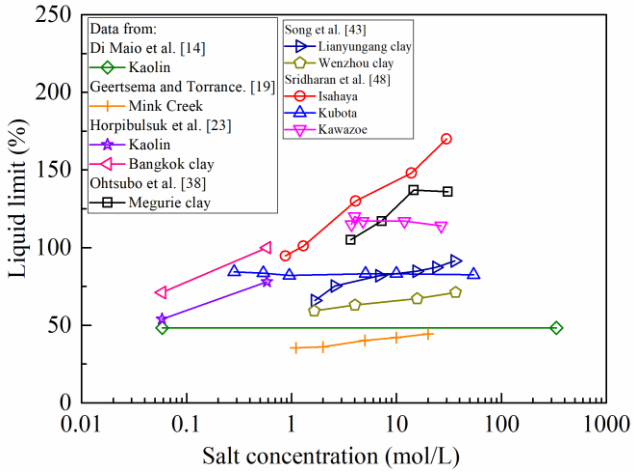

Fig. 2. Salt concentration effect on liquid limit of non-expansive soil.

From these studies, the mineralogical compositions and the clay content appeared clearly as the main factors influencing the variations of liquid limit with salt concentration. Significant decrease of liquid limit occurred with increasing salt concentration when the soil had higher quantity of montmorillonite/smectite or clay content. On the contrary, slight increase or constant value of liquid limit was observed for kaolinite, illite and chlorite, even in the case of soils

which contained a small quantity of montmorillonite/smectite. Indeed, such a clay type belongs to the three-layer minerals with 2:1 structural units, consisting of one octahedral aluminium sheet sandwiched between two tetrahedral siliceous sheets with isomorphic substitutions [35]. Thus, they exhibit high expansive capacity considering the cation exchange in interlayer coupled with water penetration in diffuse double layer [30, 35]. Sridharan et al. [48] stated that the diffuse double-layer water had a predominant role in liquid limit for expansive soils. An increase of salt concentration reduced the surface potential, leading to a decrease of the thickness of diffuse double layer [24, 35]. Thus, the inter-particle repulsive forces decreased, which led soil particles to associate with each other at a lower inter-particle distance. As a result, the liquid limit decreased [47, 57]. In other words, the shrinkage of diffuse double layer caused a reduction of liquid limit for expansive soils [7, 8, 23, 40, 46, 48, 60].

In the case of non-expansive clays such as kaolinite, illite or chlorite, the increase of salt concentration also resulted in a reduction of repulsive force and an increased or unchanged attractive force, leading to an increase of net attractive forces among soil particles [56]. According to Anson and Hawkins [7], Horpibulsuk et al. [23], Sridharan and Prakash [45], and Sridharan et al. [48], this would favour the flocculation of soil particles, leading to an increase of liquid limit because more water could be entrapped in a more flocculated structure. This explanation seems to be ambiguous and controversial because it is difficult to understand why in the case of non-expansive soils, particle flocculation might occur, while in the case of expansive soils such flocculation would not be possible. The increased liquid limit of non-expansive soils with salinity increase was also attributed to the dispersion of clay particles in salt solution [8] or explained by the formation of new expansive compounds which could increase the liquid limit [42]. On the whole, the salinity effect on the liquid limit of soils have not been well understood yet, in particular for non-expansive soils.

This study aims at clarifying the salt effect on liquid limit of soils. Two soils were considered: the MX80 Na-bentonite and a silty soil. Cone penetration method was applied to determine the liquid limit of both soils at different water salinities. Sedimentation test and rheological test were carried out on the two soils prepared with and without salt to ascertain the salt effect on liquid limit. The obtained results were analysed together with the data collected from the literature.

2. Materials and methods

2.1 Materials

A commercial MX80 Na-bentonite from Wyoming (USA) and a silty soil collected from Salin-de-Giraud (France) were used in this study. The MX80 Na-bentonite contains 92% smectite and 3% quartz [50]. The silty soil is composed of 15.7% clay minerals including 10.8% illite, 3.6% chlorite, 1.3% kaolinite and 84.3% non-clay minerals. The non-clay minerals consist of 39% quartz, 35% calcite, 9.5% feldspars and 0.8% halite NaCl. As reported by Ying et al. [59], the water salinity of natural soil pore water is 13.3‰ (g of salt/kg of salty water). The basic geotechnical properties of these two soils are given in Table 3.

Table 3. Characteristics of studied soils

Property	MX80 Na-bentonite	Silty soil
Liquid limit, w_L (%)	630	29
Plastic limit, w_p (%)	42[a]	19
Plasticity Index, I_p	478[a]	10
Specific gravity, *Gs*	2.76[a]	2.71
Specific surface area (m^2/g)	562[b]	24

[a]Data from Tang et al. [50]; [b]Data from Madsen [31].

The cone penetration method [1] and the hand method [9] were adopted to determine the liquid limit and plastic limit for MX80 Na-bentonite and for silty soil, using deionized water. The specific gravity and specific surface area of silty soil were determined by pycnometer method [2] and by spot test of methylene blue absorption measurement [5], respectively.

The grain size distributions of the two soils are presented in Fig. 3. For the silty soil, it was determined by the dry sieving method for particles larger than 80 μm and by the hydrometer method for particles smaller than 80 μm, according to the French standards AFNOR NF P 94-056 [3] and AFNOR NF P 94-057 [4], respectively. The MX80 Na-bentonite consists of 84% clay-size particles and 16% silt-size particles, while the silty soil is composed of 17% clay-size particles, 63% silt-size particles and 20% sand grains.

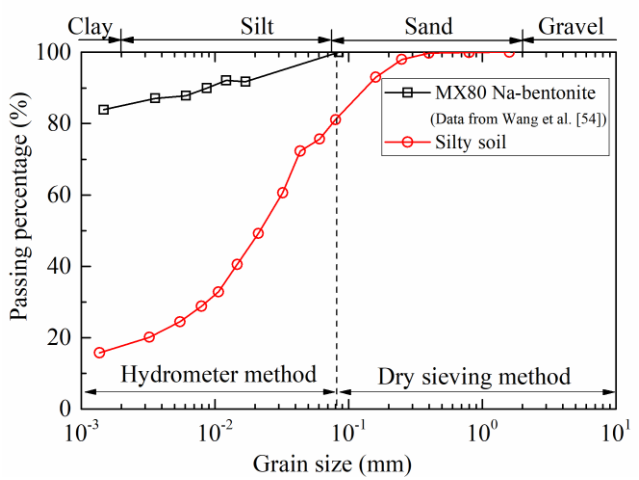

Fig. 3. Grain size distribution of MX80 Na-bentonite and silty soil.

2.2 Liquid limit

According to the French standard AFNOR NF P 94-052 [1], the natural silty soil was washed and passed through 400 μm sieve. Afterwards, the soil was oven-dried at 50°C prior to the liquid limit measurement. For the MX80 Na-bentonite powder, raw material was used directly for the liquid limit measurement.

To investigate the salt effect, considering that the MX80 Na-bentonite had a smectite content as high as 92% which was expected to be very sensitive to salinity changes, it was mixed with NaCl solution at different water salinities in a relatively small range: 0.005‰, 0.05‰, 0.5‰, 2‰ and 10‰. By contrast, the target water salinities of silty soil were chosen as 6‰, 12‰, 25‰ and 35‰, in a larger range. To guarantee the accuracy requirement in preparing the salt solution, a balance of 0.0001 g readability was used to weigh the salt mass. After mixing, the soils were stocked during 24 h for homogenization. Then, the soil was mixed again with the corresponding NaCl solutions to adjust the salty water contents allowing the falling depth of cone to be within the range from 12 mm to 25 mm. At least 5 different salty water contents were adjusted for the soil with given NaCl solution, allowing a curve of falling depth of cone versus salty water content to be satisfactorily plotted. The salty water content at falling depth of 17 mm was considered as the liquid limit of soil. The salty water content (w'), was defined as the ratio of salty water mass (m_{sw}) to dry soil mass without salt (m_s) and it was calculated by Eq. 1 [59]:

$$w' = \frac{m_{sw}}{m_s} = \frac{m - m_d}{m_d - rm} \quad (1)$$

where r is the water salinity (‰ or g of salt/kg of salty water); m_d is the oven-dried mass including soil and salt and m is the mass of wet soil before oven-drying.

3.2 Sedimentation test

The sedimentation test was the simplest way for characterising the effect of salinity on the diffuse double layer thickness and arrangement of soil particles [28, 29, 53, 55]. In the soil suspension, the soil particles tend to settle down under gravity and then reach steady state until the gravitational forces are balanced by the fluid viscosity and the (R-A) forces, where R is the double-layer repulsive force and A is the electrostatic and other attractive forces in soil-water system [44]. In this study, the soil suspensions were prepared following the procedure of grain size distribution analysis according to the French standard AFNOR NF P 94-057 [4]. The soil-water mixtures of MX80 Na-bentonite and silty soil were first prepared by adding 80 g of dry soils into 300 mL deionized water or 35‰ NaCl solution little by little. The soil-water mixtures were conserved for 15 h for salt and water homogenization. Then, they were mixed thoroughly for 3 min by a mixer. Afterwards, they were poured into 2000 mL graduated cylinders. Additional deionized water or 35‰ NaCl solution were added to obtain a suspension volume of 2000 mL. The soil suspensions were stirred for 1 min to allow complete dispersion. The sediment volume at the bottom of the cylinder was recorded with time during particle settlement, until this volume reached a stable value.

3.3 Rheological test

Rheological test was conducted on soil slurry to investigate the yield stress variations with salinity. The yield stress measurement was carried out with a C-VOR Bohlin rheometer equipped with a Vane geometry [17]. The Vane tool diameter is 25 mm. The outer cup diameter is 50 mm and its depth is 60 mm [11]. The details of the samples are listed in Table 4.

Table 4. Details of the soil-water/solution slurry used for rheological test.

Soils	Liquid limit determined by deionized water, w_L (%)	Water content or salty water content (%)	Solid content (%)	Water salinity of NaCl solution (‰)
MX80 Na-bentonite	630	500 (0.8 w_L)	20	0, 0.005, 0.05, 0.5, 2, 5, 10
Silty soil	29	43.5 (1.5 w_L)	230	0, 6, 12, 25, 35

The water content of MX80 Na-bentonite slurries was fixed at 500% (0.8 w_L, where w_L is the liquid limit determined with deionized water). The corresponding solid content, defined as the ratio of dry soil mass to solution mass, was 20%, ensuring that the soil slurries prepared with deionized water and NaCl solution at various salinities was suitable for testing (not too solid or too liquid). As shown in Fig. 4a, the MX80 Na-bentonite slurries changed from a thick state to a fluid state as water salinity increased. For the silty soil slurries, the water content was fixed at 43.5% (1.5 w_L, where w_L is the liquid limit determined with deionized water), and the corresponding solid content was 230%. Fig. 4b shows that the salinity had no significant effect on silt slurry states in comparison to MX80 Na-bentonite slurries.

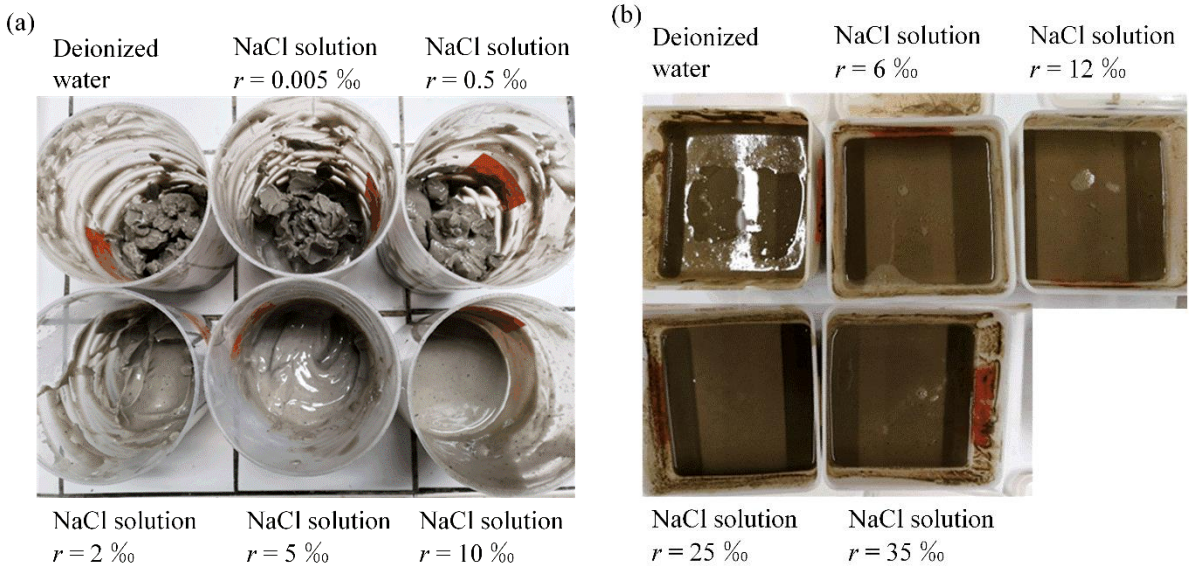

Fig. 4. Sample states with different water salinities for rheological test: (a) MX80 Na-bentonite; (b) Silty soil.

Afterwards, the soil slurries were covered and stored for at least 24 h for water and salt homogenization. The soil slurry was first mixed for 5 min by a mixer at rotate speed of 200 rpm. Then, it was introduced into the rheometer cup immediately after mixing. In rheometer,

the soil slurry was firstly stood during 1200 s prior to the testing at a constant shear rate of 0.01 s^{-1} during 500 s.

3. Results

3.1 Liquid limit

The liquid limit variations with water salinity for MX80 Na-bentonite are depicted in Fig. 5a. The liquid limit had a slight increase from 630% to 652% for the sample prepared with 0.005‰ NaCl solution in comparison to the value obtained with deionized water. Then, the liquid limit decreased with further increasing water salinity from 0.005‰ to 10‰. This phenomenon was also reported for other expansive soils and was attributed to the reduction of diffuse double layer resulting from the increase of salt concentration [12, 14, 15, 16, 34, 0, 52]. It is however worth noting that, to the authors' knowledge, no study reported the slight increase of liquid limit in the range of low water salinity.

For the silty soil, the liquid limit variations with the water salinity are depicted in Fig. 5b. The liquid limit slightly increased with the increase of salinity. This was consistent with the observations made on non-expansive soils [14, 19, 43].

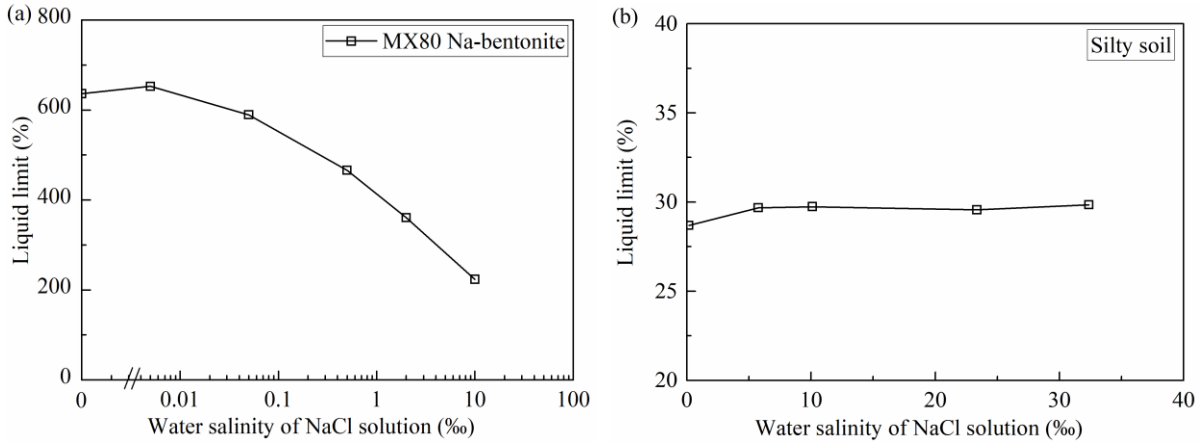

Fig. 5. Water salinity effect on liquid limit: (a) MX80 Na-bentonite; (b) Silty soil.

3.2 Sedimentation test

The variations of sediment volume with settling time are shown in Fig. 6 for MX80 Na-bentonite suspension and silty soil suspension prepared with deionized water and 35‰ NaCl

solution, respectively. The photos of the final sedimentation tests are given in Fig. 7. The sediment volume corresponded to the zone of settled particles below the zone of clean water.

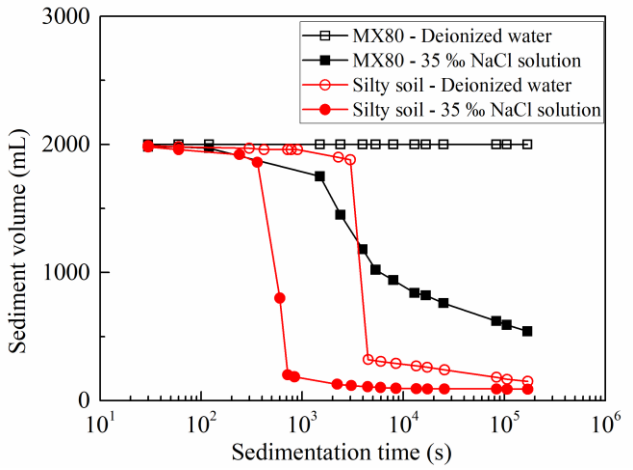

Fig. 6. Salt solution effect on sedimentation curves.

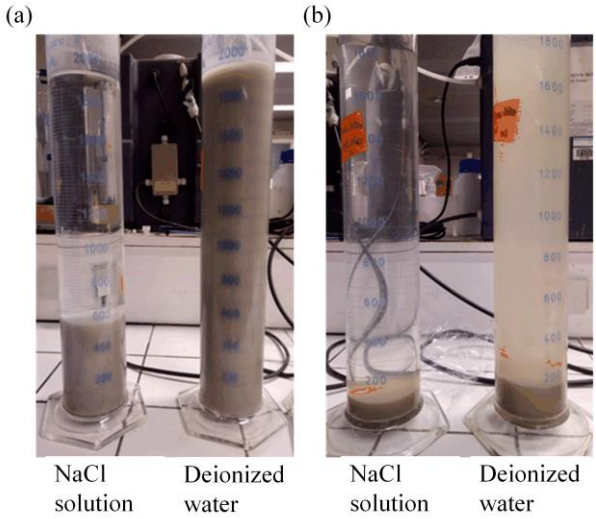

Fig. 7. Salt solution effect on final sediment volume: (a) MX80 Na-bentonite; (b) Silty soil.

The MX80 Na-bentonite suspension prepared with deionized water remained dispersed and the sediment volume was close to the initial volume of suspension. However, the MX80 Na-bentonite particles settled gradually in the suspension prepared with 35‰ NaCl solution, resulting in a separation between settled particles and clean water. From naked eye observation, the silty soil suspension prepared with deionized water kept almost stable before 3000 s, then the suspension started to settle down quickly (Fig. 6). In the case of silty soil prepared with NaCl solution, the suspension volume started to decrease drastically after a shorter time (400 s) and the silt particles formed a smaller final sediment volume than that in deionized water (Fig.6).

3.3 Rheological test

The relationships in terms of shear stress as a function of shear strain plotted in Fig. 8 show the presence of a yield stress corresponding to the stress peak. The yield stress variations with water salinity of NaCl solution for MX80 Na-bentonite and silty soil are given in Fig. 9. To check the reproducibility of tests, the yield stress measurements of MX80 Na-bentonite and silty soil were determined in duplicate and triplicate, respectively. The mean values were used in further analysis.

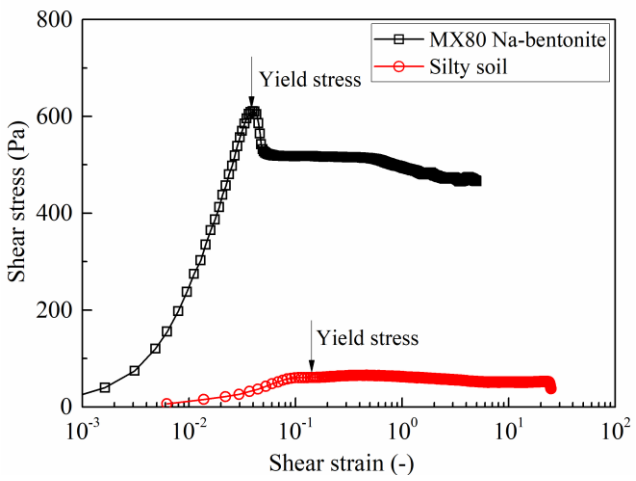

Fig. 8. Relationship between shear stress and shear strain.

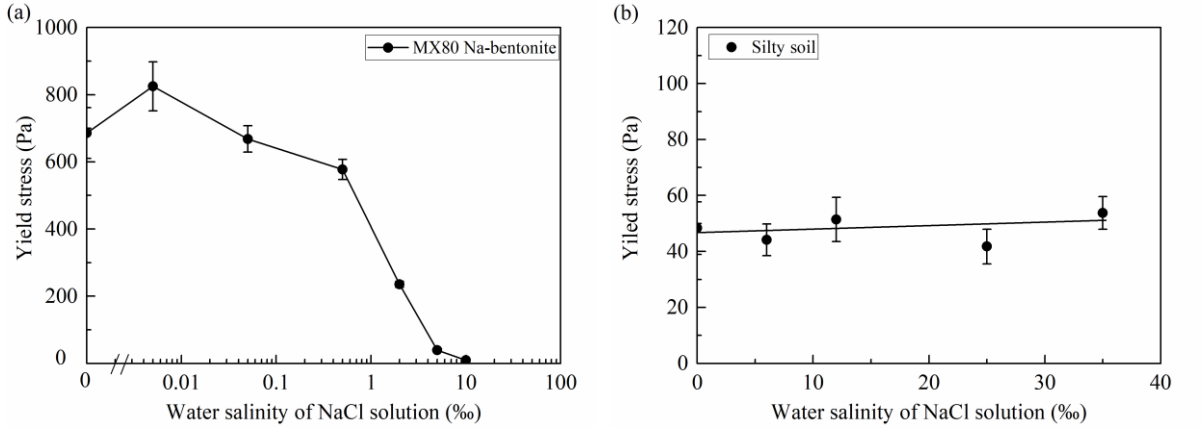

Fig. 9. Water salinity effect on yield stress: (a) MX80 Na-bentonite; (b) Silty soil.

As shown in Fig. 5a and Fig. 9a, the salinity effects on liquid limit and yield stress for MX80 Na-bentonite were in good agreement: both liquid limit and yield stress increased slightly when the water salinity of NaCl solution increased to 0.005‰, then decreased with further increase of water salinity. Interestingly, for the silty soil, the salinity effect on liquid limit was also in full agreement with the variations of yield stress: the liquid limit and yield stress had a slight

increase or kept almost constant with the increase of water salinity of NaCl solution (Fig. 5b and Fig. 9b). This confirmed that the liquid limit corresponds to a strength-based measurement [46].

4. Discussions

The liquid limit, representing the water-holding capacity of soil, is well correlated to the thickness of diffuse double layer [44]. The thickness (d) of such layer in clay particles was expressed by Eq. 2 [35]:

$$d = \sqrt{\frac{\varepsilon kT}{2n_0 e^2 v^2}} \tag{2}$$

where ε is the dielectric constant of pore water ($80\times8.85\times10^{-12}$ $C^2/(J\cdot m)$ for deionized water); k is the Boltzmann constant (1.38×10^{-23} J/K); T is the temperature (293 K in laboratory); e is the electronic charge (1.602×10^{-19} C); n_0 is the ion concentration (ion number/m^3) and v is the ionic valence.

Equation 2 shows that the thickness of diffuse double layer varies inversely with the square root of the ion concentration and it tends to be infinity in deionized water. Indeed, as shown in Fig. 7a, MX80 Na-bentonite particles swelled and dispersed thoroughly in deionized water, producing a viscous gel-like structure and thus preventing soil particles from settling, while they settled faster and formed smaller sediment volume in NaCl solution. This was consistent with the observations made by Akther et al. [6], Kondo and Torrance [28], Liu et al. [29], Luckham and Rossi [30], and Zhang et al. [61]. This sedimentation behaviour was highly related to the type of particle associations, such as dispersion, flocculation or aggregation [53]. Basically, flocculation was related to edge-to-face and edge-to-edge associations which constituted three-dimensional “house-of-card” structures, while aggregation in clay suspensions was characterized by face-to-face particle association and referred to the collapse of diffuse double layer, corresponding to thicker and larger flakes [30, 55]. The opposite of aggregation was known as dispersion [30]. Correspondingly, the state or condition of the soil dispersion in a liquid in which soil particles remained independent and un-associated with adjacent particles was termed as de-flocculation [25]. The type of particle associations was dependent on the rate of compression of diffuse double layer [30, 49]. In deionized water or dilute salt solution, montmorillonite/smectite minerals remained well dispersed in a

homogenous gel form with edge-to-face or edge-to-edge particle associations [30]. The well-developed diffuse double layer and the dominant repulsive force between montmorillonite/smectite particles made the soil particles orient themselves towards the positions of minimum free energy, preventing thus the soil particles from settling [30]. However, the development of diffuse double layer was depressed in salt solution, causing a decrease of repulsive force, which in turn, led to an increase of net attractive force [24, 35]. As a result, denser face-to-face aggregations were formed, leading to a faster sedimentation and smaller sediment volume [6, 29, 30, 49]. It was reported that the compression rate of diffuse double layer was dominated by the salt concentration for bentonite [35, 49]. During hydration, the inter-basal spacing of montmorillonite/ smectite was known to increase from 9.6 Å (0.96 nm) to complete separation due to the successive adsorption of water molecule layers [35]. This was consistent with the gel-structure for MX80 Na-bentonite in deionized water, as shown in Fig. 7a. Norrish [37] and Tessier [51] observed that the inter-basal spacing of montmorillonite gels reached 10 nm (0.3 nm for one layer of water molecules) in deionized water or dilute solution. Moore [36] stated that the diffuse double layer thickness of montmorillonite was 19.40nm, 6.2 nm and 1.94 nm for NaCl solution at 0.001, 0.01 and 0.1 mol/L concentrations, respectively. Assuming that the dielectric constant of NaCl solution at 0.005‰ (corresponding to 8.55 × 10-5 mol/L) was the same as for deionized water, the diffuse double layer thickness calculated by Eq. 2 was 33 nm, which was slightly larger than the value of 19.40 nm obtained by Moore [36] for montmorillonite in 0.001 mol/L NaCl solution and also larger than the inter-basal spacing of montmorillonite of 10 nm in deionized water or dilute solution [37, 51]. This suggested that, as the concentration varied in a lower range, the shrinkage of diffuse double layer was slight. It could be thus inferred that the produced fissures (or interlamellar or lenticullar pores) among interlayers of clay particles were in nanoscale. The compression rate of diffuse double layer in NaCl solution can be also assessed by the paste states in Fig. 4a. The similar paste states for MX80 Na-bentonite prepared with deionized water and that prepared with NaCl solution at 0.005‰ water salinity suggested that, with small increase of salinity from 0 to 0.005‰ in MX80 Na-bentonite, the development of diffuse double layer was just slightly compressed, leading to some nano-fissures between interlayers as described previously. Thus, more water was needed to fill such nano-fissures. As the size of nano-fissures was very small, the water molecule was heavily absorbed to the montmorillonite/smectite surfaces [33], improving the water-holding capacity of MX80 Na-bentonite and leading thus to an increase of liquid limit. As the diffuse double layer shrunk, the number of layers per clay particle increased, forming an aggregated structure and thus an increase of yield stress as observed for MX80 Na-

bentonite prepared with 0.005‰ NaCl solution (Fig. 9a).

With further increase of water salinity in MX80 Na-bentonite, the diffuse double layer was highly compressed, leading to thinner and denser face-to-face associations [6, 30]. This significant shrinkage of diffuse double layer caused a considerable increase of effective void size [39, 41, 58], changing some double-layer water to free water in larger pores. This was confirmed by the observation on MX80 Na-bentonite states in Fig. 4a: the MX80 Na-bentonite mixtures became much liquid at higher water salinity. It was also confirmed by the apparent interface between settled particles and clean water in Fig. 7a in MX80 Na-bentonite suspension prepared with NaCl solution. As the diffuse double layer was compressed, the bentonite particles in paste or suspension became smaller and thinner separate aggregates with increasing salinity, leading to a weaker interaction network between adjacent aggregates and thus a lower yield stress. Correspondingly, the liquid limit of MX80 Na-bentonite decreased as the expulsion of the diffuse double-layer water.

As shown in Fig. 6 and Fig. 7b, the faster settling rate and smaller sediment volume were also obtained on silty soil suspension in NaCl solution, suggesting that the thickness of diffuse double layer at clay mineral surface in silty soil also decreased and the suspension formed denser aggregated structure in salt solution. Thus, the increase of the liquid limit in silty soil as well as other non-expansive soils (as listed in Table 2) was not attributed to the flocculated particle arrangement which allowed the water entrapment within larger void space as explained in previous studies. The increase of water storage in clay aggregates was rather due to the nano-fissures in which water was subjected to the effect of diffuse double layer. Even though such nano-fissures were not directly observed on silty soil, their presence was strongly suspected as smaller sediment volume was observed for silty soil in NaCl solution. In fact, for all soils, salt solution could cause a reduction of the diffuse double layer thickness, changing the liquid limits subsequently.

In the case of silty soil, the salt effect on diffuse double layer was limited, due to a low clay-size fraction (17%) on one hand, and to its less active clay minerals (10.8% illite, 3.6% chlorite and 1.3% kaolinite) on the other hand. Indeed, the coarser particles usually presents lower specific surface area and thus less opportunity to develop particle interactions via the diffuse double layer, as suggested by the values of specific surface area in Table 3: MX80 Na-bentonite had a value of 562 m^2/g which was much higher than the value for the silty soil (24 m^2/g).

Therefore, as water salinity increased from 0 to 35‰, the diffuse double layer of silty soil had a slight shrinkage, which was similar to the MX80 Na-bentonite at 0.005‰ water salinity. It was confirmed by the similar states of silt slurries at different salinities in Fig. 4b and the visible but insignificant difference between the final sediment volumes in Fig. 7b. Consequently, the nano-fissures were expected in silty soil, improving the water storage by adsorption and giving rise to an increase of liquid limit. This aggregation process by diffuse double layer compression led to the increase of yield stress consequently, as for MX80 Na-bentonite below 0.005‰ water salinity.

5. Conclusions

The salt effect on liquid limit, sedimentation behavior and yield stress of MX80 Na-bentonite and silty soil were investigated in this paper. On the basis of the experimental results, some conclusions can be drawn, as follows:

(1) The suspensions of MX80 Na-bentonite and silty soil settled faster and formed smaller sediment volumes in NaCl solution than in deionized water. It evidenced that the thickness of diffuse double layer of clay minerals in silty soil was reduced as bentonite, leading to a denser face-to-face aggregated structure.

(2) For MX80 Na-bentonite, both liquid limit and yield stress increased slightly when the water salinity of NaCl solution increased from 0 to 0.005‰, then decreased with further increase of water salinity. As for the silty soil, the liquid limit and yield stress had a slight increase or kept almost constant with the increase of water salinity. The salinity effects on liquid limit and yield stress for MX80 Na-bentonite were in good agreement, confirming that the liquid limit measurements were strength-based tests.

(3) The variations of liquid limit with water salinity were the results of the competition of two mechanisms: (i) water storage in nano-fissures resulting from the slight shrinkage of diffuse double layer, and (ii) water expulsion with significant shrinkage of diffuse double layer. For the silty soil and MX80 Na-bentonite at low salinity, it would be the first mechanism which prevailed - the increase of liquid limit with increasing salinity could be attributed to the occurrence of nano-fissures which required more water to fill them. Meanwhile, increasing water salinity favoured the formation of aggregated structure, leading to an increase of yield stress. In contrast, for MX80 Na-bentonite at higher salinity, it would be the second mechanism

which prevailed - the diffuse double layer was compressed significantly, expelling out more double-layer water to lager pores as free water and further decreasing the liquid limit. Due to the shrinkage of diffuse double layer, the bentonite particles seemed to form separate and smaller aggregates, leading to a decrease of yield stress.

Acknowledgements

The authors would like to thank the China Scholarship Council (CSC). The supports provided by Ecole des Ponts ParisTech (ENPC) and INRAE are also greatly acknowledged.

References

1. AFNOR NF P 94-052 (1995) Standard test for soils investigation and testing-Atterberg limit determination-Part 1: Liquid limit-Cone penetrometer method.
2. AFNOR NF P 94-054 (1991) Standard test for soils investigation and testing-Determination of particle density-Pycnometer method.
3. AFNOR NF P 94-056 (1996) Standard test for soils investigation and testing-Granulometric analysis-Dry sieving method after washing.
4. AFNOR NF P 94-057 (1992) Standard test for soils investigation and testing-Granulometric analysis-Hydrometer method.
5. AFNOR NF P 94-068 (1998) Standard test for soils investigation and testing-Measuring of the methylene blue adsorption capacity of a rocky soil-Determination of the methylene blue of a soil by means of the stain test.
6. Akther S, Hwang J, Lee H (2008) Sedimentation characteristics of two commercial bentonites in aqueous suspensions. Clay Miner 43(3):449-457.
7. Anson RWW, Hawkins AB (1998) The effect of calcium ions in pore water on the residual shear strength of kaolinite and sodium montmorillonite. Géotechnique 48(6):787-800. https://doi.org/10.1680/geot.1998.48.6.787
8. Arasan S, Yetimoğlu T (2008) Effect of inorganic salt solutions on the consistency limits of two clays. Turkish J Eng Env Sci 32(2):107-115.
9. ASTM D 4318-10 (2014) Standard Test Methods for Liquid limit, Plastic limit, and Plasticity Index of Soils. ASTM International, West Conshohocken, PA.
10. Bessaies-Bey H, Baumann R, Schmitz M, Radler M, Roussel N (2015) Effect of polyacrylamide on rheology of fresh cement pastes. Cem Concr Res 76:98-106. https://doi.org/10.1016/j.cemconres.2015.05.012
11. Bessaies-Bey H, Hot J, Baumann R, Roussel N (2014) Consequences of competitive adsorption between polymers on the rheological behaviour of cement pastes. Cem Concr Compos 54:17-20. https://doi.org/10.1016/j.cemconcomp.2014.05.002
12. Calvello M, Lasco M, Vassallo R, Di Maio C (2005) Compressibility and residual shear strength of smectitic clays: influence of pore aqueous solutions and organic solvents. Italian Geotech J 1:34-46.

13. Deng YF, Yue XB, Cui YJ, Shao GH, Liu SY, Zhang DW (2014) Effect of pore water chemistry on the hydro-mechanical behaviour of Lianyungang soft marine clay. Appl Clay Sci 95:167-175. https://doi.org/10.1016/j.clay.2014.04.007

14. Di Maio C, Santoli L, Schiavone P (2004) Volume change behaviour of clays: the influence of mineral composition, pore fluid composition and stress state. Mech Mater 36(5-6):435-451. https://doi.org/10.1016/S0167-6636(03)00070-X

15. Durotoye TO, Akinmusuru JO, Ogbiye AS, Bamigboye GO (2016) Effect of common salt on the engineering properties of expansive soil. Int J Eng Technol 6(7):233-241.

16. Dutta J, Mishra AK (2015) A study on the influence of inorganic salts on the behaviour of compacted bentonites. Appl Clay Sci 116-117:85-92. https://doi.org/10.1016/j.clay.2015.08.018

17. Dzuy NQ, Boger DV (1985) Direct yield stress measurement with the vane method. J Rheol 29(3):335-347. https://doi.org/10.1122/1.549794

18. Elmashad ME, Ata AA (2016) Effect of seawater on consistency, infiltration rate and swelling characteristics of montmorillonite clay. HBRC J 12(2):175-180. https://doi.org/10.1016/j.hbrcj.2014.12.004

19. Geertsema M, Torrance JK (2005) Quick clay from the Mink Creek landslide near Terrace, British Columbia: geotechnical properties, mineralogy, and geochemistry. Can Geotech J 42(3):907-918. https://doi.org/10.1139/t05-028

20. Hajela, RB, Bhatnagar JM (1984) Rheological properties of clay pastes-Part III: surface area and thixotropy at liquid limit consistency. *Transactions of the Indian Ceramic Society* 43(4):96-100. https://doi.org/10.1080/0371750X.1984.10822691

21. Hong ZS, Yin J, Cui YJ (2010) Compression behaviour of reconstituted soils at high initial water contents. Géotechnique 60(90):691-700. https://doi.org/10.1680/geot.09. P.059

22. Hong ZS, Zeng LL, Cui YJ, Cai YQ, Lin C (2012) Compression behaviour of natural and reconstituted clays. Géotechnique 62(4):291-301. https://doi.org/10.1680/geot.10.P. 046

23. Horpibulsuk S, Yangsukkaseam N, Chinkulkijniwat A, Du YJ (2011) Compressibility and permeability of Bangkok clay compared with kaolinite and bentonite. Appl Clay Sci 52(1-2):150-159. https://doi.org/10.1016/j.clay.2011.02.014

24. Israelachvili JN (2011) Intermolecular and surface forces. 3rd edn. Academic press.

25. Jan WF (2007) Deflocculation. Encyclopedic Dictionary of Polymers. Springer New York. pp. 265. doi:10.1007/978-0-387-30160-0_3313

26. Jang J, Carlos Santamarina J (2015) Fines classification based on sensitivity to pore-fluid chemistry. J Geotech Geoenviron Eng 142(4):06015018. https://doi.org/10.1061/(ASCE)GT.1943-5606.0001420

27. Kenney TC (1963) Correspondence. Géotechnique 13(2):159-162. https://doi.org/10.1680/geot.1963.13.2.159

28. Kondo F, Torrance JK (2005) Effects of smectite, salinity and water content on sedimentation and self-weight consolidation of thoroughly disturbed soft marine clay. Paddy Water Environ 3(3):155-164.

29. Liu D, Edraki M, Berry L (2018) Investigating the settling behaviour of saline tailing suspensions using kaolinite, bentonite, and illite clay minerals. Powder Techno 326(15):228-236. https://doi.org/10.1016/j.powtec.2017.11.070

30. Luckham PF, Rossi S (1999) The colloidal and rheological properties of bentonite suspensions. Adv Colloid Interface Sci 82(1-3):43-92. https://doi.org/10.1016/S0001-8686(99)00005-6

31. Madsen FT (1998) Clay mineralogical investigations related to nuclear waste disposal. Clay Miner 33(1):109-129.

32. Marcial D, Delage P, Cui YJ (2002) On the high stress compression of bentonite. Can Geotech J 39(4):812-820. https://doi.org/10.1139/t02-019

33. Menaceur H, Delage P, Tang AM, Talandier J (2016) The status of water in swelling shales: an insight from the water retention properties of the Callovo-Oxfordian claystone. Rock Mech Rock Eng 49(12):4571-4586. https://doi.org/10.1007/s00603-016-1065-2

34. Mishra AK, Ohtsubo M, Li LY, Higashi T, Park J (2009) Effect of salt of various concentrations on liquid limit, and hydraulic conductivity of different soil-bentonite mixtures. Environ Geol 57(5):1145-1153. https://doi.org/10.1007/s00254-008-1411-0

35. Mitchell JK, Soga K (2005) Fundamentals of soil behaviour. 3rd edn. John Wiley &Sonc, Inc.

36. Moore R (1991) The chemical and mineralogical controls upon the residual strength of pure and natural clays. Géotechnique 41(1):35-47. https://doi.org/10.1680/geot.1991.41.1.35

37. Norrish K (1954) The swelling of montmorillonite. Discuss Faraday Soc 18: 120-134.

38. Ohtsubo M, Egashira K, Takayama M (1996) Mineralogy and chemistry, and their correlations with the geotechnical properties of marine clays in Ariake Bay, Japan: comparison of quick and nonquick clay sediments. Mar Georesour Geotechnol 14(3):263-282. https://doi.org/10.1080/10641199609388316

39. Petrov RJ, Kerry Rowe R (1997) Geosynthetic clay liner (GCL)-chemical compatibility by hydraulic conductivity testing and factors impacting its performance. Can Geotech J 34(6):863-885. https://doi.org/10.1139/t97-055

40. Rao SM, Sridharan A, Chandrakaran S (1993) Consistency limits behavior of bentonites exposed to sea water. Mar Georesour Geotechnol 11(3):213-227. https://doi.org/10.1080/10641199309379919

41. Rao SN, Mathew PK (1995) Effects of exchangeable cations on hydraulic conductivity of a marine clay. Clays Clay Miner 43(4):433-437. https://doi.org/10.1346/CCMN.1995.0430406

42. Sivapullaiah PV, Manju (2005) Kaolinite–alkali interaction and effects on basic properties. Geotech Geol Eng 23(5):601-614. https://doi.org/10.1007/s10706-004-1661-x

43. Song MM, Zeng LL, Hong ZS (2017) Pore fluid salinity effects on physicochemical-compressive behaviour of reconstituted marine clays. Appl Clay Sci 146(15):270-277. https://doi.org/10.1016/j.clay.2017.06.015

44. Sridharan A, Prakash K (1998) Characteristic water contents of a fine-grained soil-water system. Géotechnique 48(3):337-346. https://doi.org/10.1680/geot.1998.48.3.337

45. Sridharan A, Prakash K (1999) Mechanisms controlling the undrained shear strength behaviour of clays. Can Geotech J 36(6):1030-1038. https://doi.org/10.1139/t99-071

46. Sridharan A, Prakash K (2000) Percussion and cone methods of determining the liquid limit of soils: controlling mechanisms. Geotech Test J 23(2):236-244. https://doi.org/10.1520/GTJ11048J

47. Sridharan A, Venkatappa Rao G (1975) Mechanisms controlling the liquid limit of clays. Proc. Istanbul Conf Soil Mech Found Eng Istanbul 1:65–74.

48. Sridharan A, El-Shafei A, Miura N (2002) Mechanisms controlling the undrained strength behavior of remolded Ariake marine clays. Mar Georesour Geotechnol 20(1):21-50. https://doi.org/10.1080/106411902753556843

49. Stawiński J, Wierzchoś J, Garcia-Gonzalez MT (1990) Influence of calcium and sodium concentration on the microstructure of bentonite and kaolin. Clays Clay Miner 38(6):617-622. https://doi.org/10.1346/CCMN.1990.0380607

50. Tang AM, Cui YJ, Le TT (2008) A study on the thermal conductivity of compacted bentonites. Appl Clay Sci 41(3-4):181-189. https://doi.org/10.1016/j.clay.2007.11.001

51. Tessier D (1990) Behaviour and microstructure of clay minerals. Soil colloids and their associations in aggregates. Springer, Boston, MA, pp 387-415.

52. Tiwari B, Tuladhar GR, Marui H (2005) Variation in residual shear strength of the soil with the salinity of pore fluid. J Geotech Geoenviron Eng 131(12):1445-1456. https://doi.org/10.1061/(ASCE)1090-0241(2005)131:12(1445)

53. Vitale E, Cecconi M, Croce P, Deneele D, Pane V, Russo G, Vecchietti A (2016) Influence of pore water chemistry on hydraulic conductivity of kaolinite suspensions. Procedia Eng 158:81-86. https://doi.org/10.1016/j.proeng.2016.08.409

54. Wang Q, Tang AM, Cui YJ, Delage P, Barnichon JD, Ye WM (2013) The effects of technological voids on the hydro-mechanical behaviour of compacted bentonite-sand mixture. Soils Found 53(2):232-245. https://doi.org/10.1016/j.sandf.2013.02.004

55. Wang YH, Siu WK (2006) Structure characteristics and mechanical properties of kaolinite soils. I. Surface charges and structural characterizations. Can Geotech J 43(6):587-600. https://doi.org/10.1139/t06-026

56. Warkentin BP, Yong RN (1962) Shear strength of montmorillonite and kaolinite related to interparticle forces. Clays Clay Miner 210-218. https://doi.org/10.1016/B978-1-4831-9842-2.50014-6

57. Warkentin BP (1961) Interpretation of the upper plastic limit of clays. Nat 190:287-288.

58. Yılmaz G, Yetimoglu T, Arasan S (2008) Hydraulic conductivity of compacted clay liners permeated with inorganic salt solutions. Waste Manag Res 26(5):464-473. https://doi.org/10.1177/0734242X08091586

59. Ying Z, Duc M, Cui YJ, Benahmed N (2020) Salinity assessment for salted soil considering both dissolved and precipitated salts. Geotech Test J https://doi.org/10.1520/GTJ20190301. Accessed 29 January 2020.

60. Yukselen-Aksoy Y, Kaya A, Ören AH (2008) Seawater effect on consistency limits and compressibility characteristics of clays. Eng Geol 102(1-2):54-61. https://doi.org/10.1016/j.enggeo.2008.07.005

61. Zhang TW, Deng YF, Cui YJ, Lan HX, Zhang FY, Zhang HY (2019) Porewater salinity effect on flocculation and desiccation cracking behaviour of kaolin and bentonite considering working condition. Eng Geol 251:11-23. https://doi.org/10.1016/j.enggeo.2019.02.007

Ying, Z., Cui, Y.J., Benahmed, N., Duc, M. 2021. Journal of Rock Mechanics and Geotechnical Engineering, 13(4), 855-863.

Salinity effect on the compaction behaviour, matric suction, stiffness and microstructure of a silty soil

Zi Ying[1], Yu-Jun Cui[1], Nadia Benahmed[2], Myriam Duc[3]

Abstract: To better understand the salinity effect on the compaction behaviour of soil, standard Proctor compaction test was conducted on soil samples with different salinities. Matric suction and small strain shear modulus, G_{max}, were determined and pore size distribution was also investigated on samples statically compacted at different water contents. Results showed that with the decrease of soil salinity from initial value of 2.10‰ (g of salt/ kg of dry soil) to zero, the maximum dry density increased and the optimum water content decreased, whereas there was no significant change with the increase of soil salinity from 2.10‰ to 6.76‰. Interestingly, it was observed that, G_{max} also decreased when the soil salinity decreased from initial value of 2.10‰ to zero and kept almost constant when the soil salinity increased from 2.10‰ to 6.76‰, for dry samples with similar matric suction and also for samples compacted at optimum and on wet side whose matric suctions were slightly different due to the difference in remolded water content. Furthermore, the effect of salinity on compaction behaviour and G_{max} decreased for samples compacted from dry side to wet side. The pore size distribution exhibited bi-modal characteristics with two populations of micro-pores and macro-pores not only for samples compacted on dry side and at optimum state, but also for those compacted on wet side. Further examination showed that the modal size of micro-pores shifted to lower values and that of macro-pores shifted to higher values for saline soil compared to the soil without salt.

Keywords: silts; compaction; suction; stiffness; microstructure

1. Introduction

For the economic and environmental reasons, it is recommended to use local soils in geotechnical and geo-environmental constructions such as subgrades, dikes, dams and

[1]: Ecole des Ponts ParisTech, Laboratoire Navier/CERMES, 6 – 8 av. Blaise Pascal, Cité Descartes, Champs-sur-Marne, 77455 Marne-la-Vallée cedex 2, France
[2]: INRAE, Aix Marseille Univ, Unité de Recherche RECOVER, 3275 route Cézanne, CS 40061, 13182 Aix-en-Provence, France
[3]: Université Gustave Eiffel, IFSTTAR/GERS/SRO, 14-20 boulevard Newton, Champs-sur-Marne, 77447 Marne-la-Vallée, France

municipal waste barriers. In coastal area, soil pore water normally contains certain salinity, which can greatly affect the compaction behaviour of soils. Liu and Zhang (2014) reported that both the maximum dry density and optimum water content decreased with increasing salinity for saline soils with 3% ~ 8% clay-size fraction. Nevertheless, Ajalloeian et al. (2013) indicated that salinity had negligible effect on the compaction behaviour of fine-grained soils with 28% clay-size fraction. Abdullah et al. (1997, 1999) stated that the salt solution led to an increase in maximum dry density and a reduction of optimum water content for highly plastic clay whose main minerals were illite and smectite. The same observations were made on clayey soils with 48% clay minerals consisting of montmorillonite, polygorskite and kaolinite (Abood et al., 2007) and on expansive soils (Shariatmadari et al., 2011; Durotoye et al., 2016). They attributed this phenomenon to the decrease of diffused double layer thickness and the more oriented face-to-face clay particle contacts with the increase of salinity. From these studies, it appears that the salinity had different effect on compaction properties for soils with different clay fractions and mineral compositions. On the whole, the maximum dry density increased and the optimum water content decreased with increasing salinity for clays which had high clay fraction and swelling minerals, whereas the salinity had no significant effect on compaction behaviour or led to a reduction of both maximum dry density and optimum water content for soils with low clay fraction.

Salt can also significantly influence the strength or stiffness of compacted soils. Recent studies mainly focused on the strength variations with salinity changes (Abood et al., 2007; Ajalloeian et al., 2013; Zhang et al., 2013a; Carteret et al., 2014; Liu and Zhang, 2014). Some studies focused on the effect of salinity on the stiffness of illite (Witteveen et al., 2013) and cemented soils (Truong et al., 2012; Zhang et al., 2013b). It was reported that the unconfined compressive strength increased with increasing salinity for soils with a fraction of clay minerals as large as 48% (Abood et al., 2007) and for saline soils with only 3% ~ 8% clay-size fraction (Liu and Zhang, 2014). Liu and Zhang (2014) explained that the increased shear strength for saline soils was due to the salt crystal cementation of soil particles which improved soil mechanical behaviour. As for the samples with high quantity of clay minerals, the thickness of diffused double layer decreased with increasing salinity and this, in turn, caused repulsive force diminution and net attractive force increase (Mitchell and Soga, 2005; Israelachvili, 2011). The increased net attractive force enabled soil particles to associate with each other in an aggregated manner, which may enhance soil strength (Moore, 1991; Di Maio et al., 2004; Tiwari et al., 2005; Abood et al., 2007). In addition to salinity effect, it was also reported that the stiffness of

soil increased with the increase of matric suction but at a declining rate (Ng and Yung, 2008; Ng et al., 2009; Heitor et al., 2013). However, salinity had no significant effect on matric suction which was related to the capillary and hydration forces (Miller and Nelson, 1993; Leong et al., 2007; Sreedeep and Singh, 2011).

Concerning the correlations between microstructure and mechanical behaviour, several studies focused on the salinity effect on microstructure variations. Carteret et al. (2014) performed scanning electron microscope (SEM) and mercury intrusion porosimetry (MIP) tests on compacted saline samples with different salinities. They observed that the salt crystallization of highly saline samples caused reduction of macro-pores and increase of meso-pores and micro-pores, and these salt crystals were found to form bonds among soil particles which led to the increase of soil strength. Zhang et al. (2013a) also observed some salt bonding between clay particles of loess on SEM images, and this bonding resulted in aggregation of particles, increasing the shear strength. Sarkar and Siddiqua (2016) conducted X-ray computed tomography (X-ray CT) test on bentonite-sand materials prepared by distilled water and salt solutions, and highlighted the salt effect on pore size distribution properties of compacted samples: the pore size and number of interconnected pores increased with increasing salinity due to the reduction of diffused double layer thickness.

It appears from the above-mentioned studies that the salinity effect on either compaction behaviour or matric suction or stiffness or microstructure was conducted on different soils. However, there were few studies focusing on all these different properties of a given soil. In this study, standard Proctor compaction test was first conducted on soil samples with different salinities. To further understand the salinity effect on soil compaction behaviour, filter paper method, bender element test and MIP test were carried out on samples compacted on dry side, at optimum and on wet side. Results allowed the coupled compaction behaviour, matric suction, stiffness and microstructure to be analysed.

2. Materials and methods

2.1 Tested materials

Natural saline silty soil was taken from Salin-de-Giraud, a traditional salt exploitation site in France. Its geotechnical properties are reported in Table 1. Fig. 1 shows the grain size distribution of the soil, which was determined by the dry sieving method for particles larger

than 80 μm and by the hydrometer method for particles smaller than 80 μm, according to the French standards NF P94-056 (1996) and NF P 94-057 (1992), respectively. This soil consists of 20% sand, 63% silt-size particles (0.002 ~ 0.075 mm) and 17% clay-size fraction (< 0.002 mm). The main minerals, identified by XRD analysis, are quartz (39%), calcite (35%), feldspar (9.5%), illite (10.8%), chlorite (3.6%), kaolinite (1.3%) and NaCl crystallized on halite form (0.8%). The quantity of clay minerals (illite, chlorite and kaolinite) is 15.7%, in agreement with the clay-size fraction of 17% observed on grain size distribution curve.

Table 1. Geotechnical properties of the tested soil.

Property	Value
Specific gravity, *Gs*	2.72
Liquid limit, w_L (%)	29
Plastic limit, w_p (%)	19
Plasticity Index, I_p	10
VBS (g/100g)	0.98
Specif. surf. Area, SSA(m^2/g)	24.0

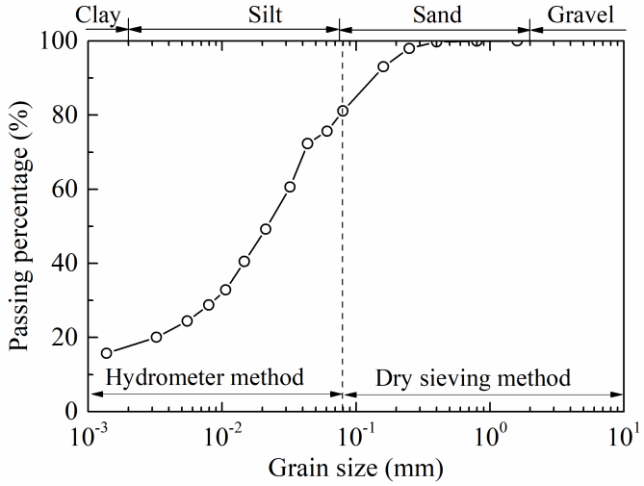

Fig. 1. Grain size distribution of natural soil.

Soil solutions were extracted by centrifugation method after several cycles of washing. The chemical compositions and ion concentration of soil solution extracts were determined by Inductively Coupled Plasma/Atomic Emission Spectroscopy (ICP/AES). As listed in Table 2, the ion concentration of soil solution extracts was transformed to ion concentration of soil pore water according to the dilution ratio. The salt concentration of soil pore water was estimated at

about 13.3 g/L. Since the salt concentration of soil pore water always changed with water content variations, the soil salinity, defined as the ratio of salt mass to dry soil mass, was adopted in this study. For the tested soil, the soil salinity was found to be 2.1‰ (g of salt/kg of dry soil).

Table 2. Chemical analysis of natural soil pore water.

Solution	Chemical compositions (mg/L) – ICP/AES method								Salt concentration, *c* (g/L)	Soil salinity, *r'* (‰ or g salt/kg of dry soil)
	Cl	Na	Ca	K	Mg	Fe	Al	Si		
Soil pore water	7521	5096	215	225	176	18	7	39	13.3	2.1

2.2 Soil salinity adjustment

Since the main ion species of soil pore water were CI^-, Na^+, Ca^{2+}, K^+, and Mg^{2+}, the same as the ion compositions of synthetic sea water (French standard NF P 18-837, 1993, as listed in Table 3), five different salts of synthetic sea water were chosen for preparing the mixed salt solution to be added to the natural saline soil in order to obtain salted soil with higher salinity. The quantity of additive salt was determined according to the initial salinity of natural saline soil and the target salinity of salted soil (Ying et al., 2020a). The total additive salt mass was adjusted to each salt mass according to the proportions of the five different salts in synthetic sea water. Mixed salt solution was prepared by dissolving the five additive salts in deionized water. Afterwards, salt solution was sprayed to natural soil in layers to reach the desired soil salinities of about 4.83‰ (or g of salt/kg of dry soil) and 6.76‰ (or g of salt/kg of dry soil), respectively. Note that the maximum target soil salinity of 6.76‰ corresponded to the salt concentration of soil pore water of 35 g/L (salt concentration of synthetic sea water) for salted soil at 20% water content.

Table 3. Chemical compositions of synthetic sea water.

salts	NaCI	$MgCI_2 \cdot 6H_2O$	$MgSO_4 \cdot 7H_2O$	$CaSO_4 \cdot 2H_2O$	$KHCO_3$
Salt mass (g) in 1000 g deionized water	30.0	6.0	5.0	1.5	0.2
Percentage (%)	70.26	14.05	11.71	3.51	0.47

To decrease the salinity of natural saline soil, leaching tests were carried out. Leaching column was filled with natural soil. Then, deionized water, with a water head of 1 m, was flushed through the column from bottom to top in order to remove the initial salt (Fig. 2). The water flow rate was controlled to be lower than 0.3 mL/s, preventing the migration of fine particles and avoiding the destruction of soil aggregates. To minimise as much as possible the soil disturbance during leaching, a layer of gravel, geotextile and filter paper were placed on the top and bottom surface of the soil. The effluent was collected and electrical conductivity (EC) was measured to verify whether the salt was washed out. The leaching of soil was repeated until the amount of salt, thus the EC, was reduced considerably. When the electrical conductivity of leaching water was close to the one of deionized water and kept almost constant, the test was stopped and a small quantity of leached soil was taken out to verify the final soil salinity. A value as low as 0.05‰ (or g of salt/kg of dry soil) was obtained, which could be regarded as zero. The natural soil, salted soil and leached soil were then air-dried, ground and sieved through 5 mm mesh. The larger soil particles which could not pass through the 5 mm sieve were ground again and rescreened until the whole soils passed through the sieve (Tang et al., 2011).

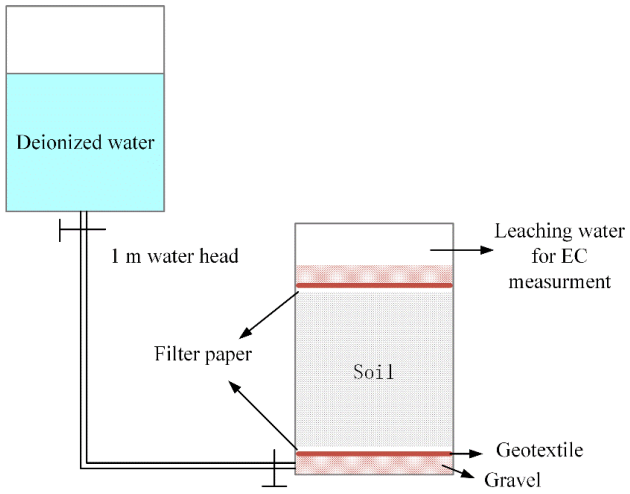

Fig. 2. Sketch of the equipment for salt leaching experiment.

2.3 Sample preparation

Air-dried soil was humidified by spraying deionized water to reach different target water contents on dry side, wet side and at optimum, and then stored in sealed plastic bag for 24 h aiming at salt and water homogenization. Afterwards, the samples were reconstituted either by dynamic compaction for proctor test or by static compaction for the matric suction and small strains shear modulus measurements as well as for the microstructure investigation. For these

cases of static compaction, the samples were reconstituted at the target dry density using double pistons acting at the top and bottom of the soil samples to ensure uniform distribution of stresses inside the sample, hence, a better soil homogeneity with respect to the dry density (Cui and Delage, 1996). The samples for matric suction measurement and MIP test had a dimension of 50 mm diameter and 20 mm height, and the samples for small strain shear modulus measurement had 50 mm in diameter and 50 mm in length.

2.4 Proctor compaction test

Standard Proctor compaction tests were conducted following the French standard NF P94-093 (1999). Air-dried soil was prepared with the procedure presented previously. Deionized water was then added into the soil to reach different water contents. At each water content, the soil was dynamically compacted in three layers into proctor mould, with 25 blows of the hammer for each layer. The compacted sample was trimmed by means of a straightedge scraping across the top of the mould. The density of compacted sample (ρ) was then determined considering the sample mass and the mould volume. A portion of sample was taken for water content determination.

When a salted sample was dried in an oven, the water evaporated but the salt remained with dry soil (Noorany, 1984). Thus, the water content (w) computed from the conventional equation (Eq. 1) was not equal to the water content (w') of saline soil which was the ratio of salty water mass (m_{sw}) to dry soil mass (m_s):

$$w = \frac{m_w}{m_d} \tag{1}$$

where m_w is the pure water mass and m_d is the solid mass after oven-drying which contained total mass of soil and salt.

The water content (w') of saline soil should be calculated by Eq. 2 taking the dissolved salt into account (Noorany, 1984; ASTM D4542-95, 2001; Ying et al., 2020a):

$$w' = \frac{m_{sw}}{m_s} = \frac{m - m_d}{m_d - rm} \tag{2}$$

where r is the water salinity, expressed as the mass ratio of salt to salty water.

To convert the salinity on the soil basis to the solution basis, the following equation was adopted (Reitemeier, 1946; Ying et al., 2020a):

$$r = \frac{r'}{w'} \tag{3}$$

where *r'* is the soil salinity on the basis of dry soil mass.

Then, the dry density (ρ_d) for saltless soil can be calculated using Eq. 4:

$$\rho_d = \frac{\rho}{1+w} \tag{4}$$

However, for saline soil, the dry density calculated by Eq. 4 was overestimated because of the consideration of the dissolved salt as soil solids. Thus, the dry density of saline soil should be calculated by Eq. 5 (Noorany, 1984; ASTM D4542-95, 2001; Siddiqua et al., 2011):

$$\rho_d' = \frac{\rho}{1+w'} \tag{5}$$

The saturation degree (S_r) of compacted samples can be determined from the water content and dry density by Eq. 6:

$$S_r = \frac{w \cdot \rho_d \cdot G_s}{\rho_w \cdot G_s - \rho_d} = \frac{w \cdot G_s}{\rho_w (G_s / \rho_d - 1)} \tag{6}$$

where G_s is the specific gravity; ρ_w is the liquid density.

Finally, based on the values of dry density and water content, the proctor compaction curves of saltless soil and saline soil with different soil salinities were plotted. The compaction states at dry and wet sides of optimum and at optimum water content with target dry densities were selected to prepare samples for matric suction, small strain shear modulus and microstructure investigations.

2.5 Matric suction measurement

Matric suction of soil sample was determined by filter paper method, according to ASTM standard D 5298-10 (2010). Whatman No. 42 filter paper was oven-dried at least 16 h prior to use in the measurements. Three stacked filter papers were sandwiched between two soil samples. The central filter paper used for matric suction measurement was slightly smaller in diameter than the outer filter papers, preventing the central filter paper from direct contact with soil. The entire sandwiched samples were wrapped by plastic film and enveloped by scotch tape. Then, they were stored in a chamber at a relative humidity of 100% and a temperature of 20 ± 2°C to allow moisture equilibration for two weeks. After equilibration, the water contents of soil

sample and central filter paper were measured.

According to ASTM standard (D5298-16, 2016), the following equations of Whatman No. 42 filter paper calibration curves were used to transform the water content of filter paper to matric suction of soil sample:

$$\log \psi_m = \begin{cases} 5.327 - 0.0779 w_f & w_f \le 45.3\% \\ 2.412 - 0.0135 w_f & w_f > 45.3\% \end{cases} \quad (7)$$

where φ_m is matric suction of soil sample (kPa), w_f is the water content of filter paper (%). Note that the mean value of matric suction and water content on the two replicated measurements was considered.

2.6 Bender element test

The bender element technique was used to measure the small strain shear modulus. The set-up of bender elements and a schematic diagram are shown in Fig. 3. This system consists of two piezo-ceramic bender elements, a function generator, an amplifier and an oscilloscope (Wang et al., 2017, 2020; Zhang et al., 2018).

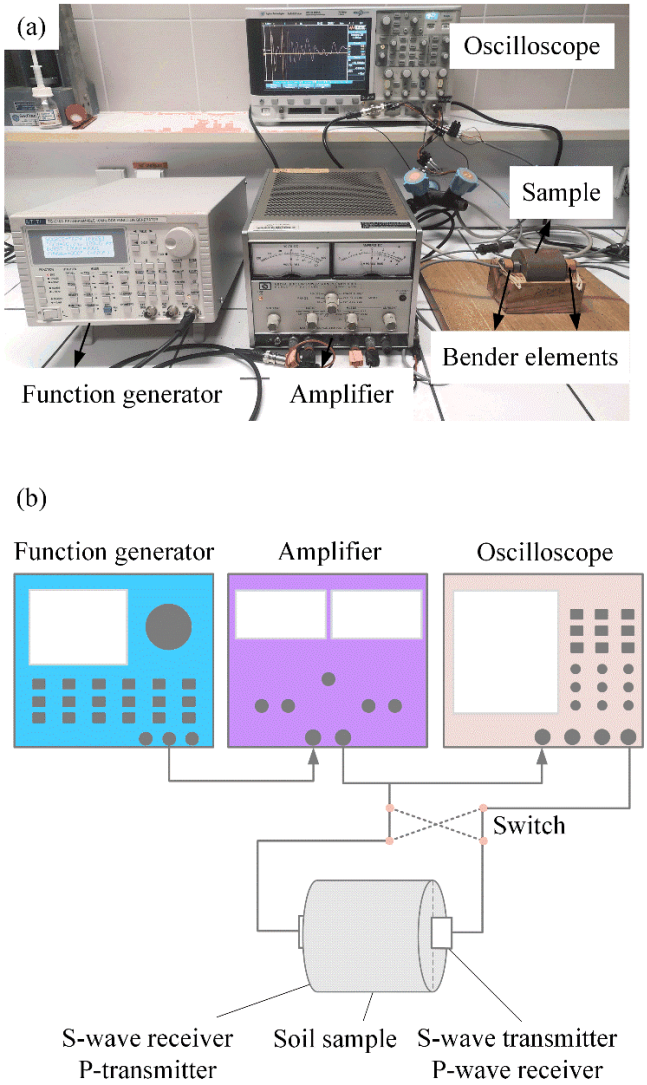

Fig. 3. Set-up of bender element test: (a) photo of the set-up; (b) sketch of the set-up (after Wang et al., 2017).

Immediately after compaction, the samples were carefully covered by paraffin to avoid water evaporation. Then, a slot was performed on the surface of the sample extremities with the same direction to install the piezo-ceramic elements and ensure a good contact with soil. The sample was then placed on a wooden holder for a good insulation and for avoiding any signal electrical perturbation (Fig. 3a). Hereafter, a simple pulse was generated by the function generator and amplified by the amplifier. The S+P method proposed by Wang et al. (2017) was adopted to determine the arrival time of shear wave (Δt). In the S+P method, both transmitted and received signals were captured by the oscilloscope through modifying the connection between the two benders (Fig. 3b). The shear wave velocity (v_s) was calculated by Eq. 8:

$$v_s = \frac{L_{tt}}{\Delta t} \tag{8}$$

where L_{tt} is the travel length or tip-to-tip distance between two bender elements.

Finally, the small strain shear modulus (G_{max}) was determined using Eq. 9:

$$G_{\max} = \rho v_s^2 \tag{9}$$

where ρ is the density of soil sample. To check the reproducibility of tests, the G_{max} measurement was determined in duplicate. And the mean value was used in this study.

2.7 Microstructure investigation

Autopore IV 9500 mercury intrusion porosimeter was used to investigate the microstructure of compacted samples. After compaction, one small piece of soil was carefully cut from the sample, then frozen using liquid nitrogen under vacuum and dried using a freeze dryer for 24 h aiming at sublimation of frozen water. To perform the MIP test, the freeze-dried piece was firstly put into a low pressure system with a pressure range varying from 3.6 kPa to 200 kPa, then transferred to a high pressure system with the maximum pressure of 230 MPa. The corresponding detectable entrance pore diameter ranged from 0.006 μm to 350 μm.

3. Results

3.1 Proctor compaction behaviour

The results of the proctor compaction curves for soil without salt and those with different soil salinities are depicted in Fig. 4. It can be observed that, with decreasing soil salinity from initial value of 2.10‰ to zero, the compaction curve moved upwards and leftwards, implying that the saltless soil had higher maximum dry density and lower optimum water content than that of natural soil with soil salinity of 2.10‰. However, as soil salinity increased from 2.10‰ to 4.83‰ and 6.76‰, the compaction curves did not exhibit distinguishable changes: the saline soil samples with different salinities had rather close values of maximum dry densities and optimum water contents. Comparison between proctor compaction curves of saltless soil and those of saline soils suggested that the salt had more significant effect on the compaction curves on dry side than that on wet side.

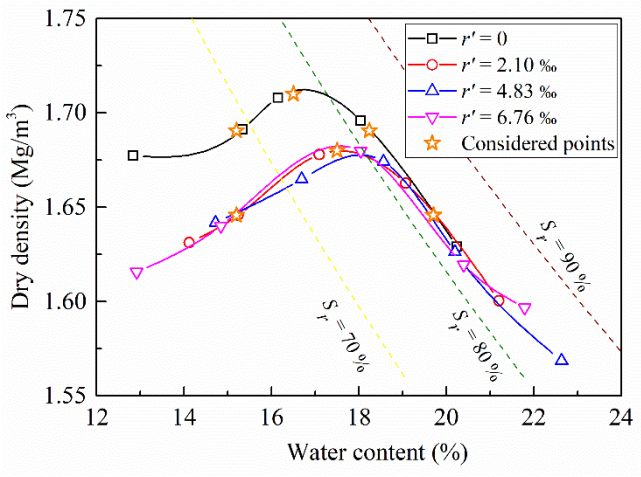

Fig. 4. Salinity effect on proctor compaction behaviour.

The properties of the compacted samples used for matric suction, small strain shear modulus and microstructure investigations are given in Table 4. The corresponding points are shown in Fig. 4. All the considered compaction states were located on the proctor compaction curves. Note that the same compaction pressure of about 2200 kPa was recorded for all samples. Note also that for a given soil salinity, the chosen points on dry and wet sides corresponded to the same dry density. The corresponding compactness which was the ratio of target dry density to maximum dry density, were 98.8% for soil without salt and 98.2% for soils with soil salinities of 2.10‰ and 6.76‰ that were almost similar.

Table 4. Properties of compacted samples.

Sample	r' = 0			r' = 2.10‰ and r' = 6.76‰		
	Dry side	Optimum	Wet side	Dry side	Optimum	Wet side
Water content (%)	15.2	16.5	18.2	15.2	17.5	19.7
Dry density (Mg/m^3)	1.69	1.71	1.69	1.65	1.68	1.65
Degree of saturation (%)	68	76	82	63	77	82
Compactness (%)	98.8	100	98.8	98.2	100	98.2

3.2 Matric suction

Figure 5 depicts the changes in matric suction of compacted samples on dry side, wet side and at optimum. It appears that all the points lay on one unique line, suggesting that the matric suction was highly related to the water content of samples, whereas the salinity had no significant effect on matric suction. This was in good agreement with previous results from

Miller and Nelson (1993), Leong et al. (2007), Sreedeep and Singh (2011) and Zhang et al. (2017). It was also observed that, for the dry samples with the same water content, the matric suctions of saltless and saline samples were quite close, while the matric suctions of saltless samples compacted at optimum and on wet side were noticeably higher than those of saline samples with soil salinity of 2.10‰ and 6.76‰.

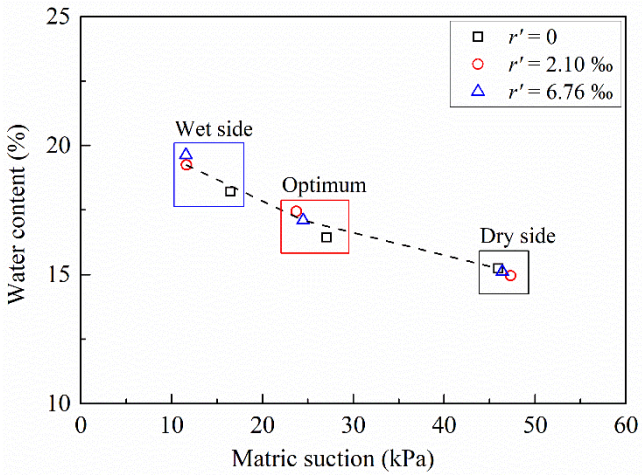

Fig. 5. Matric suction of compacted samples at dry side, wet side and optimum state.

3.3 Small strain shear modulus

The G_{max} was affected by many factors, including soil properties, compaction state, compaction stress and matric suction (Ng et al., 2009). As shown in Table 4, the compactness was almost the same for samples having different salinities which were compacted at dry, optimum and wet sides respectively, although the dry density of saltless samples was higher than that of saline samples. Moreover, as mentioned before, all samples were subjected to the same compaction pressure of around 2200 kPa. This implied that the effects of compactness (or dry density) and compaction energy on G_{max} can be ignored. Thus, there were remaining two factors affecting the G_{max} values: one was matric suction, and the other one was salinity. The variations of G_{max} with soil salinity are plotted in Fig. 6. For the samples compacted on the dry side, the matric suction was rather close (Fig. 5). Thus, the soil salinity was the sole factor to influence the G_{max} for the dry samples. As shown in Fig. 6, the G_{max} for dry samples decreased with the decrease of soil salinity from initial value of 2.10‰ to zero, whereas it kept almost constant with the increase of soil salinity from 2.10‰ to 6.76‰. The same trend of G_{max} variations were also observed for the samples compacted at optimum and wet side. However, in that case, the difference of G_{max} between the saltless samples and the saline samples was controlled by both

matric suction and soil salinity. For the samples compacted at optimum and on wet side, the matric suctions for saltless samples were higher than those of samples with soil salinities of 2.10‰ and 6.76‰ (Fig. 5). Ng et al. (2008, 2017) and Heitor et al. (2013) indicated that the G_{max} increased with increasing matric suction. This implies that, if the salinity effect was neglected, the G_{max} for the saltless samples should be higher than those of samples with soil salinity of 2.10‰ and 6.76‰, due to their higher matric suction. Nevertheless, it was observed that G_{max} for the samples compacted at optimum and on wet side decreased with the decrease of soil salinity from 2.10‰ to zero, suggesting that the decrease of salinity led a reduction of G_{max} that prevailed the increase of G_{max} as matric suction increased. This resulted in a decrease of salinity effect on G_{max} from dry side to wet side, due to the balance of the increase of G_{max} with increasing matric suction and the decrease of G_{max} with decreasing salinity for optimum and wet side samples. Specifically, as soil salinity decreased from 2.10‰ to zero, the G_{max} decreased from 27.24 MPa to 23.45 MPa (14%) for samples compacted on dry side, from 23.44 MPa to 20.80 MPa (11%) for samples compacted at optimum, and from 20.13 MPa to 19.32 MPa (4%) for samples compacted on wet side. This salinity effect on G_{max} was in full agreement with the changes of compaction curves observed previously - the salinity effect on compaction curves also decreased from dry side to wet side (Fig. 4).

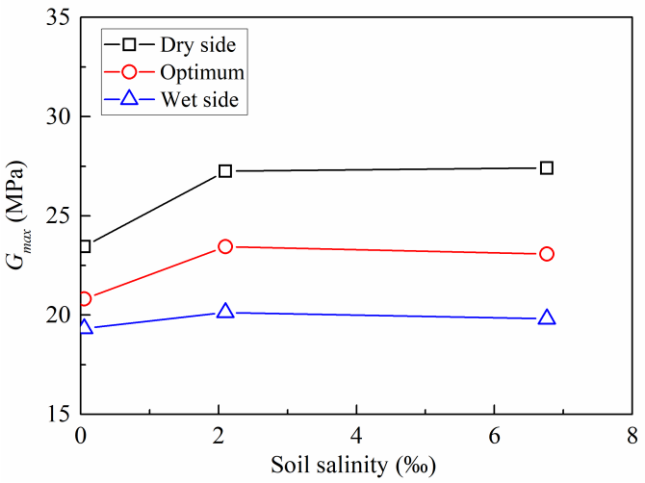

Fig. 6. Salinity effect on small strain shear modulus.

3.4 Microstructure investigation

The cumulative curves and corresponding derived curves are presented in Fig. 7 for the samples compacted on dry side, Fig. 8 for the samples compacted at optimum and Fig. 9 for the samples compacted on wet side. Based on the MIP results and the hypothesis that the water is contained

in small pores (Wan *et al*., 1995; Romero *et al*., 2011), the water ratio (i.e. void ratio of water-saturated pores, $e_w = wG_s$, where w is water content and G_s is specific gravity) and delimiting diameter between water-saturated pores and dry pores were determined, as shown in Figs. 7a, 8a and 9a. The corresponding distribution of water-saturated pores are presented in Figs. 7b, 8b and 9b. It appears from the cumulative curves that, the total intruded void ratios were relatively close to the initial void ratio of samples which were determined from sample dimension. The total intruded void ratios were almost similar for dry samples having different salinities. Concerning the optimum and wet samples, the total intruded void ratios of saltless samples were slightly lower than that of saline samples, which might be due to its relative higher dry density of saltless samples. As shown in Figs. 7b, 8b and 9b, the derived curves exhibited typical bi-modal characteristics not only for the samples compacted at dry side and optimum as usually observed, but also for the samples compacted wet of optimum, with a population of micro-pores and a population of macro-pores. For all samples on dry side, at optimum and on wet side, the water was mostly adsorbed and held in the micro-pores, leaving the most of macro-pores being dry. As for the dry samples, with decreasing soil salinity from the initial value of 2.10‰ to zero, the modal size of micro-pores increased from 0.63 μm to 0.78 μm and that of macro pores decreased from 11.63 μm to 10.23 μm, while there was no significant change when the soil salinity increased from 2.10‰ to higher value of 6.76‰ (Fig. 7b). The similar results were obtained on the samples compacted at optimum: as the soil salinity decreased from 2.10‰ to zero, the modal size of micro-pores shifted from 0.91 μm to 1.03 μm and that of macro-pores shifted from 13.17 μm to 10.86 μm, whereas the modal sizes of both macro-pores and micro-pores had no significant change with increasing soil salinity to 6.76‰ (Fig. 8b). As for the wet samples, the modal size of micro-pores increased from 0.91 μm to 1.05 μm and that of macro-pores decreased from 12.91 μm to 11.82 μm with decreasing soil salinity from 2.10‰ to zero, while the modal size of micro-pores decreased slightly and that of macro-pores increased with increasing soil salinity from initial value of 2.10‰ to 6.76‰ (Fig. 9b). Besides, as salinity increased, an increase in the frequency of macro-pores was observed on all kinds of samples.

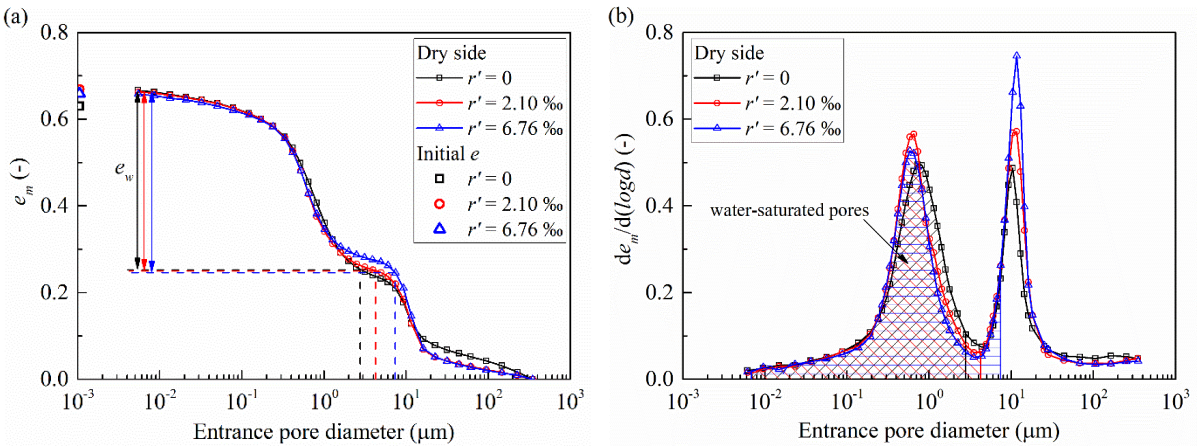

Fig. 7. MIP results of samples compacted on dry side: (a) cumulative intrusion curves; (b) derived curves.

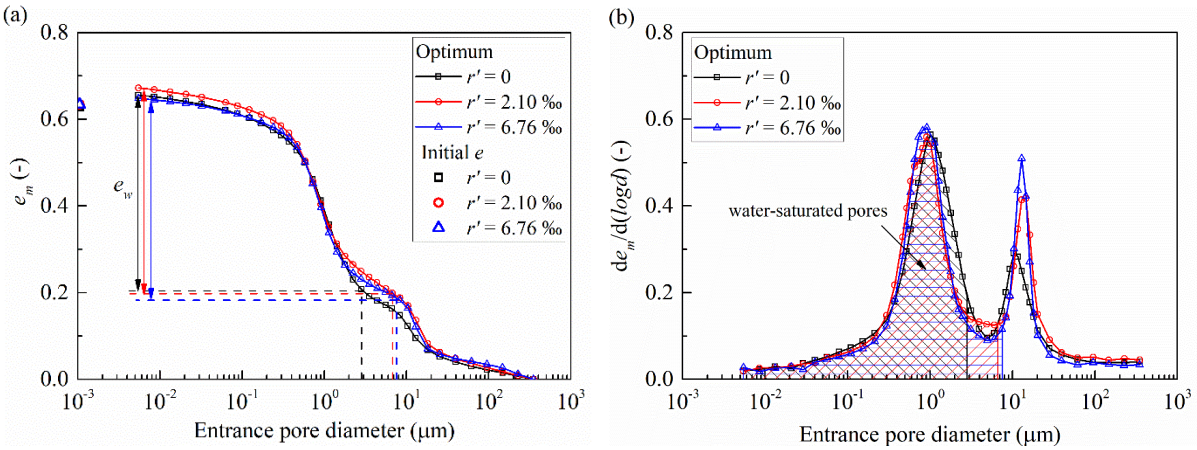

Fig. 8. MIP results of samples compacted at optimum water content: (a) cumulative intrusion curves; (b) derived curves.

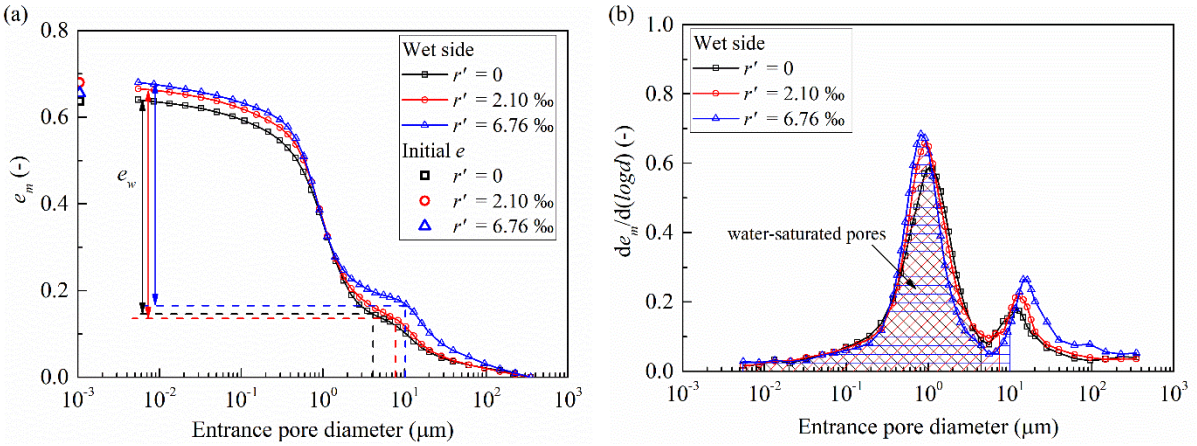

Fig. 9. MIP results of samples compacted on wet side: (a) cumulative intrusion curves; (b) derived curves.

4. Discussion

Microstructure of compacted soil was significantly dependent on the compacted water content (Delage et al., 1996). For silty soil, on dry side, the clay coated the surface of grains and the compaction cannot significantly deform the aggregates due to the high suction effect. This led to an aggregated structure characterised by bi-modal pore size distributions. On wet side, the clay fraction formed a continuous or more compact matrix around the sand or silt grains and the clay paste was able to fill the macro-pores. In that case, a uni-modal pore population was usually identified. Thus, it was not a common result that the wet samples presented aggregated structure with a high population of micro-pores and a small population of macro-pores, as shown in Fig. 9b. Russo and Modoni (2013) also observed the bi-modal pore size distribution characteristics for alluvial silty sand with only 13% clay-size fraction which was compacted on wet side. Burton et al. (2014) indicated that the wet samples can also present aggregated structure if their compaction energy and degree of saturation were low. For the tested silty soil, the clay-size fraction was only 17%. The degree of saturation of compacted samples was around 82% that was close to the value at optimum state (78%). Thus, the low clay fraction and the degree of saturation close to the one at optimum might be the possible reasons for the bi-modal pores size distribution characteristics observed on wet samples that the limited clay paste could not form a continuous matrix to fill all macro-pores.

As observed in Figs. 7b, 8b and 9b, the modal size of micro-pores decreased, while the modal size and frequency of macro-pores increased with increasing soil salinity from zero to 2.10‰ and 6.76‰. The changes in micro-pores were mainly attributed to the salinity effect which led to a decrease of diffused double layer thickness of clay minerals (Ravi and Rao, 2013; Thyagaraj and Salini, 2015). The microstructure of compacted silty soil was characterised by sand or silt grain skeleton with clay particles coating these grains, and these grains and clay particles formed aggregates (Delage et al., 1996; Lemaire et al., 2013). The pores within these aggregates were identified as micro-pores and the pores between these aggregates were regarded as macro-pores. As salinity increased, the thickness of diffused double layer decreased (Sridharan and Jayadeva, 1982; Sridharan and Prakash, 2000), leading to a reduction of micro-pore size for clay particles. Such decrease of diffused double layer thickness further induced an increase of macro-pore size and its frequency (Yılmaz et al., 2008; Shariatmadari et al., 2011). In addition, the frequency of macro-pores was also affected by the dry density: the higher the dry density, the lower the frequency of the macro-pores (Romero, 2013). It was noting that the salinity effect on the pore size distributions (especially for micro-pores) were visible with

increasing salinity from zero to 2.10‰, while this salinity effect was negligible when the salinity increased from 2.10‰ to 6.76‰. This might be attributed to the low clay fraction and its less active clay minerals (10.8 % illite, 3.6% chlorite and 1.3% kaolinite) in the tested silty soil limiting the compression of diffused double layer at higher salinity (Ying et al., 2020b), as its thickness already decreased significantly at 2.10‰ soil salinity. As most water was contained in the micro-pores, the relationship between water content and matric suction was mainly governed by the micro-pores while the dry macro-pores which were easily affected by dry density played a negligible role. Thus, the points of water content and matric suction converged to one unique line despite the different dry densities (Fig. 5). This was consistent with the results obtained by Heitor et al. (2013), showing that when the soil water retention properties of compacted silty sand were expressed in terms of water content and matric suction, the matric suctions were independent of dry density. The salinity effect on the matric suction was slight as observed in Fig. 5, which might be attributed to the visible but insignificant changes of micro-pores induced by salinity.

As soil microstructure changed with increasing salinity, the G_{max} of saline samples was expected to be higher than that of the samples without salt (Fig. 6). Since the distance between interlayers of clay decreased with the reduction of diffused double layer thickness, the inter-particle repulsive forces decreased, resulting in an increase of net attractive forces which may make clay particles attract each other and agglomerate (Warkentin and Yong, 1962; Sridharan et al., 2002; Israelachvili, 2011). This association enhanced soil strength (Warkentin and Yong, 1962; Sridharan et al., 2002). As far as the compaction behaviour was concerned, for the same compaction energy, a stiffer soil with higher G_{max} presented higher resistance to compaction. As a result, a lower maximum dry density of saline samples was obtained (Fig. 4). Meanwhile, more water was needed to destroy soil aggregates for stiffer soils. Thus, the optimum water content increased for saline soil (Fig. 4). However, the optimum degree of saturation seemed to be insensitive to salinity (Table 4), even though the microstructure and stiffness varied. This was consistent with the observations made by Tatsuoka (2015) and Tatsuoka and Correia (2018). They reported that the optimum saturation degree of compacted soil was nearly 82%, independent of soil type and compaction energy level. It can be deduced from Eq. 6 that, for the saline soil, the balance between the increased optimum water content and the decreased maximum dry density led to a negligible change in optimum saturation degree.

Regarding the saline samples with different salinities, they had rather close G_{max} and proctor

compaction curves. It was consistent with the changes in microstructure that these behaviour varied significantly when the soil salinity increased from zero to 2.10‰, while these variations were slight with increasing soil salinity from 2.10‰ to 6.76‰, due to the limited salinity effect through changes of diffused double layer thickness at higher salinity. Similar observations were made by Ajalloeian et al. (2013): the shear strength and friction angle increased then kept almost constant with increasing salinity in soils with only 28% clay-size fraction. It was also comparable to the results of saturated bentonite whose residual shear strength increased significantly in the range from 0 to 0.5 mol/L NaCl solution then had negligible variations for concentrations larger than 0.5 mol/L (Di Maio, 1996).

5. Conclusions

To better understand the salinity effect on the compaction behaviour of silty soil, standard Proctor compaction test, filter paper method and bender element test coupled with mercury intrusion porosimetry test were conducted on a silty soil with different salinities. The obtained results allowed the following conclusions to be drawn:

(1) The pore size distribution curves presented bi-modal characteristics not only for the samples compacted at dry side and optimum state as usually observed but also for the samples compacted on wet side. The smaller quantity of macro-pores for wet samples can be attributed to the low clay-size fraction whose paste could not form a continuous matrix to fill all macro-pores, and to the degree of saturation close to that of optimum.

(2) The pore size distribution of compacted samples also depended on soil salinity. For the samples with soil salinities of 2.10‰ and 6.76‰, the modal size of micro-pores shifted to smaller values, whereas the modal size of macro-pores shifted to larger values than that of samples without salt. This can be explained by the decrease of diffused double layer thickness of clay particles, leading to a reduction of the modal size of micro-pores and further inducing an increase of the frequency and modal size of macro-pores.

(3) Due to the modification of microstructure associated to salinity, the samples with soil salinities of 2.10‰ and 6.76‰ exhibited higher G_{max} than that of samples without salt. This observation was not only made on dry samples with similar matric suctions, but also for the samples compacted at optimum and on wet side, whose matric suctions were slightly different, due to the difference in remolded water content. The higher G_{max} obtained for saline soil could

be explained by the fact that, as salinity increased, the net attractive forces increased with the reduction of diffused double layer thickness that made clay particles attract each other and agglomerate, giving rise to an increase of G_{max}.

(4) The saline soil exhibited higher G_{max} and became less compactible. Thus, for the same compaction energy, the saline soil exhibited lower maximum dry density and higher optimum water content. Besides, the effect of salinity on compaction behaviour and G_{max} decreased while passing from dry side to wet side.

(5) The proctor compaction curves and G_{max} of saline samples with different soil salinities were rather similar. This could be attributed to the low clay fraction and their mineral compositions (illite, chlorite and kaolinite), which limited the salinity effect through changes in diffused double layer thickness of clay particles.

Acknowledgements

The authors would like to thank the China Scholarship Council (CSC), Ecole des Ponts ParisTech (ENPC) and INRAE for their financial support.

References

Abdullah WS, Alshibli KA, Al-Zou'bi MS. Influence of pore water chemistry on the swelling behaviour of compacted clays. Appl Clay Sci 1999;15(5-6):447-462.

Abdullah WS, Al-Zou'bi MS, Alshibli KA. On the physicochemical aspects of compacted clay compressibility. Can Geotech J 1997;34(4):551-559.

Abood TT, Kasa AB, Chik ZB. Stabilisation of silty clay soil using chloride compounds. J Eng Sci Technol 2007;2(1):102-110.

Ajalloeian R, Mansouri H, Sadeghpour AH. Effect of saline water on geotechnical properties of fine-grained soil. EJGE 2013;18:1419-1434.

ASTM D4542-95. Standard Test Method for Pore Water Extraction and Determination of the Soluble Salt Content of Soils by Refractometer. ASTM International, West Conshohocken, PA. 2001.

ASTM D5298-16. Standard Test Method for Measurement of Soil Potential (Suction) Using Filter Paper. ASTM International, West Conshohocken, PA. 2016.

Burton GJ, Sheng DC, Campbell C. Bimodal pore size distribution of a high-plasticity compacted clay. Géotechnique Lett 2014;4(2):88-93.

Carteret Rd, Buzzi O, Fityus S, Liu XF. Effect of naturally occurring salts on tensile and shear strength of sealed granular road pavements. J. Mater Civ Eng 2014;26(6):04014010.

Cui YJ, Delage P. Yielding and plastic behaviour of an unsaturated compacted silt. Géotechnique 1996;46(2):291-311.

Delage P, Audiguier M, Cui YJ, Howat MD. Microstructure of a compacted silt. Can. Geotech J 1996;33(1):150-158.

Di Maio C. Exposure of bentonite to salt solution: osmotic and mechanical effects. Géotechnique 1996;46(4):695-707.

Di Maio C, Santoli L, Schiavone P. Volume change behaviour of clays: the influence of mineral composition, pore fluid composition and stress state. Mech Mater 2004;36 (5-6):435-451.

Durotoye TO, Akinmusuru JO, Ogbiye AS, Bamigboye GO. Effect of common salt on the engineering properties of expansive soil. Int J Eng Technol 2016;6(7):233-241.

Heitor A, Indraratna B, Rujikiatkamjorn C. Laboratory study of small-strain behavior of a compacted silty sand. Can Geotech J 2013;50(2):179-188.

Israelachvili JN. Intermolecular and surface forces, 3rd edition. Academic press. 2011.

Lemaire K, Deneele D, Bonnet S, Legret M. Effects of lime and cement treatment on the physicochemical, microstructural and mechanical characteristics of a plastic silt. Eng Geol 2013;166:255-261.

Leong EC, Widiastuti S, Lee CC, Rahardjo H. Accuracy of suction measurement. Géotechnique 2007;57(6):547-556.

Liu JY, Zhang LJ. The microstructure characters of saline soil in Qarhan Salt Lake area and its behaviours of mechanics and compressive strength. Arab J Sci Eng 2014;39(12): 8649-8658.

Miller DJ, Nelson JD. Osmotic suction as a valid stress state variable in unsaturated soil mechanics. Unsaturated Soils ASCE 1993:64-76.

Mitchell JK, Soga K. Fundamentals of soil behaviour, 3rd edition. John Wiley &Sonc, Inc.2005.

Moore R. The chemical and mineralogical controls upon the residual strength of pure and natural clays. Géotechnique 1991;41(1):35-47.

NF P 18-837. Standard for special products for hydraulic concrete construction-Hydraulic binder based needling and/or sealing products-Testing of resistance against seawater and/or water with high sulphate contents. 1993.

NF P 94-056. Standard Test for Soils Investigation and Testing-Granulometric Analysis-Dry Sieving method after Washing. 1996.

NF P 94-057. Standard Test for Soils Investigation and Testing-Granulometric Analysis-Hydrometer method. 1992.

NF P 94-093. Standard Test for Soils Investigation and Testing-Dertermination of the Compaction Characteristics of a Soil-Standard Proctor test-Modified Proctro test. 1999.

Ng CWW, Yung SY. Determination of the anisotropic shear stiffness of an unsaturated decomposed soil. Géotechnique 2008;58(1):23-35.

Ng CWW, Xu J, Yung SY. Effects of wetting–drying and stress ratio on anisotropic stiffness of an unsaturated soil at very small strains. Can Geotech J 2009;46(9):1062-1076.

Ng CWW, Baghbanrezvan S, Sadeghi H, Zhou C, Jafarzadeh F. Effect of specimen preparation techniques on dynamic properties of unsaturated fine-grained soil at high suctions. Can Geotech J 2017;54(9):1310-1319.

Noorany I. Phase relations in marine soils. J Geotech Eng 1984;110(4):539-543.

Ravi K, Rao SM. Influence of infiltration of sodium chloride solutions on SWCC of compacted bentonite–sand specimens. Geotech Geol Eng 2013;31(4):1291-1303.

Reitemeier RF. Effect of moisture content on the dissolved and exchangeable ions of soils of arid regions. Soil Sci 1946;61(3):195-214.

Romero E, Della Vecchia G, Jommi C. (2011). An insight into the water retention properties of compacted clayey soils. Géotechnique. 2011;61(4):313-328.

Romero E. A microstructural insight into compacted clayey soils and their hydraulic properties. Eng. Geol. 2013;165:3-19.

Russo G, Modoni G. Fabric changes induced by lime addition on a compacted alluvial soil. Géotechnique Lett 2013;3(2):93-97.

Sarkar G, Siddiqua S. Effect of fluid chemistry on the microstructure of light backfill: An X-ray CT investigation. Eng Geol 2016;202:153-162.

Shariatmadari N, Salami M, Fard MK. Effect of inorganic salt solutions on some geotechnical properties of soil-bentonite mixtures as barriers. Int J Civ Eng 2011;9 (2):103-110.

Siddiqua S, Blatz J, Siemens J. Evaluation of the impact of pore fluid chemistry on the hydromechanical behaviour of clay-based sealing materials. Can Geotech J 2011;48(2): 199-213.

Sreedeep S, Singh DN. Critical review of the methodologies employed for soil suction measurement. Int J Geomech 2011;11(2):99-104.

Sridharan A, Jayadeva MS. Double layer theory and compressibility of clays. Géotechnique 1982;32(2):133-144.

Sridharan A, Prakash K. Percussion and cone methods of determining the liquid limit of soils: controlling mechanisms. Geotech Test J 2000;23(2):236-244.

Sridharan A, AEl-Shafei A, Miura N. Mechanisms controlling the undrained strength behaviour of remolded Ariake marine clays. Mar Georesour Geotechnol 2002;20(1):21-50.

Tang AM, Vu MN, Cui YJ. Effects of the maximum soil aggregates size and cyclic wetting-drying on the stiffness of a lime-treated clayey soil. Géotechnique 2011;61(5):421-429.

Tatsuoka F. Compaction characteristics and physical properties of compacted soil controlled by the degree of saturation. Proc. 15th Pan-American Conf. on SMGE & 6th IC on Deformation Characteristics of Geomaterials, Buenos Aires 2015:40-76.

Tatsuoka F, Correia AG. Importance of controlling the degree of saturation in soil compaction linked to soil structure design. Trans Geotech 2018;17:3-27.

Thyagaraj T, Salini U. Effect of pore fluid osmotic suction on matric and total suctions of compacted clay. Géotechnique 2015;65(11):952-960.

Tiwari B, Tuladhar GR, Marui H. Variation in residual shear strength of the soil with the salinity of pore fluid. J Geotech Geoenviron Eng 2005;131(12):1445-1456.

Truong QH, Lee C, Kim YU, Lee JS. Small strain stiffness of salt-cemented granular media under low confinement. Géotechnique 2012;62(10):949-953.

Wan AWL, Gray MN, Graham J. On the relations of suction, moisture content and soil structure in compacted clays. Proc. 1st Int. Conf. on Unsaturated Soils, Paris. Vol. 1. Balkema/Presses des Ponts et Chaussées. 1995.

Wang YJ, Benahmed N, Cui YJ, Tang AM. A novel method for determining the small-strain shear modulus of soil using the bender elements technique. Can Geotech J 2017;54(2): 280-289.

Wang YJ, Cui YJ, Benahmed N, Tang AM, Duc M. Changes of small strain shear modulus and suction for a lime-treated silt during curing. Géotechnique 2020;70(3):276-280.

Warkentin BP, Yong RN. Shear strength of montmorillonite and kaolinite related to interparticle forces. Proc. 9th Nation. Conf. Clays Clay Miner. Pergamon, 1962:210-218.

Witteveen P, Ferrari A, Laloui L. An experimental and constitutive investigation on the chemo-mechanical behaviour of a clay. Géotechnique 2013;63(3):244-255.

Yılmaz G, Yetimoglu T, Arasan S. Hydraulic conductivity of compacted clay liners permeated with inorganic salt solutions. Waste Manag Res 2008;26(5):464-473.

Ying Z, Duc M, Cui YJ, Benahmed N. Salinity assessment for salted soil considering both dissolved and precipitated salts. Geotech Test J 2020a;44(1), Online DOI: 10.1520/GTJ20190301.

Ying, Z., Cui, Y. J., Duc, M., Benahmed, N., Bessaies-Bey. H. & Chen, B. Salinity effect on the liquid limit of soils. Acta Geotechnica. 2020b. Online, DOI: 10.1007/s11440-020-01092-7.

Zhang FY, Wang GH, Kamai T, Chen WW, Zhang DX, Yang J. Undrained shear behaviour of loess saturated with different concentrations of sodium chloride solution. Eng Geol 2013a;155:69-79.

Zhang DW, Fan LB, Liu SY, Deng YF. Experimental investigation of unconfined compression strength and stiffness of cement treated salt-rich clay. Mar Georesour Geotechnol 2013b;31(4):360-374.

Zhang TW, Cui YJ, Lamas-Lopez F, Calon N, Costa D'Aguiar S. Compacted soil behaviour through changes of density, suction, and stiffness of soils with remoulding water content. Can Geotech J 2018;55(2):182-190.

Zhang Y, Ye WM, Chen YG, Chen B. Impact of NaCl on drying shrinkage behavior of low-plasticity soil in earthen heritages. Can Geotech J 2017;54(12):1762-1774.

Ying, Z., Cui, Y.J., Benahmed, N., Duc, M. 2021. Géotechnique. Doi.org/10.1680/jgeot.20.P.319.

Drying effect on the microstructure of compacted salted silt

Zi Ying[1], Yu-Jun Cui[1], Nadia Benahmed[2], Myriam Duc[3]

Abstract: This study investigates the drying-induced microstructure evolution of compacted silt with different salinities, using mercury intrusion porosimetry (MIP) and environmental scanning electron microscope (ESEM). The pore size distribution (PSD) of specimens compacted near optimum (w = 17%) exhibited bi-modal characteristics. Upon drying (w = 8%), the PSD changed to tri-modal pattern with appearance of a new nano-pore population. This suggested the development of nano-fissures which could occur in the clay fraction and at the interface between clay particles and silt/sand grains due to the clay shrinkage. With further drying (w = 3%), the nano-pores disappeared and the PSD recovered to bi-modal characteristics, suggesting that the created nano-fissures were enlarged until they became micro-fissures. The salinity seemed to decrease the frequency of the drying-induced micro-pores due to the enhanced mechanical strength of salted soil by the soil aggregation resulting from the compression of diffuse double layer and a possible cementation effect produced by precipitated salt. However, the salinity effect was relatively low, due to (i) the low clay fraction (15.7%) and the low activity clay minerals (illite, chlorite and kaolinite), (ii) the low specific surface area (24 m^2/g) which limited the salinity effect on diffuse double layer.

Keywords: Fabric/structure of soils; microscopy; partial saturation; silts; compaction

1. Introduction

Upon drying, water evaporation results in soil shrinkage and modifies soil fabric, which can greatly affect the soil hydro-mechanical behaviour and cause damage to infrastructures such as embankments, dikes, slopes, landfill liners, waste barriers etc. (Morris et al., 1992; Miller et al., 1998; Yesiller et al., 2000; Albrecht & Benson, 2001; Tay et al., 2001; Miller & Rifai, 2004; Li & Zhang, 2011; Tang et al., 2012). Therefore, understanding the microstructure evolution during drying is essential for the assessment of sustainability of geotechnical constructions in which soils are subjected to the effect of climate changes.

[1]: Ecole des Ponts ParisTech, Laboratoire Navier/CERMES, 6 – 8 av. Blaise Pascal, Cité Descartes, Champs-sur-Marne, 77455 Marne-la-Vallée cedex 2, France
[2]: INRAE, Aix Marseille Univ, Unité de Recherche RECOVER, 3275 route Cézanne, CS 40061, 13182 Aix-en-Provence, France
[3]: Université Gustave Eiffel, IFSTTAR/GERS/SRO, 14-20 boulevard Newton, Champs-sur-Marne, 77447 Marne-la-Vallée, France

MIP and ESEM have been widely applied to investigate the soil microstructure. These techniques allow identifying and quantifying the changes in micro-fabrics under the effect of suction (Simms & Yanful, 2001, 2002; Boso et al., 2005; Romero et al., 2011; Burton et al., 2015; Liu et al., 2016a, 2016b; Menaceur et al., 2016; Sun & Cui, 2018). Liu et al. (2016a) pointed out that three modes of pore size evolution existed during drying for reconstituted clayey soil. The first and second modes involved soils which exhibited initial uni-modal PSD - a significant decrease of peak pore frequency but without variations of modal size for the first mode; a decrease of the modal size by almost two orders of magnitude but without significant reduction in peak magnitude for the second mode. A third mode corresponded to a bi-modal PSD where drying resulted in a reduction of macro-pore (or inter-aggregate pore) volume and thus an increase of micro-pore (or intra-aggregate pore) volume in which the macro-pores and micro-pores were delimitated at entrance pore diameter of 0.22 μm. Zhang et al. (2017) conducted MIP tests on dried low plasticity soil slurries and reported that the uni-modal PSD curves first experienced a shift of the peak pore modal size to a lower value without much reduction of magnitude. But with further drying, the uni-modal PSD curves changed to a bi-modal pattern. Sun & Cui (2018) reported that upon drying, the soil PSD curves shifted first to a smaller diameter. Then, micro-fissures started to develop in the clay fraction and at the interface between silt grain and clay particles when the silt slurry reached the water content at air entry value. With further drying, the micro-fissures became larger and larger and finally shifted to larger pore population. This kind of micro-fissures was observed on soil slurries during drying on SEM micrographs by Bruand & Prost (1987) and Wei et al. (2013).

However, the desiccation cracks occurred not only for soil slurries (Péron et al., 2009; Tang et al., 2011a; Zhang et al., 2019), but also for compacted soils (Simms & Yanful, 2004; Romero et al., 2011). For compacted soils, it has been commonly admitted that, as the water content decreased, the reduction of macro-pores was accompanied by an increase of micro-pores, which was mainly attributed to the clay shrinkage that transformed some macro-pores to micro-pores (Simms & Yanful, 2001, 2002; Cuisinier & Laloui, 2004; Koliji et al., 2006; Romero et al., 2011).

As far as the salted soils are concerned, inhibition of macro-crack development could be caused by the cementation effect of salt crystals (Zhang et al., 2016) and by the enhanced mechanical strength of soil aggregation resulting from the shrinkage of diffuse double layer (He et al., 2016; Zhang et al., 2019). Zhang et al. (2017) investigated the microstructure of silt slurries upon

drying and reported that the sodium chloride (NaCl) solution led to a noticeable reduction of total porosity, and an increase in predominant pore entrance diameter. Liu et al. (2016b) performed MIP and SEM tests on oven-dried and freeze-dried compacted specimens which were initially immersed in distilled water or salt solutions. They observed that the total void ratio and the volume of macro-pores decreased as salt concentration increased due to the crystallization of salts: the higher the salt concentration, the more the precipitated salts and the more the pores filled by salt crystals.

The above mentioned studies showed that many studies have focused on the desiccation cracking and the drying-induced microstructure evolutions of slurries and compacted soils. Even though a few studies were devoted to the salinity effect on the microstructure changes of soil slurries during drying, there is a lack of studies that link the salinity effect on the microstructure evolutions of compacted silt upon drying. In this study, drying tests were conducted on a compacted silt with three different soil salinities. The microstructure of as-compacted specimens and dried specimens were analysed by means of MIP and ESEM. Emphasis was put on the role of clays (clay fraction and clay mineralogy) while analysing the combined effects of drying and salinity.

2. Materials and methods

2.1 Materials

The soil studied was taken from Les Salins de Giraud in southern France. It is the same soil used for the dike construction at Les Saline de Giraud. The geotechnical properties are presented in Table 1. As shown in Fig. 1, this soil contains 17% clay-size particles (< 0.002 mm), 63% silt (0.002 ~ 0.075 mm) and 20% fine sand (0.075 ~ 2 mm). According to the Unified Soil Classification System (ASTM D2487-00, 2000), this soil is a sandy silt.

Table 1. Characteristics of the tested soil.

Property	Value
Liquid limit, w_L (%)	29
Plastic limit, w_p (%)	19
Plasticity Index, I_p	10
Specific gravity, *Gs*	2.71
Specific surface area (Spot test of MB) (m^2/g)	24

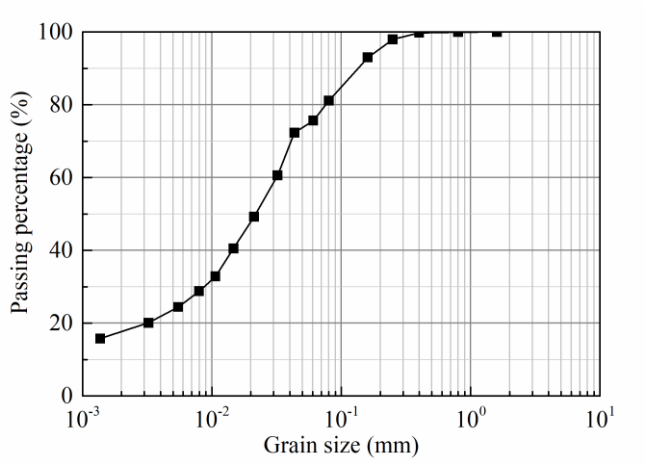

Fig. 1. Grain size distribution of the tested soil.

Mineralogical analysis shows that the main minerals of soil are 39% quartz, 35% calcite, 9.5% feldspars, 0.8% halite NaCl, and 15.7% clay minerals including 10.8% illite, 3.6% chlorite and 1.3% kaolinite. As reported by Ying *et al*. (2020a), the soil salinity (*r'*) of natural soil, defined as the mass ratio of salt to soil, is 2.1‰ (g of salt/kg of dry soil). The main ion species of soil pore water are Cl^-, Na^+, K^+, Ca^{2+}, and Mg^{2+} (Ying *et al*., 2020a), which are similar to the salt composition of synthetic sea water according to the French standard (AFNOR NF P 18-837, 1993), as shown in Table 2. Thus, for practical reasons, the five main salts of synthetic sea water were used to prepare the salted soil from initial natural soil. The target soil salinity of salted soil was 6.76‰ (g of salt/kg of dry soil), which corresponded to the near seawater salinity of r = 34‰ (g of salt/kg of salty water) when the water content of soil was fixed at 20%. More details about the salted soil preparation can be found in Ying *et al*. (2020a).

Table 2. Salt composition of synthetic sea water.

Salts	NaCI	$MgCI_2 \cdot 6H_2O$	$MgSO_4 \cdot 7H_2O$	$CaSO_4 \cdot 2H_2O$	$KHCO_3$
Concentration (g/L)	30.0	6.0	5.0	1.5	0.2

To decrease the salinity of soil, a leaching equipment was used and deionized water was flushed through natural soil from bottom to top. When the electrical conductivity of leaching water was close to that of deionized water, the leaching process ended. The soil salinity after leaching was 0.05‰ (g of salt/kg of dry soil), which could be regarded as zero. Afterwards, The natural saline soil (r' = 2.10‰), salted soil (r' = 6.76‰) and leached soil (r' = 0.05‰) were air-dried, ground and passed through 0.4 mm sieve.

2.2 Test methods

Figure 2 presents the proctor compaction curves of soils with different soil salinities, which were determined from standard proctor compaction test (AFNOR NF P 94-093, 1999). The maximum dry density of soil without salt (*r'* = 0.05‰) was 1.72 Mg/m^3, which decreased to 1.68 Mg/m^3 for soils with soil salinities of 2.10‰ and 6.76‰. The dry density of 1.63 Mg/m^3 was considered which corresponded to the compactness of 95 ~ 97% that met the requirements of dike construction at Les Salins de Giraud. The dry soil powder was humidified by deionized water to reach the water content of 17% (near optimum value) and then conserved for 24 h for salt and water homogenization. Static compaction was performed to prepare samples of 50 mm diameter and 20 mm height. Note that the water content (*w*, Eq. 1) computed from the conventional method was applied to leached soil with negligible soil salinity, while for the soil with soil salinities of 2.10‰ and 6.76‰, the water content value (*w'*, Eq. 2) was calculated by taking the dissolved salt into account (Ying *et al*., 2020a):

$$w = \frac{m - m_s}{m_s} = \frac{m_w}{m_s} \tag{1}$$

$$w' = \frac{m_{sw}}{m_s} = \frac{m_w + m_{sa}}{m_d - m_{sa}} = \frac{m - m_d}{m_d - rm} \tag{2}$$

where m is the mass of wet soil, m_s is the mass of dry soil particles, m_w is the mass of water; m_{sw} is the mass of salty water (water and salt), m_d is the mass of dry solid (soil particles and salt after oven-drying) and r is the water salinity which can be obtained from soil salinity (r') by Eq. 3 (Ying *et al*., 2020a):

$$r = \frac{r'}{w'} \tag{3}$$

After compaction, the specimens were air-dried from as-compacted state to different target water contents of around 8% and 3%. During drying, the water content of specimens was controlled by weighing the mass of specimens (m) (Tang *et al*., 2011b):

$$w = \frac{(1 + w_0)m}{m_0} - 1 \tag{4}$$

where w_0 and m_0 are respectively the initial water content and initial mass of specimens after compaction.

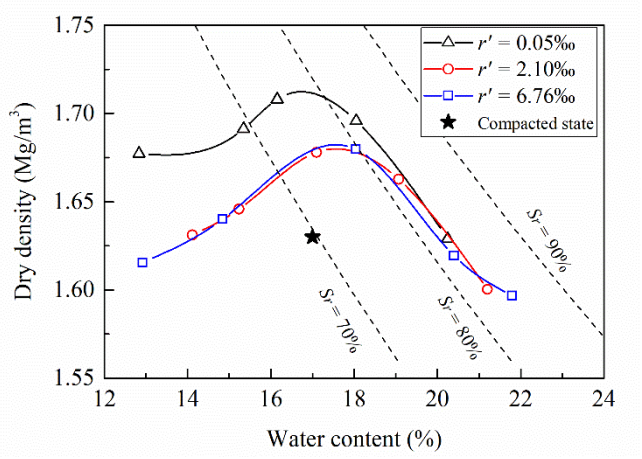

Fig. 2. Proctor compaction curves of soil with different salinities.

In order to avoid macro-cracks, the specimens were exposed to air for 2 h and then wrapped in plastic film for 1 h. The matric suction and total suction were measured by contact filter paper method and chilled-mirror dew-point hygrometer respectively prior to microstructure investigation. The suction variations during drying are plotted in Fig. 3. It appears that salinity had slight effect on the matric suction, while the total suction increased significantly with increasing soil salinity. The osmotic suction which is the difference between total and matric suctions increased with salinity increase, as expected. The soil microstructure was investigated by both MIP and ESEM. The specimens were freeze-dried prior to microstructure observations following the procedure proposed by Delage & Lefevbre (1984).

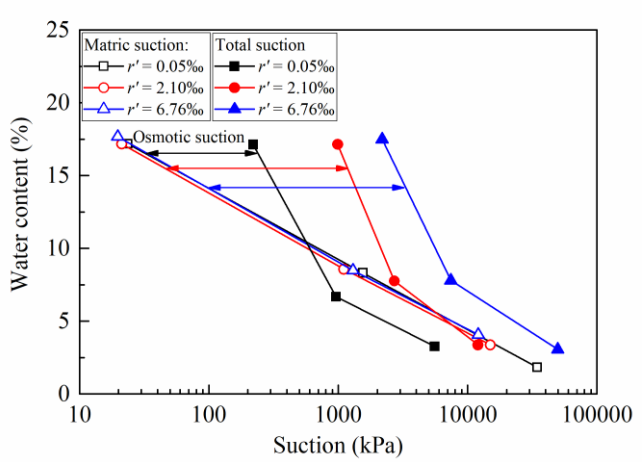

Fig. 3. Suctions variations during drying.

The mercury intrusion procedure corresponds to a desorption or drying process (Sun & Cui, 2020). Thereby, the pores which are not intruded by mercury should be regarded as filled by water. Thus, the water content and the degree of saturation of soil specimens can be obtained

as follows (Romero, 1999; Romero *et al*., 1999):

$$w = (1 - S_{rm})(w_{sat} - w_r) + w_r \tag{5}$$

$$S_r = (1 - S_{rm}) + \frac{w_r}{w_{sat}} S_{rm} \tag{6}$$

where S_{rm} is the saturation degree of mercury; w_{sat} is the water content at saturation; w_r is the residual water content.

Based on the MIP results and the hypothesis that the water is contained in small pores (Wan *et al*., 1995; Romero *et al*., 2011), the maximum diameter of water-saturated pores can be obtained according to the real water content of specimens and the relationship between entrance pore diameter and water content or degree of saturation calculated by Eqs. 5 and 6.

3. Results

3.1 Microstructural evolution during drying

The cumulative mercury intrusion curves and density function curves of the tested specimens from MIP measurements are presented in Fig. 4 for 0.05‰, 2.10‰ and 6.76‰ soil salinities, respectively. In these figures, each curve corresponds to one target water content during drying. The initial void ratio is the global one determined from the specimen dimension measured by calliper after compaction ($w \approx 17\%$) and air-drying ($w \approx 8\%$ and 3%). It can be seen that drying had negligible effect on initial void ratio. The total intruded void ratios of specimens after drying ($w \approx 8\%$ and 3%) were slightly lower than those of as-compacted specimens ($w \approx 17\%$). This slight difference was attributed to the heterogeneity of the specimen rather than the drying-induced shrinkage: the dry density of a specific small piece of specimen taken for MIP test might differ slightly from the target dry density of the whole specimen (Delage *et al*., 1996). In Figs. 4(a), (c) and (e), the dash line represents the maximum diameter of water-saturated pores. The water ratio (e_w) of specimen, defined as the void ratio corresponding to the water-saturated pores, is also indicated. As expected, the maximum diameter of water-saturated pores and the corresponding water ratio decreased with drying.

As shown in Fig. 4(b), the PSD of as-compacted specimens (w = 16.9%) exhibited bi-modal characteristics with two populations of intra-aggregate pores and inter-aggregate pores. Upon drying to 8.4% water content, the bi-modal PSD characteristics changed to tri-modal pattern with the occurrence of nano-pore population at diameters ranging from 0.1 ~ 0.4 μm. Besides,

as the water content decreased from 16.9% to 8.4%, the frequency of intra-aggregate pores decreased and its modal size shifted from 1.1 μm to 1.8 μm. Drying had negligible effect on the modal size of inter-aggregate pores, but its frequency increased when the specimens were dried to 8.4% water content. With further drying to 2.8% water content, the nano-pores disappeared and the density function curves recovered to bi-modal characteristics. The frequencies of intra-aggregate pores and inter-aggregate pores increased as compared to those at 8.4% water content.

The same observations can be made on the specimens with soil salinities of 2.10‰ and 6.76‰ (Figs. 4(d) and (f)): (i) the density functions of as-compacted specimens ($w \approx 17\%$) exhibited bi-modal characteristics; (ii) the bi-modal PSD characteristics changed to tri-modal pattern as the specimens were dried to around 8% water content; (iii) upon further drying to about 3% water content, the nano-pores disappeared and the PSD retrieved the bi-modal pattern.

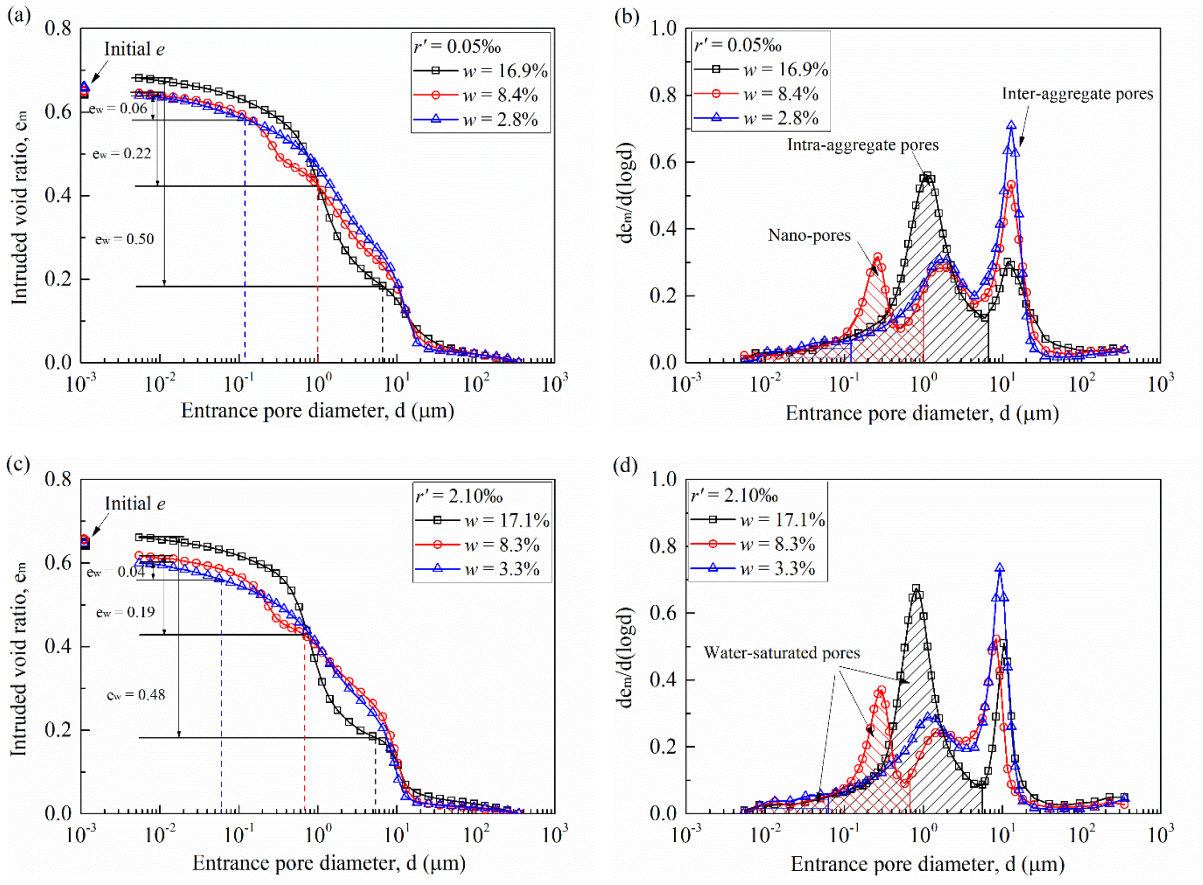

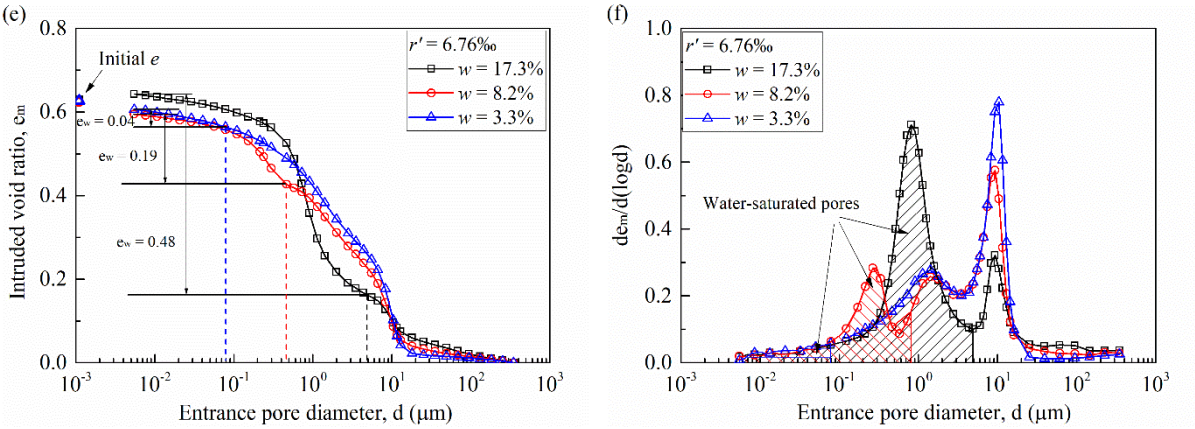

Fig. 4. Cumulative mercury intrusion curves and density function curves of compacted specimens: (a) and (b) *r'* = 0.05‰; (c) and (d) *r'* = 2.10‰; (e) and (f) *r'* = 6.76‰.

3.2 ESEM observation: microstructural changes along drying

Figures 5 show the ESEM micrographs for specimens with 2.10‰ soil salinity and water contents of 17.1%, 8.3% and 3.3%, respectively, providing an complementary insight into the MIP results. Note that almost similar observations were obtained for the specimens with different salinities. Thus, only the results of specimens at natural soil salinity (*r'* = 2.10‰) are presented here. For each specimen, two magnifications of 600× and 5000× are presented. As shown in Figs. 5(a), (c) and (e), aggregated structures were noticeable, which were mainly composed of silt/sand skeletons with some fine particles around them. This was in agreement with the observations reported on compacted Jossigny silt (Delage *et al.*, 1996) and Héricourt silt (Lemaire *et al.*, 2013). Figure 5(a) also shows that the clay fraction was not distributed homogeneously among silt/sand grains. Indeed, some grains were coated by the clay matrix, whereas some others remained quite clean, in agreement with the observations by Muñoz-Castelblanco *et al.* (2012) on an unsaturated loess with a clay fraction as low as 16%. The association of silt/sand skeletons and clay film constituted soil agglomerates (Lemaire *et al.*, 2013). The inter-aggregate pores corresponding to the porosity between agglomerates were clearly visible. The diameter of inter-aggregate pores, ranging from 5 μm to 20 μm, was in a good agreement with the size of inter-aggregate pores identified on the density function curves shown in Fig. 4(d). At a higher magnification (Fig. 5(b)), it appears that the clay particles formed a film that coated the silt/sand grains. The intra-aggregate pores with a predominant size around 1 μm, were observed at the surface of these agglomerates, confirming the obtained modal size of intra-aggregate pores by MIP test.

Comparisons of ESEM micrographs in Figs. 5(a), (c) and (e) suggested that the quantity of

inter-aggregate pores increased with the decrease of water content. This was consistent with the MIP results showing that the frequency of inter-aggregate pores increased during drying. In the micrographs with 5000× magnification (Figs. 5(b), (d) and (f)), the enlargement of intra-aggregate pores with drying was observed, in accordance with the pore size variations identified on the density function curves - the modal size of intra-aggregate pores increased as water content decreased from 17.1% to 8.3% and 3.3%. Nevertheless, the drying-induced nano-pores and the localisation of salt crystals after drying appeared indistinguishable on the ESEM images, due to the limited resolution of the apparatus.

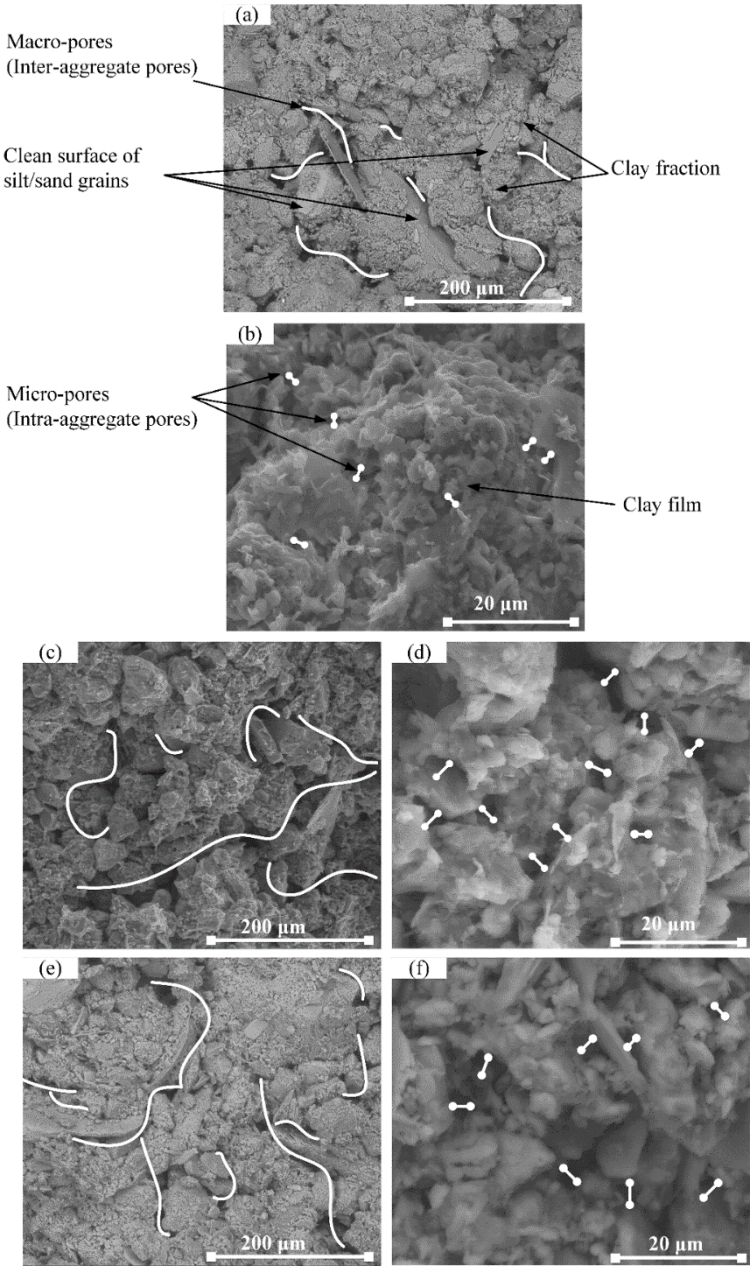

Fig. 5. ESEM micrographs of specimens with a 2.1‰ soil salinity: (a) and (b) as-compacted state at w = 17.1%; (c) and (d) after drying at w = 8.3%; (e) and (f) after drying at w = 3.3%.

3.3 Salinity effect on the microstructure

Figures 6-8 depict the PSDs of the specimens with different salinities, but at similar water content. It appears from Figs. 6(a), 7(a) and 8(a) that, at the three tested water contents, the total mercury intrusion void ratios tended to decrease with increasing soil salinity from 0.05‰ to 2.10‰ and 6.76‰. However, the intruded void ratios were slightly different from the corresponding initial void ratios. Two phenomena could be considered to explain such slight difference: (i) the heterogeneity of compacted specimens (Delage *et al*., 1996); (ii) the precipitation of salt crystals during drying which might fill the pores and reduce the pore volume (Liu *et al*., 2016b; Zhang *et al*., 2017).

Figure 6(b) shows the density function curves of as-compacted specimens ($w \approx 17\%$). With increasing soil salinity from 0.05‰ to 2.10‰, the frequency of intra-aggregate pores increased and its modal size shifted from 1.1 μm to 0.8 μm, while the modal size of inter-aggregate pores decreased from 12.9 μm to 10.5 μm. Further increase of soil salinity to 6.76‰ did not change the intra-aggregate pores significantly, but decreased the modal size of inter-aggregate pores from 10.5 μm to 9.6 μm.

The density function curves of the specimens dried to water content of around 8% are plotted in Fig. 7(b). A tri-modal characteristic was identified for all curves. With increasing soil salinity from 0.05‰ to 6.76‰, the peak pore entrance diameter of nano-pores was around 0.3 μm, and the modal size of intra-aggregate pores and inter-aggregate pores decreased slightly from 1.8 μm to 1.5 μm and from 12.9 μm to 9 μm, respectively.

Figure 8(b) depicts the density function curves for the dried specimens at about 3% water content. It was observed that, as the soil salinity increased, the modal size of intra-aggregate pores and inter-aggregate pores shifted from 1.8 μm to 1.2 μm and from 12.9 μm to 9.5 μm, respectively. Besides, with increasing soil salinity, the frequency of intra-aggregate pores decreased, while the frequency of inter-aggregate pores increased.

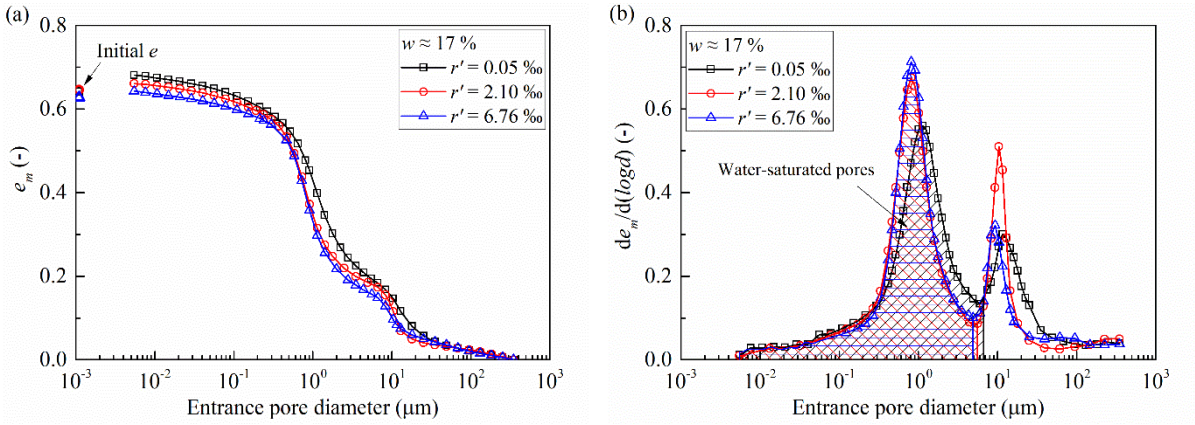

Fig. 6. Pore size distributions of as-compacted specimens at around 17% water content: (a) cumulative mercury intrusion curves; (b) density function curves.

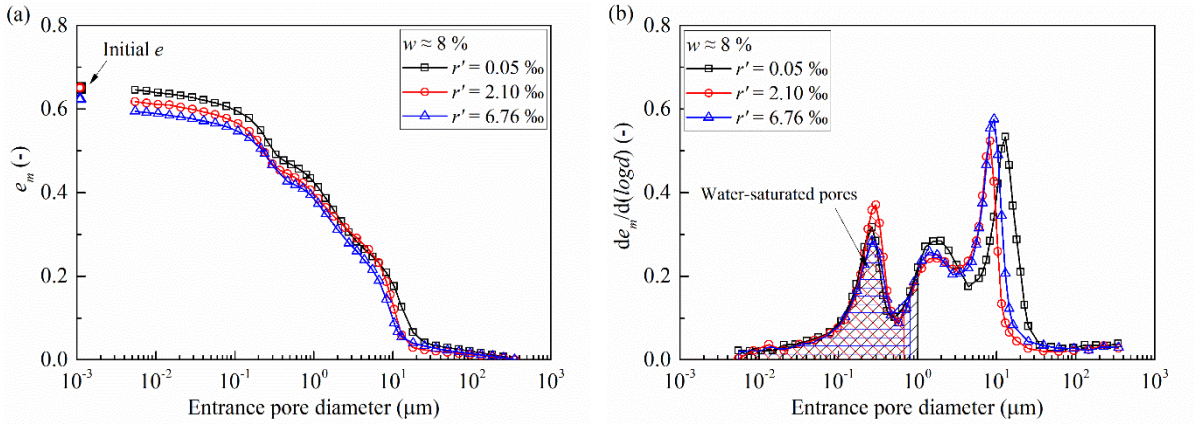

Fig. 7. Pore size distributions of air-dried specimens at around 8% water content: (a) cumulative mercury intrusion curves; (b) density function curves.

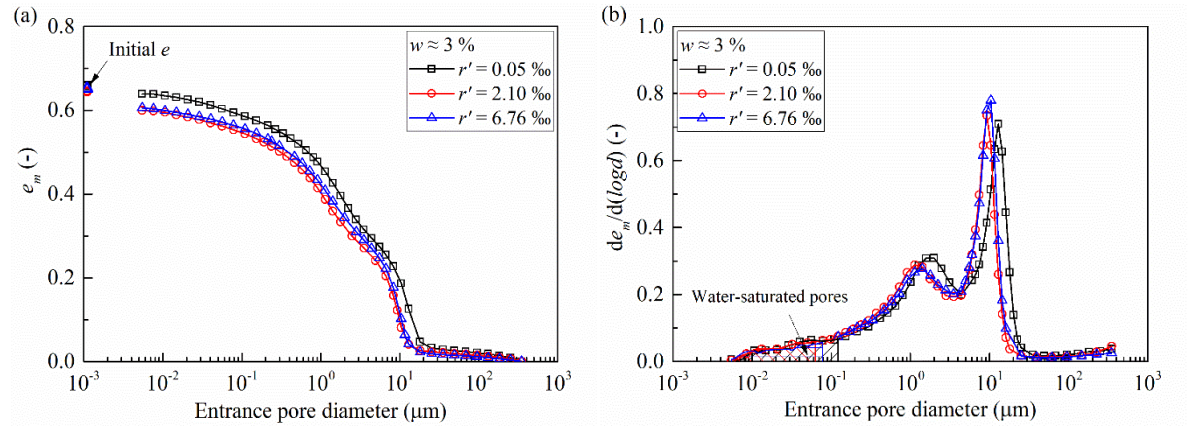

Fig. 8. Pore size distributions of air-dried specimens at around 3% water content: (a) cumulative mercury intrusion curves; (b) density function curves.

4. Discussions

4.1 Drying effect on the PSDs

Results from Figs. 4(a), (c) and (e) show that the initial void ratios of as-compacted specimens and air-dried specimens were quite similar, indicating that drying specimens from around 17% water content to lower values did not cause significant shrinkage of compacted silt, even though the PSD was significantly changed. This was consistent with the observations made by Cuisinier & Laloui (2004) on a compacted silt.

As the microstructure varied significantly during drying (Figs. 4(b), (d) and (f)), it was suspected that the micro-fissures might build up due to the shrinkage of clay. Sridharan & Prakash (1998) and Thyagaraj *et al*. (2017) pointed out that drying induced soil shrinkage through two forces acting on the soil particles: the capillary suction due to the increasing curvature of the capillary menisci and the internal resistance of soil particles to come closer to each other. It appears from Fig. 3 that the matric suction which is related to capillary suction indeed increased significantly during drying, which would induce a tensile stress acting on the surrounding particles (Tang *et al*., 2011a). Once the rising tensile stress exceeded the tensile strength or the soil shrinkage was constrained by boundary conditions, fissures/cracks would occur (Péron *et al*., 2009; Tang *et al*., 2011a; Romero 2013). As shown in the ESEM images (Fig. 5), the clay fraction in the tested silt was not uniformly distributed among the silt/sand grains, suggesting that the variations of PSD of compacted silt upon drying could be directly related to the differential shrinkage of clay fraction. Moreover, with the well-defined silt/sand skeleton, the clay shrinkage could not cause significant volume change of soil specimen.

It appeared from MIP results that the as-compacted specimens ($w \approx 17\%$) exhibited typical bi-modal pores size distribution characteristics with the almost saturated intra-aggregate pores and dry inter-aggregate pores (Fig. 6(b)). Upon drying, the water withdrawn into the smaller pores, leaving the relative larger pores being air-filled (Tarantino & De Col, 2008). Thus, the shrinkage of clay fraction could occur in the areas where grains/agglomerates changed from saturated to dry state. Owing to the clay shrinkage, some nano-fissures developed within clay fraction and at the interface between clay and silt/sand grains, explaining the appearance of nano-pores identified on the PSD curves shown in Figs. 4(b), (d) and (f). This was consistent with the observations made by Sun & Cui (2018) on Jossigny silt slurry in which a small bump appeared on the PSD curves when the slurry was dried to a water content below that at air entry

value and by Romero (2013) on compacted bentonite-sand specimens that the drying-induced cracks at the contacts between bentonite and sand grains. Meanwhile, the shrinkage of clay which coated the sand/silt grain surface also led to an increase of the intra-aggregate pore size of clay fraction (Figs. 4(b), (d) and (f); Fig. 5(d)). Upon subsequent drying to around 3% water content, the clay fraction continued to shrink, leading to larger nano-fissures. As a result, the nano-pores disappeared and the frequency of intra-aggregate pores increased. Meanwhile, the frequency of inter-aggregate pores increased as some intra-aggregate pores enlarged to inter-aggregate pores during drying (Figs. 4(b), (d) and (f)).

4.2 Salinity effect on the drying-induced microstructure evolutions

Romero (2013) reported that the frequency and modal size of inter-aggregate pores were easily affected by the dry density, while the intra-aggregate pores frequency and its dominant pore size were not affected. However, at a given dry density and water content, the modal size of intra-aggregate pores was found to decrease as the salt concentration increased (Ravi & Rao, 2013; Thyagaraj & Salini, 2015). Thus, as for the as-compacted specimens ($w \approx 17\%$) in Fig.6(b), the differences in modal size and in frequency of inter-aggregate pores were mainly attributed to the heterogeneity of compacted specimens. The higher frequency and smaller modal size of intra-aggregate pores were observed for specimens with 2.10‰ and 6.76‰ soil salinities, due to the dissolved salt in water-saturated pores. Indeed, as the salinity increased, the thickness of diffuse double layer decreased, leading to a reduction of the modal size of intra-aggregate pores (Sridharan & Jayadeva, 1982; Sridharan & Prakash, 2000; Thyagaraj & Salini, 2015). This salinity effect was visible but insignificant for the compacted silt, given that the population of intra-aggregate pores had no change with increasing soil salinity from 2.10‰ to 6.76‰. This might be attributed to (i) the low clay fraction and its less active clay minerals (10.8% illite, 3.6% chlorite and 1.3% kaolinite), and (ii) its low specific surface area of only $24 m^2/g$, limiting the development of interactions between clay particles (Ying *et al*., 2020b). This was consistent with the observations made by Zhang *et al*. (2017) on a low-plasticity loess with silt particles as high as 79.4%.

As shown in Fig. 6(b), for the as-compacted specimens, the modal sizes of intra-aggregate pores and inter-aggregate pores decreased by 0.3 μm and 3.3 μm respectively when the soil salinity increased from 0.05‰ to 2.10‰ and 6.76‰, respectively. In the case of specimens at water content of around 8% and 3% (Figs. 7(b) and 8(b)), the similar differences of 0.3 ~ 0.6 μm for

intra-aggregate pore modal size and 3.3 ~ 4 μm for inter-aggregate pore modal-size were also identified as the soil salinity increased from 0.05‰ to 2.10‰ and 6.76‰. This indicated that, as for the specimens after drying (Figs. 7(b) and 8(b)), the slightly larger modal sizes of inter-aggregate pores and intra-aggregate pores of dried specimens with 0.05‰ soil salinity resulted from the initial larger modal-sizes of these two pore populations ($w \approx 17\%$, as shown in Fig.6(b)). While drying to the water content of 8% and 3%, the salinity showed insignificant effect on the nano-pore population (Fig. 7(b)). Nonetheless, a reduction of the frequency of drying-induced micro-pores was observed when the soil salinity increased from 0.05‰ to 2.10‰ and 6.76‰ (Fig. 7(b) and 8(b)), suggesting that the salinity seemed to decrease the shrinkage of clay fraction, attenuating thus the enlargement of pore size. As the salinity increased, the inter-particle repulsive force decreased and the attractive force remained almost unchanged, resulting in an increase of the net attractive force and eventually changing the particle arrangement to aggregated structures and thus improving the mechanical strength (Warkentin & Yong, 1962). Zhang *et al*. (2019) worked on a bentonite and reported that the aggregated structure which was formed in salt solution, led to a reduction of the shrinkage volume and crack area during drying. Another possibility for lessening the development of fissures might be the cementation effect of precipitated salt which could bond the soil particles together and increased the soil resistance to cracking (Zhang *et al*., 2004; Zhang *et al*., 2016). Therefore, the specimens with soil salinities of 2.10‰ and 6.76‰ were expected to have higher mechanical strength that inhibited the clay shrinkage, leading to a smaller frequency of intra-aggregate pores, as shown in Figs. 7(b) and 8(b). This salinity effect on drying-induced microstructure variations was visible but remained quite low owing to the low clay fraction in tested silt. It was consistent with the results that salinity had insignificant effect on the matric suction even though the osmotic suction was quite higher for soils with higher salinity (Fig. 3). This was in agreement with the results obtained by Miller & Nelson (2006) and Zhang *et al*. (2017): for silty soil with less active clay fraction, the soil shrinkage during desiccation was predominantly controlled by matric suction, while the osmotic suction induced by salt solution had insignificant effect.

It appeared from above discussions that, as for the compacted silt with well-defined silt/sand skeleton, the clay shrinkage produced some internal nano/micro-fissures but without occurrence of macro-cracks and significant volume shrinkage during drying. Thus, it can be inferred that the drying-induced nano/micro-fissures could cause an increase of air permeability. Concerning the specimens at dried state, the compressibility should be lower than that at as-compacted state,

because the compressibility is mainly controlled by the increased matric suction rather than the drying-induced nano/micro-fissures. The salinity effect is expected to be slight due to its insignificant effect on matric suction. Further comprehensive investigations are needed to clarify the potential effects of the observed evolution of microstructure on the hydro-mechanical behaviour of the compacted salted silt.

5. Conclusions

In this study, the drying-induced microstructure evolution of a compacted salted silt was investigated experimentally by using MIP and ESEM techniques. Based on the obtained results, the following conclusions are drawn:

(1) The PSD of compacted silt changed upon drying without significant variations of total porosity. During drying, the PSD changed from bi-modal characteristics ($w \approx 17\%$) to tri-modal pattern with appearance of a new nano-pore population ($w \approx 8\%$), and finally retrieved the double porosity pattern ($w \approx 3\%$). The occurrence of the nano-pore populations was the result of the development of nano-fissures in the clay fraction and at the interface between clay particles and silt/sand grains due to the differential clay shrinkage when the specimens were dried to 8% water content. With further drying, the nano-fissures enlarged to micro-fissures as the clay fraction continued to shrink with drying to 3% water content, resulting in the disappearance of nano-pores and an increase of intra-aggregate pore frequency. Meanwhile, the frequency of inter-aggregate pores increased as some intra-aggregate pores enlarged and shifted to inter-aggregate pore population.

(2) Upon drying, the salinity showed negligible effect on the drying-induced nano-pores whose modal size was around 0.3 μm for specimens at different salinities. For the specimens at 8% and 3% water content, the frequency of drying-induced micro-pores decreased slightly with increasing soil salinity from 0.05‰ to 2.10‰ and 6.76‰. This could be attributed to the improved mechanical strength of salted soil due to the soil aggregation and possible cementation effect of precipitated salt, decreasing the clay shrinkage and attenuating thus the enlargement of pore size. This salinity effect on drying-induced microstructure was visible but quite low due to (i) the low clay fraction and its less active clay minerals (10.8% illite, 3.6% chlorite and 1.3% kaolinite) in silty soil, and (ii) its low specific surface area, limiting salinity effect on diffuse double layer.

Statement

Some or all data used are available from the corresponding author by request.

Acknowledgements

The authors would like to thank the China Scholarship Council (CSC). The supports provided by Ecole des Ponts ParisTech (ENPC) and INRAE are also greatly acknowledged.

References

AFNOR NF P 18-837. (1993). Standard for special products for hydraulic concrete construction-Hydraulic binder based needling and/or sealing products-Testing of resistance against seawater and/or water with high sulphate contents.

AFNOR NF P 94-093. (1999). Standard Test for Soils Investigation and Testing-Dertermination of the Compaction Characteristics of a Soil-Standard Proctor test-Modified Proctor test.

Albrecht, B. A. & Benson, C. H. (2001). Effect of desiccation on compacted natural clays. J.Geotech. Geoenviron. Eng. 127, No. 1, 67-75.

ASTM D2487-00 (2000). Standard Practice for Classification of Soils for Engineering Purposes (Unified Soil Classification System). West Conshohocken, PA: ASTM International, approved March 10, 2000.

Boso, M., Romero, E. & Tarantino, A. (2005). The use of different suction measurement techniques to determine water retention curves. Unsaturated Soils: Experimental Studies. Springer, Berlin, Heidelberg, 169-181.

Bruand, A., & Prost. R. (1987). Effect of water content on the fabric of a soil material: an experimental approach. J. Soil Sci. 38, No. 3, 461-472.

Burton, G. J., Pineda, J. A., Sheng, D. C. & Airey, D. (2015). Microstructural changes of an undisturbed, reconstituted and compacted high plasticity clay subjected to wetting and drying. Eng. Geol. 193, 363-373.

Cuisinier, O. & Laloui, L. (2004). Fabric evolution during hydromechanical loading of a compacted silt. Int. J. Numer. Anal. Methods Geomech. 28, No. 6, 483-499.

Delage, P. & Lefebvre, G. (1984). Study of the structure of a sensitive Champlain clay and of its evolution during consolidation. Can. Geotech. J. 21, No. 1, 21-35.

Delage, P., Audiguier, M., Cui, Y. J. & Howat, M. D. (1996). Microstructure of a compacted silt. Can. Geotech. J. 33, No. 1, 150-158.

He, Y., Chen, Y. G., Ye, W. M., Chen, B. & Cui, Y. J. (2016). Influence of salt concentration on volume shrinkage and water retention characteristics of compacted GMZ bentonite. Environ. Earth Sci. 75, No. 6, 535.

Koliji, A., Laloui, L., Cusinier, O. & Vulliet, L. (2006). Suction induced effects on the fabric of a structured soil. Transp. Porous Media. 64, No. 2, 261-278.

Lemaire, K., Deneele, D., Bonnet, S. & Legret, M. (2013). Effects of lime and cement treatment

on the physicochemical, microstructural and mechanical characteristics of a plastic silt. Eng. Geol. 166, 255-261.

Li, J. H. & Zhang, L. M. (2011). Study of desiccation crack initiation and development at ground surface. Eng. Geol. 123, No. 4, 347-358.

Liu, X. F., Buzzi, O., Yuan, S. Y., Mendes, J. & Fityus, S. (2016a). Multi-scale characterization of retention and shrinkage behaviour of four Australian clayey soils. Can. Geotech. J. 53, No. 5, 854-870.

Liu, X. F., de Carteret, R., Buzzi, O. P. & Fityus. S. G. (2016b). Microstructural effects of environmental salinity on unbound granular road pavement material upon drying. Acta Geotechnica. 11, No. 2, 445-451.

Menaceur, H., Delage, P., Tang, A. M. & Talandier, J. (2016). The status of water in swelling shales: an insight from the water retention properties of the Callovo-Oxfordian claystone. Rock Mech. Rock Eng. 49, No.12, 4571-4586.

Miller, C. J., Mi, H. & Yesiller, N. (1998). Experimental analysis of desiccation crack propagation in clay liners1. J. Am. Water Resour. Assoc. 34, No. 3, 677-686.

Miller, C. J. & Rifai, S. (2004). Fiber reinforcement for waste containment soil liners. J. Environ. Eng. 130, No. 8, 891-895.

Miller, D. J. & Nelson, J. D. (2006). Osmotic suction in unsaturated soil mechanics. Unsaturated Soils, 1382-1393.

Morris, P. H., Graham, J. & Williams, D. J. (1992). Cracking in drying soils. Can. Geotech. J. 29, No. 2, 263-277.

Muñoz-Castelblanco, J. A., Pereira, J. M., Delage, P. & Cui, Y. J. (2012). The water retention properties of a natural unsaturated loess from northern France. Géotechnique. 62, No. 2, 95-106.

Péron, H., Hueckel, T., Laloui, L. & Hu, L. B. (2009). Fundamentals of desiccation cracking of fine-grained soils: experimental characterisation and mechanisms identification. Can. Geotech. J. 46, No. 10, 1177-1201.

Ravi, K., & Rao, S. M. (2013). Influence of infiltration of sodium chloride solutions on SWCC of compacted bentonite–sand specimens. Geotech. Geol. Eng. 31, No. 4, 1291-1303.

Romero, E. (1999). Thermo-Hydro-Mechanical Behaviour of Unsaturated Boom Clay: an experimental study. PhD Thesis, Universidad Politécnica de Catalunya, Barcelona, Spain.

Romero, E., Gens, A., & Lloret, A. (1999). Water permeability, water retention and microstructure of unsaturated compacted Boom clay. Eng. Geol. 54, No. 1-2, 117-127.

Romero, E., Della Vecchia, G. & Jommi, C. (2011). An insight into the water retention properties of compacted clayey soils. Géotechnique. 61, No. 4, 313-328.

Romero, E. (2013). A microstructural insight into compacted clayey soils and their hydraulic properties. Eng. Geol. 165, 3-19.

Simms, P. H. & Yanful, E. K. (2001). Measurement and estimation of pore shrinkage and pore distribution in a clayey till during soil-water characteristic curve tests. Can. Geotech. J. 38, No. 4, 741-754.

Simms, P. H. & Yanful, E. K. (2002). Predicting soil-Water characteristic curves of compacted plastic soils from measured pore-size distributions. Géotechnique. 52, No. 4, 269-278.

Simms, P. H. & Yanful, E. K. (2004). A discussion of the application of mercury intrusion porosimetry for the investigation of soils, including an evaluation of its use to estimate volume change in compacted clayey soils. Géotechnique. 54, No. 6, 421-426.

Sridharan, A. & Jayadeva, M. S. (1982). Double layer theory and compressibility of clays. Géotechnique. 32, No. 2, 133-144.

Sridharan, A., & Prakash, K. (1998). Mechanism controlling the shrinkage limit of soils. Geotech. Test. J. 21, No. 3, 240-250.

Sridharan, A. & Prakash, K. (2000). Percussion and cone methods of determining the liquid limit of soils: controlling mechanisms. Geotech. Test. J. 23, No. 2, 236-244.

Sun, W. J. & Cui, Y. J. (2018). Investigating the microstructure changes for silty soil during drying. Géotechnique. 68, No. 4, 370-373.

Sun, W. J. & Cui, Y. J. (2020). Determination of soil water retention curve by mercury intrusion porosimetry tests with consideration of soil volume change. J. Rock Mech. Geotech. Eng. 12, No. 5, 1070-1079.

Tang, C. S., Shi, B., Liu, C., Suo, W. B. & Gao, L. (2011a). Experimental characterization of shrinkage and desiccation cracking in thin clay layer. Appl. Clay Sci. 52, No. 1-2, 69-77.

Tang, A. M., Vu, M. N. & Cui, Y. J. (2011b). Effects of the maximum soil aggregates size and cyclic wetting–drying on the stiffness of a lime-treated clayey soil. Géotechnique 61, No. 5, 421-429.

Tang, C. S., Shi, B., Cui, Y. J., Liu, C. & Gu, K. (2012). Desiccation cracking behavior of polypropylene fiber–reinforced clayey soil. Can. Geotech. J. 49, No. 9, 1088-1101.

Tarantino, A., & De Col, E. (2008). Compaction behaviour of clay. Géotechnique. 58, No. 3, 199-213.

Tay, Y. Y., Stewart, D. I. & Cousens, T. W. (2001). Shrinkage and desiccation cracking in bentonite–sand landfill liners. Eng. Geol. 60, No. 1-4, 263-274.

Thyagaraj, T. & Salini, U. (2015). Effect of pore fluid osmotic suction on matric and total suctions of compacted clay. Géotechnique. 65, No. 11, 952-960.

Thyagaraj, T., Thomas, S. R. & Das, A. P. (2017). Physico-chemical effects on shrinkage behavior of compacted expansive clay. Int. J. Geomech. 17, No. 2, 06016013.

Wan, A. W. L., Gray, M. N. & Graham, J. (1995). On the relations of suction, moisture content and soil structure in compacted clays. Proc. 1st Int. Conf. on Unsaturated Soils, Paris. Vol. 1. Balkema/Presses des Ponts et Chaussées.

Warkentin, B. P. & Yong, R. N. (1962). Shear strength of montmorillonite and kaolinite related to interparticle forces. Proc. 9th Nation. Conf. Clays Clay Miner. Pergamon, 210-218.

Wei, X., Hattab, M., Fleureau, J. M. & Hu, R. L. (2013). Micro–macro-experimental study of two clayey materials on drying paths. Bull. Eng. Geol. Environ. 72, No. 3-4, 495-508.

Yesiller, N., Miller, C. J., Inci, G. & Yaldo, K. (2000). Desiccation and cracking behavior of three compacted landfill liner soils. Eng. Geol. 57, No. 1-2, 105-121.

Ying, Z., Duc, M., Cui, Y. J. & Benahmed, N. (2020a). Salinity assessment for salted soil considering both dissolved and precipitated salts. Geotech. Test. J. 44, Online, 29 Jan. 2020. DOI: 10.1520/GTJ20190301.

Ying, Z., Cui, Y. J., Duc, M., Benahmed, N., Bessaies-Bey. H. & Chen, B. (2020b). Salinity

effect on the liquid limit of soils. Acta Geotechnica. Online, 28 Oct. 2020. DOI: 10.1007/s11440-020-01092-7.

Zhang, G., Germaine, J. T., Whittle, A. J. & Ladd, C. C. (2004). Index properties of a highly weathered old alluvium. Géotechnique. 54, No. 7, 441-451.

Zhang, T. W., Deng, Y. F., Cui, Y. J., Lan, H. X., Zhang, F. Y. & Zhang, H. Y. (2019). Porewater salinity effect on flocculation and desiccation cracking behaviour of kaolin and bentonite considering working condition. Eng. Geol. 251, 11-23.

Zhang, Y., Ye, W. M., Chen, B., Chen, Y. G. & Ye, B. (2016). Desiccation of NaCl-contaminated soil of earthen heritages in the Site of Yar City, northwest China. Appl. Clay Sci. 124, 1-10.

Zhang, Y., Ye, W. M., Chen, Y. G. & Chen, B. (2017). Impact of NaCl on drying shrinkage behavior of low-plasticity soil in earthen heritages. Can. Geotech. J. 54, No. 12, 1762-1774.

Chapter 4. Optimum lime content

Introduction

In practice, prior to treating a soil with lime, the optimum lime content allowing the soil to obtain the maximum mechanical performance with the minimum dosage of lime, should be determined. The optimum lime content can be determined by the variations of soil consistency limits, unconfined compression strength, pH values with increasing lime content (Eades and Grim, 1966; Kavak and Akyarlı, 2007; Al-Mukhtar et al., 2010a; Celauro et al., 2012; Moayed et al., 2012; Ciancio et al., 2014; Al-Swaidani et al., 2016). Among the three methods, the pH method was the quickest one to estimate the optimum lime content which was defined as the minimum lime content required to maintain the pH of soil-lime-water mixtures to be 12.4. The pH in the soil-lime-distilled water mixture increased gradually with the addition of lime, until it reached the maximum value (Kavak and Akyarlı, 2007; Al-Mukhtar et al., 2010a; Celauro et al., 2012; Sharma et al., 2012; Saride et al., 2013; Di Sante et al., 2014; Negawo et al., 2019). However, Emarah and Seleem (2018) reported that the pH of seawater-soil suspensions increased continuously with the increase of lime content to 3%, then it kept almost constant from 3% to 4% lime content before a second increase of pH to 12.4 with further addition of lime. This was different from the pH variations in the soil-lime-distilled water mixture. However, there is no study focusing on such difference and exploring the mechanism of salt solution effect on the optimum lime content.

This chapter aims at clarifying the salt solution effect on the pH variations with lime, hence, on the optimum lime content. The pH variations of soil-lime mixtures mixing with deionized water and synthetic seawater were investigated. To clarify the salt solution effect, the base (1-mol/L NaOH solution) titration test was performed on the soil suspensions as well. After pH measurement, the supernatants of soil-lime/NaOH suspensions were removed and acidified for chemical analysis. The results are presented in this chapter in the form of a paper submitted to “Acta Geotechnica”.

Ying, Z., Cui, Y.J., Duc, M., Benahmed, N. 2021. Submitted to Acta Geotechnica.

Effect of salt solution on the optimum lime contents of bentonite and silt

Zi Ying[1], Yu-Jun Cui[1], Myriam Duc[2], Nadia Benahmed[3]

Abstract: In practice, prior to treating a soil with lime, the optimum lime content allowing the soil to obtain the maximum mechanical performance with the minimum dosage of lime, should be determined. The optimum lime content is water chemistry and clay mineralogy dependent. In this study, the different lime dosages were added in MX-80 bentonite and silt suspensions, which were prepared with deionised water (DW) and synthetic seawater (SSW), respectively. Then, the pH measurement was conducted to determine the optimum lime contents of MX-80 bentonite and silt. The continuous base (1-mol/L NaOH solution) titration test was conducted on silt/MX80 suspensions as well, in order to highlight the lime (Ca^{2+}) role. Then, the impacts of salt solution and lime on the material behaviour such as dissolution and/or precipitation of new compounds were discussed, based on the measurement of pH followed by the quantification of the major species in the supernatants of MX80-lime/NaOH suspensions. Results showed that the optimum lime content increased with the increase of salt concentration, which could be attributed to the consumption of OH^- ions by Mg^{2+} and Ca^{2+} ions in the salt solution, producing the precipitations of $Mg(OH)_2$ and $CaCO_3$. Due to the higher cation exchange capacity and higher bentonite solubility of MX-80 compared to silt, a higher lime addition was required to reach the optimum lime dosage pH threshold for MX-80 bentonite. The pH of the tested suspensions was found to be lower than that of blank deionised water and synthetic seawater, as OH^- ions could be consumed by the material adsorption, dissolution of clay minerals and pozzolanic reaction. However, the pH of MX80-SSW-NaOH suspensions was higher than that of blank synthetic seawater in case of titration of NaOH solution from 2.5 mL to 6 mL, probably because some Mg^{2+} and Ca^{2+} ions were adsorbed on the clay mineral surface and less OH^- ions were consumed by the production of $Mg(OH)_2$ and $CaCO_3$.

Keywords: optimum lime content; silt; bentonite; salt solution; pH

[1]: Ecole des Ponts ParisTech, Laboratoire Navier/CERMES, 6 – 8 av. Blaise Pascal, Cité Descartes, Champs-sur-Marne, 77455 Marne-la-Vallée cedex 2, France
[2]: Université Gustave Eiffel, IFSTTAR/GERS/SRO, 14-20 boulevard Newton, Champs-sur-Marne, 77447 Marne-la-Vallée, France
[3]: INRAE, Aix Marseille Univ, Unité de Recherche RECOVER, 3275 route Cézanne, CS 40061, 13182 Aix-en-Provence, France

1. Introduction

Lime treatment is a traditional technique used to improve the workability and mechanical

behaviour of soils. When the lime is mixed with soil and water, lime hydration takes place rapidly, releasing some calcium (Ca^{2+}) and hydroxide (OH^-) in the pore water [9, 21]. The Ca^{2+} cations can be adsorbed on the clay minerals through cation change process by replacing the monovalent cations (i.e., Na^+, K^+, etc.) initially present on clay particles, resulting in the flocculation of soil particles and thus reducing the plasticity, swelling and shrinkage of soils [8, 9, 32]. Besides, the released OH^- ions produces a high alkaline pH environment in the soil-lime-water mixtures, inducing the dissolution of reactive silica (Si^{4+}) and alumina (Al^{3+}) ions from soils [9, 13, 44]. In the long term, the pozzolanic reaction occurs between the Ca^{2+}, Si^{4+}, Al^{3+} and OH^- ions, forming the cementitious compounds which could significantly improve the mechanical properties of soils [42, 48].

Lime treatment has been widely applied to various materials, such as quartz, silt, illite, kaolin and bentonite clay, etc. [4, 9, 15, 31, 44, 48, 51, 55]. Bell et al. [9] compared the strength increases of lime-treated montmorillonitic clay, kaolinitic clay and quartz during curing. They reported that, during curing, the fine quartz had the highest increase of strength, and the montmorillonitic clay exhibited much more rapid increase in strength than kaolinitic clay. Wang [47] indicated that, during curing, the lime-treated clay had higher small strain shear modulus (G_{max}) than the lime-treated silt, which was attributed to more pozzolanic reaction expected in lime-treated clay. Al-Mukhtar et al. [4] performed X-ray diffraction and thermogravimetric analysis on 10% lime-treated clayey soils with different clayey minerals of smectite, kaolinite and illite. They found that the lime consumption was faster and more for the clayey soil containing smectite than for those mainly consisting of illite and kaolinite. Similarly, Vitale et al. [44] reported that, compared to lime-treated kaolin, the lime-treated bentonite specimens consumed more portlandite and promoted the formation of cementitious compounds.

In practice, prior to treating a soil with lime, the optimum lime content (by weight of dry soil) which could provide sufficient Ca^{2+} ions for the cation exchange and pozzolanic reaction should be determined. In general, for the soil with similar pH, the higher the cation exchange capacity and specific surface area, the more the amount of lime required to provide sufficient Ca^{2+} ions for the cation exchange and the initiation of pozzolanic reaction [12]. Hilt and Davidson [26] proposed the definition of initial consumption of lime (ICL) which corresponded to the amount of lime participating cation exchange process. It can be determined according to the fraction of clay-size particles ($\leqslant$ 2μm), as follows:

$$ICL = \frac{Clay\ \ fraction\ (\%)}{35} + 1.25 \quad (1)$$

The initial consumption of lime is highly related to the cation exchange process. But Eq. 1 does not take the different types of clay minerals into account. For instance, the cation exchange capacities are 3-15 meq/100 g for kaolinite, 15-40 meq/100 g for illite, and up to 80-150 meq/100 g for smectite [34]. This was confirmed by the results obtained by Al-Mukhtar et al. [4] who reported that, immediately after lime addition, the smectite had the highest lime consumption, while the kaolinite had the lowest lime consumption, the illite being in between.

Hilt and Davidson [26] also indicated that the initial consumption of lime can be identified from the variation of soil consistency limits. The initial consumption of lime determined from soil plasticity was also regarded as optimum lime content [28, 35]. It was defined as the amount of lime needed for modifying the plasticity of soil, and beyond which no further change in plasticity occurred [2, 5, 10, 28, 35]. Ciancio et al. [14] indicated that the optimum lime content can be determined by measuring the unconfined compressive strength of soil samples at various lime contents, the optimum lime content being the lime content at which the unconfined compressive strength is the maximum. Nevertheless, this method is time consuming and requires preparing a large number of specimens.

The quickest procedure to estimate the optimum lime content is the pH method proposed by Eades and Grim [21]: the optimum lime content corresponds to the minimum lime content required to maintain the pH of soil-lime-water mixtures to be 12.4 which is equivalent to the pH of a lime-saturated solution. The pH in the soil-lime-distilled water mixture increases gradually with the addition of lime, until it reaches the maximum value [3, 10, 16, 28, 36, 39, 40]. This pH method is included into ASTM standard [6]. It is specified that distilled water should be used in the pH measurement for the optimum lime content determination in most cases, while the site water should be used if the pH of the site water is highly acidic (< 6) or highly basic (> 9) [6]. Emarah and Seleem [22] used the Red Sea water with a pH of 8.2~8.7 to prepare the soil suspensions for the identification of optimum lime content. Results showed that the pH of seawater-soil suspensions increased continuously with the increase of lime content to 3%, then it kept almost constant from 3% to 4% lime content before a second increase of pH to 12.4 with further addition of lime. This is different from the pH variations in the soil-lime-distilled water mixture. To the authors' knowledge, there is no study focusing on such difference and exploring the mechanism of salt solution effect on the optimum lime content.

It appears from aforementioned studies that the optimum lime content highly depends on the water chemistry and mineralogy, soil pH, specific surface area and cation exchange capacity of soils. This study aims at clarifying the salt solution effect on the pH variation with lime, hence, on the optimum lime content, with consideration of the effects of clay fraction and clay mineralogy. For this purpose, two materials were used: a MX-80 bentonite with 92% smectite and a silt with only 15.7% clay minerals. Three kinds of water were used to prepare the suspensions: deionised water, 35 g/L synthetic seawater and 70 g/L mixed salts solutions. The continuous base (1-mol/L NaOH solution) titration test with measuring pH was performed on the silt/MX80 suspensions as well. After pH measurement, the supernatants of MX80-lime/NaOH suspensions were removed and acidified for the quantification of Na, K, Ca, Mg, Al, Si and Fe species by Inductively Coupled Plasma/Optical Emission Spectroscopy (ICP/OES) analysis. The results obtained allowed the mechanisms of optimum lime content increase with the increase of salinity and the variation of pH with the addition of lime to be clarified for both MX-80 bentonite and silt. Furthermore, the salt solution and lime effects on the suspension states were also discussed.

2. Materials and methods

2.1 Materials

A commercial MX-80 bentonite from Wyoming (USA) and a silty soil sampled at Les Salins de Giraud in southern France were used. The MX-80 bentonite contains 92% smectite, 3% quartz and other 5% of feldspar, micas, sulphides and oxides [41, 46]. X-ray diffraction analysis shows that the silty soil is mainly composed of 84.3% non-clay minerals including 39% quartz, 35% calcite, 9.5% feldspars, 0.8% halite NaCl; its clay minerals include 10.8% illite, 3.6% chlorite and 1.3% kaolinite. Table 1 summarizes the basic geotechnical properties of these two materials. As expected, the MX-80 bentonite has higher liquid limit, specific surface area and cation exchange capacity than the silty soil, due to the large proportion of smectite in bentonite. The total cation exchange capacity of MX-80 bentonite is around 78 to 85 meq/100g. The main exchangeable cation is Na^+ (60-67 meq/100g), and the others such as Ca^{2+} (5-8 meq/100g), Mg^{2+} (3-4 meq/100g) and K^+ (0.2-1.3 meq/100g) are relatively low [46, 54]. The calcium consumptions of MX-80 bentonite and silt were determined by Chapelle test [23]. The calcium consumption by MX-80 bentonite was significantly higher than that by silt: the mean value of calcium consumption of MX-80 bentonite was estimated at 505 mg of CaO/g of MX-80 bentonite, against 37 mg of CaO/g of soil for the silt.

Table 1. Characteristics of the studied materials

Property	MX-80 bentonite	Silty soil
Liquid limit, w_L (%)	630[a]	29
Plastic limit, w_p (%)	42[b]	19
Plasticity Index, I_p	478[b]	10
Specific gravity, *Gs*	2.76[b]	2.71
Specific surface area (m^2/g)	562[c]	24
Total cation exchange capacity, CEC (meq/100 g)	78-85[d]	/
Calcium consumption (mg of CaO/ g of material)	505	37
pH	9.34	9.79

[a]Data from Ying et al. [52]; [b]Data Tang et al. [41]; [c]Data from Madsen [33]; [d]Data from Wang et al. [46].

As reported by Ying et al. [53], the tested silty soil is saline, with a salt concentration of 13 g/L in soil pore water. As shown in Table 2, the main ion species of soil pore water are Cl^-, Na^+, K^+, Ca^{2+}, and Mg^{2+}, which are similar to the salt composition of synthetic sea water according to the French standard [24]. Thus, for practical reason, the five main salts of synthetic seawater (Table 3) were used to prepare the salt solutions with the total concentrations of 35 g/L and 70 g/L by keeping the same proportion of each salt as for the synthetic seawater (SSW). Note that the salt solution of 35 g/L corresponds to the synthetic seawater with a pH of 7.14. According to the molar mass of ions (Na^+, Mg^{2+}, Ca^{2+} and K^+), the molar mass and the concentration of each salt, the concentration of each ion provided by synthetic seawater can be determined, as shown in Table 3.

Table 2. Chemical analysis of natural soil pore water

Solution	Chemical composition (mg/L)					Salt concentration, *c* (g/L)
	Cl^-	Na^+	Ca^{2+}	K^+	Mg^{2+}	
Soil pore water	7521	5096	215	225	176	13

Table 3. Receipt of synthetic seawater

salts	NaCl	$MgCl_2 \cdot 6H_2O$	$MgSO_4 \cdot 7H_2O$	$CaSO_4 \cdot 2H_2O$	$KHCO_3$
Salt concentration (g/L)	30.0	6.0	5.0	1.5	0.2
Ion concentration (mg/L)	Na^+: 11800	Mg^{2+}: 1200		Ca^{2+}: 350	K^+: 78

2.2 Optimum lime content determined by pH method

The optimum lime content was determined by the pH method following the procedure proposed by Eades and Grim [6, 21]. The lime used in this study was a quicklime with a CaO content as high as 97.3% [49]. A quantity of 25 g of dry silt was first mixed with various amounts of lime in a sealed container with a lid. Then, 100 mL deionised water or salt solutions (35 g/L for synthetic seawater and 70 g/L for the mixed salts solution) was added to the silt/MX80-lime mixtures. Afterwards, the silt/MX80-lime-water mixtures were shaken for 30 s every 10 min for 1 h. After shaking, the pH values of the silt/MX80-lime-water mixtures were measured immediately. By contrast with silt, only a quantity of 10 g of MX-80 bentonite was used, in order to reach a suitable consistency for the pH measurement. The photos of bentonite and silt suspension states in deionised water, deionised water with 2% lime and synthetic seawater after immediate shaking are presented in Fig. 1. It appears that the MX-80 bentonite exhibited a gel-like structure in deionised water. The addition of 2% lime made the MX-80 bentonite suspension become more fluid than that prepared with only deionised water, and the MX-80 bentonite suspensions prepared with synthetic seawater was the most fluid. In contrast, the lime and salt solution effects on the silt suspension states were found to be insignificant. A buffer solution was prepared by dissolving 2 g of lime into 100 mL deionised water or salt solutions. The optimum lime content was defined as the threshold value beyond which any further addition of lime would not change the pH of silt/MX80-lime-water mixtures. For comparison, blank tests of pH measurement were conducted on deionised water and synthetic seawater with various amounts of lime.

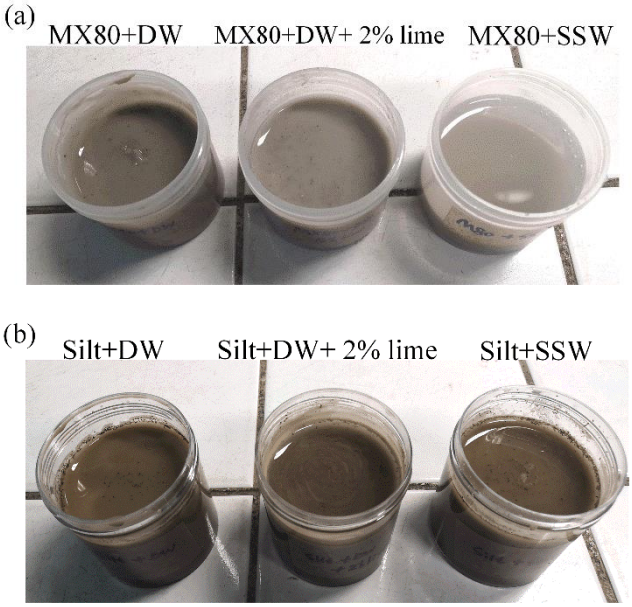

Fig. 1. Lime and salt solution effects on the suspensions states: (a) MX-80 bentonite; (b) silty soil

2.3 NaOH titration test

A 1-mol/L NaOH solution was used for the continuous base titration at 25 °C using a computer-controlled titrator (Dosino coupled with Tiamo^{TM} 2.4, Metrohm). The titration test was performed under argon atmosphere on 50 mL silt/MX80 suspension in a teflon vessel equipped with a teflon pale [18, 19]. The silt/MX80 suspension was prepared by dispersing 0.5 g material into 50 mL deionised water or 35 g/L synthetic seawater. Afterwards, the silt/MX80 suspension was shaken for 30 s every 10 min for 1 h. The 1-mol/L NaOH solution was continuously titrated into the silt/MX80 suspension at a rate of 0.1 mL/120 s until the pH reached a value of 12 or 15 mL NaOH solution was titrated. The pH of silt/MX80 suspension was measured with a combination electrode after each titration. The blank titration test was conducted on deionised water and 35 g/L synthetic seawater as well.

2.4 Chemical analysis

After pH measurement, the major elements of Na, K, Ca, Mg, Al, Si and Fe in the supernatants of MX-80 bentonite suspensions and blank solutions, were quantified by ICP/OES. To obtain the suspensions with different quantities of NaOH solution, the target volume of NaOH solution (i.e., 0.4 mL, 1 mL, 2.5 mL, 3.4 mL, 4.75 mL, 7 mL) was titrated in MX-80 bentonite suspensions and blank solutions following the same procedure in titration tests. The MX-80 bentonite suspensions and blank solutions at various lime contents and with different quantities of NaOH solutions were centrifuged to separate the supernatant and solid. Then, the supernatant was removed and filtered by a syringe filter with membrane of 0.22 μm pore size, in order to remove clay colloids in the supernatants. The clear supernatants were acidified and diluted for ICP/OES analysis. The detection limits for the analysed elements are as follows: 0.2 mg/L for Na, 0.2 mg/L for K, 0.2 mg/L for Ca, 0.05 mg/L for Mg, 0.2 mg/L for Al, 0.1 mg/L for Si, and 0.02 mg/L for Fe.

3. Results

3.1 pH variations

Figure 2 presents the pH variations with increasing lime content in MX-80 bentonite and silt suspensions which were prepared by deionised water (DW), synthetic seawater (SSW) and mixed salts solution (MSS), respectively. The pH values of buffer solutions are also shown in Fig. 2, indicating a decreasing trend with the increase of salt concentration. It is worth noting

that the pH of buffer solution prepared with deionised water was up to 12.81, which was higher than the pH of saturated lime solution of 12.4 indicated by Eades and Grim [21] and of 12.63 obtained by Chemeda et al. [11]. This might be attributed to the effects of lime purity, deionised water and ambient temperature. The purer the lime and deionised water and the lower the temperature, the higher the measured pH. In the case of suspensions with deionised water, the pH increased gradually until it reached the maximum value which was equivalent to the pH of buffer solution. With further addition of lime, the pH did not change significantly. However, in the case of silt/MX80 suspensions with salt solutions, the pH-lime content curves were quite different from those of silt/MX80 suspensions with deionised water. The pH of silt/MX80-salt suspensions increased dramatically in the beginning of lime addition. Then, it increased at a decreasing rate. Finally, it increased with a relatively higher rate and reached the maximum value close to that of buffer solution. The optimum lime contents were estimated at 5%, 7% and 10% for MX80-DW, MX80-SSW and MX80-MSS suspensions, respectively. Lower optimum lime contents of 1.5%, 3% and 4% were obtained for silt-DW suspension, silt-SSW suspension and silt-MSS suspension, respectively.

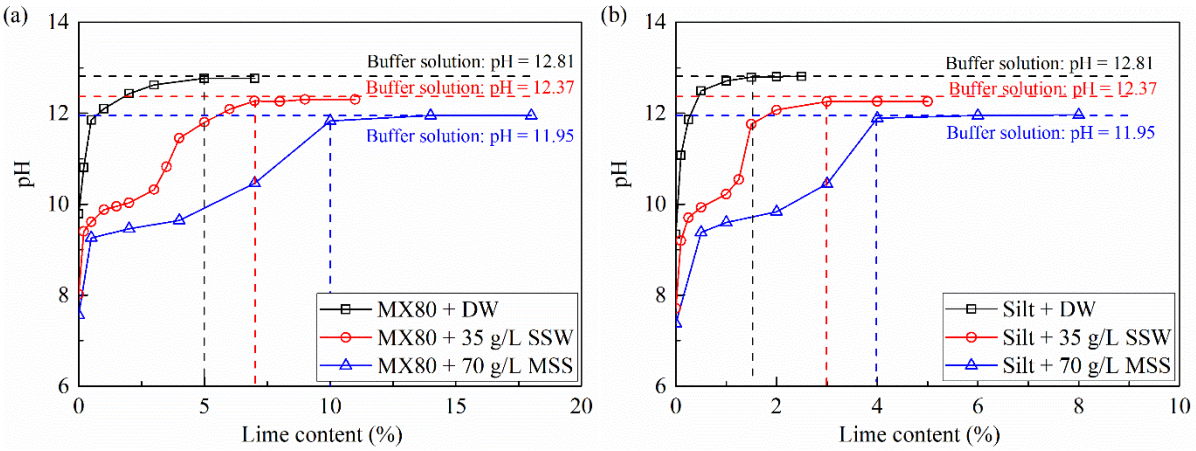

Fig. 2. Mixed salts concentration effect on the optimum lime content: (a) MX-80 bentonite; (b) silty soil

Figure 3 depicts the pH variations with lime content for silt suspensions prepared with single salt solutions (Table 3). The pH-lime content curves of silt suspensions prepared with deionised water and synthetic seawater are also presented for comparison. It is observed that at the same lime content, the pH in silt-single salt suspensions was lower than that of silt-DW suspensions, but higher than the pH of silt-SSW suspensions. The pH-lime content curves of suspensions prepared with NaCl, $CaSO_4$ and $KHCO_3$ solutions almost overlapped and lay above the curves of suspensions with $MgCl_2$ and $MgSO_4$ solutions. This suggested that the $MgCl_2$ and $MgSO_4$

in the synthetic seawater might be the main factors causing the lower increase of pH in the soil suspensions prepared with synthetic seawater and mixed salts solution.

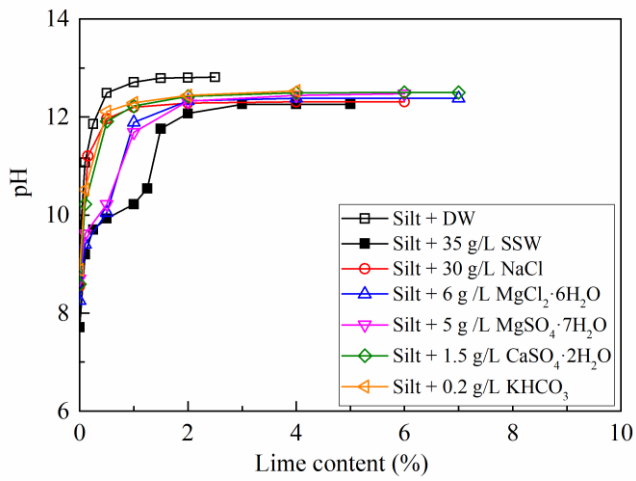

Fig. 3. Single salt solution effect on the optimum lime content of silty soil

The changes in pH of blank solutions are plotted in Fig. 4a with the pH variations of MX-80 bentonite suspensions, and in Fig. 4b with the pH variations of silt suspensions. Note that the lime dosages (g) of blank solutions in Figs. 4a and 4b are the same. To compare the pH curves of blank solutions to those of silt/MX80 suspensions, the lime contents of blank solutions in Figs. 4a and 4b were defined as the ratio of lime dosages (g) to 10 g of MX-80 bentonite and 25 g of dry silt, respectively. The pH variations for the blank deionised water and synthetic seawater were similar to those for silt/MX80 suspensions prepared with deionised water and synthetic seawater, respectively. It appears from Fig. 4a that the pH values of MX80-DW suspensions were lower than those of blank deionised water at lime content ranging from 0.1% to 5%. In the case of MX80-SSW suspensions and blank synthetic seawater, the following results were identified: when the lime content was in the range of 0.2% ~ 1.5% and 3% ~ 7%, the pH values of MX80-SSW suspensions were lower than that of blank synthetic seawater; at lime content ranging from 1.5% ~ 3% and higher than 7%, the pH-lime content curve of MX80-SSW suspensions converged to the curve of blank synthetic seawater. As shown in Fig. 4b, the difference between the pH-lime content curves of silt-DW suspensions and blank deionised water was less significant as compared to the MX80-DW suspensions. In the case of silt-SSW suspensions, lower pH values were also obtained at the lime content in the range of 0.1% ~ 0.5%. With further increase of lime content, the pH values were kept almost the same for the blank solutions and silt suspensions.

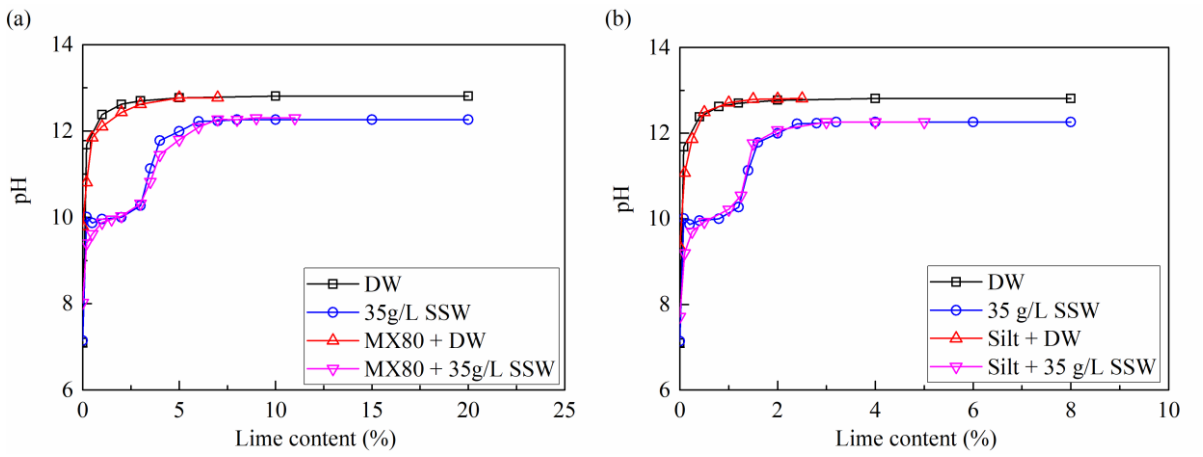

Fig. 4. pH variations with increasing lime content for suspensions and blank solutions: (a) MX-80 bentonite; (b) silty soil

The base titration curves of MX-80 bentonite suspensions and silt suspensions are presented in Figs. 5a and 5b, respectively. The titration curves of blank solutions are also presented for comparison. It appears that the variations of pH with increasing volume of NaOH solution followed the same trends as the pH variations with increasing lime content. Similarly, the pH values of the silt-DW, silt-SSW and MX80-DW suspensions were lower than those of the corresponding blank solutions, when the volumes of NaOH solution were lower than 3 mL, 1 mL and 4 mL, respectively. However, three zones were identified by comparing the pH-NaOH curves of MX80-SSW suspensions and blank synthetic seawater: i) the pH in the MX80-SSW suspensions was lower than that of blank synthetic seawater with titrating NaOH solution to 2.5 mL; ii) the reverse results were obtained with the titration of NaOH solution from 2.5 mL to 6 mL; iii) with further titration of NaOH solution, the pH of the MX80-SSW suspensions was equal to that of blank synthetic seawater (Fig. 5a).

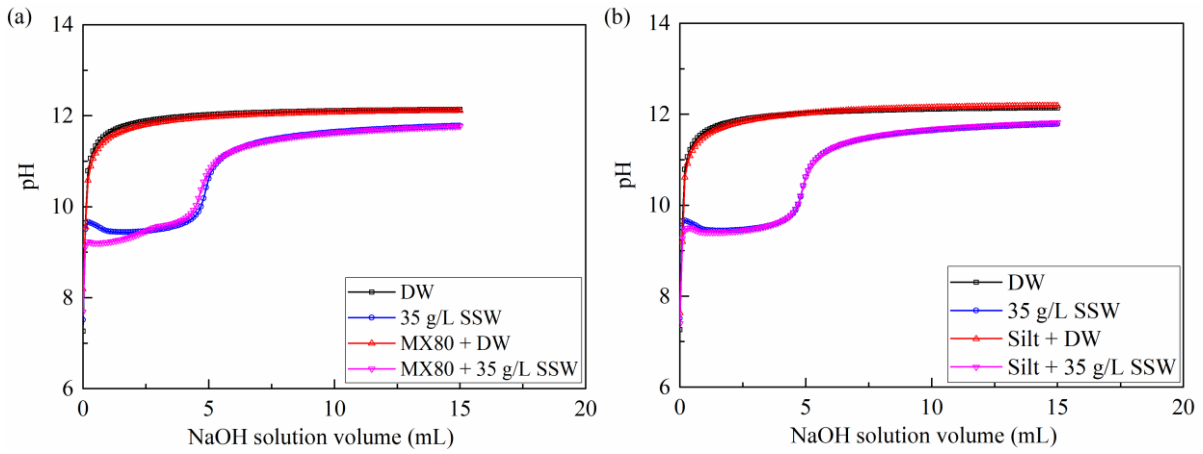

Fig. 5. pH variations with increasing NaOH solution volume for suspensions and blank solutions: (a) MX-80 bentonite; (b) silty soil

3.2 Chemical analysis

The changes in Si, K, Na, Mg and Ca concentrations with increasing NaOH solution volume or lime content are presented in Figs. 6-10, respectively. In addition to the measured concentrations, the total concentration of K, Na, Mg and Ca species in the suspensions supplied from synthetic seawater or lime/NaOH were calculated assuming that all salts and lime are dissolved and without considering the cation exchange and adsorption by clay minerals. As shown in Fig. 6, Si species were detected in the supernatants of MX-80 bentonite suspensions, but not in the supernatants of blank solutions. The Si concentration in the supernatants of MX80-DW suspensions decreased gradually from 36 mg/L to 2 mg/L with increasing lime content from 0.2% to 5%. The Si concentration in the supernatants of MX80-SSW suspensions was around 1-2 mg/L with NaOH solution or lime, which were lower than those in the supernatants of MX80-DW suspensions.

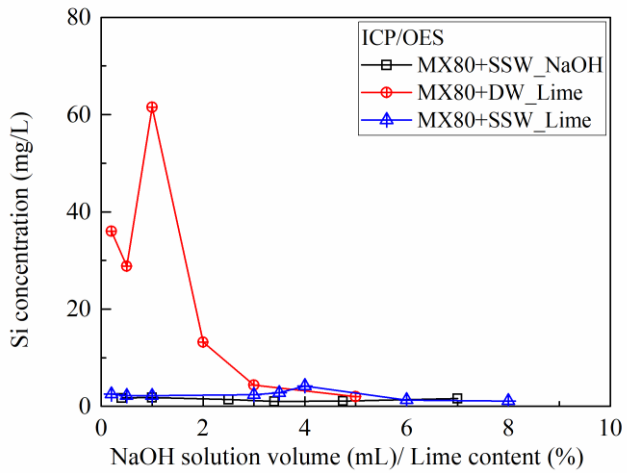

Fig. 6. Variations of Si concentration with increasing NaOH solution volume/lime content

As shown in Fig. 7a, the calculated K concentration in the supernatants of MX80-SSW suspensions and blank synthetic seawater decreased with titrating of NaOH solution, due to the dilution effect. However, the measured K concentration increased with titrating NaOH solution, probably due to the impurity of 0.5% KOH in the 1-mol/L NaOH solution. At the same titrated volume of NaOH solution, the measured K concentration in the supernatants of MX80-SSW suspensions was higher than that in the supernatants of blank synthetic seawater, suggesting that approximately 7 mg/L K^+ in the MX-80 bentonite was replaced by the Mg^{2+} or Ca^{2+} ions in the synthetic seawater through cation exchange process (Fig. 7a). Similarly, as shown in Fig. 7b, the measured K concentration in the supernatants of MX80-SSW suspensions was about 40

mg/L higher than that in the supernatants of blank synthetic seawater at different lime contents. The calculated K concentration was the lowest one as compared to that in the supernatants of MX80-SSW suspensions and synthetic seawater. With increasing lime content, the K concentration increased from 6 mg/L to 30 mg/L in the supernatants of MX80-DW suspensions, due to the cation replacement of K^+ ions by Ca^{2+} ions from lime.

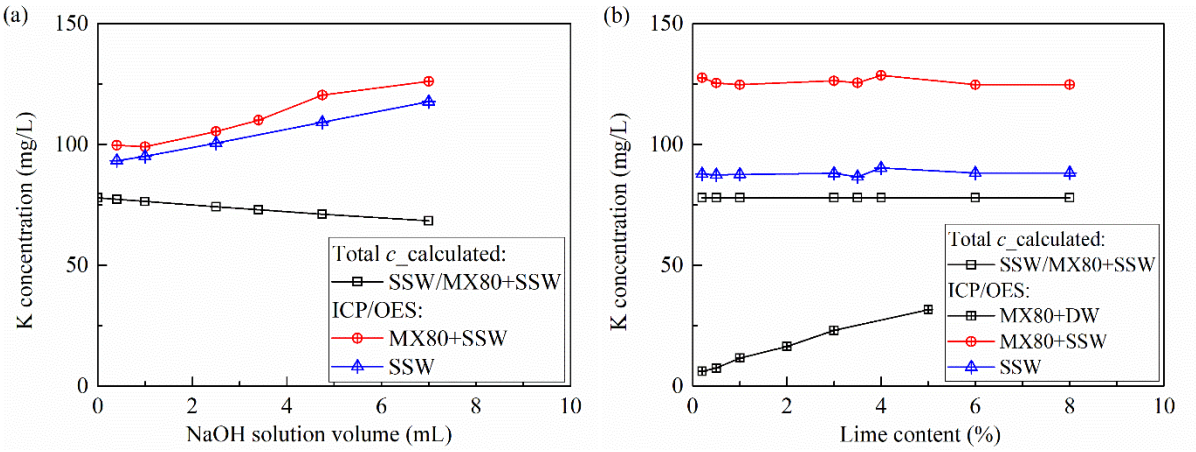

Fig. 7. Variations of K concentration with increasing: (a) NaOH solution volume; (b) lime content

With the titration of NaOH solution, the total calculated Na concentration (c) was the sum of Na from synthetic seawater (11800 mg/L in 50 mL SSW) and from NaOH solution (V mL):

$$c = \frac{11800\ mg/L \times 50\ mL}{50\ mL + V\ mL} + \frac{V\ mL \times 1\ mol/L \times 23\ g/mol}{50\ mL + V\ mL} \quad (2)$$

The calculated values increased from 11800 mg/L to 13171 mg/L, and the measured Na concentration increased from 12500 mg/L to 13800 mg/L and 14300 mg/L in the supernatants of MX80-SSW suspensions and blank synthetic seawater respectively (Fig. 8a). Unlike the K species, at a given NaOH solution volume, the difference between the measured Na concentrations in the supernatants of MX80-SSW and blank synthetic seawater was insignificant, due to the abundant supply of Na species from synthetic seawater and from NaOH solution that could mask the small amount of Na^+ ions replaced from 0.5 g of MX-80 bentonite in cation exchange process. As shown in Fig. 8b, with increasing lime content, the measured Na concentrations in the supernatants of MX80-SSW suspensions and blank synthetic seawater kept almost constant at average values of 12700 mg/L and 12300 mg/L, indicating that around 400 mg/L Na^+ ion were replaced from 10 g of MX-80 bentonite by Ca^{2+} and Mg^{2+} ions in the synthetic seawater through cation exchange process. As for the MX80-DW suspensions at lime content of 5%, approximately 1015 mg/L Na^+ ions were replaced from MX-80 bentonite by the

Ca^{2+} ions from lime. It is worth noting that, with either titrating of NaOH solution or increasing lime content, the calculated Na concentration was lower than the measured ones (Figs. 8a and 8b). Regarding the NaOH titration results, the calculated total Na concentration increased by 1371 mg/L and the measured Na concentration increased by 1234 mg/L for MX80+SSW supernatant and 1827 mg/L for blank synthetic seawater. This indicated that the increases of Na concentration of calculated and measured results were rather close. It can be thus inferred that the higher value for the measured Na concentration than the calculated one was mainly due to the experimental error from the preparation of synthetic seawater where more than 30 g/L NaCl was added. Similar phenomenon was observed on K concentration: the measured K concentration was higher than the measured one (Fig. 7a and 7b).

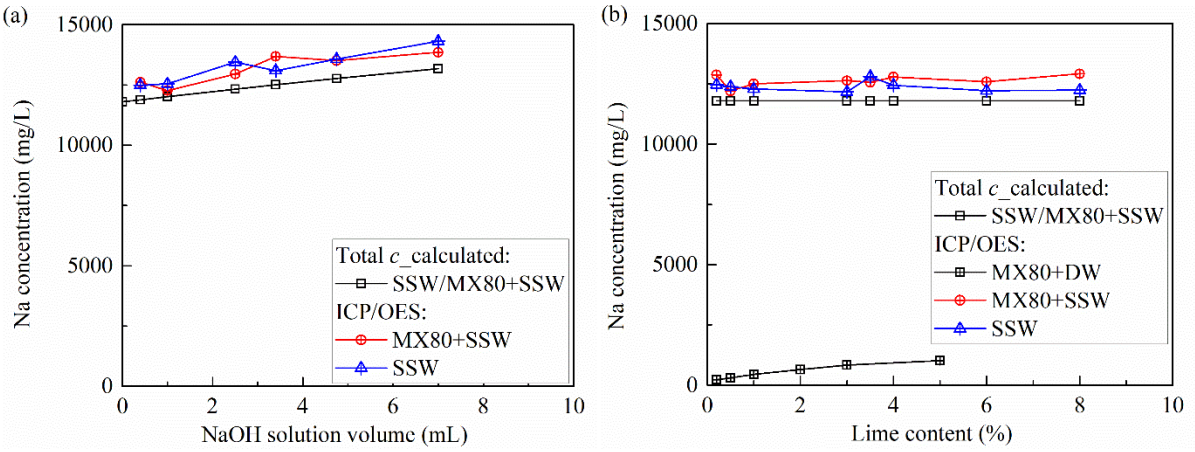

Fig. 8. Variations of Na concentration with increasing: (a) NaOH solution volume; (b) lime content

As shown in Table 3, the salts in synthetic seawater provided 1200 mg/L Mg species in the supernatants of MX80-SSW suspensions and blank synthetic seawater. The calculated Mg concentration decreased from 1200 mg/L to 1050 mg/L with titrating of 7 mL NaOH solution due to the dilution effect, while it was maintained constant with increasing lime content (Fig. 9). In contrast, the measured Mg concentration decreased gradually with the titration of NaOH solution or the increase of lime content. This was consistent with the results obtained by Renou et al. [38]. Hamidi et al. [25] stated that the precipitation of magnesium hydroxide ($Mg(OH)_2$) would occur at alkaline environment, reducing the Mg concentration, as follows:

$$Mg^{2+} + 2OH^- \rightleftharpoons Mg(OH)_2 \downarrow \quad (3)$$

Theoretically, 5 mL NaOH solution was required to eliminate Mg species originated from 50 mL synthetic seawater (Table 4). The theoretical volume of 5 mL NaOH solution was close to the titrated volume of 4.75 mL, which led the Mg concentration in the supernatants of MX80-

SSW and blank synthetic seawater to decrease to zero (Fig. 9a). In addition to the precipitation of $Mg(OH)_2$, the cation exchange would also reduce the Mg concentration in the supernatants of MX80-SSW suspensions. Thus, with the same titrated volume of NaOH solution, the Mg concentration in the supernatants of MX80-SSW suspensions was lower than that in the supernatants of blank synthetic seawater. As for the suspensions mixed with lime, the Mg species in the 100 mL synthetic seawater could consume 0.28 g CaO that corresponded to 2.8% lime content (by weight of 10 g of MX-80 bentonite) (Table 4). It was slightly lower than the lime content of 3.5% where the Mg concentrations in the supernatants of MX80-SSW suspensions and blank synthetic seawater were close to zero (Fig. 9b). This was because the OH^- ions were not only consumed by the Mg species, but also by the carbonation of Ca species, pozzolanic reaction and cation exchange in the MX80-SSW suspensions. In the supernatants of MX80-DW suspensions, there was no soluble Mg species being detected, indicating that the amount of dissolved Mg species from MX-80 bentonite was negligible (Fig. 9b).

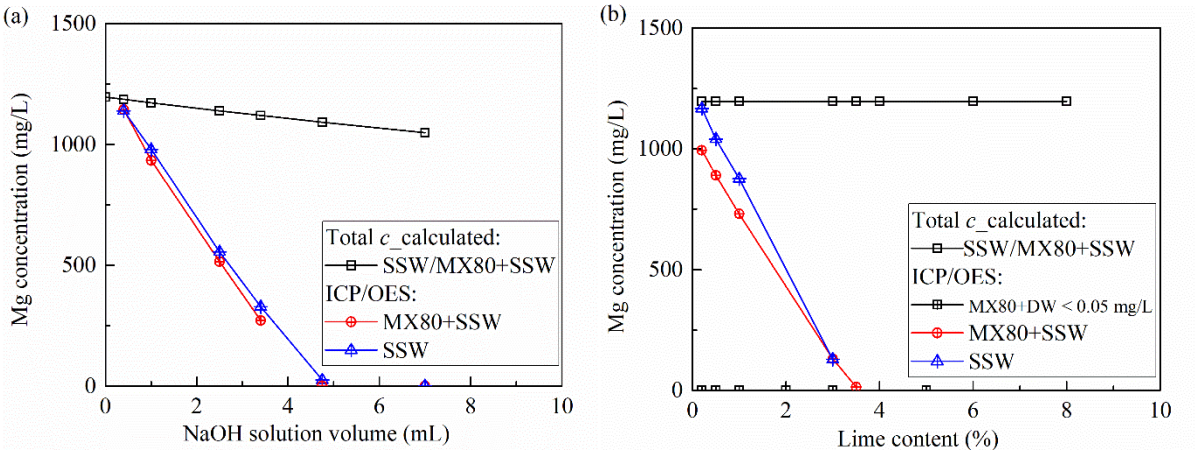

Fig. 9. Variations of Mg concentration with increasing: (a) NaOH solution volume; (b) lime content

Table 4. Consumption of NaOH solution and lime by reactions with Mg^{2+} ions

	NaOH titration test	Optimum lime content test
Volume of synthetic seawater (SSW) (mL)	50	100
Mg^{2+} ions from SSW (mol)	$\frac{1.2\ g/L}{24\ g/mol}\times 50\ ml = 0.0025\ mol$	$\frac{1.2\ g/L}{24\ g/mol}\times 100\ ml = 0.005\ mol$
Consumed OH^- ions (mol)	0.005	0.01
Consumed 1M NaOH (mL) or lime (%)	$\frac{0.005\ mol}{1\ mol/L} = 5\ ml\ NaOH$	$\frac{0.01\ mol}{2}\times 56\ g/mol = 0.28\ g\ CaO$ (2.8%)

According to the salt composition of synthetic seawater (Table 3), the total Ca concentration in the synthetic seawater was calculated, equal to 350 mg/L. This concentration decreased to 306 mg/L with the titration of NaOH solution to 7 mL (Fig. 10a), due to the dilution effect. The decrease of Ca concentration with titrating NaOH solution was not only observed in the supernatant of MX-80 bentonite suspensions but also in the supernatant of blank synthetic seawater. This indicated that the decrease of Ca concentration could be mainly attributed to the consumption of Ca by precipitation of calcium carbonate ($CaCO_3$) rather than the cation exchange of Ca^{2+} ions between MX-80 bentonite and solution. It can be inferred that even though the titration test was conducted under Argon atmosphere to prevent the carbonation, the Ca^{2+} and HCO_3^- ions in the synthetic seawater could react at alkaline environment as follows:

$$Ca^{2+} + OH^- + HCO_3^- \rightleftharpoons CaCO_3 \downarrow + H_2O \quad (4)$$

The concentration of HCO_3^- in 50 mL synthetic seawater was equal to 0.1 mmol that could consume 0.1 mmol Ca^{2+} and OH^- ions. Theoretically, the consumption of 0.1 mmol Ca species corresponded to the decrease of 70 mg/L Ca concentration. In fact, at the titration of 7 mL NaOH solution (Fig. 10a), the decrease of Ca concentrations in the supernatants of MX80-SSW suspensions and blank synthetic seawater were 84 mg/L and 88 mg/L which were close the calculated one (70 mg/L), suggesting that it was reasonable to ascribe the decrease of Ca concentration to the precipitation of $CaCO_3$. The higher decrease of measured Ca concentrations was probably due to the extra consumption of Ca^{2+} ions by cation exchange. With the titration of NaOH solution, a more significant decrease of Ca concentration from 365 mg/L to 222 mg/L in the supernatants of MX80-SSW suspensions was identified, suggesting that more Ca^{2+} ions were consumed by the cation exchange in the MX80-SSW suspensions as compared to the blank synthetic seawater.

When lime was mixed with water, the calcium hydroxide ($Ca(OH)_2$) was produced immediately, leading to an increase of pH and Ca concentration. As shown in Fig. 10b, with increasing lime content from 0.2% to 5%, the total calculated Ca concentration in the supernatants of MX80-DW suspensions increased from 140 mg/L to 3475 mg/L, while the measured Ca concentration increased slightly from 6 mg/L to 331 mg/L. This might be attributed to the solubility of $Ca(OH)_2$ with maximum value of 1800 mg/L and the consumption of Ca species through cation exchange, pozzolanic reaction, as well as the precipitation of $CaCO_3$ by adsorption of CO_2. Therefore, the measured Ca concentration in the supernatants of MX80-DW suspensions were significantly lower than the calculated Ca concentration supplied by lime (Fig. 10b).

In the case of MX80-SSW suspensions and blank synthetic seawater, the Ca species came not only from lime, but also from the salt in synthetic seawater. With increasing lime content from 0 to 8%, the total calculated Ca concentration increased from 350 mg/L to 5910 mg/L. The measured Ca concentrations were up to 2920 ~ 3240 mg/L which was significantly higher than the solubility of $Ca(OH)_2$ (1800 mg/L). This can be attributed to the OH^- release from $Ca(OH)_2$ which took part in the precipitations of $Mg(OH)_2$ and $CaCO_3$, promoting the dissolution of $Ca(OH)_2$ and thus releasing more Ca^{2+} ions in supernatants. In the case of blank synthetic seawater, the lower measured Ca concentration than the total calculated one can be attributed to the consumption of Ca^{2+} ions by carbonation with HCO_3^- in the synthetic seawater or CO_2 in the air on the one hand, and to the saturation of $Ca(OH)_2$ solution at higher lime content which could not dissociate more OH^- ions and Ca^{2+} ions on the other hand. At a given lime content, the measured Ca concentration in the supernatants of MX80-SSW suspensions was lower than that in the supernatants of blank synthetic seawater, due to the excess consumption of Ca species by cation exchange and pozzolanic reaction in MX80-SSW suspensions.

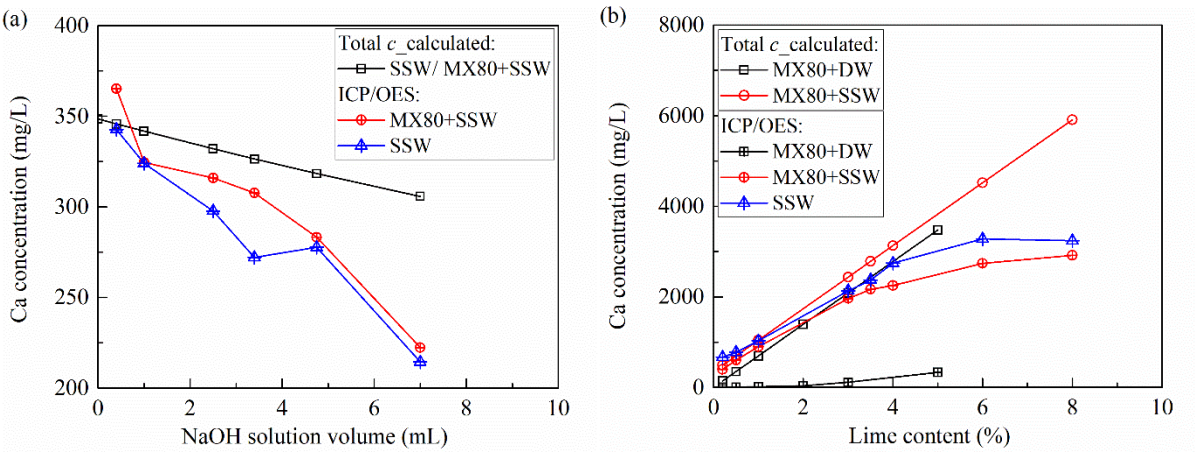

Fig. 10. Variations of Ca^{2+} concentration with increasing: (a) NaOH solution volume; (b) lime content

4. Discussions

4.1 Solubility and reactivity of MX-80 bentonite and silt

The MX-80 bentonite contains 92% smectite with a structural formula as $(Ca_{0.05}Mg_{0.02}K_{0.01}Na_{0.46})(Si_{7.94}Al_{0.06})(Al_{3.10}Ti_{0.01}Fe^{3+}_{0.37}Mg_{0.05})O_{20}(OH)_4$ [27]. This indicated that the detectable Si species in the supernatants of MX-80 bentonite suspensions can be attributed to the dissolution of MX-80 bentonite. Cherian et al. [13] and Duc et al. [20] indicated that the dissolved Si concentration increased with increasing pH. As shown in Figs. 2 and 6, the

pH at maximum Si concentration was up to 12. Regarding lime-treated soil, the high pH above 10 or 12 was indispensable to promote the dissolution of Si for pozzolanic reaction [4, 30]. It can be thus inferred that the decrease of Si concentration in the supernatants of MX80-DW suspensions with increasing lime content can be attributed to the consumption of Si by pozzolanic reaction, probably forming calcium silicate hydrates (C-S-H). Diamond and Kinter [17] reported that, in the bentonite-lime suspensions, as high as 3% lime can be absorbed on bentonite within 5 minutes, and then C-S-H can be formed over a very short period of several hours. Vitale et al. [43] performed X-ray diffraction and thermogravimetric analysis on lime-treated bentonite and evidenced that the new hydrated phase was produced at very short term (less than 1 day of curing). As compared to MX80-DW suspensions, relatively lower Si concentrations were obtained for the supernatants of MX80-SSW suspensions, which was inconsistent with the results obtained by Duc et al. [20]. They indicated that at alkaline environment, the higher the ionic strength of the solution, the higher the dissolved Si concentration. The lower Si concentration in the supernatants of MX80-SSW suspensions was probably due to the more significant pozzolanic reaction promoted by salts, consuming more Si species than in the MX80-DW suspensions. Indeed, Ramesh et al. [37] reported that the sodium salts in fly ash-lime mixtures could promote the formation of cementitious compounds. Baeyens and Bradbury [7] and Duc et al. [18, 19] stated that, in addition to the Si species, the Al and Fe can be also dissolved from MX-80 bentonite at alkaline environment. Indeed, a small amount of Fe (0.93 mg/L) and Al species (3.4 mg/L) were detected in the supernatant of MX80-DW suspension at 0.2% lime content. With increasing lime content, the soluble Al and Fe concentrations were too low to be detected by the ICP/OES apparatus.

The MX-80 bentonite had relatively higher calcium consumption and optimum lime contents than silt, which can be attributed to the different minerals in MX-80 bentonite and silt. The tested silt mainly consists of low reactivity of clay minerals (10.8% illite, 3.6% chlorite and 1.3% kaolinite) and inert phases of quartz (39%) and feldspars (9.5%), exhibiting a relatively lower specific surface area (24 m^2/g) and thus probably providing less opportunity for cation exchange and adsorption of OH^- ions by silt particles. Ying et al. [50] performed XRD tests on 2% lime-treated silt (the same silt as in this study) and found that the quantities of quartz, feldspar, illite, chlorite and kaolinite in the lime-treated silt at 150-day curing were rather similar to those of untreated soil, and no significant cementitious compounds were identified through XRD analysis. This indicates that the tested silt could not provide enough activated silica and alumina to interact with lime, limiting the consumption of Ca^{2+} and OH^- ions in the pozzolanic reaction.

In contrast, the MX-80 bentonite contains 92% smectite, which has higher specific surface area (562 m^2/g) and higher cation exchange capacity (78 to 85 meq/100 g). Al-Mukhtar et al. [4] reported that the smectite exhibited higher cation exchange capacity and softer structure (large and thin TOT layer) than illite and kaolinite, which made the smectite have higher reactivity with lime and thus faster and more lime consumption. Furthermore, Cherian and Arnepalli [12] indicated that the bentonite exhibited higher reactivity with lime due to its weaker van der Waals bonding and the availability of larger inter- and intra-layer spaces which can supply more reactive alumina and silica for pozzolanic reaction. Nevertheless, the kaolinite had lower lime reactivity due to its strong hydrogen bonding and deficiency of inter- and intra-layer spaces [12]. This suggested that, as compared to silt, the MX-80 bentonite required more lime to supply sufficient Ca species for cation exchange and pozzolanic reaction.

4.2 Salt effect on the pH variations

For improving soil with lime, the high pH environment was indispensable to enable the dissolution of silica and alumina from clay minerals in order to form cementitious compounds through pozzolanic reaction. However, for salted materials, the salts present in pore water would consume the hydroxide (OH^-), inhibiting the increase of pH (Figs. 2, 3 and 4). Lin and Lee [29] reported that the ion activity coefficient decreased with the increase of ionic strength. Thus, the maximum pH in the silt/MX80 suspensions and pH of buffer solutions decreased with the increase of salt concentration (Fig. 2). The pH of silt/MX80 suspensions kept the maximum values with further increasing lime content from the optimum one, due to the saturation of $Ca(OH)_2$ in solutions on the one hand [12], and to the balanced adsorption of OH^- ions at the positive sites of clay minerals or desorption of H^+ ions by de-protonation of surface hydroxyl groups at high pH on the other hand [1].

It appears from Figs. 4 and 5 that the pH variation in the synthetic seawater was quite different from that in deionised water with increasing lime content or titrating NaOH solution. In the deionised water, the OH^- ions originated from $Ca(OH)_2$ or from NaOH solution caused a rapid increase of pH. Then, the pH increased gradually until it reached the maximum value. However, for the synthetic seawater, the pH decreased slightly with the titration of NaOH solution from 0.2 mL to 1 mL, indicating that the consumption of OH^- ions exceeded its supply from NaOH solution. The consumption of OH^- ions can be mainly attributed to the precipitation of $Mg(OH)_2$ (Fig. 9a), and partially to the carbonation of $CaCO_3$ (Fig. 10a). With further titration of NaOH to 4.5 mL, the pH in the synthetic seawater increased slightly, also due to the consumption of

OH^- ions. As observed in Figs. 9a and 10a, the measured Mg and Ca concentrations indeed decreased significantly with titration of NaOH solution to 4.5 mL. Upon further titration, the pH in the synthetic seawater increased much significantly with less consumption of OH^- ions by Mg and Ca species. The same trend of pH variations was obtained for the synthetic seawater with increasing lime content (Fig. 4), as well as for the silt and bentonite suspensions prepared by synthetic seawater (Figs. 4 and 5). In general, due to the consumption of OH^- ions by the precipitations of $Mg(OH)_2$ and $CaCO_3$, higher lime contents (optimum lime content) were required to increase the pH of silt/MX80-SSW suspensions to the maximum value (Fig. 2).

As observed in Fig. 4a, when the lime content was in the range of 0.2% ~ 5%, the pH of MX80+DW suspensions was lower than that of blank deionised water, which can be attributed to the consumption of OH^- ions by MX-80 bentonite. This was confirmed by the decrease of Si concentration (Fig. 6) and the significant difference between the measured and total calculated Ca concentration in the supernatants of MX80-DW suspensions (Fig. 10b), where the soluble Si species reacted with Ca^{2+} and OH^- species, leading to a lower pH of MX80-DW suspensions as compared to blank deionised water. Besides, the adsorption of OH^- ions and dissolution of clay minerals could also consume OH^- ions [18], resulting in a lower pH of MX80-DW suspensions. Similarly, due to the consumption of OH^- ions by MX-80 bentonite, at the same titrated volume of NaOH solution, the pH of MX80-DW suspensions was lower than that of blank deionised water (Fig. 5a).

The pH curves were significantly different for the MX80-SSW suspensions and the blank synthetic seawater (Fig. 4a and 5a): at lime contents of 0 ~ 1.5% and 3% ~ 7% or with NaOH solution smaller than 2.5 mL, a lower pH of MX80-SSW suspensions was obtained, whereas the pH of MX80-SSW suspensions was higher than that of blank synthetic seawater with the titration of NaOH solution from 2.5 mL to 6 mL. As mentioned previously, the precipitations of $Mg(OH)_2$ and $CaCO_3$ could occur in both MX80-SSW suspensions and blank synthetic seawater. However, in the MX80-SSW suspensions, the Ca^{2+} cations can be adsorbed on the clay minerals by cation exchange process by replacing the monovalent cations (i.e., Na+, K+, etc.) previously held by the clay, lowering down the production of $Mg(OH)_2$ and $CaCO_3$ and thus leading to a less consumption of OH^- ions by precipitations. Conversely, the adsorption of OH^- ions on the surface of clay, the dissolution of clay minerals and the pozzolanic reaction could consume more OH^- ions in the MX80-SSW suspensions. It can be thus inferred that the lower pH of MX80-SSW suspensions at lime content of 0 ~ 1.5% or with titrated NaOH solution

volume lower than 2.5 mL could be attributed to the more consumption of OH^- ions by MX-80 bentonite, assuming that the consumption of OH^- ions by precipitation were similar in MX80-SSW suspensions and blank synthetic seawater in this range of lime content and NaOH solution volume. When the lime content was higher than 3%, the difference of Ca concentrations between the supernatants of MX80-SSW suspensions and blank synthetic seawater became larger (Fig. 10b). This suggested that more Ca species were consumed in the MX80-SSW suspensions by pozzolanic reaction which could also consume some OH^- ions simultaneously. The consumption of OH^- ions by pozzolanic reaction prevailed facing the consumption of OH^- ions by precipitations as some Mg and Ca species were adsorbed on clay surface, leading to a lower pH in the MX80-SSW suspensions as compared to blank synthetic seawater. In the NaOH titration test, the pozzolanic reaction between 0.5 g MX-80 bentonite and Ca^{2+} ions from synthetic seawater seemed to be insignificant because of the small amount of MX-80 bentonite inside. Nevertheless, some Mg and Ca ions species adsorbed on clay surface after cation exchange process, leading to less precipitation of $Mg(OH)_2$ and $CaCO_3$ and thus less consumption of OH^- ions in the MX-80 bentonite suspensions as compared to synthetic seawater. Thus, the MX80-SSW suspensions had higher pH with titrating NaOH solution from 2.5 mL to 6 mL.

Cherian and Arnepalli [12] indicated that the optimum lime content determined by Eades and Grim test was just the minimum lime content to produce a soil-lime-water pH of 12.4, without consideration of the availability of free Ca species to take part in the pozzolanic reaction. Indeed, as shown in Fig. 10b, the Ca concentration in the supernatant of MX80-DW suspension at 2% lime content where the pH reached 12.4, was only 37 mg/L. The soluble Si concentration in the supernatant at 2% lime content was equal to 13.3 mg/L which was lower than that of supernatants with lime content lower than 2%, suggesting that some Ca species could react with Si species at 2% lime content even though the Ca concentration was at a low level. In this study, the optimum lime content was designated as the threshold lime content which could increase the pH to the maximum value. At optimum lime contents of 5% for MX80-DW suspensions and 7% for MX80-SSW suspensions, the Ca concentrations were estimated at 330 mg/L and 3000 mg/L, respectively. The dissolved Si concentrations at optimum lime contents were close to zero. This suggested that the amount of Ca species at optimum lime content seemed to be sufficient to participate in pozzolanic reaction, allowing the soil to obtain the maximum mechanical performance, especially for saline soil which had higher Ca concentration at optimum lime content.

4.3 Salt and lime effects on the suspension states

As shown in Fig. 1, the MX-80 bentonite suspensions were gel-like, which can be attributed to the high fraction of smectite. The smectite consists of three-layer mineral with 2:1 structural unit constituted by one octahedral aluminium sheet sandwiched between two tetrahedral siliceous sheets with isomorphic substitutions [34]. During hydration, the inter-basal spacing of smectite is known to increase from 9.6 Å (0.96 nm) to infinite due to the successive adsorption of water molecule layers. In this case, the diffuse double layer was well-developed and the double-layer repulsive force was the dominant force [52]. Vitale et al. [45] indicated that the addition of lime to bentonite suspension induced a decrease of the absolute zata potential and a reduction of double layer repulsive force, which promoted the association of soil particles with each other. As a result, the diffuse double layer of bentonite was depressed with the addition of lime. As the diffuse double-layer water was expelled out, the MX-80 bentonite suspensions at 2% lime content became more liquid. In fact, the synthetic seawater played the same role as lime in influencing the interparticle force and thus the compression of diffuse double layer. As the synthetic seawater concentration of 35g/L was higher than the salt concentration provided by 2% lime, the diffuse double layer repulsive force decreased more significantly and more diffuse double-layer water was expelled out. Thus, the MX80 bentonite suspension prepared with synthetic seawater was the most liquid one as compared to that prepared with deionised water and that with 2% lime. The lime and synthetic seawater effects on the silt suspension states was negligible, because of the low clay fraction and the less active clay minerals (10.8% illite, 3.6% chlorite and 1.3% kaolinite) which limited the salinity effect on the diffuse double layer.

5. Conclusions

In this study, the salt solution effect on the pH and optimum lime content was investigated for the MX-80 bentonite and a silty soil. The continuous base (NaOH solution) titration test was also performed on the MX-80 bentonite and silt suspensions, for the purpose of comparison. The major species in the supernatants were quantified by the ICP/OES analysis. The obtained results allow the following conclusions to be drawn:

(1) The MX-80 bentonite exhibited a gel-like structure in deionised water. Due to the shrinkage of diffuse double layer induced by lime, the MX80-DW suspension prepared with 2% lime became more fluid. The synthetic seawater had more significant effect on the diffuse double

layer, leading to the most fluid state of MX80-SSW suspension. The effect of lime and salt solution on the silt suspension state was insignificant due to the low clay fraction in tested silt.

(2) As the pH of soil-lime-salt solution was lower than 12.4, the optimum lime content was defined as the threshold value of lime content at the maximum pH. At the optimum lime content, the corresponding amount of Ca species seemed to be sufficient for the cation exchange and pozzolanic reaction, especially in the case of suspensions prepared with salt solution (saline soil).

(3) The pH variation in synthetic seawater was quite different from that of deionised water with increasing lime content or titrating NaOH solution. At a given lime content (lower than optimum) or NaOH solution volume, the pH decreased with increasing salt concentration, due to the consumption of OH^- ions by the reactions with Mg^{2+} and Ca^{2+} ions in synthetic seawater. The precipitation of $Mg(OH)_2$ and $CaCO_3$ inhibited the increase of pH with the addition of lime or NaOH solution. The pH of silt/bentonite suspensions followed the same trends as those of blank synthetic seawater and deionize water. Due to the consumption of OH^- by the reactions with Mg^{2+} and Ca^{2+} ions, the optimum lime content of both silt and MX-80 bentonite increased with the increase of salt concentration.

(4) The optimum lime content of MX-80 bentonite was higher than that of silt and the difference between the pH curves of MX-80 suspensions and blank solutions was more significant than that of silt suspensions. This can be attributed to the higher cation exchange capacity and and higher bentonite solubility of MX-80 bentonite compared to silt. In the case of MX-80 bentonite, more lime was required to supply sufficient Ca species for cation exchange and pozzolanic reaction.

(5) Within a certain range of lime content or NaOH solution volume, the pH of the silt/bentonite suspensions was lower than that of blank solutions, which can be attributed to the consumption of OH^- ions by material through the adsorption of OH^- ions, dissolution of clay minerals and pozzolanic reaction. However, one exception was made for the MX80-SSW suspensions with the pH higher than that of blank synthetic seawater, in case of titration of NaOH solution from 2.5 mL to 6 mL. In the MX80-SSW-NaOH suspensions, the pozzolanic reaction was insignificant, while the adsorption of Mg^{2+} and Ca^{2+} ions on the clay surface led to a lower production of $Mg(OH)_2$ and $CaCO_3$ and thus less consumption of OH^- ions, resulting in a higher

pH of MX-80 suspensions as compared to that of blank synthetic seawater.

Author statement

Zi Ying: Validation, Investigation, Methodology, Writing - original draft. **Yu-Jun Cui:** Conceptualization, Methodology, Writing - review & editing. **Myriam Duc:** Investigation, Methodology, Resources. **Nadia Benahmed:** Investigation, Resources.

Declaration of competing interest

The authors declare that they have no known competing financial interests or personal relationships that could have appeared to influence the work reported in this paper.

Acknowledgements

The financial supports from China Scholarship Council (CSC), Ecole des Ponts ParisTech (ENPC) and INRAE are greatly acknowledged. The authors are also grateful to Denis Courtier-Murias and Nadège Caubrière for their discussion about the ICP/OES analysis.

References

1. Alkan M, Demirbaş Ö, Doğan M (2005) Electrokinetic properties of kaolinite in mono-and multivalent electrolyte solutions. Microporous Mesoporous Mater 83 (1-3): 51-59. https://doi.org/10.1016/j.micromeso.2005.03.011
2. Al-Mukhtar M, Lasledj A, Alcover JF (2010a) Behaviour and mineralogy changes in lime-treated expansive soil at 20°C. Appl Clay Sci 50 (2): 191-198. https://doi.org/10.1016/j.clay.2010.07.023
3. Al-Mukhtar M, Lasledj A, Alcover JF (2010b). Behaviour and mineralogy changes in lime-treated expansive soil at 50°C. Appl Clay Sci 50(2): 199-203. https://doi.org/10.1016/j.clay.2010.07.022
4. Al-Mukhtar M, Lasledj A, Alcover JF (2014) Lime consumption of different clayey soils. Appl Clay Sci 95: 133-145. https://doi.org/10.1016/j.clay.2014.03.024
5. Al-Swaidani A, Hammoud I, Meziab A (2016) Effect of adding natural pozzolana on geotechnical properties of lime-stabilized clayey soil. J Rock Mech Geotech Eng 8(5): 714-725. https://doi.org/10.1016/j.jrmge.2016.04.002
6. ASTM D6276-19 (2019) Standard Test Method for Using pH to Estimate the Soil-Lime Proportion Requirement for Soil Stabilization. ASTM International, West Conshohocken, PA.

7. Baeyens B, Bradbury MH (1997) A mechanistic description of Ni and Zn sorption on Na-montmorillonite Part I: Titration and sorption measurements. J Contam Hydrol 27(3-4): 199-222. https://doi.org/10.1016/S0169-7722(97)00008-9

8. Bell FG (1989) Lime stabilisation of clay soils. Bull. Int Assoc Eng Geol 39(1): 67-74. https://doi.org/10.1007/BF02592537

9. Bell FG (1996) Lime stabilization of clay minerals and soils. Eng Geol 42 (4): 223-237. https://doi.org/10.1016/0013-7952(96)00028-2

10. Celauro B, Bevilacqua A, Bosco DL, Celauro C (2012) Design procedures for soil-lime stabilization for road and railway embankments. Part 2-experimental validation. Procedia Soc Behav Sci 53: 568-579. https://doi.org/10.1016/j.sbspro.2012.09.907

11. Chemeda YC, Deneele D, Ouvrard G (2018) Short-term lime solution-kaolinite interfacial chemistry and its effect on long-term pozzolanic activity. Appl Clay Sci 161: 419-426. https://doi.org/10.1016/j.clay.2018.05.005

12. Cherian C, Arnepalli DN (2015) A critical appraisal of the role of clay mineralogy in lime stabilization. Int J Geosynth Ground Eng 1:8. https://doi.org/10.1007/s40891-015-0009-3

13. Cherian C, Kollannur NJ, Bandipally S, Arnepalli DN (2018) Calcium adsorption on clays: Effects of mineralogy, pore fluid chemistry and temperature. Appl Clay Sci 160: 282-289. https://doi.org/10.1016/j.clay.2018.02.034

14. Ciancio D, Beckett CTS, Carraro JAH (2014) Optimum lime content identification for lime-stabilised rammed earth. Constr Build Mater 53: 59-65. https://doi.org/10.1016/j.conbuildmat.2013.11.077

15. Deneele D, Le B, Cui YJ, Cuisinier O, Ferber V (2016) Experimental assessment regarding leaching of lime-treated silt. Constr Build Mater 112: 1032-1040. https://doi.org/10.1016/j.conbuildmat.2016.03.015

16. Di Sante M, Fratalocchi E, Mazzieri F, Pasqualini E (2014) Time of reactions in a lime treated clayey soil and influence of curing conditions on its microstructure and behaviour. Appl Clay Sci 99: 100-109. https://doi.org/10.1016/j.clay.2014.06.018

17. Diamond S, Kinter EB (1965) Mechanisms of soil-lime stabilization. Highway Res Rec 92: 83-102.

18. Duc M, Gaboriaud F, Thomas F (2005a) Sensitivity of the acid-base properties of clays to the methods of preparation and measurement: 1. Literature review. J Colloid Interface Sci 289(1): 139-147. https://doi.org/10.1016/j.jcis.2005.03.060

19. Duc M, Gaboriaud F, Thomas F (2005b) Sensitivity of the acid–base properties of clays to the methods of preparation and measurement: 2. Evidence from continuous potentiometric titrations. J Colloid Interface Sci 289(1): 148-156. https://doi.org/10.1016/j.jcis.2005.03.057

20. Duc M, Thomas F, Gaboriaud F (2006) Coupled chemical processes at clay/electrolyte interface: a batch titration study of Na-montmorillonites. J Colloid Interface Sci 300(2): 616-625. https://doi.org/10.1016/j.jcis.2006.04.081

21. Eades JL, Grim RE (1966) A quick test to determine lime requirements for lime stabilization. Highway Res Rec 139: 61-72.

22. Emarah DA, Seleem SA (2018) Swelling soils treatment using lime and sea water for roads construction. Alexandria Eng J 57(4): 2357-2365. https://doi.org/10.1016/j.aej.2017.08.009

23. French standard AFNOR NF P 18-513 (2012) Pozzolanic addition for concrete-Metakaolin-Definitions, Specifications and Conformity Criteria. Association Francaise de Normalisation.

24. French standard AFNOR NF P 18-837 (1993) Standard for special products for hydraulic concrete construction-Hydraulic binder based needling and/or sealing products-Testing of resistance against seawater and/or water with high sulphate contents. Association Francaise de Normalisation.

25. Hamidi R, Kahforoushan D, Fatehifar E, Arehjani M, Farmanbordar S (2011) Simultaneous removal of Ca and Mg Salts using chemical precipitation with lime. The 7th International Chemical Engineering Congress & Exhibition. Kish, Iran, 21-24 November, 2011.

26. Hilt GH, Davidson DT (1960) Lime fixation in clayey soils. Highway Res Board Bul. 262: 20-32.

27. Karnland O (2010) Chemical and mineralogical characterization of the bentonite buffer for the acceptance control procedure in a KBS-3 repository. Technical report, SKB-TR-10-60. Sweden.

28. Kavak A, Akyarlı A (2007) A field application for lime stabilization. Environ Geol 51(6): 987-997. https://doi.org/10.1007/s00254-006-0368-0

29. Lin CL, Lee LS (2003) A two-ionic-parameter approach for ion activity coefficients of aqueous electrolyte solutions. Fluid Phase Equilib 205(1): 69-88. https://doi.org/10.1016/S0378-3812(02)00275-3

30. Little DN (1999) Evaluation of Structural Properties of Lime Stabilized Soils and Aggregates. Prepared for the National Lime Association: Arlington, Virginia, USA.

31. Liu XF, de Carteret R, Buzzi OP, Fityus SG (2016) Microstructural effects of environmental salinity on unbound granular road pavement material upon drying. Acta Geotechnica 11(2): 445-451. https://doi.org/10.1007/s11440-015-0393-9

32. Locat J, Bérubé MA, Choquette M (1990) Laboratory investigations on the lime stabilization of sensitive clays: shear strength development. Can Geotech J 27(3): 294-304. https://doi.org/10.1139/t90-040

33. Madsen FT (1998) Clay mineralogical investigations related to nuclear waste disposal. Clay Miner. 33(1): 109-129. https://doi.org/10.1180/000985598545318

34. Mitchell JK, Soga K (2005) Fundamentals of soil behaviour. 3rd edn. John Wiley &Sonc, Inc.

35. Moayed RZ, Izadi E, Heidari S (2012) Stabilization of saline silty sand using lime and micro silica. Journal of Central South University. 19 (10): 3006-3011. https://doi.org/10.1007/s11771-012-1370-1

36. Negawo WJ, Di Emidio G, Bezuijen A, Verastegui Flores RD, François B (2019) Lime-stabilisation of high plasticity swelling clay from Ethiopia. Eur J Environ Civ Eng 23(4): 504-514. https://doi.org/10.1080/19648189.2017.1304272

37. Ramesh HN, Mohan MS, Sivapullaiah PV (1999) Improvement of strength of fly ash with lime and sodium salts. Gr Improv 3: 163-167. https://doi.org/10.1680/gi.1999.030403

38. Renou S, Poulain S, Givaudan JG, Moulin P (2008) Treatment process adapted to stabilized leachates: Lime precipitation-prefiltration-reverse osmosis. J Membr Sci 313(1-2): 9-22. https://doi.org/10.1016/j.memsci.2007.11.023

39. Saride S, Puppala AJ, Chikyala SR (2013) Swell-shrink and strength behaviors of lime and cement stabilized expansive organic clays. Appl Clay Sci 85: 39-45. https://doi.org/10.1016/j.clay.2013.09.008

40. Sharma NK, Swain SK, Sahoo UC (2012) Stabilization of a clayey soil with fly ash and lime: a micro level investigation. Geotech Geol Eng 30(5): 1197-1205. https://doi.org/10.1007/s10706-012-9532-3

41. Tang AM, Cui YJ, Le TT (2008) A study on the thermal conductivity of compacted bentonites. Appl Clay Sci 41(3-4): 181-189. https://doi.org/10.1016/j.clay.2007.11.001

42. Tang AM, Vu MN, Cui YJ (2011) Effects of the maximum soil aggregates size and cyclic wetting-drying on the stiffness of a lime-treated clayey soil. Géotechnique 61: 421-429. https://doi.org/10.1680/geot.SIP11.005

43. Vitale E, Deneele D, Russo G (2016) Multiscale analysis on the behaviour of a lime treated bentonite. Procedia Engineering 158: 87-91. https://doi.org/10.1016/j.proeng.2016.08.410

44. Vitale E, Deneele D, Paris M, Russo G (2017) Multi-scale analysis and time evolution of pozzolanic activity of lime treated clays. Appl Clay Sci 141: 36-45. https://doi.org/10.1016/j.clay.2017.02.013

45. Vitale E, Deneele D, Russo G (2020) Microstructural investigations on plasticity of lime-treated soils. Minerals 10(5): 386. https://doi.org/10.3390/min10050386

46. Wang Q, Cui YJ, Tang AM, Delage P, Gatmiri B, Ye WM (2014) Long-term effect of water chemistry on the swelling pressure of a bentonite-based material. Appl Clay Sci 87: 157-162. https://doi.org/10.1016/j.clay.2013.10.025

47. Wang YJ (2016) Investigation the thermo-hydro-mechanical properties of lime-treated fine-grained soils. PhD Dissertation, Ecole Nationale des Ponts et Chaussées, France.

48. Wang YJ, Cui YJ, Tang AM, Benahmed N, Duc M (2017a) Effects of aggregate size on the compressibility and air permeability of lime-treated fine-grained soil. Eng Geol 228: 167-172. https://doi.org/10.1016/j.enggeo.2017.08.005

49. Wang YJ. Duc M, Cui YJ, Tang AM, Benahmed N, Sun WJ, Ye WM (2017b). Aggregate size effect on the development of cementitious compounds in a lime-treated soil during curing. Appl Clay Sci 136: 58-66. https://doi.org/10.1016/j.clay.2016.11.003

50. Ying Z, Cui YJ, Benahmed N, Duc M (2020) Changes in mineralogy and microstructure of a lime-treated silty soil during curing time. 4th European Conference on Unsaturated soils. Lisbon. 2020. https://doi.org/10.1051/e3sconf/202019503044

51. Ying Z, Cui YJ, Benahmed N, Duc M (2021) Changes of microstructure and water retention property of a lime-treated saline soil during curing. Acta Geotech https://doi.org/10.1007/s11440-021-01218-5

52. Ying Z, Cui YJ, Duc M, Benahmed N, Bessaies-Bey H, Chen B (2021) Salinity effect on the liquid limit of soils. Acta Geotech 16: 1101-1111. https://doi.org/10.1007/s11440-020-01092-7

53. Ying Z, Duc M, Cui YJ, Benahmed N (2021) Salinity assessment for salted soil considering both dissolved and precipitated salts. Geotech Test J 44(1): 130-147. https://doi.org/10.1520/GTJ20190301

54. Zeng ZX, Cui YJ, Zhang F, Conil N, Talandier J (2019). Investigation of swelling pressure of bentonite/claystone mixture in the full range of bentonite fraction. Appl Clay Sci 178: 105137. https://doi.org/10.1016/j.clay.2019.105137

55. Zhang XW, Mavroulidou M, Gunn MJ (2017) A study of the water retention curve of lime-treated London Clay. Acta Geotech 12(1): 23-45. https://doi.org/10.1007/s11440-015-0432-6

Chapter 5. Mineralogy, microstructure and water retention property of lime-treated saline soils

Introduction

When the soil, lime and water were mixed together, the cation exchanges were expected to take place rapidly, leading to the flocculation of soil particles and the formation of coarser aggregates (Locat et al., 1990; Bell, 1996; Cuisinier et al., 2011a; Wang et al., 2016). During curing, the silicon ions (Si^{4+}) and aluminium ions (Al^{3+}) ions dissolved from clay minerals, quartz, and feldspar, reacted with Ca^{2+} ions from lime, producing calcium silicate hydrate (C-S-H), calcium aluminate hydrate (C-A-H) and calcium aluminium silicate hydrate (C-A-S-H) (Bell, 1996; Guney et al., 2007; Al-Mukhtar et al., 2010a, 2010b; Lemaire et al., 2013; Di Sante et al., 2014; Vitale et al., 2017). The cementitious compounds coated the surface of aggregates and filled the pores gradually, leading to a decrease of the modal sizes of lime-treated soils (Gueny et al., 2007; Tedesco and Russo, 2008; Wang et al., 2017a, 2017b). Due to the modification of soil microstructure by the production of cementitious compounds, the water retention property of lime-treated soils increased during curing, as more water could be retained in the inner pores (Cecconi and Russo, 2008; Khattab and Al-Taie, 2006; Tedesco and Russo, 2008; Wang et al., 2015). The above-mentioned studies mainly involved the mineralogy, microstructure and water retention property of lime-treated saltless soils. To date, no study has paid attention to lime-treated saline soils.

This chapter in three parts, aims at investigating the effects of curing time, salinity and maximum soil aggregate size on the mineralogy, microstructure and water retention property of lime-treated saline soils. In the first part, the evolutions of mineralogy and microstructure of lime-treated specimens were studied, and the results were presented in a conference paper. The second part dealt with the aggregate size effect on the microstructure and water retention property of lime-treated soil during curing. The relevant results were presented in a paper published in “Acta Geotechnica”. The third part investigated the the salinity effect on the water retention property (total and matric suctions) during curing and the changes of microstructure along water retention curve (during drying) for lime-treated soils. This constituted a paper published in “Construction and Building Materials”. The articles are presented here in their original versions.

Ying, Z., Cui, Y.J., Benahmed, N., Duc, M. 2020. 4th European Conference on Unsaturated soils. Lisbon.

Changes in mineralogy and microstructure of a lime-treated silty soil during curing time

Zi Ying[1], Yu-Jun Cui[1], Nadia Benahmed[2], Myriam Duc[3]

Abstract: Lime treatment is widely applied to improve the workability and long-term durability of soils. In this study, the curing time effect on the mineralogy and microstructure of lime-treated soil was investigated. The soil samples were prepared with 2% lime and statically compacted at dry (w = 17%) and wet (w = 20%) sides of optimum. X-ray diffraction (XRD) and mercury intrusion porosimetry (MIP) were performed on lime-treated soil at various curing times. The presence of XRD peaks attributed to portlandite even after 150 days curing time indicated that it was not totally converted in cementitious compounds after reaction with silica and alumina from clay minerals. By contrast, no obvious XRD reflections of well-crystallized cementitious compounds were identified. Furthermore, all samples compacted at dry and wet side of optimum exhibited bi-modal pore size distribution, with a decrease of macro-pore frequency with increasing water content. The microstructure changes with increasing curing time did not follow monotonic tendency. On the whole, the quantities of pores less than 0.006 μm and micro-pores increased and the quantity of macro-pores decreased with increasing curing time due to the possible creation of poorly crystallized or amorphous cementitious compounds.

Keywords: lime-treated soil, mineralogy, microstructure; curing time

1. Introduction

Lime stabilization is a widespread technique applied in recent years to soils with poor physical and mechanical characteristics. Lime can significantly improve soil hydro-mechanical behaviour owing to series of physical-chemical reactions, including lime hydration, cation exchange and pozzolanic reaction [1-3]. The cementitious compounds produced in pozzolanic reaction play a major role in improving soil hydro-mechanical behaviour [3-4].

The production of cementitious compounds is strongly dependent on curing time and mineral

[1]: Ecole des Ponts ParisTech, Laboratoire Navier/CERMES, 6 – 8 av. Blaise Pascal, Cité Descartes, Champs-sur-Marne, 77455 Marne-la-Vallée cedex 2, France
[2]: INRAE, Aix Marseille Univ, Unité de Recherche RECOVER, 3275 route Cézanne, CS 40061, 13182 Aix-en-Provence, France
[3]: Université Gustave Eiffel, IFSTTAR/GERS/SRO, 14-20 boulevard Newton, Champs-sur-Marne, 77447 Marne-la-Vallée, France

composition of soils. For the lime-treated Impersol soil which contained 86% clay minerals (48% bentonite and 38% kaolinite), the products from pozzolanic reaction were observed in the form of calcium aluminate hydrate (C-A-H) after 1 day and in the form of calcium silicate hydrate (C-S-H) after 7 days of curing [5]. The C-S-H phase was detected for lime-treated silty soil with 27% clay-size fraction after 1 year curing [6]. Finally, the formation of C-S-H was identified for lime-treated quartz SiO_2 [1]. Indeed, the cementitious compounds were not only produced from the reactions of lime and alumino-silicate such as clay minerals but also from the reactions of lime and silicate such as fine quartz (or feldspars). The presence of a low amount of amorphous silica mixed with quartz and characterized by higher dissolution ability than well crystallized quartz may explain such result. Note that the carbonation of lime hydration products were usually put aside considering that the soil was under compacted form prevented in major case from air contact.

Microstructure changes of lime-treated soil were also analysed in several studies. Lemaire et al.[7] reported that for lime-treated silty soil, the cementitious compounds produced by the pozzolanic reaction were distributed continuously around the agglomerates which were constituted by clay and large-sized quartz particles. They pointed out that the pores within these agglomerates were identified as micro-pores and the pores between agglomerates were regarded as macro-pores. Lime addition caused the creation of smaller pores due to the formation of cementitious compounds [6-9]. Indeed, the cementitious compounds gradually coated the surface of soil aggregates and bonded the soil particles together, leading to a reduction of the modal sizes and the frequencies of micro-pores and macro-pores. As these cementitious compounds filled the pores and blocked some entrances of micro-pores, the total intrusion value decreased with curing time [6, 10-11].

The above studies highlighted the mineralogy and microstructure evolutions of lime-treated soil with curing time. However, few studies have been focused on lime-treated silty soil with low amount of clay. In this study, the changes of mineralogy and microstructure of lime-treated silty soil during curing time were analysed. Two groups of samples were prepared at dry and wet sides of optimum. X-ray diffraction (XRD) and mercury intrusion porosimetry (MIP) were carried out to investigate the mineral composition and the pore size distribution of lime-treated soil.

2. Materials and methods

The tested soil was taken from Salin-de-Giraud, a traditional salt exploitation site in France. Its geotechnical properties are reported in Table 1. The natural soil was air-dried, gently ground and passed through the 0.4 mm sieve. The grain size and aggregate size distribution of natural soil and dry sieved soil powder are presented in Fig. 1. The natural soil was composed of 63% silt particles (0.002 ~ 0.075 mm) while the dry soil powder mainly consisted of 62% sand particles (0.075 ~ 2 mm). The soil salinity, defined as the mass ratio of salt to dry soil, was 2.1‰ (g of salt/ kg of dry soil).

Table 1. Geotechnical properties of the tested soil

Property	Value
Specific gravity, G_s	2.71
Liquid limit, w_L (%)	29
Plastic limit, w_p (%)	19
Plasticity Index, I_p	10
VBS (g/100g)	0.98
Specif. surf. Area, SSA(m^2/g)	24.0

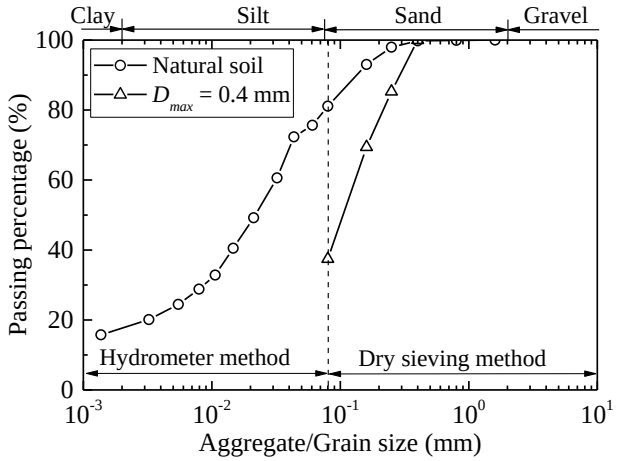

Fig. 1. Aggregate/Grain size distribution of dry sieved soil (D_{max} = 0.4 mm) and natural soil.

Dry soil powder and 2% quicklime (by weight of dry soil) were mixed thoroughly. Then, the soil-lime mixture was humidified by spraying deionized water to reach different target water contents. After mellowing for 1 h, static compaction was performed to prepare samples at the target dry density. Both dry (w = 17%) and wet sides (w = 20%) of optimum water content with

the same dry density (ρ_d = 1.63 Mg/m^3) were considered, according to the normal proctor compaction curve of 2% lime-treated soil presented in Fig. 2. After compaction, the samples were wrapped and cured at different times. At a given curing time, the samples were freeze-dried following the procedure proposed by Delage and Pellerin [12].

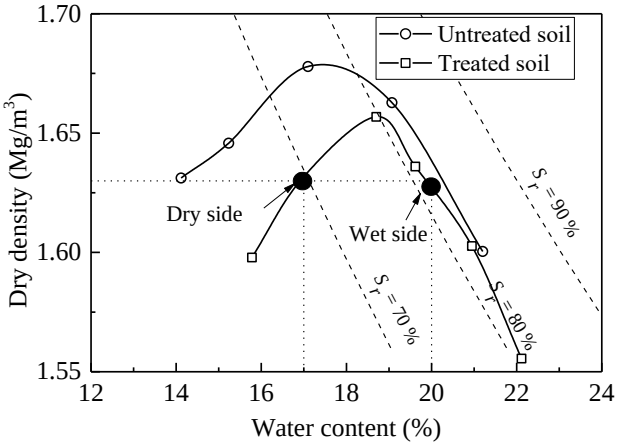

Fig. 2. Normal proctor curve of untreated and 2% lime-treated soil.

X-ray diffraction (XRD) analysis was performed on both untreated and lime-treated soil for mineralogy investigation. The freeze-dried samples were first crushed to pass entirely through 80 μm sieve prior to XRD analysis. Samples were loaded into XRD sample holder by sprinkling the powder through a 200 μm sieve. Then, the superfluous soil was removed by cutting the surface with a thin razor blade that prevented the particles from preferential orientation. XRD patterns were collected with a D8 Advance diffractometer (from Bruker) equipped with Cobalt anode, no momochromator, and a lynx eye rapid detector (acquisition during 1s per 0.01° 2theta). Minerals were identified with EVA software coupled with ICDDPdf2 database and the quantification was established with TOPAS software.

Autopore IV 9500 mercury intrusion porosimeter (from Micromeritics) was used to investigate the microstructure of lime-treated soil. The applied pressure ranged from 3.6 kPa to 230 MPa, and the corresponding intruded diameter varied from 0.006 μm to 350 μm. According to the MIP results, the delimiting diameter between micro-pores and macro-pores can be determined following the method proposed by Zhang et al. [13]. This method based on the water retention curve deduced from MIP results and the soil suction considering the higher sensitivity of micro-pores than macro-pores as water content changed.

3. Results

3.1. Mineralogical analysis

Fig. 3a shows the XRD patterns of the untreated soil and lime-treated soil compacted on dry side. Note that mineralogical analysis was only conducted on dry samples. Measurement on wet side should confirm similar mineralogy. The main minerals of untreated soil were found to be quartz (39%), calcite (35%) and clay (15.7%) with small amount of feldspars (9.5%) and halite NaCl (0.8%). The clay compositions were identified as illite (10.8%), chlorite (3.6%) and kaolinite (1.3%) and the whole content (15.7%) was consistent with the clay-size fraction (< 2μm) estimated at 17.4% on Fig 1. These clay minerals were also present in the lime-treated soil and no clear changes in their content were measured even after 150 days. To better identify the mineralogy changes for lime-treated soil during curing, the XRD patterns between 20° to 25° (2θ) and 32° to 41° (2θ) are depicted in Fig. 3b and 3c. For the lime-treated soil at curing time of 1, 90 and 150 days, three new reflections at 2θ equal to 21.0° (d ~ 4.90 Å), 33.4° (d ~ 3.09 Å) and 39.8° (d ~ 2.63 Å) were identified, suggesting the appearance of portlandite. The portlandite, namely calcium hydroxide $Ca(OH)_2$, was produced immediately when soil, lime and water were mixed together. Calcium hydroxide provided an alkaline environment in soil, inducing the dissolution of the silica and alumina present in the clay minerals. Then, the released Si and Al may react with Ca from the $Ca(OH)_2$ and form cementitious compounds [4-5]. However, the portlandite XRD reflections were still observed after 150-day curing, suggesting that the portlandite consumption was not complete and might extend longer. Furthermore, following the observations by Wang et al. [6], a reflection corresponding to cementitious compounds at 2θ equal to 34.2° (d ~ 3.04 Å) was identified for a lime-treated soil after 1-year curing. However, for the tested soil in this study, the reflection at 34.2° 2θ was occupied by the main XRD peak of calcite, as shown in Fig. 3a. A small heave around the reflection at 34.2° 2θ may be associated with the formation of poorly crystallized or amorphous cementitious compounds (Fig. 3c).

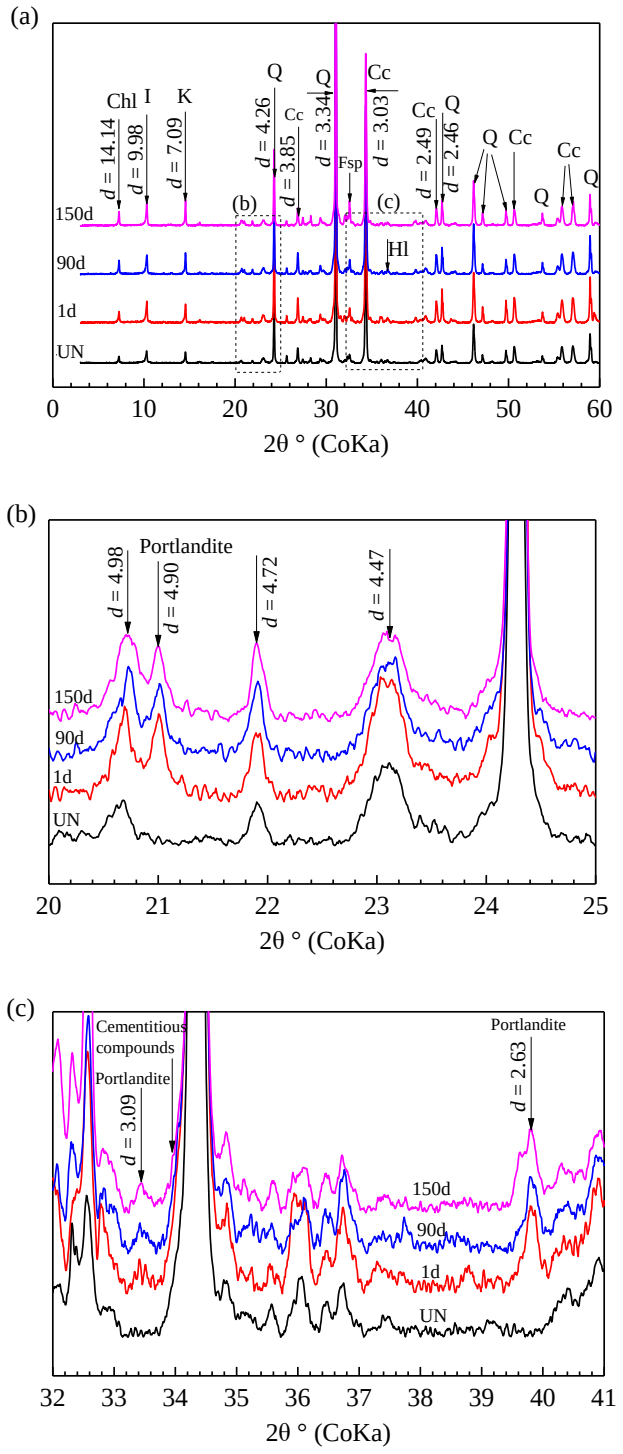

Fig. 3. X-ray diffraction patterns of untreated and lime-treated samples compacted on dry side: (a) 2θ 0°-60°; (b) 2θ 20°-25°; (c) 2θ 32°-41° (UN: untreated; Chl: chlorite; I: illite; K: kaolinite; Q: quartz; Cc: calcite; Fsp: feldspar; Hl: halite).

3.2 Pore size distribution

The cumulative curves and the corresponding derived curves of lime-treated samples compacted on dry and wet sides of optimum are presented in Fig. 4 and in Fig. 5, respectively.

With increasing curing time, the total intruded void ratio for dry samples decreased from 0.64 at 1 day curing to 0.59 at 28 days, whereas the total intruded void ratio for samples at 90 days was slightly larger than the sample at 1 day curing (Fig. 4a). The total intruded void ratio for the wet samples at 90 days was smaller than for the sample at 1 day. However, for the samples at 7 days and 28 days, it was slightly larger than for the samples at 1-day curing (Fig. 5a).

The pore size distribution of lime-treated samples compacted on both dry and wet sides of optimum presented bi-modal characteristics, with a population of macro-pores and a population of micro-pores. The frequency of macro-pores decreased with increasing water content. The microstructure changes for the lime-treated samples with increasing curing time did not follow a monotonic tendency. For the dry samples (Fig. 4b), the modal size of micro-pores decreased from 0.89 μm to 0.63 μm after 90-day curing while for the population of macro-pores, its modal size decreased from 7.50 μm after 1-day curing to 4.99 μm after 28-day curing, then increased to 7.00 μm at 90-day curing. As for the samples compacted on wet side (Fig. 5b), the modal size of micro-pores was around 1.04 μm for all samples at different curing times. The modal size of macro-pores decreased from 5.63 μm at 1-day curing to 5.00 μm after 90-day curing, whereas the modal sizes of macro-pores for samples at 7 days and 28 days were larger than those of samples at curing time of 1 day and 90 days.

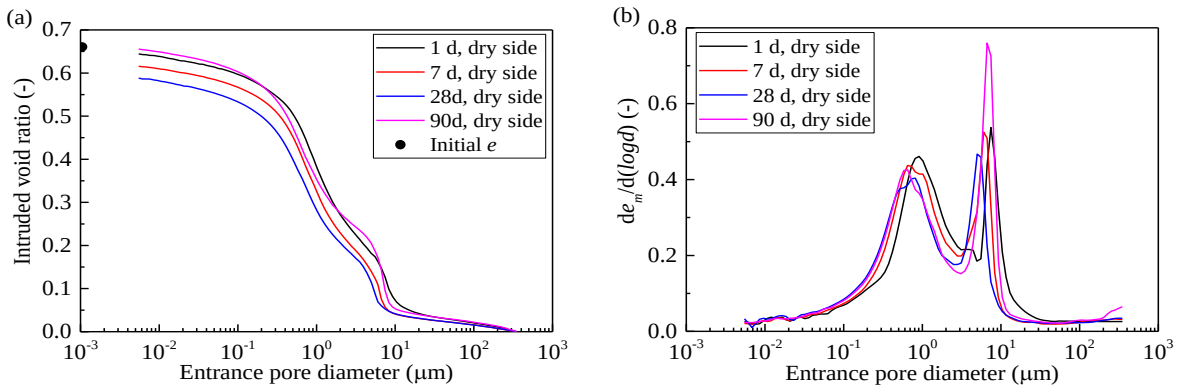

Fig. 4. MIP results of samples compacted on dry side: (a) cumulative curves, (b) derived curves.

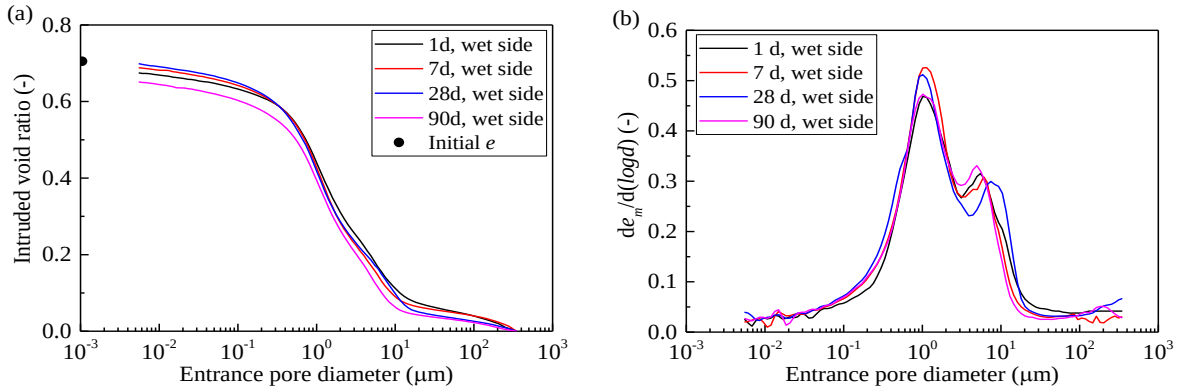

Fig. 5. MIP results of samples compacted on wet side: (a) cumulative curves, (b) derived curves.

To better distinguish the change tendency of the microstructure for lime-treated soil during curing time, the quantity of each pore population was given as the ratio of intruded void ratio to the initial void ratio which was calculated from the global parameters of compacted samples, as illustrated in Table 2. Note that the void ratio of pores < 0.006 μm was not quantified by porosimeter but its value was estimated by the value of initial void ratio minus the total mercury intruded void ratio. If the total intruded void ratio was larger than the initial value, the void ratio of pores < 0.006 μm was regarded as zero. On the whole, the quantities of pores < 0.006 μm and micro-pores increased, whereas the quantity of macro-pores decreased with curing time, except for the dry sample at 90 days.

Table 2. Quantity of the different pore populations.

Samples		Delimiting diameter d_L(μm)	Pores < 0.006 μm (%)	Micro-pores 0.006 μm - d_L(%)	Macro-pores > d_L(%)
Dry side	1 d	1.32	2.7	47.2	50.1
	7 d	1.16	7.1	58.2	34.7
	28 d	1.05	11.2	54.8	34.0
	90 d	1.03	1.1	46.0	52.9
Wet side	1 d	1.66	0	49.1	50.9
	7 d	1.57	0	51.0	49.0
	28 d	1.57	0	51.6	48.4
	90 d	1.59	2.7	52.3	45.0

4. Discussions

XRD patterns of lime-treated soil showed new peaks at d ~ 4.90 Å, ~ 3.09 Å and ~ 2.63 Å corresponding to portlandite produced during lime hydration process. The presence of remaining portlandite in lime-treated soil after 150-day curing indicated that the lime was not consumed completely. This can be explained both by the slow pozzolanic process and by the low clay fraction present in the tested soil. Low water content in dry or wet soil was in favour of low portlandite dissolution in soil pore water, followed by diffusion. Then, the low amount of clay, especially clay with low ability to dissolve such as illite and chlorite, cannot provide enough activated silica and alumina in order to interact with calcium and form cementitious compound. Other phases present in soil such as quartz and feldspars could also contribute but their usual low ability to dissolve compared to clay one, limited their role in pozzolanic reaction. Furthermore, as for a silty soil, the clay coated the granular quartz grains to constitute agglomerates and lime powder was solely distributed at the surface of these agglomerates without penetrating them [7, 14]. Therefore, the lime could preferentially react with soluble silica and alumina in clay minerals but not with the inert quartz minerals.

Concerning the cementitious compounds, the lack of XRD observations was usually attributed to the absence of well-crystallized cementitious compounds [6, 15]. Besides, the high intensity of natural calcite on XRD patterns may also mask the potential reflections of cementitious compounds (Fig. 3c).

Considering the pore size distribution of lime-treated soil, the curing time effect was consistent with the mineralogical analysis. The insignificant microstructure changes with increasing curing time did correspond to the formation of a low quantity of cementitious compounds probably in poorly crystallized or amorphous form. On the whole, the quantity of pores < 0.006 µm and micro-pores for samples compacted on wet and dry sides increased, and the quantity of macro-pores decreased with curing time. The pores < 0.006 µm were correlated with the formation of poorly crystallized or amorphous cementitious compounds produced in pozzolanic reaction, whose small internal pores were undetectable by MIP measurement due to the apparatus detection limit. This was in agreement with the observations made by Wang et al. [6]. Such new cementitious compounds gradually covered soil aggregates, and bonded adjacent soil particles together parallel to the filling of macropores. Then, it shifted the modal sizes to lower values, leading to a decrease of the quantity of macro-pores and an increase in the quantity of micro-pores [6-7, 10-11].

In general, the samples compacted on dry side exhibited aggregated structure with larger macro-pores and smaller micro-pores, while the samples compacted on wet side exhibited dispersed (or continuous) structure with only micro-pores [11, 16]. Thus, a bi-modal pore size distribution curves for wet samples as observed in this study was not a common result. However, Burton et al. [17] indicated that the bi-modal pore size distribution characteristics was not limited to samples compacted on dry side, but may also concern samples compacted on wet side if their compaction energy and degree of saturation were low. Delage et al. [16] indicated also that the volume of clay phase at equal dry density was an important parameter to understand the water content effect on compaction structure. On the dry side, the clay fraction was not well expanded and clays were coated on the surface of grains, leading to an aggregated structure characterized by populations of micro-pores and macro-pores. With increasing water content, the clay fraction formed a continuous or more compact matrix around the silt grains and clays were able to fill the macro-pores.

As for the lime-treated soil, the compacted dry density was estimated at 1.63 Mg/m^3, close to the maximum dry density of 1.66 Mg/m^3 and the compacted water content was only 1.5% larger than the optimum water content of 18.5%. Thus, the compaction water content and the low clay fraction of the tested soil might be the possible reasons for the bi-modal pore size distribution identified on wet samples. The degree of saturation of wet samples was close to that at optimum state, but the compacted dry density was lower than the maximum dry density. Thus, wet samples at this compaction state preferentially exhibited bi-modal pore size distribution with a population of micro-pores and a small population of macro-pores, similar to the samples at optimum observed by Delage et al. [16]. Besides, the low fraction of clay paste surrounding partially silt grains, led to a decrease in the frequency of macro-pores but not eliminated them.

5. Conclusions

XRD and MIP tests were performed on lime-treated soil compacted at dry and wet sides of optimum. The curing time effect on mineralogy and microstructure of lime-treated soil was investigated. The obtained results allowed the following conclusions to be drawn:

• Portlandite observed on XRD pattern of lime-treated soil after curing time until 150 days, might be attributed to the limited water content in wet and dry samples combined with the low clay fraction that couldn’t provide sufficient silica and alumina to interact with calcium from portlandite. Furthermore, no cementitious compounds in significant quantity were detected on

XRD patterns even after a curing time as long as 150 days. The high intensity of calcite peak overlapping the reflection of hydrated products may explain such result. The formation of low amount of poorly crystallized or amorphous cementitious compounds might be the other possibility.

• The insignificant microstructure changes with increasing curing time were consistent with the formation of poorly crystallized or amorphous cementitious compounds whose pores were smaller than 0.006 μm and the quantity of these pores increased with curing time. Cementitious compounds gradually coated soil particles and bonded them together parallel to the filling of macropores, leading to a decrease of the quantity of macro-pores and an increase of the quantity of micro-pores.

• The samples compacted on dry and wet sides of optimum exhibited bi-modal pore size distribution characteristics with two populations of micro-pores and macro-pores. The smaller frequency of macro-pores for wet samples can be attributed to the slightly higher water content than optimum and the low clay fraction. The limited amount of clay paste surrounding the silt particles led to a decrease of the quantity of macro-pores but it did not eliminate them.

Acknowledgements

The authors would like to thank the China Scholarship Council (CSC), Ecole des Ponts ParisTech and IRSTEA for their financial support.

References

1. Bell, F.G., 1996. Lime stabilization of clay minerals and soils. Eng. Geol. 42 (4), 223-237.
2. Tang, A.M., Vu, M.N., Cui, Y.J., 2011. Effects of the maximum soil aggregates size and cyclic wetting-drying on the stiffness of a lime-treated clayey soil. Géotechnique 61, 421-429.
3. Wang, Y.J., Cui, Y.J., Benahmed, N., Tang, A.M., Duc, M., 2020. Changes of small strain shear modulus and suction for a lime-treated silt during curing. Géotechnique 70, 276-280.
4. Guney, Y., Sari, D., Cetin, M., Tuncan, M., 2007. Impact of cyclic wetting-drying on swelling behavior of lime-stabilized soil. Build. Environ. 42 (2), 681-688.
5. Al-Mukhtar, M., Lasledj, A., Alcover, J.F., 2010. Behaviour and mineralogy changes in lime-treated expansive soil at 20°C. Appl. Clay Sci. 50, 191-198.
6. Wang, Y.J., Duc, M., Cui, Y.J., Tang, A.M., Benahmed, N., Sun, W.J., Ye, W.M., 2017. Aggregate size effect on the development of cementitious compounds in a lime-treated soil during curing. Appl. Clay Sci. 136, 58-66.

7. Lemaire, K., Deneele, D., Bonnet, S., Legret, M., 2013. Effects of lime and cement treatment on the physicochemical, microstructural and mechanical characteristics of a plastic silt. Eng. Geol. 166, 255-261.

8. Cuisinier, O., Auriol, J.C., Le Borgne, T., Deneele, D., 2011a. Microstructure and hydraulic conductivity of a compacted lime-treated soil. Eng. Geol. 123, 187-193.

9. Russo, G., Modoni, G., 2013. Fabric changes induced by lime addition on a compacted alluvial soil. Geotech. Lett. 3, 93-97.

10. Wang, Y.J., Cui, Y.J., Tang, A.M., Tang, C.S., Benahmed, N., 2015. Effects of aggregate size on water retention capacity and microstructure of lime-treated silty soil. Geotech. Lett. 5, 269-274.

11. Wang, Y.J., Cui, Y.J., Tang, A.M., Tang, C.S., Benahmed, N., 2016. Changes in thermal conductivity, suction and microstructure of a compacted lime-treated silty soil during curing. Eng. Geol. 202, 114-121.

12. Delage, P., Pellerin, F.M. 1984. Influence de la lyophilisation sur la structure d'une argile sensible du Québec. Clay Miner. 19(2), 151-160.

13. Zhang, F., Cui, Y.J., Ye, W.M., 2018. Distinguishing macro-and micro-pores for materials with different pore populations. Géotechnique Lett. 8(2), 102-110.

14. Shi, B., Liu, Z.B., Cai, Y., Zhang, X.P., 2007. Micropore structure of aggregates in treated soils. J. Mater. Civ. Eng. 19(1), 99-104.

15. Al-Mukhtar, M., Lasledj, A., Alcover, J.F., 2014. Lime consumption of different clayey soils. Appl. Clay Sci. 95, 133-145.

16. Delage, P., Audiguier, M., Cui, Y.J. Howat, M.D., 1996. Microstructure of a compacted silt. Can. Geotech. J. 33(1), 150-158.

17. Burton, G.J., Sheng, D.C., Campbell, C., 2014. Bimodal pore size distribution of a high-plasticity compacted clay. Géotechnique Lett. 4(2), 88-93.

Ying, Z., Cui, Y.J., Benahmed, N., Duc, M. 2021. Acta Geotechnica. Doi: org/10.1007/s11440-021-01218-5.

Changes of microstructure and water retention property of a lime-treated saline soil during curing

Zi Ying[1], Yu-Jun Cui[1], Nadia Benahmed[2], Myriam Duc[3]

Abstract: This study aims at investigating the lime treatment effect on the changes in microstructure and water retention property of compacted saline soil, with consideration of the aggregate size effect. Two soil powders with different maximum aggregate sizes (D_{max} = 0.4 mm and 5 mm) were prepared and stabilised by 2% lime. The microstructure, total suction and matric suction were determined at various curing times. Results showed that the lime treatment caused a rapid decrease of micro-pores and an increase of macro-pores due to the flocculation of soil particles. During curing, the percentage of micro-pores decreased and that of nano-pores increased slightly. Due to the modification of microstructure, the matric suction increased significantly at 90-day curing. However, the curing time effect on the total suction was insignificant. This was due to the fact that the Ca^{2+} and Mg^{2+} in soil pore water and the Ca^{2+} from hydrated lime were consumed in the precipitations of $CaCO_3$ and $Mg(OH)_2$, cation exchanges and pozzolanic reaction, resulting in a reduction of osmotic suction. Therefore, the increase of total suction was slight, as the increase in matric suction was balanced by the decrease of osmotic suction. The treated specimens with larger aggregates exhibited a larger modal size and thus had a smaller air entry value. The aggregate size effect on the water retention property of total suction and matric suction was found to be insignificant, which could be explained by the similar pore size distribution at micro-pore range and the same soil mineralogy for specimens with different aggregates.

Keywords: Lime-treated saline soil; curing time; microstructure; suction; aggregate size

1. Introduction

Lime treatment is recognised as an effective improvement technique widely applied to soils with poor physical and mechanical characteristics. It can significantly modify the geotechnical

[1]: Ecole des Ponts ParisTech, Laboratoire Navier/CERMES, 6 – 8 av. Blaise Pascal, Cité Descartes, Champs-sur-Marne, 77455 Marne-la-Vallée cedex 2, France
[2]: INRAE, Aix Marseille Univ, Unité de Recherche RECOVER, 3275 route Cézanne, CS 40061, 13182 Aix-en-Provence, France
[3]: Université Gustave Eiffel, IFSTTAR/GERS/SRO, 14-20 boulevard Newton, Champs-sur-Marne, 77447 Marne-la-Vallée, France

properties and mechanical behaviours of soils through a series of physical-chemical reactions, such as lime hydration, cation exchanges and pozzolanic reaction [1, 6, 28, 34].

To days, most studies have been focused on the effect of lime treatment on the changes in microstructure and water retention property of soils. It was widely admitted that lime addition resulted in rapid hydration and cation exchanges that flocculated the soil particles, forming coarser aggregates [13, 17, 18, 29, 30]. Further pozzolanic reaction decreased the modal pore sizes due to the formation of cementitious compounds which coated the surface of aggregates [13, 17, 18, 29, 30]. Cuisinier et al. [8] and Le Runigo et al. [16] indicated that the main consequence of lime treatment on soil fabric was the formation of a new pore population below 0.2/0.3 μm. Similar observations were made by Wang et al. [33] – the formation of cementitious compounds led to the creation of nano-pores ranging from 0.006 μm to 0.1 μm. All these changes of soil microstructure would increase the water retention capacity of lime-treated soil, as more water could be retained in the inner the inner pores [7, 15, 29, 31, 32].

Concerning the aggregate size effect, Wang et al. [33] reported that the well-crystallized cementitious compounds can be detected by X-ray diffraction (XRD) technique on lime-treated soil with larger aggregates, while poorly crystallized or amorphous cementitious compounds were observed on soil with smaller aggregates. As a result, a higher reduction of total mercury intruded void ratio was found in lime-treated soil with smaller aggregates due to the creation of more undetected pores (d < 0.006 μm) in poorly crystallized or amorphous cementitious compounds [33]. In addition, Wang et al. [31] indicated that the lime-treated silt with smaller aggregates had relatively smaller modal size of macro-pores and consequently exhibited a higher air entry value and higher water retention capacity.

The above-mentioned studies mainly involved the microstructure and water retention property of lime-treated saltless soils. To the authors' knowledge, no study has paid attention to lime-treated saline soils, especially for the water retention property in which both matric and osmotic suctions were involved. In this study, mercury intrusion porosimetry (MIP) was used to investigate the microstructure of untreated and lime-treated soils with two different maximum aggregate sizes (D_{max} = 0.4 mm and 5 mm). Water retention curves in terms of total suction and matric suction were determined by the chilled-mirror dew-point hygrometer (WP4C) and contact filter paper method (FP), respectively. The results obtained were analysed to understand the changes of microstructure and water retention property of lime-treated saline soils during

curing.

2. Materials and methods

2.1 Materials

A plastic silt sampled at Les Salins de Giraud in southern France was used in this study. The basic geotechnical properties of natural soil are presented in Table 1. XRD analysis shows that this soil is mainly composed of quartz (39%) and calcite (35%); its clay fraction (15.7%) contains 10.8% illite, 3.6% chlorite and 1.3% kaolinite. The water salinity of soil pore water is 13.3‰ (g of salt/kg of salty water) for the soil at 15.6% water content, and the main ion species in soil pore water are Cl^-, Na^+, K^+, Ca^{2+} and Mg^{2+} [36]. The corresponding soil salinity is 2.10‰ (g of salt/kg of dry soil) that does not vary with the changes of water quantity [36]. The grain size distribution of natural soil determined by the wet sieving method for particles larger than 80 μm [11] and by the hydrometer method for particles smaller than 80 μm [12] is presented in Fig. 1. This natural soil contains 17% clay-size particles (< 0.002 mm), 53% silt (0.002 ~ 0.075 mm) and 30% fine sand (0.075 ~ 2 mm). To prepare the soil specimens, the natural soil was air-dried, ground and passed through the target sieves to get two different powders with different maximum aggregate sizes (D_{max} = 0.4 mm for S0.4 and 5 mm for S5). The soil aggregates which could not pass through the target sieves were ground again until all the soil aggregates passed through. The aggregate size distributions of dry soil powders (S0.4 and S5) obtained by dry sieving are also shown in Fig. 1. It appears that the soil powders S0.4 and S5 contain all soil particles of natural soil, suggesting that this preparation of soil powders ensured the soil samples S0.4 and S5 to have the same mineral composition, clay faction and salinity as natural soil.

Table 1. Characteristics of the tested soil.

Property	Value
Liquid limit, w_L (%)	29
Plastic limit, w_p (%)	19
Plasticity Index, I_p	10
Specific gravity, *Gs*	2.71
Specific surface area (m^2/g)	24
Optimum lime dosage (% of lime)	0.5
Optimum water content of 2% lime- treated soil (%)	18.7
Maximum dry density of 2% lime-treated soil (Mg/m^3)	1.66

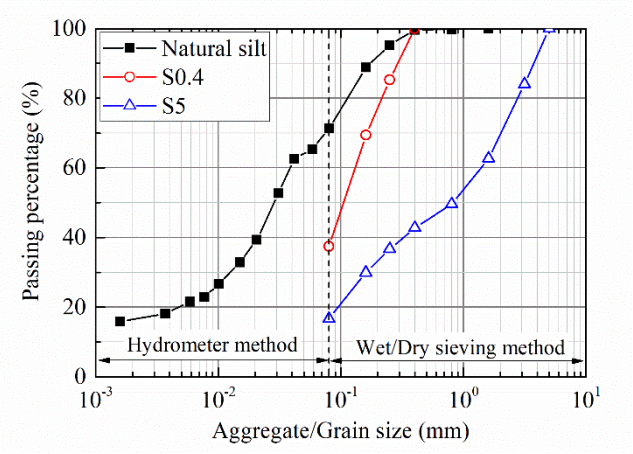

Fig. 1. Aggregate/Grain size distributions of dry soil powders and natural silt.

The lime used in this study was a quicklime with CaO content as high as 97.3% [33]. The optimum lime dosage of the soil was determined by pH method according to ASTM standard D6276-19 [5] and the value was found to be 0.5% (by dry weight of soil). Based on the dosage applied for the construction of dike at Les Salins de Giraud, a lime content of 2% by weight of dry soil was selected.

After grinding, the dry soil powder was first mixed with lime and then humidified by deionized water to obtain the target water content (w = 17%, dry side of optimum). After a period of mellowing of 1 h, the soil-lime mixture was statically compacted to the target dry density (1.63Mg/m^3) using double pistons acting at the top and bottom of the soil specimen to ensure uniform distribution of stresses inside the specimen. A compaction rate of 0.3 mm/min was adopted. The specimens for MIP test and matric suction measurement had 50 mm in diameter and 20 mm in height, and the specimens for total suction measurement were statically compacted in five layers to the dimensions of 38 mm in diameter and 100 mm in height. After compaction, the specimens were wrapped by plastic film and scotch tape, covered by wax and then cured for 1, 28, 90 days, respectively.

2.2 Test method

Autopore IV 9500 mercury intrusion porosimeter (from Micromeritics) was used to investigate the microstructure of untreated and lime-treated specimens. Small pieces of specimens were rapidly frozen using vacuumed liquid nitrogen, and then lyophilised [9]. In MIP test, the applied pressure increased from 3.6 kPa to 230 MPa in steps, and the corresponding intruded diameter varied from 350 μm to 0.006 μm [32].

Based on the MIP results, the matric suction (u_a - u_w) can be deduced from mercury intrusion pressure p by Eq. 1 [22]:

$$u_a - u_w = -\frac{T_w \cos\theta_w}{T_m \cos\theta_m} p \quad (1)$$

where subscript m denotes mercury while subscript w denotes water; T is the surface tension (T_w = 0.073 N/m, T_m = 0.485 N/m); θ is the contact angle (θ_w = 0°, θ_m = 130°).

The water content of soil specimens can be obtained from MIP results as follows [23,27]:

$$w = (1 - S_{rm})(w_{sat} - w_r) + w_r = \frac{e}{G_S}(1 - \frac{e_{MIP}}{e}) \quad (2)$$

where S_{rm} is the saturation degree of mercury; w_{sat} is the water content at saturation; w_r is the residual water content; e is the global void ratio of compacted specimens; e_{MIP} is the mercury intruded void ratio; G_s is the specific gravity.

Thus, the soil water retention curves can be derived from MIP results by calculating the matric suction and water content using Eqs.1 and 2. Moreover, based on the pore size distribution of specimen and its water content measured by oven drying, the distribution of soil pore water can be estimated assuming that water is contained in the smaller pores.

WP4C device was used to measure the total suction. At a given curing time, one specimen was cut into several small pieces. They were air-dried for different durations in order to obtain different total suctions. Then, they were covered and stored for one night for water homogenization. Afterwards, the total suction of each piece was measured by WP4C device. The corresponding water content was determined by oven-drying at 105 °C.

The matric suction was determined by the contact filter paper method [4]. Filter papers (Whatman No. 42) were oven-dried for at least 16 h prior to the measurements. The untreated specimens and lime-treated specimens at given curing time were air-dried to reach different water contents in order to obtain different matric suctions. Once the target water content reached, the three stacked filter papers were sandwiched between two specimens for the measurement of matric suction.

According to ASTM D5298-16 [4], the filter paper calibration relationships expressed by Eq. 3 were used to determine the soil matric suction (ψ_m) from the water content of filter paper (w_f):

$$\log \psi_m = \begin{cases} 5.327 - 0.0779 w_f & w_f \le 45.3\% \\ 2.412 - 0.0135 w_f & w_f > 45.3\% \end{cases} \quad (3)$$

3. Results and discussions

3.1 Microstructure

Figures 2 and 3 show the pore size distributions of untreated and lime-treated specimens at 1, 28 and 90 days for S0.4 and S5, respectively. Note that the data obtained for lime-treated specimen S0.4 were reported previously in Ying et al. [35], for microstructure analysis. It can be observed that the curing time effect on the total intruded void ratio was insignificant. The density function curves of both S0.4 (Fig. 2b) and S5 (Fig. 3b) exhibited bi-modal characteristics with two populations of micro-pores and macro-pores which were delimited at diameter of 2 μm, the same as the delimiting diameter adopted by Wang et al. [33] for a lime-treated silt. As shown in Figs. 2b and 3b, the lime-treatment decreased the frequency of micro-pores, while the frequency of macro-pores increased and its modal size shifted to lower values. Specifically, the modal sizes of micro-pores were around 0.91 μm, 0.66 μm and 0.58 μm for the lime-treated specimens S0.4 at curing time of 1, 28 and 90 days, respectively. A higher value of 0.92 μm was observed for the untreated specimen S0.4. For the population of macro-pores, its modal size decreased from 10.56 μm for untreated specimen to 7.50 μm, 5.40 μm and 6.65 μm for lime-treated specimens at curing time of 1, 28 and 90 days, respectively. Similar results were obtained on the specimens S5. In addition, as shown in Figs. 2b and 3b, an increase in the frequency at diameters ranging from 0.1 to 0.5 μm was observed on lime-treated specimens S0.4 and S5. The density function curves at range of nano-pores (0.006-0.1 μm) were also magnified in Figs. 2b and 3b. It appears that the frequency of lime-treated specimens at diameters ranging from 0.006 to 0.1 μm was higher than that of untreated specimens.

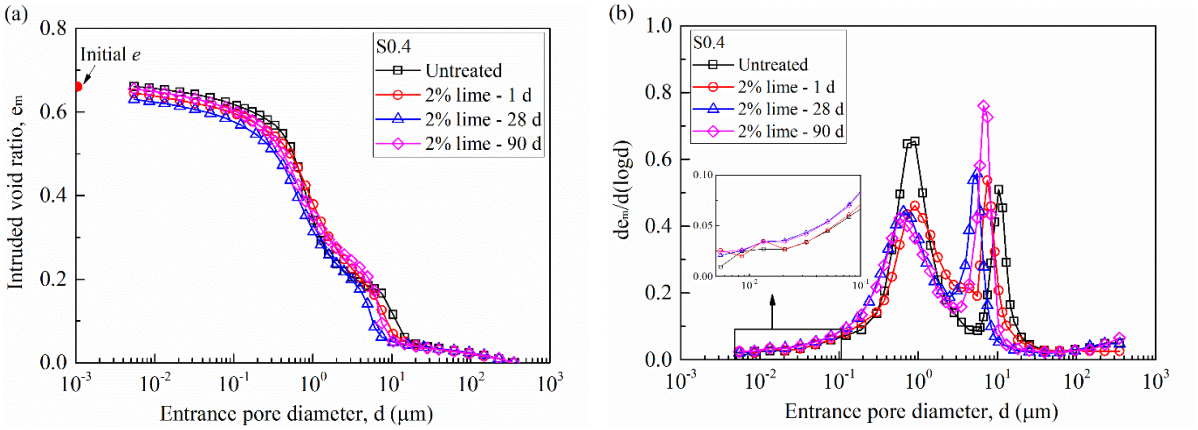

Fig. 2. MIP results of lime-treated soil and untreated soil, S0.4: (a) cumulative intruded void ratio curves; (b) density function curves.

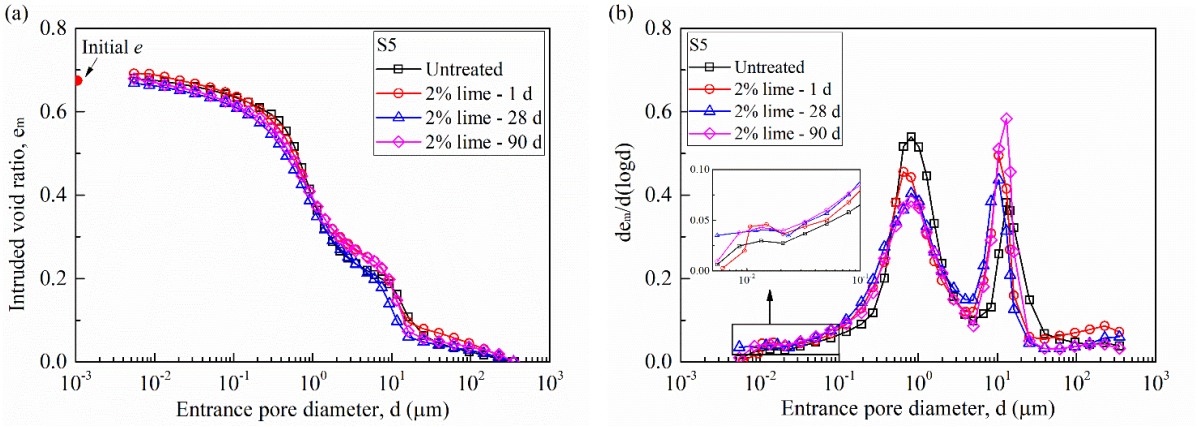

Fig. 3. MIP results of lime-treated soil and untreated soil, S5: (a) cumulative intruded void ratio curves; (b) density function curves.

Figure 4 presents the quantity of different pore populations of S0.4 and S5, which was given as the ratio of intruded void ratio at corresponding diameters to the total intruded void ratio. It can be observed that, the S5 had more macro-pores and less micro-pores as compared to S0.4, while the quantity of nano-pores was almost similar for S0.4 and S5. Comparison of the different pore populations of lime-treated specimens during curing and of untreated specimens indicated that the microstructure modification induced by lime treatment was mainly attributed to the rapid flocculation of soil particles but not the formation of cementitious compounds produced in the pozzolanic reaction.

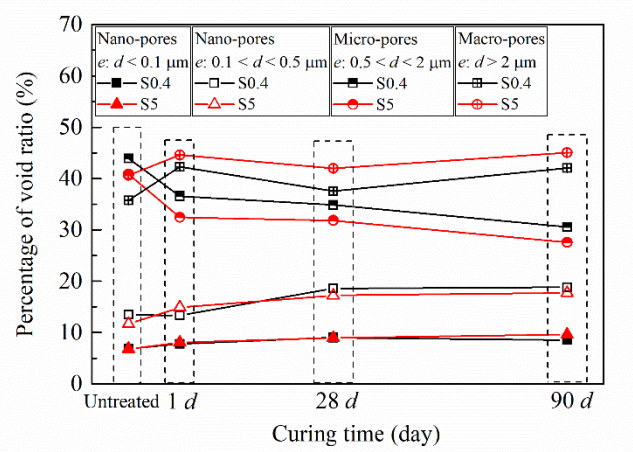

Fig. 4. Variations of different pore populations with curing time.

When the soil, lime and water were mixed together, the cation exchanges were expected to take place rapidly [1, 10, 13], leading to the flocculation of soil particles and the formation of coarser aggregates [6, 8, 18, 32]. Consequently, the percentage of macro-pores (d > 2 μm) increased, while the percentage of micro-pores (0.5 < d < 2 μm) decreased (Fig. 4). The specimens S5 with larger maximum aggregate size presented higher quantity of macro-pores as compared to specimens S0.4. During curing, the percentage of micro-pores (0.5 < d < 2 μm) decreased and that of nano-pores (d < 0.1 μm and 0.1 < d < 0.5 μm) increased slightly, probably due to the formation of cementitious compounds. This was consistent with the observations obtained by Wang et al. [33]. They reported that, for the lime-treated Héricourt silt, the formation of cementitious compounds led to the creation of nano-pores ranging from 0.006 to 0.1 μm and such nano-porous compounds filled the micro-pores gradually (0.1 to 2 μm), leading to a reduction of the micro-pore frequency. Indeed, after lime treatment, a new pore population of 0.007-0.2/0.3 μm was also observed on other low-plasticity soils [8, 16, 26]. Alvarez et al. [2] ascribed the new pore population below 0.01 μm to the gel pores of calcium silicate hydrate (C-S-H) in nanosilica-treated aerial lime binding material. Muller [20] reported that the C-S-H interlayer space was around 1 nm and the C-S-H gel pores were about 2.5 nm that were too small to be detected by MIP test. Thus, it can be concluded that, for the tested lime-treated silt with 15.7% clay fraction, the increased percentage of nano-pores (d < 0.1 μm and 0.1 < d < 0.5μm) with increasing curing time was mainly attributed to the filling effect of cementitious compounds. The cementitious compounds can be produced not only from the reactions of lime and alumina-silicate from clay minerals, but also slightly from the reactions of lime and silicate from fine quartz or feldspars [6]. As for the tested silt, it mainly consisted of less active clay minerals (10.8% illite, 3.6% chlorite and 1.3% kaolinite) and inert phases of quartz (39%) and

feldspars (9.5%). Thus, it can be inferred that the insignificant curing time effect on the pore size distribution was due to the small quantity of activated silicate and alumina in the soil to interact with lime and form cementitious compounds. It was confirmed by the XRD test that the quantities of quartz, feldspar, illite, chlorite and kaolinite in lime-treated soil after 90-day curing were rather similar to that of untreated soil, and the percentage of portlandite decreased slightly from 2.1% to 1.9% [35]. As observed in Fig. 4, the percentages of nano-pores of specimens S0.4 and S5 were rather similar during curing. This suggested that the aggregate size effect on the production of cementitious compounds was slight in the tested silt, as the soil mineral composition was almost the same for specimens S0.4 and S5.

3.2 Water retention property

Due to the modification of soil microstructure by the lime addition and the formation of cementitious compounds, the water retention property was expected to increase during curing as more water could be retained in the inner pores [15, 29, 31, 32]. As shown in Fig. 5, the lime-treated specimens cured at 90 days exhibited much higher matric suctions than that of untreated specimens and lime-treated specimens at 28-day curing. This could be attributed to the slight increase of nano-pores and the production of cementitious compounds at longer curing time which could improve the water capacity of soil. However, the curing time effect on the total suction was slight (Fig. 6), suggesting that the effect of lime treatment on the water retention property of saline soil was mainly reflected on the changes in matric suction rather than total suction which consisted of both matric and osmotic suctions.

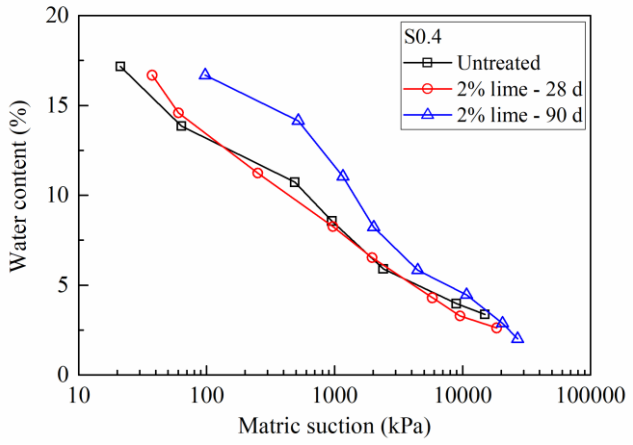

Fig. 5. Water retention curves in terms of matric suction.

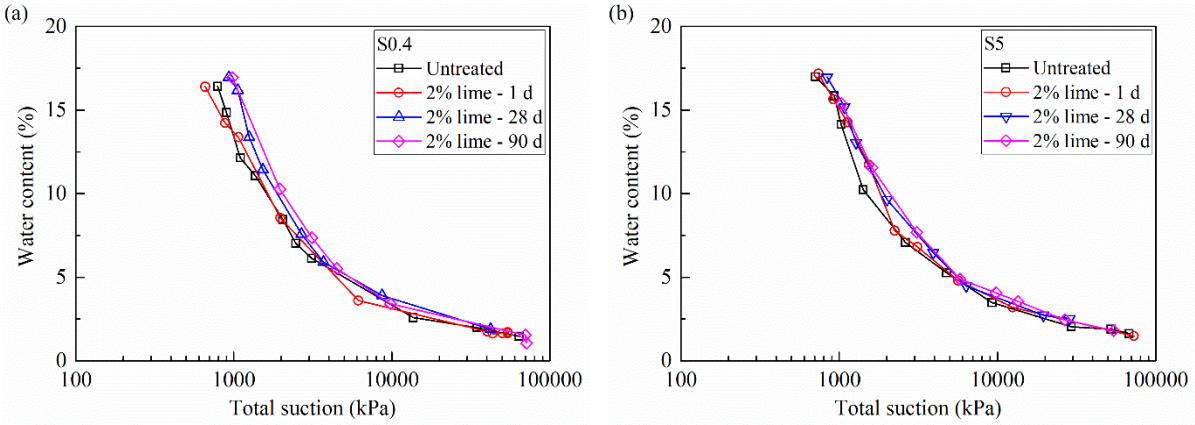

Fig. 6. Water retention curves in terms of total suction: (a) S0.4; (b) S5.

The matric suction was controlled by the capillary component and adsorption mechanisms [19, 21], while the osmotic suction was related to the dissolved salt in soil pore water [3]. As for the lime-treated saline soil, the presence of cations (Ca^{2+} and Mg^{2+}) in soil pore water and Ca^{2+} from hydrated lime would participate in cation exchanges immediately after mixing soil, lime and water together. In the long-term, the silicate and alumina dissolved from silt minerals reacted with Ca^{2+} to form cementitious compounds. Meanwhile, the precipitations of $CaCO_3$ and $Mg(OH)_2$ could occur in alkaline environment [14], consuming the Ca^{2+} and Mg^{2+} in soil pore water. Thus, with the Ca^{2+} and Mg^{2+} being consumed, the quantity of dissolved salt in soil pore water tended to decrease, leading to a reduction of osmotic suction. The decrease of salt concentration during curing was confirmed by Al-Mukhtar et al. [1]. They reported that the electrical conductivity (EC) of soil-lime mixtures decreased during the first 7 days due to the cation exchanges, and the reduction of EC after 7 days was attributed to the consumption of Ca^{2+} and OH^- in the pozzolanic reaction. As a result, the total suction increased slightly during curing, due to the balance of the decrease of osmotic suction and the increase in matric suction.

The water retention curves and pore size distributions for specimens S0.4 and S5 (t = 28 days) are depicted in Fig. 7. The water retention curves shown in Fig. 7 in terms of total suction and matric suction were obtained separately by WP4C device and contact filter paper method (FP). The water retention curves in terms of matric suction, deduced from MIP results are also presented in Fig. 7. The curves of matric suction obtained from contact filter paper method were slightly different from that of matric suction deduced from MIP Model. This difference can be attributed to the fact that the curves from MIP test deduced from the as-compacted specimens (w = 17%) did not consider the microstructure changes, while the curves from the filter paper measurements involved the microstructure evolutions during drying. This was consistent with

the observations made by Wang et al. [31]. Note that the effect of volume change on the water retention curve was described and modelled by Sun and Cui [27].

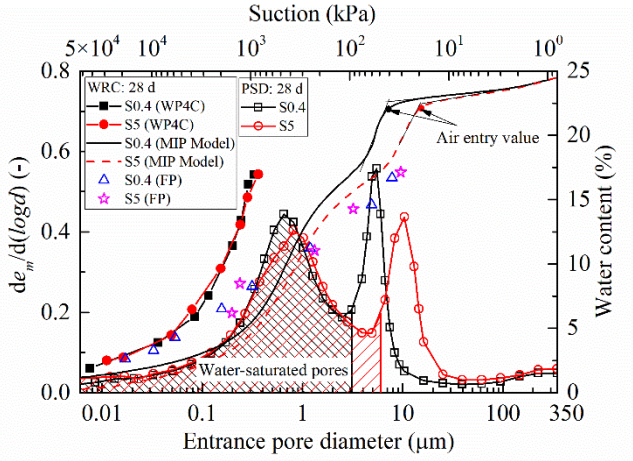

Fig. 7. Aggregate size effect on the pore size distribution and water retention property.

It appears from Fig. 7 that the aggregate size had negligible effect on the micro-pore population whose modal size was around 0.84 μm for S5 and 0.66 μm for S0.4. Nevertheless, the population of macro-pores was highly affected by aggregate size: its modal size for S5 was up to 10.5 μm and a lower value of 5.3 μm was obtained for S0.4. Due to the lager entrance pore size of S5, a lower air entry value (20 kPa) was observed for S5 than that of S0.4 (40 kPa).

It is noting that the water retention curves in terms of total suction (WP4C) and matric suction (FP) were insensitive to the aggregate size. As shown in Fig. 7, almost all water was contained in the micro-pores. Thus, along the drying path, the main de-saturation took place in the micro-pores. With first drying, both capillarity and adsorption contributed to the water retention property [19]. Then, the capillarity was exceeded by the adsorption at the high range of suction beyond the residual state [21, 25]. The capillarity was highly related to the pore size distribution, while the adsorption was associated with soil mineralogy [19] and the specific surface of the clayey fraction [24]. This explains why the effect of aggregate size on the water retention curves of matric suction (FP) was insignificant as the drying path was started from the unsaturated state where the water retention capacity was dominated by the similar pore size distribution at micro-pore range and by the almost same soil mineralogy for S5 and S0.4. Moreover, as the specimens S5 and S0.4 had the same salinity, hence, the same osmotic suction, the water retention curves of total suction (WP4C) were insensitive to aggregate size as well.

4. Conclusions

The microstructure and water retention property of untreated and lime-treated saline soils were studied, with consideration of the aggregate size effect. Based on the obtained results, the following conclusions are drawn:

(i) Lime treatment caused a reduction of the percentage of micro-pores and an increase of macro-pore quantity due to the flocculation of soil particles. With increasing curing time, the percentage of micro-pores ($0.5 < d < 2$ μm) decreased and that of nano-pores below 0.5 μm increased slightly, probably due to the production of cementitious compounds which coated the surface of aggregates and filled the pores gradually. The effect of cementitious compounds was insignificant due to the low fraction of active clay minerals and the inert phases of quartz and feldspars in the silty soil, which cannot provide enough activated silica and alumina to interact with calcium and form significant cementitious compounds.

(ii) Because of the increase of nano-pores, the matric suction increased significantly at 90- day curing. However, the total suction increased slightly. This was explained by the fact that during curing, the Ca^{2+} and Mg^{2+} in soil pore water and the Ca^{2+} dissolved from hydrated lime were consumed in the precipitations of $CaCO_3$ and $Mg(OH)_2$, cation exchanges and pozzolanic reaction, leading to a decrease of osmotic suction. As the increase of matric suction was almost balanced by the decrease of osmotic suction, the change in total suction was insignificant.

(iii) The lime-treated specimens with larger aggregates had a smaller air entry value due to its relatively larger modal size as observed by MIP test. Nevertheless, the aggregate size effect on the total suction (WP4C) and matric suction (FP) was insignificant. Because the similar micro-pore size distribution and almost same soil mineralogy for S5 and S0.4 dominated the water retention capacity with the specimens being dried from unsaturated state, leading to an insignificant effect of aggregate size.

Acknowledgements

The authors would like to thank the China Scholarship Council (CSC). The support provided by Ecole des Ponts ParisTech (ENPC) and INRAE is also greatly acknowledged.

References

1. Al-Mukhtar M, Lasledj A, Alcover JF (2010) Behaviour and mineralogy changes in lime-treated expansive soil at 20 ℃. Appl Clay Sci 50(2):191-198. https://doi.org/10.1016/j.clay.2010.07.023
2. Alvarez JI, Fernandez JM, Navarro-Blasco I, Duran A, Sirera R (2013) Microstructural consequences of nanosilica addition on aerial lime binding materials: Influence of different drying conditions. Mater Charact 80:36-49. https://doi.org/10.1016/j.matchar.2013.03.006
3. Arifin YF, Schanz T (2009) Osmotic suction of highly plastic clays. Acta Geotech 4(3):177-191. https://doi.org/10.1007/s11440-009-0097-0
4. ASTM D5298-16 (2016) Standard Test Method for Measurement of Soil Potential (Suction) Using Filter Paper. ASTM International, West Conshohocken, PA.
5. ASTM D6276-19 (2019) Standard Test Method for Using pH to Estimate the Soil-Lime Proportion Requirement for Soil Stabilization. ASTM International, West Conshohocken, PA.
6. Bell FG (1996) Lime stabilization of clay minerals and soils. Engineering geology 42(4):223-237. https://doi.org/10.1016/0013-7952(96)00028-2
7. Cecconi M, Russo G (2008) Prediction of soil-water retention properties of a lime stabilised compacted silt. In: Toll, et al. (EDs), Unsaturated Soils: Advances in Geo-Engineering. 2008. Taylor & Fransic Group. London 271-276. (ISBN 978-0-415-47692-8).
8. Cuisinier O, Auriol JC, Borgne TL, Deneele D (2011) Microstructure and hydraulic conductivity of a compacted lime-treated soil. Eng Geol 123(3):187-193. https://doi.org/10.1016/j.enggeo.2011.07.010
9. Delage P, Lefebvre G (1984) Study of the structure of a sensitive Champlain clay and of its evolution during consolidation. Can. Geotech. J 21(1):21-35. https://doi.org/10.1139/t84-003
10. Di Sante M, Fratalocchi E, Mazzieri F, Pasqualini E (2014) Time of reactions in a lime treated clayey soil and influence of curing conditions on its microstructure and behaviour. Appl Clay Sci 99:100-109. https://doi.org/10.1016/j.clay.2014.06.018
11. French standard AFNOR NF P 94-056 (1996) Standard Test for Soils Investigation and Testing-Granulometric Analysis-Dry Sieving method after Washing.
12. French standard AFNOR NF P 94-057 (1992) Standard Test for Soils Investigation and Testing-Granulometric Analysis-Hydrometer method.
13. Guney Y, Sari D, Cetin M, Tuncan M (2007) Impact of cyclic wetting–drying on swelling behavior of lime-stabilized soil. Build Environ 42(2):681-688. https://doi.org /10.1016/j.buildenv.2005.10.035
14. Hamidi R, Kahforoushan D, Fatehifar E, Arehjani M, Farmanbordar S (2011) Simultaneous removal of Ca and Mg Salts using chemical precipitation with lime. The 7th International Chemical Engineering Congress & Exhibition. Kish, Iran, 21-24 November, 2011.
15. Khattab SAA, Al-Taie LKhI (2006) Soil-water characteristic curves (SWCC) for lime treated expansive soil from Mosul City. Unsaturated soils 1671-1682. https://doi.org/10.1061/40802(189)140

16. Le Runigo B, Cuisinier O, Cui YJ, Ferber V, Deneele D (2009) Impact of initial state on the fabric and permeability of a lime-treated silt under long-term leaching. Can Geotech J 46(11):1243-1257. https://doi.org/10.1139/T09-061

17. Liu YW, Wang Q, Liu SW, ShangGuan YL, Fu HC, Ma B, Chen H, Yuan XQ (2019) Experimental investigation of the geotechnical properties and microstructure of lime-stabilized saline soils under freeze-thaw cycling. Cold Reg Sci Technol 161:32-42. https://doi.org/10.1016/j.coldregions.2019.03.003

18. Locat J, Bérubé MA, Choquette M (1990) Laboratory investigations on the lime stabilization of sensitive clays: shear strength development. Can Geotech J 27(3):294-304. https://doi.org/10.1139/t90-040

19. Lu N, Khorshidi M (2015) Mechanisms for soil-water retention and hysteresis at high suction range. J Geotech Geoenviron Eng 141(8):04015032. https://doi.org/10.1061/(ASCE)GT.1943-5606.0001325

20. Muller ACA (2014) Characterization of porosity & CSH in cement pastes by ^{1}H NMR. PhD Thesis, École Polytechnique Fédérale de Lausanne, Lausanne, Suisse.

21. Ng CWW, Sadeghi H, Belal Hossen SK, Chiu CF, Alonso EE, Baghbanrezvan S (2016) Water retention and volumetric characteristics of intact and re-compacted loess. Can Geotech J 53(8):1258-1269. https://doi.org/10.1139/cgj-2015-0364

22. Prapaharan S, Altschaeffl AG, Dempsey BJ (1985) Moisture curve of compacted clay: mercury intrusion method. J Geotech Eng 111(9):1139-43. https://doi.org/10.1061/(ASCE) 0733-9410(1985)111:9(1139)

23. Romero E (1999) Thermo-Hydro-Mechanical Behaviour of Unsaturated Boom Clay: an experimental study. PhD Thesis, Universidad Politécnica de Catalunya, Barcelona, Spain.

24. Romero E, Vaunat J (2000) Retention curves of deformable clays. Experimental Evidence and Theoretical Approaches in Unsaturated Soils 91-106.

25. Romero E, Della Vecchia G, Jommi C (2011) An insight into the water retention properties of compacted clayey soils. *Géotechnique* 61(4):313-328. https://doi.org/10.1680/geot.2011.61.4.313

26. Russo G, Modoni G (2013) Fabric changes induced by lime addition on a compacted alluvial soil. Géotechnique Lett 3(2):93-97. https://doi.org/10.1680/geolett.13.026

27. Sun WJ, Cui, YJ (2020) Determination of soil water retention curve by mercury intrusion porosimetry tests with consideration of soil volume change. J Rock Mech Geotech Eng 12(5):1070-1079. https://doi.org/10.1016/j.jrmge.2019.12.022

28. Tang AM, Vu MN, Cui YJ (2011) Effects of the maximum soil aggregates size and cyclic wetting-drying on the stiffness of a lime-treated clayey soil. Géotechnique 61(5):421-429. https://doi.org/10.1680/geot.SIP11.005.

29. Tedesco DV, Russo G (2008) Time dependency of the water retention properties of a lime stabilised compacted soil. In: Toll, et al. (EDs), Unsaturated Soils: Advances in Geo-Engineering. 2008 Taylor & Francis Group, London, pp. 277-282. (ISBN 978-0-415-47692-8).

30. Tran TD, Cui YJ, Tang AM, Audiguier M, Cojean R (2014) Effects of lime treatment on the microstructure and hydraulic conductivity of Héricourt clay. J Rock Mech Geotech Eng 6(5):399-404. https://doi.org/10.1016/j.jrmge.2014.07.001

31. Wang YJ, Cui YJ, Tang AM, Tang CS, Benahmed N (2015) Effects of aggregate size on water retention capacity and microstructure of lime-treated silty soil. Géotechnique Lett 5(4):269-274. https://doi.org/10.1680/jgele.15.00127

32. Wang YJ, Cui YJ, Tang AM, Tang CS, Benahmed N (2016) Changes in thermal conductivity, suction and microstructure of a compacted lime-treated silty soil during curing. Eng Geol 202:114-121. https://doi.org/10.1016/j.enggeo.2016.01.008

33. Wang YJ, Duc M, Cui YJ, Tang AM, Benahmed N, Sun WJ, Ye WM (2017) Aggregate size effect on the development of cementitious compounds in a lime-treated soil during curing. Appl Clay Sci 136:58-66. https://doi.org/10.1016/j.clay.2016.11.003

34. Wang YJ, Cui YJ, Benahmed N, Tang AM, Duc M (2020) Changes of small strain shear modulus and suction for a lime-treated silt during curing. Géotechnique 70(3):276-280. https://doi.org/10.1680/jgeot.18.T.018

35. Ying Z, Cui YJ, Benahmed N, Duc M (2020) Changes in mineralogy and microstructure of a lime-treated silty soil during curing time. 4th European Conference on Unsaturated soils. Lisbon. 2020.

36. Ying Z, Duc M, Cui Y J, Benahmed N (2021) Salinity assessment for salted soil considering both dissolved and precipitated salts. Geotech. Test. J. 44(1):130-147.

Ying, Z., Cui, Y.J., Benahmed, N., Duc, M. 2021. Construction and Building Materials, 303: 124564. Doi.org/10.1016/j.conbuildmat.2021.124564.

Investigating the salinity effect on water retention property and microstructure changes along water retention curves for lime-treated soil

Zi Ying[1], Yu-Jun Cui[1], Nadia Benahmed[2], Myriam Duc[3]

Abstract: Lime treatment is a widely applied technique in improving the workability and geotechnical properties of soil. The water retention property and microstructure are highly related to the hydro-mechanical behaviour of unsaturated lime-treated soil. In this study, the water retention property and the evolution of pore size distribution (PSD) along the water retention curves (during drying) were studied for a lime-treated soil, with emphasis put on the curing time and salinity effects. Two soil powders with different soil salinities were prepared and stabilised by 2% lime. The chilled-mirror dew-point hygrometer and the contact filter paper method were used to measure the total and matric suctions, respectively. The PSD of lime-treated soil at various water contents was obtained using mercury intrusion porosimetry (MIP). Results showed that the matric suction increased significantly, while the total suction varied slightly during curing. At a given curing time, the specimens with higher salinity exhibited higher matric and total suctions. The difference between the soil water retention curves (SWRCs) determined by the filter paper method and from the PSD became more significant at longer curing time, as the production of cementitious compounds did not contribute to the SWRC from PSD, but contributed to the increase of matric suction measured by the filter paper method. The PSD of lime-treated soil changed from bi-modal characteristics (w > 14%) to tri-modal pattern ($w \approx 8\%$), and finally recovered to bi-modal characteristics ($w \approx 3\%$), due to the shrinkage-related cracking of the clay fraction. The lime treatment inhibited the clay shrinkage, whereas the curing time and salinity effects on the drying-induced microstructure were insignificant.

Keywords: lime-treated soil; salinity; total suction; matric suction; microstructure

[1]: Ecole des Ponts ParisTech, Laboratoire Navier/CERMES, 6 – 8 av. Blaise Pascal, Cité Descartes, Champs-sur-Marne, 77455 Marne-la-Vallée cedex 2, France
[2]: INRAE, Aix Marseille Univ, Unité de Recherche RECOVER, 3275 route Cézanne, CS 40061, 13182 Aix-en-Provence, France
[3]: Université Gustave Eiffel, IFSTTAR/GERS/SRO, 14-20 boulevard Newton, Champs-sur-Marne, 77447 Marne-la-Vallée, France

1. Introduction

From a socio-economic point of view, there is an increasing need of using local soils in geotechnical and geo-environmental constructions such as embankments, dikes, slopes and municipal waste barriers. However, when the natural soils involved have low physical and mechanical properties and cannot be directly used in the constructions, lime treatment is often applied to improve the workability and the mechanical properties of soils through a series of physical-chemical reactions, including lime hydration, cation exchanges and long-term pozzolanic reaction [1-3].

The water retention property describing the relationship between suction and either water content or degree of saturation was widely used to predict the permeability [4,5], shear strength [6], deformation [7] for unsaturated soils. It is also an important factor affecting the hydro-mechanical behaviour of lime-treated soils. In general, the lime addition first resulted in the flocculation of soil particles, forming coarser aggregates with larger macro-pores [8]. During curing, the cementitious compounds produced from the pozzolanic reaction coated the surface of aggregates and filled some pores, leading to the reduction of pore size and interconnectivity [9–13], giving rise to higher water retention property and mechanical performance of lime-treated soil. The production of cementitious compounds was affected by the existence of salts in soil. Ramesh et al. [14] reported that the sodium salts in fly ash-lime mixtures could promote the formation of sodium calcium silicate hydrate as compared to calcium silicate hydrate. Saldanha et al. [15] found that 1% NaCl was the optimum salt content in lime-treated soil, while a higher concentration would decrease the rate of lime dissociation. Nevertheless, Xing et al. [16] indicated that the Al^{3+} and Ca^{2+} ions in cemented salt-rich soil improved the formation of cementitious compounds, while the Mg^{2+}, Cl^{-} and SO_4^{2-} ions impeded such formation.

The soil water retention curves (SWRCs) can be determined experimentally by the chilled-mirror dew-point hygrometer [17] and non-contact filter paper method [18,19] for the total suction measurement, as well as by contact filter paper method [19], insertion tensiometer [20] and axis-translation technique [21,22] for the matric suction measurement. The SWRCs in terms of matric suction can be also derived from the pore size distribution (PSD) curves obtained from mercury intrusion porosimetry (MIP) test [5]. However, some difference between the SWRCs from direct measurements and from MIP tests was often observed. This difference was mainly attributed to the volume change due to suction changes, because the SWRC determined directly involved the effect of volume change, while the SWRC derived from MIP

test did not [9,23,24].

In most cases, the lime-treated soils are exposed to natural environment and unavoidably subjected to water evaporation effect. Drying can generate soil shrinkage and desiccation cracks, which might have a detrimental effect on the sustainability of infrastructures. For the compacted untreated soil, under the effect of drying, the frequency and modal size of macro-pores decreased while the frequency of micro-pores increased, due to the clay shrinkage that transformed some macro-pores to micro-pores [25–29]. Stoltz et al. [30] found that the lime treatment did not prevent the soil shrinkage. However, Nabil et al. [31] and Poncelet and François [32] indicated that the lime treatment would reduce the shrinkage potential and attenuated the propagation of desiccation macro-cracks of silty clay, due to the formation of cementitious compounds limiting the development of cracks.

It appears from the aforementioned studies that although the water retention property and desiccation cracks of lime-treated soils were investigated, few attention has been paid to the salinity effect on the water retention property during curing and to the changes of microstructure along the water retention curve (during drying) for lime-treated soil. However, while dealing with constructions involving salted soils, the salinity effect becomes an essential parameter for the assessment of the effectiveness of lime treatment. This constitutes the main objective of this study. In this paper, the chilled-mirror dew-point hygrometer (WP4C) and the contact filter paper (FP) method were employed to determine the SWRCs of lime-treated soil with different salinities. The evolution of PSD along SWRC was investigated by MIP tests. The SWRCs were also derived from PSD curves, for the purpose of comparison with the direct measured ones. The results obtained revealed the different evolution of matric suction and total suction with curing time, and the effect of microstructure changes on SWRC during drying, for lime-treated soil with different salinities.

2. Materials and methods

2.1 Materials

The soil used was a plastic silt, taken from Les Salins de Giraud in southern France, which was used for a dike construction. This natural soil (w = 15.6%) was saline with soil salinity of 2.1‰ (g of salt/kg of dry soil) and water salinity of 13.3‰ (g of salt/kg of salty water) [33]. The geotechnical properties are presented in Table 1. As shown in Fig. 1, this soil contains 17%

clay-size particles, 53% silt and 30% fine sand. X-Ray diffraction (XRD) analysis shows that the soil is composed of 15.7% clay minerals and 84.3% non-clay minerals. The non-clay minerals are identified as 39% quartz, 35% calcite, 9.5% feldspar and 0.8% halite NaCl, and the clay minerals consists of 10.8% illite, 3.6% chlorite and 1.3% kaolinite. The main ion species in soil pore water are Cl^-, Na^+, K^+, Ca^{2+}, and Mg^{2+}, which are similar to the salt composition of synthetic seawater. Thus, to prepare the salted soil, five different salts of synthetic seawater were used according to the French standard [34], as shown in Table 2. The target soil salinity of salted soil was selected as 6.8‰ (g of salt/kg of dry soil) which corresponded to the water salinity of 34‰ (g of salt/kg of salty water) for soil at 20% water content. This water salinity was exactly the salinity of synthetic seawater. More details about the salted soil preparation can be found in Ying et al. [33]. The natural saline soil (r' = 2.1‰) and salted soil (6.8‰) were air-dried, ground and passed through 0.4 mm sieve.

Table 1. Characteristics of the tested soil.

Property	Value
Liquid limit, w_L (%)	29
Plastic limit, w_p (%)	19
Plasticity Index, I_p	10
Specific gravity, *Gs*	2.71
Specific surface area (m^2/g)	24

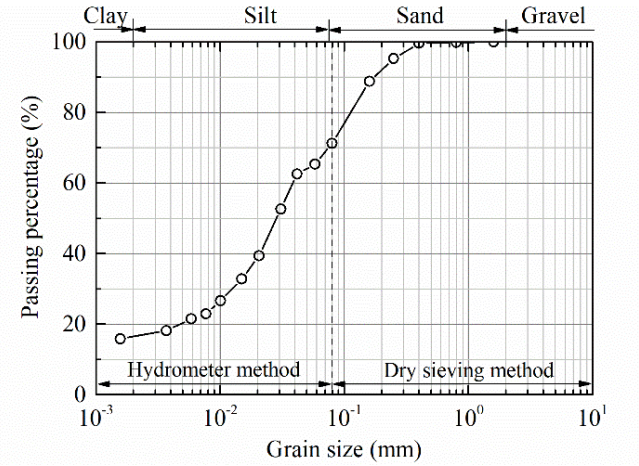

Fig. 1. Grain size distribution of the tested soil.

Table 2. Salt composition of synthetic seawater.

Salts	NaCl	$MgCl_2 \cdot 6H_2O$	$MgSO_4 \cdot 7H_2O$	$CaSO_4 \cdot 2H_2O$	$KHCO_3$
Concentration (g/L)	30.0	6.0	5.0	1.5	0.2

A quicklime with CaO content as high as 97.3% was used as additive. Based on the dosage applied for the construction of dike at Les Salins de Giraud, a lime content of 2% by weight of dry soil was selected.

To prepare the soil specimen, the dry soil powder was first mixed with lime and then humidified by deionized water to obtain the target water content (w = 17%). According to the proctor compaction curve of lime-treated natural soil with soil salinity of 2.1‰ (Fig. 2), all the specimens with different soil salinities were statically compacted to the same dry density (1.63Mg/m^3). A compaction rate of 0.3 mm/min was adopted. After compaction, the specimens were wrapped by plastic film and scotch tape, covered by wax, confined in a hermetic box and cured for different times.

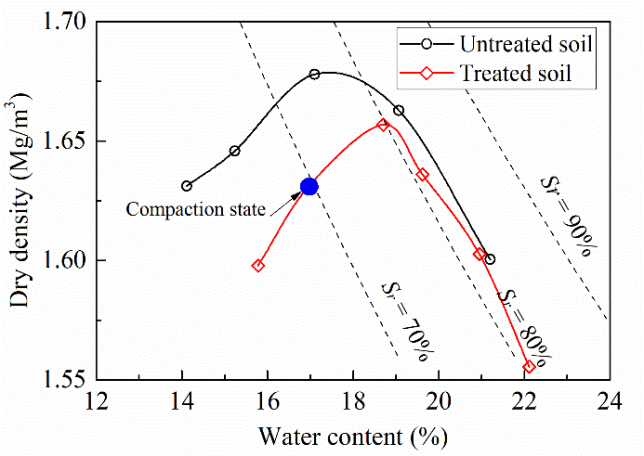

Fig. 2. Proctor compaction curves of untreated and lime-treated soils with soil salinity of 2.1‰.

2.2 Test methods

The soil total suction was determined by WP4C device [17]. The specimen (38 mm in diameter and 100 mm in height) was cut into several small pieces at given curing time. Each small piece was air-dried for different durations to reach different water contents. Then, they were covered and stored for one night for water homogenization. Afterwards, one small piece was put into the WP4C device for total suction measurement. Immediately after suction measurement, the

small piece was oven-dried to determine the water content.

Matric suction was measured using contact filter paper method [19]. At given curing time, the lime-treated specimens (50 mm in diameter and 20 mm in height) were air-dried for different times to reach different target water contents, in order to obtain the soil specimens with different matric suctions. During drying, the water contents of specimens were controlled by weighing the masses of specimens. Once the target water content reached, the three stacked filter papers were sandwiched between two specimens with the same water content for one matric suction measurement. Two replicated tests were conducted and the mean value was used.

After matric suction measurement, one specimen was directly oven-dried to determine its water content, while the second one was cut into small pieces for the MIP test. The small pieces were rapidly frozen using vacuumed liquid nitrogen, and lyophilised following the procedure proposed by Delage and Lefebvre [35]. Then they were subjected to MIP test.

In the MIP test, the entrance pore diameter can be deduced from the mercury intrusion pressure according to Laplace's law and a relationship between mercury and water can be established:

$$d = -\frac{4T_m \cos\theta_m}{p_m} = \frac{4T_w \cos\theta_w}{p_w} \tag{1}$$

where subscript m denotes mercury while subscript w denotes water; T is the surface tension (T_w = 0.073 N/m, T_m = 0.485 N/m); p_m is the mercury intrusion pressure; p_w is the soil matric suction; θ is the contact angle ($\theta_w = 0°$, $\theta_m = 130°$).

The pore size density function can be determined as follows [36]:

$$f(\log r_i) = \frac{dv_i}{d(\log d)} \tag{2}$$

where $f(\log r_i)$ is the frequency of density function; dv_i is the intruded mercury volume at a given incremental intrusion pressure. The intruded mercury volume can be transformed to the intruded void ratio by multiplying the density of soil particles.

The matric suction can be deduced from entrance pore diameter:

$$p_w = \frac{4T_w \cos\theta_w}{d} \tag{3}$$

The corresponding water content of soil specimens can be obtained from MIP results [24,37]:

$$w_{MIP} = (1 - S_{rm})(w_{sat} - w_r) + w_r = \frac{e}{G_S}(1 - \frac{e_{MIP}}{e}) \quad (4)$$

where S_{rm} is the saturation degree of mercury; w_{sat} is the water content at saturation; w_r is the residual water content; e is the global void ratio of compacted specimens; e_{MIP} is the mercury intruded void ratio; G_s is the specific gravity.

Based on the matric suction and water content calculated by Eqs. (3) and (4), the water retention curves can be deduced from the pore size distribution curves.

3. Results

3.1 Water retention property

The SWRCs in terms of total and matric suctions are depicted in Figs. 3a and 3b for lime-treated specimens with soil salinities of 2.1‰ and 6.8‰, respectively. Note that the data of lime-treated specimens with 2.1‰ at curing times of 1-, 28- and 90-day were reported previously in Ying et al. [38]. It appears that the curing time had insignificant effect on the SWRCs of total suction, whereas the SWRCs of matric suction shifted rightwards with the increase of curing time from 28 days to 90 days. This suggested that the effect of curing time on the water retention property of lime-treated saline soil was mainly reflected on the changes in matric suction rather than total suction. The difference between the total and matric suctions can be considered as osmotic suction which was resulted from the dissolved salts in soil pore water [39]. As the total suction varied slightly while the matric suction increased significantly with increasing curing time, the osmotic suction of lime-treated specimens seemed to decrease over curing. With decreasing water content, the SWRCs of matric suction converged gradually to the total suction curves. This was consistent with the results of untreated soil obtained by Sreedeep and Singh [39] and Arifin and Schanz [40].

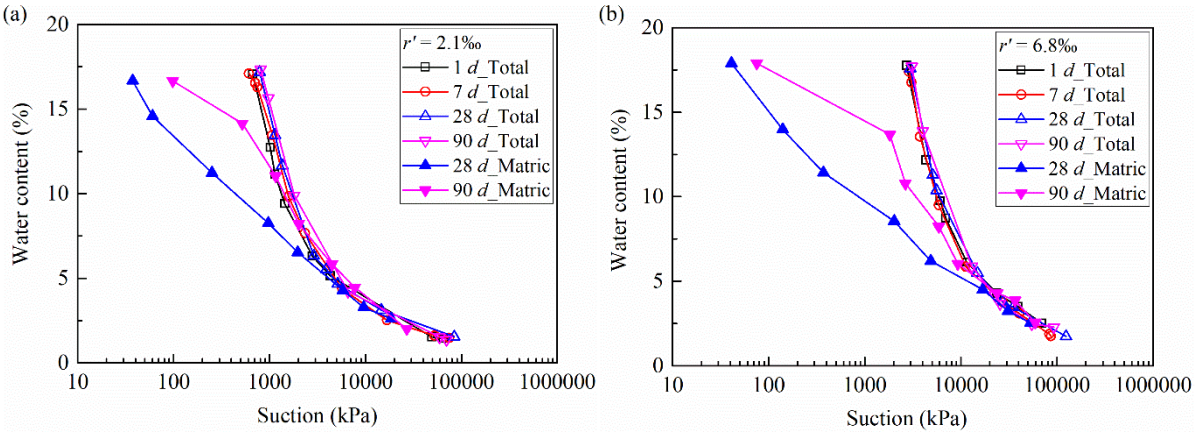

Fig. 3. Water retention curves in terms of total and matric suctions for the lime-treated specimens: (a) r' = 2.1‰; (b) r' = 6.8‰.

The SWRCs of total and matric suctions for the lime-treated specimens with different salinities of 2.1‰ and 6.8‰ are presented in Fig. 4a for the specimens at 28-day curing, and in Fig. 4b for the specimens at 90-day curing. It can be observed that, at a given water content, the total suction increased significantly with increasing soil salinity, which can be attributed to the contribution of higher osmotic suction for the specimens with higher soil salinity (6.8‰ against 2.1‰). The matric suction of lime-treated specimens also increased with increasing soil salinity, which was different from the results of untreated soil that the salinity had negligible effect on the matric suction [41–43].

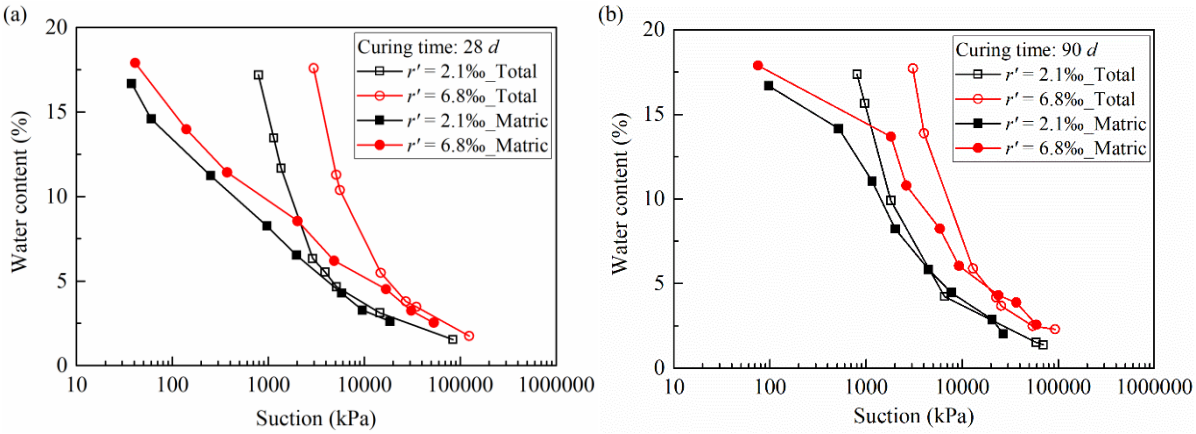

Fig. 4. Salinity effect on the total and matric suctions for the lime-treated specimens: (a) t = 28 days; (b) t = 90 days.

3.2 Microstructure variations along SWRCs

The PSD curves in terms of density function are presented in Figs. 5a and 5b for the specimens cured for 28 days with 2.1‰ soil salinity, and in Figs. 5c and 5d for the specimens at curing

time of 90 days with soil salinities of 2.1‰ and 6.8‰, respectively. Three pore populations of micro-pores, meso-pores and macro-pores can be defined. The boundary between the meso-pores and macro-pores was considered as 3 μm, which was at the minima of PSD curves between two peaks for all the specimens. The delimiting diameter between micro-pores and meso-pores was chosen as 0.5 μm which corresponded to the minima between the two peaks of micro-pores and meso-pores for the specimens at around 8% water content in which the drying-induced micro-pores and meso-pores were well-developed. As shown in Fig. 5a, the as-compacted specimens (w = 17.1%) exhibited bi-modal pore size distribution with two dominant peaks. Upon drying to water content of 14.4% and 11.2%, the peak pore entrance diameter between micro-pores and meso-pores decreased from 0.7 μm to 0.6 and 0.5 μm, while the modal size of macro-pores increased from 5.3 μm to 6.1 μm and 8.2 μm (Fig. 5a). Moreover, an interesting phenomenon was identified from Fig. 5a: a third peak at diameters ranging from 0.9 μm to 3 μm started to appear on the PSD curves of specimens at water content of 11.2%. With drying to 8.3% water content, the two peaks of micro-pores and meso-pores were well developed and the PSD exhibited tri-modal characteristics (Fig. 5b). Upon further drying from 8.3% to 6.5%, the peak frequency ($de_m/d(logd)$) of micro-pores decreased gradually, and the peak of micro-pores disappeared as the specimen was air-dried to 3.3% water content. As shown in Figs. 5c and 5d, the similar evolution trends of PSD during drying were observed for the lime-treated specimens at 90-day curing time with soil salinities of 2.1‰ and 6.8‰: the pore size distribution changed from bi-modal pattern for specimens at higher water content (w > 14%) to tri-modal pattern with drying close to 8% water content; it finally recovered to bi-modal pattern with further drying (w ≈ 3%) as the peak of micro-pores disappeared for both specimens at 90-day curing (r' = 2.1‰ and 6.8‰), in similar manner to the specimens at 28-day curing.

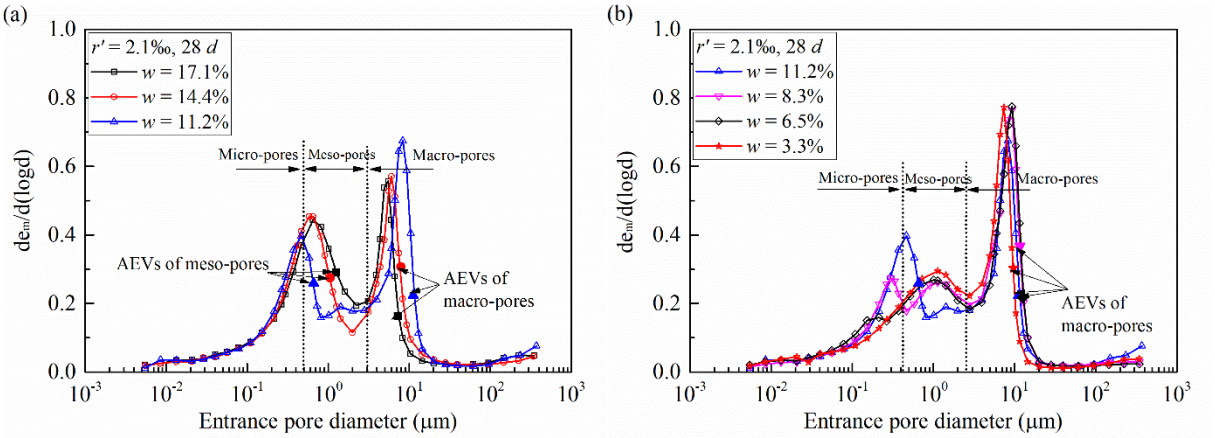

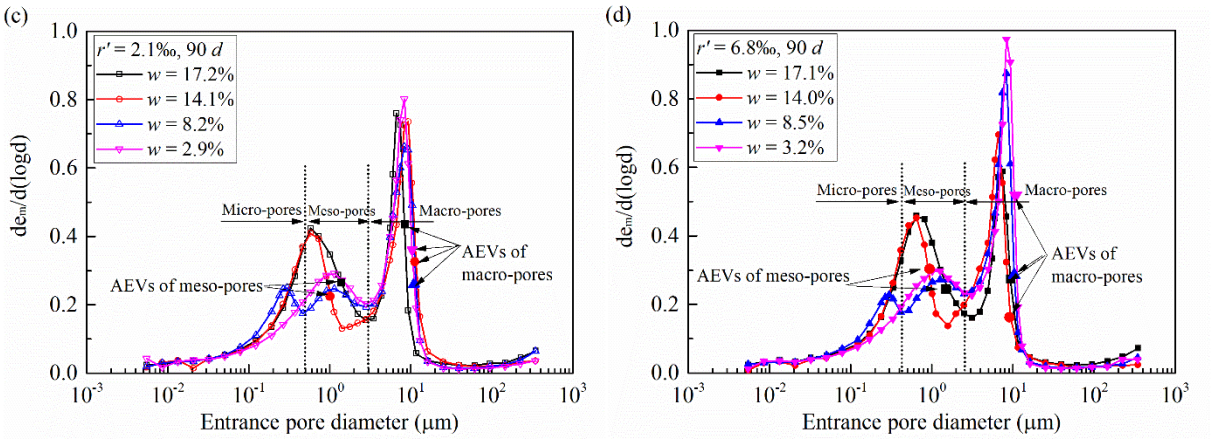

Fig. 5. Pore size distribution of lime-treated specimens during drying: (a) r' = 2.1‰, t = 28 days ($w \geq$ 11.2%); (b) r' = 2.1‰, t = 28 days ($w \leq$ 11.2%); (c) r' = 2.1‰, t = 90 days; (d) r' = 6.8‰, t = 90 days.

Figure 6 shows the variations of void ratio of different pore populations (micro-, meso- and macro-pores) during drying. The global void ratio and water ratio (water volume over solid volume, $e_w = wG_s$, where w is the water content and G_s is the specific gravity) are also presented for comparison. The stacked value of micro-pores, meso-pores and macro-pores represented the total intruded void ratio. For most specimens, the total intruded void ratio coincided well with the global one. Romero et al. [29] and Wan et al. [44] indicated that the smaller pores would be saturated before water began to be stored in the larger pores. Thus, it can be observed that the micro-pores and meso-pores were saturated before drying, as the water ratio was higher than the sum of void ratio of micro-pores and meso-pores at water content of 17% (Fig. 6). During drying, the water ratio decreased gradually, indicating that water withdrew toward the smaller pores. It appears from Fig. 6a that the void ratio of micro-pores increased when the specimens (r' = 2.1‰, t = 28 days) were dried to 11.2% water content, then it decreased with decreasing water content to 3.3%. By contrast, the void ratio of meso-pores decreased, then increased during drying. The void ratio of macro-pores increased with drying to around 8%, then kept almost constant with further drying. As for the specimens (r' = 2.1‰) at 90-day curing (Fig. 6b), the void ratio of micro-pores, meso-pores and macro-pores exhibited similar variations to the specimens at 28-day curing time (Fig. 6a). Concerning the specimens with higher salinity (r' = 6.8‰, t = 90 days), it appears from Fig. 6c that drying had slight effect on the micro-pore void ratio, while it led to a decrease of meso-pore void ratio and an increase of macro-pore void ratio.

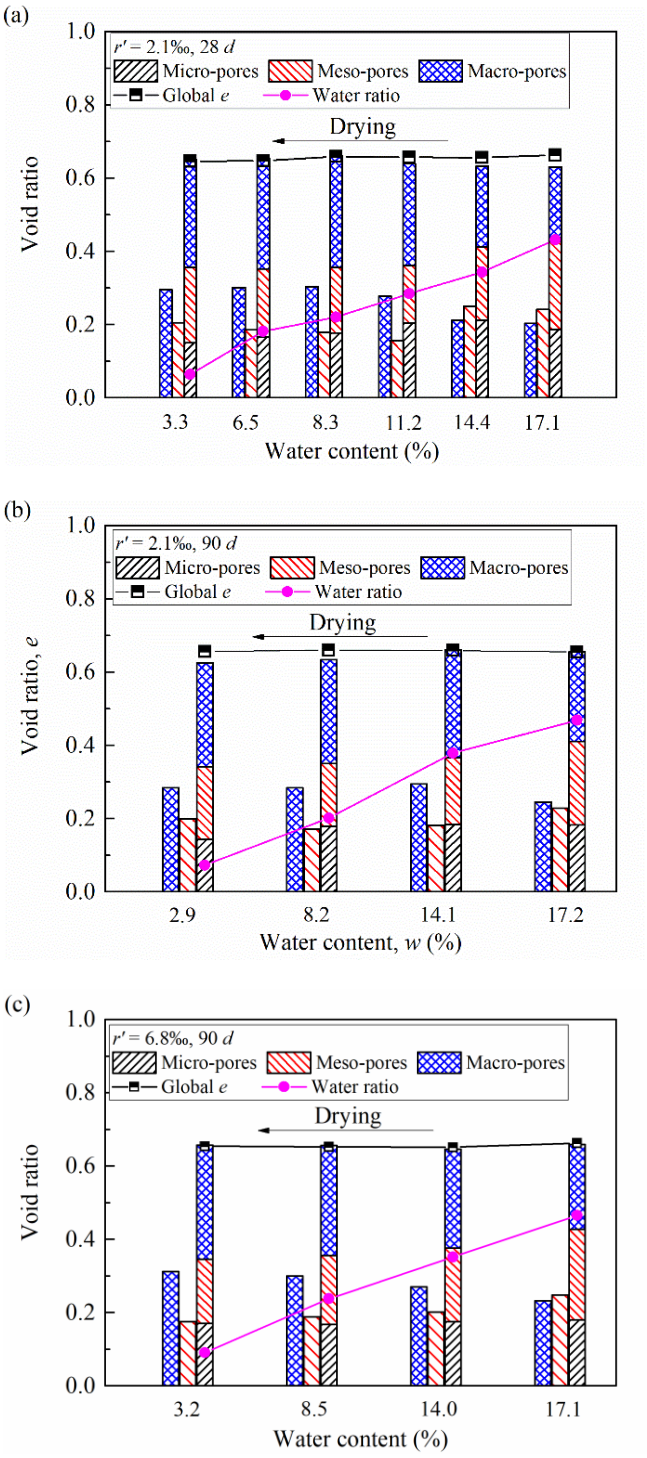

Fig. 6. Variations of void ratio of different pore populations during drying: (a) r' = 2.1‰, t = 28 days; (b) r' = 2.1‰, t = 90 days; (c) r' = 6.8‰, t = 90 days.

The PSD curves of lime-treated soil (r' = 2.1‰) at different curing times are plotted in Figs. 7a and 7b for the specimens at around 8% and 3% water contents respectively. The PSD curves of untreated specimens are also presented for comparison. It appears that, as for the specimens at water content of around 8%, the PSD curves of lime-treated soil at curing times of 28-day and

90-day were almost overlapped, while the curve of untreated soil deviated from that of lime-treated soil. Specifically, the modal sizes of micro-pores and macro-pores were almost identical for untreated and lime-treated specimens, whereas the modal size of meso-pores of lime-treated specimens was smaller than that of untreated specimens. Besides, the lime-treated specimens exhibited a smaller frequency of micro-pores and a higher frequency of macro-pores. As for the specimens at around 3% water content, the PSD curves of lime-treated specimens (t = 28 days and 90 days) exhibited similar modal sizes of meso-pores and macro-pores, while the PSD curves of untreated specimen shifted rightwards slightly, giving rise to larger modal sizes.

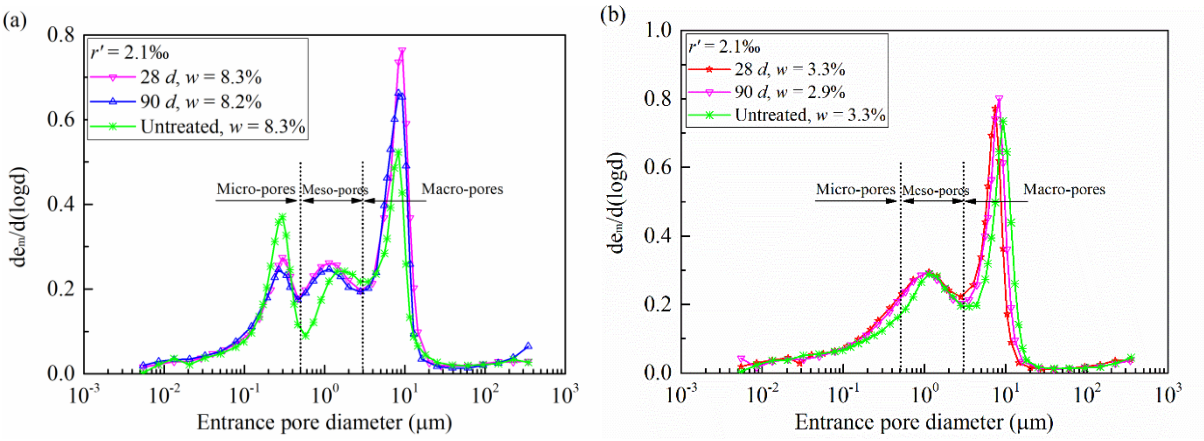

Fig. 7. Lime treatment effect on the pore size distribution of untreated and lime-treated specimens after drying: (a) $w \approx 8\%$; (b) $w \approx 3\%$.

Figure 8 depicts the PSD curves of lime-treated specimens (t = 90 days) with different salinities, but similar water contents ($w \approx 8\%$ in Fig. 8a and $w \approx 3\%$ in Fig. 8b). It can be observed that the salinity effect on the entrance diameter of peak pores was slight, but the salinity had a low but visible effect on the frequencies of peak pores. Specifically, higher frequencies of meso-pores and macro-pores were observed for specimens with higher salinity of 6.8‰ at 8% water content. For specimens at 3% water content, the frequency of meso-pores was rather similar for different salinities, while the frequency of macro-pores was found higher for 6.8‰ soil salinity.

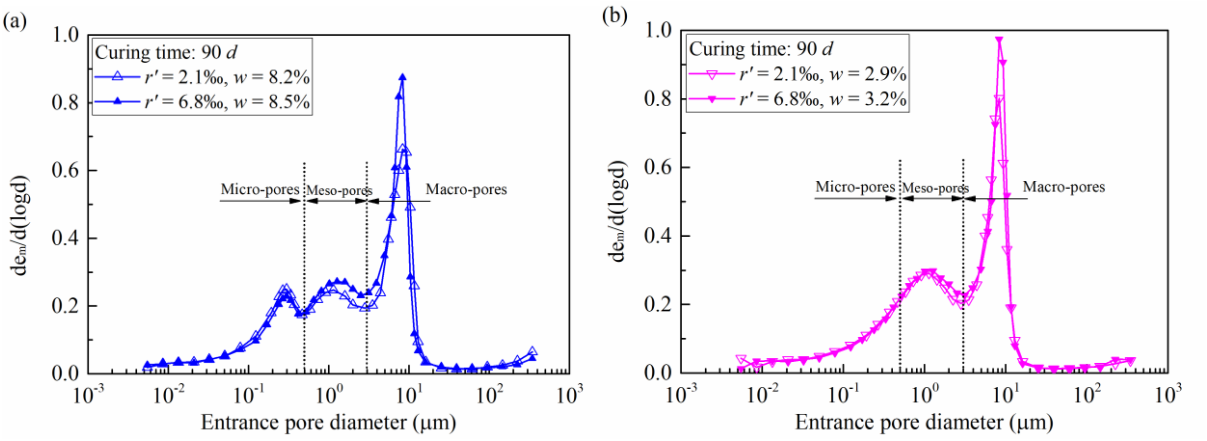

Fig. 8. Salinity effect on the pore size distribution for the lime-treated specimens after drying: (a) $w \approx 8\%$; (b) $w \approx 3\%$.

4. Discussions

4.1 Water retention capacity

Based on the PSD curves, the SWRCs of lime-treated specimens were deduced and presented in Figs. 9a and 9b for the specimens at 28-day and 90-day curing, respectively. The SWRCs of specimens at different water contents derived from the MIP tests are shown in dash/dot lines (MIP), and the curves of matric suction which was measured by filter paper method are presented in hollow signs (FP). It is observed that the SWRCs (MIP) of specimens at water content higher than 14% were characterized by two air entry values (AEVs) at suctions in the ranges of 30 ~ 40 kPa and 200 ~ 300 kPa, respectively. The corresponding entrance pore diameters at AEVs are shown in Fig. 5. It indicates that the two AEVs corresponded to the points at which the density function curves of macro-pores and meso-pores increased dramatically. With drying (w < 14%), only one AEV of macro-pores at low suction could be observed, while the AEV of meso-pores was not obvious due to the enlargement of meso-pores which exhibited a relatively lower increase in density function. It appears from Fig. 9b that the salinity effect on the SWRCs (MIP) was insignificant, whereas the specimens with higher soil salinity had relatively higher matric suctions measured by the filter paper method. Comparison between the SWRCs in Figs. 9a and 9b indicates that the curing time had insignificant effect on the SWRCs derived from the MIP results, which was different from the matric suction measured by filter paper method that increased noticeably as curing time increased from 28 days to 90 days (Fig. 3). Thus, a larger difference between the SWRCs from MIP tests and from filter paper measurements was observed for specimens at 90-day as compared to those at 28-

day curing. Wang et al. [9] and Sun and Cui [24] attributed this difference to the effect of volume change: the curve from MIP results did not include any effect of volume change, while that determined directly using filter paper method for suction measurement did. Indeed, as explained in the materials and methods section, each SWRC that consisted of several points in terms of matric suction versus water content, was derived from the MIP result of one specimen without considering the volume change. The points of specimens at different water contents (during drying) can be selected on the SWRCs (MIP) at the corresponding water contents and these points constituted the SWRCs in solid signs, namely SWRCs (MIP at each *w*). These SWRCs were considered involving the microstructure variations, as these points corresponded to different specimens during drying but not from one specimen. Nevertheless, these SWRCs (MIP at each *w*) were also different from the ones directly measured by the filter paper method.

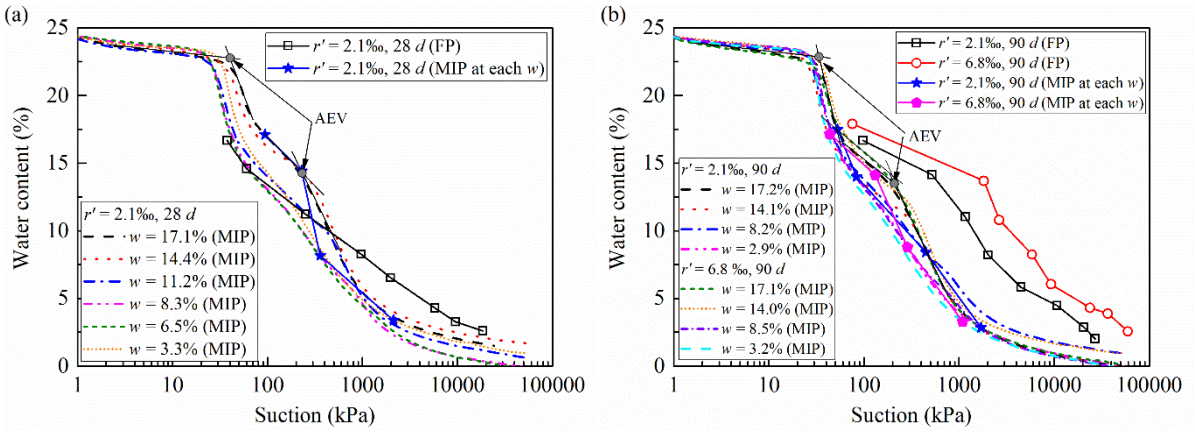

Fig. 9. Water retention curves in terms of matric suction from MIP tests and by filter paper method for suction measurement: (a) t = 28 days; (b) t = 90 days.

It appears from Eq. (3) that the value of the contact angle between the water-soil interface and the value of the surface tension of soil pore water might affect the matric suction deduced from the MIP results. The water-soil contact angle, θ_w, was widely taken as zero, assuming that the soil was a perfect hydrophilic material [45–48]. Li et al. [49] indicated that, when the contact angle of soil-water interface was taken as 70° and 50° for the wetting and drying process of loess, the SWRCs derived from MIP results agreed well with the measured ones. It was noting that the larger the contact angle, the lower the matric suction. As a result, a larger difference between the water retention curves derived from MIP results and filter paper measurement was obtained if a higher value of contact angle (> 0°) was taken. Sghaier et al. [50] and Leelamanie [51] indicated that the surface tension (T) and the contact angle (θ) increased with increasing salt concentration. However, the product of $T\cos\theta$ did not change appreciably with the salt

concentration. This suggested that the salinity effect on the surface tension and contact angle was not the main reason for the difference between the SWRCs derived from MIP results and filter paper measurement.

Romero et al. [5,29] indicated that the water retention property was dominated by the capillary force in low suction range, whereas the adsorptive force was the important factor in high suction range. The capillarity was highly related to the soil mineralogy and pore size distribution [52,53], while the adsorption was associated with soil mineralogy [52] and the specific surface area of the clayey fraction [54,55]. Tuller and Or [55] reported that the soil with higher specific surface area presented higher water adsorption capacity. The specific surface area of lime-treated soil was found to increase over curing time as the cementitious compounds were produced in the long-term reaction [56-58]. Muller [59] calculated the specific surface area of cementitious compounds (C-S-H) in cement paste using the results from Nuclear Magnetic Resonance (NMR) test. It was reported that the specific surface areas were 91 m^2/cm^3 for C-S-H gel pores and 175 m^2/cm^3 for interlayer spaces [59], which were higher than that of untreated soil. Ying et al. [60] performed XRD tests on the lime-treated soil (the same silt as in this study) and reported that the hydrated lime decreased from 2.1% at 1-day curing to 1.9% at 90-day curing, suggesting that the soil-lime reaction was developed and small amount of cementitious compounds was produced in this kind of silt. Thus, the difference between the water retention curves derived from MIP results and measured by contact filter paper method could be mainly attributed to the production of cementitious compounds which could improve the water adsorption capacity of soils. However, the cementitious compounds had slight effect on the PSD, and hence the SWRCs derived from MIP results. This was due to the low quantity of cementitious compounds which could only coat some surfaces of aggregates, leading to a slight decrease of micro-pores for this studied silt [38]. The longer the curing time, the more the production of cementitious compounds, thus the higher the matric suction measured. Therefore, the difference between the matric suctions from the filter paper measurement and derived from MIP results increased with increasing curing time from 28 days to 90 days. Moreover, at given curing time, this difference was larger for lime-treated soil with higher soil salinity (6.8‰ against 2.1‰). By contrast, it was found that the salinity had no or negligible effect on the matric suction of untreated soil, such as compacted kaolin and residual soil [22], fine sandy silt [41], and fine-grained soil [42]. This suggested that the increased matric suction of lime-treated soil with higher salinity might be due to the promotion of cementitious compounds production by salts.

Unlike the matric suction, the total suction did not exhibit significant changes over curing time, while it increased appreciably as the soil salinity increased (Figs. 3 and 4). Note that the total suction was determined through the measurement of relative humidity [17,21,22]. Leong et al. [22] measured the relative humidity of filter papers which were soaked with distilled water or sodium chloride (NaCl) solutions, and reported that the relative humidity decreased with the increase of salt concentration. This explains why the total suction which was composed of both matric and osmotic suctions increased significantly as soil salinity increased (Fig. 4). Al-Mukhtar et al. [61] stated that the electrical conductivity of soil-lime mixtures decreased during curing due to the cation exchanges and the consumption of Ca^{2+} and OH^- in the long-term pozzolanic reaction, suggesting that the osmotic suction of lime-treated specimens should decrease during curing. In addition, Hamidi et al. [62] reported that the precipitation of $CaCO_3$ and $Mg(OH)_2$ could occur in alkaline environment, consuming the Ca^{2+} and Mg^{2+} ions in soil pore water. Thus, at given water content, the insignificant effect of curing time on total suction can be attributed to the balance between the increased matric suction resulted from the production of cementitious compounds and the decreased osmotic suction due to the consumption of salts. Furthermore, upon drying, the matric suction increased, while the osmotic suction decreased due to the precipitation of salts, making the matric suction curves converge to the total suction curves at low water content (Fig. 3).

4.2 Microstructure

The MIP results showed that the PSD varied significantly during drying despite the similar global void ratio of specimens (Figs. 5 and 6). This can be attributed to the large amount of silt/sand grains (83%) constituting the skeleton of compacted specimens which can maintain the macro-pores and the global volume unchanged during drying. Indeed, Shi and Zhao [63] indicated that, for the soil with low clay fraction, the behaviour was dominant by the silt/sand grains. The association of silt/sand skeleton and clay film constituted soil aggregates. The macro-pores corresponded to the porosity between aggregates, and the micro-pores and meso-pores were related to the porosity of clays on the surface of these aggregates. The shrinkage of clay fraction led to an enlargement of the pore size between the aggregates on the one hand, and induced the development of some fissures in the clay fraction and at the interface between clay and silt/sand grains on the other hand [64–66]. Therefore, with the specimens being dried to 11.2% water content, the following phenomena were observed (Fig. 5): the peak pore entrance diameter between the micro-pores and meso-pores decreased as the nano-fissures (micro-pores) developed; a dominant peak of meso-pores started to emerge at around 1.5 μm

as some initial relative smaller meso-pores or micro-pores of the clay fraction became larger; the modal size of macro-pores enlarged and its frequency increased due to the enlargement of inter-aggregate pores which might be meso-pores initially. Correspondingly, the void ratio of micro-pores increased with the development of nano-fissures, while the void ratio of meso-pores decreased and that of macro-pores increased with decreasing water content to 11% due to the prevailing enlargement of meso-pores to macro-pores rather than the evolution of micro-pores to meso-pores (Fig. 6). Upon drying to 8% water content, the tri-modal pattern with populations of micro-pores, meso-pores and macro-pores was well formed, in which the micro-pores were mostly composed of drying-induced fissures. With further drying, the drying-induced fissures became larger and larger due to the continuous shrinkage of clay fraction, making the peak of micro-pores disappear gradually and the frequency of meso-pores increase (Fig. 5). Thus, the void ratio of micro-pores decreased, while the void ratio of meso-pores increased upon drying from 11.2% to 3.3% water content (Fig. 6).

When soil, lime and water were mixed together, the cation exchanges took place rapidly, making soil particles flocculate and forming coarser aggregates [1,3]. Bell [1,2] indicated that these modifications of soil particles induced by lime addition would largely reduce the plasticity and shrinkage of soil. Therefore, the lower frequency of drying-induced micro-pores and the smaller modal size of drying-induced meso-pores were observed on lime-treated specimens in comparison to the untreated specimens at water content of around 8% (Fig. 7a). The lime-treated specimens presented a higher frequency of macro-pores at 8% water content, which could be attributed to the flocculation of soil particles that produced more macro-pores in the lime-treated specimens. With further drying to 3% water content, the clay fraction in the untreated specimens suffered more significant shrinkage, giving rise to an increase of the frequency of macro-pores in the untreated specimens to the level of lime-treated specimens (Fig.7b). Nevertheless, the similar PSD curves were observed for the lime-treated specimens at different curing times (t = 28 days and 90 days). The insignificant effect of curing time on the drying-induced microstructure indicated that the production of cementitious compounds by pozzolanic reaction was limited due to the low reactivity of clay minerals (10.8% illite, 3.6% chlorite and 1.3% kaolinite), and inert phases of quartz (39%) and feldspar (9.5%) in the tested silt. It could not provide enough activated silica and alumina to interact with calcium to produce a significant amount of cementitious compounds. Indeed, Ying et al. [60] showed that the quantities of quartz, feldspar, illite, chlorite and kaolinite in the lime-treated soil (the same silt as in this study) after 90-day curing were rather similar to those of untreated soil, and no

significant cementitious compounds were identified through XRD analysis. Wang et al. [67] reported that the well-crystallized cementitious compounds could be identified in the lime-treated soil with large aggregates (D_{max} = 5 mm) after one year curing, while no XRD signal of cementitious compounds was detected on soil with smaller aggregates (D_{max} = 0.4 mm) due to the low quantity and low degree of crystallisation of cementitious compounds. Thus, it can be inferred that the low quantity of cementitious compounds produced in the tested silt might be in poorly-crystallized or amorphous phase that played a limited role in inhibition of clay shrinkage. This was consistent with the results obtained by Wang et al. [68], showing that the curing time effect was insignificant on the shrinkage behaviour of lime-treated soil. Ying et al. [33] indicated that, for the same silt with soil salinity of 6.32‰, some salts started to precipitate when the water content deceased to 8%, which might reduce the pore size. However, the slightly higher frequencies of macro-pores were obtained for the specimens with higher salinity (Fig. 8). This indicated that the enlargement of macro-pores due to the shrinkage of the diffuse double layer of clay minerals induced from salts prevailed over the decreased pore size due to the precipitated salts. However, this salinity effect was quite low owing to the low clay fraction (15.7%) in the tested silt [69].

5. Conclusions

The water retention property of lime-treated specimens was studied, with consideration of the curing time and salinity effects. The PSD variations in the lime-treated specimens along the SWRC were investigated by MIP tests. The difference between the SWRCs from filter paper measurement and from MIP tests was analyzed. On the basis of the results obtained, the following conclusions are drawn:

(1) The soil matric suction increased significantly during curing, due to the production of cementitious compounds which exhibited higher specific surface area, giving rise to an increase of water adsorption capacity of soils. Higher matric suctions were observed for the lime-treated specimens having higher salinity, suggesting that salts promoted the production of cementitious compounds. However, the curing time effect on the total suction was insignificant, which can be attributed to the balance between the increased matric suction and the decreased osmotic suction induced by the consumption of cations in the cation exchanges, pozzolanic reaction and salt precipitation.

(2) The SWRCs derived from MIP results of specimens at different water contents considering

the microstructure variations during drying were still different from those curves from direct measurement. This difference was mainly attributed to the production of cementitious compounds: the cementitious compounds with higher adsorption capacity did not contribute to the matric suctions derived from the MIP tests, but they significantly contributed to the matric suctions measured by the filter paper method.

(3) The PSD presented bi-modal characteristics for as-compacted specimens ($w \approx 17\%$) and air-dried specimens at water contents higher than 14%. Upon drying to 8% water content, a new peak pore developed gradually and the PSD changed to tri-modal pattern with three populations of micro-pores, meso-pores and macro-pores. With further drying to a water content of about 3%, the frequency of micro-pores decreased gradually, finally making the peak of the micro-pores disappear and the PSD recover to bi-modal characteristics. These variations of PSD could be attributed to the clay shrinkage of the clay fraction in the tested silt which was mainly constituted by silt/sand skeletons, leading to an enlargement of the meso-pore size and inducing the development of some fissures in the clay fraction and at the interface between clay and silt/sand grains.

(4) The curing time effect was found insignificant on the drying-induced microstructure changes, while the lime treatment effect was noticeable. Lime treatment resulted in rapid cation exchanges that made the soil particles flocculate and forming larger aggregates, inhibiting the clay shrinkage and attenuating the enlargement of pore size. The insignificant effect of curing time on the drying-induced microstructure could be attributed to the low reactivity of silty soil wilt lime, forming low quantity cementitious compounds that played a limited role in inhibiting clay shrinkage. The salinity effect on the drying-induced microstructure was visible but not significant, due to the low clay fraction in the tested silt.

It can be concluded that, for this lime-treated silt used for dike construction, drying resulted in shrinkage of clay fraction that altered the microstructure of soils, but did not induce the macro-cracks which could influence the sustainability of structures. The salts in synthetic seawater promoted the production of cementitious compounds which improved the water retention capacity of lime-treated soil and thus gave rise to higher resistance to climate changes, such as rainfall and water evaporation, etc. These results can be further used to interpret the hydro-mechanical behaviour of lime-treated silt.

CRediT authorship contribution statement

Zi Ying: Validation, Investigation, Writing - original draft. Yu-Jun Cui: Conceptualization, Methodology, Writing - review & editing. Nadia Benahmed: Investigation, Resources. Myriam Duc: Investigation.

Declaration of competing interest

The authors declare that they have no known competing financial interests or personal relationships that could have appeared to influence the work reported in this paper.

Acknowledgements

The authors would like to thank the China Scholarship Council (CSC). The supports provided by Ecole des Ponts ParisTech (ENPC) and INRAE are also greatly acknowledged.

References

[1] F.G. Bell, Lime stabilization of clay minerals and soils, Eng. Geol. 42 (1996) 223-237. https://doi.org/10.1016/0013-7952(96)00028-2.

[2] F.G. Bell, Lime stabilisation of clay soils, Bull. Int. Assoc. Eng. Geol. 39 (1989) 67-74. https://doi.org/10.1007/BF02592537.

[3] J. Locat, M.A. Berube, M. Choquette, Laboratory investigations on the lime stabilization of sensitive clays: shear strength development, Can. Geotech. J. 27 (1990) 294-304. https://doi.org/10.1139/t90-040.

[4] Y. Gao, Z. Li, D.A. Sun, H.H. Yu, A simple method for predicting the hydraulic properties of unsaturated soils with different void ratios, Soil Tillage Res. 209 (2021). 104913. https://doi.org/10.1016/j.still.2020.104913.

[5] E. Romero, A. Gens, A. Lloret, Water permeability, water retention and microstructure of unsaturated compacted Boom clay, Eng. Geol. 54 (1999) 117-127. https://doi.org/10.1016/S0013-7952(99)00067-8.

[6] W.S. Kim, R.H. Borden, Influence of soil type and stress state on predicting shear strength of unsaturated soils using the soil-water characteristic curve, Can. Geotech. J. 48 (2011) 1886-1900. https://doi.org/10.1139/T11-082.

[7] H. Tu, S.K. Vanapalli, Prediction of the variation of swelling pressure and one-dimensional heave of expansive soils with respect to suction using the soil-water retention curve as a tool, Can. Geotech. J. 53 (2016) 1213-1234. https://doi.org/10.1139/cgj-2015-0222.

[8] B. Le Runigo, O. Cuisinier, Y.J. Cui, V. Ferber, D. Deneele, Impact of initial state on the fabric and permeability of a lime-treated silt under long-term leaching, Can. Geotech. J. 46 (2009) 1243-1257. https://doi.org/10.1139/T09-061.

[9] Y.J. Wang, Y.J. Cui, A.M. Tang, C.S. Tang, N. Benahmed, Effects of aggregate size on water retention capacity and microstructure of lime-treated silty soil, Geotech. Lett. 5 (2015) 269-274. https://doi.org/10.1680/jgele.15.00127.

[10] G. Russo, G. Modoni, Fabric changes induced by lime addition on a compacted alluvial soil, Geotech. Lett. 3 (2013) 93-97. https://doi.org/10.1680/geolett.13.026.

[11] S.A.A. Khattab, L.K.I. Al-Taie, Soil-water characteristic curves (SWCC) for lime treated expansive doil from Mosul city, Unsaturated Soils (2006) 1671-1682. https://doi.org/10.1061/40802(189)140.

[12] D. V. Tedesco, G. Russo, Time dependency of the water retention properties of a lime stabilised compacted soil, Unsaturated Soils: Advances in Geo-Engineering. Taylor & Francis Group, London (2008) 277-282. https://doi.org/10.1201/9780203884430.ch33.

[13] X. Bian, L.L. Zeng, X.Z. Li, X.S. Shi, S.M. Zhou, F.Q. Li, Fabric changes induced by super-absorbent polymer on cement–lime stabilized excavated clayey soil, J. Rock Mech. Geotech. Eng. (2021). https://doi.org/10.1016/j.jrmge.2021.03.006.

[14] H.N. Ramesh, M.S. Mohan, P. V. Sivapullaiah, Improvement of strength of fly ash with lime and sodium salts, Gr. Improv. 3 (1999) 163-167. https://doi.org/10.1680/gi. 1999.030403.

[15] R.B. Saldanha, H.C.S. Filho, J.L.D. Ribeiro, N.C. Consoli, Modelling the influence of density , curing time , amounts of lime and sodium chloride on the durability of compacted geopolymers monolithic walls, Constr. Build. Mater. 136 (2017) 65-72. https://doi.org/10.1016/j.conbuildmat.2017.01.023.

[16] H.F. Xing, X.M. Yang, C. Xu, G.B Ye, Strength characteristics and mechanisms of salt-rich soil-cement, Eng. Geol. 103 (2009) 33-38. https://doi.org/10.1016/j.enggeo.2008. 07.011.

[17] E.C. Leong, S. Tripathy, H. Rahardjo, Total suction measurement of unsaturated soils with a device using the chilled-mirror dew-point technique, Géotechnique. 53 (2003) 173-182. https://doi.org/10.1680/geot.53.2.173.37271.

[18] T. Thyagaraj, U. Salini, Effect of pore fluid osmotic suction on matric and total suctions of compacted clay, Géotechnique. 65 (2015) 952-960. https://doi.org/10.1680/jgeot. 14.P.210.

[19] ASTM D5298-16. Standard Test Method for Measurement of Soil Potential (Suction) Using Filter Paper. ASTM International, West Conshohocken, PA. 2016.

[20] S. Sreedeep, D.N. Singh, A study to investigate the influence of soil properties on suction, J. Test. Eval. 33 (2005) 61-66. https://doi.org/10.1520/jte11981.

[21] D.G. Fredlund, H. Rahardjo, Soil mechanics for unsaturated soils, John Wiley & Sons, New York, 1993.

[22] E.C. Leong, S. Widiastuti, C.C. Lee, H. Rahardjo, Accuracy of suction measurement, Géotechnique. 57 (2007) 547-556. https://doi.org/10.1680/geot.2007.57.6.547.

[23] J.A. Muñoz-Castelblanco, J.M. Pereira, P. Delage, Y.J. Cui, The water retention properties of a natural unsaturated loess from northern France, Géotechnique. 62 (2012) 95-106. https://doi.org/10.1680/geot.9.P.084.

[24] W.J. Sun, Y.J. Cui, Determining the soil-water retention curve using mercury intrusion porosimetry test in consideration of soil volume change, J. Rock Mech. Geotech. Eng. 12 (2020) 1070-1079. https://doi.org/10.1016/j.jrmge.2019.12.022.

[25] P.H. Simms, E.K. Yanful, Measurement and estimation of pore shrinkage and pore distribution in a clayey till during soil-water characteristic curve tests, Can. Geotech. J. 38 (2001) 741-754. https://doi.org/10.1139/cgj-38-4-741.

[26] P.H. Simms, E.K. Yanful, Predicting soil-water characteristic curves of compacted plastic soils from measured pore-size distributions, Géotechnique. 52 (2002) 269-278. https://doi.org/10.1680/geot.2002.52.4.269.

[27] O. Cuisinier, L. Laloui, Fabric evolution during hydromechanical loading of a compacted silt, Int. J. Numer. Anal. Methods Geomech. 28 (2004) 483-499. https://doi.org/10.1002/nag.348.

[28] A. Koliji, L. Laloui, O. Cusinier, L. Vulliet, Suction induced effects on the fabric of a structured soil, Transp. Porous Media. 64 (2006) 261-278. https://doi.org/10.1007/s11242-005-3656-3.

[29] E. Romero, G. Della Vecchia, C. Jommi, An insight into the water retention properties of compacted clayey soils, Géotechnique. 61 (2011) 313-328. https://doi.org/10.1680/geot.2011.61.4.313.

[30] G. Stoltz, O. Cuisinier, F. Masrouri, Multi-scale analysis of the swelling and shrinkage of a lime-treated expansive clayey soil, Appl. Clay Sci. 61 (2012) 44-51. https://doi.org/10.1016/j.clay.2012.04.001.

[31] M. Nabil, A. Mustapha, S. Rios, Long term evaluation of wetting-drying cycles for compacted soils treated with Lime, In Conference of the Arabian Journal of Geosciences. (2018) 277-281. https://doi.org/10.1007/978-3-030-01665-4.

[32] N. Poncelet, B. François, Desiccation crack in lime-treated silty clay: Experimental evaluation and constitutive interpretation, E3S Web Conf. 92 (2019) 1-6. https://doi.org/10.1051/e3sconf/20199211002.

[33] Z. Ying, M. Duc, Y.J. Cui, N. Benahmed, Salinity assessment for salted soil considering both dissolved and precipitated salts, Geotech. Test. J. 44 (2021) 130-147. https://doi.org/10.1520/GTJ20190301.

[34] French standard AFNOR NF P 18-837, Standard for special products for hydraulic concrete construction-Hydraulic binder based needling and/or sealing products-Testing of resistance against seawater and/or water with high sulphate contents. Association Francaise de Normalisation. (1993).

[35] P. Delage, G. Lefebvre, Study of the structure of a sensitive Champlain clay and of its evolution during consolidation, Can. Geotech. J. 21 (1984) 21-35. https://doi.org/10.1139/t84-003.

[36] C.H. Juang, R.D. Holtz, A probabilistic permeability model and the pore size density function, Int. J. Numer. Anal. Methods Geomech. 10 (1986) 543-553. https://doi.org/10.1002/nag.1610100506.

[37] E. Romero, Thermo-hydro-mechanical behaviour of unsaturated boom clay: an experimental study. PhD Thesis, Universidad Politécnica de Catalunya, Barcelona, Spain. (1999).

[38] Z. Ying, Y.J. Cui, N. Benahmed, M. Duc, Changes of microstructure and water retention property of a lime-treated saline soil during curing, Acta Geotech. (2021). https://doi.org/10.1007/s11440-021-01218-5.

[39] S. Sreedeep, D.N. Singh, Methodology for determination of osmotic suction of soils,

Geotech. Geol. Eng. 24 (2006) 1469-1479. https://doi.org/10.1007/s10706-005-1882-7.

[40] Y.F. Arifin, T. Schanz, Osmotic suction of highly plastic clays, Acta Geotech. 4 (2009) 177-191. https://doi.org/10.1007/s11440-009-0097-0.

[41] D.J. Miller, J.D. Nelson, Osmotic suction in unsaturated soil mechanics, in: Unsaturated Soils 2006, American Society of Civil Engineers, Reston, VA, 2006: pp. 1382-1393. https://doi.org/10.1061/40802(189)114.

[42] S. Sreedeep, D.N. Singh, Critical review of the methodologies employed for soil suction measurement, Int. J. Geomech. 11 (2011) 99-104. https://doi.org/10.1061/(asce)gm.1943-5622.0000022.

[43] Z. Ying, Y.J. Cui, N. Benahmed, M. Duc, Salinity effect on the compaction behaviour, matric suction, stiffness and microstructure of a silty soil, J. Rock Mech. Geotech. Eng. (2021). https://doi.org/10.1016/j.jrmge.2021.01.002.

[44] A.W.L. Wan, M.N. Gray, J. Graham, On the relations of suction , moisture content and soil structure in compacted clays, Proc. 1st Int. Conf. on Unsaturated Soils, Paris. Vol. 1. Balkema/Presses des Ponts et Chaussées. (1995).

[45] K.K. Aung, H. Rahardjo, E.C. Leong, D.G. Toll, Relationship between porosimetry measurement and soil-water characteristic curve for an unsaturated residual soil, Geotech. Geol. Eng. 19 (2001) 401-416. https://doi.org/10.1023/A:1013125600962.

[46] X. Li, L.M. Zhang, Characterization of dual-structure pore-size distribution of soil, Can. Geotech. J. 46 (2009) 129-141. https://doi.org/10.1139/T08-110.

[47] Y.J. Wang, Y.J. Cui, A.M. Tang, C.S. Tang, N. Benahmed, Changes in thermal conductivity, suction and microstructure of a compacted lime-treated silty soil during curing, Eng. Geol. 202 (2016) 114-121. https://doi.org/10.1016/j.enggeo.2016.01.008.

[48] G. Niu, D.A. Sun, L.T. Shao, L.F. Zeng, The water retention behaviours and pore size distributions of undisturbed and remoulded complete-intense weathering mudstone, Eur. J. Environ. Civ. Eng. (2019) 1233-1250. https://doi.org/10.1080/19648189.2019.1572544.

[49] H. Li, T.L. Li, P. Li, Y.G. Zhang, Prediction of loess soil-water characteristic curve by mercury intrusion porosimetry, J. Mt. Sci. 17 (2020) 2203-2213. https://doi.org/10.1007/s11629-019-5929-2.

[50] N. Sghaier, M. Prat, S. Ben Nasrallah, On the influence of sodium chloride concentration on equilibrium contact angle, Chem. Eng. J. 122 (2006) 47-53. https://doi.org/10.1016/j.cej.2006.02.017.

[51] D.A.L. Leelamanie, J. Karube, Soil-water contact angle as affected by the aqueous electrolyte concentration, Soil Sci. Plant Nutr. 59 (2013) 501-508. https://doi.org/10.1080/00380768.2013.809601.

[52] N. Lu, M. Khorshidi, Mechanisms for Soil-Water Retention and Hysteresis at High Suction Range, J. Geotech. Geoenviron. Eng. 141 (2015) 04015032. https://doi.org/10.1061/(asce)gt.1943-5606.0001325.

[53] C.W.W. Ng, H. Sadeghi, S.K.B. Hossen, C.F. Chiu, E.E. Alonso, Water retention and volumetric characteristics of intact and re-compacted loess, Can. Geotech. J. 53 (2016) 1258-1269. https://doi.org/doi.org/10.1139/cgj-2015-0364.

[54] E. Romero, J. Vaunat, Retention curves of deformable clays, Experimental Evidence and Theoretical Approaches in Unsaturated Soils. (2000) 91-106.

[55] M. Tuller, D. Or, Water films and scaling of soil characteristic curves at low water contents, Water Resour. Res. 41 (2005) 1-6. https://doi.org/10.1029/2005WR004142.

[56] E. Vitale, D. Deneele, M. Paris, G. Russo, Multi-scale analysis and time evolution of pozzolanic activity of lime treated clays, Appl. Clay Sci. 141 (2017) 36-45. https://doi.org/10.1016/j.clay.2017.02.013.

[57] L.K. Sharma, N.N. Sirdesai, K.M. Sharma, T.N. Singh, Experimental study to examine the independent roles of lime and cement on the stabilization of a mountain soil: A comparative study, Appl. Clay Sci. 152 (2018) 183-195. https://doi.org/10.1016/j.clay.2017.11.012.

[58] W.P. Halperin, J.Y. Jehng, Y.. Song, Application of spin-spin relaxation to measurement of surface area and pore size distributions in a hydrating cement paste, Magn. Reson. Imaging. 12 (1994) 169-173. https://doi.org/doi.org/10.1016/0730-725X(94)91509-1.

[59] A.C.A. Muller, Characterization of porosity & C-S-H in cement pastes by 1H NMR, PhD Thesis, École Polytechnique Fédérale de Lausanne, Lausanne, Suisse. (2014).

[60] Z. Ying, Y.J. Cui, N. Benahmed, M. Duc, Changes in mineralogy and microstructure of a lime-treated silty soil during curing time, 4th European Conference on Unsaturated soils. Lisbon. (2020). https://doi.org/10.1051/e3sconf/202019503044.

[61] M. Al-Mukhtar, A. Lasledj, J.F. Alcover, Behaviour and mineralogy changes in lime-treated expansive soil at 20°C, Appl. Clay Sci. 50 (2010) 191-198. https://doi.org/10.1016/j.clay.2010.07.023.

[62] R. Hamidi, D. Kahforoushan, E. Fatehifar, M. Arehjani, S. Farmanbordar, Simultaneous removal of Ca and Mg salts using chemical precipitation with lime, The 7th International Chemical Engineering Congress & Exhibition. Kish, Iran, 21-24 November, (2011).

[63] X.S. Shi, J.D. Zhao, Practical estimation of compression behavior of clayey/silty sands using equivalent void-ratio concept, J. Geotech. Geoenviron. Eng. 146 (2020) 04020046. https://doi.org/10.1061/(asce)gt.1943-5606.0002267.

[64] C.S. Tang, B. Shi, C. Liu, W. W.B. Suo, L. Gao, Experimental characterization of shrinkage and desiccation cracking in thin clay layer, Appl. Clay Sci. 52 (2011) 69-77. https://doi.org/10.1016/j.clay.2011.01.032.

[65] W.J. Sun, Y.J. Cui, Investigating the microstructure changes for silty soil during drying, Géotechnique. 68 (2018) 370-373. https://doi.org/10.1680/jgeot.16.P.165.

[66] Z. Ying, Y. Cui, N. Benahmed, M. Duc, Drying effect on the microstructure of compacted salted silt, Géotechnique. (2021) Accepted for publication.

[67] Y.J. Wang, M. Duc, Y.J. Cui, A.M. Tang, N. Benahmed, W.J. Sun, W.M. Ye, Aggregate size effect on the development of cementitious compounds in a lime-treated soil during curing, Appl. Clay Sci. 136 (2017) 58-66. https://doi.org/10.1016/j.clay.2016.11.003.

[68] Y.J. Wang, Y.J. Cui, A.M. Tang, N. Benahmed, M. Duc, W.J. Sun, Shrinkage behaviour of a compacted lime-treated clay, Geotech. Lett. 10 (2020) 174-178. https://doi.org/10.1680/jgele.19.00006.

[69] Z. Ying, Y.J. Cui, M. Duc, N. Benahmed, H. Bessaies-Bey, B. Chen, Salinity effect on the liquid limit of soils, Acta Geotech. 16 (2021) 1101-1111. https://doi.org/10.1007/s11440-020-01092-7.

Chapter 6. Mechanical behaviour and durability of lime-treated saline soils

Introduction

Lime treatment can enhance the workability and hydro-mechanical properties of soils through different physical-chemical reactions, such as cation exchange and pozzolanic reaction (Sivapullaiah et al., 2000; Rao and Shivananda, 2005; Al-Mukhtar et al., 2010a, 2010b; Tang et al., 2011a; Muntohar et al., 2013; Vitale et al., 2017; Wang et al., 2020). Nevertheless, the beneficiary effect of lime treatment can be altered when the soils were exposed to wetting and drying cycles, due to the softening of soil structure and cementitious compounds (Aldaood et al., 2014; Stoltz et al., 2014; Rosone et al., 2016, 2018; Cuisinier et al., 2020; Nabil et al., 2020).

In order to understand the lime treatment effect on the mechanical behaviour and the durability of lime-treated saline soils subjected to wetting-drying cycles, bender element and oedometer tests as well as mercury intrusion porosimetry tests were conducted on untreated/lime-treated specimens and those specimens subjected to wetting-drying cycles. Different wetting fluids (deionized water and synthetic seawater) and maximum soil aggregate sizes (D_{max} = 0.4 mm for S0.4 and D_{max} = 5 mm for S5) were considered in the wetting-drying tests.

This chapter consists of two papers. The first paper, published “Engineering Geology”, presented the changes of small strain shear modulus and microstructure of lime-treated soil subjected to wetting-drying cycles. The second paper, submitted to “Journal of Rock Mechanics and Geotechnical Engineering”, presented the results of oedometer tests. The articles are presented here in their original versions.

Ying, Z., Cui, Y.J., Benahmed, N., Duc, M. 2021. Engineering Geology, 293: 106334. Doi.org/10.1016/j.enggeo.2021.106334.

Changes of small strain shear modulus and microstructure for a lime-treated silt subjected to wetting-drying cycles

Zi Ying[1], Yu-Jun Cui[1], Nadia Benahmed[2], Myriam Duc[3]

Abstract: Lime treatment can enhance the workability and hydro-mechanical properties of soil through different physical-chemical reactions. Nevertheless, the beneficiary effect of lime treatment can be altered when the soil was exposed to wetting-drying cycles, depending on the wetting fluid and soil state. In the present study, the changes in small strain shear modulus (G_{max}) and microstructure of a compacted lime-treated silt under wetting-drying cycles were studied. The untreated state of soil was also considered for comparison. Meanwhile, the effects of wetting fluid (deionized water and synthetic seawater) and maximum soil aggregate size (D_{max} = 0.4 mm for S0.4 and 5 mm for S5) were investigated. Results showed that G_{max} increased significantly for the lime-treated soil over curing, and increased slightly for the untreated soil. The untreated specimens were softened and damaged by wetting-drying cycles, while the lime-treated specimens exhibited good resistance with the pore size distributions almost kept reversible along the wetting-drying paths. The subsequent more intensive drying resulted in a significant fabric alteration with occurrence of shrinkage-related fissures of the clay part. However, these fissures were almost healed with rewetting. Thereby, the G_{max} of lime-treated soil showed a constant decreasing trend with wetting and an increasing trend with drying. Moreover, G_{max} decreased slightly with wetting-drying cycles for the lime-treated specimens wetted by deionized water, suggesting that the wetting-drying indeed softened the soil. However, G_{max} increased for the lime-treated specimens wetted by synthetic seawater, due to the more production of cementitious compounds promoted by salts. The lime-treated specimens S0.4 wetted by synthetic seawater had higher G_{max} than those wetted by deionized water, while the wetting fluid had insignificant effect on the G_{max} of specimens S5 due to the limited promotion of pozzolanic reaction and negligible soil aggregation induced by salts.

Keywords: Lime treatment; small strain shear modulus; microstructure; wetting-drying; wetting fluid

[1]: Ecole des Ponts ParisTech, Laboratoire Navier/CERMES, 6 – 8 av. Blaise Pascal, Cité Descartes, Champs-sur-Marne, 77455 Marne-la-Vallée cedex 2, France
[2]: INRAE, Aix Marseille Univ, Unité de Recherche RECOVER, 3275 route Cézanne, CS 40061, 13182 Aix-en-Provence, France
[3]: Université Gustave Eiffel, IFSTTAR/GERS/SRO, 14-20 boulevard Newton, Champs-sur-Marne, 77447 Marne-la-Vallée, France

1. Introduction

In most geological, geotechnical and geo-environmental applications, it is encouraged to use local soils in order to reduce the economic cost and carbon emission. When clayey soils are involved, they must be improved prior to use. Lime treatment was widely used in that case, allowing improvement of the workability and the hydro-mechanical behaviour of soils (Bell, 1989, 1996; Locat et al., 1990). It is generally accepted that lime hydration and cation exchange took place rapidly after mixing soil with water and lime, leading to the flocculation of soil particles (Guney et al., 2007; Al-Mukhtar et al., 2010a; Di Sante et al., 2014), and further improving the soil workability by reducing the soil plasticity, shrinkage, and swelling (Bell, 1996; Khattab and Fleureau, 2007; Al-Mukhtar et al., 2012; al-Swaidani et al., 2016). In the long term, the pozzolanic reaction developed, producing some cementitious compounds which coated the surface of aggregates and connected the adjacent soil particles (Bell, 1996). This resulted in an enhancement of soil mechanical behaviour, as evidenced by the increase of unconfined compressive strength (Al-mukhtar et al., 2010b; Muntohar et al., 2013), stiffness (Tang et al., 2011a; Wang et al., 2020) and shear strength (Sivapullaiah et al., 2000), and also by the decrease of compressibility (Rao and Shivananda, 2005; Vitale et al., 2017; Wang et al., 2017a).

Several studies reported that, as compared to the specimens prepared in the laboratory, the lime-treated soil in field condition usually exhibited lower strength and stiffness, but higher swelling potential and hydraulic conductivity (Puppala et al., 2006; Cuisinier and Deneele, 2008; Dong, 2013). This could be ascribed to the different sizes of aggregates used in the field and laboratory. Tang et al. (2011a) performed bender element tests on lime-treated soil with different maximum aggregate sizes and reported that the lime-treated specimens with smaller aggregates had higher small strain shear modulus (G_{max}). Wang et al. (2017b) reported that lime was more concentrated in the specimens with larger aggregates and formed well-crystallized cementitious compounds by pozzolanic reaction, while the distribution of lime was diffused in the small soil aggregate-lime mixture and poorly crystallized or amorphous cementitious compounds were produced in that case.

Even though the soil properties were improved by lime treatment, the long-term durability of lime-treated soils might be altered when the soils were exposed to cyclic climate loadings such as wetting-drying cycles. Several studies revealed that the imposition of wetting-drying cycles on lime-treated soil would partially destroy the cementitious bonds and alter the soil

microstructure, leading to progressive loss of soil strength (Aldaood et al., 2014; Stoltz et al., 2014; Cuisinier et al., 2020; Nabil et al., 2020), and an increase in compressibility and hydraulic conductivity (Rosone et al., 2016, 2018; Cuisinier et al., 2020). Nevertheless, Anggraini et al. (2016) indicated that wetting-drying cycles could make the curing time longer, and therefore the durability of stabilized soils was enhanced. Similar strengthening behaviour was observed on untreated soil - G_{max} increased with increasing wetting-drying cycles due to the effect of suction history-related decrease of saturation degree and void ratio (Heitor et al., 2015; Ngoc et al., 2019; Khosravi et al., 2020). Estabragh et al. (2013) investigated the wetting fluid (distilled water, saline water and acidic water) effect on the volume change of swelling soil during wetting-drying cycles. They found that the specimens inundated with saline water and acidic water showed compressive deformation, while the specimens wetted by distilled water showed expansive deformation. To the authors' knowledge, there is no study focusing on the wetting fluid effect on the mechanical behaviour of lime-treated soils subjected to wetting-drying cycles.

Small strain shear modulus, G_{max} is an important parameter for describing the elastic properties of soils, and for predicting the dynamic response and deformation of geotechnical structures (Zhou and Chen, 2005; Ng and Yung, 2008; Tang et al., 2011a; Chakraborty et al., 2018). In this study, the changes of G_{max} with time were investigated using bender element method for a silt with two different maximum aggregate sizes (D_{max} = 0.4 mm and 5 mm). Both untreated and lime-treated compacted specimens were prepared for this purpose. When the stabilization of G_{max} was reached, cyclic wetting-drying tests were performed with either deionized water or synthetic seawater as wetting fluid. At each wetting or drying stage, G_{max} was measured. Moreover, mercury intrusion porosimetry (MIP) tests were conducted on the lime-treated specimens which had been subjected to different wetting-drying cycles. The results obtained were analyzed to understand the changes of G_{max} during wetting-drying cycles for different wetting fluids and different maximum soil aggregate sizes.

2. Materials and methods

2.1 Materials

The tested soil was sampled at Les Salins de Giraud in southern France, which was used for a dike construction. According to the results obtained by Ying et al. (2021a), this soil was naturally saline with a soil salinity (r') of 2.1‰ (g of salt/kg of dry soil) and the corresponding

water salinity of soil pore water is 13.3‰ (g of salt/kg of salty water) for the soil at 15.6% water content. The main ion species in soil pore water are Cl^-, Na^+, K^+, Ca^{2+} and Mg^{2+}. This soil has a liquid limit of 29%, a plastic limit of 19% and a specific gravity of 2.71. The specific surface area of soil is 24 m^2/g, which was measured by the spot test of methylene blue following the procedure proposed by Santamarina et al. (2002). The main minerals of this soil are quartz (39%), calcite (35%), feldspars (9.5%), halite NaCl (0.8%), illite (10.8%), chlorite (3.6%) and kaolinite (1.3%). The grain size distribution of natural soil is presented in Fig. 1. It is observed that the soil contains 17% clay-size particles (< 0.002 mm), 53% silt (0.002 ~ 0.075 mm) and 30% fine sand (0.075 ~ 2 mm).

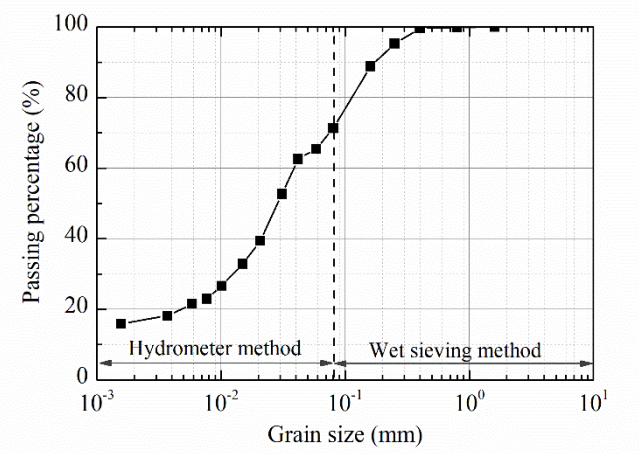

Fig. 1. Grain size distribution of the tested soil.

To prepare the soil specimens, the natural soil was air-dried, ground and sieved through two meshes with two different sizes of 0.4 mm and 5mm. Thus, two soil powders with different maximum aggregate sizes (D_{max} = 0.4 mm and 5 mm) were obtained, namely S0.4 and S5, respectively. The soil aggregates were ground again until all the soil aggregates passed through, enabling the soil powders S0.4 and S5 to have the same mineral composition as natural soil.

A quicklime with 97.3% CaO was used. The optimum lime dosage was determined by the pH method following the Eades and Grim test procedure (ASTM Standard D6276-19, 2019). The value was found to be 0.5% (by dry weight of soil) at which the pH of soil-lime-deionized water mixture reached 12.4. To keep consistent with the lime dosage in the dike construction at Les Salins de Giraud, a lime content of 2% was selected.

2.2 Sample preparation

After the dry soil powders were prepared, 2% lime was first mixed with dry soil. Then, deionized water was used to humidify the soil-lime mixture to reach different target water contents: 17% on dry side and 19% on wet side. Note that the dry side corresponded to the left side of optimum water content, while the wet side corresponded to the right side of optimum water content, as shown in Fig. 2. Note also that no water content higher than 19% was selected because water would flow out of soil during compaction at higher water contents. The soil-lime-water mixture was mellowed for 1 h to allow the development of rapid soil-lime reactions. Afterwards, static compaction was performed at a rate of 0.3 mm/min to prepare the specimens at a target dry density of 1.63 Mg/m^3 (Fig. 2). The specimens for bender element test had 50 mm diameter and 50 mm height, and the specimens for MIP tests had 50 mm diameter and 20 mm height. After compaction, the specimens were covered by paraffin to avoid water evaporation. Then, they were wrapped by plastic membrane and scotch tape, and cured in a hermetic box.

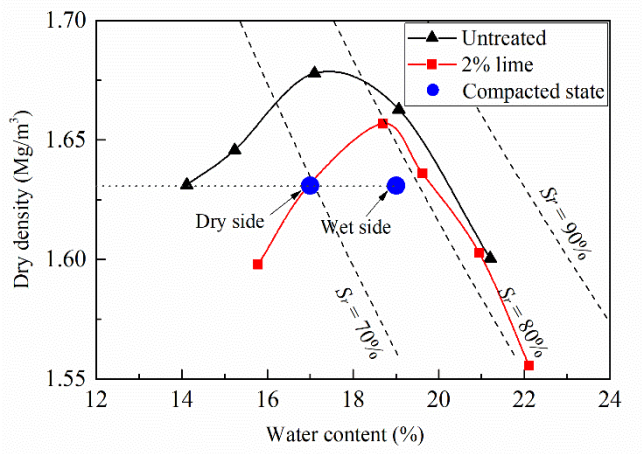

Fig. 2. Standard proctor compaction curves of untreated and lime-treated soils, as well as the soil states considered in the tests.

2.3 Bender element tests

The small strain shear modulus was measured by bender element technique (Fig. 3), which consists of a pair of piezo-ceramic elements, a function generator, an amplifier and an oscilloscope (Ying et al., 2021b). Prior to use, the bender elements were calibrated by connecting the two benders directly without soil sample. The delay time between two bender elements was found to be 2 μs that was considered in the calculation of travel time of shear

wave through specimens.

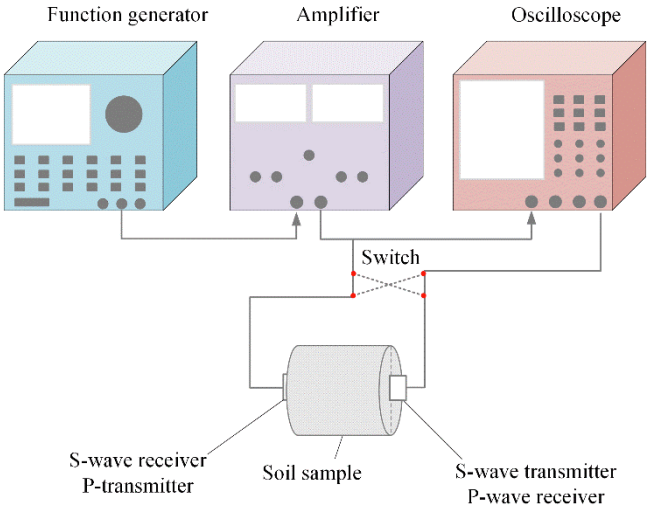

Fig. 3. Set-up of bender element test (after Ying et al., 2021b).

As the specimens for the bender elements tests were covered by paraffin, prior to testing, two slots were performed on the top and bottom surfaces of specimen with the same position to enable a good contact between the bender elements and specimen. The ground connection was applied during testing in order to eliminate the crosstalk and near-field effects (Lee and Santamarina, 2005). Afterwards, an excitation signal (±14V sine pulse) was emitted by the function generator and amplified by the amplifier. Both input (transmitted) and output (received) signals were acquired and visualized by oscilloscope. The arrival time of shear wave was determined by the S+P method which needed to capture both the input and output signals of S-wave and P-wave by oscilloscope through switching the connections of the two piezo-ceramic elements (Wang et al., 2017c). As shown in Fig. 4, Point S was selected as the arrival point of shear wave, which corresponded to the initial main excursion (Point S_p) in the received signal of P-wave (Wang et al., 2017c). Equation 1 was used to calculate the shear wave velocity (v_s):

$$v_s = \frac{L_{tt}}{\Delta t} \tag{1}$$

where L_{tt} is the travel length (the height of specimen minus the depth of the two slots), Δt is the travel time of shear wave (the arrival time minus the delay time between two benders).

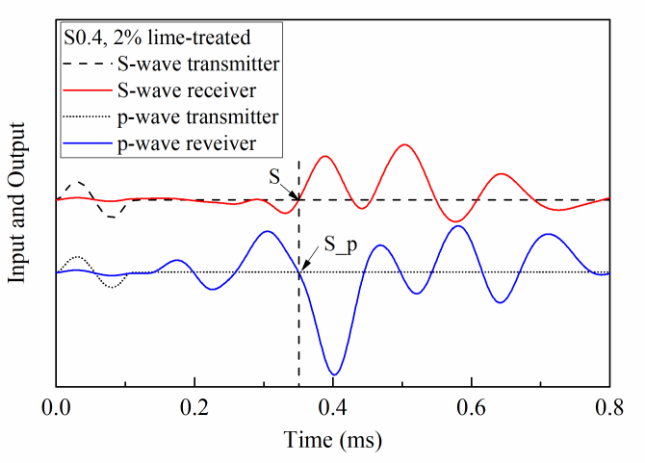

Fig. 4. Determination of the arrival point of shear wave by S+P method.

Equation 2 was used to determine the small strain shear modulus (G_{max}):

$$G_{max} = \rho v_s^2 \quad (2)$$

where ρ is the density of soil sample.

This G_{max} measurements were repeated on the same specimens over curing. Two replicated tests were conducted on the lime-treated specimens and four replicated measurements were performed on the untreated specimens. At a given time, the mean value of the measurements on the replicated specimens was used for further analysis.

2.4 Wetting-drying tests for G_{max} measurement

When the G_{max} kept stable with time, the wetting-drying cycles were applied on the specimens with deionized water and 35 g/L synthetic seawater as wetting fluids. The salt composition of synthetic seawater is presented in Table 1 (AFNOR NF P 18-837, 1993). Prior to the wetting process, the paraffin on the top and bottom surfaces of the specimens was scraped off, allowing for water infiltration. Then, two filter papers and two porous stones were placed on the top and bottom sides, respectively. The specimens were wetted by adding water on the top surface using a plastic dropper until a constant mass of specimen was obtained. The water contents after wetting were found to be 21% for the lime-treated specimens, and 25% for the untreated specimens. For drying, the specimens were air-dried to the initial soil mass before wetting. At the end of the seventh wetting, the lime-treated specimens were subjected to an intensive drying to the water contents of 8% and 3%. Afterwards, the lime-treated specimens were rewetted to the water content of 21%. At the end of each wetting and drying stage, the specimens were

wrapped in plastic film for at least 24 h for water equilibration. Then, G_{max} was measured by the bender element technique. The soil dimensions were measured using a calliper. Because the changes in soil volume were found to be negligible for the lime-treated specimens, they were ignored in the calculation of soil density and shear wave velocity. However, a swelling phenomenon was observed on untreated soil during wetting. Hence, the volume changes were considered in that case while calculating the soil density and shear wave velocity.

Table 1. Salt composition of synthetic seawater.

Salts	NaCl	$MgCl_2 \cdot 6H_2O$	$MgSO_4 \cdot 7H_2O$	$CaSO_4 \cdot 2H_2O$	$KHCO_3$
Concentration (g/L)	30.0	6.0	5.0	1.5	0.2

2.5 Wetting-drying tests for microstructure investigation

The microstructure variations during wetting-drying cycles were investigated by Autopore IV 9500 mercury intrusion porosimeter. Because the microstructure of the studied silt was affected slightly by salts (Ying et al., 2021b) and the untreated soil was easily softened by wetting, only the lime-treated specimens S0.4 (w_i = 17%, t = 600 d) were used for MIP tests, which were subjected to different wetting-drying cycles with deionized water as wetting fluid. Note that specimens S5 had the same microstructure variations as specimens S0.4. Thus, specimens S5 were not selected for MIP test for clarity. In total, eleven soil states of specimens S0.4 were considered for MIP tests (Fig. 5), which corresponded to the specimens' states for bender element tests. State "A" represented the as-compacted condition with an initial water content of 17% and dry density of 1.63 Mg/m^3. After wetting, the water content of lime-treated specimens increased to 21%. Then, the specimens were air-dried to the water content of 17%. States "B", "C", "D", "E" and "F" corresponded to the ends of the first wetting (B), first drying (C), second wetting (D), seventh wetting (E) and seventh drying (F) cycles, respectively. Four specimens (w = 17%), after seven wetting-drying cycles, were subjected to more intensive drying to reach the water contents of around 8% (G) and 3% (H). Then, three specimens at water contents of 17%, 8% and 3% respectively were rewetted to the water content of 21%, namely specimens "I", "J" and "K", respectively. The freeze-dried specimens were used for the MIP tests, which were rapidly frozen in liquid nitrogen and then dried with a freeze-dryer for 24h.

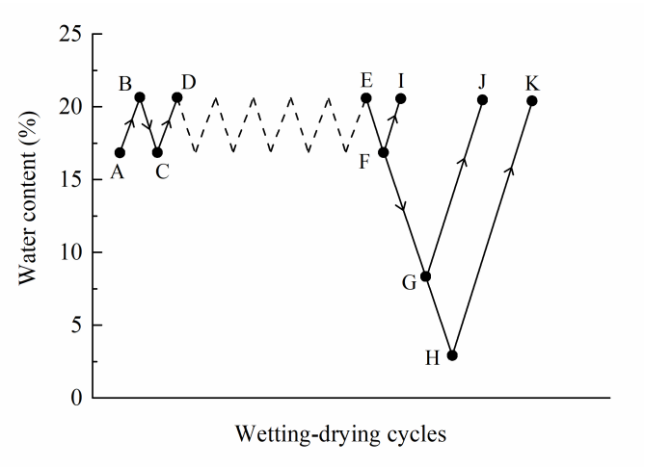

Fig. 5. The conditions of specimens for MIP tests.

3. Results

3.1 Stiffness variations during curing time

The variations of G_{max} are plotted against curing time on the semi-logarithmic scale for specimens S0.4 in Fig. 6a, and for specimens S5 in Fig. 6b. After compaction, the lime-treated specimens had higher G_{max} values as compared to the untreated specimens. G_{max} of the untreated specimens S0.4 and S5 increased slightly from 20 MPa at 1 h to 23 MPa at 2000 h, while it increased much significantly for the lime-treated specimens. As shown in Fig. 6a, when the curing time was less than 100 h, G_{max} of the lime-treated specimens S0.4 compacted on dry side was higher than those of specimens S0.4 compacted on wet side. Upon further curing, G_{max} of the lime-treated specimens S0.4 compacted wet of optimum increased and approached the values of specimens compacted dry of optimum. Then, G_{max} increased with time and stabilized after 10 000 h (417 d) at around 60 MPa (Fig. 6a) for the lime-treated specimens S0.4 on both dry and wet sides. In the case of lime-treated specimens S5 (Fig. 6b), G_{max} of the specimens on dry side was higher than those on wet side. Specifically, G_{max} increased from 26 MPa (1 h) to 59 MPa (6900 h) for the specimens S5 compacted dry of optimum, while it increased from 23 MPa (1 h) to 49 MPa (6700 h) for the specimens S5 compacted wet of optimum.

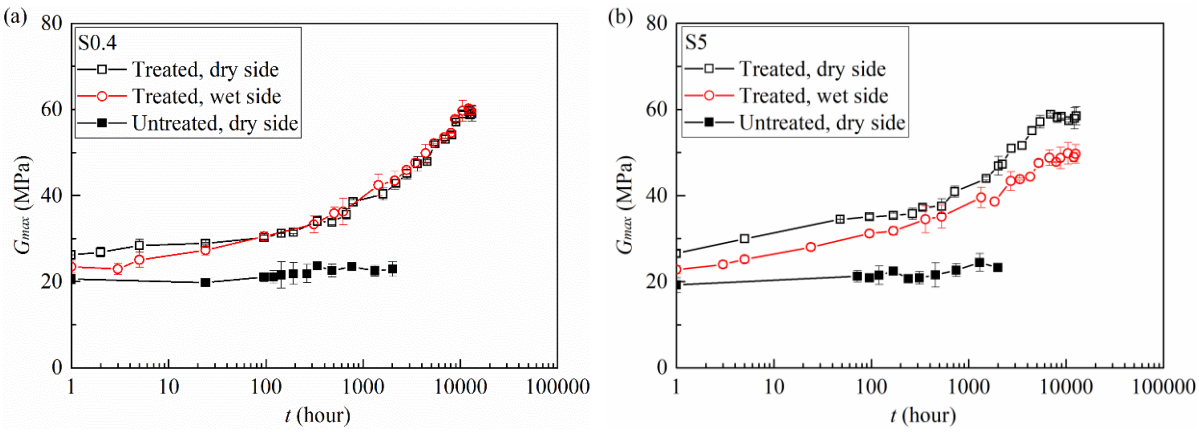

Fig. 6. Evolutions of small strain shear modulus after compaction: (a) S0.4; (b) S5.

3.2 G_{max} variations under wetting-drying cycles

The imposition of wetting-drying cycles had different effects on the morphology of untreated and lime-treated specimens. As shown in Fig. 7, some cracks initiated on the surface of untreated specimens after the first wetting. This was in agreement with the observations by Wang et al. (2014) on compacted bentonite, by Zeng et al. (2020) on compacted bentonite/claystone mixture, and by Zeng et al. (2017) on stiff Teguline clay. This phenomenon was attributed to the division of aggregates with wetting. Upon the second wetting, more and more cracks with larger width and length were observed on the untreated specimens. The third wetting cycle resulted in significant loss of soil and thus the destruction of untreated specimen. Nevertheless, the lime-treated specimens could well resist the wetting-drying cycles without appearance of any macro-cracks and specimen destruction.

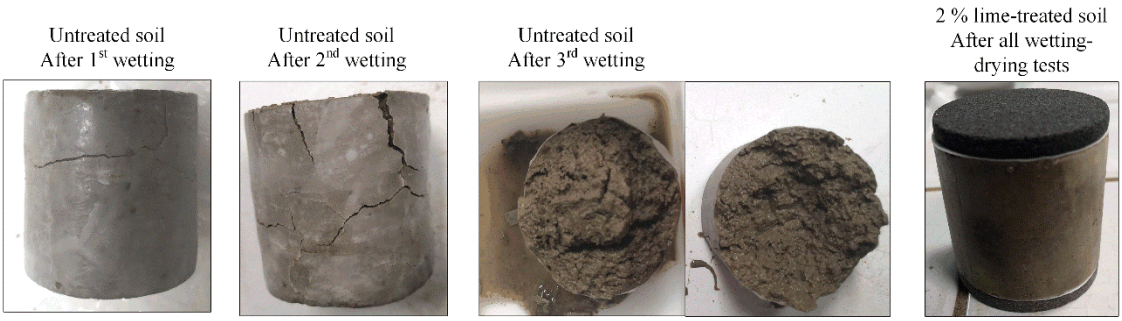

Fig. 7. The photos of specimens at different wetting-drying states.

Figures 8a and 8b present the variations of G_{max} with time under wetting-drying cycles for the untreated specimens S0.4 and S5, respectively. The corresponding water content at each wetting-drying stages are also presented. The starting point of G_{max} (t = 0) corresponded to the last point in Fig. 6, and the starting point of water content was the value of compacted water

content. It appears from Fig. 8 that, during wetting-drying cycles, the wetting fluid effect on the G_{max} was insignificant for the untreated specimens. For both specimens S0.4 and S5, the first wetting reduced G_{max} values from 23 MPa to 10 MPa. Despite of some cracks on the surface of untreated specimens, G_{max} could recover to the value of 23 MPa upon the subsequent drying. In the second wetting-drying cycle, the G_{max} variations were similar to those in the first cycle. The untreated specimens were destroyed after the third wetting and no further measurement of G_{max} was possible. When the water contents were kept unchanged (w = 17% in drying stage; w = 25% in wetting stage), the G_{max} of untreated specimens varied slightly with time.

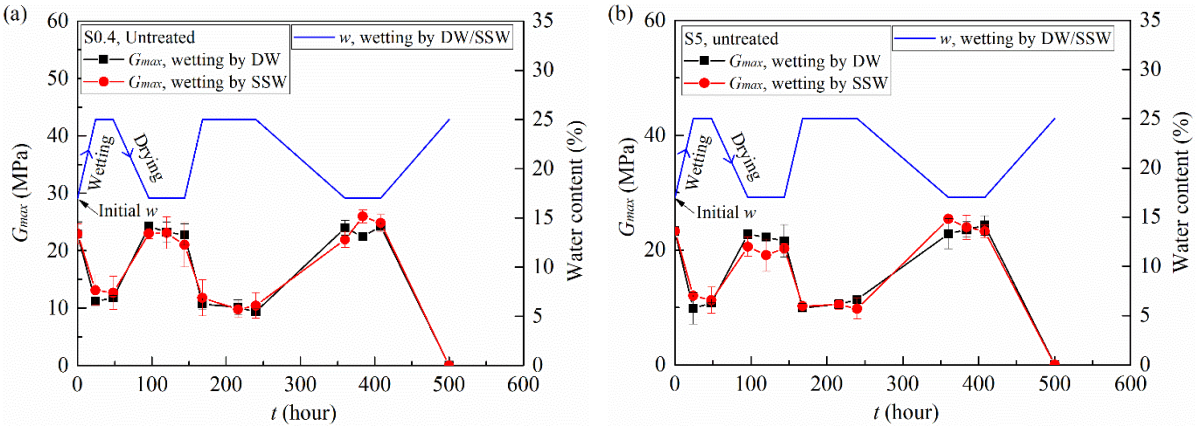

Fig. 8. G_{max} changes during wetting-drying cycles for untreated soil: (a) S0.4; (b) S5.

The changes in G_{max} with time under wetting-drying cycles are plotted in Figs. 9a and 9b for the lime-treated specimens S0.4 and S5, respectively. Because of the limited number of replicated specimens, the two replicated specimens compacted on dry side (w = 17%) were wetted by deionized water, and the two replicated specimens compacted on wet side (w = 19%) were wetted by synthetic seawater. For both lime-treated specimens S0.4 and S5, G_{max} decreased with wetting, while it increased in the subsequent drying process, regardless of the wetting fluid used. Generally, upon wetting or drying, G_{max} increased with wetting-drying cycles for the lime-treated specimens wetted by synthetic seawater, whereas it decreased slightly for the specimens wetted by deionized water. Moreover, the specimens wetted by synthetic seawater had higher G_{max} as compared to the specimens wetted by deionized water, especially for specimens S0.4 at both wetting and drying conditions (Fig. 9a). After a total of seven wetting-drying cycles, all the lime-treated specimens were subjected to an intensive drying process. It appears that G_{max} increased significantly to around 120 ~ 126 MPa at 8% water content, then it continued to increase to 150 ~ 160 MPa with decreasing water content to 3%, regardless of the soil aggregate sizes (S0.4 and S5) and the wetting fluids (deionized water

and synthetic seawater). Rewetting the specimens from water content of 3% to 21% reduced G_{max} to the values at the seventh wetting stage (20 ~ 23 MPa for specimens wetted by deionized water, 26 ~ 30 MPa for specimens wetted by synthetic seawater).

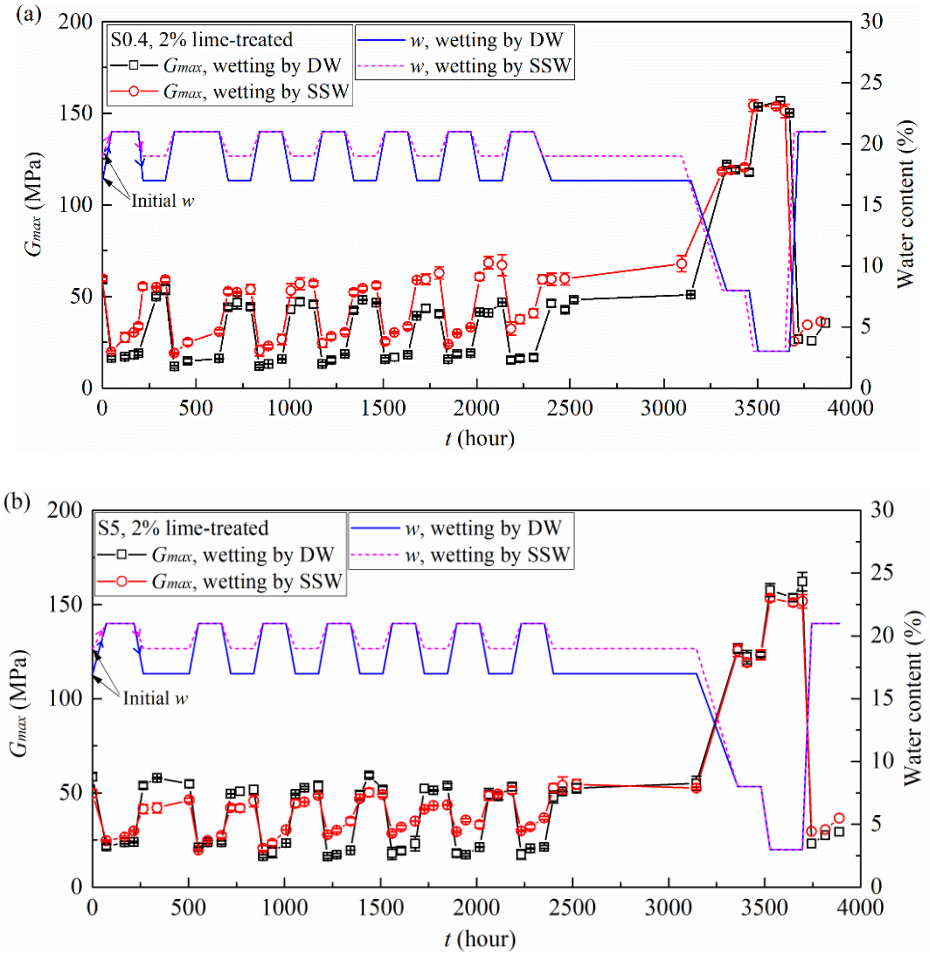

Fig. 9. G_{max} changes during wetting-drying cycles for lime-treated soil: (a) S0.4; (b) S5.

It is worth noting that, when the specimens were maintained at the end of wetting stage or drying stage, G_{max} increased significantly over time for the specimens wetted by synthetic seawater, whereas it increased slightly in the case of wetting by deionized water (Fig. 9a and 9b). To characterise the G_{max} variations, the increase of G_{max} (ΔG_{max}) at each wetting or drying stage was calculated, as follows (Eq. 3):

$$\Delta G_{\max} = G_{\max L_{iW/D}} - G_{\max F_{iW/D}} \quad (3)$$

where $G_{maxFiW/D}$ is the first measured value at number i wetting or drying stage, and $G_{maxLiW/D}$ is the last measured value at number i wetting or drying stage.

The increase of G_{max} against the number of cycles are plotted in Figs. 10a and 10b for the lime-treated specimens S0.4 and S5 in wetting stage, and in Figs. 10c and 10d in drying stage, respectively. It appears that, when the water content was maintained at the high value in wetting stage (Figs. 10a and 10b), the specimens wetted by synthetic seawater had higher increase of G_{max} as compared to the specimens wetted by deionized water. Nevertheless, under the drying condition, the wetting fluid effect on the increase of G_{max} was negligible (Figs. 10c and 10d). For the lime-treated specimens wetted by synthetic seawater, the increase of G_{max} was much more significant for the specimens under wetting condition (5 ~ 15 MPa) than for the specimens under drying condition (0 ~ 5 MPa).

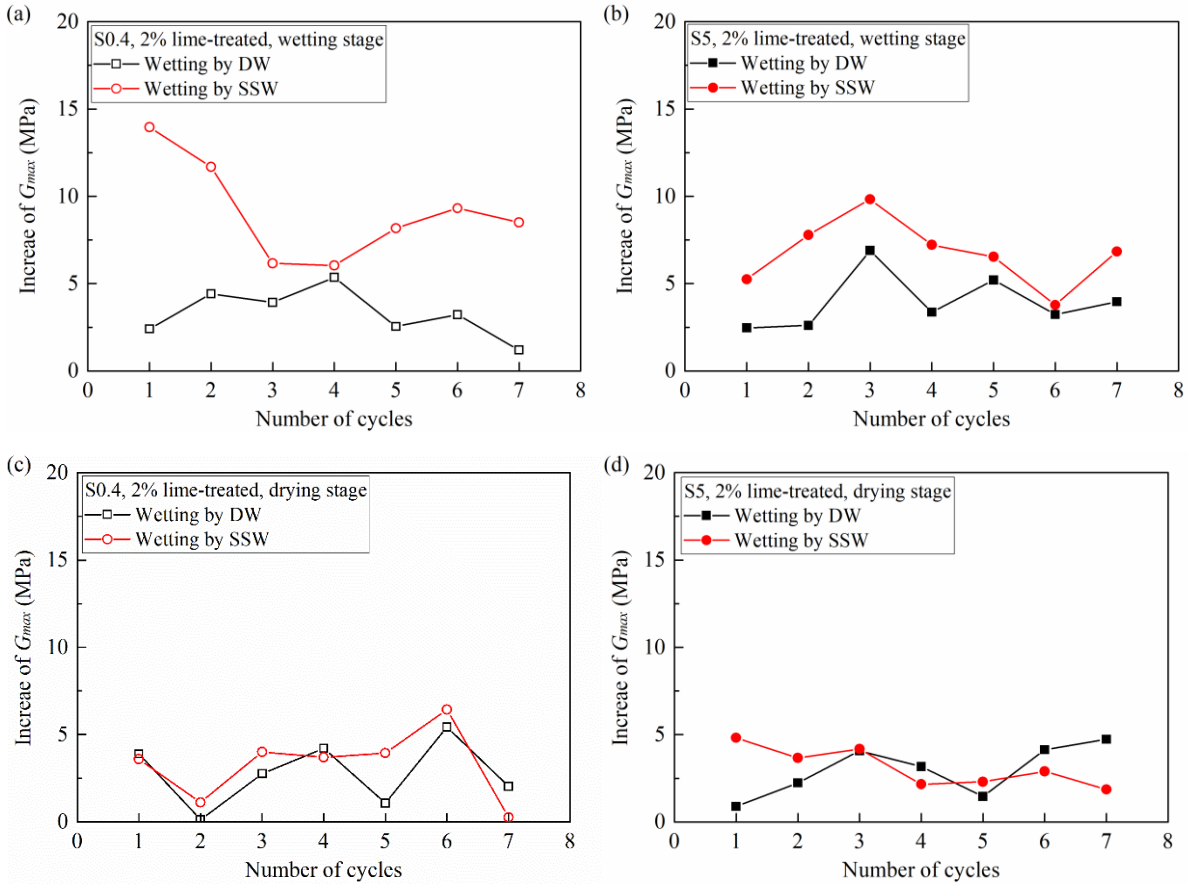

Fig. 10. Increase of G_{max} with wetting-drying cycles.

3.3 MIP results

Figure 11 presents the MIP results of lime-treated specimens S0.4 subjected to different wetting-drying cycles. It appears from Fig. 11a that the specimens at water contents of 17% and 21% exhibited bi-modal pore size distribution characteristics with two populations of micro-pores and macro-pores. The first wetting cycle resulted in an increase in the micro-pore modal

size and a decrease in the macro-pore modal size. Upon subsequent drying (from B to C), the modal size of micro-pores recovered to the value of specimen "A", while that of macro-pores was enlarged to a higher value. The second wetting cycle made the modal sizes of micro-pores and macro-pores of specimen "D" shift to the similar values of specimen "B". Similarly, the pore size distribution curve of specimen "E" at the seventh wetting stage approached the curves of specimens "B" and "D", suggesting that the variations of pore size distribution of lime-treated specimens were almost reversible under cyclic wetting-drying. As shown in Fig. 11b, the pore size distribution curves varied significantly with the intensive drying: the pore size distribution changed from bi-modal pattern to tri-modal pattern with drying to 8% water content, and finally retrieved the bi-modal pattern with further drying to 3% water content. As expected, upon the subsequent wetting, the tri-modal pore size distribution pattern at 8% water content recovered to bi-modal pattern (Fig. 11c). Nevertheless, slight irreversible changes were observed for specimens "I", "J" and "K" after rewetting - the pore size distribution shifted rightwards in turn with the specimens being previously dried to the water contents of 17%, 8% and 3% (Fig. 11c).

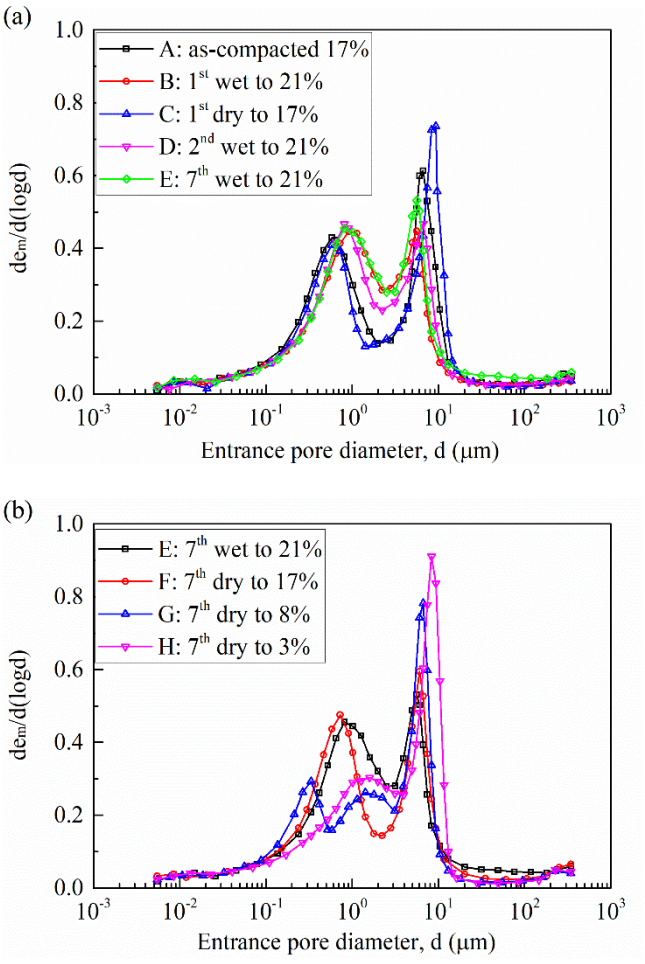

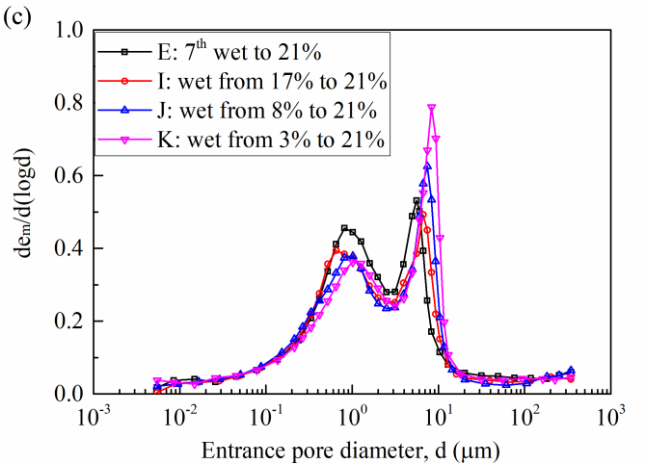

Fig. 11. Pore size distributions of lime-treated specimens (S0.4, t = 600 d) subjected to wetting-drying cycles.

4. Discussions

4.1 Curing time effect on the G_{max}

Figure 6 showed that, after compaction, the G_{max} of lime-treated soil was around 6 MPa higher than that of untreated soil, whatever the maximum soil aggregate size. This can be attributed to the increase of suction resulting from the lime-treatment on the one hand, and to the flocculation of soil particles resulting from the cation exchange on the other hand (Tang et al., 2011a; Wang et al., 2020). Indeed, the matric suction was found to be 41 kPa for lime-treated specimens at curing time of 14 days (14 days for filter paper measurement after compaction) that was higher than that of untreated specimens (22 kPa according toYing et al., 2021c). For the lime-treated soil, the flocculation of soil particles gave rise to an increase of G_{max} in short curing period, while the increase of G_{max} in the long term was due to the formation of cementitious compounds in the pozzolanic reaction, which bonded the adjacent soil particles and thus improved the soil stiffness (Tang et al., 2011a; Wang et al., 2020). Unlike the lime-treated soil, the G_{max} of untreated soil increased slightly over curing, which can be attributed to the aging effect of compacted soil: the amount of micro-pores increased with the exchange of water between the micro-pores and macro-pores with time (Delage et al., 2006), which could increase the soil capillarity, and hence soil matric suction and stiffness.

4.2 Factors influencing the stabilized values of G_{max}

For the lime-treated specimens S0.4, the stabilized values of G_{max} were found to be insensitive to the moulding water content (Fig. 6a), in agreement with the observation by Tang et al. (2011a).

However, in the case of lime-treated specimens S5, the specimens compacted dry of optimum had relatively higher G_{max} than the specimens compacted wet of optimum (Fig. 6b), which was consistent with the observations made by Wang et al. (2020). Tang et al. (2011a) and Wang et al. (2020) indicated that the G_{max} of dry side specimens was mainly governed by the contact surface of aggregates and cementitious bonds, while that of wet side specimens was dominated by suction and cementitious bonds. Ying et al. (2020) conducted MIP tests on the lime-treated specimens (the same silt as in this study) which were compacted on both dry and wet sides. They found that both dry and wet specimens exhibited aggregated structures with two populations of micro-pores and macro-pores, giving rise to similar contact surfaces of aggregates for dry and wet side specimens. Thus, the suction and cementitious bonds seemed to be the main factors influencing G_{max} for this lime-treated silt.

For a given soil, the formation of cementitious compounds was affected by the soil aggregate size and the moulding water content. It was reported that sufficient water was needed for the hydration and pozzolanic reaction in lime-treated soil (Muntohar et al., 2013; Russo and Modoni, 2013; Anggraini et al., 2016). This implied that much cementitious compounds might be formed for the specimens compacted wet of optimum, contributing more to the soil stiffness. However, the specimens compacted wet of optimum had lower suction, leading to a lower soil stiffness. Thus, for the lime-treated specimens compacted wet of optimum, there was competition between the positive contribution from the more significant formation of cementitious bonds and the negative contribution from the lower suction. Besides, the specimens with smaller aggregate size had a larger total contact surface between soil and lime, probably producing much more cementitious compounds (Tang et al., 2011a; Wang et al., 2017b). Thus, it can be inferred that, for specimens S0.4 compacted wet of optimum, much more cementitious bonds were created, which could compensate the degradation of G_{max} caused by the lower suction, making G_{max} increase to the level of specimens S0.4 compacted dry of optimum over curing. Nevertheless, as regards specimens S5, the promotion of pozzolanic reaction for the wet specimens was limited due to the smaller contact surface between soil and lime. Therefore, the lower suction for specimens S5 compacted wet of optimum led to lower G_{max} as compared to specimens S5 compacted dry of optimum.

4.3 Wetting-drying cycle effect on the microstructure and G_{max}

When the specimens were exposed to wetting, the untreated specimens could uptake more water than lime-treated soil, in agreement with the results obtained by Stoltz et al. (2012). For

untreated soil, wetting induced a significant expansion of soil specimens, giving rise to an appreciable increase of water content to 25%. On the contrary, the swelling potential was highly inhibited by lime treatment, leading to a lower water adsorption and thus small water uptake during wetting.

The untreated specimens were easily softened and damaged with wetting, while the lime-treated specimens survived from the cyclic wetting-drying tests and G_{max} seemed to undergo repeated decreasing and increasing cycles along the wetting and drying paths. This indicated that the lime treatment indeed improved the soil workability and long-term durability. The repetitive variations of G_{max} can be attributed to the suction effect induced from the water content variations (Ng et al., 2009; Tang et al., 2011a; Heitor et al., 2015; Ngoc et al., 2019). Generally, soil suction was reduced with wetting, leading to a reduction of soil stiffness. Nevertheless, upon drying, soil suction was increased. This corresponded to an increase in the mean effective stress which held the soil particles together and enhanced the soil mechanical behaviour, giving rise to an increase of G_{max} (Ng et al., 2009; Ngoc et al. 2019). The total suction was measured by chilled-mirror dew-point hygrometer (WP4C) for the lime-treated specimens S0.4 (t = 90 days) with two different soil salinities of 0.05‰ (g of salt/kg of dry soil) and 6.8‰, and for the lime-treated specimens S0.4 (t = 90 days) subjected to seven wetting-drying cycles. Note that the soil salinity of 6.8‰ corresponded to the salt concentration of 35 g/L in soil pore water, which was also the concentration of synthetic seawater. The osmotic suction of synthetic seawater was estimated at 2.4 MPa by the WP4C device. The total suctions were found to be 0.8 MPa and 3.2 MPa for the lime-treated specimens S0.4 (t = 90 days) with soil salinities of 0.05‰ and 6.8‰, respectively. For the specimens at the end of the seventh drying cycle, the total suctions were found to be 0.9 MPa for the specimens with deionized water, and 3.2 MPa in the case of synthetic seawater. This indicated that the total suctions of specimens after seven wetting-drying cycles were approximately equivalent to the values of as-compacted specimens (wetted by deionized water against soil salinity of 0.05‰, wetted by synthetic seawater against soil salinity of 6.8‰), respectively. This suggested that the suction variations were almost reversible during wetting-drying cycles as water content varied slightly in the range of 17% to 21%, in agreement with the G_{max} changes. It is also interesting to note that the difference between the total suctions of specimens with two different salinities (0.05‰ against 6.8‰, wetted by deionized water against by synthetic seawater) was around 2.3 ~ 2.4 MPa which was exactly equal to the osmotic suction of synthetic seawater, indicating that there was no precipitated salts as water content varied between 17% and 21%.

The changes in G_{max} of lime-treated specimens during wetting-drying cycles were in agreement with the microstructure variations in which the pore size distribution showed almost reversible pattern in the total seven wetting-drying cycles with the water content varying from 17% to 21% (Fig. 11a). During wetting, the expansion of soil aggregates led to an increase of the micro-pore size and a decrease of macro-pore size, while the subsequent drying resulted in the shrinkage of soil aggregates which made the pore size distribution recover to the state of specimens at water content of 17%. The almost reversible fabric changes of lime-treated soil were mainly attributed to the coarser aggregates and the cementitious bonds resulting from the soil-lime reaction, which could maintain the soil microstructure stable during wetting-drying cycles with water content varying slightly between 17% and 21%, and thus the repetitive decreasing and increasing phenomena of G_{max}. Nevertheless, the intensive drying to the water contents of 8% and 3% altered the microstructure significantly, which could be attributed to the shrinkage-related cracking of the clay part (Sun and Cui, 2018; Ying et al., 2021d). Indeed, some fissures/cracks would occur during drying, as the rising tensile stress exceeded the tensile strength or the soil shrinkage was constrained by boundary conditions (Péron et al., 2009; Tang et al., 2011b; Romero 2013). As shown in Fig. 11b, the pore size distribution changed from bi-modal characteristics (w = 17%) to tri-modal pattern (w = 8%) with three populations of nano-pores, micro-pores and macro-pores, in which the nano-pores were mostly composed of drying-induced nano-fissures. With further drying to 3% water content, the nano-pores became lager and lager with the continuous shrinkage of the clay part, making the nano-pores disappear. Tang et al. (2011a) worked on a lime-treated silt and reported that the drying-induced micro-cracks would result in a decrease of G_{max}. It appears from Fig. 9 that G_{max} increased significantly with the specimens being dried to 8% and 3%, indicating that the soil suction played a dominant role in the increase of G_{max} which prevailed facing the adverse effect of drying-induced fissures. Ying et al. (2021a) performed salinity assessment on this silt (soil salinity = 6.32‰) with decreasing water content and reported that when the water content decreased to 8%, some salts started to precipitate. It can be inferred that for this lime-treated silt wetted by synthetic seawater, some salts could precipitate with more intensive drying. This salt precipitation between soil particles played the role of bridge connection, contributing to soil stiffness (Truong et al., 2012). The subsequent wetting of specimens induced the healing of drying-induced fissures, as evidenced clearly by the disappearance of nano-pores on the pore size distribution curves when the specimen was wetted from water content of 8% to 21%. The similar phenomena of fissure healing were observed on the other specimens upon wetting which were previously dried to 17% and 3% water contents. This rewetting made G_{max} approach the values at wetting state

prior to the intensive drying. This was inconsistent with the results obtained by Tang et al. (2011a), who observed a significant reduction of G_{max} during the last wetting path after an intensive drying.

4.4 Wetting fluid effect on the G_{max} during wetting-drying cycles

As shown in Fig. 10, the increase of G_{max} with time at the end of each wetting or drying stage was much significant for the specimens wetted by synthetic seawater as compared to those wetted by deionized water. This indicated that synthetic seawater might enhance the soil stiffness. The similar results were obtained by Ying et al. (2021b) on untreated soil - the G_{max} of saline soil was higher than those of saltless soil due to the slight modification of microstructure by salts. Besides, the production of cementitious compounds might be promoted by salts. Indeed, Ramesh et al. (1999) reported that the sodium salts in fly ash-lime mixtures promoted the formation of sodium calcium silicate hydrate, and Saldanha et al. (2017) indicated that NaCl within 1% increased the dissolution of lime and gave rise to an increase of unconfined compressive strength. Thus, it can be inferred that the cations in synthetic seawater could promote pozzolanic reaction, and hence the formation of cementitious compounds. Nevertheless, it was also reported that wetting-drying cycles would resulted in a breakage or softening of the bonds of cementitious compounds, leading to a decrease of soil strength (Rao et al., 2001; Guney et al., 2007; Stoltz et al., 2014; Rosone et al., 2018; Cuisinier et al., 2020). For the specimens wetted by synthetic seawater, upon wetting (w = 21%) or drying (w = compacted water content), G_{max} followed an increasing trend during wetting-drying cycles (Fig. 9), suggesting that the contribution of cementitious compounds to G_{max} exceeded the reduction caused by the breakage or the softening of cementitious bonds. Nevertheless, in the case of the specimens wetted by deionized water, G_{max} followed a decreasing trend with wetting-drying cycles, as the destruction or softening of bonds prevailed facing the positive effect of cementitious compounds.

4.5 Aggregate size effect on the G_{max} during wetting-drying cycles

As mentioned previously, the specimens S0.4 with smaller aggregates had larger contact surface for soil-lime reaction. Thus, the promotion of pozzolanic reaction by synthetic seawater was much more significant for specimens S0.4 than for specimens S5. Besides, when the specimens were wetted by synthetic seawater, the thickness of diffuse double layer of clay fraction should decrease, causing a reduction of repulsive force, which in turn, led to an increase of net

attractive force (Mitchell and Soga, 2005; Israelachvili, 2011). This promoted the soil particles to associate with each other at a lower inter-particle distance (Sridharan and Jayadeva, 1982; Thyagaraj and Salini, 2015). Consequently, the G_{max} values of specimens S0.4 wetted by synthetic seawater were rather higher than those of the specimens wetted by deionized water (Fig. 9a). However, the larger aggregates of specimens S5 exhibited smaller contact surface between soil and lime, limiting the promotion of pozzolanic reaction by salts. Furthermore, the soil aggregation induced by salts can be neglected as compared to the initial larger aggregates in specimens S5. Thus, the difference between G_{max} of specimens S5 wetted by synthetic seawater and deionized water was insignificant (Fig. 9b).

5. Conclusions

The changes in small strain shear modulus (G_{max}) of untreated and lime-treated soils during curing and cyclic wetting-drying were studied, with consideration of the effects of maximum soil aggregate size and wetting fluid. The microstructure observations were made using MIP technique to investigate the effect of wetting-drying cycles on the soil fabric alteration. Based on the obtained results, the following conclusions were drawn:

(1) Lime treatment significantly increased G_{max} of soil due to the effects of soil flocculation and the production of cementitious compounds, and the G_{max} of untreated soil increased slightly due to the aging effect which would increase the soil suction slightly. The stabilized G_{max} values were independent of moulding water content for the treated specimens S0.4, because the much more production of cementitious compounds on wet side of optimum compensated the degradation of G_{max} induced from the lower suction. For the specimens S5 compacted on wet side, the lower suction effect prevailed the promotion of pozzolanic reaction by higher water content due to the smaller contact surface for soil-lime reaction, leading to lower G_{max} as compared to the specimens S5 compacted on dry side.

(2) The wetting-drying cycles had a significantly detrimental effect on the untreated specimens that induced some cracks on the soil surface and destroyed the soil samples at the third wetting cycle, whereas no significant volume variations and cracks were observed on lime-treated specimens, indicating the beneficiary effect of lime treatment in terms of long-term durability. The microstructure characterization showed that the pore size distributions of lime-treated soil were almost reversible with water content varying from 17% to 21%. The subsequent intensive drying altered the pore size distribution significantly, which changed from bi-modal pattern to

tri-modal pattern with drying from water content of 17% to 8%, and finally recovered to bi-modal pattern as water content decreased to 3%. Such fabric variations could be attributed to the clay shrinkage, producing some drying-induced fissures. However, the rewetting of lime-treated specimens could induce healing of fissures, making the pore size distribution exhibit similar pattern.

(3) Due to the almost reversible microstructure variations, the G_{max} of lime-treated soil followed the repeated decreasing and increasing trends with wetting and drying paths. Wetting reduced the soil matric suction and thus the soil stiffness, while drying increased the soil suction and stiffness. Upon intensive drying, G_{max} increased significantly, indicating that the negative effect of the drying-induced fissures can be neglected. As the fissures were healed, the rewetting led the G_{max} to approach the values at wetting state prior to the intensive drying.

(4) At each wetting or drying stage, G_{max} of lime-treated soil increased with time at the constant water content, which was attributed to the pozzolanic reaction. The increase of G_{max} was much significant for the specimens at wetting state, especially for the treated specimens wetted by synthetic seawater, suggesting that the production of cementitious compounds was promoted by salts. Nevertheless, under wetting or drying condition, G_{max} decreased slightly with the wetting-drying cycles in the case of deionized water as wetting fluid, indicating that the wetting-drying indeed induced softening of soil structure that exceeded the contribution of cementitious compounds. On the contrary, for the specimens wetted by synthetic seawater, G_{max} increased with wetting-drying cycles due to the much more significant effect of cementitious bonds.

(5) The lime-treated specimens S0.4 wetted by synthetic seawater had higher G_{max} than the specimens wetted by deionized water. By contrast, the wetting fluid had insignificant effect on G_{max} of lime-treated specimens S5. This could be attributed to the limited promotion of pozzolanic reaction by salts in specimens S5 which exhibited smaller contact surface between soil and lime, and to the negligible effect of soil aggregation induced by salts as compared to the initial lager aggregates.

Author statement

Zi Ying: Validation, Investigation, Writing - original draft. Yu-Jun Cui: Conceptualization, Methodology, Writing - review & editing. Nadia Benahmed: Investigation, Resources. Myriam Duc: Investigation.

Declaration of competing interest

The authors declare that they have no known competing financial interests or personal relationships that could have appeared to influence the work reported in this paper.

Acknowledgements

The authors would like to thank the China Scholarship Council (CSC). The supports provided by Ecole des Ponts ParisTech (ENPC) and INRAE are also greatly acknowledged.

References

Al-Mukhtar, M., Lasledj, A., Alcover, J.F., 2010a. Behaviour and mineralogy changes in lime-treated expansive soil at 20°C. Appl. Clay Sci. 50, 191-198. https://doi.org/10.1016/j.clay.2010.07.023

Al-Mukhtar, M., Lasledj, A., Alcover, J. F., 2010b. Behaviour and mineralogy changes in lime-treated expansive soil at 50°C. Appl. Clay Sci. 50, 199-203. https://doi.org/10.1016/j.clay.2010.07.022

Al-Mukhtar, M., Khattab, S., Alcover, J.F., 2012. Microstructure and geotechnical properties of lime-treated expansive clayey soil. Eng. Geol. 139/140, 17–27. https://doi.org/10.1016/j.enggeo.2012.04.004

Al-Swaidani, A., Hammoud, I., Meziab, A., 2016. Effect of adding natural pozzolana on geotechnical properties of lime-stabilized clayey soil. J. Rock Mech. Geotech. Eng. 8, 714-725. https://doi.org/10.1016/j.jrmge.2016.04.002

Aldaood, A., Bouasker, M., Al-mukhtar, M., 2014. Impact of wetting – drying cycles on the microstructure and mechanical properties of lime-stabilized gypseous soils. Eng. Geol. 174, 11-21. https://doi.org/10.1016/j.enggeo.2014.03.002

Anggraini, V., Asadi, A., Farzadnia, N., Jahangirian, H., Huat, B.B.K., 2016. Reinforcement Benefits of Nanomodified Coir Fiber in Lime-Treated Marine Clay. J. Mater. Civ. Eng. 28, 06016005. https://doi.org/10.1061/(asce)mt.1943-5533.0001516

ASTM D6276-19, 2019. Standard Test Method for Using pH to Estimate the Soil-Lime Proportion Requirement for Soil Stabilization. ASTM International, West Conshohocken, PA.

Bell, F.G., 1989. Lime stabilisation of clay soils. Bull. Int. Assoc. Eng. Geol 39, 67-74. https://doi.org/ 10.1007/BF02592537

Bell, F.G., 1996. Lime stabilization of clay minerals and soils. Eng. Geol. 42, 223-237. https://doi.org/10.1016/0013-7952(96)00028-2

Chakraborty, S., Banerjee, A., Das, J.T., Mosadegh, L., Puppala, A.J., 2018. Impact of variation of small strain shear modulus on seismic slope stability analysis of a levee: A Sensitivity Analysis. In IFCEE 2018, 302-313. https://doi.org/10.1061/9780784481608.029

Cuisinier, O., Deneele, D., 2008. Impact of cyclic wetting and drying on the swelling properties of a lime-treated expansive clay. In: Jourées Nationales de Géotechnique et de Géologie de l'Ingénieur JNGG'08, Nantes, pp. 18-20.

Cuisinier, O., Masrouri, F., Mehenni, A., 2020. Alteration of the hydromechanical performances of a stabilized compacted soil exposed to successive wetting-drying cycles. J. Mater. Civ. Eng. 32, 04020349. https://doi.org/10.1061/(asce)mt.1943-5533.0003270

Delage, P., Marcial, D., Cui, Y.J., Ruiz, X., 2006. Ageing effects in a compacted bentonite: A microstructure approach. Géotechnique 56, 291-304. https://doi.org/10.1680/geot. 2006.56.5.291

Di Sante, M., Fratalocchi, E., Mazzieri, F., Pasqualini, E., 2014. Time of reactions in a lime treated clayey soil and influence of curing conditions on its microstructure and behaviour. Appl. Clay Sci. 99, 100-109. https://doi.org/10.1016/j.clay.2014.06.018

Dong, J., 2013. Investigation of aggregates size effect on the stiffness of lime and/or cement treated soil: from laboratory to field conditions. PhD Dissertation. France, Ecole des Ponts ParisTech.

Estabragh, A.R., Moghadas, M., Javadi, A.A., 2013. Effect of different types of wetting fluids on the behaviour of expansive soil during wetting and drying. Soils Found. 53, 617-627. https://doi.org/10.1016/j.sandf.2013.08.001

French standard AFNOR NF P 18-837. 1993. Standard for special products for hydraulic concrete construction-Hydraulic binder based needling and/or sealing products-Testing of resistance against seawater and/or water with high sulphate contents.

Guney, Y., Sari, D., Cetin, M., Tuncan, M., 2007. Impact of cyclic wetting-drying on swelling behavior of lime-stabilized soil. Build. Environ. 42, 681-688. https://doi.org/10.1016/j.buildenv.2005.10.035

Heitor, A., Indraratna, B., Rujikiatkamjorn, C., 2015. The role of compaction energy on the small strain properties of a compacted silty sand subjected to drying-wetting cycles. Géotechnique. 65 (9), 717–727. https://doi.org/10.1680/geot.14.P.053

Israelachvili, J.N., 2011. Intermolecular and surface forces. 3rd edn. Academic press.

Khattab, S.A.A., Fleureau, J., 2007. Long-Term Stability Characteristics of a lime-treated plasric soil. J. Mater. Civ. Eng. 19(4), 358-366. https://doi.org/10.1061/(ASCE)0899-1561(2007)19:4(358)

Khosravi, A., Hashemi, A., Ghadirianniari, S., Khosravi, M., 2020. Variation of small-strain shear modulus of unsaturated silt under successive cycles of drying and wetting. J. Geotech. Geoenviron. Eng. 146, 1-13. https://doi.org/10.1061/(ASCE)GT.1943-5606.0002275

Lee, J. S., Santamarina, J. C., 2005. Bender elements: performance and signal interpretation. J. Geotech. Geoenviron. Eng. 131(9), 1063-1070. https://doi.org/10.1061/(ASCE)1090-0241(2005)131:9(1063)

Locat, J., Berube, M.A., Choquette, M., 1990. Laboratory investigations on the lime stabilization of sensitive clays: shear strength development. Can. Geotech. J. 27, 294-304. https://doi.org/10.1139/t90-040

Mitchell, J.K., Soga, K., 2005. Fundamentals of soil behaviour. 3rd edn. John Wiley &Sonc, Inc.

Muntohar, A.S., Widianti, A., Hartono, E., Diana, W., 2013. Engineering properties of silty soil stabilized with lime and rice husk ash and reinforced with waste plastic fiber. J. Mater. Civ. Eng. 25, 1260–1270. https://doi.org/10.1061/(asce)mt.1943-5533.0000659

Nabil, M., Mustapha, A., Rios, S., 2020. Impact of wetting-drying cycles on the mechanical properties of lime-stabilized soils. Int. J. Pavement Res. Technol. 13, 83-92. https://doi.org/10.1007/s42947-019-0088-y

Ng, C.W.W., Xu, J., Yung, S.Y., 2009. Effects of wetting-drying and stress ratio on anisotropic stiffness of an unsaturated soil at very small strains. Can. Geotech. J. 46, 1062-1076. https://doi.org/10.1139/T09-043

Ng, C.W.W., Yung, S.Y., 2008. Determination of the anisotropic shear stiffness of an unsaturated decomposed soil. Géotechnique. 58(1), 23-35. https://doi.org/10.1680/geot.2008.58.1.23

Ngoc, T.P., Fatahi, B., Khabbaz, H., 2019. Impacts of Drying-Wetting and Loading-Unloading Cycles on Small Strain Shear Modulus of Unsaturated Soils. Int. J. Geomech. 19(8), 04019090. https://doi.org/10.1061/(ASCE)GM.1943-5622.0001463

Péron, H., Hueckel, T., Laloui, L., Hu, L.B., 2009. Fundamentals of desiccation cracking of fine-grained soils: Experimental characterisation and mechanisms identification. Can. Geotech. J. 46, 1177-1201. https://doi.org/10.1139/T09-054

Puppala, A.J., Kadam, R., Madhyannapu, R.S., Hoyos, L.R. 2006. Small-strain shear moduli of chemically stabilized sulfate-bearing cohesive soils. J. Geotech. Geoenviron. Eng. 132(3), 322-336. https://doi.org/10.1061/(ASCE)1090-0241(2006)132:3(322)

Ramesh, H.N., Mohan, M.S., Sivapullaiah, P. V., 1999. Improvement of strength of fly ash with lime and sodium salts. Gr. Improv. 3, 163-167. https://doi.org/10.1680/gi.1999.030403

Rao, S.M., Reddy, B.V.V., Muttharam, M., 2001. The impact of cyclic wetting and drying on the swelling behaviour of stabilized expansive soils. Eng. Geol. 60, 223-233. https://doi.org/10.1016/S0013-7952(00)00103-4

Rao, S.M., Shivananda, P., 2005. Compressibility behaviour of lime-stabilized clay. Geotech. Geol. Eng. 23, 309-319. https://doi.org/10.1007/s10706-004-1608-2

Romero, E., 2013. A microstructural insight into compacted clayey soils and their hydraulic properties. Eng. Geol. 165, 3-19. https://doi.org/10.1016/j.enggeo.2013.05.024

Rosone, M., Airò Farulla, C., Ferrari, A., Torta, C., Celauro, C., 2016. Suction controlled drying and wetting cycle effects on the volumetric behaviour of a lime-treated high plasticity clay. E3S Web Conf. 9, 0-5. https://doi.org/10.1051/e3sconf/20160914020

Rosone, M., Ferrari, A., Celauro, C., 2018. On the hydro-mechanical behaviour of a lime-treated embankment during wetting and drying cycles. Geomech. Energy Environ. 14, 48-60. https://doi.org/10.1016/j.gete.2017.11.001

Russo, G., Modoni, G., 2013. Fabric changes induced by lime addition on a compacted alluvial soil. Geotech. Lett. 3, 93-97. https://doi.org/10.1680/geolett.13.026

Saldanha, R.B., Scheuermann Filho, H.C., Ribeiro, J.L.D., Consoli, N.C., 2017. Modelling the influence of density, curing time, amounts of lime and sodium chloride on the durability of compacted geopolymers monolithic walls. Constr. Build. Mater. 136, 65-72. https://doi.org/10.1016/j.conbuildmat.2017.01.023

Santamarina, J.C., Klein, K.A., Wang, Y.H., Prencke, E., 2002. Specific surface: Determination and relevance. Can. Geotech. J. 39, 233-241. https://doi.org/10.1139/t01-077

Sivapullaiah, P. V., Sridharan, A., Ramesh, H.N., 2000. Strength behaviour of lime-treated soils in the presence of sulphate. Can. Geotech. J. 37, 1358-1367. https://doi.org/10.1139/t00-052

Sridharan, A., Jayadeva, M.S., 1982. Double layer theory and compressibility of clays. Géotechnique 32, 133-144. https://doi.org/10.1680/geot.1982.32.2.133

Stoltz, G., Cuisinier, O., Masrouri, F., 2012. Multi-scale analysis of the swelling and shrinkage of a lime-treated expansive clayey soil. Appl. Clay Sci. 61, 44-51. https://doi.org/10.1016/j.clay.2012.04.001

Stoltz, G., Cuisinier, O., Masrouri, F., 2014. Weathering of a lime-treated clayey soil by drying and wetting cycles. Eng. Geol. 181, 281-289. https://doi.org/10.1016/j.enggeo.2014.08.013

Sun, W.J., Cui, Y.J., 2018. Investigating the microstructure changes for silty soil during drying. Géotechnique 68, 370-373. https://doi.org/10.1680/jgeot.16.P.165

Tang, A.M., Vu, M.N., Cui, Y.J., 2011a. Effects of the maximum soil aggregates size and cyclic wetting-drying on the stiffness of a lime-treated clayey soil. Géotechnique 61, 421-429. https://doi.org/10.1680/geot.SIP11.005

Tang, C.S., Shi, B., Liu, C., Suo, W. Bin, Gao, L., 2011b. Experimental characterization of shrinkage and desiccation cracking in thin clay layer. Appl. Clay Sci. 52, 69–77. https://doi.org/10.1016/j.clay.2011.01.032

Thyagaraj, T., Salini, U., 2015. Effect of pore fluid osmotic suction on matric and total suctions of compacted clay. Géotechnique 65, 952-960. https://doi.org/10.1680/jgeot.14.P.210

Truong, Q.H., Lee, C., Kim, Y.U., Lee, J.S., 2012. Small strain stiffness of salt-cemented granular media under low confinement. Géotechnique 62, 949-953. https://doi.org/10.1680/geot.10.T.004

Vitale, E., Deneele, D., Paris, M., Russo, G., 2017. Multi-scale analysis and time evolution of pozzolanic activity of lime treated clays. Appl. Clay Sci. 141, 36-45. https://doi.org/10.1016/j.clay.2017.02.013

Wang, Q., Cui, Y.J., Tang, A.M., Li, X.L., Ye, W.M., 2014. Time-and density-dependent microstructure features of compacted bentonite. Soils Found. 54(4), 657-666. https://doi.org/10.1016/j.sandf. 2014.06.021

Wang, Y.J., Cui, Y.J., Tang, A.M., Benahmed, N., Duc, M., 2017a. Effects of aggregate size on the compressibility and air permeability of lime-treated fine-grained soil. Eng. Geol. 228, 167-172. https://doi.org/10.1016/j.enggeo.2017.08.005

Wang, Y.J., Duc, M., Cui, Y.J., Tang, A.M., Benahmed, N., Sun, W.J., Ye, W.M., 2017b. Aggregate size effect on the development of cementitious compounds in a lime-treated soil during curing. Appl. Clay Sci. 136, 58-66. https://doi.org/10.1016/j.clay.2016.11.003

Wang, Y.J., Benahmed, N., Cui, Y. J., Tang, A. M. 2017c. A novel method for determining the small-strain shear modulus of soil using the bender elements technique. Can. Geotech. J. 54(2), 280-289. https://doi.org/10.1139/cgj-2016-0341

Wang, Y.J, Cui, Y.J., Benahmed, N., Tang, A.M., Duc, M., 2020. Changes of small strain shear modulus and suction for a lime-treated silt during curing. Géotechnique 70, 276-280. https://doi.org/10.1680/jgeot.18.T.018

Ying, Z., Cui, Y.J., Benahmed, N., Duc, M., 2020. Changes in mineralogy and microstructure of a lime-treated silty soil during curing time. E3S Web Conf. 195. https://doi.org/10.1051/e3sconf/202019503044

Ying, Z., Duc, M., Cui, Y.J., Benahmed, N., 2021a. Salinity assessment for salted soil considering both dissolved and precipitated salts. Geotech. Test. J. 44, 130-147. https://doi.org/10.1520/GTJ20190301

Ying, Z., Cui, Y.J., Benahmed, N., Duc, M., 2021b. Salinity effect on the compaction behaviour, matric suction, stiffness and microstructure of a silty soil. J. Rock Mech. Geotech. Eng. https://doi.org/10.1016/j.jrmge.2021.01.002

Ying, Z., Cui, Y.J., Benahmed, N., Duc, M., 2021c. Changes of microstructure and water retention property of a lime-treated saline soil during curing. Acta Geotech. https://doi.org/10.1007/s11440-021-01218-5

Ying, Z., Cui, Y.J., Benahmed, N., Duc, M., 2021d. Drying effect on the microstructure of compacted salted soil. Géotechnique. https://doi.org/10.1680/jgeot.20.P.319

Zeng, L.L., Cui, Y.J., Conil, N., Zghondi, J., Armand, G., Talandier, J., 2017. Experimental study on swelling behaviour and microstructure changes of natural stiff Teguline clays upon wetting. Can. Geotech. J. 54(5), 700-709. https://doi.org/10.1139/cgj-2016-0250

Zhou, Y.G., Chen, Y.M, 2005. Influence of seismic cyclic loading history on small strain shear modulus of saturated sands. Soil Dyn. Earthq. Eng. 25, 341-353. https://doi.org/10.1016/j.soildyn.2005.03.001

Zeng, Z.X., Cui, Y.J., Zhang, F., Conil, N., Talandier, J., 2020. Effect of technological voids on swelling behaviour of compacted bentonite–claystone mixture. Can. Geotech. J. 57(12), 1881-1892. https://doi.org/10.1139/cgj-2019-0339.

Ying, Z., Benahmed, N., Cui, Y.J., Duc, M. 2021. Submitted to Journal of Rock Mechanics and Geotechnical Engineering.

Wetting-drying cycle effect on the compressibility of lime-treated soil accounting for wetting fluid nature and aggregate size

Zi Ying[1], Nadia Benahmed[2], Yu-Jun Cui[1], Myriam Duc[3]

Abstract: The durability, which refers to the ability of earthen structures to ensure their functionality over time while maintaining their required mechanical performance, is a key issue in evaluating the effectiveness of lime treatment. In this study, the effect of wetting-drying cycles on the compressibility and the microstructure was investigated with untreated and lime-treated specimens considering the wetting fluid and maximum aggregate size (0.4 mm for S0.4 and 5 mm for S5) effects. Results showed that the wetting-drying cycles caused an increase of void ratio and changed the bi-modal porosity to tri-modal pattern for the untreated specimens, while it led to a reversible variation of void ratio and a conservation of bi-modal pore size distribution characteristics for lime-treated specimens, indicating the beneficiary effect of lime treatment in terms of durability. Thereby, the wetting-drying cycles made the compression curve of untreated specimens change from convex to linear without evident yield point, while their effect was visible but not significant for the lime-treated soil. Lower yield stress and higher decrease of macro-pore void ratio with loading were obtained on the lime-treated specimens under wetting-drying cycles compared to the as-compacted specimens, indicating a slight softening of soil structure by the wetting-drying cycles. Regarding the effect of wetting fluid nature, synthetic seawater, compared to deionized water, resulted in a higher compressibility. This was attributed to the presence of higher quantity of macro-pores in the specimens wetted by synthetic seawater induced by the shrinkage of the clay fraction. The aggregate size had insignificant effect on the compressibility of as-compacted specimens due to their similar production of cementitious compounds and matric suction. Nevertheless, after wetting-drying cycles, the lime-treated specimens S5 had higher yield stress and lower decrease of macro-pore void ratio than the lime-treated specimens S0.4, due to the significant reduction of macro-pore population with wetting-drying cycles.

Keywords: Lime-treatment; durability; compressibility; microstructure; wetting-drying cycles; wetting fluid; aggregate size

[1]: Ecole des Ponts ParisTech, Laboratoire Navier/CERMES, 6 – 8 av. Blaise Pascal, Cité Descartes, Champs-sur-Marne, 77455 Marne-la-Vallée cedex 2, France
[2]: INRAE, Aix Marseille Univ, Unité de Recherche RECOVER, 3275 route Cézanne, CS 40061, 13182 Aix-en-Provence, France
[3]: Université Gustave Eiffel, IFSTTAR/GERS/SRO, 14-20 boulevard Newton, Champs-sur-Marne, 77447 Marne-la-Vallée, France

1. Introduction

Nowadays, in order to move towards more sustainable engineering practice and reduce economic, environmental and ecological impacts, there is an increasing requirement to re-use the soils located at the site of constructions such as embankments, roads, highways, landfills, dikes, etc. However, in most cases, the local soils cannot meet the required mechanical performance. In this context, geotechnical improvement enhancing the resistance of soils becomes indispensable prior to their use. Stabilization with lime treatment is often used in that case to improve the soil mechanical performance through different physical-chemical reactions (Locat et al., 1990; Bell, 1996; Tang et al., 2011; Mavroulidou et al., 2013; Vitale et al., 2017; Wang et al., 2017; Cuisinier et al., 2020; Bian et al., 2021).

It is widely recognised that the compressibility is an important parameter to evaluate the mechanical performance of soils (Olson and Mesri, 1970; Burland, 1990; Hong et al., 2010; Zeng et al., 2015). Delage and Lefebvre (1984) and Marcial et al. (2002) reported that, when the clayey soils was compressed in oedometer, the decrease of volume corresponded to the collapse of macro-pores (or inter-aggregate pores) at low pressure and to the modification of micro-pores (intra-aggregate pores) at higher stress level, which made the soil particles denser and led to more oriented microstructure. As for the granular soils, the volume change during compression was characterised by the re-arrangement of silt/sand particles at low stress level and by the breakage of grains at higher stress stage (Mesri and Vardhanabhuti, 2009; Mun and McCartney, 2017; Zhao et al., 2020). Wang et al. (2021) indicated that, for soil containing fine and coarse soil particles, the compressibility was related to both collapse of pores and breakage of grains.

As far as the lime effect on the soil compression behaviour is concerned, it was reported that the lime treatment led to a decrease of soil compressibility and an increase of yield stress due to the flocculation of soil particles and the production of cementitious compounds in long-term pozzolanic reaction (Rajasekaran and Rao, 2002; Rao and Shivananda, 2005; Mavroulidou et al., 2013; Vitale et al., 2017; Wang et al., 2017). In general, the higher the lime content or the longer the curing time, the lower the compressibility. Wang et al. (2017) indicated that the compression behavior of lime-treated soil is affected by the soil aggregate size - the specimens with smaller aggregates exhibited lower compressibility and higher oedometer modulus, as lime was distributed more homogeneously inside the soil in the case of smaller aggregates, resulting in more cementitious compounds production.

Beyond the beneficial effects induced by lime treatment, the durability or long-term stability characteristics of lime-treated soils upon the influence of environmental factors has attracted particular attention. Indeed, lime-treated soil might be altered by cyclic climate loadings, such as wetting-drying cycles which may result in the softening/destruction of cementitioud bonds and soil structure, decreasing the mechanical performance and thus compromising the durability of lime-treated soil (Rao et al., 2001; Aldaood et al., 2014; Cuisinier et al., 2020; Nabil et al., 2020). Indeed, Stoltz et al. (2014) and Rosone et al. (2018) performed oedometer tests on the lime-treated specimens which were subjected to wetting-drying cycles and reported that the wetting-drying cycles led to an increase of compressibility and a significant reduction of yield stress. It appears from the above-mentioned studies that, although numerous studies had been focused on the compressibility of lime-treated soil, few studies involved the effects of wetting fluids nature and aggregate sizes while investigating the effect of wetting-drying cycles on the compression behaviour of lime-treated soils.

The aim of this study is to clarify the effect of wetting-drying cycles on the compression behaviour of lime-treated soils with consideration of soil aggregate size and wetting fluid effects. For this purpose, two soil powders with two different maximum aggregate sizes of 0.4 mm and 5 mm (S0.4 and S5 respectively) were used. Both untreated and lime-treated specimens were prepared by static compaction. At a given curing time of 90 days, wetting-drying cycles were performed on specimens with either deionized water or synthetic seawater as wetting fluids. Oedometer tests were conducted on the specimens at as-compacted state and the specimens after wetting-drying cycles. Furthermore, after compression, the specimens were subjected to mercury intrusion porosimetry (MIP) tests, allowing the interpretation of compression behaviour by considering the microstructure changes.

2. Materials and methods

2.1 Materials

A plastic silt, which was taken from Les Salins de Giraud, a traditional salt exploitation site in southern France, was used in this study. According to the grain size distribution in Fig. 1, this silt is made up mostly of 83% silt/sand fraction and 17% clay-size particles (< 0.002 mm). Mineral analysis showed that the non-clay minerals consists of 39% quartz, 35% calcite, 9.5% feldspar and 0.8% halite, and the clay minerals includes 10.8% illite, 3.6% chlorite and 1.3% kaolinite. Table 1 presents the geotechnical properties of this silt (Ying et al., 2021a). The soil

salinity, defined as the mass ratio of salt to dry soil, was estimated at 2.1‰ (g of salt/kg of dry soil) (Ying et al., 2021b). To remove the salt present in the natural soil, the latter was washed by deionized water in a leaching equipment (Ying et al., 2021c). The final soil salinity of leached soil was down to 0.05‰ (g of salt/kg of dry soil), which is rather low and can be neglected in further analysis. Afterwards, the leached soil was air-dried, ground and sieved through two sieves to obtain two soil powders with two different maximum aggregate sizes which were S0.4 with D_{max} = 0.4 mm and S5 with D_{max} = 5 mm. The aggregate size distributions of these two soil powders were presented in Fig. 1.

Table 1. Geotechnical properties of tested silt.

Property	Atterberg limits			Specific gravity	Compaction behaviour of 2% lime-treated soil	
	Liquid limit (%)	Plastic limit (%)	Plasticity index		Maximum dry density (Mg/m^3)	Optimum water content (%)
Value	29	19	20	2.71	1.66	18.7

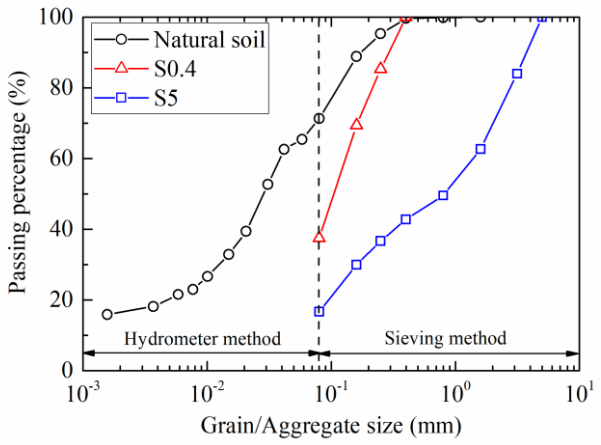

Fig. 1. Grain/Aggregate size distributions of the natural soil and dry soil powders.

After grinding, the dry soil powders were mixed with 2% quicklime (97.3% CaO) which was the same lime dosage used for the dike construction at Les Salins de Giraud, and then humidified by deionized water to reach a water content w = 17% which corresponded to the dry side of optimum water content determined by the Standard Proctor Compaction Test (AFNOR NF P94-093, 1999). After the soil-lime-water mixtures being mellowed for 1h, the specimens were prepared by static compaction at a rate of 0.3 mm/min to a target dry density equal to 1.63Mg/m^3 (98% compactness of Standard Proctor maximum dry density). It is worth underlining that the dry density of 1.63 Mg/m^3 was selected as the compaction state in the dike construction. The untreated specimens were prepared at the same water content and dry density

as for the lime-treated specimens. The final dimensions of specimens were 50 mm in diameter and 20 mm in height. The compaction stresses were around 2000 kPa for the untreated specimens and 3500 kPa for the lime-treated specimens. Immediately after compaction, the lime-treated specimens were wrapped with a plastic film and adhesive tape, and covered by paraffin. Then, they were stored in a hermetic box and cured for 90 days.

2.2 Test methods

At curing time of 90 days, wetting-drying cycles were performed on the specimens in a standard oedometer cell. Prior to the installation of a specimen, the inner side surface of the cell was smeared with silicone grease to avoid any leakage between the specimens and the cell. Two porous stones and two filter papers which were fully saturated were placed on the top and bottom of the specimen in the oedometer cell (Fig. 2). Previously, the height of the cell and the stacked two porous stones and filter papers were measured by a calliper in order to determine the variation of specimen's height during wetting-drying cycles. Before starting the wetting step, the masses of the cell, porous stones and filter papers were weighted in order to determine the specimen's mass at each wetting-drying stage. Then, the specimen was wetted by carefully dropping water on the top surface of porous stone and monitoring the changes of the total mass of the wetting-drying oedometer system using a balance. Deionized water and 35 g/L synthetic seawater with an osmotic suction of 2.4 MPa were used as wetting fluids, respectively. Table 2 illustrates the salt composition of synthetic seawater according to the French standard (AFNOR NF P 18-837, 1993). The wetting process was considered to be completed when a constant total mass was maintained with further wetting. In the drying process, the specimens were air-dried to the initial soil mass. Both untreated and lime-treated specimens were subjected to a total of seven wetting-drying cycles. At the end of each wetting or drying cycle, the soil mass was determined, and the height variation of the specimen was measured by taking the height between the top of the cell and the upper side of the top porous stone (h_i, as shown in Fig. 2). Note that the lateral deformation during wetting was ignored because the specimens were laterally constrained in oedometer cell. During drying, the lateral deformation of lime-treated specimens was also ignored due to their negligible shrinkage, while that of untreated specimens were measured by a calliper. Then, the void ratios of the specimens at each wetting-drying stage were calculated using Eq. (1):

$$e = \frac{\rho_s (1+w)}{\rho} - 1 \tag{1}$$

where ρ_s is the density of soil particle (2.71 Mg/m^3), ρ is the density of soil specimen, and w is the water content.

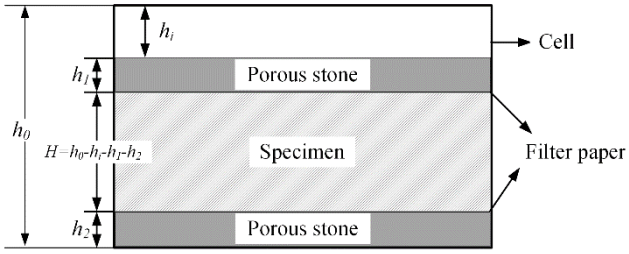

Fig. 2. Sketch of wetting-drying system.

Table 2. Salt composition of synthetic seawater.

Salts	NaCl	$MgCl_2 \cdot 6H_2O$	$MgSO_4 \cdot 7H_2O$	$CaSO_4 \cdot 2H_2O$	$KHCO_3$
Concentration (g/L)	30.0	6.0	5.0	1.5	0.2

At the end of the seventh drying stage for each specimen, oedometer test was carried out following the procedure described in ASTM standard (ASTM 2435-04, 2004). The specimen was first loaded to 10 kPa, then subjected to incremental loadings until reaching a maximum load of 3250 kPa. The loading during each stage was maintained constant for 24 h to ensure the final displacement rate to be lower than 0.01 mm/h as suggested in the ASTM standard. For the untreated specimens after wetting-drying cycles, loading time of 48 h was selected at the first loading because of their larger displacement. The vertical displacements were measured by the micrometer dial gauge with an accuracy of 0.001 mm. The sample height and the void ratio were then determined. For comparison, the as-compacted untreated specimens and lime-treated specimens at 90-day curing were subjected to oedometer tests as well.

Once the oedometer test was completed, the specimens were unloaded and taken out of the oedemeter cells for mercury intrusion porosimetry (MIP) tests. Meanwhile, the specimens at as-compacted state and at the end of wetting-drying cycles were also subjected to MIP tests, for comparison. Prior to testing, the specimens were cut into several small pieces, then rapidly frozen using vacuumed liquid nitrogen and dried by a freeze dryer for at least 24 h. In the MIP test, the freeze-dried piece was firstly put into a low pressure system, and then transferred to a high pressure system with applied pressure ranging from 3.6 kPa to 230 MPa. The corresponding entrance pore diameter varied from 350 μm to 6 nm.

3. Results

3.1 Void ratio change during wetting-drying cycles

Figure 3 presents the void ratio variations under wetting-drying cycles for both untreated specimens and lime-treated specimens at 90-day curing. It appears that for lime-treated soil, the void ratio increased slightly with wetting, then decreased to the value at previous drying state, leading to almost reversible variations of void ratio with wetting-drying cycles. However, the void ratios of untreated specimens changed significantly with cycles. In general, the wetting paths induced more significant increase of void ratio for untreated specimens as compared to lime-treated specimens. For untreated specimens, the drying paths induced limited decrease of void ratio especially for the third drying path, which prevented the specimens from recovering to the state at previous wetting. This finally resulted an increase of void ratio for untreated specimens at the end of cyclic tests. Regarding the nature of the wetting fluids, it had insignificant effect on the void ratio variations of lime-treated soil, while the final void ratio of untreated specimens wetted by synthetic seawater was slightly higher than that of specimens wetted by deionized water.

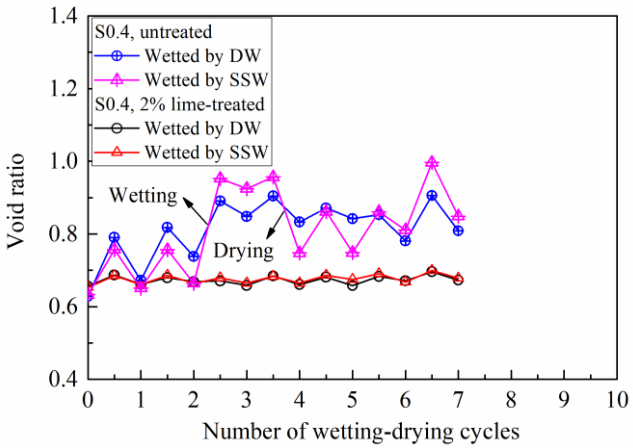

Fig. 3. Void ratio variations during wetting-drying cycles.

3.2 Effect of wetting-drying cycles on compression behaviour

The compression curves of untreated specimens S0.4 and S5 and lime-treated specimens S0.4 and S5 at 90-day curing and subjected to seven wetting-drying cycles with deionized water and synthetic seawater as wetting fluids are presented in Figs. 4a, 4b, 4c and 4d, respectively. They were also compared with those of as-compacted specimens without undergoing wetting-drying cycles. It appears from Figs. 4a and 4b that the wetting-drying cycles had a significant effect

on the compression behaviour of untreated specimens: i) the void ratio decreased much more significantly with loading for the untreated specimens subjected to wetting-drying cycles than for the as-compacted specimens; ii) the as-compacted specimens exhibited obvious yield stress (σ_y) of about 380 kPa for S0.4 and 340 kPa for S5 which was determined using Casagrande method, while the yield points of untreated specimens subjected wetting-drying cycles were indistinguishable. Besides, the effect of wetting fluids nature seemed to be slight for the untreated specimens S0.4, whereas the synthetic seawater led to a higher decrease of void ratio of untreated specimens S5 than the deionized water. As regards the lime-treated specimens at 90-day curing, the wetting-drying cycles resulted in a reduction of yield stress. Specifically, the yield stresses of as-compacted lime-treated specimens S0.4 and S5 were around 460 kPa and 515 kPa respectively; these values decreased to 317 kPa and 319 kPa for specimens S0.4 and S5 with deionized water as wetting fluid, and to 230 kPa and 265 kPa for those specimens S0.4 and S5 wetted by synthetic seawater, respectively.

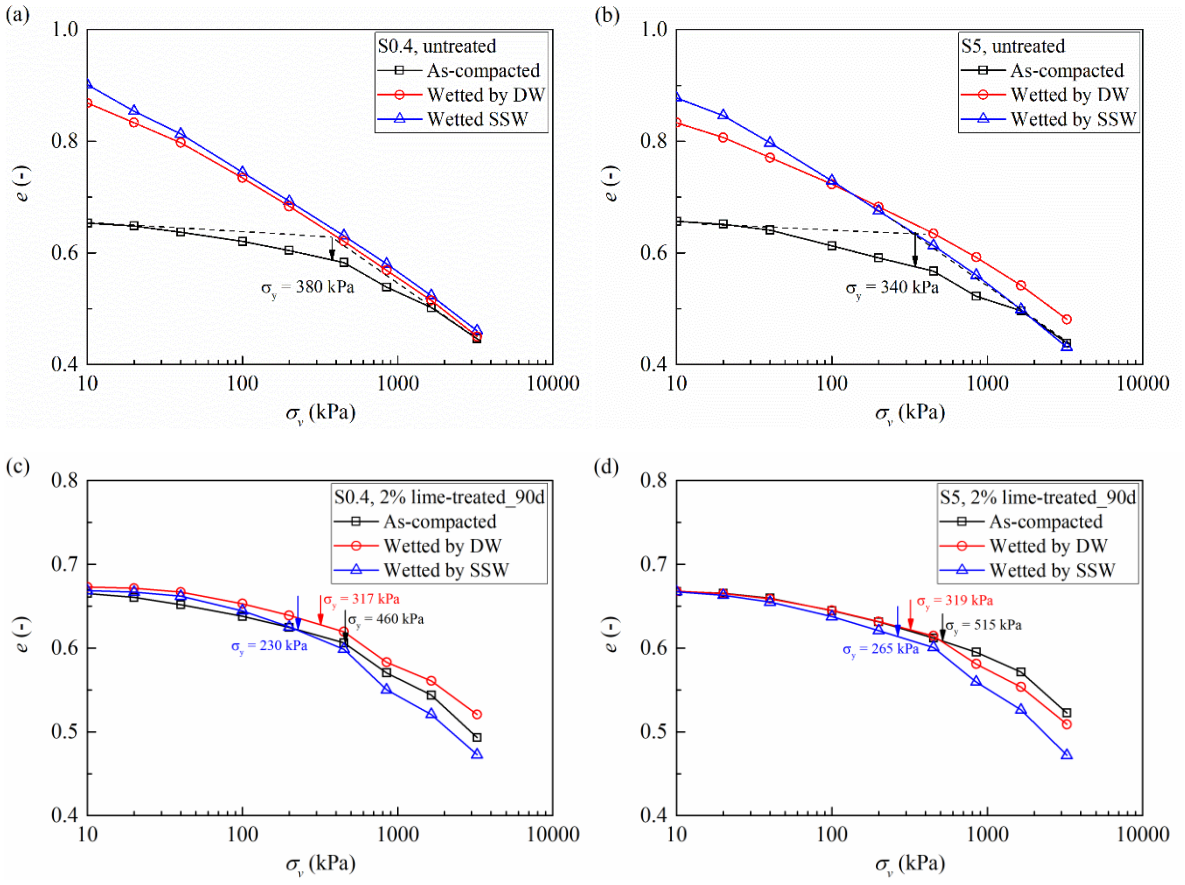

Fig. 4. Compression curves e-logσ_v: (a) untreated S0.4; (b) untreated S5; (c) 2% lime-treated S0.4_90 days; (d) 2% lime-treated S5_90 days.

To further analyze the effect of wetting-drying cycles on the compression behaviour, the total

volume strain (ε_v) with loading was determined (Eq. 2). In addition, the compression index (C_c^*) and the oedometer modules (E_{oed}) at each loading step were determined by Eq. 3 and 4 respectively, as these parameters varied with loading (Deng et al., 2014):

$$\varepsilon_v = \frac{de}{1+e_0} \tag{2}$$

$$C_c^* = \frac{de}{d\log\sigma_v} \tag{3}$$

$$E_{oed} = \frac{d\sigma_v}{d\varepsilon_v} = (1+e_0)\frac{d\sigma_v}{de} \tag{4}$$

where e_0 is the initial void ratio of specimens before compression; de is the change in void ratio under an increment of vertical stress of $d\sigma_v$.

The changes in volumetric strain, compression index and oedometer modulus with vertical stress are plotted in Figs. 5, 6 and 7, respectively. In the case of untreated specimens, the volumetric strain of the specimens subjected to wetting-drying cycles was rather larger than that of as-compacted specimens, regardless of the soil maximum aggregate sizes (Figs. 5a and 5b). For instance, at the maximum vertical load of 3250 kPa, the total volumetric strain was up to 0.2 ~ 0.25 for the untreated specimens subjected to wetting-drying cycles, while it was around 0.13 for the as-compacted untreated specimens. Moreover, the untreated specimens S0.4 and S5 wetted by synthetic seawater had higher volumetric strain as compared to the specimens wetted by deionized water. The similar results were obtained for the lime-treated specimens - both specimens S0.4 and S5 wetted by synthetic seawater had the highest volumetric strain as compared to the specimens with deionized water as wetting fluid and to the as-compacted specimens (Figs. 5c and 5d).

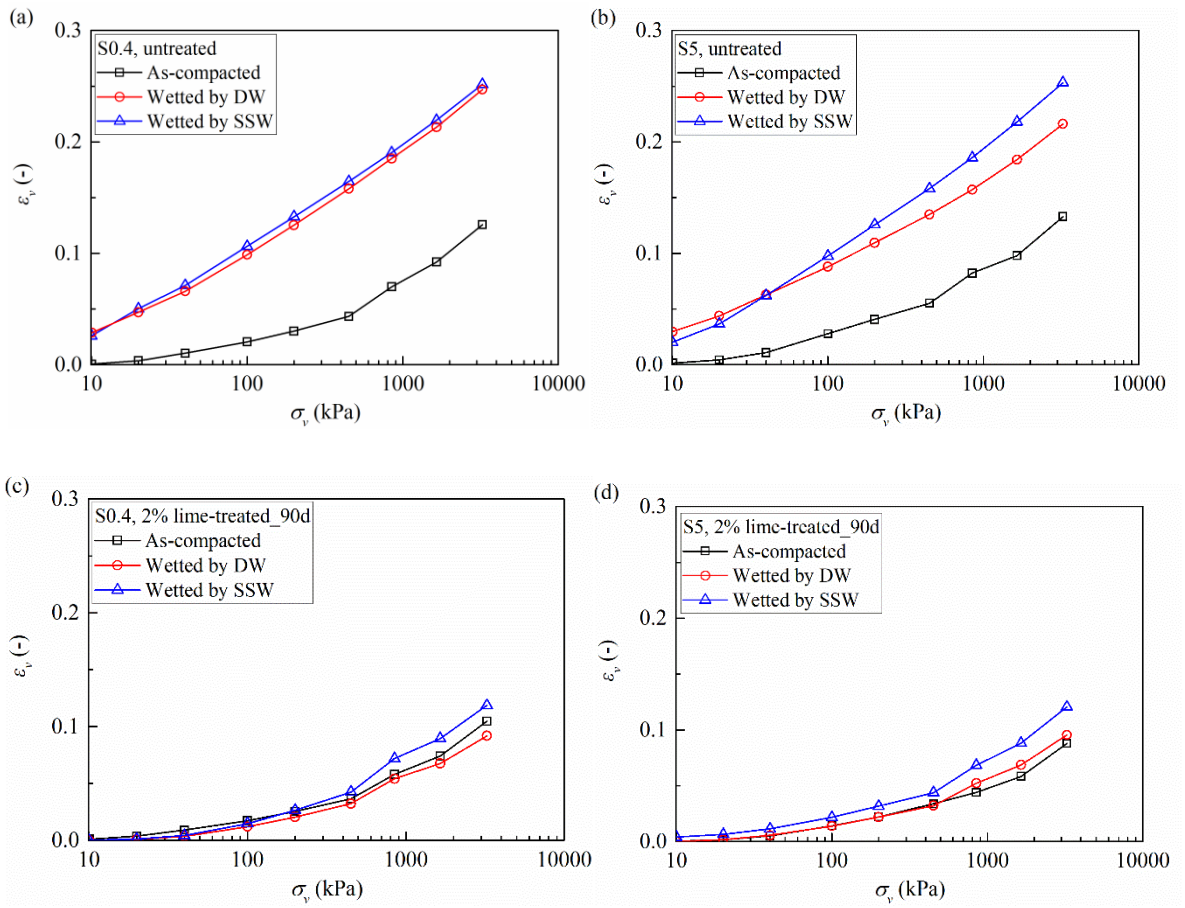

Fig. 5. Volume strain versus vertical stress: (a) untreated S0.4; (b) untreated S5; (c) 2% lime-treated S0.4_90 days; (d) 2% lime-treated S5_90 days.

As shown in Figs. 6a and 6b, the compression index C_c^* of untreated specimens subjected to wetting-drying cycles was rather larger than that of as-compacted specimens, suggesting that the wetting-drying cycles resulted in a higher compressibility of untreated specimens. For the untreated specimens S0.4 and S5 at as-compacted state, the C_c^* increased slightly from around 0.016 to 0.06 as the vertical stress increased from 20 kPa to 450 kPa; then, it increased significantly up to 0.19 at vertical stress of 3250 kPa. Regarding the untreated specimens S0.4 subjected to wetting-drying cycles, the C_c^* increased gradually from 0.12 (deionized water as wetting fluid) and 0.16 (synthetic seawater as wetting fluid) to around 0.22 with loading. However, for the untreated specimens S5, the C_c^* of specimens wetted by synthetic seawater was larger than that of specimens wetted by deionized water at each loading step. In the case of lime-treated specimens, the difference of C_c^* between the as-compacted specimens and the specimens under wetting-drying cycles was not as significant as for the untreated specimens. On the whole, the specimens S0.4 and S5 wetted by synthetic seawater had the largest C_c^*. Similar to the untreated specimens at as-compacted state, the C_c^* increased slightly to 0.05 at

vertical stress of 450 kPa, then increased with a relatively higher rate with further loading to 3250 kPa.

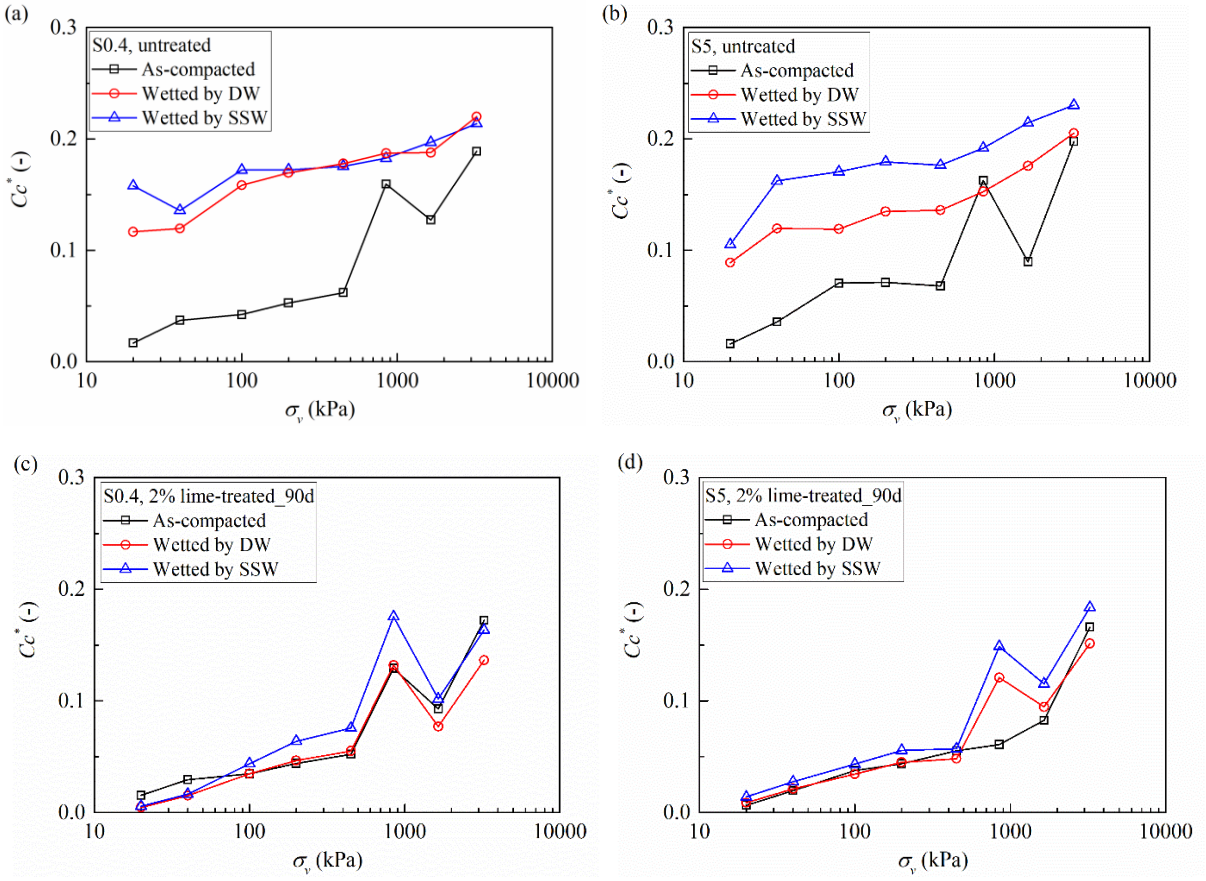

Fig. 6. Compression index versus vertical stress: (a) untreated S0.4; (b) untreated S5; (c) 2% lime-treated S0.4_90 days; (d) 2% lime-treated S5_90 days.

Figure 7 presents the relationships between oedometer modulus and vertical stress on the semi-logarithmic scale. For the untreated specimens, the E_{oed} of as-compacted specimens was slightly higher in the beginning of loading than those of specimens subjected to wetting-drying cycles, then increased with higher rate and finally converged to those of specimens with wetting-drying cycles when the vertical stress reached 850 kPa, and followed fairly the same evolution beyond this value. Regarding the wetting fluids type, it had insignificant effect on the E_{oed} of untreated specimens S0.4 as indicated by the two overlapped curves, while the synthetic seawater led to lower E_{oed} for the specimens S5 as compared to deionized water (Figs. 7a and 7b). Similarly, the E_{oed} of lime-treated specimens S0.4 and S5 wetted by synthetic seawater was slightly lower than those of specimens wetted by deionized water and of as-compacted specimens (Figs. 7c and 7d). Furthermore, the evolution rate of E_{oed} of lime-treated specimens can be divided into two zones: a first zone with E_{oed} increasing slightly from 5 ~ 10 MPa to around 20 MPa with

loading to 450 kPa, and a second zone with E_{oed} increasing rapidly to 50 ~ 60 MPa with further loading to 3250 kPa.

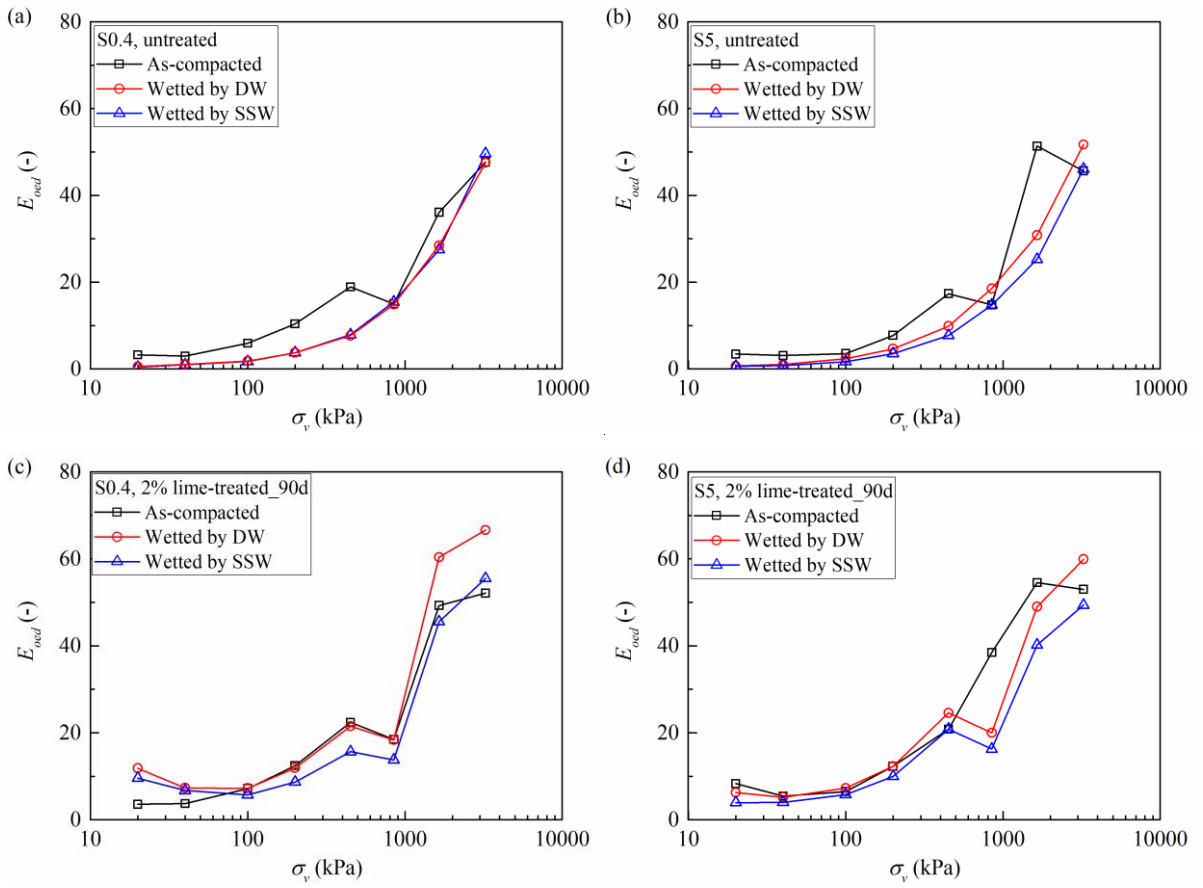

Fig. 7. Oedometer modulus versus vertical stress: (a) untreated S0.4; (b) untreated S5; (c) 2% lime-treated S0.4_90 days; (d) 2% lime-treated S5_90 days.

3.3 Effect of lime treatment and aggregate size on compression behaviour

To compare the effects of lime treatment and maximum aggregate size on the compression behaviour, the compression index and oedometer modulus against vertical stress are plotted in Fig. 8. From Figs. 8a and 8b, it was observed that for the as-compacted specimens, the points of C_c^* of lime-treated specimens lay slightly below those of untreated specimens, regardless of the soil maximum aggregate sizes (S0.4 and S5). Conversely, the E_{oed} of lime-treated specimens were higher than those of untreated specimens. As compared to the untreated specimens S5, the untreated specimens S0.4 seemed to exhibit lower C_c^* and slightly higher E_{oed} when the vertical stress was lower than 450 kPa, whilst beyond this stress, the reverse results were obtained. For the lime-treated specimens, the specimens S0.4 seemed to have larger C_c^* and lower E_{oed} in the range of vertical stress either below 100 kPa or beyond 850 kPa (Figs. 8a and 8b).

As regards the specimens subjected to wetting-drying cycles, the lime-treated specimens exhibited relatively smaller C_c^* and higher E_{oed} than the untreated specimens (Figs. 8c-8f). Regarding the aggregate size effect, smaller C_c^* and higher E_{oed} were observed on lime-treated specimens S0.4 when the vertical stresses were either lower than 100 kPa or higher than 850 kPa, whatever the wetting fluid (Figs. 8c-8f). For the untreated specimens, specimens S0.4 seemed to have larger C_c^* and slightly lower E_{oed} as compared to specimens S5 in the case of deionized water, whereas the reverse results were obtained in the case of synthetic seawater.

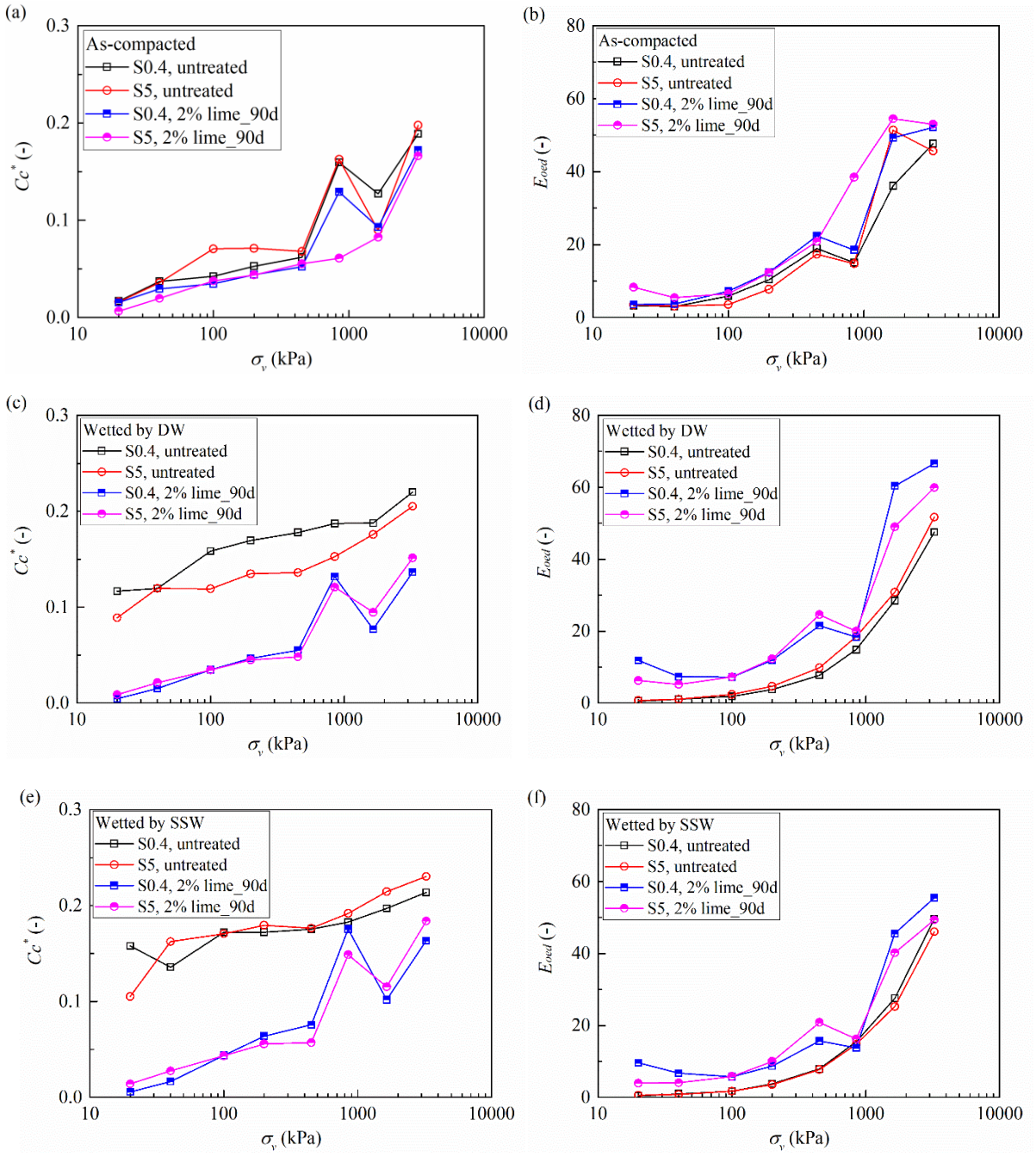

Fig. 8. Lime treatment and aggregate size effect on the compression behaviour.

3.4 Microstructure analysis

The cumulative mercury intrusion curves and density function curves from MIP tests are presented in Figs. 9 and 10 for the untreated and lime-treated specimens S0.4 and S5, respectively. It can be observed that the total intruded void ratio increased after wetting-drying cycles for untreated specimens, while it had no significant change for lime-treated specimens, which was in agreement with the results of global void ratios obtained by measurement. As expected, the total intruded void ratio became smaller after compression. Moreover, after compression, the specimens wetted by synthetic seawater had the lowest total intruded void ratio as compared to the specimens wetted by deionized water and to the as-compacted specimens (Fig. 9).

As shown in Fig. 10, for both untreated and lime-treated specimens at as-compacted state, the pore size distribution exhibited bi-modal characteristic with micro-pores and macro-pores. The macro-pores corresponded to the pores between aggregates which were constituted by silt/sand grains with clay matrix coating them, while the micro-pores related to the pores within aggregates (Ying et al., 2021d). From Figs. 10a and 10b, it appears that the untreated specimens S0.4 and S5 had similar modal size of micro-pores at 0.85 μm, while the specimens S0.4 exhibited lower modal size of macro-pores than specimens S5 (10.7 μm against 13.8 μm). Moreover, in the case of untreated specimens S0.4, the wetting-drying cycles made the pore size distribution change to tri-modal pattern with a new population of larger pores at diameters ranging from 30 μm to 200 μm and a reduction of macro-pore frequency. This suggested that the fabric of untreated soil might be altered by wetting-drying cycles (Fig. 10a). Furthermore, for untreated soil either at as-compacted state or after wetting-drying cycles, the frequency of macro-pores was reduced significantly by compression, while the micro-pores were affected slightly.

In the case of lime-treated specimens at as-compacted state (Figs. 10c and 10d), the modal sizes of micro-pores (0.7 μm) were close for specimens with different aggregate sizes, while those of macro-pores were found to be larger for specimens S5 than for specimens S0.4 (12.2 μm against 7 μm). After wetting-drying cycles, the microstructure of lime-treated soil kept bi-modal characteristics in which the modal size of macro-pores became smaller and that of micro-pores remained almost unchanged. The compression resulted in a reduction of the frequency and modal size of macro-pore for the treated specimens at as-compacted state. However, after

wetting-drying cycles, loading made the macro-pores almost disappear for treated specimens S5, while a small quantity of macro-pores still existed for treated specimens S0.4.

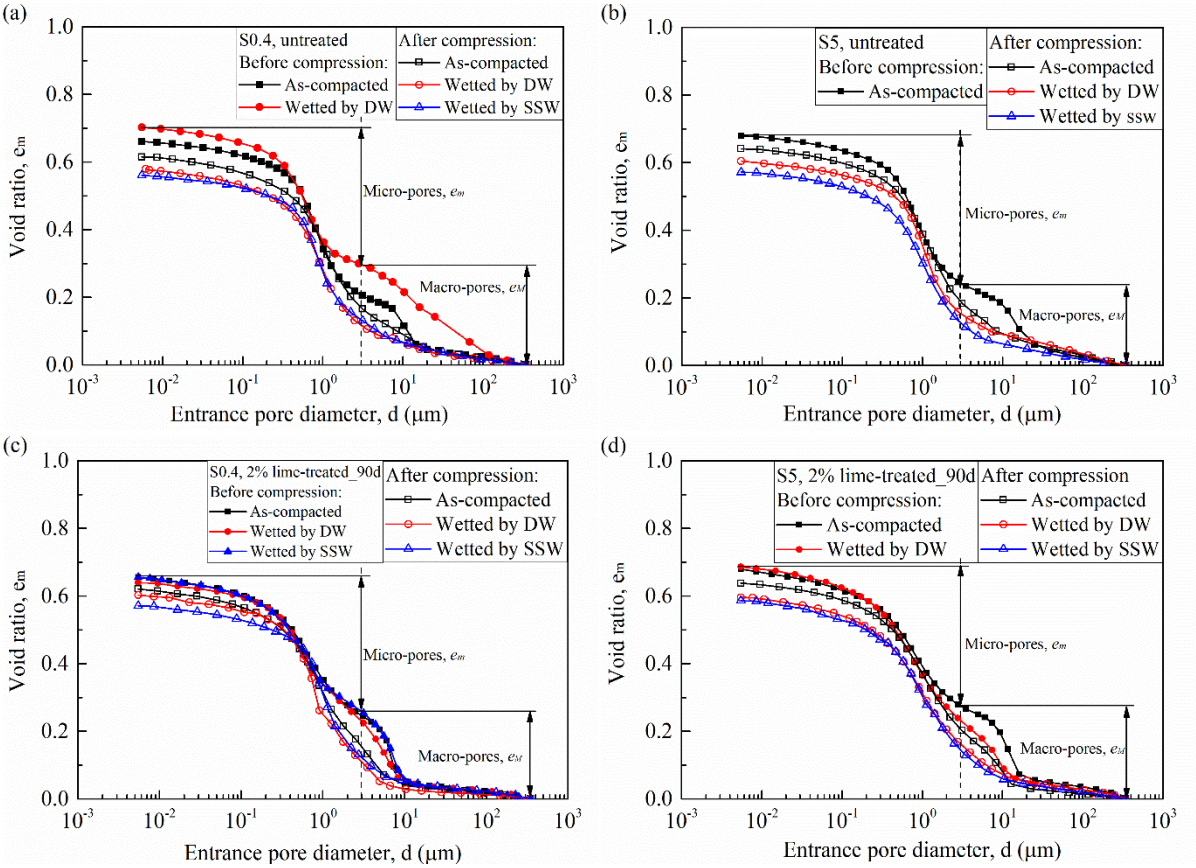

Fig. 9. Cumulative mercury intrusion curves from MIP tests: (a) untreated S0.4; (b) untreated S5; (c) 2% lime-treated S0.4_90 days; (d) 2% lime-treated S5_90 days.

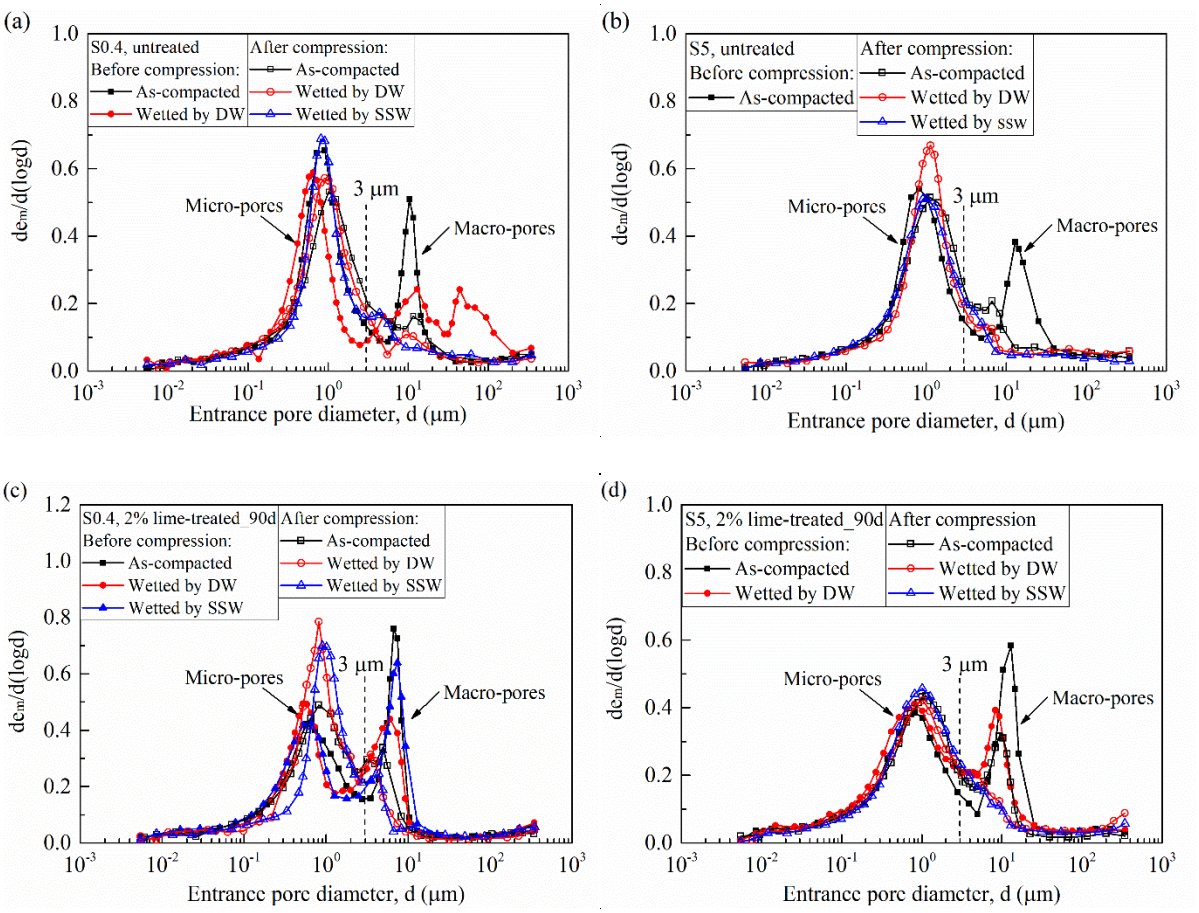

Fig. 10. Density function curves from MIP tests: (a) untreated S0.4; (b) untreated S5; (c) 2% lime-treated S0.4_90 days; (d) 2% lime-treated S5_90 days.

The void ratio variations induced by compression were quantified and presented in Table 3. The delimiting diameter between micro-pores and macro-pores was selected as 3 μm, which corresponded to the minima between two peaks (Fig. 10). The void ratios of micro-pores and macro-pores can be determined from the cumulative mercury intrusion curves (Fig. 9). As shown in Table 3, compression caused a reduction of macro-pore void ratio and led to an increase of micro-pore void ratio. For both untreated and lime-treated specimens S0.4 and S5 after compression, the specimens subjected to wetting-drying cycles exhibited a higher decrease of the macro-pore void ratio as compared to the specimens at as-compacted state. The results from lime-treated specimens S0.4 showed that compression led to a slightly higher decrease of macro-pore void ratio for the specimens wetted by synthetic seawater than for the specimens wetted by deionized water (53.2% against 50.7%). The maximum soil aggregate size had insignificant effect on the variation of macro-pores for untreated specimens. Nevertheless, regarding the lime-treated specimens, the specimens S5 with larger aggregates seemed to have lower decrease of macro-pore void ratio.

Table 3. Void ratio variations after compression.

Specimens	Micro-pores: d < 3 μm			Macro-pores: d > 3 μm		
	Before compression e_{m1}	After compression e_{m2}	$\frac{e_{m1}-e_{m2}}{e_{m1}}$ (%)	Before compression e_{M1}	After compression e_{M2}	$\frac{e_{M1}-e_{M2}}{e_{M1}}$ (%)
S0.4, untreated_as-compacted	0.453	0.447	1.3	0.213	0.168	21.2
S0.4, untreated_7W/D by DW	0.405	0.463	-14.5	0.298	0.117	60.8
S5, untreated_as-compacted	0.435	0.453	-4.1	0.245	0.188	22.9
S0.4, lime-treated_as-compacted	0.409	0.464	-13.6	0.247	0.156	36.7
S0.4, Lime-treated_7WD by DW	0.410	0.489	-19.3	0.230	0.114	50.7
S0.4, Lime-treated_7WD by SSW	0.396	0.449	-13.5	0.260	0.122	53.2
S5, lime-treated_as-compacted	0.404	0.432	-6.7	0.275	0.206	24.9
S5, Lime-treated_7WD by DW	0.454	0.453	0.2	0.233	0.143	38.7

4. Discussions

As expected, the lime treatment induced a reduction of soil compressibility and an increase of yield stress, as shown in Fig. 4. The decrease of compressibility of lime-treated soil was mainly attributed to soil-lime reactions during curing (Rajasekaran and Rao, 2002; Rao and Shivananda, 2005; Mavroulidou et al., 2013; Wang et al., 2017; Vitale et al., 2017): i) the short-term lime hydration and cation exchanges led to the flocculation of soil particles, leading to a reduction of soil plasticity; ii) the long-term pozzolanic reaction produced cementitious compounds which coated the surface of soil particles and bonded them together, giving rise to higher mechanical performance. For this tested silt, the production of cementitious compounds cannot be detected by X-ray diffraction (XRD) analysis, probably due to its low quantity (Ying et al., 2020). This low quantity of cementitious compounds might be in well-crystallized phase which could bond the adjacent soil particles together, leading to a decrease of compressibility. On the other hand, the cementitious compounds might be in poorly-crystallized or amorphous phase which had a higher specific surface area (Vitale et al., 2017), giving rise to an increase of water retention capacity and thus matric suction. Indeed, Ying et al., (2021a) performed suction measurement on this silt (the same silt as in this study) and reported that the matric suction of lime-treated specimens at 90-day curing was 103 kPa, which was higher than that of untreated specimens (22 kPa). The increase of matric suction induced from lime treatment also played a role in reducing the compressibility. Thus, the lime-treated specimens had higher resistance to

compression, exhibiting higher yield stress and oedometer modulus E_{oed}, but lower compressibility index C_c^* and volumetric strain ε_v. For both untreated and lime-treated specimens at as-compacted state, the aggregate size had insignificant effect on the compression behaviour (Figs. 8a and 8b), as the aggregate size had negligible effect on the production of cementitious compounds and matric suction (Ying et al., 2021a).

As shown in Fig. 4, the yield stresses of as-compacted specimens determined from the low-pressure oedometer tests were significantly lower than the compaction pressure of specimens (2000 kPa for the untreated specimens and 3500 kPa for the lime-treated specimens). This was consistent with the results obtained by Wang et al. (2017) on untreated and 2% lime-treated Héricourt silt. Honda et al. (2006) indicated that the yield stress of static specimens should be almost the same as the compaction stress if the suction was kept constant after compaction. It can be this inferred that the yield stresses identified in Fig. 4 are just due to the significant non linearity of the curves. They are far from the compaction stress. It can be expected that if the specimens were loaded to higher pressures, the yield point determined using Casagrande method might shift rightwards, exhibiting higher yield stress probably close to the compaction stress.

It appears from the compression curves (except for the untreated specimens after wetting-drying cycles) that the vertical stress of 450 kPa seemed to be a critical stress that divided the curves of ε_v-logσ_v, C_c^*-logσ_v, E_{oed}-logσ_v into two zones: below the critical stress, the ε_v, C_c^* and E_{oed} increased at a lower rate; beyond this critical stress, these variations became more significant. This critical stress was close to the yield stress of the untreated specimens (380 kPa for S0.4 and 340 kPa for S5) and lime-treated specimens (460 kPa for S0.4 and 515 kPa for S5), but higher than those of lime-treated specimens subjected to wetting-drying cycles with the yield stress in the range of 230 kPa to 319 kPa. When the vertical stress was lower than the critical stress of 450 kPa or yield stress, the structure of soil skeleton could resist the compression, generating a small displacement and lower increase of C_c^*. As the vertical stress exceeded the critical stress or yield stress, the macro-pores experienced significant collapse (Delage and Lefebvre, 1984; Marcial et al., 2002; Delage, 2010; Zeng et al., 2021), and partially shifted to micro-pore population, giving rise to an increase of micro-pore void ratio (Table 3). Meanwhile, the C_c^* increased at a higher rate revealing higher compressibility, and the variations of ε_v and E_{oed} became much more significant as compared to those at vertical stress below 450 kPa. It is worth noting that the compression with loading to 3250 kPa did not change the micro-pore

population significantly, indicating that there was no breakage of silt/sand grains which was usually observed under higher pressures (Mesri and Vardhanabhuti, 2009; Mun and McCartney, 2017; Zhao et al., 2020).

Due to the modification induced by lime treatment, the swelling of lime-treated soil was inhibited during wetting, which was consistent with the observations made by Stoltz et al. (2012, 2014) and Rosone et al. (2018). The small swelling of lime-treated specimens was balanced by the subsequent drying-induced shrinkage, leading to reversible variations of void ratio with wetting-drying cycles. Correspondingly, the bi-modal pore size distribution of lime-treated specimens was preserved after seven wetting-drying cycles (Figs. 10c and 10d). Nevertheless, for the untreated specimens, the soil aggregations were easily softened during the wetting process, accompanied by significant swelling, which could not be balanced by the subsequent drying-induced shrinkage, leading hence, to an accumulation of irrecoverable swelling strains and an increase of void ratio. This was confirmed by the MIP results on the untreated specimens - the total intruded void ratio was increased after wetting-drying cycles and the bi-modal porosity changed to tri-modal characteristics, sign of soil disaggregation. These results evidenced the beneficial effect of lime treatment which reduced the volumetric deformations and microstructure variations during wetting-drying cycles, and thus improved the workability and long-term durability of soil.

As shown in Fig. 4, the shape of compression curves (e-logσ_v) of untreated specimens changed from convex for as-compacted specimens to almost linear without evident yield point for the specimens after wetting-drying cycles. This indicated that the soil structure of untreated specimens produced by static compaction was destroyed by wetting-drying cycles. As a result, higher ε_v and C_c^*, and lower E_{oed} were obtained on untreated specimens subjected to wetting-drying cycles as compared to the as-compacted specimens (Figs. 5, 6 and 7). Nevertheless, in the case of lime-treated specimens subjected to wetting-drying cycles, the convex e-logσ_v curves were preserved and close to those of as-compacted specimens (Fig. 4). It can be thus inferred that the soil flocculation, cementitious bonding and increase of matric suction induced from lime treatment enabled the structure of lime-treated specimens to remain stable, hence reducing the detrimental effect of wetting-drying cycles on soil compressibility. In fact, the wetting-drying cycles also led to a decrease of yield stress and more significant reduction of macro-pore void ratio for lime-treated specimens, indicating a slight softening of soil structure induced by wetting-drying cycles.

As far as the wetting fluids was concerned, it appeared that the deionized water and synthetic seawater had similar effect on the void ratio variations, especially for the lime-treated specimens (Fig. 3). This was inconsistent with the observations made by Mokni et al. (2014) on compacted boom clay and by Rao and Thyagaraj (2007) on compacted expansive clay. They reported that, when the compacted specimens were inundated with salt solution, the diffused double layer of clay particles decreased, causing a reduction of repulsive force and thus an increase of net attractive force. This, in turn, enabled the soil particles to move close to each other, exhibiting osmotic consolidation which decreased the void ratio. Regarding the studied silt, the compacted specimen was mainly constituted by 83% silt/sand grains and 15.6% clay minerals (illite, chlorite and kaolinite) and the behaviour was mainly controlled by coarse grains (Shi et al., 2020). Thus, salt solution had slight effect on the thickness of diffuse double layer of clay minerals in this soil (Ying et al., 2021e), giving rise to similar global void ratios of specimens wetted by deionized water and synthetic seawater. Nevertheless, the limited shrinkage of diffused double layer in clay fraction led to a higher frequency of macro-pores for the lime-treated specimens wetted by synthetic seawater as compared to those wetted by deionized water (Fig. 10c and Table 3). Similarly, Ying et al. (2021c) performed MIP tests on this untreated silt (the same silt as in this study) and reported that the global void ratios were almost similar for the specimens with different salinities while the frequency of macro-pores increased with increasing salinity. Furthermore, the total suctions were found to be 0.9 MPa for lime-treated specimens S0.4 at the end of seventh wetting-drying cycles in case of deionized water, and 3.2 MPa for treated S0.4 after seven wetting-drying cycles by synthetic seawater. Note that the total suction for the lime-treated specimens wetted by deionized water were close to those of specimens prior to wetting (0.8 MPa), indicating that wetting-drying cycles had negligible effect on the suction variations. The difference of total suctions between these two specimens after wetting-drying cycles with deionized water and synthetic seawater was 2.3 MPa which was close to the osmotic suction of synthetic seawater (2.4 MPa). This indicated that the matric suctions (the difference between total and osmotic suction) were almost the same for the specimens after wetting-drying cycles with either deionized water or synthetic seawater as wetting fluids, if the total suction of specimen wetted by deionized water was also taken as matric suction. Thus, it can be inferred that, as compared to the specimens wetted by deionized water, the higher compressibility of untreated and lime-treated specimens wetted by synthetic seawater was due to the larger quantity of macro-pores. Indeed, Delage and Lefebvre (1984) indicated that the soil compressibility was highly related to the existing largest pore size at the given vertical pressure - the larger the pore size, the higher the compressibility. One can

conclude that the osmotic suction induced by synthetic seawater affected the soil microstructure and thus the soil compressibility. The lime-treated specimens wetted by deionized water had similar compression parameters (ε_v, C_c^*, and E_{oed}) to the as-compacted specimens, implying that the wetting-drying cycles with deionized water as wetting fluid had less detrimental effect on the durability of lime-treated soil as compared to synthetic seawater. This can be attributed to the balance between the positive contribution of reduction of macro-pores with wetting-drying cycles (Fig. 10 and Table 3) and the negative contribution from the softening of soil structure.

In comparison with the lime-treated specimens S5 subjected to wetting-drying cycles, the lime-treated specimens S0.4 exhibited lower yield stress and higher decrease of macro-pore void ratio with compression. This suggested that the treated specimens S0.4, after the wetting-drying cycles, had lower resistance to compression, even though this aggregate size effect was not evidently observed on the compression curves (ε_v-logσ_v, C_c^*-logσ_v, E_{oed}-logσ_v). This behaviour was possibly due to the fact that the wetting-drying cycles led to a more significant decrease of macro-pore void ratio for specimens S5 than specimens S0.4. For examples, the void ratio of macro-pores decreased from 0.275 to 0.233 for treated specimens S5 after seven wetting-drying cycles with deionized water, while that of treated specimens S0.4 decreased slightly from 0.247 to 0.230, as shown in Table 3. Thus, after wetting-drying cycles, the treated specimens S5 had lower compressibility as compared to the treated specimens S0.4.

5. Conclusions

This study investigated the wetting-drying cycle effect on the compression behaviour of lime-treated specimens, considering the effects of wetting fluids nature and maximum soil aggregates size. The volume variations during wetting-drying cycles were recorded. Microstructure characterization was conducted by MIP tests on the specimens prior to compression and on those after compression. The experimental results allowed the following conclusions to be drawn:

(1) The lime-treated specimens exhibited reversible volume (void ratio) variations with wetting-drying cycles, whereas the latter led to an accumulation of swelling strains, and thus higher void ratio, for untreated specimens. The microstructure investigations showed that the bi-modal pore size distribution of lime-treated specimens remained unchanged after wetting-drying cycles, while that of untreated specimens changed to tri-modal pattern with a new larger pore population due to the possible softening and breakage of aggregates. This suggested that the

soil flocculation, the production of cementitious compounds and the increase of matric suction of lime-treated specimens gave rise to higher resistance to wetting-drying cycles.

(2) The wetting-drying cycles had a significant effect on the compression behaviour of untreated specimens that made the e-logσ_v curve change from convex to almost linear, indicating that cyclic tests on untreated specimens induced a significant destruction of soil structure. By contrast, the convex e-logσ_v curve of the lime-treated specimens was preserved after wetting-drying cycles. However, the lime-treated specimens exhibited a decrease of yield stress as compared to the as-compacted specimens, indicating that the wetting-drying cycles indeed caused some softening of soil structure for lime-treated soil. For both untreated and lime-treated specimens, the volume change during compression mainly corresponded to the collapse of macro-pores. The decrease of macro-pore void ratio with loading was higher for the specimens subjected to wetting-drying cycles than for the as-compacted specimens.

(3) The compression curves (e-logσ_v, ε_v-logσ_v, C_c^*-logσ_v and E_{oed}-logσ_v) of the lime-treated specimens wetted by deionized water almost converged to those of as-compacted specimens. This could be attributed to the balance between the positive contribution of macro-pores reduction with wetting-drying cycles and the negative contribution related to the softening of soil structure. Nevertheless, the specimens wetted by synthetic seawater exhibited higher compressibility than those wetted by deionized water, probably due to the larger quantity of macro-pores with the shrinkage of diffuse double layer caused by synthetic seawater. This result indicated that the wetting-drying cycles by synthetic seawater had more detrimental effect on the soil compression behaviour and thus on the durability, as compared to deionized water.

(4) The aggregate size had insignificant effect on the compression behaviour and the variation of macro-pore void ratio of as-compacted specimens, due to the insignificant effect of aggregate sizes on the production of cementitious compounds and matric suctions. Regarding the lime-treated specimens after wetting-drying cycles, the specimens S0.4 exhibited lower yield stress and higher decrease of macro-pore void ratio with loading as compared to the specimens S5. This was due to the fact that the wetting-drying cycles caused a higher decrease of macro-pore void ratio in specimens S5, which in turn, afforded them lower compressibility as compared to the specimens S0.4.

Author statement

Zi Ying: Validation, Investigation, Writing - original draft. Nadia Benahmed: Investigation, Resources, Writing - review & editing. Yu-Jun Cui: Conceptualization, Methodology, Writing - review & editing. Myriam Duc: Investigation, Resources.

Declaration of competing interest

The authors declare that they have no known competing financial interests or personal relationships that could have appeared to influence the work reported in this paper.

Acknowledgements

The authors would like to thank the China Scholarship Council (CSC). The supports provided by Ecole des Ponts ParisTech (ENPC) and INRAE are also greatly acknowledged.

References

Aldaood, A., Bouasker, M., Al-mukhtar, M., 2014. Impact of wetting – drying cycles on the microstructure and mechanical properties of lime-stabilized gypseous soils. Eng. Geol. 174, 11-21. https://doi.org/10.1016/j.enggeo.2014.03.002

ASTM D2435-04. 2004. Standard test method for one-dimensional consolidation properties of soils using incremental loading. ASTM International, West Conshohocken, PA.

Bell, F.G., 1996. Lime stabilization of clay minerals and soils. Eng. Geol. 42, 223–237. https://doi.org/10.1016/0013-7952(96)00028-2

Bian, X., Zeng, L.L., Li, X.Z., Shi, X.S., Zhou, S.M., & Li, F.Q., 2021. Fabric changes induced by super-absorbent polymer on cement–lime stabilized excavated clayey soil. J. Rock Mech. Geotech. Eng. https://doi.org/10.1016/j.jrmge.2021.03.006

Burland, J.B., 1990. On the compressibility and shear strength of natural clays. Géotechnique 40, 329-378. https://doi.org/10.1680/geot.1990.40.3.329

Cuisinier, O., Masrouri, F., Mehenni, A., 2020. Alteration of the hydromechanical performances of a stabilized compacted soil exposed to successive wetting-drying cycles. J. Mater. Civ. Eng. 32, 04020349. https://doi.org/10.1061/(asce)mt.1943-5533.0003270

Delage, P., 2010. A microstructure approach to the sensitivity and compressibility of some eastern Canada sensitive clays. Géotechnique 60, 353-368. https://doi.org/10.1680/geot.2010.60.5.353

Delage, P., Lefebvre, G., 1984. Study of the structure of a sensitive Champlain clay and of its evolution during consolidation. Can. Geotech. J. 21, 21-35. https://doi.org/10.1139/t84-003

Deng, Y. F., Yue, X. B., Cui, Y. J., Shao, G. H., Liu, S. Y., Zhang, D. W. (2014). Effect of pore water chemistry on the hydro-mechanical behaviour of Lianyungang soft marine clay.

Appl. Clay Sci. 95, 167-175. https://doi.org/10.1016/j.clay.2014.04.007

French standard AFNOR NF P 18-837. 1993. Standard for special products for hydraulic concrete construction-Hydraulic binder based needling and/or sealing products-Testing of resistance against seawater and/or water with high sulphate contents.

French standard AFNOR NF P 94-093. 1999. Standard test for soils investigation and testing-dertermination of the compaction characteristics of a soil-standard proctor test-modified proctro test.

Honda, M., Iizuka, A., Ohno, S., Kawai, K., Wang, W., 2006. An evaluation method for the volume change characteristics of compacted soil. Fourth International Conference on Unsaturated Soils, 837-848. https://doi.org/10.1061/40802(189)66

Hong, Z.S., Yin, J., Cui, Y.J., 2010. Compression behaviour of reconstituted soils at high initial water contents. Géotechnique 60, 691-700. https://doi.org/10.1680/geot.09.P.059

Locat, J., Berube, M.A., Choquette, M., 1990. Laboratory investigations on the lime stabilization of sensitive clays: shear strength development. Can. Geotech. J. 27, 294-304. https://doi.org/10.1139/t90-040

Marcial, D., Delage, P., Cui, Y.J., 2002. On the high stress compression of bentonites. Can. Geotech. J. 39, 812-820. https://doi.org/10.1139/t02-019

Mavroulidou, M., Zhang, X., Gunn, M.J., Cabarkapa, Z., 2013. Water Retention and Compressibility of a Lime-Treated, High Plasticity Clay. Geotech. Geol. Eng. 31, 1171-1185. https://doi.org/10.1007/s10706-013-9642-6

Mesri, G., Vardhanabhuti, B., 2009. Compression of granular materials. Can. Geotech. J. 46, 369-392. https://doi.org/10.1139/T08-123

Mokni, N., Romero, E., Olivella, S., 2014. Chemo-hydro-mechanical behaviour of compacted Boom Clay: Joint effects of osmotic and matric suctions. Géotechnique 64, 681-693. https://doi.org/10.1680/geot.13.P.130

Mun, W., McCartney, J.S., 2017. Roles of Particle Breakage and Drainage in the Isotropic Compression of Sand to High Pressures. J. Geotech. Geoenviron. Eng. 143, 04017071. https://doi.org/10.1061/(asce)gt.1943-5606.0001770

Nabil, M., Mustapha, A., Rios, S., 2020. Impact of wetting-drying cycles on the mechanical properties of lime-stabilized soils. Int. J. Pavement Res. Technol. 13, 83-92. https://doi.org/10.1007/s42947-019-0088-y

Olson, R. E., Mesri, G., 1970. Mechanisms controlling compressibility of clays. J. Soil Mech. Found. Div, 96, 1863-1978.

Rajasekaran, G., Rao, S.N., 2002. Compressibility behaviour of lime-treated marine clay. Ocean Eng. 29, 545-559. https://doi.org/10.1016/S0029-8018(01)00010-5

Rao, S.M., Reddy, B.V.V., Muttharam, M., 2001. The impact of cyclic wetting and drying on the swelling behaviour of stabilized expansive soils. Eng. Geol. 60, 223-233. https://doi.org/10.1016/S0013-7952(00)00103-4

Rao, S.M., Shivananda, P., 2005. Compressibility behaviour of lime-stabilized clay. Geotech. Geol. Eng. 23, 309-319. https://doi.org/10.1007/s10706-004-1608-2

Rao, S.M., Thyagaraj, T., 2007. Swell-compression behaviour of compacted clays under chemical gradients. Can. Geotech. J. 44, 520-532. https://doi.org/10.1139/T07-002

Rosone, M., Ferrari, A., Celauro, C., 2018. On the hydro-mechanical behaviour of a lime-

treated embankment during wetting and drying cycles. Geomech. Energy Environ. 14, 48-60. https://doi.org/10.1016/j.gete.2017.11.001

Shi, X.S., Zhao, J.D., 2020. Practical estimation of compression behavior of clayey/silty sands using equivalent void-ratio concept. J. Geotech. Geoenviron. Eng. 146, 04020046. https://doi.org/10.1061/(ASCE)GT.1943-5606.0002267

Stoltz, G., Cuisinier, O., Masrouri, F., 2012. Multi-scale analysis of the swelling and shrinkage of a lime-treated expansive clayey soil. Appl. Clay Sci. 61, 44-51. https://doi.org/10.1016/j.clay.2012.04.001

Stoltz, G., Cuisinier, O., Masrouri, F., 2014. Weathering of a lime-treated clayey soil by drying and wetting cycles. Eng. Geol. 181, 281-289. https://doi.org/10.1016/j.enggeo.2014.08.013

Tang, A.M., Vu, M.N., Cui, Y.J., 2011. Effects of the maximum soil aggregates size and cyclic wetting-drying on the stiffness of a lime-treated clayey soil. Géotechnique 61, 421-429. https://doi.org/10.1680/geot.SIP11.005

Vitale, E, Deneele, D., Paris, M., Russo, G., 2017. Multi-scale analysis and time evolution of pozzolanic activity of lime treated clays. Appl. Clay Sci. 141, 36-45. https://doi.org/10.1016/j.clay.2017.02.013

Wang, H., Cui, Y. J., Zhang, F., Liu, J. 2021. Effect of grain breakage on the compressibility of soils. Acta Geotech. 1-10. https://doi.org/10.1007/s11440-021-01256-z

Wang, Y.J., Cui, Y.J., Tang, A.M., Benahmed, N., Duc, M., 2017. Effects of aggregate size on the compressibility and air permeability of lime-treated fine-grained soil. Eng. Geol. 228, 167-172. https://doi.org/10.1016/j.enggeo.2017.08.005

Ying, Z., Cui, Y.J., Benahmed, N., Duc, M., 2020. Changes in mineralogy and microstructure of a lime-treated silty soil during curing time. E3S Web Conf. 195. https://doi.org/10.1051/e3sconf/202019503044

Ying, Z., Cui, Y.J., Benahmed, N., Duc, M., 2021a. Changes of microstructure and water retention property of a lime-treated saline soil during curing. Acta Geotech. https://doi.org/10.1007/s11440-021-01218-5

Ying, Z., Duc, M., Cui, Y.J., Benahmed, N., 2021b. Salinity assessment for salted soil considering both dissolved and precipitated salts. Geotech. Test. J. 44, 130-147. https://doi.org/10.1520/GTJ20190301

Ying, Z., Cui, Y.J., Benahmed, N., Duc, M., 2021c. Salinity effect on the compaction behaviour, matric suction, stiffness and microstructure of a silty soil. J. Rock Mech. Geotech. Eng. https://doi.org/10.1016/j.jrmge.2021.01.002

Ying, Z., Cui, Y.J., Benahmed, N., Duc, M., 2021d. Drying effect on the microstructure of compacted salted soil. Géotechnique. Accepted for publication.

Ying, Z., Cui, Y.J., Duc, M., Benahmed, N., Bessaies-Bey, H., Chen, B., 2021e. Salinity effect on the liquid limit of soils. Acta Geotech. 16, 1101-1111. https://doi.org/10.1007/s11440-020-01092-7

Zeng, L.L., Hong, Z.S., Cui, Y.J., 2015. Determining the virgin compression lines of reconstituted clays at different initial water contents. Can. Geotech. J. 52, 1408-1415. https://doi. org/10.1139/cgj-2014-0172

Zeng, Z.X, Cui, Y. J., Talandier, J., 2021. Compaction and sealing properties of bentonite/claystone mixture: Impacts of bentonite fraction, water content and dry density.

Eng. Geol, 287, 106122. https://doi.org/10.1016/j.enggeo.2021.106122

Zhao, B.D., Wang, J.F., Andò, E., Viggiani, G., Coop, M.R., 2020. Investigation of particle breakage under one-dimensional compression of sand using x-ray microtomography. Can. Geotech. J. 57, 754-762. https://doi.org/10.1139/cgj-2018-0548

Conclusions and perspectives

Conclusions

A study on the hydro-mechanical behaviour of untreated and lime-treated soils had been conducted. The first part of this study assessed the changes in dissolved salinity with water content variations and the induced osmotic suction. Then, the salinity effect on the liquid limit and compaction behaviour of untreated soils were investigated, and drying effect on the evolution of microstructure of compacted saline soils was studied. Afterwards, the salt solution effect on the optimum lime content was clarified by performing pH measurement test, base titration test and ICP/OES analysis. The effects of salinity and aggregate size on the mineralogy, microstructure and water retention property of lime-treated saline soils were investigated. The mercury intrusion porosimetry, oedometer and bender element tests were carried out on untreated/lime-treated specimens and the specimens subjected to wetting-drying cycles, to investigate the mechanical behaviour and the durability of lime-treated soils. Different wetting fluids and maximum soil aggregate sizes were considered in the wetting-drying tests. Based on the obtained results, the following conclusion can be drawn.

Assessment of dissolved salinity and osmotic suction

(i) Assessment of dissolved salinity

As regards the unsaturated saline soils, the description of the soil composition was first revised, taking dissolved and precipitated salts into account. Then, the relationship between dissolved water salinity (the mass ratio of dissolved salt to salty water) and dissolved soil salinity (the mass ratio of dissolved salt to dry solid) was established. For mixed salts solution having the same salt composition as synthetic seawater, the relationship between electrical conductivity (EC) and either total water salinity or dissolved water salinity (r) was investigated. Afterwards, three approaches were proposed to determine the dissolved water salinity and dissolved soil salinity of salt-amended soils with decreasing water content by combining the EC-r relationship of mixed salts solution and the relationship between dissolved water salinity and dissolved soil salinity. Results showed that the measured salinities of salt-amended soils coincided well with the calculated values. Using the proposed method, the dissolved water salinity and the dissolved soil salinity at any salty water content can be determined for a soil with a certain amount of salt.

(ii) Determination of soil osmotic suction

The matric and total suctions of compacted specimens were determined by the contact filter paper method and chilled-mirror dew-point hygrometer (WP4C), respectively. Then, the osmotic suction was determined as the difference between the total (T) and matric (M) suctions. Furthermore, a relationship between osmotic suction and electrical conductivity was established for a mixed salts solution, and a new equation was proposed taking dissolved and precipitated salts into account. It appeared that the indirectly determined osmotic suctions (T-M) and calculated osmotic suctions were in good agreement for soil specimens with 2.10‰ soil salinity when water content was higher than 8%, and for soil specimens with 6.76‰ soil salinity in the whole considered range of water contents. This highlighted that the osmotic suction can be accurately determined from electrical conductivity, ion and salt concentrations, which were transformed from the established relationships and not from the experimental measurements. By this method, the osmotic suction can be determined more easily for saturated soils and especially unsaturated soils which had no enough soil pore water for chemical analysis.

Geotechnical property and drying-induced microstructure of untreated soils:

(i) Liquid limit

The salt effect on liquid limit, sedimentation behavior and yield stress of MX80 Na-bentonite and silty soil were investigated. The sedimentation test evidenced the shrinkage of diffused double layer and the formation of denser aggregated structure. This indicated that the change of liquid limit is the result of two mechanisms in competition, which depends on the compression rate of diffused double layer: (i) the water storage in nano-fissures which correspond to the nanoscale spaces among interlayers of clay particles resulting from the slight shrinkage of diffused double layer, and (ii) the water expulsion into larger pores with significant shrinkage of diffused double layer. For the MX80 at low salinity and for the silty soil, the first mechanism prevailed and the increasing liquid limit was attributed to the requirement of more water to fill the nano-fissures. Meanwhile, increasing water salinity favored the formation of aggregated structure, leading to an increase of yield stress. In contrast, for MX80 at high salinity, the second mechanism prevailed - the diffused double layer was compressed significantly, changing the double-layer water to free water and giving rise to the decrease of liquid limit. Due to the shrinkage of diffused double layer, the bentonite particles seemed to form separate and smaller aggregates, leading to a decrease of yield stress.

(ii) Compaction behaviour

The standard Proctor compaction test, bender element test coupled with mercury intrusion porosimetry test were conducted on the soils with different salinities. Results showed that, for the specimens with soil salinities of 2.10‰ and 6.76‰, the modal size of micro-pores shifted to smaller values, whereas the modal size of macro-pores shifted to larger values than that of specimens without salt. The specimens with soil salinities of 2.10‰ and 6.76‰ exhibited higher G_{max} than that of samples without salt. This can be explained by the fact that, as salinity increased, the net attractive forces increased with the reduction of diffused double layer thickness that made clay particles attract each other and agglomerate, giving rise to an increase of G_{max}. The saline soils exhibited higher G_{max} and became less compactible. Thus, for the same compaction energy, the saline soils exhibited lower maximum dry density and higher optimum water content.

(iii) Drying-induced microstructure

The drying-induced microstructure evolution of compacted silt with different salinities was studied by performing MIP and ESEM tests. During drying, the pore size distribution changed from bi-modal characteristics ($w \approx 17\%$) to tri-modal pattern with appearance of a new nano-pore population ($w \approx 8\%$), and finally retrieved the double porosity pattern ($w \approx 3\%$). The occurrence of the nano-pore populations was the result of the development of nano-fissures in the clay fraction and at the interface between clay particles and silt/sand grains due to the differential clay shrinkage. With further drying ($w \approx 3\%$), the nano-fissures enlarged to micro-fissures as the clay fraction continued to shrink, resulting in the disappearance of nano-pores and an increase of intra-aggregate pore frequency. The salinity seemed to decrease the frequency of the drying-induced micro-pores due to the enhanced mechanical strength of salted soils by the soil aggregation resulting from the compression of diffused double layer and a possible cementation effect produced by precipitated salt.

Optimum lime content:

The optimum lime content increased with the increase of salt concentration, which can be attributed to the consumption of OH^- ions by Mg^{2+} and Ca^{2+} ions in the salt solution, producing the precipitations of $Mg(OH)_2$ and $CaCO_3$ in the alkaline environment. This finding should be accounted for when applying the widely used pH method for the determination of the optimum

lime content for saline soils. Due to the higher specific surface area, cation exchange capacity and more soluble Si^{4+} and Al^{3+} ions in the MX80 Na-bentonite, a higher optimum lime content was required to supply sufficient Ca^{2+} ions for cation exchange and pozzolanic reaction as compared to silt.

Mineralogy, microstructure and water retention property of lime-treated soils:

(i) Mineralogy:

XRD analysis was performed on both untreated specimens and lime-treated specimens at curing times of 1 day, 90 days and 150 days. Results showed that the portlandite was observed on XRD pattern of lime-treated soils after curing time 150 days. This was due to the low clay fraction and inert phases of quartz and feldspar in tested silt which cannot provide sufficient silica and alumina to interact with calcium from portlandite. Furthermore, no cementitious compounds in significant quantity were detected on XRD patterns even after a curing time as long as 150 days. The high intensity of calcite peak overlapping the reflection of hydrated products and the formation of low amount of poorly crystallized or amorphous cementitious compounds might be explain such result.

(ii) Microstructure:

Lime treatment caused a reduction of the percentage of micro-pores and an increase of macro-pore quantity due to the flocculation of soil particles. With increasing curing time, the percentage of micro-pores ($0.5 < d < 2$ μm) decreased and that of nano-pores below 0.5 μm increased slightly, probably due to the production of cementitious compounds which coated the surface of aggregates and filled some pores gradually. The insignificant effect of curing time on microstructure evolution was due to the low quantity of cementitious compounds produced from pozzolanic reaction.

All lime-treated specimens compacted at dry and wet side of optimum exhibited bi-modal pore size distribution, with a decrease of macro-pore frequency with increasing water content. The treated specimens with larger aggregates exhibited a larger modal size.

The evolution of microstructure of lime-treated soils during drying followed the same tendency as untreated soils. The curing time effect was found insignificant on the drying-induced microstructure changes, while the lime treatment effect was noticeable. Lime treatment resulted

in rapid cation exchanges that made the soil particles flocculate and form larger aggregates, inhibiting the clay shrinkage and attenuating the enlargement of pore size. The insignificant effect of curing time on the drying-induced microstructure could be attributed to the low reactivity of silty soil with lime, forming low quantity of cementitious compounds that played a limited role in inhibiting clay shrinkage. The salinity effect on the drying-induced microstructure was visible but not significant, due to the low clay fraction in the tested silt.

(iii) Water retention property

The matric suction of lime-treated specimens increased significantly during curing, due to the production of poorly crystallized or amorphous cementitious compounds which exhibited higher specific surface area, giving rise to an increase of water adsorption capacity of soils. Higher matric suctions were observed for the lime-treated specimens with higher salinity, suggesting that salts promoted the production of cementitious compounds.

The total suction of lime-treated specimens increased slightly during curing. This was explained by the fact that during curing, the Ca^{2+} and Mg^{2+} in soil pore water and the Ca^{2+} dissolved from hydrated lime were consumed in the precipitations of $CaCO_3$ and $Mg(OH)_2$, cation exchanges and pozzolanic reaction, leading to a decrease of osmotic suction. As the increase of matric suction was almost balanced by the decrease of osmotic suction, the change in total suction was insignificant.

The soil water retention curves (SWRCs) derived from MIP results of treated specimens at different water contents considering the microstructure variations during drying were still different from those curves from direct measurement. This difference was mainly attributed to the production of cementitious compounds: the cementitious compounds with higher adsorption capacity did not contribute to the matric suctions derived from the MIP tests, but they significantly contributed to the matric suctions measured by the filter paper method.

The aggregate size effect on the total suction (WP4C) and matric suction (FP) was insignificant, because the similar micro-pore size distribution and almost same soil mineralogy for lime-treated specimens S5 (D_{max} = 5 mm) and S0.4 (D_{max} = 0.4 mm) dominated the water retention capacity with the specimens being dried from unsaturated state, leading to an insignificant effect of aggregate size. On the SWRCs derived from MIP results, the higher the maximum soil aggregates, the smaller the air entry value.

Mechanical behaviour

Lime treatment increased the yield stress and small strain shear modulus (G_{max}), but reduced the compressibility of soils, which can be attributed to the effects of soil flocculation, the production of cementitious compounds and the increase of matric suction. The aggregate size had insignificant effect on the compression behaviour, as the aggregate size had negligible effect on the production of cementitious compounds and matric suction.

The stabilized G_{max} values were independent of moulding water content for treated specimens S0.4 (D_{max} = 0.4 mm) with smaller aggregates, because the much more production of cementitious compounds at wet side compensated the degradation of G_{max} induced from the lower suction. For the specimens S5 (D_{max} = 5 mm) with larger aggregates on wet side, the lower suction effect prevailed the pozzolanic reaction promoted by higher water content, leading to lower G_{max} as compared to the specimens S5 at dry side.

Durability of lime-treated soils:

(i) Wetting-drying cycle effect on soil morphology and microstructure

The wetting-drying cycles induced swelling strain and some cracks on the soil surface, whereas no significant volume variations and cracks were observed on lime-treated specimens. The bi-modal pore size distribution of untreated specimens changed to tri-modal pattern with a new larger pore population due to the possible softening and breakage of aggregates, while that of lime-treated soils were unchanged and almost reversible with water content varying from 17% to 21%. The subsequent intensive drying induced some fissures in lime-treated soils, whereas the rewetting of lime-treated specimens could induce the healing of them.

(ii) Wetting-drying effect on the small strain shear modulus

The G_{max} of lime-treated soils showed a constant decreasing trend with wetting and an increasing trend with drying. Moreover, G_{max} decreased slightly with wetting-drying cycles for the lime-treated specimens wetted by deionized water, suggesting that the wetting-drying cycles indeed softened the soils. However, G_{max} increased for the lime-treated specimens wetted by synthetic seawater, due to the more production of cementitious compounds promoted by salts. The lime-treated specimens S0.4 (D_{max} = 0.4 mm) wetted by synthetic seawater had higher G_{max} than those wetted by deionized water, while the wetting fluid had insignificant effect on the

G_{max} of specimens S5 (D_{max} = 5 mm) due to the limited promotion of pozzolanic reaction and negligible soil aggregation induced by salts.

(iii) Wetting-drying cycle effect on the compression behaviour

Lower yield stress and higher decrease of macro-pore void ratio with loading were obtained on the lime-treated specimens under wetting-drying cycles compared to the as-compacted specimens, indicating a slight softening of soil structure by the wetting-drying cycles. Regarding the effect of wetting fluid nature, synthetic seawater, compared to deionized water, resulted in a higher compressibility. This was attributed to the presence of higher quantity of macro-pores in the specimens wetted by synthetic seawater induced by the shrinkage of the clay fraction. After wetting-drying cycles, the lime-treated specimens S5 (D_{max} = 5 mm) had higher yield stress and lower decrease of macro-pore void ratio than the lime-treated specimens S0.4 (D_{max} = 0.4 mm), due to the significant reduction of macro-pore population with wetting-drying cycles.

Recommendation for the dike construction at Les Saline-de-Giraud:

(i) The optimum lime contents were estimated at 1.5%, 3% and 4% for soil-lime mixtures mixing with deionized water, 35 g/L synthetic seawater and 70 g/L mixed salts solution. It appears that, while preparing lime-treated soils using seawater, a lime content as high as 3-4% is required for the modification and stabilization of soils.

(ii) The maximum dry density decreased and the optimum water content increased as salinity increased. This indicated that, for the same compaction energy, the specimens with higher salinity exhibited lower dry density. Thus, while compacting saline soils for dike construction, it is necessary to use higher compaction energy for the soils with higher salinity, in order to obtain the desired dry density.

(iii) Because the tested soils is mainly composed of inert phases of quartz (39%) and feldspar (9.5%) and the low fraction of clay minerals (10.8% illite, 3.6% chlorite and 1.3% kaolinite, which cannot provide enough activated silica and alumina to interact with calcium to produce a significant amount of cementitious compounds, the curing time effect on the mineralogy, microstructure, water retention property, as well as the mechanical behaviour was insignificant. In order to improve the soil behaviour by lime treatment more significantly and thus the

mechanical performance of dike, metakaolin consisting of high quantities of SiO_2 and Al_2O_3 can be used as additive to promote the pozzolanic reaction.

(iv) The salinity had significant effect on the matric and total suctions of lime-treated soils, while its effect on the microstructure was visible but not significant due to the low clay fraction in the tested silt. Thus, concerning the dike construction on the soils taken from les Salin-de-Giraud with lime treatment, the salinity effect on the total suction and microstructure can be ignored.

(v) As regards the durability of dike, the wetting-drying cycles slightly softened the structure of lime-treated specimens, while the untreated specimens were damaged with wetting-drying cycles. During wetting-drying cycles, the different effects induced from synthetic seawater and deionized water were insignificant. It appears thus that the lime treatment is essential in the dike construction which can improve the durability significantly and reduce the detrimental effect of seawater during wetting-drying cycles.

Perspectives

The present study allowed a better understanding of the hydro-mechanical behaviour of untreated and lime-treated saline soils, accounting for the effects of salinity, soil maximum aggregate size and wetting-drying cycles. In light of the findings obtained, the following issues are proposed in future exploration:

(i) The proposed method of assessing dissolved salinity and osmotic suction was only applicable for silty soils or other low plasticity soils without consideration of cation exchange between soil and soil pore water. It appears interesting to extend this method to high plasticity soils.

(ii) The production of cementitious compounds was not detected by XRD test, due to their low quantity. High-resolution ESEM should be employed on lime-treated specimens cured for longer time. This will provide some evidence supporting the discussions on the effect of cementitious compounds on the microstructure, water retention property and mechanical performance of lime-treated soils.

(iii) This work mainly focused the fundamental soil behaviour of untreated and lime-treated

soils. It would be interesting to investigate other mechanical behaviour such as shear strength, unconfined compressive strength, etc., in order to investigate the mechanical stability of dike.

(iv) It appears also interesting to perform some experimental tests on undisturbed samples taken from the DIGUE 2020 experimental dike, in order to assess the possibility of upscaling from laboratory data to field data.

(v) Based on the experimental results obtained in this work, a constitutive model accounting for the effects of salinity and lime treatment can be developed and then implemented in a numerical code for numerically analysing the hydro-mechanical behaviour of dike.

References

Abdullah, W.S., Alshibli, K.A., Al-Zou'bi, M.S., 1999. Influence of pore water chemistry on the swelling behaviour of compacted clays. Appl. Clay Sci. 15(5-6), 447-462.

Abdullah, W.S., Al-Zou'bi, M.S., Alshibli, K.A., 1997. On the physicochemical aspects of compacted clay compressibility. Can. Geotech J. 34(4), 551-559.

Abedi-Koupai, J., Mehdizadeh, H., 2008. Estimation of osmotic suction from electrical conductivity and water content measurements in unsaturated soils. Geotech. Test. J. 31(2), 142-148.

Abood, T.T., Kasa, A.B., Chik, Z.B., 2007. Stabilisation of silty clay soil using chloride compounds. J. Eng. Sci. Technol. 2(1), 102-110.

AFNOR NF P 11-300, 1992. Standard for classification of materials for use in the construction of embankments and capping layers of road infrastructures.

AFNOR NF P 18-513. 2012. Pozzolanic addition for concrete-Metakaolin-Definitions, Specifications and Conformity Criteria. Association Francaise de Normalisation.

AFNOR NF P 18-837. 1993. Standard for special products for hydraulic concrete construction-Hydraulic binder based needling and/or sealing products-Testing of resistance against seawater and/or water with high sulphate contents.

AFNOR NF P 94-052. 1995. Standard test for soils investigation and testing-Atterberg limit determination-Part 1: Liquid limit-Cone penetrometer method.

AFNOR NF P 94-054. 1991. Standard test for soils investigation and testing-Determination of particle density-Pycnometer method.

AFNOR NF P 94-056. 1996. Standard test for soils investigation and testing-Granulometric analysis-Dry sieving method after washing.

AFNOR NF P 94-057. 1992. Standard test for soils investigation and testing-Granulometric analysis-Hydrometer method.

AFNOR NF P 94-068. 1998. Standard test for soils investigation and testing-Measuring of the methylene blue adsorption capacity of a rocky soil-Determination of the methylene blue of a soil by means of the stain test.

AFNOR NF P 94-093. 1999. Standard Test for Soils Investigation and Testing-Dertermination of the Compaction Characteristics of a Soil-Standard Proctor test-Modified Proctor test.

Afrin, H., 2017. A review on different types soil stabilization techniques. Int. J. Transp. Eng. Technol. 3, 19-24.

Ajalloeian, R., Mansouri, H., Sadeghpour, A.H., 2013. Effect of saline water on geotechnical properties of fine-grained soil. EJGE 18, 1419-1434.

Akther, S., Hwang, J., Lee, H., 2008. Sedimentation characteristics of two commercial bentonites in aqueous suspensions. Clay Miner. 43(3), 449-457.

Albrecht, B.A. Benson, C.H., 2001. Effect of desiccation on compacted natural clays. J.Geotech. Geoenviron. Eng. 127(1), 67-75.

Aldabaa, A.A.A., Weindorf, D.C., Chakraborty, S., Sharma, A., Li, B., 2015. Combination of proximal and remote sensing methods for rapid soil salinity quantification. Geoderma 239-240, 34-46.

Aldaood, A., Bouasker, M., Al-mukhtar, M., 2014a. Impact of wetting-drying cycles on the microstructure and mechanical properties of lime-stabilized gypseous soils. Eng. Geol. 174, 11-21.

Aldaood, A., Bouasker, M., Al-Mukhtar, M., 2014b. Free swell potential of lime-treated gypseous soil. Appl. Clay Sci. 102, 93-103.

Alkan, M., Demirbaş, Ö., Doğan, M., 2005. Electrokinetic properties of kaolinite in mono-and multivalent electrolyte solutions. Microporous Mesoporous Mater. 83 (1-3), 51-59.

Al-Mukhtar, M., Khattab, S., Alcover, J.F., 2012. Microstructure and geotechnical properties of lime-treated expansive clayey soil. Eng. Geol. 139-140, 17-27.

Al-Mukhtar, M., Lasledj, A., Alcover, J.F., 2010a. Behaviour and mineralogy changes in lime-treated expansive soil at 20°C. Appl. Clay Sci. 50, 191-198.

Al-Mukhtar, M., Lasledj, A., Alcover, J.F., 2010b. Behaviour and mineralogy changes in lime-treated expansive soil at 50°C. Appl. Clay Sci. 50, 199-203.

Al-Mukhtar, M., Lasledj, A., Alcover, J.F., 2014. Lime consumption of different clayey soils. Appl. Clay Sci. 95, 133-145.

Al-Swaidani, A., Hammoud, I., Meziab, A., 2016. Effect of adding natural pozzolana on geotechnical properties of lime-stabilized clayey soil. J. Rock Mech. Geotech. Eng. 8 (5), 714-725.

Alvarez, J.I., Fernandez, J.M., Navarro-Blasco, I., Duran, A., Sirera, R., 2013. Microstructural consequences of nanosilica addition on aerial lime binding materials: Influence of different drying conditions. Mater. Charact. 80, 36-49.

Andavan, S., Maneesh Kumar, B., 2020. Case study on soil stabilization by using bitumen emulsions - A review. Mater. Today Proc. 22, 1200-1202.

Anggraini, V., Asadi, A., Farzadnia, N., Jahangirian, H., Huat, B.B.K., 2016. Reinforcement benefits of nanomodified coir fiber in lime-treated marine clay. J. Mater. Civ. Eng. 28, 06016005.

Anson, R.W.W., Hawkins, A.B., 1998. The effect of calcium ions in pore water on the residual shear strength of kaolinite and sodium montmorillonite. Géotechnique 48, 787-800.

Arasan, S., Yetimoğlu, T., 2008. Effect of inorganic salt solutions on the consistency limits of two clays. Turkish J. Eng. Environ. Sci. 32, 107-115.

Arifin, Y.F., Schanz, T., 2009. Osmotic suction of highly plastic clays. Acta Geotech, 4(3), 177-191.

Aung, K.K., Rahardjo, H., Leong, E.C., Toll, D.G., 2001. Relationship between porosimetry measurement and soil-water characteristic curve for an unsaturated residual soil, Geotech. Geol. Eng. 19, 401-416.

ASTM D 2435-04. 2004. Standard test method for one-dimensional consolidation properties of soils using incremental loading. ASTM International, West Conshohocken, PA.

ASTM D 2487-00. 2000. Standard Practice for Classification of Soils for Engineering Purposes (Unified Soil Classification System). West Conshohocken, PA: ASTM International, approved March 10, 2000.

ASTM D 4318-10. 2014. Standard Test Methods for Liquid limit, Plastic limit, and Plasticity Index of Soils. ASTM International, West Conshohocken, PA.

ASTM D 4542-95. 2001. Standard Test Method for Pore Water Extraction and Determination of the Soluble Salt Content of Soils by Refractometer. ASTM International, West Conshohocken, PA.

ASTM D 5298-16. 2016. Standard Test Method for Measurement of Soil Potential (Suction) Using Filter Paper. ASTM International, West Conshohocken, PA.

ASTM D 6276-19. 2019. Standard Test Method for Using pH to Estimate the Soil-Lime Proportion Requirement for Soil Stabilization. ASTM International, West Conshohocken, PA.

Baeyens, B., Bradbury, M.H., 1997. A mechanistic description of Ni and Zn sorption on Na-montmorillonite Part I: Titration and sorption measurements. J. Contam. Hydrol. 27 (3-4), 199-222.

Baldovino, J.A., Moreira, E.B., Teixeira, W., Izzo, R.L.S., Rose, J.L., 2018. Effects of lime addition on geotechnical properties of sedimentary soil in Curitiba, Brazil. J. Rock Mech. Geotech. Eng. 10, 188-194.

Barbour, S.L., Fredlund, D.G., 1989. Mechanisms of osmotic flow and volume change in clay soils. Can. Geotech. J. 26(4), 551-562.

Basha, E.A., Hashim, R., Mahmud, H.B., Muntohar, A.S., 2005. Stabilization of residual soil with rice husk ash and cement. Constr. Build. Mater. 19, 448-453.

Behnood, A., 2018. Soil and clay stabilization with calcium- and non-calcium-based additives: A state-of-the-art review of challenges, approaches and techniques. Transp. Geotech. 17, 14-32.

Bell, F.G., 1989. Lime stabilisation of clay soils. Bull. Int. Assoc. Eng. Geol. 39 (1), 67-74.

Bell, F.G., 1996. Lime stabilization of clay minerals and soils. Eng. Geol. 42 (4), 223-237.

Bessaies-Bey, H., Baumann, R., Schmitz, M., Radler, M., Roussel, N., 2015. Effect of polyacrylamide on rheology of fresh cement pastes. Cem. Concr. Res. 76, 98-106.

Bessaies-Bey, H., Hot, J., Baumann, R., Roussel, N., 2014. Consequences of competitive adsorption between polymers on the rheological behaviour of cement pastes. Cem. Concr. Compos. 54, 17-20.

Bhuvaneshwari, S., Robinson, R.G., Gandhi, S.R., 2013. Behaviour of lime treated cured expansive soil composites. Indian Geotech. J. 44(3), 278-293.

Bian, X., Cui, Y.J., Li, X.Z., 2019. Voids effect on the swelling behaviour of compacted bentonite. Géotechnique 69, 593-605.

Bian, X., Zeng, L.L, Li, X.Z., Shi, X.S., Zhou, S.M., Li, F.Q., 2021. Fabric changes induced by super-absorbent polymer on cement-lime stabilized excavated clayey soil. J. Rock Mech. Geotech. Eng.

Bisanal, M.G., Badiger, R., 2007. Study on stabilization of soil using sea shell and bitumen emulsion. Int. J. Innov. Res. Sci. Eng. Technol. 3297, 58755882.

Boso, M., Romero, E., Tarantino, A., 2005. The use of different suction measurement techniques to determine water retention curves. Unsaturated Soils: Experimental Studies Springer, Berlin, Heidelberg, 169-181.

Brooks, R.M., 2009. Soil stabilization with fly ash and rice husk ash. Int. J. Res. Rev. Appl. Sci. 1, 2076-734.

Bruand, A., Prost. R., 1987. Effect of water content on the fabric of a soil material: an experimental approach. J. Soil Sci. 38(3), 461-472.

Bulut, R., Hineidi. S.M., Bailey, B., 2002. Suction measurements-filter paper and chilled mirror psychrometer. In Proceedings of the Texas section American Society of Civil Engineers, Fall Meeting, Waco, Texas, October, 2002, 2-5.

Burland, J.B., 1990. On the compressibility and shear strength of natural clays. Géotechnique 40, 329-378.

Burton, G.J., Sheng, D.C., Campbell, C., 2014. Bimodal pore size distribution of a high-plasticity compacted clay. Géotechnique Lett. 4(2), 88-93.

Burton, G.J., Pineda, J.A., Sheng, D.C., Airey, D., 2015. Microstructural changes of an undisturbed, reconstituted and compacted high plasticity clay subjected to wetting and drying. Eng. Geol. 193, 363-373.

Calvello, M., Lasco, M., Vassallo, R., Di Maio, C., 2005. Compressibility and residual shear strength of smectitic clays: influence of pore aqueous solutions and organic solvents. Italian Geotech J 1:34-46.

Carteret, R.d., Buzzi, O., Fityus, S., Liu, X.F., 2014. Effect of naturally occurring salts on tensile and shear strength of sealed granular road pavements. J. Mater. Civ. Eng. 26(6), 04014010.

Cecconi, M., Russo, G., 2008. Prediction of soil-water retention properties of a lime stabilised compacted silt. Unsaturated Soils Adv. Geo-Engineering - Proc. 1st Eur. Conf. Unsaturated Soils, E-UNSAT 2008, 271-276.

Celauro, B., Bevilacqua, A., Lo, D., Celauro, C., 2012. Design procedures for soil-lime stabilization for road and railway embankments. Part 2- Experimental Validation. Procedia - Soc. Behav. Sci. 53, 568-579.

Celik, E., Nalbantoglu, Z., 2013. Effects of ground granulated blastfurnace slag (GGBS) on the swelling properties of lime-stabilized sulfate-bearing soils. Eng. Geol. 163, 20-25.

Chakraborty, S., Banerjee, A., Das, J.T., Mosadegh, L., Puppala, A.J., 2018. Impact of variation of small strain shear modulus on seismic slope stability analysis of a levee: A Sensitivity Analysis. In IFCEE 2018, 302-313.

Chemeda, Y.C., Deneele, D., Ouvrard, G., 2018. Short-term lime solution-kaolinite interfacial chemistry and its effect on long-term pozzolanic activity. Appl Clay Sci 161: 419-426.

Cherian, C., Arnepalli, D.N., 2015. A critical appraisal of the role of clay mineralogy in lime stabilization. Int. J. Geosynth. Ground Eng. 1:8.

Cherian, C., Kollannur, N.J., Bandipally, S., Arnepalli, D.N. 2018. Calcium adsorption on clays: Effects of mineralogy, pore fluid chemistry and temperature. Appl. Clay Sci. 160, 282-289.

Chi, C.M., Wang, Z.C., 2010. Characterizing salt-affected soils of Songnen Plain using saturated paste and 1: 5 soil-to-water extraction methods. Arid Land Res Manag 24(1), 1-11.

Ciancio, D., Beckett, C.T.S., Carraro, J.A.H., 2014. Optimum lime content identification for lime-stabilised rammed earth. Constr. Build. Mater. 53, 59-65.

Cokca, E., Yazici, V., Ozaydin, V., 2009. Stabilization of expansive clays using granulated blast furnace slag (GBFS) and GBFS-Cement. Geotech. Geol. Eng. 27, 489-499.

Consoli, N.C., Lopes, L. da S., Prietto, P.D.M., Festugato, L., Cruz, R.C., 2011. Variables controlling stiffness and strength of lime-stabilized soils. J. Geotech. Geoenviron. Eng. 137, 628-632.

Consoli, N.C., Prietto, P.D.M., Lopes, L. da S., Winter, D., 2014. Control factors for the long term compressive strength of lime treated sandy clay soil. Transp. Geotech. 1, 129-136.

Consoli, N.C., Saldanha, R.B., Scheuermann Filho, H.C., 2019. Short-and long-term effects of sodium chloride on strength and durability of coal fly ash stabilized with carbide lime. Can. Geotech. J. 56, 1929-1939.

Cui, Y.J., Delage, P., 1996. Yielding and plastic behaviour of an unsaturated compacted silt. Géotechnique 46(2), 291-311.

Cuisinier, O. Laloui, L., 2004. Fabric evolution during hydromechanical loading of a compacted silt. Int. J. Numer. Anal. Methods Geomech. 28(6), 483-499.

Cuisinier, O., Deneele, D., 2008. Impact of cyclic wetting and drying on the swelling properties of a lime-treated expansive clay. In: Jourées Nationales de Géotechnique et de Géologie de l'Ingénieur JNGG'08, Nantes, pp. 18-20.

Cuisinier, O., Auriol, J.C., Le Borgne, T., Deneele, D., 2011a. Microstructure and hydraulic conductivity of a compacted lime-treated soil. Eng. Geol. 123, 187-193.

Cuisinier, O., Le Borgne, T., Deneele, D., Masrouri, F., 2011b. Quantification of the effects of nitrates, phosphates and chlorides on soil stabilization with lime and cement. Eng. Geol. 117, 229-235.

Cuisinier, O., Masrouri, F., Mehenni, A., 2020. Alteration of the hydromechanical performances of a stabilized compacted soil exposed to successive wetting-drying cycles. J. Mater. Civ. Eng. 32, 04020349.

Dao, V.N.T., Morris, P.H., and Dux, P.F., 2008. On equations for the total suction and its matric and osmotic components. Cem. Concr. Res. 38(11), 1302-1305.

De Baecque, M., 2019. Caractérisation multi-physique de la durabilité d'un sol traité à la chaux pour une application aux digues maritimes. PhD Dissertation, Université Paris-Est.

De Brito Galvão, T.C., Elsharief, A., Simões, G.F., 2004. Effects of lime on permeability and compressibility of two tropical residual soils. J. Environ. Eng. 130(8), 881-885.

Delage, P., Lefebvre, G., 1984. Study of the structure of a sensitive Champlain clay and of its evolution during consolidation. Can. Geotech. J. 21, 21-35.

Delage, P., Pellerin, F.M. 1984. Influence de la lyophilisation sur la structure d'une argile sensible du Québec. Clay Miner. 19(2), 151-160.

Delage, P., Audiguier, M., Cui, Y.J. Howat, M.D., 1996. Microstructure of a compacted silt. Can. Geotech. J. 33(1), 150-158.

Delage, P., Marcial, D., Cui, Y.J., Ruiz, X., 2006. Ageing effects in a compacted bentonite: A microstructure approach. Géotechnique 56, 291-304.

Delage, P., 2010. A microstructure approach to the sensitivity and compressibility of some eastern Canada sensitive clays. Géotechnique 60, 353-368. https://doi.org/10.1680/geot.2010.60.5.353

Deneele, D., Le, B., Cui, Y., Cuisinier, O., Ferber, V., 2016. Experimental assessment regarding leaching of lime-treated silt. Constr. Build. Mater. 112, 1032-1040.

Deng, Y.F., Yue, X.B., Cui, Y.J., Shao, G.H., Liu, S.Y., Zhang, D.W., 2014. Effect of pore water chemistry on the hydro-mechanical behaviour of Lianyungang soft marine clay. Appl. Clay Sci. 95, 167-175.

Deng, Y.F., Zhang, T.W., Zhao, Y., Liu, Q.W., W. Q., 2017. Mechanical behaviour and microstructure of steel slag-based composite and its application for soft clay stabilisation. Eur. J. Environ. Civ. Eng. 8189, 1-16.

Di Maio, C., 1996. Exposure of bentonite to salt solution: Osmotic and mechanical effects. Géotechnique 46, 695-707.

Di Maio, C., Santoli, L., Schiavone, P., 2004. Volume change behaviour of clays: the influence of mineral composition, pore fluid composition and stress state. Mech Mater 36(5-6), 435-451.

Di Sante, M., Fratalocchi, E., Mazzieri, F., Pasqualini, E., 2014. Time of reactions in a lime treated clayey soil and influence of curing conditions on its microstructure and behaviour. Appl. Clay Sci. 99, 100-109.

Diamond, S., 1970. Pore size distributions in clays. Clays Clay. Min. 18, 7-23.

Diamond, S., Kinter, E.B., 1965. Mechanisms of soil-lime stabilization An Interpretive Review. Highw. Res. Rec. 83-102.

Dong, J.C, 2013. Investigation of aggregates size effect on the stiffness of lime and/or cement treated soil: from laboratory to field conditions. PhD Dissertation, Ecole Nationale des Ponts et Chaussées, France.

Duc, M., Gaboriaud, F., Thomas, F., 2005a. Sensitivity of the acid-base properties of clays to the methods of preparation and measurement: 1. Literature review. J. Colloid Interface Sci. 289 (1), 139-147.

Duc, M., Gaboriaud, F., Thomas, F., 2005b. Sensitivity of the acid–base properties of clays to the methods of preparation and measurement: 2. Evidence from continuous potentiometric titrations. J. Colloid Interface Sci. 289 (1), 148-156.

Duc, M., Thomas, F., Gaboriaud, F., 2006. Coupled chemical processes at clay/electrolyte interface: a batch titration study of Na-montmorillonites. J. Colloid Interface Sci. 300 (2), 616-625.

Durotoye, T.O., Akinmusuru, J.O., Ogbiye, A.S., Bamigboye, G.O., 2016. Effect of common salt on the engineering properties of expansive soil. Int J Eng Technol 6(7), 233-241.

Dutta, J., Mishra, A.K., 2015. A study on the influence of inorganic salts on the behaviour of compacted bentonites. Appl. Clay Sci. 116-117, 85-92.

Dzuy, N.Q., Boger, D.V., 1985. Direct yield stress measurement with the vane method. J. Rheol. 29(3), 335-347.

Eades, J.L., Grim, R.E., 1966. A quick test to determine lime requirements for lime stabilization. Highway Res. Rec. 139, 61-72.

Edil, T.B., Motan, S.E. 1984. Laboratory evaluation of soil suction components. Geotech. Test. J. **7**(4), 173-181.

Elmashad, M.E., Ata, A.A., 2016. Effect of seawater on consistency, infiltration rate and swelling characteristics of montmorillonite clay. HBRC J. 12(2), 175-180.

Emarah, D.A., Seleem, S.A., 2018. Swelling soils treatment using lime and sea water for roads construction. Alexandria Eng. J. 57, 2357-2365.

Estabragh, A.R., Moghadas, M., Javadi, A.A., 2013. Effect of different types of wetting fluids on the behaviour of expansive soil during wetting and drying. Soils Found. 53, 617-627.

Faisant, T., Peyras, L., Jeanniot, C., Tekatlian, A., et al., 2019. Projet de R&D DIGUE 2020: réalisation d'une plateforme de recherche en site maritime pour l'étude des actions de la mer sur les digues, la durabilité, et la perception du risque de submersion. In Digues maritimes et fluviales de protection contre les inondations-3e colloque-Digues 2019.

Ferreira, C., Martins, J.P., Gomes Correia, A., 2014. Determination of the small-strain Stiffness of hard soils by means of bender elements and accelerometers. Geotech. Geol. Eng. 32, 1369-1375.

Firoozi, A.A., Guney Olgun, C., Firoozi, A.A., Baghini, M.S., 2017. Fundamentals of soil stabilization. Int. J. Geo-Engineering 8.

Fredlund, D.G., Rahardjo, H., 1993. Soil mechanics for unsaturated soils. John Wiley & Sons, New York.

Fredlund, D.G., Xing, A.Q., Huang, S.Y., 1994. Predicting the permeability function for unsaturated soils using the soil-water characteristic curve. Can. Geotech. J. 31, 533-546.

Gao, Y., Li, Z., Sun, D.A., Yu, H.H., 2021. A simple method for predicting the hydraulic properties of unsaturated soils with different void ratios. Soil Tillage Res. 209, 104913

Geertsema, M., Torrance, J.K., 2005. Quick clay from the Mink Creek landslide near Terrace, British Columbia: geotechnical properties, mineralogy, and geochemistry. Can. Geotech. J. 42(3), 907-918.

Ghobadi, M.H., Abdilor, Y., Babazadeh, R., 2014. Stabilization of clay soils using lime and effect of pH variations on shear strength parameters. Bull. Eng. Geol. Environ. 73, 611-619.

Golnabi, H., Matloob, M. R., Bahar, M., Sharifian, M., 2009. Investigation of electrical conductivity of different water liquids and electrolyte solutions. Iran. Phys. J. 3(2), 24-28.

Guney, Y., Sari, D., Cetin, M., Tuncan, M., 2007. Impact of cyclic wetting-drying on swelling behavior of lime-stabilized soil. Build. Environ. 42 (2), 681-688.

Hajela, R.B., Bhatnagar, J.M., 1984. Rheological properties of clay pastes-Part III: surface area and thixotropy at liquid limit consistency. Transactions of the Indian Ceramic Society 43(4), 96-100

Halperin, W.P., Jehng, J.Y., Song, Y., 1994. Application of spin-spin relaxation to measurement of surface area and pore size distributions in a hydrating cement paste. Magn. Reson. Imaging 12, 169-173.

Hamidi, R., Kahforoushan, D., Fatehifar, E., Arehjani, M., Farmanbordar, S., 2011 Simultaneous removal of Ca and Mg Salts using chemical precipitation with lime. The 7th International Chemical Engineering Congress & Exhibition. Kish, Iran, 21-24 November, 2011.

Hardie, M., Doyle, R., 2012. Measuring soil salinity. In Plant Salt Tolerance. Humana Press, Totowa, NJ: 415-425.

Harichane, K., Ghrici, M., Kenai, S., Grine, K., 2011. Use of natural pozzolana and lime for stabilization of cohesive soils. Geotech. Geol. Eng. 29, 759-769.

He, Y., Chen, Y.G., Ye, W.M., Chen, B., Cui, Y.J., 2016a. Influence of salt concentration on volume shrinkage and water retention characteristics of compacted GMZ bentonite. Environ. Earth Sci. 75, 1-10.

He, Y., Ye, W.M., Chen, Y.G., Chen, B., Ye, B., Cui, Y.J., 2016b. Influence of pore fluid concentration on water retention properties of compacted GMZ01 bentonite. Appl. Clay Sci. 129, 131-141.

Heitor, A., Indraratna, B., Rujikiatkamjorn, C., 2013. Laboratory study of small-strain behavior of a compacted silty sand. Can. Geotech. J. 50, 179-188.

Heitor, A., Indraratna, B., Rujikiatkamjorn, C., 2015. The role of compaction energy on the small strain properties of a compacted silty sand subjected to drying-wetting cycles. Géotechnique. 65 (9), 717-727.

Herrier, G., Group, L., Lesueur, D., Puiatti, D., Auriol, J.C., Chevalier, C., Haghighi, I., Cuisinier, O., Bonelli, S., Fry, J.J., 2012. Lime treated materials for embankment and hardfill dam Lime treated materials for embankment and hardfill dam. In ICOLD 2012 - International Symposium On Dams For A Changing World, Kyoto 5-8 June 2012.

Hilt, G.H., Davidson, D.T., 1960. Lime fixation in clayey soils. Highway Res. Board Bull. 262, 20-32.

Honda, M., Iizuka, A., Ohno, S., Kawai, K., Wang, W., 2006. An evaluation method for the volume change characteristics of compacted soil. Fourth International Conference on Unsaturated Soils, 837-848.

Hong, Z.S., Yin, J., Cui, Y.J., 2010. Compression behaviour of reconstituted soils at high initial water contents. Géotechnique 60, 691-700.

Hong, Z.S., Zeng, L.L., Cui, Y.J., Cai, Y.Q., Lin, C., 2012. Compression behaviour of natural and reconstituted clays. Géotechnique 62, 291-301.

Horpibulsuk, S., Yangsukkaseam, N., Chinkulkijniwat, A., Du, Y.J., 2011. Compressibility and permeability of Bangkok clay compared with kaolinite and bentonite. Appl. Clay Sci. 52, 150-159.

Israelachvili, J.N., 2011. Intermolecular and surface forces. 3rd edn. Academic press.

Jan, W.F., 2007. Deflocculation. Encyclopedic Dictionary of Polymers. Springer New York. pp. 265.

Jang, J., Carlos Santamarina, J., 2015. Fines classification based on sensitivity to pore-fluid chemistry. J. Geotech. Geoenviron. Eng. 142 (4), 06015018.

Jha, A.K., Sivapullaiah, P.V., 2015. Mechanism of improvement in the strength and volume change behavior of lime stabilized soil. Eng. Geol. 198, 53-64.

Jha, A.K., Sivapullaiah, P.V., 2016. Volume change behavior of lime treated gypseous soil - influence of mineralogy and microstructure. Appl. Clay Sci. 119, 202-212.

Juang, C.H., Holtz, R.D., 1986. A probabilistic permeability model and the pore size density function, Int. J. Numer. Anal. Methods Geomech. 10, 543-553.

Kassim, K.A., Chern, K.K., 2004. Lime stabilized Malaysian cohesive soils. Jurnal Kejuruteraan Awam. 16(1), 13-23.

Kavak, A., Akyarlı, A., 2007. A field application for lime stabilization. Environ. Geol. 51 (6), 987-997.

Karnland, O., 2010. Chemical and mineralogical characterization of the bentonite buffer for the acceptance control procedure in a KBS-3 repository. Sweden: N. p., 2010. Web.

Kenney, T.C., 1963. Correspondence. Géotechnique. 13(2):159-162.

Keramatikerman, M., Chegenizadeh, A., Nikraz, H., 2016. Effect of GGBFS and lime binders on the engineering properties of clay. Appl. Clay Sci. 132-133, 722-730.

Khattab, S.A.A., Al-Taie, L.K.I., 2006. Soil-water characteristic curves (SWCC) for lime treated expansive soil from mosul city, in: Forth International Conference on Unsaturated Soils 2006, 1671-1682.

Khattab, S.A.A., Fleureau, J., 2007. Long-term stability characteristics of a lime-treated plastic soil. J. Mater. Civ. Eng. 19, 358-366.

Khosravi, A., Hashemi, A., Ghadirianniari, S., Khosravi, M., 2020. Variation of small-strain shear modulus of unsaturated silt under successive cycles of drying and wetting. J. Geotech. Geoenviron. Eng. 146, 1-13.

Kim, W.S., Borden, R.H., 2011. Influence of soil type and stress state on predicting shear strength of unsaturated soils using the soil-water characteristic curve. Can. Geotech. J. 48, 1886-1900.

Koliji, A., Laloui, L., Cusinier, O. Vulliet, L., 2006. Suction induced effects on the fabric of a structured soil. Transp. Porous Media. 64(2), 261-278.

Kondo, F., Torrance, J.K., 2005. Effects of smectite, salinity and water content on sedimentation and self-weight consolidation of thoroughly disturbed soft marine clay. Paddy Water Environ, 3(3), 155-164.

Krahn, J., Fredlund, D.G., 1972. On total, matric and osmotic suction. Soil Sci. 114(5), 339-348.

Kwak, Jan C.T., Hayes, R.C., 1975. Electrical conductivity of aqueous solutions of salts of polystyrenesulfonic acid with univalent and divalent counterions. J. Phys. Chem. 79(3), 265-269.

Le Runigo, B., Cuisinier, O., Cui, Y.J., Ferber, V., Deneele, D., 2009. Impact of initial state on the fabric and permeability of a lime-treated silt under long-term leaching. Can. Geotech. J. 46, 1243-1257.

Le Runigo, B., Ferber, V., Cui, Y.J., Cuisinier, O., Deneele, D., 2011. Performance of lime-treated silty soil under long-term hydraulic conditions. Eng. Geol. 118, 20-28.

Lee, J. S., Santamarina, J. C., 2005. Bender elements: performance and signal interpretation. J. Geotech. Geoenviron. Eng. 131(9), 1063-1070.

Leelamanie, D.A.L., Karube, J., 2013. Soil-water contact angle as affected by the aqueous electrolyte concentration. Soil Sci. Plant Nutr. 59, 501-508.

Lemaire, K., Deneele, D., Bonnet, S., Legret, M., 2013. Effects of lime and cement treatment on the physicochemical, microstructural and mechanical characteristics of a plastic silt. Eng. Geol. 166, 255-261.

Leong, E. C., He, L., Rahardjo, H., 2002. Factors affecting the filter paper method for total and matric suction measurements. Geotech. Test. J. 25(3), 322-333.

Leong, E.C., Tripathy, S., Rahardjo, H., 2003. Total suction measurement of unsaturated soils with a device using the chilled-mirror dew-point technique. Géotechnique. 53, 173-182.

Leong, E.C., Widiastuti, S., Lee, C.C., Rahardjo, H., 2007. Accuracy of suction measurement. Géotechnique. 57, 547-556.

Leong, E.C., Abuel-Naga, H., 2018. Contribution of osmotic suction to shear strength of unsaturated high plasticity silty soil. Geomech. Energy Environ. 15, 65-73.

Li, H., Li, T.L., Li, P., Zhang, Y.G., 2020. Prediction of loess soil-water characteristic curve by mercury intrusion porosimetry. J. Mt. Sci. 17, 2203-2213.

Li, J. H., Zhang, L. M., 2011. Study of desiccation crack initiation and development at ground surface. Eng. Geol. 123(4), 347-358.

Li, M., Chai, S.X., Du, H.P., Wang, C., 2016. Effect of chlorine salt on the physical and mechanical properties of inshore saline soil treated with lime. Soils Found. 56, 327-335.

Li, X., Zhang, L.M., 2009. Characterization of dual-structure pore-size distribution of soil. Can. Geotech. J. 46, 129-141.

Lin, C.L., Lee, L.S., 2003. A two-ionic-parameter approach for ion activity coefficients of aqueous electrolyte solutions. Fluid Phase Equilib. 205(1), 69-88.

Little, D. N., 1999. Evaluation of Structural Properties of Lime Stabilized Soils and Aggregates. Prepared for the National Lime Association: Arlington, Virginia, USA.

Little, D.N., Nair, S., Herbert, B., 2010. Addressing sulfate-induced heave in lime treated soils. J. Geotech. Geoenviron. Eng. 136(1), 110-118.

Liu, M.D., Pemberton, S., 2010. A study of the strength of lime treated soft clays. Int. Symp. Exhib. Geotech. Geosynth. Eng. Challenges Oppor. Clim. Chang. 245-251.

Liu, J.Y., Zhang, L.J., 2014. The microstructure characters of saline soil in Qarhan Salt Lake area and its behaviours of mechanics and compressive strength. Arab. J. Sci. Eng. 39(12), 8649-8658.

Liu, X.F., de Carteret, R., Buzzi, O.P., Fityus, S.G., 2016a. Microstructural effects of environmental salinity on unbound granular road pavement material upon drying. Acta Geotech. 11, 445-451.

Liu, X.F., Buzzi, O., Yuan, S.Y., Mendes, J., Fityus, S., 2016b. Multi-scale characterization of retention and shrinkage behaviour of four Australian clayey soils. Can. Geotech. J. 53(5), 854-870.

Liu, J., Bai, Y.X., Feng, Q., Song, Z.Z., Wei, J.H., Sun, S.R., Kanungo, D.P., 2018a. Strength properties of sand reinforced with a mixture of organic polymer stabilizer and polypropylene fiber. J. Mater. Civ. Eng. 30, 04018330.

Liu, L.L., Li, Z., Liu, X.Y., Li, Y.Y., 2018b. Effect of salt content on freezing temperature and uncon fined compression strength of lime-treated subgrade clay. Appl. Clay Sci. 158, 65-71.

Liu, D., Edraki, M., Berry, L., 2018c. Investigating the settling behaviour of saline tailing suspensions using kaolinite, bentonite, and illite clay minerals. Powder Techno. 326(15), 228-236.

Liu, J.J., Zha, F.S., Xu, L., Kang, B., Tan, X.Z., Deng, Y.F., Yang, C.B., 2019a. Mechanism of stabilized/solidified heavy metal contaminated soils with cement-fly ash based on electrical resistivity measurements. Meas. 141, 85-94.

Liu, Y.W., Wang, Q., Liu, S.W, ShangGuan, Y.L., Fu, H.C., Ma, B., Chen, H., Yuan, X.Q., 2019b. Experimental investigation of the geotechnical properties and microstructure of lime-stabilized saline soils under freeze-thaw cycling. Cold Reg. Sci. Technol. 161, 32-42.

Locat, J., Bérubé, M.A., Choquette, M., 1990. Laboratory investigations on the lime stabilization of sensitive clays: shear strength development. Can. Geotech. J. 27 (3), 294-304.

Locat, J., Trembaly, H., Leroueil, S., 1996. Mechanical and hydraulic behaviour of a soft inorganic clay treated with lime. Can. Geotech. J. 33(4), 654-669.

Loret, B., Hueckel, T., Gajo, A., 2002. Chemo-mechanical coupling in saturated porous media: Elastic-plastic behaviour of homoionic expansive clays. Int. J. Solids Struct. 39, 2773-2806.

Lu, N., Khorshidi, M., 2015. Mechanisms for Soil-Water Retention and Hysteresis at High Suction Range. J. Geotech. Geoenviron. Eng. 141, 04015032.

Luckham, P.F., Rossi, S., 1999. The colloidal and rheological properties of bentonite suspensions. Adv. Colloid Interface Sci. 82(1-3), 43-92.

Madsen, F.T., 1998. Clay mineralogical investigations related to nuclear waste disposal. Clay Miner. 33 (1), 109-129.

Magistad, O.C., Reitemeier, R.F. Wilcox, L.V., 1945. Determination of soluble salts in soils. Soil Sci. 59(1), 65-76.

Makki-Szymkiewicz, L., Hibouche, A., Taibi, S., Herrier, G., Lesueur, D., Fleureau, J.M., 2015. Evolution of the properties of lime-treated silty soil in a small experimental embankment. Eng. Geol. 191, 8-22.

Marcial, D., Delage, P., Cui, Y.J., 2002. On the high stress compression of bentonites. Can. Geotech. J. 39, 812820.

Marks, B. D., Haliburton, T. A., 1972. Acceleration of lime-clay reactions with salt. J. Soil Mech. Found. Div. 98(4), 327-339.

Mata, C., Romero, E., Ledesma, A. 2002. Hydro-chemical effects on water retention in bentonite-sand mixtures. In Proceeding of the 3rd International Conference on Unsaturated soil. Recife, Brazil, Swets & Zeitlinger, Lisse, 2002, 283-288.

Mavroulidou, M., Zhang, X.W., Gunn, M.J., Cabarkapa, Z., 2013. Water retention and compressibility of a lime-treated, high plasticity clay. Geotech. Geol. Eng. 31, 1171-1185.

McCallister, L.D., Petry, T.M., 1990. Property changes in lime treated expansive clays under continuous leaching. TEXAS UNIV AT ARLINGTON.

McCallister, L.D., Petry, T.M., 1992. Leach tests on lime-treated clays. Geotech. Test. J. 15(2), 106-114.

McLaughlin, M, J., Palmer, L.T., Tiller, K. G., Beech, T. A., Smart, M. K., 1994. Increased soil salinity causes elevated cadmium concentrations in field-grown potato tubers. J. Environ. Qual. 23(5), 1013-1018.

McRobert, J., Foley, G., 1999. The impacts of waterlogging and salinity on road assets: a Western Australian case study (No. 57).

Menaceur, H., Delage, P., Tang, A.M., Talandier, J., 2016. The status of water in swelling shales: an insight from the water retention properties of the Callovo-Oxfordian claystone. Rock Mech. Rock Eng. 49(12), 4571-4586.

Mesri, G., Vardhanabhuti, B., 2009. Compression of granular materials. Can. Geotech. J. 46, 369-392.

Miller, C.J., Mi, H. Yesiller, N., 1998. Experimental analysis of desiccation crack propagation in clay liners[1]. J. Am. Water Resour. Assoc. 34(3), 677-686.

Miller, C.J., Rifai, S., 2004. Fiber reinforcement for waste containment soil liners. J. Environ. Eng. 130(8), 891-895.

Miller, D J., Nelson, J.D., 1993. Osmotic suction as a valid stress state variable in unsaturated soil mechanics. Unsaturated Soils, 64-76

Miller, D.J. Nelson, J.D., 2006. Osmotic suction in unsaturated soil mechanics. Unsaturated Soils, 1382-1393.

Mishra, A.K., Ohtsubo, M., Li, L.Y., Higashi, T., Park, J., 2009. Effect of salt of various concentrations on liquid limit, and hydraulic conductivity of different soil-bentonite mixtures. Environ. Geol. 57, 1145-1153.

Mishra, P.N., Scheuermann, A., Bore, T., Li, L., 2019. Salinity effects on soil shrinkage characteristic curves of fine-grained geomaterials. J. Rock Mech. Geotech. Eng. 11(1), 181-191.

Mitchell, J.K., Soga, K., 2005. Fundamentals of soil behaviour. 3rd edn. John Wiley &Sonc, Inc.

Moayed, R.Z., Izadi, E., Heidari, S., 2012. Stabilization of saline silty sand using lime and micro silica. Journal of Central South University. 19(10), 3006-3011.

Modmoltin, C., Voottipruex, P., 2009. Influence of salts on strength of cement-treated clays. Proc. Inst. Civ. Eng. Gr. Improv. 162, 5-26.

Moghal, A.A.B., Obaid, A.A.K., Al-Refeai, T.O., 2014. Effect of accelerated loading on the compressibility characteristics of lime-treated semiarid soils. J. Mater. Civ. Eng. 26, 1009-1016.

Mohamed, A.M.O., 2000. The role of clay minerals in marly soils on its stability. Eng. Geol. 57(3), 193-203

Mokni, N., Romero, E., Olivella, S., 2014. Chemo-hydro-mechanical behaviour of compacted Boom Clay: Joint effects of osmotic and matric suctions. Géotechnique 64, 681-693.

Monteleone, M., Lacolla, G., Caranfa, G., Cucci, G., 2016. Indirect measurement of electrical conductivity and exchangeable cations on soil water extracts: Assessing the precision of the estimates. Soil Sci. 181(9/10), 465-471.

Moore, R., 1991. The chemical and mineralogical controls upon the residual strength of pure and natural clays. Géotechnique 41(1), 35-47.

Morris, P.H., Graham, J., Williams, D.J., 1992. Cracking in drying soils. Can. Geotech. J. 29 (2), 263-277.

Muller, A.C.A., 2014. Characterization of porosity & C-S-H in cement pastes by 1H NMR. PhD Thesis, École Polytech. Fédérale Lausanne, Lausanne, Suisse.

Mun, W., McCartney, J.S., 2017. Roles of particle breakage and drainage in the isotropic compression of sand to high pressures. J. Geotech. Geoenviron. Eng. 143, 04017071.

Muñoz-Castelblanco, J.A., Pereira, J.M., Delage, P., Cui, Y.J., 2012. The water retention properties of a natural unsaturated loess from northern France. Géotechnique. 62, 95-106.

Muntohar, A.S., Widianti, A., Hartono, E., Diana, W., 2013. Engineering properties of silty soil stabilized with lime and rice husk ash and reinforced with waste plastic fiber. J. Mater. Civ. Eng. 25, 1260-1270.

Musso, G., Romero Morales, E., Gens, A., Castellanos, E., 2003. The role of structure in the chemically induced deformations of FEBEX bentonite. Appl. Clay Sci. 23, 229-237.

Nabil, M., Mustapha, A., Rios, S., 2018. Long term evaluation of wetting-drying cycles for compacted soils treated with lime. In Conference of the Arabian Journal of Geosciences (pp. 277-281). Springer, Cham.

Nabil, M., Mustapha, A., Rios, S., 2019. Impact of wetting-drying cycles on the mechanical properties of lime-stabilized soils. Int. J. Pavement Res. Technol. 13, 83-92

Nabil, M., Mustapha, A., Rios, S., 2020. Impact of wetting-drying cycles on the mechanical properties of lime-stabilized soils. Int. J. Pavement Res. Technol. 13, 83-92.

Nalbantoglu, Z., Tuncer, E.R., 2001. Compressibility and hydraulic conductivity of a chemically treated expansive clay. Can. Geotech. J. 38(1), 154-160.

Negawo, W.J., Emidio, G. D., Bezuijen, A., Daniel, R., Flores, V., François, B., 2019. Lime-stabilisation of high plasticity swelling clay from Ethiopia. Eur. J. Environ. Civ. Eng. 23(4), 504-514.

Nelson, J., Miller, D. J., 1997. Expansive soils: problems and practice in foundation and pavement engineering. John Wiley & Sons.

Niu, G., Sun, D.A., Shao, L.T., Zeng, L.F., 2019. The water retention behaviours and pore size distributions of undisturbed and remoulded complete-intense weathering mudstone, Eur. J. Environ. Civ. Eng. 1233-1250.

Ng, C.W.W., Baghbanrezvan, S., Sadeghi, H., Zhou, C., Jafarzadeh, F., 2017. Effect of specimen preparation techniques on dynamic properties of unsaturated fine-grained soil at high suctions. Can. Geotech. J. 54(9), 1310-1319.

Ng, C.W.W., Sadeghi, H., Hossen, S.K.B., Chiu, C.F., Alonso, E.E., 2016. Water retention and volumetric characteristics of intact and re-compacted loess. Can. Geotech. J. 53, 1258-1269.

Ng, C.W.W., Xu, J., Yung, S.Y., 2009. Effects of wetting-drying and stress ratio on anisotropic stiffness of an unsaturated soil at very small strains. Can. Geotech. J. 46, 1062-1076.

Ng, C.W.W., Yung, S.Y., 2008. Determination of the anisotropic shear stiffness of an unsaturated decomposed soil. Géotechnique. 58(1), 23-35.

Ngoc, T.P., Fatahi, B., Khabbaz, H., 2019. Impacts of Drying-Wetting and Loading-Unloading Cycles on Small Strain Shear Modulus of Unsaturated Soils. Int. J. Geomech. 19(8), 04019090.

Nguyen, X.P., Cui, Y.J., Tang, A.M., Deng, Y.F., Li, X.L., Wouters, L., 2013. Effects of pore water chemical composition on the hydro-mechanical behavior of natural stiff clays. Eng. Geol. 166(8), 52-64.

Noorany, I. 1984. Phase relations in marine soils. J. Geotech. Eng. 110(4), 539-543.

Norrish, K., 1954. The swelling of montmorillonite. Discuss. Faraday Soc. 18, 120-134.

Ohtsubo. M, Egashira, K., Takayama, M., 1996. Mineralogy and chemistry, and their correlations with the geotechnical properties of marine clays in Ariake Bay, Japan: comparison of quick and nonquick clay sediments. Mar. Georesour. Geotechnol. 14(3),

263-282.

Olson, R.E., Mesri, G., 1970. Mechanisms controlling compressibility of clays. J. Soil Mech. Found. Div. 96, 1863-1978.

Osinubi, K.J., 1998. Permeability of lime-treated lateritic soil. J. Transp. Eng. 124(5), 465-469.

Péron, H., Hueckel, T., Laloui, L., Hu, L.B., 2009. Fundamentals of desiccation cracking of fine-grained soils: Experimental characterisation and mechanisms identification. Can. Geotech. J. 46, 1177-1201.

Petrov, R.J., Kerry Rowe, R., 1997. Geosynthetic clay liner (GCL)-chemical compatibility by hydraulic conductivity testing and factors impacting its performance. Can Geotech J 34(6), 863-885.

Petry, T.M., Jiang, C.P., 2007. Soil suction and behavior of chemically treated clays. Transp. Res. Rec. 30-38.

Poncelet, N., François, B., 2019. Desiccation crack in lime-treated silty clay: Experimental evaluation and constitutive interpretation, E3S Web Conf. 92, 1-6.

Prapaharan, S., Altschaeffl, A.G., Dempsey, B.J., 1985. Moisture curve of compacted clay: mercury intrusion method. J. Geotech.. Eng 111(9), 1139-43.

Puppala, A.J., Kadam, R., Madhyannapu, R.S., Hoyos, L.R., 2006. Small-strain shear moduli of chemically stabilized sulfate-bearing cohesive soils. J. Geotech. Geoenviron. Eng. 132, 322-336.

Puppala, A.J., Mohammad, L.N., Allen, A., 1996. Engineering behavior of lime-treated Louisiana subgrade soil. Transp. Res. Rec. 24-31.

Quang, N.D., Chai, J.C., 2015. Permeability of lime- and cement-treated clayey soils. Can. Geotech. J. 52, 1221-1227.

Rajasekaran, G., Murali, K., Srinivasaraghavan, R., 1997. Effect of chlorides and sulphates on lime treated marine clays. Soils Found. 37(2), 105-115.

Rajasekaran, G., Rao, S.N., 2000. Strength characteristics of lime-treated marine clay. Gr. Improv. 4, 127-136.

Rajasekaran, G., Rao, S.N., 2001. Permeability characteristics of lime treated marine clay. Ocean Eng. 29, 113-127.

Rajasekaran, G., Rao, S.N., 2002. Compressibility behaviour of lime-treated marine clay. Ocean Eng. 29, 545–559.

Ramesh, H.N., Mohan, M.S., Sivapullaiah, P. V., 1999. Improvement of strength of fly ash with lime and sodium salts. Gr. Improv. 3, 163-167.

Rao, S.M., Sridharan, A., Chandrakaran, S., 1993. Consistency limits behavior of bentonites exposed to sea water. Mar. Georesour. Geotechnol. 11(3), 213-227.

Rao, S.N., Mathew, P.K., 1995. Effects of exchangeable cations on hydraulic conductivity of a marine clay. Clays Clay Miner. 43(4), 433-437.

Rao, S.M., Reddy, B.V.V., Muttharam, M., 2001. The impact of cyclic wetting and drying on the swelling behaviour of stabilized expansive soils. Eng. Geol. 60, 223-233.

Rao, S.M., Shivananda, P., 2005a. Compressibility behaviour of lime-stabilized clay. Geotech. Geol. Eng. 23, 309319.

Rao, S.M., Shivananda, P., 2005b. Role of osmotic suction in swelling of salt-amended clays. Can. Geotech. J. 42, 307315.

Rao, S.M., Thyagaraj, T. 2007a. Role of direction of salt migration on the swelling behaviour of compacted clays. Appl. Clay. Sci. 38(1-2), 113-129.

Rao, S.M., Thyagaraj, T. 2007b. Swell-compression behaviour of compacted clays under chemical gradients. Can. Geotech. J. 44(5), 520-532.

Rao, S.M., Thyagaraj, T., Thomas, H.R., 2006. Swelling of compacted clay under osmotic gradients. Géotechnique 56, 707-713.

Ravi, K., Rao, S. M., 2013. Influence of infiltration of sodium chloride solutions on SWCC of compacted bentonite–sand specimens. Geotech. Geol. Eng. 31(4), 1291-1303.

Reitemeier, R.F., 1946. Effect of moisture content on the dissolved and exchangeable ions of soils of arid regions. Soil Sci. 61(3), 195-214.

Renou, S., Poulain, S., Givaudan, J.G., Moulin, P., 2008. Treatment process adapted to stabilized leachates: Lime precipitation-prefiltration-reverse osmosis. J. Membr. Sci. 313 (1-2), 9-22.

Rhoades, J.D., 1981. Predicting bulk soil electrical conductivity versus saturation paste extract electrical conductivity calibrations from soil properties. Soil Sci. Soc. Am. J. 45(1), 42-44.

Rhoades, J.D., 1982. Soluble salts. Methods of soil analysis Part 2.2, 167-178.

Romero, E., 1999. Thermo-Hydro-Mechanical Behaviour of Unsaturated Boom Clay: an experimental study. PhD Thesis, Universidad Politécnica de Catalunya, Barcelona, Spain.

Romero, E., Gens, A., Lloret, A., 1999. Water permeability, water retention and microstructure of unsaturated compacted Boom clay. Eng. Geol. 54, 117-127.

Romero, E., Vaunat, J., 2000. Retention curves of deformable clays, in: Experimental Evidence and Theoretical Approaches in Unsaturated Soils. 91-106.

Romero, E., Della Vecchia, G., Jommi C., 2011. An insight into the water retention properties of compacted clayey soils. Géotechnique. 61(4), 313-328.

Romero, E., 2013. A microstructural insight into compacted clayey soils and their hydraulic properties. Eng. Geol. 165, 3-19.

Rosone, M., Farulla, C.A., Ferrari, A., Torta, C., Celauro, C., 2016. Suction controlled drying and wetting cycle effects on the volumetric behaviour of a lime-treated high plasticity clay. In E3S Web of Conferences (Vol. 9, p. 14020).

Rosone, M., Ferrari, A., Celauro, C., 2018. On the hydro-mechanical behaviour of a lime-treated embankment during wetting and drying cycles. Geomech. Energy Environ. 14, 48-60.

Rosone, M., Celauro, C., Ferrari, A., 2020. Microstructure and shear strength evolution of a lime-treated clay for use in road construction. Int. J. Pavement Eng. 21, 1147-1158.

Roy, A., 2017. Soil Stabilization using Rice Husk Ash and Cement. Int. Res. J. Eng. Technol. 4, 49-54.

Russo, G., Modoni, G., 2013. Fabric changes induced by lime addition on a compacted alluvial soil. Geotech. Lett. 3, 93-97.

Russo, G., Vecchio, S., Mascolo, G., 2007. Microstructure of a lime stabilised compacted silt. In T. Schanz, ed. Experimental Unsaturated Soil Mechanics. Springer Berlin Heidelberg, pp. 49-56.

Sakr, M.A., Shahin, M.A., Metwally, Y.M., 2009. Utilization of lime for stabilizing soft clay soil of high organic content. Geotech. Geol. Eng. 27, 105-113.

Saldanha, R.B., Scheuermann Filho, H.C., Ribeiro, J.L.D., Consoli, N.C., 2017. Modelling the influence of density, curing time, amounts of lime and sodium chloride on the durability of compacted geopolymers monolithic walls. Constr. Build. Mater. 136, 65-72.

Santamarina, J.C., Klein, K.A., Wang, Y.H., Prencke, E., 2002. Specific surface: Determination and relevance. Can. Geotech. J. 39, 233-241.

Saride, S., Puppala, A.J., Chikyala, S.R., 2013. Swell-shrink and strength behaviors of lime and cement stabilized expansive organic clays. Appl. Clay Sci. 85, 39-45.

Sarkar, G., Siddiqua, S., 2016. Effect of fluid chemistry on the microstructure of light backfill: An X-ray CT investigation. Eng. Geol. 202, 153-162.

Sghaier, N., Prat, M., Ben Nasrallah, S., 2006.On the influence of sodium chloride concentration on equilibrium contact angle. Chem. Eng. J. 122, 47-53.

Shariatmadari, N., Salami, M., Karimpour, F.M., 2011. Effect of inorganic salt solutions on some geotechnical properties of soil-bentonite mixtures as barriers. Int. J. Civ. Eng. 9(2), 103-110.

Sharma, L.K., Sirdesai, N.N., Sharma, K.M., Singh, T.N., 2018. Experimental study to examine the independent roles of lime and cement on the stabilization of a mountain soil: A comparative study. Appl. Clay Sci. 152, 183-195.

Sharma, N.K., Swain, S.K., Sahoo, U.C., 2012. Stabilization of a clayey soil with fly ash and lime: A Micro Level Investigation. Geotech. Geol. Eng. 30(5), 1197-1205.

Shi, B., Liu, Z.B., Cai, Y., Zhang, X.P., 2007. Micropore structure of aggregates in treated soils. J. Mater. Civ. Eng. 19(1), 99-104.

Shi, X.S., Zhao, J.D., 2020. Practical estimation of compression behavior of clayey/silty sands using equivalent void-ratio concept. J. Geotech. Geoenviron. Eng. 146, 04020046.

Siddiqua, S., Blatz, J., Siemens, G., 2011. Evaluation of the impact of pore fluid chemistry on the hydromechanical behaviour of clay-based sealing materials. Can. Geotech. J. 48, 199-213.

Simms, P.H., Yanful, E.K., 2001. Measurement and estimation of pore shrinkage and pore distribution in a clayey till during soil-water characteristic curve tests. Can. Geotech. J. 38(4), 741-754.

Simms, P.H., Yanful, E.K., 2002. Predicting soil-Water characteristic curves of compacted plastic soils from measured pore-size distributions. Géotechnique. 52(4), 269-278.

Simms, P.H. Yanful, E.K., 2004. A discussion of the application of mercury intrusion porosimetry for the investigation of soils, including an evaluation of its use to estimate volume change in compacted clayey soils. Géotechnique. 54(6), 421-426.

Sivapullaiah, P.V., Manju, 2005. Kaolinite - Alkali interaction and effects on basic properties. Geotech. Geol. Eng. 23, 601-614.

Sivapullaiah, P.V., Sridharan, A., Ramesh, H.N., 2000. Strength behaviour of lime-treated soils in the presence of sulphate. Can. Geotech. J. 37, 1358-1367.

Sivapullaiah, P.V., Sridharan, A., Ramesh, H.N., 2006. Effect of sulphate on the shear strength of lime-treated kaolinitic soil. Gr. Improv. 10, 23-30.

Smith, A.K., Gortner, R.A., 1933. The Electrical Conductivity of Mixed Salt Solution. J. Phys. Chem. 37(1), 79-86.

Song, M.M., Zeng, L.L., Hong, Z.S., 2017. Pore fluid salinity effects on physicochemical-compressive behaviour of reconstituted marine clays. Appl. Clay Sci. 146(15), 270-277.

Sreedeep, S., Singh, D.N., 2005. A study to investigate the influence of soil properties on suction. J. Test. Eval. 33, 61-66.

Sreedeep, S., Singh, D.N., 2006. Methodology for determination of osmotic suction of soils. Geotech. Geol. Eng. 24(5), 1469-1479.

Sreedeep, S., Singh, D.N., 2011. Critical review of the methodologies employed for soil suction measurement. Int. J. Geomech., 11(2), 99-104.

Sridharan, A., Venkatappa Rao, G., 1975. Mechanisms controlling the liquid limit of clays. Proc. Istanbul Conf Soil Mech Found Eng Istanbul 1, 65–74.

Sridharan, A. Jayadeva, M.S., 1982. Double layer theory and compressibility of clays. Géotechnique. 32(2), 133-144.

Sridharan, A., Prakash, K., 1998a. Characteristic water contents of a fine-grained soil-water system. Géotechnique. 48(3), 337-346.

Sridharan, A., Prakash, K., 1998b. Mechanism controlling the shrinkage limit of soils. Geotech. Test. J. 21(3), 240-250.

Sridharan, A., Prakash, K., 1999. Mechanisms controlling the undrained shear strength behaviour of clays. Can. Geotech. J. 36(6), 1030-1038.

Sridharan, A., Prakash, K., 2000. Percussion and cone methods of determining the liquid limit of soils: Controlling Mechanisms. Geotech. Test. J. 23, 236-244.

Sridharan, A., El-Shafei, A., Miura, N., 2002. Mechanisms controlling the undrained strength behavior of remolded Ariake marine clays. Mar. Georesour. Geotechnol. 20(1), 21-50.

Stawiński, J., Wierzchoś, J., Garcia-Gonzalez, M.T., 1990. Influence of calcium and sodium concentration on the microstructure of bentonite and kaolin. Clays Clay. Miner. 38(6), 617-622.

Stevens, D.P., McLaughlin, M.J., Smart, M.K., 2003. Effects of long-term irrigation with reclaimed water on soils of the Northern Adelaide Plains, South Australia. Soil Res. 41(5), 933-948.

Stoltz, G., Cuisinier, O., Masrouri, F., 2012. Multi-scale analysis of the swelling and shrinkage of a lime-treated expansive clayey soil. Appl. Clay Sci. 61, 44-51.

Stoltz, G., Cuisinier, O., Masrouri, F., 2014. Weathering of a lime-treated clayey soil by drying and wetting cycles. Eng. Geol. 181, 281-289.

Sun, D.A., Sun, W.J., Yan, W., Li, J., 2010. Hydro-mechanical behaviours of highly compacted sand-bentonite mixture. J. Rock Mech. Geotech. Eng. 2(1), 79-85.

Sun, D.A., Zhang, J.Y., Song, G.S., 2013. Experimental study of soil-water characteristic curve of chlorine saline soil (in Chinese). Rock Soil .Mech. 34(4), 955-960.

Sun, H.L., Weng, Z.Q., Liu, S.J., Geng, X.Y., Pan, X.D., Cai, Y.Q, 2020. Compression and consolidation behaviors of lime-treated dredging slurry under vacuum pressure. Eng. Geol. 270, 105573.

Sun, W.J., Sun, D.A., Fang, L., Liu, S.Q., 2014. Soil-water characteristics of Gaomiaozi bentonite by vapour equilibrium technique. J. Rock Mech. Geotech. Eng. 6(1), 48-54.

Sun, W.J., Cui, Y.J., 2018. Investigating the microstructure changes for silty soil during drying. Géotechnique 68, 370-373.

Sun, W.J., Cui, Y.J., 2020. Determining the soil-water retention curve using mercury intrusion porosimetry test in consideration of soil volume change. J. Rock Mech. Geotech. Eng. 12, 1070-1079.

Tang, A.M., Cui, Y.J., Le, T.T., 2008. A study on the thermal conductivity of compacted bentonites. Appl. Clay Sci. 41 (3-4), 181-189.

Tang, A.M., Vu, M.N., Cui, Y.J., 2011a. Effects of the maximum soil aggregates size and cyclic wetting-drying on the stiffness of a lime-treated clayey soil. Géotechnique 61, 421-429.

Tang, C.S., Shi, B., Liu, C., Suo, W. Bin, Gao, L., 2011b. Experimental characterization of shrinkage and desiccation cracking in thin clay layer. Appl. Clay Sci. 52, 69-77.

Tang, C.S., Shi, B., Cui, Y.J., Liu, C. Gu, K., 2012. Desiccation cracking behavior of polypropylene fiber–reinforced clayey soil. Can. Geotech. J. 49, No. 9, 1088-1101.

Tang. G.X., Graham, J., and Blat, J., 2002. Suctions, stresses and strengths in unsaturated sand-bentonite. Eng. Geol, 64(2-3), 147-156.

Tarantino, A., De Col, E., 2008. Compaction behaviour of clay. Géotechnique. 58, No. 3, 199-213.

Tatsuoka, F., 2015. Compaction characteristics and physical properties of compacted soil controlled by the degree of saturation. Proc. 15th Pan-American Conf. on SMGE & 6th IC on Deformation Characteristics of Geomaterials, Buenos Aires. 40-76.

Tatsuoka, F., Correia, A.G., 2018. Importance of controlling the degree of saturation in soil compaction linked to soil structure design. Trans. Geotech. 17, 3-27.

Tay, Y.Y., Stewart, D.I. Cousens, T.W. 2001. Shrinkage and desiccation cracking in bentonite–sand landfill liners. Eng. Geol. 60(1-4), 263-274.

Tedesco, D.V., 2006. Hydro-mechanical behaviour of lime-stabilised soils. PhD dissertation, Universitá degli Studi di Cassino, Facoltá di Ingegneria, Cassino, Italy.

Tedesco, D.V., Russo, G., 2008. Time dependency of the water retention properties of a lime stabilised compacted soil. Unsaturated Soils Adv. Geo-Engineering - Proc. 1st Eur. Conf. Unsaturated Soils, E-UNSAT 2008 277-282.

Tessier, D., 1990. Behaviour and microstructure of clay minerals. Soil colloids and their associations in aggregates. Springer, Boston, MA, pp 387-415.

Thomas, A., Tripathi, R.K., Yadu, L.K., 2018. A laboratory investigation of soil stabilization using enzyme and alkali-activated ground granulated blast-furnace slag. Arab. J. Sci. Eng. 43, 5193-5202.

Thyagaraj, T. Rao, S.M., 2013. Osmotic swelling and osmotic consolidation behaviour of compacted expansive clay. Geotech. Geol. Eng., 31(2). 435-445.

Thyagaraj, T., Rao, S.M., 2010. Influence of osmotic suction on the soil-water characteristic curves of compacted expansive clay. J. Geotech. Geoenviron. Eng. 136, 1695-1702.

Thyagaraj, T., Salini, U., 2015. Effect of pore fluid osmotic suction on matric and total suctions of compacted clay. Géotechnique, 65(11), 952-960.

Thyagaraj, T., Thomas, S.R. Das, A.P., 2017. Physico-chemical effects on shrinkage behavior of compacted expansive clay. Int. J. Geomech. 17(2), 06016013.

Tiwari, B., Tuladhar, G.R., Marui, H., 2005. Variation in residual shear strength of the soil with the salinity of pore fluid. J. Geotech. Geoenviron. Eng. 131(12), 1445-1456.

Tran, T.D., Cui, Y.J., Tang, A.M., Audiguier, M., Cojean, R., 2014. Effects of lime treatment on the microstructure and hydraulic conductivity of Héricourt clay. J. Rock Mech. Geotech. Eng. 6, 399-404.

Trefalt, G., Borkovec, M., 2014. Overview of DLVO theory. Lab. Colloid Surf. Chem. Univ. Geneva. 1-10.

Truong, Q.H., Lee, C., Kim, Y.U., Lee, J.S., 2012. Small strain stiffness of salt-cemented granular media under low confinement. Géotechnique 62, 949-953.

Tu, H., Vanapalli, S.K., 2016. Prediction of the variation of swelling pressure and one-dimensional heave of expansive soils with respect to suction using the soil-water retention curve as a tool. Can. Geotech. J. 53, 1213-1234.

Tuller, M., Or, D., 2005. Water films and scaling of soil characteristic curves at low water contents. Water Resour. Res. 41, 1-6.

United States Salinity Laboratory Staff, 1954. Diagnosis and improvement of saline and alkali soils. USDA Agriculture Handbook no. 60. U.S. Government Printing Office, Washington, D.C. 1954.

Vitale, E., Cecconi, M., Croce, P., Deneele, D., Pane, V., Russo, G., Vecchietti, A., 2016. Influence of pore water chemistry on hydraulic conductivity of kaolinite suspensions. Procedia Eng. 158, 81-86.

Vitale, E., Deneele, D., Paris, M., Russo, G., 2017. Multi-scale analysis and time evolution of pozzolanic activity of lime treated clays. Appl. Clay Sci. 141, 36-45.

Vitale, E., Deneele, D., Russo, G., 2020. Microstructural investigations on plasticity of lime-treated soils. Minerals. 10(5), 386.

Walton, N.R.G. 1989. Electrical conductivity and total dissolved solids-what is their precise relationship?. Desalination. 72(3), 275-292.

Wan, A.W.L., Gray, M.N., Graham, J., 1995. On the relations of suction, moisture content and soil structure in compacted clays. 1st International Conference on Unsaturated Soils, Paris, France, 1995, 215-222.

Wang, H., Cui, Y. J., Zhang, F., Liu, J. 2021. Effect of grain breakage on the compressibility of soils. Acta Geotech. 1-10.

Wang, Q., Tang, A.M., Cui, Y.J., Delage, P., Barnichon, J.D., Ye, W.M., 2013. The effects of technological voids on the hydro-mechanical behaviour of compacted bentonite-sand mixture. Soils Found. 53(2), 232-245.

Wang, Q., Cui, Y.J., Tang, A.M., Delage, P., Gatmiri, B., Ye, W.M., 2014a. Long-term effect of water chemistry on the swelling pressure of a bentonite-based material. Appl. Clay Sci. 87, 157-162.

Wang, Q., Cui, Y.J., Tang, A.M., Li, X.L., Ye, W.M., 2014b. Time-and density-dependent microstructure features of compacted bentonite. Soils Found. 54(4), 657-666. https://doi.org/10.1016/j.sandf. 2014.06.021

Wang, Y.H., Siu, W.K., 2006. Structure characteristics and mechanical properties of kaolinite soils. I. Surface charges and structural characterizations. Can. Geotech. J. 43(6), 587-600.

Wang, Y.J., 2016. Investigation the thermo-hydro-mechanical properties of lime-treated fine-grained soils. PhD Dissertation, Ecole Nationale des Ponts et Chaussées, France.

Wang, Y.J., Cui, Y.J., Tang, A.M., Tang, C.S., Benahmed, N., 2015. Effects of aggregate size on water retention capacity and microstructure of lime-treated silty soil. Geotech. Lett. 5, 269-274.

Wang, Y.J., Cui, Y.J., Tang, A.M., Tang, C.S., Benahmed, N., 2016. Changes in thermal conductivity, suction and microstructure of a compacted lime-treated silty soil during curing. Eng. Geol. 202, 114-121.

Wang, Y.J., Cui, Y.J., Tang, A.M., Benahmed, N., Duc, M., 2017a. Effects of aggregate size on the compressibility and air permeability of lime-treated fine-grained soil. Eng. Geol. 228, 167-172.

Wang, Y.J., Duc, M., Cui, Y.J., Tang, A.M., Benahmed, N., Sun, W.J., Ye, W.M., 2017b. Aggregate size effect on the development of cementitious compounds in a lime-treated soil during curing. Appl. Clay Sci. 136, 58-66.

Wang, Y.J., Benahmed, N., Cui, Y. J., Tang, A. M. 2017c. A novel method for determining the small-strain shear modulus of soil using the bender elements technique. Can. Geotech. J. 54(2), 280-289.

Wang, Y.J., Cui, Y.J., Benahmed, N., Tang, A.M., Duc, M., 2020a. Changes of small strain shear modulus and suction for a lime-treated silt during curing. Géotechnique 70, 276-280.

Wang, Y.J., Cui, Y.J., Tang, A.M., Benahmed, N., Duc, M., Sun, W.J., 2020b. Shrinkage behaviour of a compacted lime-treated clay, Geotech. Lett. 10, 174-178.

Warkentin, B.P., 1961. Interpretation of the upper plastic limit of clays. Nat. 190, 287-288.

Warkentin, B.P., Yong, R.N., 1962. Shear strength of montmorillonite and kaolinite related to interparticle forces. Proc. 9th Nation. Conf. Clays Clay Miner. Pergamon, 210-218.

Wei, X., Hattab, M., Fleureau, J.M., Hu, R.L., 2013. Micro-macro-experimental study of two clayey materials on drying paths. Bull. Eng. Geol. Environ. 72(3-4), 495-508.

Wicaksono, R.I., Kuwano, R., 2009. Small strain shear stiffness of Toyoura sand obtained from various wave measurement techniques. Bull. ERS 42, 107-120.

Wild, S., Arabi, M., Leng-Ward, G., 1986. Soil-lime reaction and microstructural development at elevated temperatures. Clay Miner. 21(3), 279-292.

Wild, S., Arabi, M., Rowlands, G.O., 1987. Relation between pore size distribution, permeability, and cementitious gel formation in cured clay-lime systems. Mater. Sci. Technol. 3(12), 1005-1011.

Wild, S., Kinuthia, J. M., Jones, G.I., Higgins, D.D., 1999. Suppression of swelling associated with ettringite formation in lime stabilized sulphate bearing clay soils by partial substitution of lime with ground granulated blastfurnace slag (GGBS). Eng. Geol. 51(4), 257-277.

Witteveen, P., Ferrari. A., Laloui, L., 2013. An experimental and constitutive investigation on the chemo-mechanical behaviour of a clay. Géotechnique. 63(3), 244-255.

Wu, Y.C., Berezansky, P.A., 1995. Low electrolytic conductivity standards." J. Res. Natl. Inst. Stand. Technol. 100(5), 521-527.

Xing, H., Yang, X.M., Xu, C., Ye, G.B., 2009. Strength characteristics and mechanisms of salt-rich soil - cement. Eng. Geol. 103, 33-38.

Yao, K., Chen, Q.S., Xiao, H.W, Liu, Y.Y, Lee, F.H., 2020. Small-strain shear modulus of cement-treated marine clay. J. Mater. Civ. Eng. 32, 04020114.

Ye, W.M., Zhang, F., Chen, B., Chen, Y.G., Wang, Q., Cui, Y.J., 2014. Effects of salt solutions on the hydro-mechanical behavior of compacted GMZ01 Bentonite. Environ. Earth. Sci. 72(7), 2621-2630.

Ye, W.M., Zhang, F., Chen, Y.G., Chen, B., Cui, Y.J., 2017. Influences of salt solutions and salinization-desalinization processes on the volume change of compacted GMZ01 bentonite. Eng. Geol. 222(18), 140-145.

Yesiller, N., Miller, C.J., Inci, G. Yaldo, K., 2000. Desiccation and cracking behavior of three compacted landfill liner soils. Eng. Geol. 57(1-2), 105-121.

Yılmaz. G., Yetimoglu, T., Arasan, S., 2008. Hydraulic conductivity of compacted clay liners permeated with inorganic salt solutions. Waste. Manag. Res. 26(5), 464-473.

Yong, R.N., Ouhadi, V.R., 2007. Experimental study on instability of bases on natural and lime/cement-stabilized clayey soils. Appl. Clay Sci. 35(3-4), 238-49.

Youn, J.U., Choo, Y.W., Kim, D.S., 2008. Measurement of small-strain shear modulus G_{max} of dry and saturated sands by bender element, resonant column, and torsional shear tests. Can. Geotech. J. 45, 1426-1438.

Yukselen-Aksoy, Y., Kaya, A., Ören, A.H., 2008. Seawater effect on consistency limits and compressibility characteristics of clays. Eng. Geol. 102, 54-61.

Yunus, N.M., Wanatowski, D., Stace, L.R. 2013. The influence of chloride salts on compressibility behaviour of lime-treated organic clay. Int. J. GEOMATE. 5(1), 640-646.

Yunus, N.M., Marto, A., Pakir, F., Kasran, K., Jamal, M.A.A., Jusoh, S.N., Abdullah, N., 2015. Performance of lime-treated marine clay on strength and compressibility chracteristics. Int. J. GEOMATE. 8, 1232-1238.

Zeng, L.L., Cui, Y.J., Conil, N., Zghondi, J., Armand, G., Talandier, J., 2017. Experimental study on swelling behaviour and microstructure changes of natural stiff teguline clays upon wetting. Can. Geotech. J. 54, 700-709.

Zeng, L.L., Hong, Z.S., Cui, Y.J., 2015. Determining the virgin compression lines of reconstituted clays at different initial water contents. Can. Geotech. J. 52, 1408-1415.

Zeng, Z.X., Cui, Y.J., Zhang, F., Conil, N., Talandier, J., 2020. Effect of technological voids on swelling behaviour of compacted bentonite–claystone mixture. Can. Geotech. J. 57(12), 1881-1892. https://doi.org/10.1139/cgj-2019-0339

Zeng, Z.X, Cui, Y. J., Talandier, J., 2021. Compaction and sealing properties of bentonite/claystone mixture: Impacts of bentonite fraction, water content and dry density. Eng. Geol, 287, 106122.

Zeng, Z.X., Cui, Y. J., Zhang, F., Conil, N., Talandier, J., 2019. Investigation of swelling pressure of bentonite/claystone mixture in the full range of bentonite fraction. Appl. Clay

Sci. 178, 105137.

Zhang, G., Germaine, J.T., Whittle, A.J. Ladd, C.C., 2004. Index properties of a highly weathered old alluvium. Géotechnique. 54(7), 441-451.

Zhang, D.W., Cao, Z.G., Fan, L.B., Liu, S.Y., Liu, W.Z., 2014. Evaluation of the influence of salt concentration on cement stabilized clay by electrical resistivity measurement method. Eng. Geol. 170, 80-88.

Zhang, F.Y., Wang, G.H., Kamai, T., Chen, W.W., Zhang, D.X., Yang, J., 2013a. Undrained shear behaviour of loess saturated with different concentrations of sodium chloride solution. Eng. Geol. 155, 69-79.

Zhang, D.W., Fan, L.B., Liu, S.Y., Deng, Y.F., 2013b. Experimental investigation of unconfined compression strength and stiffness of cement treated salt-rich clay. Mar. Georesour. Geotechnol. 31(4), 360-374.

Zhang, F., Ye, W.M., Chen, Y.G., Chen, B., Cui, Y.J., 2016a. Influences of salt solution concentration and vertical stress during saturation on the volume change behavior of compacted GMZ01 bentonite. Eng. Geol. 207(3), 48-55.

Zhang, Y., Ye, W.M., Chen, B., Chen, Y.G., Ye, B., 2016b. Desiccation of NaCl-contaminated soil of earthen heritages in the Site of Yar City, northwest China. Appl. Clay Sci. 124-125, 1-10.

Zhang, X.W., Mavroulidou, M., Gunn, M.J., 2017a. A study of the water retention curve of lime-treated London Clay. Acta Geotech. 12, 23-45.

Zhang, Y., Ye, W.M., Chen, Y.G., Chen, B., 2017b. Impact of NaCl on drying shrinkage behavior of low-plasticity soil in earthen heritages. Can. Geotech. J. 54(12), 1762-1774.

Zhang, F., Cui, Y.J., Ye, W.M., 2018a. Distinguishing macro-and micro-pores for materials with different pore populations. Géotechnique Lett. 8(2), 102-110.

Zhang, T.W., Cui, Y.J., Lamas-Lopez, F., Calon, N., Costa D'Aguiar, S., 2018b. Compacted soil behaviour through changes of density, suction, and stiffness of soils with remoulding water content. Can. Geotech. J. 55(2), 182-190.

Zhang, T.W., Deng, Y.F., Cui, Y.J., Lan, H.X., Zhang, F.Y., Zhang, H.Y., 2019. Porewater salinity effect on flocculation and desiccation cracking behaviour of kaolin and bentonite considering working condition. Eng. Geol. 251:11-23.

Zhao, B.D., Wang, J.F., Andò, E., Viggiani, G., Coop, M.R., 2020. Investigation of particle breakage under one-dimensional compression of sand using x-ray microtomography. Can. Geotech. J. 57, 754-762.

Zhou, Y.G., Chen, Y.M, 2005. Influence of seismic cyclic loading history on small strain shear modulus of saturated sands. Soil Dyn. Earthq. Eng. 25, 341-353.

Zou, D.G, Liu, X.Y., Liu, J.M., Zhang, H., Zhou, C.G., Pei, H.F., 2019. A torsional vibration device for shear wave velocity measurement of coarse grained soils. Meas. J. Int. Meas. Confed. 148, 106972.